This work was performed for the Jet Propulsion Laboratory, California Institute of Technology, sponsored by the National Aeronautics and Space Administration under Contract NAS7-100.

N68-18661

Surveyor Spacecraft System

SURVEYOR VI FLIGHT PERFORMANCE FINAL REPORT

JPL Contract 950056/January 1968

SSD 68189-6

J. D. Cloud

J. D. CLOUD
Manager
System Engineering and Analysis Laboratory

T B Van Horne

T. B. VAN HORNE
Manager
Analysis Department

W B McIntyre

W. B. MC INTYRE
Project Engineer
Analysis Department

HUGHES

HUGHES AIRCRAFT COMPANY
SPACE SYSTEMS DIVISION

CONTENTS

					Page
1.0	INTRODUCTION AND SCOPE				1-1
2.0	DESCRIPTION OF SURVEYOR SYSTEM				
	2.1	Surveyor VI Mission Objectives			2-1
	2.2	Surveyor VI Flight Configuration			2-1
	2.3	References			2-9
3.0	SYSTEM SUMMARY				
	3.1	Summary of Significant Anomalies			3-1
	3.2	Conclusions			3-2
4.0	SYSTEM PERFORMANCE ANALYSIS				
	4.1	General Mission Summary			4-1
		4.1.1	Spacecraft Transit Phase Command Log		4-1
		4.1.2	Prelaunch Countdown		4-1
		4.1.3	Launch, Injection, and Separation		4-2
		4.1.4	DSIF Acquisition		4-2
		4.1.5	Coast Phase I Including Canopus Acquisition		4-2
		4.1.6	Midcourse Correction and Coast Phase II		4-3
		4.1.7	Terminal Descent Phase		4-3
		4.1.8	Initial Lunar Operation		4-19
	4.2	Reliability Analysis			4-19
		4.2.1	Surveyor VI Reliability Estimates		4-19
		4.2.2	Future Reliability Predictions		4-21
	4.3	References and Acknowledgments			4-31
5.0	PERFORMANCE ANALYSIS				
	5.1	THERMAL CONTROL SUBSYSTEM			
		5.1.1	Introduction: Surveyor Thermal Control Techniques		5.5-1
		5.1.2	Thermal Anomalies - Failure of Thermal Switches to Open in Lunar Night		5.1-2
		5.1.3	Thermal Subsystem Summary		5.1-2
			5.1.3.1	Transit	5.1-2
			5.1.3.2	Lunar	5.1-2

PRECEDING PAGE BLANK NOT FILMED.

	5.1.4	Thermal Performance in Transit	5.1-3
		5.1.4.1 Prelaunch Phase	5.1-3
		5.1.4.2 Postlaunch Phase	5.1-11
		5.1.4.3 Midcourse	5.1-11
		5.1.4.4 Coast Phases	5.1-12
		5.1.4.5 Terminal Descent Phase	5.1-15
	5.1.5	Thermal Performance – First Lunar Day	5.1-16
		5.1.5.1 Touchdown and Orientation	5.1-16
		5.1.5.2 Heater Performance	5.1-16
		5.1.5.3 Compartment System	5.1-16
		5.1.5.4 Surveyor Environmental Test Laboratory (SETL) Spacecraft Model	5.1-16
		5.1.5.5 Television Camera Operation	5.1-19
		5.1.5.6 Alpha Scattering System	5.1-19
	5.1.6	Lunar Night Thermal Performance	5.1-21
	5.1.7	References	5.1-25
	5.1.8	Acknowledgment	5.1-25
	APPENDICES TO SECTION 5.1		
		A. Transit Temperature Plots	5.1-A1
		B. Lunar Day Temperature Plots	5.1-B1
5.2	ELECTRICAL POWER SUBSYSTEM		
	5.2.1	Introduction	5.2-1
	5.2.2	Anomaly Description	5.2-4
	5.2.3	Summary	5.2-4
		5.2.3.1 Transit	5.2-4
		5.2.3.2 Lunar	5.2-4
	5.2.4	Analysis	5.2-4
		5.2.4.1 Mission Telemetry Plots	5.2-7
		5.2.4.2 Power Loads and Sources Budget	5.2-7
		5.2.4.3 Comparison of Flight Loads and Flight Acceptance Test Loads	5.2-8
		5.2.4.4 Lunar Translation Plots	5.2-8
	5.2.5	Reference	5.2-17
	5.2.6	Acknowledgment	5.2-17
5.3	RF DATA LINK SUBSYSTEM		
	5.3.1	Introduction	5.3-1
	5.3.2	Anomaly Discussion	5.3-4
		5.3.2.1 Loss of Two-Way Lock During Canopus Acquisition	5.3-4
		5.3.2.2 Down Link Signal Levels Larger Than Expected	5.3-4
		5.3.2.3 Spacecraft Not Reacting to Transmitted Command	5.3-21
	5.3.3	Summary and Conclusions	5.3-22

5.3.4	Subsystem Performance Analysis		5.3-26
	5.3.4.1	General Discussion	5.3-26
	5.3.4.2	Mission Phase 1: Prelaunch to Spacecraft Acquisition	5.3-33
	5.3.4.3	Mission Phase 2: Coast	5.3-38
	5.3.4.4	Mission Phase 3: Canopus Acquisition Maneuver	5.3-42
	5.3.4.5	Mission Phase 4: Midcourse Maneuver	5.3-51
	5.3.4.6	Mission Phase 5: Terminal Maneuver	5.3-52
	5.3.4.7	Mission Phase 6: Descent and Touchdown	5.3-53
	5.3.4.8	Mission Phase 7: Lunar	5.3-53
	5.3.4.9	Mission Data Plots	5.3-55
5.3.5	References		5.3-55
5.3.6	Acknowledgments		5.3-56

5.4	SIGNAL PROCESSING			
	5.4.1	Introduction		5.4-1
	5.4.2	Anomalies		5.4-1
	5.4.3	Summary		5.4-1
	5.4.4	Signal Processing Analysis		5.4-2
		5.4.4.1	Unbalance Current Corrections	5.4-2
		5.4.4.2	Potentiometer Reference Voltage Corrections	5.4-2
		5.4.4.3	Current Calibration Signals	5.4-3
		5.4.4.4	Touchdown Strain Gage Data	5.4-3
	5.4.5	Documentation		5.4-4
	5.4.6	Acknowledgments		5.4-4
5.5	FLIGHT CONTROL			
	5.5.1	Introduction		5.5-1
		5.5.1.1	Attitude Control	5.5-1
		5.5.1.2	Angular Maneuvers	5.5-1
		5.5.1.3	Velocity Correction	5.5-1
		5.5.1.4	Soft Landing	5.5-2
		5.5.1.5	Mission Performance	5.5-2
		5.5.1.6	Analysis	5.5-2
	5.5.2	Anomaly Description		5.5-2
	5.5.3	Summary		5.5-2
	5.5.4	Subsystem Performance Analysis		5.5-9
		5.5.4.1	Prelaunch	5.5-9
		5.5.4.2	Launch Through Separation From Centaur	5.5-9
		5.5.4.3	Sun Acquisition	5.5-11
		5.5.4.4	Canopus (Star Aquisition)	5.5-14
		5.5.4.5	Coast Phase Attitude Control	5.5-23
		5.5.4.6	Premidcourse Attitude Maneuvers	5.5-24
		5.5.4.7	Postmidcourse Attitude Maneuvers	5.5-29

		5.5.4.8	Midcourse Velocity Correction	5.5-31
		5.5.4.9	Preretro Maneuvers	5.5-37
		5.5.4.10	Main Retro Phase	5.5-43
		5.5.4.11	Terminal Descent Phase	5.5-49
	5.5.5	References		5.5-51
	5.5.6	Acknowledgments		5.5-51
5.6	VERNIER PROPULSION			
	5.6.1	Introduction		5.6-1
		5.6.1.1	Description	5.6-1
		5.6.1.2	Purpose	5.6-1
	5.6.2	Anomalies		5.6-3
	5.6.3	Summary and Recommendations		5.6-3
	5.6.4	Subsystem Performance Analysis		5.6-3
		5.6.4.1	Prelaunch	5.6-3
		5.6.4.2	Launch	5.6-4
		5.6.4.3	Coast Phase I	5.6-4
		5.6.4.4	Midcourse	5.6-5
		5.6.4.5	Coast Phase II	5.6-7
		5.6.4.6	Terminal Descent	5.6-11
		5.6.4.7	First Lunar Day	5.6-11
	5.6.5	References		5.6-17
	5.6.6	Acknowledgments		5.6-17
	APPENDIX A TO SECTION 5.6. FIRST LUNAR DAY VERNIER SYSTEM PRESSURE LOSS STUDY			
		Introduction		5.6-A1
		Conclusions		5.6-A1
		Discussion		5.6-A1
5.7	PROPULSION – MAIN RETRO			
	5.7.1	Introduction		5.7-1
	5.7.2	Anomaly Description		5.7-2
	5.7.3	Summary and Recommendations		5.7-2
	5.7.4	Subsystem Performance Analysis		5.7-3
		5.7.4.1	Thrust Versus Time	5.7-3
		5.7.4.2	Specific Impulse	5.7-5
		5.7.4.3	Retro Disturbance Torques	5.7-5
		5.7.4.4	T_{3500}	5.7-6
	5.7.5	References		5.7-6
	5.7.6	Acknowledgments		5.7-6
5.8	ALTITUDE MARKING RADAR			
	5.8.1	Introduction		5.8-1
	5.8.2	Anomalies		5.8-2
	5.8.3	Summary		5.8-2
	5.8.4	Subsystem Performance Analysis		5.8-3
		5.8.4.1	Event Times	5.8-3
		5.8.4.2	Load Current Signals	5.8-3
		5.8.4.3	Late Gate Signals	5.8-4
		5.8.4.4	DB Budget	5.8-4

		5.8.4.5	Expected Marking Range	5.8-6
		5.8.4.6	Marking Range Dispersion	5.8-7
		5.8.4.7	AMR Parameter Reconstruction	5.8-9
		5.8.4.8	AMR AGC Evaluation	5.8-11
	5.8.5	References and Documentation		5.8-11
	5.8.6	Acknowledgments		5.8-15
5.9	RADVS PERFORMANCE			
	5.9.1	Introduction		5.9-1
	5.9.2	Anomalies		5.9-4
	5.9.3	Summary		5.9-4
	5.9.4	Subsystem Performance Analysis		5.9-4
		5.9.4.1	RADVS Turn-on	5.9-4
		5.9.4.2	Velocity Acquisition Conditions	5.9-4
		5.9.4.3	Range Acquisition Conditions	5.9-5
		5.9.4.4	Revised Nominal db Budget	5.9-6
		5.9.4.5	Surveyor VI Event Times	5.9-6
		5.9.4.6	Descent Reconstruction	5.9-6
		5.9.4.7	Radar Reflectivity Analysis	5.9-6
		5.9.4.8	Reflectivity Model	5.9-14
	5.9.5	RADVS Documentation		5.9-14
	5.9.6	Acknowledgments		5.9-15
5.10	STRUCTURES PERFORMANCE			
	5.10.1	Introduction		5.10-1
	5.10.2	Anomaly Description		5.10-1
	5.10.3	Summary		5.10-2
	5.10.4	Performance Analysis		5.10-2
		5.10.4.1	Launch Phase	5.10-2
		5.10.4.2	Touchdown	5.10-2
	5.10.5	References		5.10-5
	5.10.6	Acknowledgments		5.10-6
5.11	MECHANISMS SUBSYSTEM			
	5.11.1	Introduction		5.11-1
	5.11.2	Anomaly Description		5.11-3
	5.11.3	Summary and Recommendations		5.11-3
	5.11.4	Subsystem Performance Analysis		5.11-3
		5.11.4.1	Landing Gear Deployment	5.11-3
		5.11.4.2	Omnidirectional Antenna Deployment	5.11-3
		5.11.4.3	A/SPP Performance	5.11-3
	5.11.5	References		5.11-13
	5.11.6	Acknowledgments		5.11-13

5.12	TERMINAL DESCENT TRAJECTORY PERFORMANCE		
	5.12.1	Introduction	5.12-1
	5.12.2	Anomaly Description	5.12-2
	5.12.3	Summary and Recommendations	5.12-2
	5.12.4	Performance Analysis	5.12-2
	5.12.4.1	Introduction	5.12-2
	5.12.4.2	Postflight Analysis Computer Programs	5.12-7
	5.12.4.3	Velocity Change Due to Thrusting During Retro Phase	5.12-8
	5.12.4.4	Main Retro Thrust Versus Time Curve	5.12-13
	5.12.4.5	Retro Thrust Misalignment	5.12-17
	5.12.4.6	6DOF Simulation of Doppler Data	5.12-19
	5.12.4.7	Vernier Propellant Consumption	5.12-21
	5.12.4.8	Spacecraft Landing Location	5.12-23
	5.12.4.9	Trajectory Reconstruction	5.12-23
	5.12.5	Acknowledgments	5.12-33
5.13	TELEVISION		
	5.13.1	Introduction	5.13-1
	5.13.2	Anomalies	5.13-1
	5.13.3	Summary	5.13-1
	5.13.4	Subsystem Performance	5.13-1
	5.13.5	References	5.13-8
	5.13.6	Acknowledgments	5.13-8
5.14	ALPHA SCATTERING EXPERIMENT		
	5.14.1	Introduction	5.14-1
	5.14.1.1	Purpose	5.14-1
	5.14.1.2	Description	5.14-1
	5.14.2	Anomalies	5.14-4
	5.14.3	Recommendations	5.14-4
	5.14.4	Subsystem Performance Analysis	5.14-4
	5.14.5	Reference	5.14-15
	5.14.6	Acknowledgment	5.14-15

1.0 INTRODUCTION AND SCOPE

On day 311 at 07:39:01.075 GMT, the sixth Surveyor spacecraft was launched from pad 36B at AFETR at a launch azimuth of 82.955 degrees. The launch into parking orbit was near perfect, with the spacecraft being injected into its translunar trajectory after the second Centaur burn at 311:08:04:30 GMT. Subsequent transit operations were nominal, and terminal descent to a soft landing on the moon was accomplished on 10 November 1967. Over 30,000 high quality television pictures were taken, and approximately 59 hours were accumulated by the alpha scattering device. In addition to further experimental information concerning the chemical composition of the lunar surface, the first powered flight translation of a Surveyor spacecraft was accomplished at 10:32:02 GMT on day 321. Over 10,000 of the television pictures were taken from the post-translation position, providing valuable stereo views of surface objects.

The basic purpose of this report is to document the actual performance of this spacecraft throughout the mission, compare its performance with that predicted from spacecraft design, summarize preliminary failure investigations, and recommend any changes or modifications that should be made to the spacecraft design. This report is based on both real time and post-mission data analysis.

2.0 DESCRIPTION OF SURVEYOR SYSTEM

The Surveyor spacecraft is designed and built by Hughes Aircraft Company for the National Aeronautics and Space Administration under the direction of the California Institute of Technology Jet Propulsion Laboratory. It has been conceived and designed to effect a transit from earth to the moon, perform a soft landing, and transmit to earth basic scientific and engineering data relative to the moon's environment and characteristics.

2.1 SURVEYOR VI MISSION OBJECTIVES

The primary objectives of the Surveyor VI spacecraft system were as follows:

1) Accomplish a soft landing near the center of the moon at 0.42°N and 1.33°W

2) Demonstrate spacecraft capability to soft land on the moon with an oblique approach angle of 25 degrees

3) Obtain postlanding television pictures

4) Obtain data on radar reflectivity, thermal characteristics, touchdown dynamics, and other measurements of the lunar surface through use of various payload equipment, including the alpha scattering device.

Surveyor VI achieved these objectives. A soft landing occurred near the center of the moon at an approach angle of 24.5 degrees. Television pictures were transmitted from the lunar surface, extensive use was made of the alpha scattering device, and the first lunar powered flight translation was accomplished.

2.2 SURVEYOR VI FLIGHT CONFIGURATION

For a summary description of the major Surveyor functions and design mechanization, consult the "Surveyor I Flight Performance Final Report" or Section 2.3 of the "Surveyor Spacecraft Equipment Specification" (References 1

TABLE 2-1. MAJOR SURVEYOR V DESIGN CHANGES

Subsystem	Change
RF	Elimination of power dropoff with temperature Elimination of microswitches in transfer and SPDT switches
Signal Processing	Data channel reassignment
Solar Panel	Use of flat cell mounting Lower voltage output
Power	Elimination of auxiliary battery Elimination of OCR in battery charge regulator Higher efficiency and current limiting in boost regulator
Flight Control	Separation latch Increased midcourse timing capability Terminal descent staging Nitrogen tank thermal characteristics
Radars	Improved AMR noise figure RADVS 3-beam crosscoupled sidelobe logic RADVS crosscoupled sidelobe logic at low altitudes RADVS on/off relay
Propulsion	Helium check and relief valve assembly Pressure and temperature transducers on fuel lines
A/SPP	High torque motors Strengthened axes locks Strengthened sector gear Solar axis support tube
Television	Removable mirror assembly — Strengthened drive ring gear and drive shaft Potentiometers — New dry lube and thicker wiper Vidicons — Survival heater and optical front porch Spherical viewing mirrors
Alpha Scattering System	Instrument sensor Deployment mechanism Compartment C — Instrument electronics, instrument auxiliary, and thermal control

and 2). Surveyor VI is a reconfigured spacecraft (as compared to Surveyors I through 4). Major design changes were first made on Surveyor V, and Table 2-1 provides a summary of these (from Reference 3). In Table 2-2, additional changes to the reconfigured design, which occurred first on Surveyor VI, have been given (summarized from Reference 4). To define the spacecraft configuration at launch, a list of Surveyor VI control items, separated by subsystem or function, is given in Table 2-3 (Reference 5).

TABLE 2-2. SIGNIFICANT DESIGN CHANGES FROM SURVEYOR V TO VI

Change flight compartment B thermal blankets, permitting their installation and use for STV. Test access installed in compartment.
A third auxiliary TV viewing mirror was added to permit viewing of the lunar surface where the alpha scattering experiment is deployed.
A/SPP position potentiometer drive was changed to eliminate slippage.
Survey camera incorporates survivable vidicon and gain change.
Change in manufacturer source of subcarrier oscillators.

TABLE 2-3. SPACECRAFT UNIT CONFIGURATION AT LAUNCH

Subsystem	Part Name, Number, S/N
Electrical Power	Main battery, 237900, S/N 150
	Thermal control and heater A, 283724-1, S/N 14
	Thermal control and heater B, 283724-2, S/N 11
	Boost regulator, 3024240-1, S/N 15
	Battery charge regulator, 3024260-1, S/N 13
	Solar panel, 251167, S/N 2
	Main power switch, 254112, S/N 14
	Engineering mechanisms auxiliary, 263500-10, S/N 16
Flight Control	Flight control sensor group, 3023450-2, S/N 3
	Roll actuator, 235900-3, S/N 10
	Gas supply, attitude jet, 235600-3, S/N 1
	Attitude jets, 235700-2, S/N 12 and 18
	Attitude jet, 235700-3, S/N 8
	Secondary solar sensor, 235450-1, S/N 3
Radar	Altitude marking radar, 283810, S/N 13
	KPSM (RADVS), 232909, S/N 12
	SDC (RADVS), 232908-6, S/N 8
	Altitude velocity sensor antenna (RADVS), 232910, S/N 13
	Velocity sensor antenna (RADVS), 232911, S/N 13
	Waveguide assembly (RADVS), 232912, S/N 12
	RADVS on/off switch, 274153, S/N 14

Table 2-3 (continued)

Subsystem	Part Name, Number, S/N
Telecommunications	Transmitter A, 3024400-1, S/N 17
	Transmitter B, 3024400-1, S/N 19
	Command receiver A, 231900-3, S/N 18
	Command receiver B, 231900-3, S/N 26
	Omnidirectional antennas A and B, 232400, S/N 13 and 26
	Telemetry buffer amplifiers A and B, 290780-1, A/N 23 and 22
	Planar array antenna, 232300, S/N 14
	Low pass filters A and B, 233466, S/N 28 and 27
	RF switch, SPDT, 284344, S/N 14
	RF transfer switch, 284345, S/N 12
Signal Processing	Signal processing auxiliary, 232540-1, S/N 8
	Central command decoder, 232000-5, S/N 7
	Low data rate auxiliary, 264875-2, S/N 8
	Engineering signal processor, 233350-10, S/N 3
	Auxiliary engineering signal processor, 264900-7, S/N 2
	Central signal processor, 232200-7, S/N 2
	TV auxiliary, 232106-7, S/N 14
Television	Survey camera, 290512-3, S/N 14
	Photo chart, antenna B, 231051, S/N 17
	Photo chart, leg 1, 230992, S/N 17
	Viewing mirror, 3035010, S/N 3
	Viewing mirror, 3035000, S/N 3
	Viewing mirror, 3035080, S/N 2

Table 2-3 (continued)

Subsystem	Part Name, Number, S/N
Propulsion	Oxidizer tank, 287119, S/N 5
	Oxidizer tank, 287121, S/N 4
	Oxidizer tank, 287120, S/N 5
	Fuel tank, 287117, S/N 9
	Fuel tank, 287118, S/N 4
	Fuel tank, 287117, S/N 10
	Check and relief valve assembly 1, 287290-30, S/N 1
	Check and relief valve assembly 2, 287290-50, S/N 18
	Helium tank and valve assembly, 3026042, S/N 3
	Thrust chamber assembly, 285063-4 (Hughes), S/N 564
	Thrust chamber assembly, 285063-7 (Hughes), S/N 540
	Thrust chamber assembly, 285063-6 (Hughes), S/N 562
	Main retro, 238612, S/N A21-29
Mechanisms	Spaceframe, 3025093-1, S/N 1
	Omnidirectional antenna A mechanism, 3028000-1, S/N 3
	Omnidirectional antenna B mechanism, 273880-2, S/N 2
	Antenna/solar panel positioner, 3035092-1, S/N 1
	Leg position pots, 988684-1, S/N 337, 338, and 339
	Retro-rocket release mechanisms, 230069-1, S/N 19, 20, and 21

Table 2-3 (continued)

Subsystem	Part Name, Number, S/N
Mechanisms (continued)	Separation sensing and arming devices, 293400, S/N 22, 23, and 25
	Shock absorbers, legs 1 through 3, 238927, S/N 13, 15, and 16
	Magnet assembly, leg 2, 3050836-1, S/N 7
	Footpad leg 1, 263947, S/N 572
	Footpads legs 2 and 3, 263947-1, S/N 569 and 573
	Landing gear, 261278, S/N 9
	Landing gear, 261279, S/N 8
	Landing gear, 3025100, S/N 2
	Crushable block, 261281-2, S/N 406
	Crushable block, 3050736,
	Crushable block, 3050697
	Strain gauge amplifier, 238930, S/N 9
Alpha Scattering	Auxiliary, 274350-1, S/N 4
	Electronics, 239305, S/N FU-1
	Deployment mechanism, 3024801, S/N 2
	Sensor head, 239304, S/N FU-1
	Standard sample, 239397, S/N F1
	Heater, compartment C, 290900, S/N 2
	Passive simulator, 3024506, S/N 4
Thermal Control	Thermal switch A, 3028200-2, S/N 7
	Thermal switch A, 3028200-1, S/N 21, 22, 23, 25, 27, 28, 29, and 32
	Thermal switch B, 3028200-4, S/N 6

Table 2-3 (continued)

Subsystem	Part Name, Number, S/N
Thermal Control (continued)	Thermal switch B, 3028200-3, S/N 7, 13, 15, 16, and 18
	Thermal shell, compartment A, 3025262, S/N 2
	Thermal shell, compartment B, 3025288, S/N 2
	Thermal tray, compartment A, 3025094, S/N 3
	Thermal tray, compartment B, 3025096, S/N 3
Harness	Wiring harness compartment B, 3025790, S/N 1
	Wiring harness compartment A, 3025637, S/N 2
	Wiring harness basic bus 1, 3020797, S/N 1
	Wiring harness TV camera, 285833, S/N 2
	Wiring harness basic bus 2, 3020799, S/N 1
	Wiring harness TV auxiliary, 3025391, S/N 2
	Wiring harness retro motor, 285832, S/N 2
	Wiring harness battery cell volt, 3025155, S/N 8
	Wiring harness separation squibs, 285831, S/N 3
	Wiring harness A/SPP, 3025420, S/N 3
	Cable, retro igniter, 286927, S/N 2
	Wiring harness ASI, 3025641, S/N 2

2.3 REFERENCES

1) "Surveyor I Flight Performance Final Report," Hughes Aircraft Company, SSD 68189R, October 1966.

2) "Surveyor Spacecraft Equipment Specification," Hughes Aircraft Company 224832, Revision A.

3) "Surveyor V Flight Performance Final Report," Hughes Aircraft Company, SSD 68189-5, November 1967.

4) "Minutes of SC-6 Consent to Ship Meeting," Hughes Aircraft Company, SSD 74092, 5 September 1967.

5) "Spacecraft Configuration Index, Spacecraft SC-6," Hughes Aircraft Company, Engineering Order 239606, Revision F, 2 November 1967.

3.0 SYSTEM SUMMARY

3.1 SUMMARY OF SIGNIFICANT ANOMALIES

There were no anomalies during the transit portion of Mission F. Table 3-1 summarizes the three problems that occurred on the lunar surface. For this report, an anomaly is defined as an unexpected occurrence that might be indicative of a spacecraft trouble or failure.

TABLE 3-1. SPACECRAFT ANOMALIES

GMT, day:hr:min:sec	Anomaly	Effect on Mission
321:10:32:04	During lunar translation, the first of two vernier engine off commands (0735) did not shut down the engines (see subsection 5. 3. 2. 3), probably due to an RF multipath null.	None. Engines were shut down by the second 0735 command.
After day 323	The vernier system developed a leak which eventually resulted in complete loss of helium and oxidizer pressure. There was probably a slow liquid leak on oxidizer tank 1 initially, followed by a rapid gas leak (see Appendix A to subsection 5. 6).	None on normal operations. Any attempts at lunar translation should be modified if telemetry indicates a vernier system pressure loss.
Day 329 and after	Several thermal switches in compartments A and B stuck closed, or did not actuate at proper temperature (TFR 18271). (See subsection 5. 1. 2.)	The extent of spacecraft operations into lunar night was shortened, and the probability of lunar night survival was reduced.

PRECEDING PAGE BLANK NOT FILMED.

3.2 CONCLUSIONS

Performance of the Surveyor VI spacecraft was excellent during flight and on the moon. A selected group of performance parameters which could be directly determined through analysis of spacecraft telemetry for the six Surveyor flights are summarized in Table 3-2. Required or predicted values of these parameters for Surveyor VI are included in this summary.

TABLE 3-2. SUMMARY PERFORMAN

Spacecraft		Actual				
		1	2	3	4	
Parameters	Units					
LAUNCH TO ACQUI						
Ignition-liftoff	GMT	0 second is 1966 150:14:41:00.99	0 second is 1966 263:12:31:59.824	0 second is 1967 107:07:05:01.059	0 second is 1967 195:11:53:29.215	0 second is 1967 251:07:57:01.257
Booster engine cutoff	seconds from liftoff	142.2	142.29	142.5	141.88	153.4
Booster jettison		145.6	145.75	145.5	145.38	156.8
Insulation panel jettison		176.2	176.06	176.2	176.18	198.4
Nose fairing jettison		203.0	202.90	203.5	203.38	228.6
Sustainer engine cutoff		239.3	235.17	237.7	237.98	246.4
Atlas/Centaur separation		241.8	237.03	239.6	241.58	248.7
Centaur main engine cutoff 1		689.3	686.3	569	687.98	587.0
Centaur main engine cutoff 2		None	None	2028.8	None	1103.9
Surveyor:						
Extend landing gear		715.5	710.7	2051.8	715.78	1124.2
Extend omnidirectional antenna		725.7	720.7	2061.8	725.28	1134.4
Transmitter to high power		745.4	741.4	2072.5	745.98	1154.7
Electrical disconnect from Centaur		752.3	742.08	2087.8	751.28	1160.9
Centaur separation		757.1	752.58	2093.4	756.88	1165.5
Time to null rates to 0.1 deg/sec	seconds	≤15	<4	<11	<13	<20
Pitch	degrees	≈0	–	–	+0.35	
Yaw	degrees	≈2.3	–	–	-2.0	
Roll	degrees	≈0	–	–	~0	
Centaur retro maneuver time	seconds	L + 996.0	L + 992.8	L + 2355.5	L + 996.88	L + 1405.5
Solar axis deployment time	seconds	617	360	358	348	298
Spacecraft separated weight	pounds	~2192.8	2203	2281.3	2294.9	2216.8
Spacecraft cg location						
X	inch	-0.116	-0.101	+0.058	+0.044	-0.070
Y	inch	-0.092	+0.010	+0.179	-0.188	+0.779
Z	inch	~59.185	59.16	58.95	58.88	59.69
Spacecraft moment of inertia						
I_{xx}	slug-ft^2	195.4	200	202	204	210
I_{yy}	slug-ft^2	191.7	196	198	200	211
I_{zz}	slug-ft^2	213.3	215	223	225	211
COAST						
Sun acquisition						
Roll angle	degrees	-87	-71.5	-181	-59.4	-342
Yaw angle	degrees	+99	+15	+38	+42.1	+18.0
Total time	seconds	372	174.8	438.2	203	722
Star acquisition						
Proper acquisition and Canopus verification		Manual	Manual	Automatic	Automatic	Automatic
Roll angle from beginning of maneuver to Canopus	degrees	580.6	240	+205	+210.5	+179
Objects identified		Alpha Doradus Phi Eridani Markab Pi Cygni Alderamin Regulus Alpha Hydrae Naos Canopus	Zeta Draconis Beta Draconis Ras Alhague Shaula Theta Scorpii Gamma Arae Alpha Tr. Australis Alpha Arae Zeta C Majoris Canopus	Canopus Moon Jupiter Earth Procyon Altair Adhara	Eta U Majoris Delta Velorum Gamma Casiopeiae Canopus Moon Earth	Zeta Ophiuchi (Antares, Tau Sco Gamma Tr. Austr Canopus (Alnitak, Alnilam, Alpha Leporis Earth Bellatrix Polaris
Mean roll rate during star map phase	deg/sec	+0.5004	+0.4998	0.5011	0.5003	0.5007
Effective gain of Canopus sensor	X Canopus	1.5	>1.5	1.03 - 1.22	1.16	1.32
Attitude orientation						
Average error from sunline						
Pitch	degree	-0.058	-0.07	0	+0.009	Very small
Yaw	degree	-0.053	-0.1	+0.02	+0.08	
Roll	degree	-0.055	-0.08	-0.06	~0	

FOLDOUT FRAME

ICE PARAMETERS

5	6	Subsection or Reference	Predicted or Specified for Surveyor VI	Reference	Comments
SITION SUMMARY					
	0 second is 1967 311:07:39:01. 075				
	153. 4	FPAC	153. 5	Preflight nominal trajectory	
	156. 7		156. 6		
	198. 3		198. 5		
	228. 6		228. 5		
	245. 6		248. 5		
	248. 2		250. 2		
	581. 0		579. 6		
	1468. 7		1465. 9		
	1487. 9		1487		
	1498. 4		1497. 5		
	1518. 9		1518		
	1524		1523. 5		
	1528. 9		1529		
	<17		Within 50 seconds		
	≈ 0				
	L+1532. 3	FPAC	L + 1534		
	337	5. 11. 4	337		
	2220.				Spacecraft weight,cg and moments of inertia at separation
	-0. 063				
	+0. 732				
	59. 7				
	210				
	211				
	211				
SUMMARY					
	-264 +22 572	5. 5. 4. 3	18 minutes maximum	224832A (7.3.3.3.4)	Roll maneuver until activation of acquisition sun sensor and then a yaw maneuver until primary sun sensor illumination
	Automatic	5. 5. 4. 4		224832A (7.3.3.3.5)	
	+298				
	Deneb				
rpii)	Canopus				
alis	Earth				
Mintaka)					
	0. 5009		0. 5		
	1. 10			Design	Normally the gain setting is 1 x Canopus
	Very small		Within 0. 2 degree	224832A (7. 3. 3. 3. 6)	Sensor group roll axis shall be held within 0. 2 degree of sun-spacecraft line

Table 3-2 (continued)

Spacecraft Parameters	Units	Actual 1	2	3	4	5			
COAST SUMMARY (continued)									
Average error from Canopus line of sight									
Pitch	degree	-0.058	-0.07	0	~0	Very small			
Yaw	degree	-0.053	-0.1	+0.02	~0				
Roll	degree	-0.055	-0.08	-0.06	+0.104				
Limit cycle optical mode									
Average amplitude – roll	degrees	0.441	0.441	0.55	0.6	0.46			
Average amplitude – pitch	degrees	0.470	0.45	0.51	0.44	0.37			
Average amplitude – yaw	degrees	0.457	0.37	0.54	0.41	0.50			
Average period	seconds	65	64	68.5	64				
Limit cycle inertial mode									
Average amplitude – roll	degrees	0.415	0.47	0.46	0.48	0.30			
Average amplitude – pitch	degrees	0.443	0.42	0.48	0.46	0.31			
Average amplitude – yaw	degrees	0.417	0.43	0.50	0.53	0.36			
Average period	seconds	50	61	68.5	61				
Gyro drift									
Roll	deg/hr	0.2	-0.78	+1.1	-0.5	+0.85			
Pitch	deg/hr	0	+0.24	+0.6	-1.0	+0.60			
Yaw	deg/hr	0.75	+1.09	-0.8	+0.15	-0.60			
MIDCOURSE SUMMARY									
Time of initiation of vernier burn	GMT	151:06:45:03.801	264:05:00:02	108:05:00:03.433	197:02:30:00	252:01:45:02.3			
Duration of burn(s)	seconds	20.815	NA	4.245	10.48	(1) 14.22	(2) 10.04	(3) 23.04	(4) 12.32
Command of first maneuver	GMT	151:06:30:12.888	264:04:44:00	108:04:46:49.8	197:02:15:28.9	252:01:32:57.0			Prior to Midcourse
First maneuver	degrees	86.6 roll	+75.4 roll	+56.7 roll	+72.5 roll	+71.9 roll			
Command of second maneuver	GMT	151:06:34:48,861	264:04:48:05	108:04:50:08.2	197:02:21:09.9	252:01:36:27.3			
Second maneuver	degrees	58.0 yaw	+110.6 yaw	-39.1 pitch	-64.3 yaw	-35.5 yaw			
Command of third maneuver	GMT	NA	NA	NA	NA	NA			
Third maneuver	degrees	NA	NA	NA	NA	NA			
Midcourse ΔV	m/sec	20.26	NA	4.2	10.13	(1) 14.2	(2) 9.78	(3) 22.54	(4) 13.02
Midcourse ΔV error	m/sec	-0.081	NA	0.176	-0.17				
Peak attitude transients at ignition									
Roll	degrees	-0.43	NA	-1.0	–	-0.88	-0.88	-0.84	-0.90
Pitch	degrees	0	NA	-0.125	-0.17	-0.24	0	-0.13	-0.05
Yaw	degrees	-0.08	NA	+0.30	+0.19	+0.08	+0.25	+0.19	+0.20
Peak angular error at shutdown			NA			(1)	(2)	(3)	(4)
Roll	degrees	–		+0.58	+1.18	+1.2	+1.0	+1.1	-0.44
Pitch	degrees	–		+0.96	+1.09	+0.13	+0.16	+0.58	+0.14
Yaw	degrees	–		+1.97	+0.10	+0.50	+0.90	+0.48	+1.3
Roll actuator position									
Peak at ignition	degrees	+0.9		-0.8	-1.22	–			
Mean during burn	degrees	+0.65		–	–				
Engine shutoff impulse									
Engine 1	lbs/sec	0.27		-0.31	-0.18	-0.06	-0.10	-0.13	-0.07
Engine 2	lbs/sec	-0.37		+0.42	+0.03	+0.05	+0.18	+0.11	+0.1
Engine 3	lbs/sec	0.10		-0.11	+0.15	+0.01	+0.08	+0.02	-0.03
Shutdown angular rate									
Pitch	deg/sec	–			+0.24	+0.06	+0.06	+0.13	+0.06
Yaw	deg/sec	–			-0.01	+0.06	+0.23	+0.12	+0.17
TERMINAL DESCENT SUMMARY									
Landing location		2.41°S, 43.35°W	5.5°N, 12.00°S	2.94°S, 23.34°W	0.47°N, 1.44°W	1.50°N, 23.19°E			
Approach flight-path angle	degrees	6.13	NA	23.6	31.5	46.4			
Goldstone visibility									
Pre-touchdown	hours	4		~4.5	NA				
Post-touchdown	hours	5		~10	NA				
Transmitter high power on		153:05:20:18.3		109:23:09:40.7	198:01:09:26.8	253:23:51:41.3			
Telemetry mode	NA	2/3		6	6	6			
Bit rate	bps	1100		1100	1100	1100			
Touchdown strain gages	NA	Yes		Yes	Yes	Yes			

FOLDOUT FRAME

	6	Subsection or Reference	Predicted or Specified for Surveyor VI	Reference	Comments
:d)					
	Very small		Within 0.2 degree	224832A (7.3.3.3.6)	Canopus sensor null with respect to sensor group roll pitch plane
	0.41 0.52 0.52 —	5.5.4.6	±0.44 degree	224832A (7.3.3.3.3)	
	0.48 0.37 0.20 —	5.5.4.6	±0.44 degree	224832A (7.3.3.3.3)	
	-0.64 0 +1.4	5.5.4.9		224832A (7.3.3.3.3C)	Non g-sensitive
	312:02:20:02.1	5.5.4.8 and 4.1.6			First burn only Surveyor V
(5) (6) 3.07 | 5.40	10.242				
No. 1	312:02:02:59 +91.8 roll 312:02:09:08 +127.4 yaw NA NA				
(5) (6) .32 | 5.28	10.1217 +0.058		10.06		
.0 | -0.82 .05 | +0.1 .22 | -0.18	— 0.17 0.17	5.5.4.8			
(5) (6) .2 | +0.36 .71 | +1.2 .5 | -2.2	+0.77 -0.33 -0.47	5.5.4.8			( ) refers to particular mid-course of Surveyor V
—	— —				
.53 | -0.29 .65 | +0.15 .12 | +0.14	+0.085 -0.09 +0.015	5.5.4.8	Δ Impulse <0.66 lb/sec	224832A (8.3.1.3.2.4.2)	
.46 | +0.13 .76 | ≈0	-0.08 -0.1	5.5.4.8			
RY					
	0.470°N, 1.480°W 24.5 ~3 — 314:00:07:32.2 6 1100 Yes				SC-2 impacted moon. SC-4 impacted moon. Last signal on terminal descent.

FOLDOUT FRAME

3-6

Table 3-2 (continued)

Spacecraft Parameters	Units	Actual 1	2	3	4	5
TERMINAL DESCENT SUMMARY (continued)						
Command of first maneuver	GMT		NA	109:23:23:30	198:01:24:44.2	254:00:12:15.1
First maneuver	degrees	+89.3 roll		-158 yaw	+80.8 roll	+73.8 roll
Command of second maneuver	GMT			109:23:30:17	198:01:29:34.2	254:00:16:20.5
Second maneuver	degrees	+60.0 yaw		-76.8 pitch	+92.7 yaw	+119.6 yaw
Command of third maneuver	GMT			109:23:34:35	198:01:35:04.6	None
Third maneuver	degrees	+94.4 roll		-64 roll	-25.4 roll	None
AMR enabled (station time)	GMT	153:06:12:57.684		109:23:59:35.252	198:02:00:16.99	254:00:43:00.9
AMR mark (station time)	GMT	153:06:14:39.708		110:00:01:12.829	198:02:01:56.08	254:00:44:39.081
AMR backup mark (station time)	GMT			110:00:01:13.439	198:02:01:56.35	254:00:44:46.38
Ignition delay time	seconds	7.85		5.09	2.73	12.33
Retro delay time	seconds	1.1		1.1	1.12	1.07
Retro action time (T3500)	seconds	38.9		41.02	≈42	38.56
Maximum retro thrust	pounds	9900		9550	9250	9950
Thrust to velocity vector	degrees	0.26		0.34	0.17°	0.30
Retro thrust to cg offset	inch	< 0.02		0.024	–	-0.048
Start RADVS – controlled descent						
Slant range	feet	27820		36158	NA	6300
Altitude	feet	27800		32900	49420	4139
V_z	fps	425		462	NA	+46
V_x	fps	71.3		171	NA	-41
V_y	fps	-4.1			NA	+50
V-Total	fps	430		483	1092	79
Flight-path angle	degrees			26.8	26.8	-35.67
Peak attitude transient at retro ignition						
Roll	degree	–		-0.22	~0	-0.16
Pitch	degree	-0.41		-0.10	-0.09	+0.5
Yaw	degree	-1.03		~0	-0.35	-0.5
RODVS acquire condition						
Slant range	feet	55000		63900	78000	
Velocity	fps	3280		3230	3414	
RORA acquire condition						
Slant range	feet	36000		43700	NA	
Velocity	fps	690		640	NA	
Beam loss of locks						
Retro case	NA	No. 3 once		No. 4 once	None	Nos. 4, 3 once
Other	NA	None		Nos. 3, 4 once	None	None
Segment acquisition					NA	
Slant range	feet	18000		22300		806
Velocity	fps	442		495		97
1000 foot mark conditions						
Time	GMT	153:06:17:10.494		110:00:03:53.023		254:00:46:19.697
Velocity	fps	103.1		103.27		96.03
Attitude	degree	1.11		0.51		-7.5
10-fps mark conditions						
Slant range	feet	43		46		46
Time	GMT	153:06:17:28.719		110:00:04:10.623		254:00:46:37.097
Attitude	degree	0.7		0.025		-0.53
Δ Time 1000 foot mark to 10-fps mark	seconds	18.22		17.6		17.4
Δ Time 10 fps mark to 14-foot mark	seconds	6.45		NA		5.6
Vernier engine shutoff						
14 foot mark	GMT	153:06:17:34.169		NA		254:00:46:42.697
Altitude (from foot pads)	feet	13		NA		14.5
Vertical velocity	fps	5		NA		5.2
Lateral velocity	fps	≈0		NA		~0
Angle to local vertical	degree	≈0.3		NA		-0.11
Time to touchdown	seconds	1.53		NA		1.7
Touchdown condition trajectory						
Vertical velocity	fps	12.2		6-8		13.5
Lateral velocity	fps	≈0.6		≈0		0.5
Attitude	degree	≈0		≈0		≈0
Touchdown conditions (strain gages)						
Vertical velocity	fps	10		6		12 to 13
Lateral velocity	fps	2		0.5		< 1
Attitude	degree	1		≈0		≈0
Spacecraft attitude after landing						
Roll orientation (+ x-axis to north)	degrees	179 clockwise		134.2 clockwise		114.5 clockwise
Tilt magnitude	degrees			12		19.5
Tilt direction	degrees			277 clockwise		7.6 clockwise
Vernier fuel used	pounds	139.0		140.1		136.62

FOLDOUT FRAME

	6	Subsection or Reference	Predicted or Specified for Surveyor VI	Reference	Comments
	314:00:25:20				
	+82.0 roll				
	314:00:29:38				
	+111.8 yaw				
	314:00:34:56				
	+120.5 roll				
	314:00:56:19.6				AMR times received at DSS
	314:00:57:57.038				
	314:00:57:58.99				
	5.900				
	1.100			224832A	
	39.37	5.7.3		(7.3.3.3.9)	SC-4 loss of signal at
	9700	5.7.3			198:02:02:41.018
	0.8	5.5.3			
	0.04	5.5.3			
	40574	5.12.3		5.12.3	Burnout data for SC-4
	36625		37,005		is at signal loss
	463		468		
	225		105		
	0		36		
	515		482		
	8.1		10.82		
	-0.77	5.5.3		224832A	
	-0.17			(7.3.3.3.10)	
	-0.08				
	68022				
	3202				
	35924				
	515				
	None				
	24730	5.12.3	23,000		
	522	5.12.3	494		
	314:01:00:40.534				
	106	5.12.3	106		
	1.04	5.12.3	1.3		
	50	5.12.3	43		
	314:01:00:57.634				
	0.03	5.12.3	0.02		
	17.1				
	6.5				
	314:01:01:04.133				
	14	5.12.3	13.0		
	5	5.12.3	5		
	~0		~0		
	0.03	5.12.3	0.01		
	1.33				
	12.5	5.12.3	12.5		
	0	5.12.3	0		
	≈0	5.12.3	—		
	11.5	5.10.4.2			
	<1	5.10.4.2			
	≈2				
	148.99 clockwise				
	0.86				
	335.04 clockwise				
	146.33	5.12.3	136.65		

4.0 SYSTEM PERFORMANCE ANALYSIS

4.1 GENERAL MISSION SUMMARY

Surveyor VI was launched from pad 36B at Cape Kennedy on a parking orbit lunar intercept trajectory at a launch azimuth of 82.995 degrees; this launch culminated in a soft landing on the moon. The flight of Surveyor VI began on 7 November 1967 (311:07:39:01.075 GMT) and soft landed on 10 November 1967 (314:01:01:05.467 GMT). A total of 30,065 television pictures were received and 59 hours of lunar science data were accumulated by the alpha scattering experiment. At 321:10:32:02 GMT, lunar liftoff and translation were successfully accomplished. Performance of the Atlas and Centaur (AC-14) launch vehicles appeared excellent throughout the flight period as mark events occurred very close to predicted times. No anomalies were noted during transit.

A summary of the mission event history is contained in Table 4-1. Injection of the spacecraft occurred at 311:08:04:30 GMT on a trajectory that with a midcourse correction provided a total miss of 7.2 kilometers from the targeted aiming point of 1.133°W longitude and 0.417°N latitude for a landing site estimated to be 0.437°N latitude and 1.373°W longitude from final post-touchdown orbit determination. Lunar Orbiter evaluation gave 470°N latitude and 1.480°W longitude. During transit, sun acquisition, solar panel deployment, DSIF acquisition, initial commanding and interrogations, star acquisition and verification, and midcourse and terminal descent maneuvers were all successfully executed.

The earth track traced by Surveyor VI is shown in Figure 4-1, and predicted view periods for the tracking stations are given in Table 4-2.

4.1.1 Spacecraft Transit Phase Command Log

A detailed list of spacecraft commands sent during the transit portion is presented in Table 4-3. This table includes the time the command was sent, bit rate, telemetry mode, and tracking station originating the command.

4.1.2 Prelaunch Countdown

During countdown, an apparent real time anomaly occurred when the AMR heater on command (0624) sent in step 004, substep 011 was not indicated by the command printer. Subsequent investigation showed that the command was sent and received at the spacecraft but was missed by the command printer. The countdown proceeded to a successful launch.

4.1.3 Launch, Injection, and Separation

The parking orbit boost phase was normal, with the Atlas roll and pitch programs and the normal opening and closing of the spacecraft inertia switch being confirmed by spacecraft telemetry. Figure 4-2 shows the major events of the trajectory through separation as seen in profile. Table 4-4 contains Atlas/Centaur mark events, as well as spacecraft telemetry verification of Centaur-initiated commands. Subsequent to injection and just prior to its separation from the spacecraft, the Centaur issued the preprogrammed commands "extend landing gears," "extend omni antennas," and "transmitter high power on," all of which are verified by spacecraft telemetry. Separation of Centaur and Surveyor occurred immediately thereafter.

Following separation, solar panel stepping was initiated, the cold gas jets were enabled, and the roll-yaw sequence to acquire the sun was initiated. The poor quality of data prevented effective monitoring of the solar panel stepping and the spacecraft maneuvers to acquire the sun. Verification of solar-panel-axis stepping to the transit position, A/SPP roll-axis stepping to the transit position, and achievement of sun lock on were finally accomplished.

4.1.4 DSIF Acquisition

At 311:08:10 GMT, the spacecraft became visible to DSS 51 (Johannesburg), which achieved one-way lock at this time. At 311:08:13 GMT, the acquisition was completed when two-way lock was established between DSS 51 and the spacecraft.

The first ground-controlled sequence (initial spacecraft operations) was initiated at L+40M31S by commanding off the transmitter high voltage and filament power. In addition, commands were sent to the spacecraft to turn off other equipment required only for the launch-to-DSIF-acquisition phase (e.g., solar panel deployment logic off and A/D isolation amplifier off); to seat the solar panel and roll axis locking pins securely (i.e., by rocking the axes back and forth); to switch from the 550-bps, low modulation index mode to the 1100-bps, normal modulation index mode; and to interrogate telemetry commutator modes so that the overall condition of the spacecraft could be assessed. All spacecraft responses to commands were normal.

4.1.5 Coast Phase I Including Canopus Acquisition

During star map, while performing a sun-locked roll maneuver with the spacecraft in high power, DSS 61 lost receiver lock at a signal level about 10 db above threshold. Star mapping was terminated by commanding sun mode on to stop the roll and turning the transponder off. The problem was apparently caused by the transponder dropping phase lock, resulting in the shift to NBVCXO and loss of DSS lock, then reacquiring a command sideband and causing an in and out of lock condition which resulted in an intermittent signal at the DSS. This signal was steady in AFC mode (transponder off). At 311:16:14:24, roll was resumed in one-way lock (transponders off). Earth, Deneb, Canopus, and two other objects were identified until automatic Canopus lockon was achieved. Two-way lock (transponder on) was regained, the spacecraft was returned to low power mode, and the spacecraft systems continued to operate normally.

4.1.6 Midcourse Correction and Coast Phase II

The midcourse velocity correction was executed at 312:02:20:02.1 for 10.3 seconds after successful predmidcourse roll (+91.8 degrees) and yaw (+127.4 degrees) maneuvers. The attitude rotations were initiated at limit cycle nulls to further minimize pointing errors. Following successful execution of the midcourse correction, the postmidcourse maneuvers were performed in a nominal manner. Sun lockon was achieved at 312:02:31, Canopus lockon was indicated at 312:02:35, and cruise mode on was commanded at 312:02:37:39.

In addition to normal spacecraft operations in the second coast phase, the alpha scattering instrument was operated successfully for calibration purposes. Fourteen gyro drift checks were performed during transit to provide accurate gyro rates for terminal operations planning. The gyro drift rates provided prior to terminal descent were: roll (-0.64 deg/hr), pitch (0.0 deg/hr), and yaw (+1.40 deg/hr).

The retro engine temperature at retro ignition was predicted (52.55°F), and a resulting engine burn time of 39.60 seconds (from ignition to the 3500-pound thrust level) was provided.

4.1.7 Terminal Descent Phase

Terminal descent closely followed design and predicted performance. An initial roll of +82.0 degrees, followed by a yaw of +111.8 degrees, and then a final roll of +120.5 degrees, aligned the retro engine thrust axis to the desired direction. The three attitude maneuvers, as well as other preretro ignition spacecraft operations (e.g., loading the proper altitude mark to vernier ignition delay quantity — 5.875 seconds, establishing the retro sequence mode for ensuring that the desired automatic flight control sequences would occur in response to the altitude radar mark, establishing the proper vernier engine thrust level for the retro burning phase, turning on flight control thrust phase power, etc.), were executed on schedule. Retro separation was smooth, vernier descent contour acquisition was obtained, and vernier descent control was normal. Event times occurred at the proper time (Table 4-1). The engines were turned off automatically by the 14-foot mark, and a soft landing was verified from the retention of the communication link and continued nominal spacecraft performance, and later by the touchdown strain gage data.

TABLE 4-1. SURVEYOR VI MISSION MILESTONES

Event	GMT, day:hr:min:sec
Launch	311:07:39:01.075
Separation — electrical disconnect*	311:08:04:24.626
Separation — mechanical*	311:08:04:29.995
A/SPP solar panel unlocked*	311:08:04:31.4 ± 2.0
A/SPP solar panel locked in transit position*	311:08:10:07.4 ± 2.0
A/SPP roll axis locked in transit position*	311:08:14:07.4 ± 2.0
Automatic sun acquisition complete*	311:08:16
Initial DSS acquisition (one-way) confirmed*	311:08:10:16
Initial DSS acquisition (two-way lock) confirmed*	311:08:13:27
First ground command sent to spacecraft	311:08:19:32.7
Canopus verification begins	311:15:42:33
Canopus lockon (automatic)*	311:16:28:30
First premidcourse (roll) maneuver executed	312:02:02:59.5
Second premidcourse (yaw) maneuver executed	312:02:09:08.0
Midcourse correction executed	312:02:20:02.1
Sun reacquired	312:02:31:44
Canopus reacquired	312:02:35:53
Transmitter high power on	314:00:07:32.2
1100 bps	314:00:08:20.0
Mode 5 on	314:00:11:44.2
Transponder off	314:00:16:58.6
Start roll maneuver	314:00:25:19.8
Start yaw maneuver	314:00:29:38.1
Start roll maneuver	314:00:34:55.8
Reset nominal thrust	314:00:40:59.5
Retro sequence delay	314:00:41:41.5
Retro sequence mode on	314:00:52:04.9
AMR power on	314:00:53:16.9
FC thrust phase power on	314:00:54:16.9
Enable AMR	314:00:56:16.9
Emergency AMR signal	314:00:57:56.4
AMR on (R 1)*	314:00:53:19.604 ± 0.6
AMR enabled (R 11)*	314:00:56:19.600 ± 0.6
AMR mark (FC-64)*	314:00:57:57.038 ± 0.05
Vernier ignition (FC-28)*	314:00:58:02.938 ± 0.05
Retro ignition (FC-29)*	314:00:58:04.038 ± 0.05
RADVS pyro switch (EP-33)*	314:00:58:04.396 ± 0.6
RADVS on (R-28)*	314:00:58:05.798 ± 0.6
RODVS (FC-34)*	314:00:58:34.098 ± 0.6
Inertial switch signal (FC-63)*	314:00:58:43.397 ± 0.30
Retro burn out (FC-30)*	314:00:58:43.637 ± 0.05

Table 4-1 (continued)

Event	GMT, day:hr:min:sec
Start maximum thrust (FC-78)*	314:00:58:53.297 ± 0.6
Retro eject signal (FC-31)*	314:00:58:55.637 ± 0.05
Retro ejected (V-4)*	314:00:58:55.942 ± 0.255
Start RADVS-controlled descent (FC-42)	314:00:58:57.737 ± 0.05
RORA (FC-33)*	314:00:58:59.297 ± 0.6
Segment acqusition*	314:00:59:21.276 ± 0.14
1000-foot mark (FC-37)*	314:01:00:40.534 ± 0.05
10-fps mark (FC-36)*	314:01:00:57.634 ± 0.05
14-foot mark (FC-38)*	314:01:01:04.133 ± 0.05
Touchdown*	314:01:01:05.467 ± 0.003
Selected Lunar Events	
First 200-line picture	314:01:51
Initial sun acquisition (azimuth)	314:03:18
Initial earth acquisition	314:03:39
First 600-line picture	314:04:04
Alpha scattering turned on	314:05:38
A/SPP fine positioning (start)	314:12:01
Alpha scattering instrument deployed	314:12:07
Modulation interrupt sequence	314:20:42
Attitude jet firing experiment	315:03:22
Attitude jet firing experiment	315:03:46
Static firing	315:03:57
Alpha scattering instrument deployed	315:12:07
RF communication test	318:14:23
Telecommunication signal processing test	318:15:30
DSS antenna axial ratio test	320:10:00
Lunar translation	321:10:32:02
Combined RF and signal processing (start)	325:21:37
Combined RF and signal processing (end)	325:23:25
Optimum antenna pointing for lunar surface operations	326:00:28
Lock landing gear	326:16:08
Day/night terminator (predict)	328:14:42
To standby	330:09:34

*Telemetry time at ground station.

TABLE 4-2. PREDICTED VIEW PERIOD SUMMARY

Station	Event	GMT Time		
		November 1967	Hour	Minute
DSS 51 Johannesburg	5^{o} elevation rise	7	8	9
DSS 42 Tidbinbilla	5^{o} elevation rise	7	8	34
DSS 72 Ascension	0^{o} elevation rise	7	12	38
DSS 42 Tidbinbilla	5^{o} elevation set	7	14	13
DSS 61 Madrid	5^{o} elevation rise	7	14	31
DSS 11 Goldstone	5^{o} elevation rise	7	21	51
DSS 51 Johannesburg	90^{o} hour angle set	7	22	23
DSS 61 Madrid	5^{o} elevation set	7	22	43
DSS 72 Ascension	0^{o} elevation set	8	1	29
DSS 42 Tinbinbilla	5^{o} elevation rise	8	2	13
DSS 11 Goldstone	5^{o} elevation set	8	6	51
DSS 51 Johannesburg	270^{o} hour angle rise	8	10	56
DSS 61 Madrid	5^{o} elevation rise	8	14	43
DSS 42 Tinbinbilla	5^{o} elevation set	8	15	8
DSS 11 Goldstone	5^{o} elevation rise	8	22	1
DSS 51 Johannesburg	90^{o} hour angle set	8	22	54
DSS 61 Madrid	5^{o} elevation set	8	23	29
DSS 42 Tinbinbilla	5^{o} elevation rise	9	2	37
DSS 11 Goldstone	5^{o} elevation set	9	7	19
DSS 51 Johannesburg	270^{o} hour angle rise	9	11	8
DSS 61 Madrid	5^{o} elevation rise	9	14	45
DSS 42 Tinbinbilla	5^{o} elevation set	9	15	16
DSS 11 Goldstone	5^{o} elevation rise	9	22	3
DSS 51 Johannesburg	90^{o} hour angle set	9	23	2
DSS 61 Madrid	5^{o} elevation set	9	23	42

TABLE 4.3 SURVEYOR VI COMMAND SEQUENCE

Command Number	Description	GMT, hr:min:sec	Telemetry Mode	Bit Rate
		Day 311 – DSS-51		
0107	Xmtr Hi Volt Off	08:19:32.7	5	550
0110	Xmtr Fil Pwr Off	19:40.5		
0130	Xfer Sw B Lo Pwr	19:41.0		
0236	A/D Iso Amp Off	22:40.0		
0316	SP Deploy Logic Off	22:40.5		
0126	Xfer Sw A Lo Pwr	22:41.0		
0402	Step SP Minus (x10)	23:20.0		
0401	Step SP Plus (x5)	23:26.0		
0405	Step Roll Axis Plus (x10)	24:28.0		
0406	Step Roll Axis Minus (x5)	24:34.0		
0510	AESP Off	25:23.5		
0226	Mode 1	25:31.0	1	
0237	Low Mod SCOs Off	25:32.0		
0216	7.35 kc SCO On	25:32.5		
0205	1100 bps	25:33.0		1100
0231	Mode 4	30:27.0	4	
0227	Mode 2	33:18.0	2	
0232	ESP Off	36:43.5		
0507	Mode 6	36:51.0	6	
0506	Mode 5	38:35.3	5	
0510	AESP Off	12:14:39.3		
0231	Mode 4	14:46.3	4	
0227	Mode 2	20:29.7	2	
0226	Mode 1	25:01.7	1	
0232	ESP Off	28:11.7		
0506	Mode 5	28:12.3	5	
		Day 311 – DSS-61		
0510	AESP Off	15:30:00.1		
0231	Mode 4	30:00.6	4	
0227	Mode 2	36:07.1	2	
0226	Mode 1	39:24.5	1	
0105	Xmtr B Fil Pwr On	42:35.6		
0127	Xfer Sw B Hi Pwr	44:20.5		
0106	Xmtr Hi Volt On	44:20.6		
0220	7.35 kc SCO Off	44:57.8		
0217	33 kc SCO On	44:57.9		
0206	4400 bps	44:58.9		4400
0704	Cruise Mode	45:51.9		
0715	Man Delay Mode	45:52.9		
0710	Pos Angle Maneuver	45:53.9		
0120	Select Omni A	46:31.3		

Table 4.3 (continued)

Command Number	Description	GMT, hr:min:sec	Telemetry Mode	Bit Rate
0714	Sun and Roll	15:50:21.9	1	4400
0121	Select Omni B	56:39.7		
0702	Sun Acq Mode	58:44.0		
0124	Xponder Pwr Off	16:04:38.6		
0231	Mode 4	06:51.5	4	
0226	Mode 1	12:12.0	1	
0704	Cruise Mode	13:00.9		
0715	Man Delay Mode	13:01.9		
0710	Pos Angle Maneuver	13:02.9		
0714	Sun and Roll	14:22.3		
0703	Sun-Star Acq Mode On	25:27.6		
0704	Cruise Mode	29:12.0		
0232	ESP Off	30:04.6		
0506	Mode 5	30:10.6	5	
0123	Xponder B Pwr On	32:07.4		
0205	1100 bps	36:16.4		1100
0220	Hi Data Rate SCOs Off	36:17.4		
0216	7.35 kc SCO On	36:18.4		
0107	Xmtr Hi Volt Off	37:15.6		
0110	Xmtr Fil Pwr Off	37:27.8		
0130	Xfer Sw B Lo Pwr	37:28.8		
0700	Inertial Mode	43:04.9		
0306	SP Sw On, Bypass Off	52:57.5		
0307	Bypass On, SP Sw Off	57:42.0		
	Day 311 – DSS-51			
0704	Cruise Mode	18:04:10.6		
0700	Inertial Mode	18:21.5		
0306	Sp Sw On, Bypass Off	19:31.6		
0306	Sp Sw On, Bypass Off	19:20:46.4		
0704	Cruise Mode	22:31.9		
0700	Inertial Mode	24:24.9		
0306	SPSw On, Bypass Off	20:23:32.2		
0704	Cruise Mode	38:57.6		
0700	Inertial Mode	44:52.5		
0306	SPSw On, Bypass Off	22:00:29.0		
0704	Cruise Mode	03:03.0		
	Day 311 – DSS-11			
0510	AESP Off	22:16:17.6		
0231	Mode 4	16:23.6	4	
0504	137.5 bps	19:54.8		137.5
0204	Coast Phase Clock Rates	20:00.9		

Table 4.3 (continued)

Command Number	Description	GMT, hr:min:sec	Telemetry Mode	Bit Rate
0205	1100 bps	22:23:32.3	4	1100
0227	Mode 2	25:33.9	2	
0226	Mode 1	29:01.3	1	
0232	ESP Off	32:02.8		
0506	Mode 5	32:09.0	5	
0306	SPSw On, Bypass Off	48:04.4		
Day 312 – DSS-11				
0510	AESP Off	00:12:01.0		1100
0231	Mode 4	12:14.7	4	
0227	Mode 2	14:26.2	2	
0226	Mode 1	16:24.4	1	
0232	ESP Off	18:36.7		
0506	Mode 5	18:43.7	5	
0220	33, 7.35, 3.9 kc SCOs Off	24:42.6		
0221	Gyro Spd Sig Pro On	24:46.1		
0222	Next Gyro	26:40.2		
0222	Next Gyro	28:10.1		
0222	Next Gyro	29:57.6		
0223	Gyro Spd Sig Pro Off	31:34.7		
0216	7.35 kc SCO On	31:45.1		
0510	AESP Off	01:36:51.8		
0231	Mode 4	36:58.2	4	
0227	Mode 2	39:20.7	2	
0226	Mode 1	42:48.6	1	
0105	Xmtr B Fil Pwr On	49:27.2		
0127	Xfer Sw B Hi Pwr	51:18.6		
0106	Xmtr Hi Volt On	51:19.1		
0220	37, 7.35, 3.9 kc SCOs Off	52:04.2		
0217	33 kc SCO On	52:04.7		
0206	4400 bps	52:05.2		4400
0704	Cruise Mode	56:47.7		
0710	Pos Angle Maneuver	56:51.7		
3617	Interlock	57:00.2		
M 1614	Magnitude (460 BCD) (+91.8 degrees)	57:00.7		
0714	Sun and Roll	02:02:59.5		
3617	Interlock	07:03.7		
M 2335	Magnitude (637 BCD) (+127.4 degrees)	07:04.2		
0713	Yaw	09:08.0		
0521	Prop S-Gage Pwr On	14:14.0		4400
0700	Inertial Mode	14:14.5		
0720	Reset – Set IV Outputs	14:28.0		

Table 4.3 (continued)

Command Number	Description	GMT, hr:min:sec	Telemetry Mode	Bit Rate
0604	AMR Htr Off	02:15:56.7	1	4400
0613	VL2 FT2 Ther Pwr Off	15:57.2		
0616	VL1 OT2 Ther Pwr Off	15:57.7		
0621	VL3 OT3 Ther Pwr Off	15:57.9		
3617	Interlock	15:58.5		
0605	Unlk Roll Act, Press VPS	15:58.9		
0727	FC T-φ Pwr On	17:16.7		
3617	Interlock	17:41.9		
M0307	Magnitude (103 BCD)	17:42.4		
3617	Interlock	20:01.6		
0721	Vernier Ignition	20:02.1		
0735	Emer Vernier Eng Off	20:15.1		
0735	Emer Vernier Eng Off	20:16.6		
0737	FC T-φ Pwr Off	20:42.0		
0737	FC T-φ Pwr Off	20:44.0		
0522	Prop S-Gage Pwr Off	20:11.1		
0516	TD S-Gage Pwr Off	20:14.6		
0232	ESP Off	22:12.5		
0506	Mode 5	22:17.9	5	
0611	VL2 Ther Pwr On	23:20.1		
0614	VL1 Ther Pwr On	23:20.6		
0617	VL3 Ther Pwr On	23:21.6		
0624	AMR Htr On	23:22.1		
03617	Interlock	24:53.1		
M2335	Magnitude (637 BCD) (-127.4 degrees)	24:53.6		
0713	Yaw	26:06.5		
0702	Sun Acq. Mode On	31:44.0		
3617	Interlock	32:08.9		
M1614	Magnitude (460 BCD) (-91.8 degrees)	32:09.4		
0714	Sun and Roll	32:56.9		
0704	Cruise Mode	37:38.8		
0510	AESP Off	38:17.0		
0227	Mode 2	38:23.5	2	
0231	Mode 4	42:06.9	4	
0232	ESP Off	45:01.8		
0506	Mode 5	45:09.8	5	
0205	1100 bps	46:07.9		1100
0220	Hi Data Rate SCOs Off	46:08.3		
0216	7.35 kc SCO On	46:08.8		
0107	Xmtr Hi Volt Off	47:07.8		
0110	Xmtr Fil Pwr Off	47:08.3		
0130	Xfer Sw B Lo Pwr	47:08.8		

Table 4.3 (continued)

Command Number	Description	GMT, hr:min: sec	Telemetry Mode	Bit Rate
0515	TD S-Gage Pwr On	03:12: 28.0	5	1100
0517	TD S-Gage Data Chan On	12: 42.4		
0520	TD S-Gage Data Chan Off	28: 20.0		
0516	TD S-Gage Pwr Off	28: 26.2		
0522	Prop S-Gage Pwr Off	28: 34.6		
Day 312 – DSS-42				
0510	AESP Off	04:22: 41.3		
0231	Mode 4	22: 46.3	4	
0227	Mode 2	28: 50.3	2	
0226	Mode 1	33: 38.8	1	
0232	ESP Off	36: 12.8		
0506	Mode 5	36: 18.8	5	
0700	Inertial Mode	37: 42.8		
0704	Cruise Mode	05:42: 51.0		
0702	Sun Acq Mode On	08:32: 26.5		
0510	AESP Off	12:25: 23.8		
0231	Mode 4	25: 27.8	4	
0227	Mode 2	29: 15.8	2	
0226	Mode 1	32: 00.5	1	
0232	ESP Off	36: 27.5		
0506	Mode 5	36: 32.5	5	
0704	Cruise Mode	46: 28.8		
Day 312 – DSS-51				
0700	Inertial Mode	16:18: 39.3		
0510	AESP Off	17:14: 55.1		
0231	Mode 4	15: 02.1	4	
0227	Mode 2	23: 32.7	2	
0226	Mode 1	27: 46.6	1	
0232	ESP Off	32: 14.1		
0506	Mode 5	32: 21.6	5	
0704	Cruise Mode	53: 41.0		
0702	Sun Acq Mode On	18:59: 38.9		
Day 312 – DSS-61				
0510	AESP Off	21:16: 38.6		
0231	Mode 4	16: 43.6	4	
0227	Mode 2	19: 55.7	2	
0232	ESP Off	24: 49.2		
0506	Mode 5	24: 55.2	5	
0510	AESP Off	37: 09.1		

Table 4.3 (continued)

Command Number	Description	GMT, hr:min:sec	Telemetry Mode	Bit Rate
0226	Mode 1	21:37:13.6	1	1100
0232	ESP Off	41:59.7		
0506	Mode 5	42:03.7	5	
0704	Cruise Mode	42:27.6		
Day 312 – DSS-11				
0700	Inertial Mode	22:45:01.3		
Day 313 – DSS-11				
0704	Cruise Mode	00:11:17.9		
0700	Inertial Mode	01:11:24.9		
0510	AESP Off	50:32.7		
0231	Mode 4	50:39.6	4	
0227	Mode 2	53:03.3	2	
0226	Mode 1	54:48.4	1	
0232	ESP Off	57:32.4		
0506	Mode 5	57:39.6	5	
0704	Cruise Mode	02:25:36.5		
0700	Inertial Mode	03:29:51.6		
0704	Cruise Mode	04:48:09.4		
Day 313 – DSS-42				
0510	AESP Off	06:13:59.6		
0231	Mode 4	14:04.6	4	
0227	Mode 2	19:51.5	2	
0226	Mode 1	23:06.3	1	
0232	ESP Off	25:02.5		
0506	Mode 5	25:07.5	5	
0700	Inertial Mode	25:57.1		
0704	Cruise Mode	07:38:32.2		
0700	Inertial Mode	09:04:07.7		
0704	Cruise Mode	10:42:28.3		
0510	AESP Off	46:46.3		
0231	Mode 4	46:51.8	4	
0227	Mode 2	50:35.8	2	
0226	Mode 1	53:25.0	1	
0232	ESP Off	57:47.3		
0506	Mode 5	57:52.8	5	
0702	Sun Acq Mode On	11:01:22.1		
0411	Comp A Htr Pwr On	03:55.9		

Table 4.3 (continued)

Command Number	Description	GMT, hr:min:sec	Telemetry Mode	Bit Rate
	Day 313 — DSS-51			
0510	AESP Off	13:52:56:2		1100
0231	Mode 4	53:03.7	4	
0227	Mode 2	56:55.4	2	
0226	Mode 1	14:00:00.6	1	
0232	ESP Off	02:33.1		
0506	Mode 5	02:41.6	5	
0612	FT2 Ther Pwr On	53:17.0		
0615	OT2 Ther Pwr On	53:22.0		
0620	OT3 Ther Pwr On	53:28.0		
0704	Cruise Mode	15:26:55.4		
0510	AESP Off	17:58:16.4		
0231	Mode 4	58:24.4	4	
0227	Mode 2	18:01:51.9	2	
0226	Mode 1	04:59.9	1	
0232	ESP Off	07:06.9		
0506	Mode 5	07:14.9	5	
0503	550 bps	08:43.3		550
0204	Coast Phase Clk Rates	08:52.3		
0220	33, 7.35, 3.9 kc SCOs Off	08:55.9		
0215	3.9 kc SCO On	09:03.8		
1136	Sur Camera ETC On	19:55:38.5		
0136	Comp C Temp Cont On	20:25:07.4		
0510	AESP Off	37:13.9		
0231	Mode 4	37:21.9	4	
0232	ESP Off	43:09.9		
0506	Mode 5	43:17.9	5	
0510	AESP Off	21:35:39.0		
0231	Mode 4	35:56.0	4	
0227	Mode 2	50:09.0	2	
0226	Mode 1	53:04.0	1	
0232	ESP Off	58:28.0		
0506	Mode 5	58:35.0	5	
	Day 313 — DSS-11			
3503	Alpha Scat Htr Pwr On	22:27:26.7		
0510	AESP Off	39:25.2		
0231	Mode 4	39:32.7	4	
0227	Mode 2	42:10.1	2	
0226	Mode 1	46:04.4	1	
0232	ESP Off	48:51.6		
0506	Mode 5	49:00.1	5	
0220	33, 7.35, 3.9 kc SCOs Off	51:23.1		

Table 4.3 (continued)

Command Number	Description	GMT, hr:min:sec	Telemetry Mode	Bit Rate
0221	Gyro Spd Sig Pro On	22:51:28.6	5	550
0222	Next Gyro	52:32.1		
0222	Next Gyro	53:15.1		
0222	Next Gyro	53:53.1		
0223	Gyro Spd Sig Pro Off	54:40.1		
0215	3.9 kc SCO On	54:50.6		
0124	Xpdr Pwr Off	56:43.1		
0123	Xpdr B Pwr On	58:04.1		
0413	Comp A Htr Pwr Off	23:13:13.5		
0507	Mode 6	52:11.3	6	
0510	AESP Off	54:59.8		
0231	Mode 4	55:07.3	4	
Day 314 — DSS-11				
0105	Xmtr B Fil Pwr On	00:05:51.7		
0127	Xfer Sw B Hi Pwr	07:31.7		
0106	Xmtr Hi Volt On	07:32.2		
0220	33, 7.35, 3.9 kc SCOs Off	08:19.0		
0216	7.35 kc SCO On	08:19.5		
0205	1100 bps	08:20.0		1100
0214	Sum Amps Off	09:03.8		
0211	Phase Sum Amp B On	09:04.3		
0227	Mode 2	09:21.2	2	
0232	ESP Off	11:36.2		
0506	Mode 5	11:11.2	5	
0521	Prop S-Gage Pwr On	14:34.2		
0515	TD S-Gage Pwr On	15:00.6		
0517	TD S-Gage D-Ch On	15:01.1		
1133	Sur Camera VTC On	15:41.6		
0124	Xpdr Pwr Off	16:58.6		
0704	Cruise Mode	18:38.1		
0710	Pos Angle Maneuver	18:38.6		
3617	Interlock	18:39.1		
M1431	Magnitude (409 BCD) (+82.0 degrees)	18:39.6		
0714	Sun and Roll	25:19.8		
3617	Interlock	28:30.1		
M2117	Magnitude (559 BCD) (+111.8 degrees)	28:30.6		
0713	Yaw	29:38.1		
3617	Interlock	33:58.5		
M2233	Magnitude (603 BCD) (+120.5 degrees)	33:59.0		
0711	Roll	34:55.8		

Table 4.3 (continued)

Command Number	Description	GMT, hr:min:sec	Telemetry Mode	Bit Rate
0207	Pre Sum Amp On	00:40:02.5	5	1100
0723	Reset Nom Thr Bias	40:59.5		
3617	Interlock	41:41.0		
M0326	Retro Seq Delay (118 BCD) (5.875 seconds)	41:41.5		
0507	Mode 6	48:57.5	6	
0720	Reset Set IV Outputs	50:30.0		
0720	Reset Set IV Outputs	51:31.9		
3617	Interlock	52:04.4		
0724	Retro Seq Mode On	52:04.9		
0613	VL2 FT2 Ther Pwr Off	52:27.0		
0616	VL1 OT2 Ther Pwr Off	52:27.5		
0621	VL3 OT3 Ther Pwr Off	52:28.0		
1134	Sur Camera VTC Off	52:28.5		
1137	Sur Camera ETC Off	52:29.0		
0604	AMR Htr Off	52:29.5		
0135	Comp C Temp Cont Off	52:30.0		
3504	Aplha Scat Htr Off	52:30.5		
0625	AMR Pwr On	53:16.9		
0727	FC T-φ Pwr On	54:16.9		
0626	Enable AMR	56:16.9		
0730	Emer AMR Signal	57:56.4		
0730	Emer AMR Signal	57:56.9		
0730	Emer AMR Signal	57:57.4		
0737	FC T-φ Pwr Off	01:01:37.9		
0737	FC T-φ Pwr Off	01:39.4		
3617	Interlock	02:00.6		
0630	RADVS Pwr Off	02:01.1		
3617	Interlock	02:01.6		
0630	RADVS Pwr Off	02:02.1		
3617	Interlock	02:02.6		
0311	All FC Pwr Off	02:03.1		
3617	Interlock	02:03.6		
0311	All FC Pwr Off	02:04.6		
0506	Mode 5	02:45.0		
0510	AESP Off	04:46.2		
0227	Mode 2	05:07.4	2	
0516	TD S-Gage Pwr Off	06:10.4		
0520	TD S-Gage Data Chan Off	06:20.9		
0522	Prop S-Gage Pwr Off	06:25.4		

TABLE 4-4. SURVEYOR VI LIFTOFF AND BOOST EVENTS

Mark Number	Event	Actual Time, GMT, Day 311 hr:min:sec	Actual Time From Launch, seconds	Nominal Time From Launch, seconds	Nominal Time From Separation, seconds
	Liftoff (2-inch motion)	07:39:01.075	0	0	
1	Atlas boost engine cutoff (BECO)	07:41:34.475	153.42	153.5	
2	Atlas boost engine jettison	07:41:37.805	156.73	156.6	
3	Centaur insulation panel jettison	07:42:19.405	198.33	198.5	
4	Centaur nose fairing jettison	07:42:49.635	228.56	228.5	
5	Atlas SECO and VECO	07:43:06.625	245.55	248.5	
6	Atlas/Centaur separation	07:43:09.305	248.23	250.2	
7	Centaur main engine start (1)	07:43:19.795	258.72	259.7	
8	Centaur main engine cutoff (1)	07:48:42.095	581.02	579.6	
—	Centaur burn duration (1)	—	(322.3)	(319.9)	
9	100-pound thrust on	07:48:44.295	583.22	579.6	
10	100-pound thrust off			655.6	
11	6-pound thrust on	07:49:58.895	657.82	655.6	
12	100-pound thrust on	08:00:56.995	1315.92	1313.0	-216.0
13	Centaur main engine start (2) C2			1353.0	-176.0
14	Centaur main engine start (2) C1	08:01:34.995	1353.92	1353.0	-176.0
15	Centaur main engine cutoff (2)	08:03:29.745	1468.67	1465.9	- 63.1
—	Centaur burn duration (2)	—	(114.75)	(112.9)	—
16	Extend landing gear command	08:03:48.995	1487.92	1487.0	- 42.0
—	Legs down (telemetry)				
17	Unlock omnidirectional antenna command	08:03:59.495	1498.42	1497.5	- 31.5
—	Omnidirectional antennas extended (telemetry)	—			
18	Surveyor high power transmitter on	08:04:19.995	1518.92	1518.0	- 11.0
—	High power on (telemetry)	—			
19	Centaur/Surveyor electrical disconnect	08:04:25.095	1524.02	1523.5	- 5.5
—	Vehicle electrical separation (telemetry)	08:04:24:626			
20	Spacecraft separation	08:04:29.995	1528.92	1529.0	0
21	Begin Centaur turn around maneuver	08:04:33.395	1532.32	1534.0	5.0
22	Start Centaur lateral thrust	—	—	1574.0	45.0
23	End Centaur lateral thrust	—	—	1594.0	65.0
24	Start Centaur tank blowdown	08:08:29.995	1768.92	1769.0	240.0
25	End Centaur tank blowdown	08:12:40.195	2019.12	2019.0	490.0
26	Power changeover switch	08:14:20.095	2119.02	2119.0	590.0

78176-7 (U)

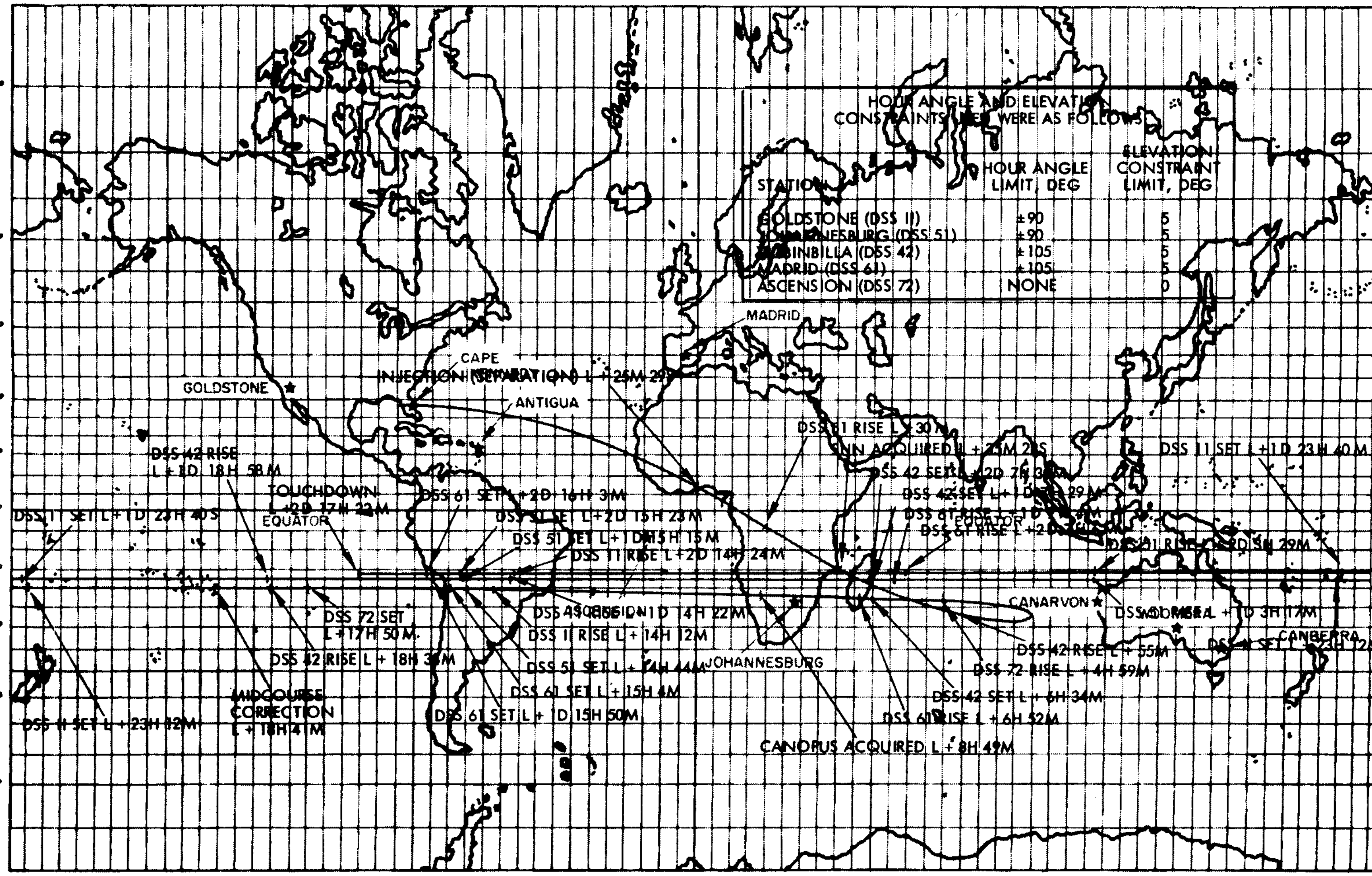

Figure 4-1. Surveyor VI Earth Track

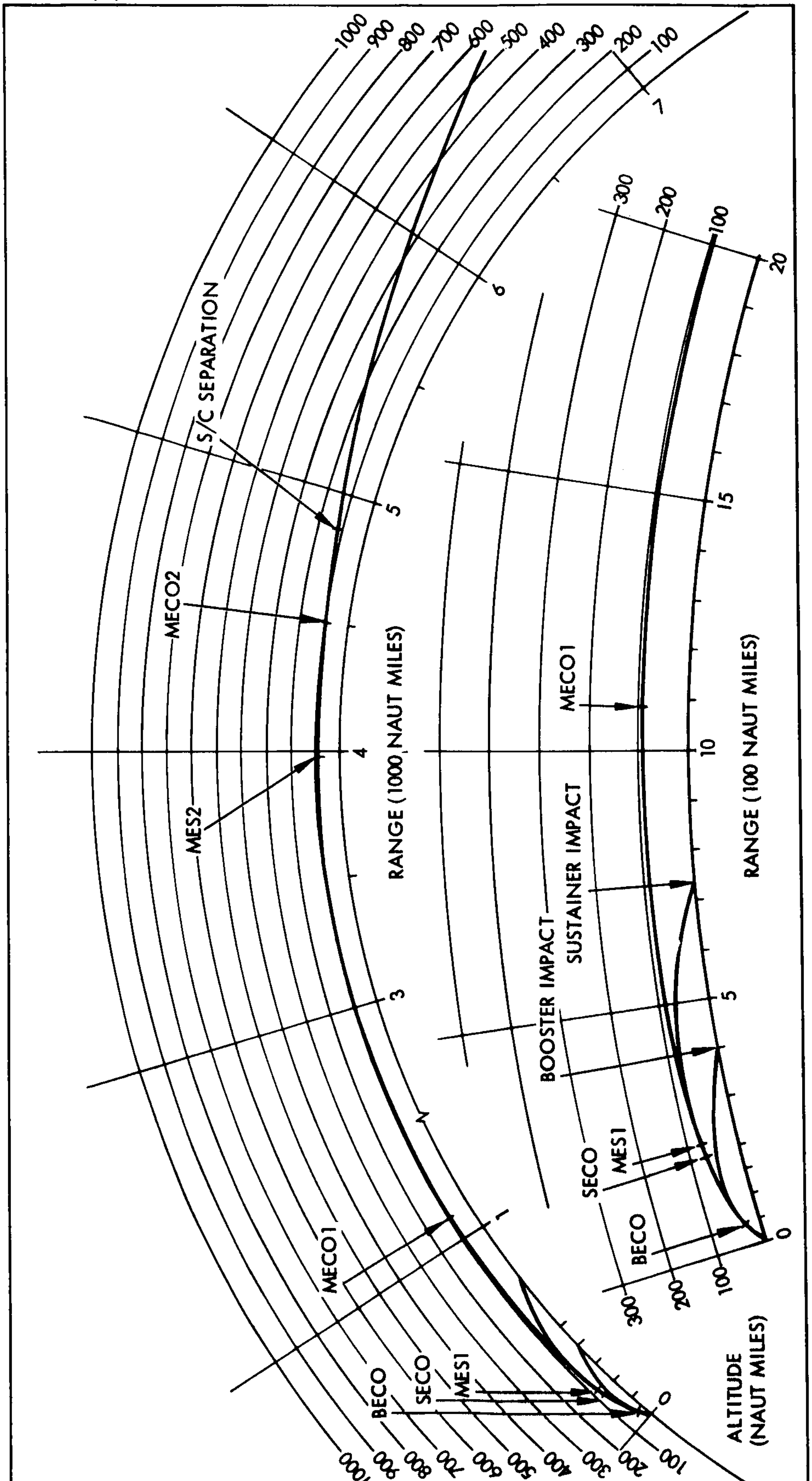

Figure 4-2. AC-14 Launch Phase Trajectory Profile

Strain gage data indicated that touchdown occurred at approximately 314:01:01:05.467 GMT, with leg 1 touching the surface first, followed by legs 2 and 3, in that order. The peak loads experienced by legs 1, 2, and 3 were approximately 1590, 1810, and 1590 pounds, respectively. These levels are indicative of a landing velocity of approximately 11.5 fps on a surface with a 5-psi static bearing strength and a slope of approximately 0.8 degree.

4.1.8 Initial Lunar Operation

After the initial engineering assessment, a 200-line television survey was conducted. The first 200-line picture was obtained at 314:01:51. The first command of the initial sun/earth acquisition was sent at 314:02:55:26. Thereafter, the sun was acquired in azimuth at 314:03:18:55, and earth acquisition with the planar array was completed at 314:03:39:42. The spacecraft was then configured for 600-line television, the first such picture being received at 314:04:04.

The primary method of Surveyor VI attitude determination on the lunar surface was based on sun and earth position data obtained via the A/SPP. Attitude determination before and after the lunar translation at 321:10:01.741 is presented in Figure 4-3.

4.2 RELIABILITY ANALYSIS

4.2.1 Surveyor VI Reliability Estimates

4.2.1.1 System and Subsystem Reliability

The final reliability point estimate for Surveyor VI is 0.75. This estimate is based upon Surveyor VI flight and systems test data and applicable Surveyor I through V system test and flight experience. Final reliability point estimates for each subsystem are given in Table 4-5.

TABLE 4-5. SUBSYSTEM FINAL RELIABILITY POINT ESTIMATES

Subsystem		Reliability Estimates
Telecommunications		0.991
Vehicle and mechanisms		0.880
Propulsion		0.927
Electrical power		0.988
Flight control		0.940
Spacecraft	0.751	
Systems interaction reliability factor	1.0	
Spacecraft reliability (0.751)(1.0) =	0.75	

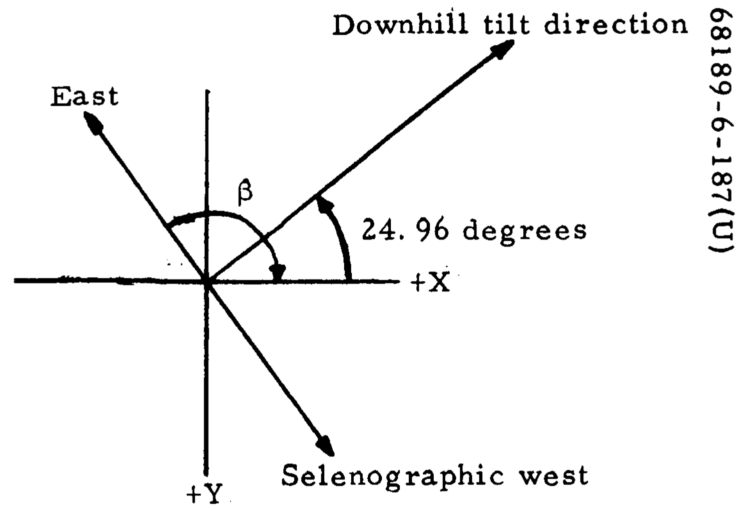

Magnitude of tilt = 0.86 degree, direction = 335.04 degrees

X_{tilt} = 0.78 degree

Y_{tilt} = 0.36 degree

Roll orientation (X axis CW from selenographic east)

β = 121.01 degrees

a) Pretranslation

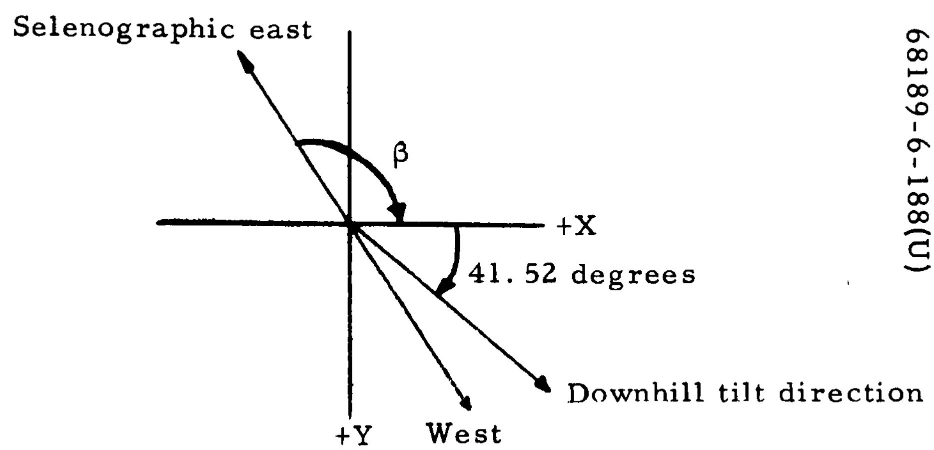

Magnitude of tilt = 4.05 degrees, direction = 41.52 degrees

X_{tilt} = 3.03 degrees

Y_{tilt} = 2.69 degrees

Roll orientation (X axis CW from selenographic east)

β = 113.64 degrees

b) Post-translation

Figure 4-3. Spacecraft Attitude

4.2.1.2 Summary of Data Base for Surveyor VI Reliability Estimates

The primary source of data for reliability estimates is the operating time and cycles experienced by Surveyor VI units during systems tests and flight and the accumulated reliability relevant failure data provided by TFRs. Data from Surveyor I through V test and flight experience are included where there are no significant design differences between the units. A failure is considered relevant if it affects equipment reliability and could occur during a mission. Relevance of failures is based upon a joint reliability-systems engineering decision. In addition, relevant failures are weighted as follows:

1.0 Critical – Would normally cause a safety hazard, mission abort, or failure of mission objective.

0.6 Major – Would significantly degrade system performance but not cause mission abort or failure.

0.1 – Would not significantly affect ability of system to function as designed.

A data base for Surveyor VI reliability estimates is summarized in Table 4-6.

4.2.1.3 Time/Cycle/Reliability History for Surveyors I Through V

Table 4-7 presents a history of time/cycle/reliability data for each major control item for Surveyors I through V.

4.2.2 Future Reliability Predictions

Table 4-8 presents results of a special analysis on the trend direction of Surveyor VI reliability. In the development of the data base used in estimating reliability, normal Surveyor practice is to retain applicable data from all prior spacecraft in a pooled data base which is used for estimating reliability of subsequent spacecraft. The advantage of this technique is that it strengthens the statistical inference by increasing the sample (data base) size. However, because a spacecraft begins systems level testing before all prior spacecraft have completed their missions, operating time and failure experience of prior spacecraft has a definite effect upon the trend direction of the latter spacecraft. This is not inaccurate, since only applicable data are pooled; hence, each estimate is a reflection of the total experience of similar units. Nonetheless, it does not provide a ready answer to the question of the extent to which Surveyor VI experience directly affected the trend direction of the reliability estimates for the spacecraft.

In response to this question, a special analysis of Surveyor VI reliability was conducted as follows:

TABLE 4-6. SUMMARY OF DATA BASE FOR SURVEYOR VI RELIABILITY ESTIMATES

Units	Total Weighted Revelant Failures	Test Time, hours or cycles	Reliability
Receiver-decoder select	0	9,849.0	1.0
Central decoder	0.6	9,848.0	0.995
Subsystem decoder	0	49,245.0	1.0
Engineering signal processor	0.3	2,980.0	0.998
Auxiliary engineering signal processor	2.5	4,268.6	0.964
Signal processing auxiliary	0	945.0	1.0
Central signal processor	0.7	8,908.6	0.993
Low data rate auxiliary	1.0	2,629.1	0.998
Omnidirectional antenna	0	5,707.2	1.0
Omnidirectional mechanisms	0	872 cycles	1.0
Diplexer	0	17,442.7	1.0
Transmitter	2.7	7,309.3	0.969
Low pass filter	0	18,374.0	1.0
Telemetry buffer amplifier	0	16,654.5	1.0
Receiver	0.2	18,849.1	0.999
Transponder	0	2,822.5	1.0
RF transfer switch	0	7,309.3	1.0
SPDT switch	0	7,309.3	1.0
Thermal sensors	0.3	230,232.8	0.994
Passive controls	0	4,204.7	1.0
Thermal control and heater assembly	0.6	4,813.5	0.979
Thermal switch	0.1	22,687.5	0.994
Thermal shell	0	8,409.4	1.0
Space frame	0	24 mission cycles	1.0
Landing gear structure	0	181 mission cycles	1.0

Table 4-6 (continued)

Units	Total Weighted Revelant Failures	Test Time, hours or cycles	Reliability
Compartment A thermal tray	0	24 mission cycles	1. 0
Compartment B thermal tray	0	24 mission cycles	1. 0
Wiring harness			
Wiring harness separation squibs	0	1, 596. 9	1. 0
Wiring harness compartment A	1. 0	3, 912. 9	0. 978
Wiring harness compartment B	0	7, 579. 8	1. 0
Wiring harness basic bus 1	1. 0	10, 117. 0	0. 992
Wiring harness basic bus 2	1. 0	10, 117. 0	0. 992
Wiring harness A/SPP	1. 4	2, 220. 8	0. 948
Wiring harness RF cabling	0	9, 847. 9	1. 0
Wiring harness retro motor	0	1, 072. 4	1. 0
Retro-rocket release	0	587 cycles	1. 0
Engineering mechanism auxiliary	0. 2	9, 134. 2	0. 998
Antenna/solar panel positioner*			
Roll	0	237, 760 cycles	1. 0
Solar	0. 2	190, 044 cycles	0. 999
SS and A device*	0	269 actuations	1. 0
Retro rocket system	0	18 mission cycles	1. 0
Solar panel	0	565. 7	1. 0
Battery charge regulator	0	2, 738. 5	1. 0
Boost regulator	1. 4	10, 251. 7	0. 988
Main power switch	0	9, 130. 2	1. 0
Main battery	0	5, 080. 1	1. 0
Flight control sensor group	2. 1	4, 737. 3	0. 963
Altitude marking radar	0. 2	166. 2	0. 999

Table 4-6 (continued)

Units	Total Weighted Revelant Failures	Test Time, hours or cycles	Reliability
RADVS			
SDC	3.3	557.0	0.994
KPSM	2.8	554.8	0.995
AVSA	2.6	554.8	0.995
VSA	2.2	556.8	0.996
Waveguide	0	535.4	1.0
Roll actuator	0	222.4	1.0
Attitude jet system	0.2	611,556 cycles	0.998
Pin puller*	0	16,131 cycles	1.0
Pin puller cartridge*	0	16,131 equivalent firings	1.0
Helium tank and valves assembly*	1.1	38 mission cycles	0.971
Propellant tank assembly*			
Fuel tank	0	70 mission cycles	1.0
Oxidizer tank	0.6	88 mission cycles	0.993
Lines and fittings	0.1	102 mission cycles	0.999
Thrust chamber assembly (JPL-supplied)			
Propellant shutoff valve	0	7,971 cycles	1.0
Throttle valve	2.0	704 mission cycles	0.997
Thrust chamber and injector assembly	1.0	266 cycles	0.996
Helium release valves*	0	18 firings	1.0
Valve cartridge*	0	16,066 equivalent firings	1.0
Shock absorber*	0	406 cycles	1.0
Crushable structure*	0	76 cycles	1.0
System**	0	1,063.5	1.0

*Includes unit flight acceptance and type approval test data.

**Based on main power switch operating time in system test.

TABLE 4-7. TIME/CYCLE/RELIABILITY HISTORY FOR SURVEYORS I THROUGH V

	Time, hours, or Cycles					Failures					Reliability				
	I	2	III	4	V	I	2	III	4	V	I	2	III	4	V
Receiver decoder select	2,137.3	4,073.4	5,602.1	6,776.5	8015.9	0	0	0	0	0	1.0	1.0	1.0	1.0	1.0
Central Decoder	2,137.3	4,073.4	5,602.1	6,776.5	8015.9	0.6	0.6	0.6	0.6	0.6	0.972	0.987	0.990	0.992	0.994
Subsystem Decoder	10,686.5	20,367.0	28,010.5	33,882.5	40,079.5	0	0	0	0	0	1.0	1.0	1.0	1.0	1.0
Engineering signal processor	691.3	1,300.5	1,711.8	1,954.2	2,360.0	2.2	2.3	0.8	1.1	0.3	0.752	0.861	0.960	0.955	0.997
Auxiliary engineering signal Processor	838.0	1,478.2	2,290.4	2,862.4	3,472.1	1.0	2.4	2.8	4.8	4.1	0.893	0.870	0.901	0.866	0.928
Signal Processing auxiliary	292.7	461.8	530.4	620.7	762.0	0	0	0	0	0	1.0	1.0	1.0	1.0	1.0
Central signal processor	1,828.3	3,133.0	4,661.7	5,836.1	7,075.5	0.7	1.4	0.7	0.7	0.7	0.960	0.963	0.990	0.994	0.992
Low data rate auxiliary	449.9	847.1	1,484.3	1,637.9	1,938.3	0	0	0.1	1.1	1.1	1.0	1.0	0.994	1.0	0.997
Omnidirectional antenna	716.7	1,068.4	2,075.4	2,310.6	2,632.8	0	0	0	0	0	1.0	1.0	1.0	1.0	1.0
Omnidirectional mechanism	42 cycles	510 cycles	663 cycles	784 cycles	824	0	0.2	0	0	0	1.0	0.999	1.0	1.0	1.0
Diplexer	2,173.8	5,891.5	8,948.9	11,297.7	13,776.5	0	0	0	0	0	1.0	1.0	1.0	1.0	1.0
Transmitter	1,019.1	2,373.0	3,685.9	4,527.1	5,699.3	2.3	1.0	2.4	1.4	2.5	0.874	0.961	0.942	0.971	0.964
Low pass filter	3,176.6	6,822.8	9,880.2	12,229.0	14,707.8	0	0	0	0	0	1.0	1.0	1.0	1.0	1.0
Telemetry buffer amplifier	1,874.4	5,103.3	8,160.7	10,509.5	12,988.3	0	0	0	0	0	1.0	1.0	1.0	1.0	1.0
Receiver	3,580.2	7,297.9	10,355.3	12,704.1	15,182.9	0.2	0.2	0.1	0.1	0.2	0.995	0.998	0.999	0.999	0.999
Transponder	529.1	1,153.4	1,663.2	2,054.8	2,467.9	0	0	0	0	0	1.0	1.0	1.0	1.0	1.0
RF Transfer switch	1,019.1	2,373.0	3,685.9	4,527.1	5,699.3	0	0	0	0	0	1.0	1.0	1.0	1.0	1.0
SPDT switch	1,019.1	2,373.0	3,685.9	4,527.1	5,699.3	0	0	0	0	0	1.0	1.0	1.0	1.0	1.0
Thermal sensors	40,953.8	76,038.0	104,180.8	118,431.6	165,065.6	0	0	0	0.1	0.3	1.0	1.0	1.0	0.997	0.991
Thermal control and heater assembly	1,455.9	1,591.7	2,359.7	2,664.4	3,011.9	0	0	0	0	0.6	1.0	1.0	1.0	1.0	0.967
Thermal switch	14,755.5	26,196.0	35,373.0	4,647.0	10,242.0	0	1.2	1.2	1.2	0.1	1.0	0.943	0.958	0.973	0.988
Thermal shell	1,967.4	3,492.8	4,716.4	5,336.0	6,082.0	0	0	0	0	0	1.0	1.0	1.0	1.0	1.0
Spaceframe	8 cycles	11 cycles	16 cycles	18 cycles	22 cycles	0	0	0	0	0	1.0	1.0	1.0	1.0	1.0
Landing gear	21 cycles	139 cycles	160 cycles	166 cycles	178 cycles	0	0	0	0	0	1.0	1.0	1.0	1.0	1.0
Compartment A thermal tray	8 cycles	11 cycles	17 cycles	18 cycles	22 cycles	0	0	0	0	0	1.0	1.0	1.0	1.0	1.0
Compartment B thermal tray	8 cycles	11 cycles	17 cycles	18 cycles	22 cycles	0	0	0	0	0	1.0	1.0	1.0	1.0	1.0
Auxiliary battery compartment	8 cycles	11 cycles	17 cycles	18 cycles	DNA	0	0	0	0	—	1.0	1.0	1.0	1.0	—
Wire harness compartment A	2,587.2	1,868.5	3,332.9	1,174.4	2,413.8	1.0	0	0	1.0	1.0	0.963	1.0	1.0	0.930	0.965
Wire harness compartment B	2,587.2	1,868.5	3,332.9	4,507.3	5,746.7	0.1	0	0	0	0	0.997	1.0	1.0	1.0	1.0
Wire harness basic bus 1	2,537.2	4,405.7	5,870.1	7,044.5	8,283.9	0.1	2.1	2.1	3.0	1.0	0.996	0.960	0.970	0.963	0.990
Wiring harness basic bus 2	2,537.2	4,405.7	5,870.1	7,044.5	8283.9	1.0	2.0	1.0	1.0	1.0	0.962	0.962	0.986	0.988	0.990
Wiring harness ASPP	1,063.9	1,111.7	1,121.2	1,128.6	1,135.9	0	0	0	0	0.6	1.0	1.0	1.0	1.0	0.956
Wiring harness auxiliary battery	1,129.1	1,333.8	1,440.2	1,482.4	DNA	0	0	0	0	—	1.0	1.0	1.0	1.0	—

Table 4-7 (continued)

Unit	Time, hours, or Cycles					Failures					Reliability				
	I	2	III	4	V	I	2	III	4	V	I	2	III	4	V
Wiring Harness RF cabling	2,601.3	4,227.5	5,601.0	6,775.4	8,014.8	0.1	0	0	0	0	0.996	1.0	1.0	1.0	1.0
Wiring harness retro rocket	1,053.2	1,059.5	1,070.8	1,070.8	1,072.8	0	0	0	0	0	1.0	1.0	1.0	1.0	1.0
Nitrogen lines	1,147.0	1,963.0	2,814.7	3,395.9		0	0	0	0	—	1.0	1.0	1.0	1.0	—
Retro rocket release	540 cycles	575 cycles	578 cycles	581 cycles	584 cycles	0	0	0	0	0	1.0	1.0	1.0	1.0	1.0
Engineering mechanical auxiliary	1,576.3	3,358.6	4,887.3	6,061.7	7,301.1	0	0	0	0.2	0.2	1.0	1.0	1.0	0.998	0.998
Antenna/solar panel positioner	240,504 cycles	511,506 cycles	482,446 cycles	581,520 cycles	165,831 cycles	22.7	1.4	1.4	0.1	0.1	0.891	0.995	0.995	0.997	0.999
Separation sensing and arming device	75 cycles	72 cycles	178 cycles	212 cycles	230 cycles	0	0	0	0	0	1.0	1.0	1.0	1.0	1.0
Retro rocket system	13 cycles	14 cycles	15 cycles	16 cycles	17 cycles	0	0	0	0	0	1.0	1.0	1.0	1.0	1.0
Solar panel	375.1	402.7	467.7	529.3	64	0	0	0	0	0	1.0	1.0	1.0	1.0	1.0
Battery charge regulator	1,128.4	3,072.0	4,600.7	5,775.1	1,230.4	0.1	0.7	0.7	0	0	0.989	0.980	0.987	1.0	1.0
Boost regulator	2,457.8	4,476.1	6,004.8	7,179.2	8,418.6	0.8	1.4	1.4	1.4	1.4	0.968	0.974	0.982	0.984	0.986
Auxiliary battery control	1,929.3	3,998.0	5,526.7	6,701.1	DNA	0	0.6	0.7	0.7	—	1.0	0.998	0.998	0.998	—
Main power switch	1,475.4	3,354.6	4,883.3	6,057.7	7,297.1	0	0	0	0	0	1.0	1.0	1.0	1.0	1.0
Main battery	1,037.4	1,553.8	2,685.5	3,220.2	3,673.4	1.0	1.0	0	0	0	0.882	0.994	1.0	1.0	1.0
Auxiliary battery	90.7	113.6	248.5	291.3	DNA	0.6	0.6	0.6	0.6	—	0.880	0.924	0.962	0.967	—
Boost regulator input choke	937.2	2,623.9	4,152.6	5,327.0	DNA	0	0	0	0	—	1.0	1.0	1.0	1.0	—
Boost regulator unregulated filter	937.2	2,627.9	4,152.6	5,331.0	DNA	0	0	0	0	—	1.0	1.0	1.0	1.0	—
Flight control sensor group	1,147.2	1,963.2	2,815.1	3,396.5	4,065.5	0	2.0	0	1.8	1.4	1.0	0.917	1.0	0.956	0.971
Altitude marking radar	62.9	92.9	106.3	131.9	162.1	0	0	0	0.1	0.1	1.0	1.0	1.0	0.999	0.999
RADVS -signal data converter	595.1	987.1	1,131.7	1,504.4	1,790.0	6.5	10.3	11.1	13.1	17.9	0.982	0.989	0.989	0.990	0.989
Klystron power supply modulator	311.5	725.7	921.0	1,090.5	1,246.3	5.4	5.9	5.9	6.9	6.9	0.981	0.991	0.993	0.993	0.994
Attitude velocity sensing antenna	295.9	522.7	823.9	987.8	1,182.0	2.2	2.2	4.4	4.4	5.0	0.992	0.996	0.994	0.995	0.995
Velocity sensing antenna	266.6	424.1	652.5	955.2	1,142.0	0	1.6	2.2	2.8	2.8	1.0	0.996	0.996	0.996	0.997
RADVS waveguide	194.1	278.0	424.2	530.1	633.7	0	0	0	0	0	1.0	1.0	1.0	1.0	1.0
Roll actuator	56.6	98.1	148.6	190.5	195.4	0	0	0	0	0	1.0	1.0	1.0	1.0	1.0
Attitude jet system	147,381 cycles	269,576 cycles	370,756 cycles	444,675 cycles	559,208 cycles	0.1	0.1	0.1	0.1	0.2	0.995	0.998	0.998	0.999	0.998
Pin pullers	16,071 cycles	16,080 cycles	16,092 cycles	16,101 cycles	16,110 cycles	0	0	0	0	0	1.0	1.0	1.0	1.0	1.0

Table 4-7 (continued)

Unit	Time, hours, or Cycles					Failures					Reliability				
	I	2	III	4	V	I	2	III	4	V	I	2	III	4	V
Pin puller cartridge	16,071 cycles	16,429 cycles	16,441 cycles	16,101 cycles	16,110 cycles	0	0	0	0	0	1.0	1.0	1.0	1.0	1.0
Helium tank and valve assembly	30 cycles	33 cycles	34 cycles	36 cycles	37 cycles	0	0.1	0.1	0.1	0.7	1.0	0.997	0.977	0.977	0.981
Fuel tanks	46 cycles	49 cycles	52 cycles	58 cycles	64 cycles	0	0	0	0	0	1.0	1.0	1.0	1.0	1.0
Oxidizer tanks	64 cycles	67 cycles	70 cycles	76 cycles	82 cycles	0	0	0	0.6	0.6	1.0	1.0	1.0	0.977	0.993
Lines and fittings	54 cycles	60 cycles	66 cycles	78 cycles	90 cycles	0	0	0.1	0.1	0.1	1.0	1.0	0.998	0.999	0.999
Propellant shutoff valve	7,944 cycles	7,947 cycles	7,953 cycles	7,956 cycles	7,965 cycles	0	0	0	0	0	1.0	1.0	1.0	1.0	1.0
Throttle valve	693 cycles	694 cycles	697 cycles	698 cycles	701 cycles	2.0	2.0	2.0	2.0	2.0	0.997	0.997	0.997	0.997	0.997
Thrust chamber and injection assembly	255 cycles	256 cycles	259 cycles	260 cycles	263 cycles	0	1.0	1.0	1.0	1.0	1.0	0.995	0.996	0.996	0.996
Helium release valve	13 cycles	14 cycles	15 cycles	16 cycles	17 cycles	0	0	0	0	0	1.0	1.0	1.0	1.0	1.0
Valve cartridges	16,061 cycles	16,062 cycles	16,063 cycles	16,064 cycles	16,065 cycles	0	0	0	0	0	1.0	1.0	1.0	1.0	1.0
Shock absorber	391 cycles	391 cycles	400 cycles	400 cycles	403 cycles	0.2	0	0	0	0	0.999	1.0	1.0	1.0	1.0
Crushable structures	61 cycles	61 cycles	70 cycles	70 cycles	73 cycles	0	0	0	0	0	1.0	1.0	1.0	1.0	1.0
System interaction	1,717.1	1,013.2	1,528.7	1,174.4	1,239.4	5.0	0.6	0.6	0.3	0.2	0.736	0.949	0.967	0.978	0.986

TABLE 4-8. RELATIVE SUBSYSTEM RELIABILITY FOR SURVEYOR VI – INITIAL ESTIMATE VERSUS FINAL ESTIMATE

Subsystem	Initial	Final	Ratio of Final to Initial
Telecommunications	0.990	0.991	1.001
Vehicle and mechanisms	0.897	0.888	0.891
Propulsion	0.924	0.927	1.003
Electrical power	0.988	0.988	1.0
Flight control	0.935	0.940	1.005
Systems interaction factor	1.0	1.0	1.0
Spacecraft	0.758	0.751	0.991

1) All poolable data from Surveyor I through the end of the Surveyor V mission were collected and totaled. This provided a constant data base upon which Surveyor VI experience could be superimposed. Since Surveyor V (and earlier) data are constant throughout, the resulting trend direction is a function of Surveyor VI experience only.

2) The data base used in the initial Surveyor VI estimate was then examined, and only the Surveyor VI operating time and failure experience was extracted. These data were then combined with the constant data developed in item 1 above to produce a new initial Surveyor VI reliability estimate.

3) The new initial estimate was then compared with the final Surveyor VI reliability estimate to produce the reliability trend of Surveyor VI as a single variable function of the spacecraft's performance. It is to be noted that the final estimate, computed either way, must, of necessity, converge to the same value.

As shown in Table 4-9, the trend of Surveyor VI reliability was slightly downward. This drop is a result of three failures within the vehicle mechanisms subsystem: two failures to the wire harness antenna/solar panel positioner and one failure to the A/SPP itself.

TFR 85664 reported a cut in cable insulation. The cause was traced to excessive epoxy potting in a connector that was in contact with the cable. The epoxy had subsequently damaged the insulation. Repair was effected by removing the excessive epoxy and applying a shrink sleeve patch to the cable

TABLE 4-9. SURVEYOR SPACECRAFT RELIABILITY GROWTH

Subsystem	I	2	III	4	V	VI	SC-7
Telecommunications	0.925	0.944	0.965	0.929	0.987	0.991	0.991
Vehicle and mechanism	0.816	0.868	0.907	0.854	0.853	0.880	0.880
Propulsion	0.991	0.991	0.968	0.947	0.934	0.927	0.927
Electrical power	0.870	0.958	0.935	0.954	0.985	0.988	0.975
Flight control	0.953	0.889	0.971	0.931	0.945	0.940	0.928
Systems interaction factor	0.737	0.950	0.967	0.978	0.986	1.0	0.897
Spacecraft	0.457	0.658	0.745	0.653	0.723	0.751	0.656

insulation. The basic cause of the problem was poor workmanship; corrective action implemented includes closer inspection. No corrective engineering action was necessary.

TFR 85664 reported the failure of a connector pin to pass pin retention testing. Such test failures have been a recurring problem on all harnesses. The requirement for all connectors to pass pin retention test prior to final mating significantly reduces the probability of this failure occurring during the mission.

TFR 85692 reported an intermittent output from the solar drive position potentiometer. The intermittency existed only in the launch position. The tendency of position potentiometers to produce short-term intermittent signals has been a recurring problem. The cause of this situation has been traced to the accumulation of lubrication in a localized area of the pot windings such that the wiper arm rides up on the lubricant, producing the intermittent signal. Past experience has shown that these accumulations are localized, and that they disappear after repeated operation of the pot. As a result, no corrective action is required.

The Surveyor spacecraft realized a steady reliability growth through Surveyor III, dipped for Surveyor 4, resumed the upward direction for Surveyors V and VI, and has dipped significantly again for SC-7. This can readily be seen from Table 4-9 which presents reliability figures for Surveyor I through SC-7. Principal cause of the drop in SC-7 reliability figures is reported in TFR 87191. During preparation for solar thermal vacuum phase A, application of gyro pre-heat power produced a full-scale reading on the ammeter monitoring gyro pre-heat current. Power was immediately turned off. Extensive troubleshooting and analysis of both the spacecraft and the STEA failed to uncover the source of the problem. All efforts to duplicate the problem failed. The flight controls were subsequently removed for electronic conversion unit repairs and successfully passed all flight acceptance testing. The TFR was closed as cause unknown, reliability revelant,and with a failure weighting of 1.0. The cause unknown nature of the failure requires that the failure be considered as part of the systems interaction reliability factor which has a very direct impact upon reliability numerics. SC-7 reliability without the systems interaction factor is 0.732.

4.2.2.1 SC-7 Reliability

Estimated reliability for SC-7 at launch for a 66-hour flight and landing mission is 0.66. This projected estimate is based upon SC-7 systems test data and applicable Surveyor I through VI test and flight experience.

4.2.2.2 Reliability Estimate Basis

Reliability estimates are based on equipment failure data and operating time and cycle data generated during spacecraft mission and systems testing, which are combined in accordance with Hughes "Reliability Math Model Surveyor Spacecraft A-21," SSD 64002-3R, 1 May 1967. The model describes the spacecraft system in terms of block diagrams, mission profile, time/cycle data, and probabilistic equations appropriate to the functional interaction of all spacecraft units. For convenience, the spacecraft is referred to at three basic levels: systems, set, and control item or unit. Reliability is defined as follows:

> Reliability of the A-21 Surveyor spacecraft for the flight and landing phase is the probability that the spacecraft equipment will operate successfully as required from launch through soft landing. Successful soft landing is assumed if two-way communications is established and there is no apparent damage to spacecraft equipment required to support intended lunar operations.

In the derivation of the model, the following general assumptions were made:

1) No human error will occur during the mission which will cause failure.

2) All equipment inspection and test procedures are perfect and comprehensive, and all equipment will be used only in applications within the boundaries of its design parameters.

3) Every performance characteristic is verified up to the instant of no return in launch operations, and the launch will be aborted if fault exists.

4) All parts and designs are used in applications proven by test.

5) All scheduled changes to improve reliability of performance have been physically incorporated and tested prior to launch.

6) Natural hazards, such as meteorites and deep lunar dust, are nonexistent.

4.3 REFERENCES AND ACKNOWLEDGMENTS

The material in Sections 1, 2, 3, and 4 was coordinated (and originated or compiled) by W. McIntyre from the following sources:

1) W. McIntyre, "Surveyor VI Preliminary Post Mission Data," Hughes IDC 2292/429, 4 December 1967.

2) "Surveyor VI Flight Path Analysis and Command Operations Report," Hughes Aircraft Company, SSD 78176, December 1967.

3) "Surveyor Mission F Space Flight Operations Report," Hughes Aircraft Company, SSD 78187, December 1967.

Mention is also due to the following people:

R. L. Lackman for information concerning postlanding attitude determination.

L. K. Cooley for the reliability analysis in subsection 4.2.

5.0 PERFORMANCE ANALYSIS

5.1 THERMAL CONTROL SUBSYSTEM

5.1.1 INTRODUCTION: SURVEYOR THERMAL CONTROL TECHNIQUES

The Surveyor thermal design utilizes a variety of temperature control techniques. Active, passive, and semiactive mechanisms are employed to provide the required temperature control (storage, operational, and/or survival) throughout the transit and lunar phases of the mission. Each spacecraft subsystem is individually controlled, and the thermal coupling between subsystems is minimized by using conduction and radiation isolation wherever advantageous. Subsystem analyses are accomplished by evaluating in detail the thermal environment for each subsystem, with consideration being given to all significant thermal interactions between the subsystems whenever a high degree of isolation is not possible.

The following temperature control techniques are used on the Surveyor spacecraft:

1) Passive thermal control utilizing combinations of paints and metal processes to provide surfaces with solar absorptance and infrared emittance characteristics to produce the required subsystem temperatures. Solar energy reflections are used to provide energy in cases where insufficient direct solar illumination exists.

2) Active thermal control systems utilizing heaters and radiation shields provide energy in cases where:

   a) Sufficient solar illumination is not available

   b) The unit's storage temperature is significantly different from its optimum operational temperature

3) Subsystems having large heat capacities are thermally decoupled from the transit and lunar environments by utilizing superinsulation blankets to minimize radiative heat transfer and thermal isolators to minimize conductive heat transfer. Such systems never reach equilibrium conditions and therefore depend on heat capacity and a controlled rate of heat rejection to provide optimum operational temperatures.

4) Bimetallically activated thermal switches control the temperature of the electronics compartments during transit and lunar operations.

Combinations of the above techniques are used on many of the subsystems to optimize the temperature control system.

5.1.2 THERMAL ANOMALIES – FAILURE OF THERMAL SWITCHES TO OPEN IN LUNAR NIGHT

As the spacecraft entered lunar night, at least eight of the nine thermal switches on compartment A and two of the six switches on compartment B were stuck. At spacecraft shutdown 41 hours after sunset, six thermal switches on compartment A and one on compartment B remained closed. This anomaly was documented in TFR 18271 and is discussed in subsection 5.1.6, "Lunar Night Thermal Performance."

5.1.3 THERMAL SUBSYSTEM SUMMARY

5.1.3.1 Transit

The thermal response of the spacecraft during the Mission F transit was excellent. All steady-state temperatures were close to the nominal predictions except one: oxidizer line 1 temperature (sensor P-8) was 51°F during the coast phase II steady-state condition compared to the prediction range of 21° to 41°F, but was well within the required limits of 0° to 110°F. Of the 74 temperature sensors, 69 were within 10°F of their predicted nominal steady-state values.

The Surveyor VI television camera differed from its predecessors in that it had the new, larger, square-shaped hood and mirror assembly. The camera warmup during the last 5 hours of transit was slower than on previous missions, resulting in a delay of 23 minutes from nominal in the turn-on of the television vidicon heater. (The electronics temperature, TV-16, is required to be above -20°F prior to enabling of the vidicon thermal control.)

5.1.3.2 Lunar

Spacecraft temperatures during lunar operations were nominal throughout the first lunar day. Telecommunication electronics operation was restricted by the temperature levels for 1-1/2 days in the lunar noon interval. The alpha scattering system and TV camera temperatures were nominal throughout the lunar day. Shadowing of critical spacecraft units with the solar panel and planar array was accomplished to great advantage:

1) Main battery temperature was maintained below 70°F during the entire lunar morning.

2) Vernier engine and flight control temperatures stayed below their upper limits, satisfying thermal requirements for liftoff and translation.

3) Alpha scattering system operation was facilitated by keeping compartment C electronics and instrument temperatures within operating limits. Lunar night operations had to be terminated only 41 hours after sunset because of stuck thermal switches in compartments A and B (TFR 18271).

5. 1. 4 THERMAL PERFORMANCE IN TRANSIT

A summary of equilibrium temperatures for Missions A through F, along with Mission F predictions, is presented in Table 5. 1-1. All temperature signals were plotted in real time during the mission (see Figures 5. 1-A1 through 5. 1-A6).

A table of events for Mission F is presented in Table 5. 1-2. This table primarily includes events that may affect the thermal response of the spacecraft, but does not include spacecraft commutator mode changes.

Only thermal responses which were unique or of special interest are discussed in this report. For those units with temperature histories consistent with previous missions, the equilibrium temperature summary and transit plots are supplied in lieu of further discussion.

5. 1. 4. 1 Prelaunch Phase

All spacecraft heaters were properly configured prior to launch, as follows:

Vernier line heaters	Enabled
AMR heater	Enabled
Survey TV electronics and mirror heaters	Not enabled
Survey TV vidicon heater	Not enabled
Propellant tank heaters	Not enabled
Alpha scattering head heater	Not enabled
Compartment A heater	Not enabled
Compartment B heater	Not enabled
Compartment C heater	Not enabled

Prelaunch air-conditioning was provided as required. Conditioned air was maintained at approximately 70°F until 2 hours and 17 minutes prior to launch, whereupon the inlet air temperature control was raised to 85°F. During the last hour prior to launch, the payload adapter temperature was maintained at 82. 5°F.

All temperature sensors were within their respective required launch temperature ranges at launch.

TABLE 5.1-1, SURVEYOR TRANSIT STEADY-STATE TEMPERATURE DATA, FLIGHT PREDICTIONS, AND LIMITS

Flight Sensor Location by Subsystem		Transit Steady-State Temperature, °F							Temperature Limits, °F	
		Mission A Actual	Mission B Actual	Mission C Actual	Mission D Actual	Mission E Actual	Mission F Predicted	Mission F Actual	Operational	Survival
Vehicle and mechanisms										
Compartment A										
Upper tray	V-15	70	74	49	58	46	40	41	125/0	135/-10
Lower tray	V-16	93	94	70	76	56	52	51	125/0	135/-10
Transmitter A	D-13	68	71	49	55	42	37	39	185/5	210/0
Transmitter B	D-14	68	73	48	57	44	40	41	185/5	210/0
Main battery	EP-8	97	99	69	75	58	54	52	125/40	125/0
Battery charge regulator	EP-34	123	118	94	98	64	60	60	170/5	190/0
Radiators										
No. 5	V-20	42	31	30	25	-3	15	21	145/-300	150/-320
No. 8	V-25	44	28	36	42	29	26	31	145/-300	150/-320
No. 2	V-47	35	34	19	22	-31	8	15	145/-300	150/-320
No. 3	V-49	*	*	*	*	4	5	9	145/-300	150/-320
Thermal shell inside	V-17	92	92	68	74	*	*	*	125/0	130/-10
Thermal shell outside	V-18	-85	-82	-84	-87	-93	-90	-82	160/-210	DNA
Thermal switch No. 5 inside	V-19	66	69	47	56	43	37	39	130/-5	150/-15
Compartment B										
Upper tray	V-21	93	99	76	77	74	70	78	140/0	150/-10
Lower tray	V-22	98	103	81	81	77	71	81	140/0	150/-10
Boost regulator	EP-13	115	128	94	97	82	76	83	175/5	190/0
Radiators										
No. 4	V-24	67	70	55	54	52	46	53	145/-300	150/-320
No. 1	V-45	73	84	61	62	58	53	61	145/-300	150/-320
No. 5	V-46	66	70	56	53	51	48	55	145/-300	150/-320
Thermal shell outside	V-23	-70	-72	-64	-72	-78	-82	-76	160/-210	DNA
Thermal switch No. 4 inside	V-26	88	93	74	72	68	62	73	130/-5	150/-15
Wiring harness	V-29	89	91	72	74	67	72	68	125/0	135/-10
Auxiliary battery	EP-26	35	64**	54	60	*	*	*	130/40	145/15
Auxiliary battery outer compartment canister	V-48	2	9**	12	*	*	--	--	60/-140	DNA

*Not on spacecraft.

**Steady state not obtained.

Table 5.1-1 (continued)

Flight Sensor Location by Subsystem		Transit Steady-State Temperature, °F							Temperature Limits, °F	
		Mission A Actual	Mission B Actual	Mission C Actual	Mission D Actual	Mission E Actual	Mission F Predicted	Mission F Actual	Operational	Survival
Landing gear assembly										
Leg 2	V-31	83	74	77	65	*	*	*	160/-140	DNA
Crushable block	V-44	-62	-48	-63	-55	-68	-76	-76	160/-140	DNA
Shock absorber										
No. 1	V-30	84	76	74	77	80	80	79	125/20	125/-25
No. 2	V-32	72	73	76	76	76	76	84	125/20	125/-25
No. 3	V-33	82	82	79	74	70	80	76	125/20	125/-25
Antenna/solar panel positioner mechanism										
Solar panel drive	M-10	60	45	51	46	45	50	63	260/-225	265/-235
Elevation axis drive	M-12	1	-17	-11	-20	-23	-12	-8	260/-225	265/-235
Solar cell array	EP-12	109	111	112	110	126	128	128	150/-150	235/-260
Planar array	M-8	-50	-50	-50	-52	-50	-50	-43	275/-225	280/-225
A/SPP mast	V-34	-84	-88	-88	-90	*	*	*	264/-225	DNA
Spaceframe and substructure										
Upper spaceframe										
Near leg 1	V-27	60	53	57	52	56	59	59	160/-140	DNA
Near leg 2	V-35	-79	-81	-82	-84	-82	-80	-80	160/-140	DNA
Lower spaceframe										
Under compartment B	V-28	48	42	43	38	39	40	40	160/-140	DNA
Under compartment A	V-36	-27	-24	-32	-34	-31	-30	-25	160/-140	DNA
Retro attach points										
Leg 1	V-37	39	44	42	37	38	38	42	120/-95	140/-100
Leg 2	V-38	-36	-32	-52	-53	-41	-40	-37	120/-95	140/-100
Leg 3	V-39	44	44	46	37	41	40	42	120/-95	140/-100
Flight control										
Flight control electronics										
Chassis board 1	FC-44	90	90	71	66	67	65	69	150/0	165/-20
Chassis board 6	FC-45	124	137	60	59	61	60	62	127/30	132/0
Canopus sensor	FC-47	78	85	74	76	70	68	73	130/-20	145/-20

*Not on spacecraft.

Table 5.1-1 (continued)

Flight Sensor Location by Subsystem		Transit Steady-State Temperature, °F							Temperature Limits, °F	
		Mission A Actual	Mission B Actual	Mission C Actual	Mission D Actual	Mission E Actual	Mission F Predicted	Mission F Actual	Operational	Survival
Roll gyro†	FC-46	170	175	173	175	175	175	173	185/165	190/120
Pitch gyro†	FC-54	175	175	172	175	174	174	173	185/165	190/120
Yaw gyro†	FC-55	180	174	172	174	174	174	173	185/165	190/120
Roll actuator	FC-71	79	82	83	80	88	82	94	190/10	200/0
Nitrogen tank	FC-48	45	40	50	41	45	53	53	130/0	135/-10
Attitude control jet No. 2	FC-70	88	86	105	91	94	96	103	150/-40	160/-50
Radars										
RADVS										
KPSM	R-8	12	11	17	18	20	17	23	100/-22	125/-49
SDC	R-9	56	63	55	53	60	60	66	105/15	125/5
Velocity sensor preamplifier	R-10	22	14	16	15	16	20	27	109/-50	112/-58
Altitude/velocity sensor preamplifier	R-13	33	20	27	36	25	24	35	107/-50	110/-58
Altitude marking radar										
Electronics	R-7	15	18	17	16	22	20	17-20	60/-5	75/-10
Antenna dish	R-6	-12	-14	3	-7	-6	-5	+2	100/-25	105/-30
Edge of dish	R-27	-185	-191	-202	-183	*	*	*	200/-300	300/-300
Propulsion										
Vernier engine thrust chamber assembly										
No. 1	P-7	59	54	58	50	60	58	65	145/0	DNA/0
No. 2	P-10	72	84	81	80	72	74	80	145/0	DNA/0
No. 3	P-11	59	63	69	66	68	65	74	145/0	DNA/0
Propellant tanks††										
Oxidizer 1	P-15	75/41	76/50	76/41	76/42	75/39	76/41	76/42	100/0	120/-10
Fuel 1	P-13	76/52	77/57	76/55	76/56	75/57	75/55	75/53	100/0	120/-10
Oxidizer 2	P-16	77/24	75/35	75/18	75/19	74/14	75/21	75/21	100/0	120/-10
Fuel 2	P-5	75/34	83/47	74/33	74/32	74/25	74/29	74/30	100/0	120/-10
Oxidizer 3	P-6	79/40	75/46	77/30	76/42	74/34	74/40	74/38	100/0	120/-10
Fuel 3	P-14	76/53	75/53	76/52	76/51	75/52	75/53	75/53	100/0	120/-10

*Not on spacecraft

†Corrected for bit rate errors.

††Launch temperature/touchdown temperature for Missions A, C, D, E, and F; launch temperature/midcourse temperature for Mission B.

Table 5.1-1 (continued)

Flight Sensor Location by Subsystem		Transit Steady-State Temperature, °F							Temperature Limits, °F	
		Mission A Actual	Mission B Actual	Mission C Actual	Mission D Actual	Mission E Actual	Mission F Predicted	Mission F Actual	Operational	Survival
Propellant lines										
Oxidizer line 1	P-8	26	23	30	39	30	31	51	110/0	120/-10
Oxidizer line 2	P-4	24	14	21	22	18-22	18-28	20-26	110/0	120/-10
Oxidizer line 3	P-9	24	24	22	22	21-25	18-28	18-22	110/0	120/-10
Fuel line 1	P-23	*	*	*	*	60	50	55	110/0	120/-10
Fuel line 2	P-24	*	*	*	*	25	10-20	25-31	110/0	120/-10
Fuel line 3	P-25	*	*	*	*	71	61-71	58	110/0	120/-10
Helium tank	P-17	60	72	73	76	79	75	84	110/0	110/-10
Main retro										
Upper case††	P-3	73/67	72/73	73/64	73/66	72/64	72/65	74/67	75/55	100/10
Lower case††	P-12	74/46	76/59	78/41	77/44	76/43	76/43	76/41	75/35	100/10
Nozzle	P-22	-124	-118	-130	-127	-123	-127	-122	300/-300	DNA
Television, SM/SS, and alpha scattering device										
TV 3 mirror assembly	TV-17	-120	-120	-120	-125	-126	-125	-124	180/-50	185/-220
TV 3 ECU	TV-16	-134	-128**	-128	-130	-136	-136	-135	165/-20	165/-250
Auxiliary electronics	SS-12	*	*	-35	-35	*	*	*	158/-4	185/-67
SM/SS substructure	SS-13	*	*	*	-104	*	*	*	0 minimum	-
Compartment C electronics†	AS-4	*	*	*	*	-20	-25	-10	131/-4	185/-67
Sensor head electronics†	AS-3	*	*	*	*	35	35	44	122/-40	167/-300

*Not on spacecraft.

**Steady state not obtained.

†Corrected for bit rate errors.

††Launch temperature/touchdown temperature for Missions A, C, D, E, and F; launch temperature/midcourse temperature for Mission B.

TABLE 5.1-2. SURVEYOR VI TRANSIT THERMAL EVENT LOG

Day	GMT, hr:min:sec	Mission Time, hr:min:sec	Event
311	07:39:01	0	Launch
	07:43	00:04	Shroud jettison
	07:43:19	00:04:18	MEIG 1
	07:48:42	00:09:41	MECO 1
	07:53:22	00:14:22	Out of earth shadow
	08:04:19	00:25:18	Omni B high power on
	08:04:30	00:25:29	Surveyor-Centaur separation
	08:14:24	00:37	Sun acquisition
	08:19	00:40	Omni B high power off
	09:29	01:50	Line 2 heater cycling
	15:01	07:22	AMR heater cycling
	15:44	08:05	Omni B high power on
	16:27	08:48	Star acquisition
	16:37	08:58	Transmitter B high power off
	16:43	09:04	Gyro drift check 1 (three-axis)
	18:04	10:25	End gyro drift check
	18:18	10:39	Initiate gyro drift check (three-axis)
	19:22	11:43	End gyro drift check 2
	19:24	11:45	Initiate gyro drift check (three-axis)
	20:38	13:00	End gyro drift check 3
	20:45	13:06	Initiate gyro drift check (three-axis)
	21:58	14:19	Solar panel switch off
	22:00	14:21	Solar panel switch on
	22:03	14:24	End gyro drift check 4
	22:20	14:41	137.5 bps
	22:24	14:45	1100 bps
	22:32	14:53	Solar panel switch off
	22:48	15:09	Solar panel switch on
312	01:51	18:12	Omni B high power on
	01:52	18:13	4400 bps
	02:03	18:24	Initiate midcourse roll (+91.8 degrees)
	02:06	18:27	Terminate roll
	02:09	18:30	Initiate yaw (+127.3 degrees)
	02:13	18:34	End of yaw
	02:16	18:37	Disable heaters: AMR, oxidizer lines 2, 1, and 3
	02:20	18:41	Midcourse (10.25-second burn)
	02:23	18:44	Enable heaters on: AMR, oxidizer lines 2, 1, and 3
	02:26	18:47	Initiate reverse yaw (-127.3 degrees)

Table 5.1-2 (continued)

Day	GMT, hr:min:sec	Mission Time, hr:min:sec	Event
312 (cont)	02:30	18:51	Terminate reverse yaw
	02:33	18:54	Initiate reverse roll (-91.8 degrees)
	02:36	18:57	Terminate roll
	02:46	19:07	1100 bps
	02:47	19:08	Omni B high power off
	04:37	20:58	Initiate gyro drift 5 (all axes)
	05:42	22:03	End gyro drift 5
	08:32	24:53	Initiate gyro drift 6 (roll)
	12:46	29:07	End gyro drift 6
	16:18	32:39	Initiate gyro drift 7 (all axes)
	17:18	33:39	Line 3 heater cycling
	17:53	34:14	Terminate gyro drift 7
	18:59	35:20	Initiate gyro drift 8 (roll only)
	21:42	38:03	Terminate gyro drift 8
	22:45	39:06	Initiate gyro drift 9 (all axes)
313	00:11	40:32	Terminate gyro drift 9
	01:11	41:32	Initiate gyro drift 10 (all axes)
	02:25	42:46	Terminate gyro drift 10
	03:30	43:51	Initiate gyro drift check 11 (all axes)
	04:48	45:09	Terminate gyro drift 11
	06:25	46:46	Initiate gyro drift check 12 (all axes)
	07:38	47:59	End gyro drift check 12
	09:04	49:25	Initiage gyro drift 13 (all axes)
	10:42	51:03	Terminate gyro drift 13
	11:01	51:22	Initiate gyro drift 14 (roll only)
	11:04	51:25	Compartment A heater on
	14:53	55:14	Enable heaters on fuel tank 2 and oxidizer tanks 2 and 3
	15:27	55:48	Terminate gyro drift check 14
	19:55	60:16	TV electronics heater on
	20:25	60:46	Compartment C heater on
	22:27	62:48	Alpha scattering instrument heater on
	23:13	63:34	Compartment A heater off

Table 5.1-2 (continued)

Day	GMT, hr:min:sec	Mission Time, hr:min:sec	Event
314	00:07	64:28	Omni B high power on
	00:15	63:37	TV vidicon heater on
	00:25	63:46	Initiate roll (+81.7 degrees)
	00:28	64:49	End roll
	00:29	64:50	Start yaw (+111.7 degrees)
	00:33	64:54	End yaw
	00:35	64:56	Start roll (+120.5 degrees)
	00:39	65:00	End roll
	00:52	65:13	Heaters off: vernier lines and tanks, TV, AMR, Compartment C, and alpha scattering
	00:53	65:14	AMR power on
	00:54	65:15	Thrust phase power on
	00:56	65:17	AMR enable
	00:57:57	65:18:50	AMR mark
	00:58:04	65:19:04	Retro ignition, ≈ RADVS on, ≈ vernier ignition
	00:58:41	65:19:43	Retro burnout
	01:01:05	65:22:04	Touchdown
	00:01	65:22	RADVS power off
	00:02	65:23	Flight control power off
	01:23	00:22	Omni B high power off

5.1.4.2 Postlaunch Phase

The spacecraft was injected into a parking orbit for 15 minutes and was in an earth shadow for 14.4 minutes from launch. This time interval was small enough that most components were not subjected to any large temperature variations. The solar panel was an exception: the minimum recorded temperature was 36°F at 11 minutes after launch. No data were available from this time to sun acquisition at 36 minutes after launch. It is estimated that the minimum temperature occurred at the time of earth shadow exit and that the solar panel did not go below 0°F.

5.1.4.3 Midcourse

The spacecraft thermal response during midcourse was nominal. A maximum engine temperature of 368°F was observed on engine 3. A summary of propulsion system temperature excursions due to midcourse operations is presented in Table 5.1-3.

The spacecraft was oriented off-sun for about 21 minutes and 19 seconds during which time the midcourse engine firing was executed. During this period, all spacecraft temperature signals remained within appropriate limits.

TABLE 5.1-3. SURVEYOR VI MIDCOURSE THERMAL RESPONSE (°F)

Sensor	Preignition Temperature	Peak Temperature Observed	Temperature Increase
Engine 1 (P-7)	65	335	270
Engine 2 (P-10)	84	265	181
Engine 3 (P-11)	77	368	291
Oxidizer line 1 (P-8)	60	71	11
Oxidizer line 2 (P-4)	37	58	21
Oxidizer line 3 (P-9)	58	88	30
Oxidizer tank 1 (P-15)	60	71	11
Oxidizer tank 2 (P-16)	37	56	19
Oxidizer tank 3 (P-6)	55	62	7
Fuel tank 1 (P-13)	56	65	9
Fuel tank 2 (P-5)	43	56	13
Fuel tank 3 (P-14)	56	66	10

All cyclic heater loads (except the gyro heaters) were commanded off for approximately 7 minutes. The heaters are commanded off in order to remove cyclic loads so that critical electrical loads could be observed without ambiguity during the vernier burn.

Propellant tank temperature stratification was observed on this flight as in all previous flights. Temperature changes induced at the temperature sensor locations due to propellant motion within the tanks are also presented in Table 5. 1-3.

5. 1. 4. 4 Coast Phases

Heater Performance

All heaters performed as expected and no anomalies occurred. The gyro heaters were on before launch and continued to cycle until after touchdown when flight control power was commanded off. The duty cycles for the gyros at 5 hours after launch are as follows:

Roll: 12. 8 percent

Pitch: 28 percent

Yaw: 16. 9 percent

The first vernier propellant line to cycle after launch was oxidizer line 2 at L+1:50. It cycled between the values of 18° and 26°F with the duty cycles as listed in Table 5. 1-4 during the rest of the transit phase. The altitude marking radar heater started cycling at L+7:22 and remained between 17° and 20°F thereafter. The duty cycles are listed in Table 5. 1-4.

TABLE 5. 1-4. HEATER DUTY CYCLES

Mission Time, hr:min	Oxidizer Line 2, percent	AMR, percent	Oxidizer Line 3, percent
09:00	26.4		
11:00			
28:00	35.4	47.9	
52:50	40.5		
62:00	45.0		
53:53		56.1	7.4

Vernier oxidizer line 3 started cycling at 33 hours and 39 minutes into the mission, and the temperature ranged from 18° to 22°F after it started cycling. The duty cycle is listed in Table 5. 1-4.

The propellant tank heaters were all enabled at 55:14 hours mission time, but none of them cycled during the mission as the temperatures were above the thermostat set point. The television electronics and compartment C heater were enabled at 60:16 and 60:46 mission time, respectively, and the alpha head heater was commanded on at 62:48. The television vidicon heater was commanded on at 63:37.

Gyro Drift Check and Effects

The most notable thermal effect during the 14 gyro drift checks was on engine 2, caused by the +1. 2 deg/hr yaw. The increased solar energy raised this engine 18 degrees above its steady-state temperature of 80°F. This engine is known to be sensitive to the gyro drift, and therefore this was considered a nominal condition. The pitch gyro drift rate was very small and had a negligible thermal effect on the spacecraft.

The thermal effect of gyro drift checks on other subsystems may be seen on the temperature histories of the nitrogen tank (FC-48), the A/V preamplifier (R-13), the compartment A canister (V-18), and the spaceframe at retro attach point 2 (V-38).

Vernier Oxidizer Line 1

The transit steady-state temperature range of 51° to 57°F (Figure 5. 1-A5) on oxidizer line 1 (P-8), while within limits, was unexpected. Based on solar thermal vacuum test data and the experience of previous flights, the predicted temperature for Mission F was 31°F. The temperature sensor is remotely located from the maximum temperature location at the upper portion of the feed line. The maximum temperature at this localized region was estimated to be 110°F or at the upper temperature limit.

During the terminal maneuvers when solar energy illuminated the bottom of the spacecraft, the temperature of oxidizer line 1 at the flight sensor increased steadily, reaching 103°F at retro ignition.

Several other investigations were made to validate the oxidizer line 1 temperature measurement. Scaling coefficients were checked; the temperature in the prelaunch air-conditioning environment compared exactly with the other two oxidizer lines; and a temperature of 20°F (the set point of the thermostat) was measured when the line 1 heater cycled starting at 6 hours and 23 minutes after touchdown. The pre-encapsulation photographs and thermal inspection did not indicate any discrepancies in the line thermal finish or to the sunshade. Power considerations indicated the line 1 heater was not drawing current during the transit.

It must be concluded that no reason for the higher than predicted temperature of oxidizer line 1 could be found.

Alpha Scattering Instrument

The thermal performance of the alpha scattering units is summarized in Table 5. 1-5 and Figure 5. 1-A5. All temperatures were corrected for bit rate errors of 2°F at 550 bps, 5°F at 1100 bps, and approximately 16°F at 4400 bps. The Surveyor VI preterminal descent warmup of compartment C was initiated at approximately L+60:46 (less warmup time was required for Surveyor VI than for Surveyor V because compartment C and instrument head equilibrium temperatures were 10°F higher than Surveyor V). After a 2-hour warmup of compartment C to above -4°F, the alpha scattering instrument heater was enabled. The head temperature increased from an equilibrium of 43°F to the heater thermostat set point of 50°F, and the heater began cycling within 0. 5 hour after being enabled. One hour before retro ignition, the ASI head temperature was at 52°F, and the compartment C temperature was 17°F.

The alpha scattering system temperatures after landing were of interest because of the low sun elevation. It was predicted that the instrument steady-state temperature with the heater on would be above the operational temperature limit after touchdown. Compartment C temperature was predicted to be above the operational limit even with the heater disabled. The sun illuminated the compartment radiator directly in the landed orientation. The alpha scattering temperatures after landing were 50°F for the sensor head and 15°F for compartment C.

Television System

The television camera electronics heater was enabled at the normally scheduled time of L+60: 16. On previous missions, the electronics temperature (TV-16) had warmed up to the required -20°F for vidicon heater turn-on 1/2 hour in advance of the nominal turn-on time. In Mission F, the electronics temperature was -27°F at that time, and vidicon heater turn-on was delayed for 23 minutes. No television problems resulted from this delay as the camera had achieved the desired operational temperatures prior to use of the television system.

The new enlarged television hood and mirror assembly was flown for the first time on Mission F and may have caused the slower thermal response.

Compartment System

The thermal performance of compartments A and B agreed well with predictions for Mission F during steady-state operations. Compartment A performed exactly as predicted, whereas compartment B was approximately 9°F warmer than predicted.

The thermal response of compartments A and B to high power operation was as expected. Table 5. 1-5 presents data from the four high power transmitter operation intervals and indicates the temperature responses of all critical sensors in compartments A and B. Transmitter B was utilized for all transit high power operations.

TABLE 5. 1-5. COMPARTMENTS A AND B THERMAL RESPONSE TO HIGH POWER OPERATION (°F)

	Sun Acquisition			Canopus Search			Midcourse			Terminal Descent		
	Peak Temperature	Temperature Rise										
		Predicted	Actual	Peak Temperature	Predicted	Actual	Peak Temperature	Predicted	Actual	Peak Temperature	Predicted	Actual
Compartment A												
D-13	83	4	3	67	15	16	62	38	18	58	28	19
D-14	122	49	41	110	55	56	106	61	58	115	22	19
EP-8	84	1	4	77	4	4	72	8	2	79	39	27
EP-34	94	6	6	82	6	6	77	11	6	102	50	42
V-15	100	18	20	87	32	32	80	37	33	62	37	21
V-16	86	1	4	73	5	3	69	8	5	87	31	36
Compartment B												
EP-13	83	0	0	79	8	0	84	9	4	83	7	0
V-21	88	0	0	74	4	1	74	4	6	77	3	0
V-22	85	0	0	79	3	0	77	4	1	81	3	0

During launch, aerodynamic heating on compartments A and B negligibly affected the compartment internal temperatures. Unfortunately, no data were available from 07:50 to 08:10 GMT on day 311, the critical period of aerodynamic heating, to observe the temperature response of the thermal switches.

5. 1. 4. 5 Terminal Descent Phase

The thermal response during terminal descent was nominal. The maximum temperatures recorded on the vernier engines were 450°, 345°, and 451°F on engines 1, 2, and 3, respectively. The klystron power supply modulator temperature increased from 14° to 92°F during RADVS operation. At retro ignition, the retro bulk temperature was 53°F.

Incorporation of the battery warmup procedure resulted in a battery temperature of 90. 4°F at the time of RADVS turn-on. Thus, the battery was at the most desired temperature to support the loads associated with terminal descent.

The spacecraft was in an off-sun attitude for approximately 31. 5 minutes prior to touchdown. All temperatures remained within proper temperature limits during this period (see Figures 5. 1-A1 through 5. 1-A6).

Transmitter B high power operation was initiated 53. 5 minutes before touchdown and terminated 22 minutes after touchdown (approximately 1 hour and 16 minutes of continuous high power). During this period, transmitter B temperature increased to 115°F and remained steady at that temperature for the last 44 minutes of the operation.

5. 1. 5 THERMAL PERFORMANCE – FIRST LUNAR DAY

A summary of maximum lunar day temperatures and minimum temperatures during an eclipse is shown in Table 5. 1-6. Plots of thermal parameters during the lunar day are presented in Appendix B to this section.

5. 1. 5. 1 Touchdown and Orientation

Surveyor VI touchdown occurred at 01:01 GMT on day 314. The spacecraft +X axis was pointing nominally downhill at an inclination of 0. 9 degree. The sun vector was 59 degrees from -X towards -Y. A comparison of landing orientation for Surveyors I, III, V, and VI is given in Table 5. 1-7.

5. 1. 5. 2 Heater Performance

Performances of all heaters during the lunar phase were within tolerances, and no anomalies occurred. Table 5. 1-8 gives the times that heaters were enabled and disabled during lunar operations. The use of compartment heaters towards the end of the lunar day served two purposes: 1) to serve as a load for a near fully charged battery to keep the solar panel switch on, 2) to warm the compartment interior prior to sunset for additional operating time into the lunar night from the compartment heat capacity.

5. 1. 5. 3 Compartment System

Compartment A behaved better thermally in the lunar morning than any prior spacecraft. For a period of 7 days during the lunar morning, the main battery never exceeded 75°F. These low temperatures were caused by shadowing of compartment A radiators by the solar panel and planar array. During the afternoon, compartment A could not be shadowed without loss of earth lock, and the main battery reached 115°F twice: at 323:13:00 GMT (solar elevation angle = 62 degrees), and 324:19:00 GMT (solar elevation angle = 46 degrees). A standby mode had to be initiated from 323:10:00 to 324:23:00 to cool down the main battery to ensure future ability to take pictures at each Goldstone rise. Engineering interrogations were made every 2 hours during this period.

Compartment B never exceeded its operational temperature limits. The maximum temperatures observed in compartment B were 115°F for the lower thermal tray and 111°F for the upper thermal tray.

5. 1. 5. 4 Surveyor Environmental Test Laboratory (SETL) Spacecraft Model

During lunar operations, it became essential to determine the shading on spacecraft components for a variety of solar panel and planar array locations and sun positions. This was necessary because of the special requirements of the lunar hopper experiment. The SETL model of the spacecraft was used, along with a collimated light source to simulate the spacecraft in the lunar environment. Polaroid pictures were taken of the shadow patterns on the model. Actual spacecraft television pictures of shaded areas were used to verify the effectiveness of this method.

TABLE 5.1-6. MAXIMUM QUASI-STEADY STATE TEMPERATURES AND MINIMUM TEMPERATURES OF SPACECRAFT ON LUNAR SURFACE

Sensor and Location	Maximum Temperature, °F				Eclipse Minimum Temperature, °F	
	Surveyor I	Surveyor III	Surveyor V	Surveyor VI	Surveyor III	Surveyor V
AS-3 Alpha scattering sensor head	—	—	143/146*	163	—	14
AS-4 Compartment C electronics	—	—	132/138	147	—	23
D-13 Transmitter A	185	118	120/112	110	47	64
D-14 Transmitter B	106	110	109/111	110	43	64
EP-8 Main battery	118	116	114/118	115	74	101
EP-12 Solar panel	217	220	248/250	241	-185	-166
EP-13 Boost regulator	132	132	124/127	115	32	66
EP-26 Auxiliary battery	155	166	—	—	140	—
EP-34 Battery charge regulator	142	125	124/125	136	72	99
FC-44 Flight control electronics	192	202	180/184	196	53	25
FC-45 Flight control electronics	200	201	185/190	197	-3	31
FC-46 Roll gyro	167	198	157/290**	160	11	116
FC-47 Canopus	180	194	170/177	200	-20	6
FC-48 Nitrogen tank	173	165	195/187	225	—	16
FC-54 Pitch gyro	188	—	157/289**	159	—	112
FC-55 Yaw gyro	170	—	157/291**	161	—	114
FC-70 Attitude jet 2	205	210	219/226	214	-52	-66
FC-71 Roll actuator	224	239	230/238	244	-16	28
M-8 Planar array	228	230	296/296	290	-140	-133
M-10 Solar motor	218	230	242/245	222	-43	-52
M-12 Elevation motor	190	201	210/208	223	14	-3
P-4 Oxidizer line 2	203	203	210/207	182	76	81
P-5 Fuel tank 2	164	197	206/201	194	165	136
P-6 Oxidizer tank 3	154	179	173/181	179	108	136
P-7 Vernier engine 1	244	256	250/250	246	-12	40
P-8 Oxidizer line 1	221	202	220/226	213	8	52
P-9 Oxidizer line 3	184	200	182/186	195	62	-1
P-10 Vernier engine 2	229	256	272/252	256	36	-12
P-11 Vernier engine 3	227	232	210/219	271	22	12
P-13 Fuel tank 1	190	208	209/204	200	83	174
P-14 Fuel tank 3	171	188	166/160	195	137	124
P-15 Oxidizer tank 1	173	183	192/187	180	96	149
P-16 Oxidizer tank 2	166	185	182/183	166	153	129
P-17 Helium tank	145	178	197/213	186	21	-19
P-23 Fuel line 1	—	—	213/210	214	—	142
P-24 Fuel line 2	—	—	219/208	208	—	84
P-25 Fuel line 3	—	—	210/210	245	—	33
R-8 Klystron power supply modulator	225	214	222/227	247	23	43
R-9 Signal data converter	149	168	174/180	161	8	42

*First day/second day values.

**IRU radiator damaged during lunar night.

Table 5.1-6 (continued)

Sensor and Location	Maximum Temperature, °F				Eclipse Minimum Temperature, °F	
	Surveyor I	Surveyor III	Surveyor V	Surveyor VI	Surveyor III	Surveyor V
R-10 Doppler preamplifier	235	260	260/260	215	-33	31
R-13 Altitude preamplifier	214	232	243/226	243	2	-31
SS-12 Surface sampler electronics	–	144	–	–	-18	–
TV-16 TV electronics	127	140	150/157	143	-10	0
TV-17 TV hood	124	148	152/155	136	-12	-1
V-15 Compartment A tray top	110	109	109/117	110	41	64
V-16 Compartment A tray bottom	118	117	119/124	124	68	89
V-17 Compartment A shell, retainer	–	120	–	–	69	–
V-18 Compartment A shell, canister	–	108	100/110	119	-170	-160
V-19 Compartment A switch 5, base	–	112	108/115	110	45	62
V-20 Compartment A switch 5, radiator	78	101	100/104	97	18	24
V-21 Compartment B tray top	118	117	117/122	112	21	59
V-22 Compartment B tray bottom	124	122	124/127	115	29	70
V-23 Compartment B shell canister	111	152	105/114	100	-154	-153
V-24 Compartment B switch 4, radiator	99	100	100/106	96	-16	11
V-25 Compartment A switch 8, radiator	88	100	100/110	98	13	8
V-26 Compartment B switch 4, base	–	114	114/118	109	21	52
V-27 Upper spaceframe	138	156	160/168	159	-75	-70
V-28 Lower spaceframe	190	186	196/201	182	-32	-8
V-29 Thermal tunnel	–	115	130/134	126	47	73
V-30 Shock absorber 1	193	190	178/187	184	-51	-65
V-31 Leg 2 upper web	148	158	–	–	–	–
V-32 Shock absorber 2	171	183	195/201	183	-57	-67
V-33 Shock absorber 3	175	186	189/195	184	-35	-55
V-34 Antenna/solar panel positioner mast	130	142	–	–	-102	–
V-35 Upper spaceframe	125	154	168/172	154	-70	-81
V-36 Lower spaceframe	166	179	187/188	192	-45	-46
V-37 Retro bolt 1	222	202	219/222	234	-2	14
V-38 Retro bolt 2	175	227	222/206	206	32	-29
V-39 Retro bolt 3	185	200	185/188	214	-11	-7
V-44 Crushable block 3 heat shield	189	193	210/211	236	-29	-15
V-45 Compartment B switch 1, radiator	104	105	108/112	102	-95	25
V-46 Compartment B switch 5, radiator	96	100	100/105	95	-5	-30
V-47 Compartment A switch 2, radiator	–	104	105/110	100	18	9
V-49 Compartment A switch 3, radiator	–	–	105/110	102	–	18

TABLE 5.1-7. COMPARISON OF LANDING ORIENTATIONS FOR SURVEYOR SPACECRAFT

Spacecraft	Sun Elevation Angle to Spacecraft X-Y Plane, degrees	Sun Direction at Touchdown
I	29	Sun vector 1 degree from -Y towards +X
III	12	Sun vector 44 degrees from +X towards -Y
V	20-1/2	Sun vector 24 degrees from +X towards -Y
VI	4-1/2	Sun vector 59 degrees from -X towards -Y

5.1.5.5 Television Camera Operation

The camera was within operational temperature limits throughout the entire lunar day. It was not necessary to go to a standby mode during the lunar noon interval to maintain proper camera thermal control. The solar panel was positioned to partially shade the camera at 09:00 GMT on day 318. The camera had the thermal capability to operate almost continuously at 2-hour operating periods with engineering interrogations interspersed. This was the best television camera thermal performance experienced on any spacecraft during the lunar noon period.

5.1.5.6 Alpha Scattering System

Continuous alpha scattering operation from thermal considerations was possible for nearly 3 days after touchdown. It was necessary to command the alpha scattering system off at 316:23:39 because the temperatures of the instrument (AS-3) and the compartment C electronics (AS-4) were 122° and 125°F, respectively. The upper operational limits are 122° and 131°F.

At this point, alpha scattering system operation had to be suspended for 3-1/2 days until the sun elevation angle was 79 degrees, at which time, as indicated by the SETL spacecraft model and the shadow plots, solar panel shading was possible. The temperatures of the instrument and the compartment C electronics had both increased to 142°F in this period. At 320:06:00 the solar panel was repositioned to accomplish the required shading and bring the alpha scattering system temperature within operational limits. Alpha scattering experimentation was resumed at 320:13:01 with instrument

TABLE 5.1-8. HEATER ENABLE/DISABLE TIMES FOR FIRST LUNAR DAY

Day	GMT, hr:min	Propellant Lines	Propellant Tanks	Compart-ment C	Alpha Scattering Head	TV		AMR Logic	(Gyros) Flight Control Power	Compart-ment A	Compart-ment B
						Electronics	Video				
314	01:12	On	On	On	On	On	On		Off		
	01:18							Off			
	05:47			Off							
	06:34	Off	Off								
	06:35	Line 1 on									
315	06:16	Off			Off	Off					
	20:30						Off			Off	Off
321	09:45								On		
	10:34								Off		
322	01:55				On						
	12:06				Off						
326	00:14				On						
	08:00							On			
	19:06									On	
	20:16							Off			
327	00:15									Off	
	00:16										On
	04:55									On	Off
	07:07							On			
	16:12					On	On	Off			
	18:46									Off	On
	20:45									On	Off
328	01:54			On							
	02:09			Off							
	04:13			On							
	14:04									Off	
	16:01					On					
	16:28					On					
	16:43					On					
	17:53					On					
	18:03			Off	Off						
	19:48						Off				
329	07:08									On	
	18:25									Off	
	21:05									On	
330	01:09									Off	
(S/C shutdown)	01:10					Off					

and electronic temperatures at 100° and 92°F, respectively. The system was commanded off at 321:03:32 after sufficient data were obtained to allow preparations for the lunar translation.

After the lunar translation, the alpha instrument was found to be upside down. The instrument temperature is hotter in this position than upright as the cavity absorbs most of the incident solar energy and the radiator (primary temperature control surface) is in contact with the hot lunar surface. The instrument temperature rose to 163°F subsequent to the translation (321:17:00), an increase of 20 degrees.

The alpha scattering device temperature changes with bit rate. On several occasions, the bit rate was lowered to determine the magnitude of the temperature error associated with the higher bit rate of 1100 bps. Table 5. 1-9 gives readings taken at various times during the mission. The average 1100-bps correction for AS-3 and AS-4, respectively, was 5. 6° and 5. 7°F.

TABLE 5. 1-9. EFFECT OF BIT RATE ON ALPHA SCATTERING TEMPERATURES

GMT, day:hr:min	Instrument Temperature (AS-3), °F			Compartment C Electronics Temperature (AS-4), °F		
	137. 5 bps	1100 bps	Difference	137. 5 bps	1100 bps	Difference
316:18:21	118. 7	125. 9	+7. 2	122. 6	128. 8	+6. 2
318:17:00	139	146	+7	88	93	+5
319:06:30	142	147	+5	94	100	+6
319:18:00	141	147	+6	97	102	+5
320:14:32	96. 6	101. 8	+5. 2	93. 2	98. 5	+5. 3
322:13:56	48. 6	53. 9	+5. 3	64	70. 2	+6. 2

5. 1. 6 LUNAR NIGHT THERMAL PERFORMANCE

An analysis was made to determine the performance of the compartment A and B thermal switches during the Surveyor VI first lunar night. Figure 5. 1-1 shows the power and temperature history of both compartments and an estimate of the number of closed (stuck) switches during this period. It was determined that at last contact with the spacecraft (330:06:41 GMT) there were six switches closed in compartment A and one closed in compartment B. This problem was documented in TFR 18271.

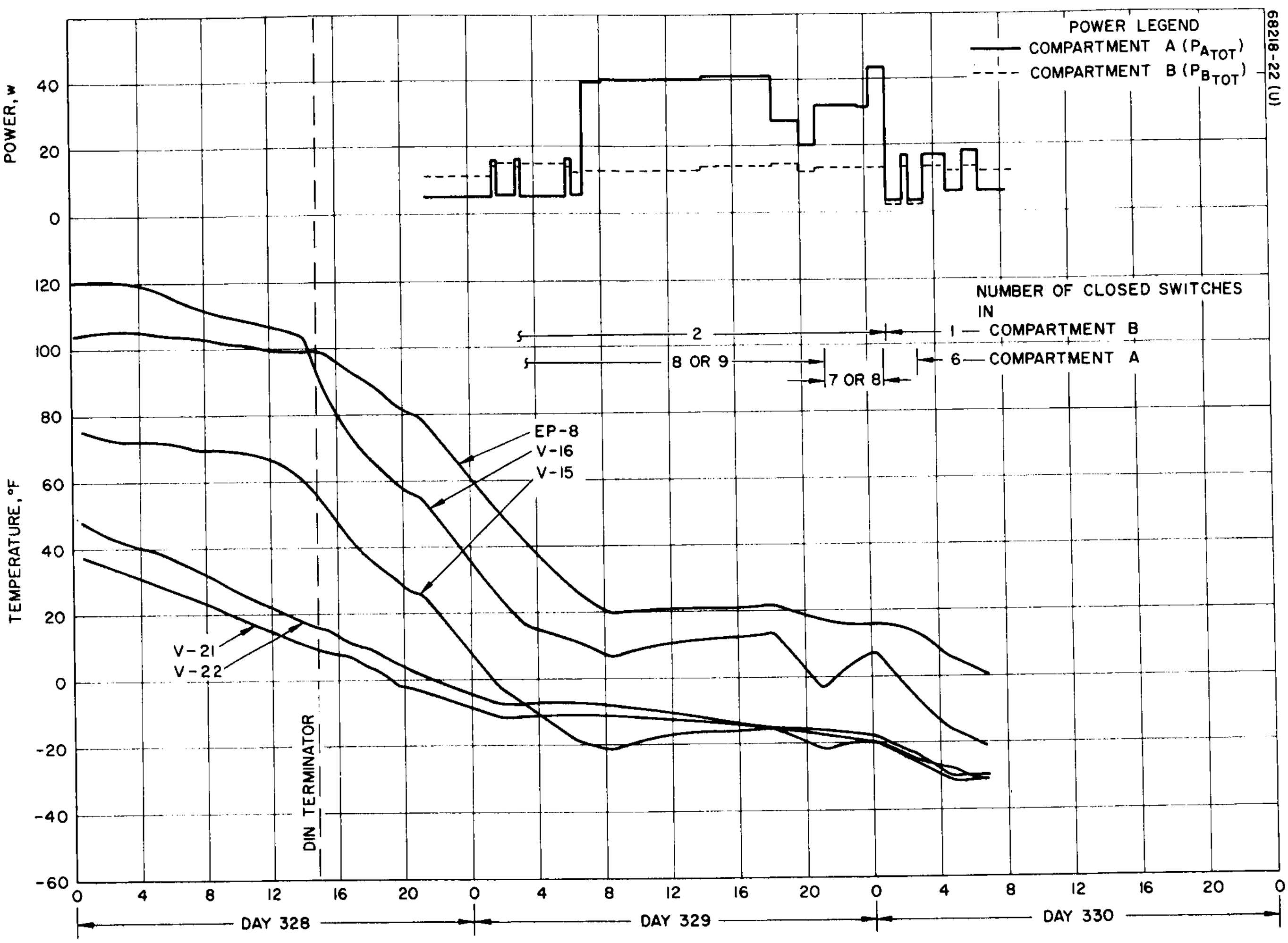

Figure 5.1-1. Surveyor VI Thermal Switch Closures During Lunar Night

The number of closed switches was determined by performing heat balances on each compartment during specific time periods. The unit power dissipations in the compartments were obtained from Reference 1. The battery dissipation was calculated by

$$P_{Batt} = (25.77 - \text{bus voltage}) \times \text{unregulated current}$$

The data shown in Figure 5.1-1 represents all the spacecraft power configurations during the time period shown, based on information found in the detailed command log and/or real time records.

The general method of analysis used postulates that any heat input above that required to maintain the compartment at steady state when all switches are open (based on Surveyor V experience) is lost through closed switches. During the Surveyor VI first lunar night, no true steady-state temperature condition was obtained in either compartment. For this reason, it became necessary to account for the heat capacity of the compartments. Since the analysis is based on the bulk temperature of the compartment, the necessity of using the rate of change of temperature introduces considerable uncertainty in the calculations when the compartment internal temperature gradients are significant. Due to temperature gradients in the compartment A and B trays, the bulk temperatures were assumed to be given by

$$T_c(A) = 0.75\ T_{EP-8} + 0.25\ T_{V-15}$$

$$T_c(B) = 0.5\ T_{V-21} + 0.5\ T_{V}\text{-}22$$

The method of calculating the number of stuck switches is outlined in Table 5.1-10.

Results using this analysis are somewhat uncertain. The limiting conditions associated with this method of estimating the number of closed switches are as follows:

1) Analysis indicates that prior to 329:21:30 GMT, all nine switches on compartment A were closed. However, there is other evidence that indicates that switch 6 would be open in the specified temperature range. This switch definitely opened during Surveyor VI solar thermal vacuum testing; also, TV pictures taken of compartment A soon after touchdown indicate that this switch was open at that time.

2) Results obtained by this analysis are sensitive to the selection of the time interval over which the calculations are made. This is due to the combined effects of using average internal power levels, bulk compartment temperatures, and average temperature slopes.

TABLE 5.1-10. METHOD OF CALCULATING STUCK THERMAL SWITCHES

$$P = \frac{\Sigma P_i \, \Delta \theta_i}{\Sigma \Delta \theta_i}$$

$$Q_r = \sigma \epsilon \left(T_r^4 - T_b^4\right), \text{ watts/ft}^2$$

$$Q_1 = \Delta Q \Big|_{\text{steady state}}^{\text{actual}} = P - Q_s - G \frac{\Delta T}{\Delta \theta}$$

$$A_r = \frac{Q_1}{Q_r}$$

$$N_s = \frac{A_r}{A_s}$$

where:

$\Delta\theta$ = time interval

P = average power level during $\Delta\theta$

T_r = average closed switch radiator temperature during $\Delta\theta$

T_b = radiator background temperature (assumed equal to average open switch radiator temperature)

Q_r = heat flux from closed switch radiators

Q_s = heat loss from compartment at steady state at T_c with all switches open

G = compartment "heat rate" — watts/°F/hr (6.2 for compartment A, 2.2 for compartment B)

Q_1 = heat loss in excess of steady-state conditions (watts)

A_r = area required to radiate excess heat (ft^2)

A_s = radiating area per switch (0.313 ft^2 for compartment A, 0.33 ft^2 for compartment B)

N_s = number of closed switches

Due to the existence of the uncertainties mentioned above, the compartment A results (Figure 5.1-1) indicate a range of switches closed rather than a unique number of switches.

Telemetry provided the following information:

1) Compartment A switch 5 opened at approximately 330:03:00 GMT at an out of specification tray temperature of -26°F.

2) All three telemetered switches (1, 4, and 5) on compartment B opened.

3) Two switches (1 and 5) on compartment B opened out of the specified temperature range (1 at ~ 11°F and 5 at ~ 9°F).

The following conclusions regarding the thermal switches can be made:

1) Seven switches remained closed at the time of last contact with the spacecraft (six on compartment A and one on compartment B).

2) One switch opened within the specified temperature range (compartment B switch 4).

3) Six switches opened out of the specified temperature range (three on each compartment).

4) One additional switch on compartment B opened but it is not known whether or not it was within the specified temperature range.

5.1.7 REFERENCES

1) "Power Management Data Summary," Hughes Aircraft Company, Surveyor System Specification 3023931, 25 August 1967.

2) L. L. Gamer, "SC-VI Spacecraft Shadow Plots For First Lunar Day Using Actual A/SPP Stepping History," Hughes Aircraft Company, IDC 2292/438, 21 December 1967.

5.1.8 ACKNOWLEDGMENT

This section was coordinated by J.S. Tuchscher of the Surveyor Thermal Control Section.

APPENDIX A
TO SECTION 5.1

TRANSIT TEMPERATURE PLOTS

Appendix A contains Figures 5.1-A1 to 5.1-A6 which are transit thermal plots.

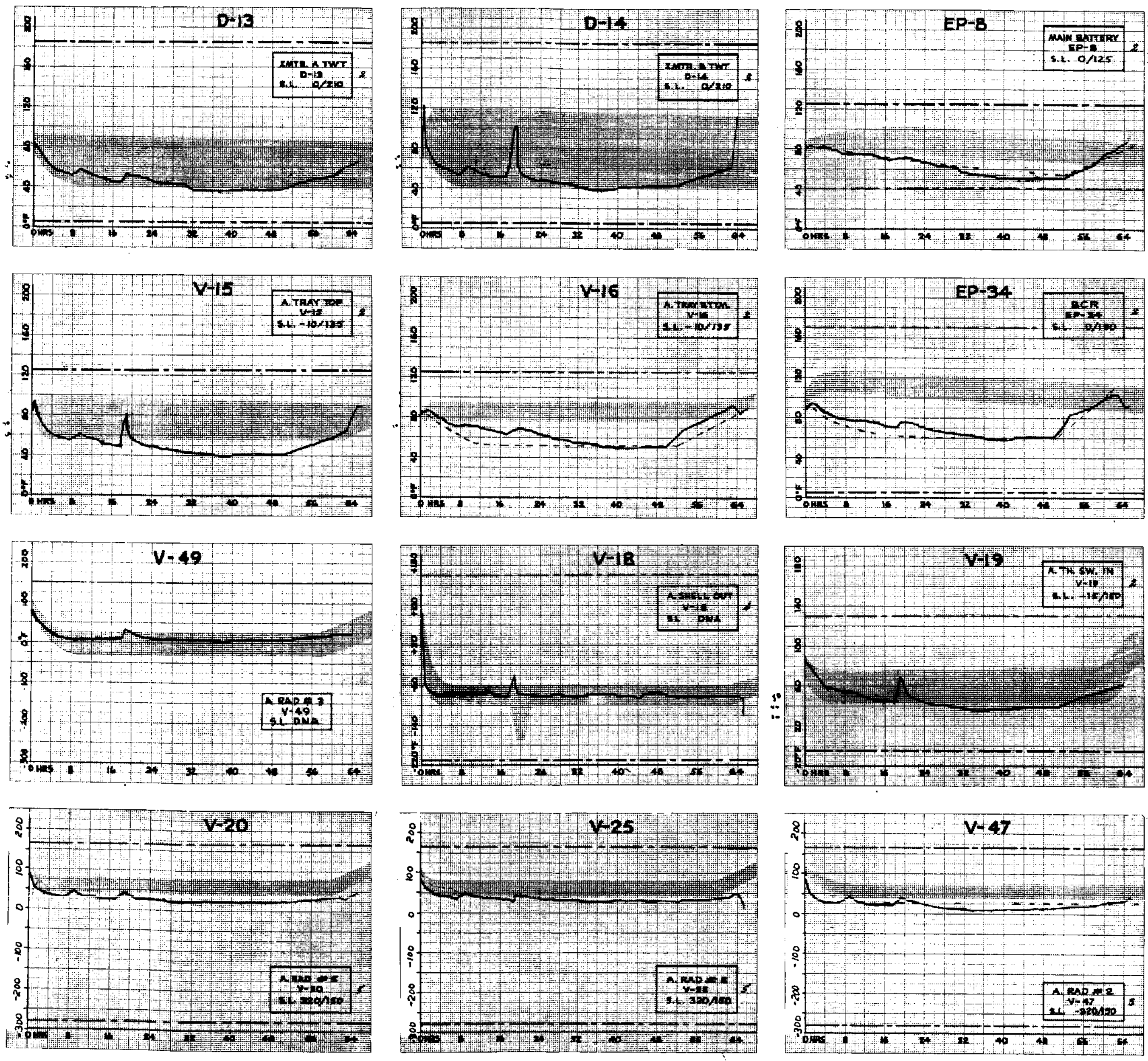

Figure 5. 1-A1. Compartment A

PRECEDING PAGE BLANK NOT FILMED.

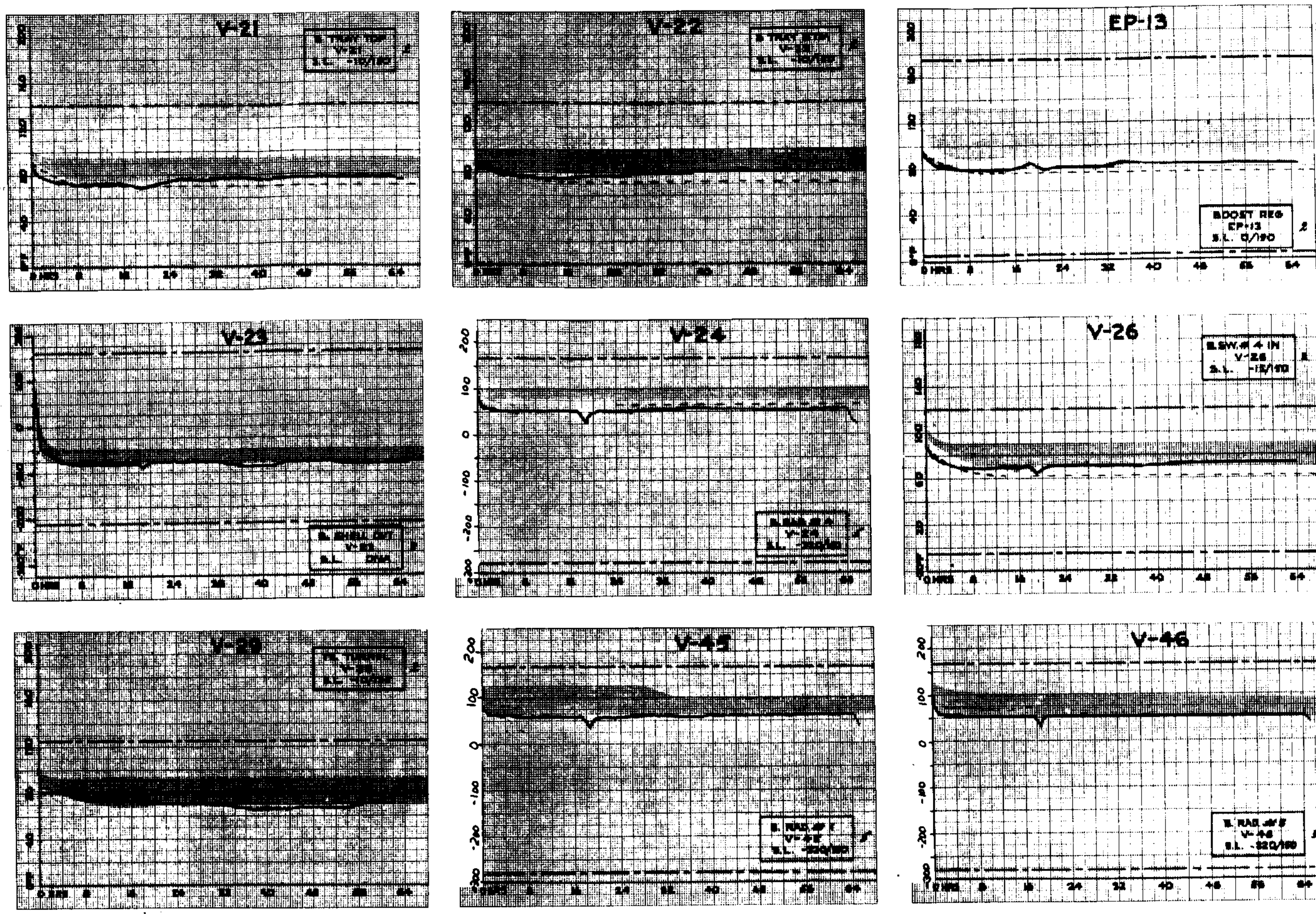

Figure 5.1-A2. Compartment B

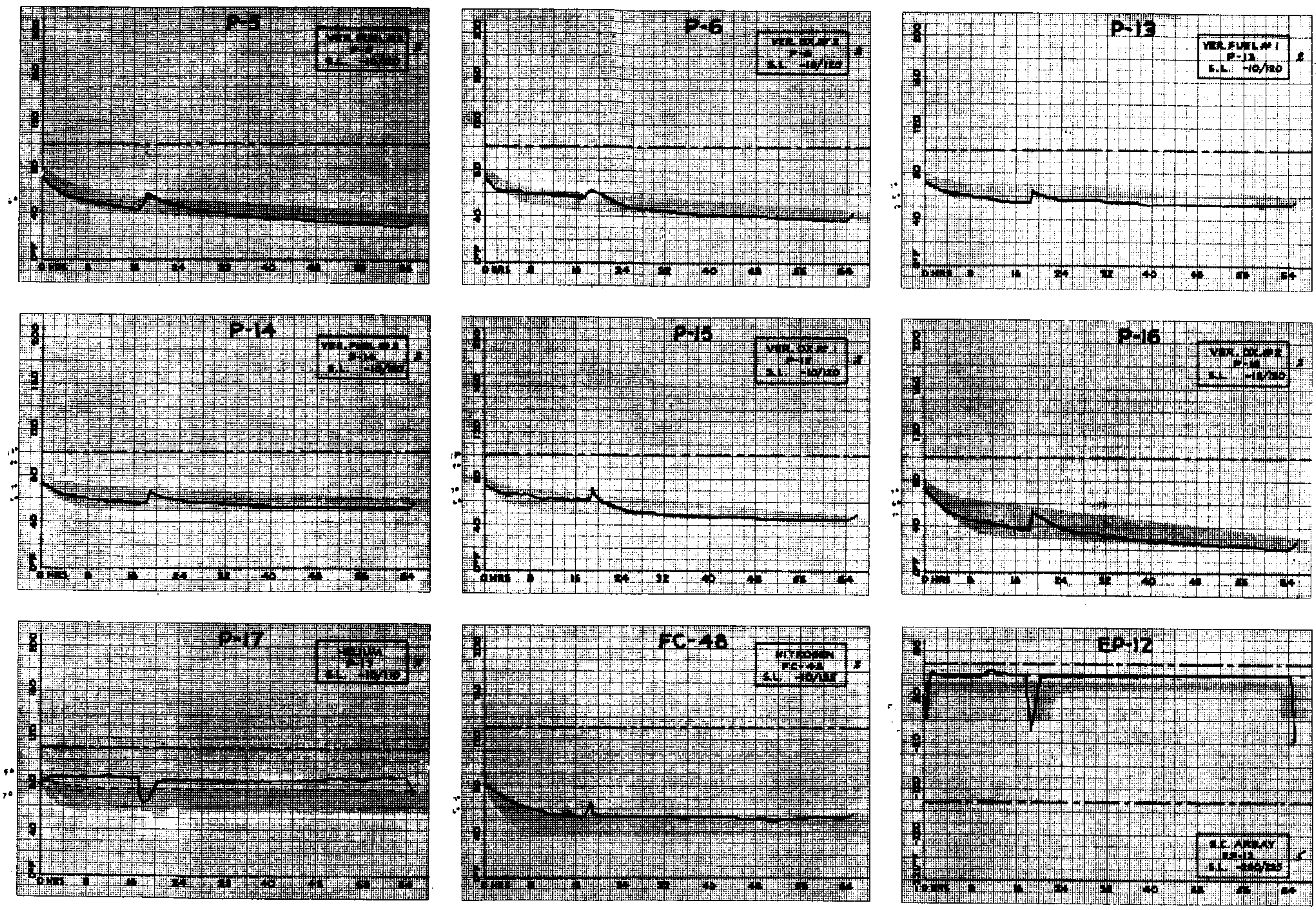

Figure 5.1-A3. Tanks

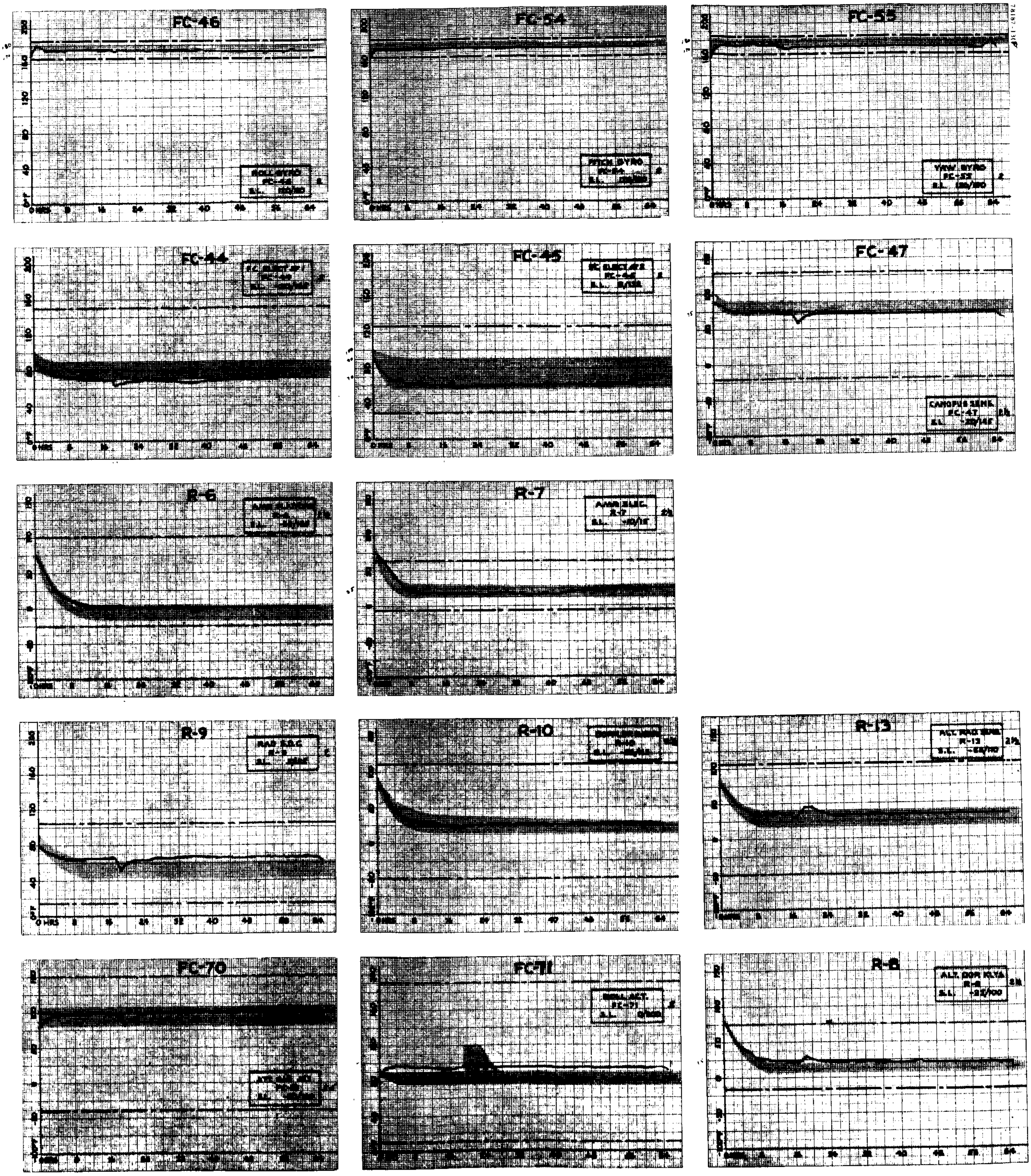

Figure 5.1-A4. Flight Control

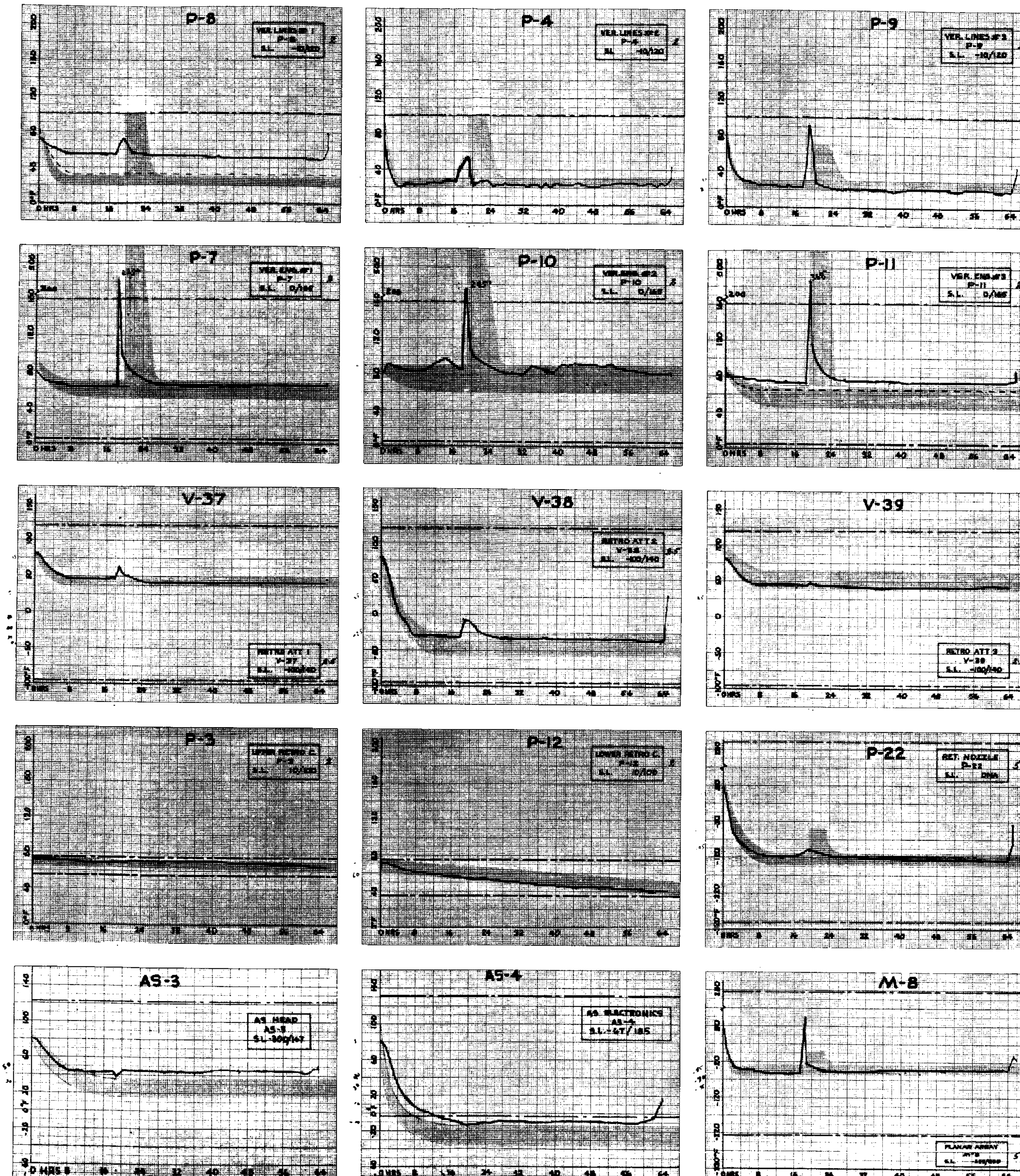

Figure 5. 1-A5. Propulsion

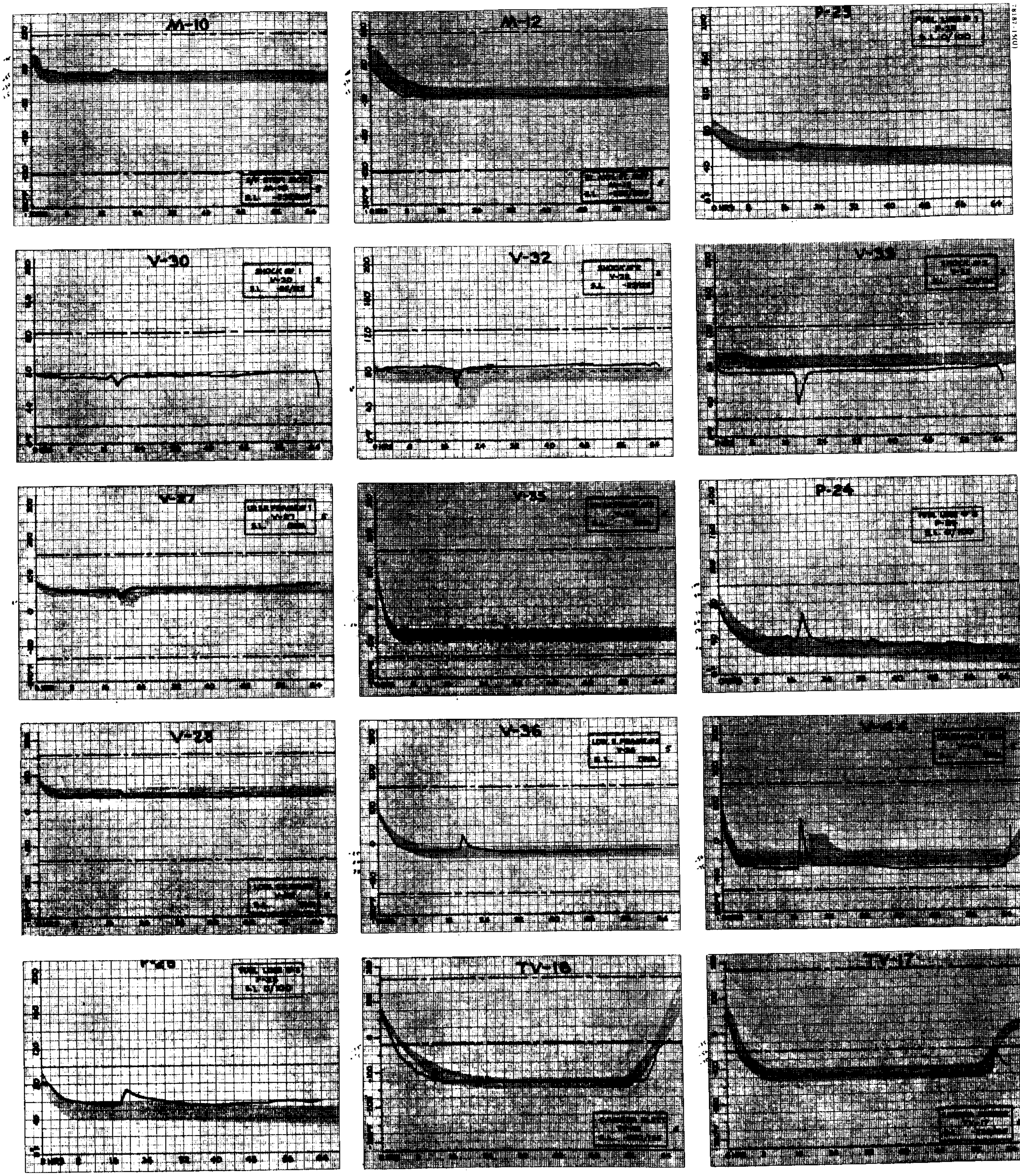

Figure 5.1-A6. Space Frame

APPENDIX B
TO SECTION 5.1
LUNAR DAY TEMPERATURE PLOTS

Appendix B contains Figures 5.1-B1 to 5.1-B69 which are the first lunar day temperature plots. The sun incidence angle is noted on these plots. Reference 2 contains shadow plots for the first lunar day using the actual A/SPP stepping history.

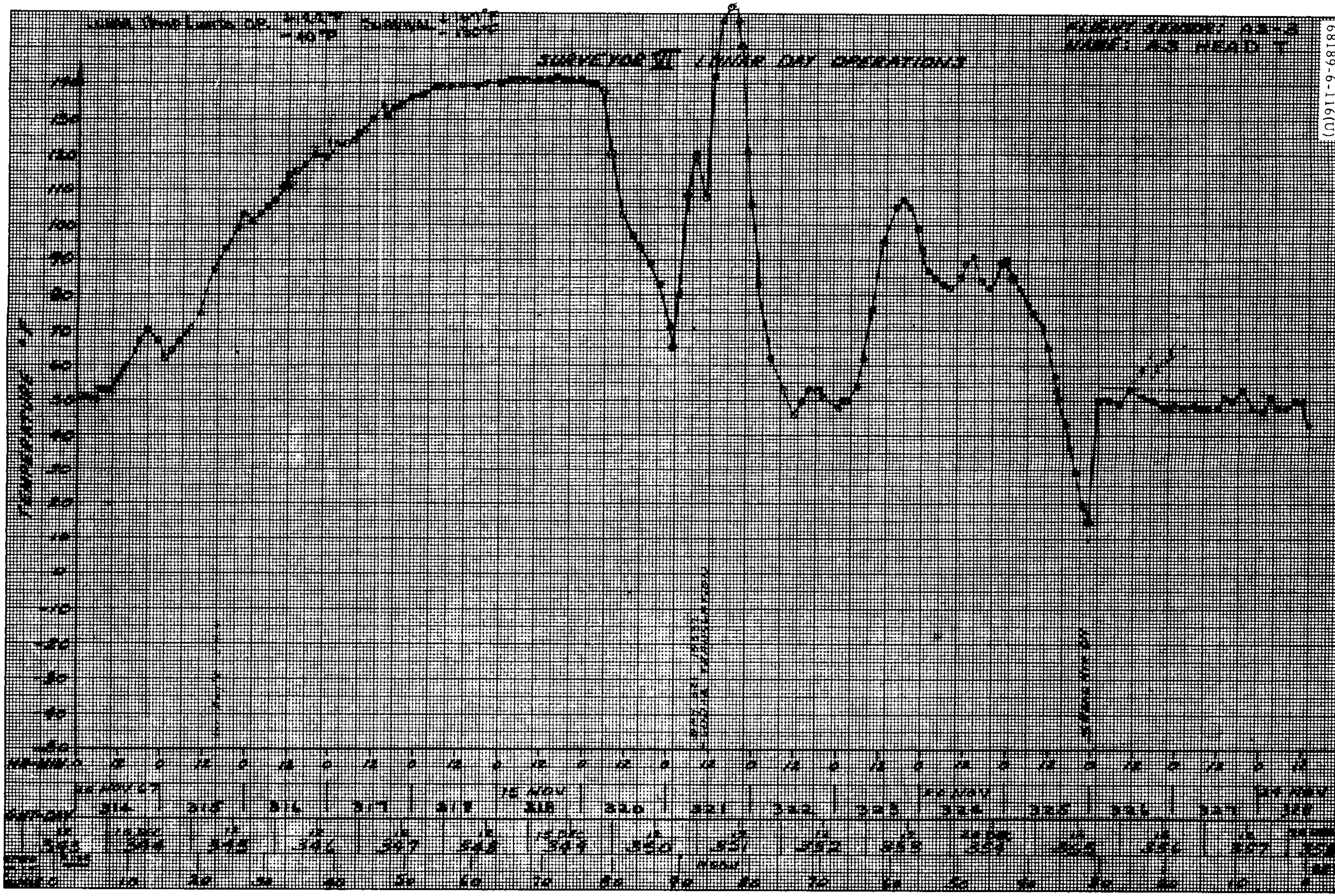

Figure 5.1-B1. Sensor AS-3: Alpha Scattering Head

PRECEDING PAGE BLANK NOT FILMED.

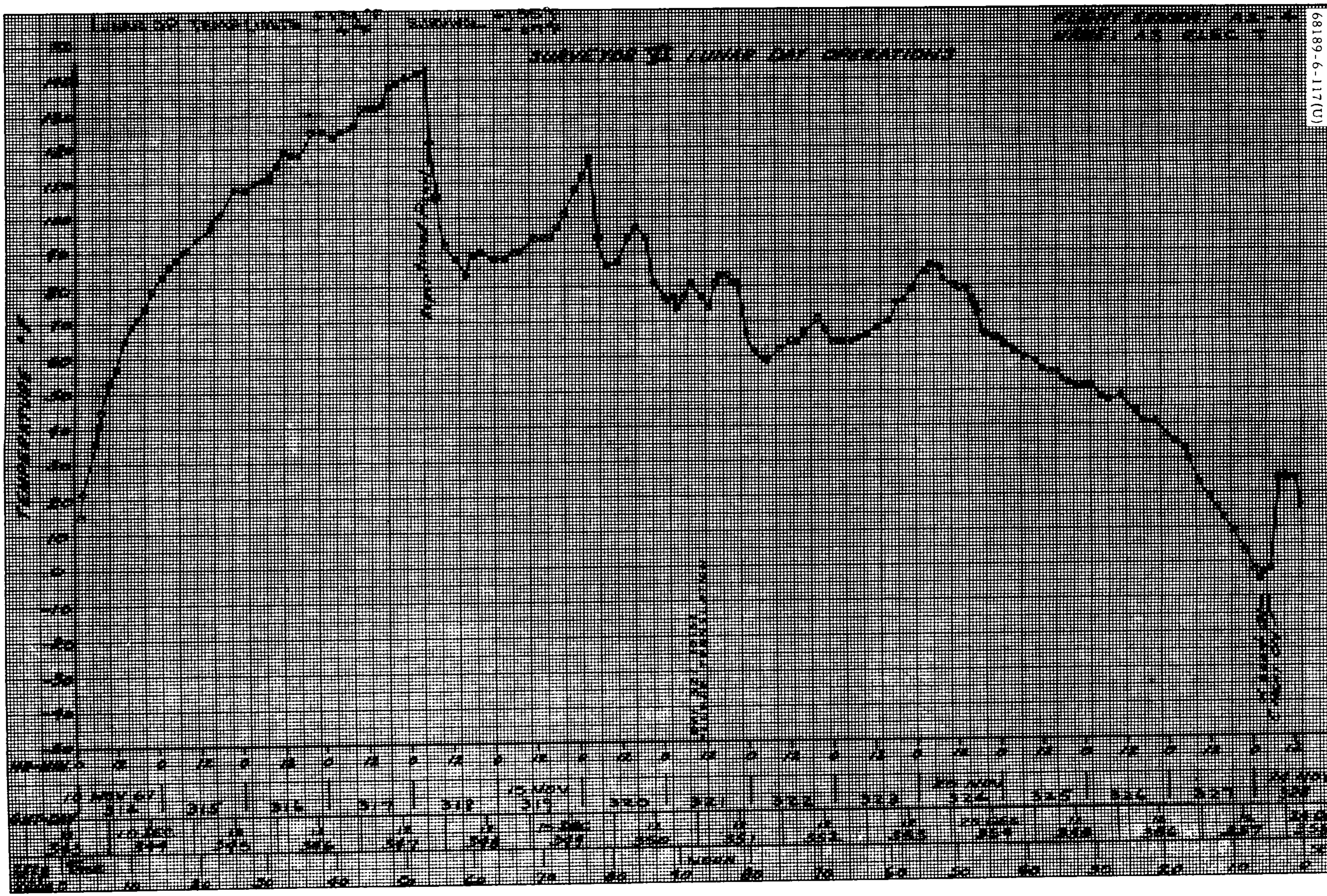

Figure 5. 1-B2. Sensor AS-4: Compartment C

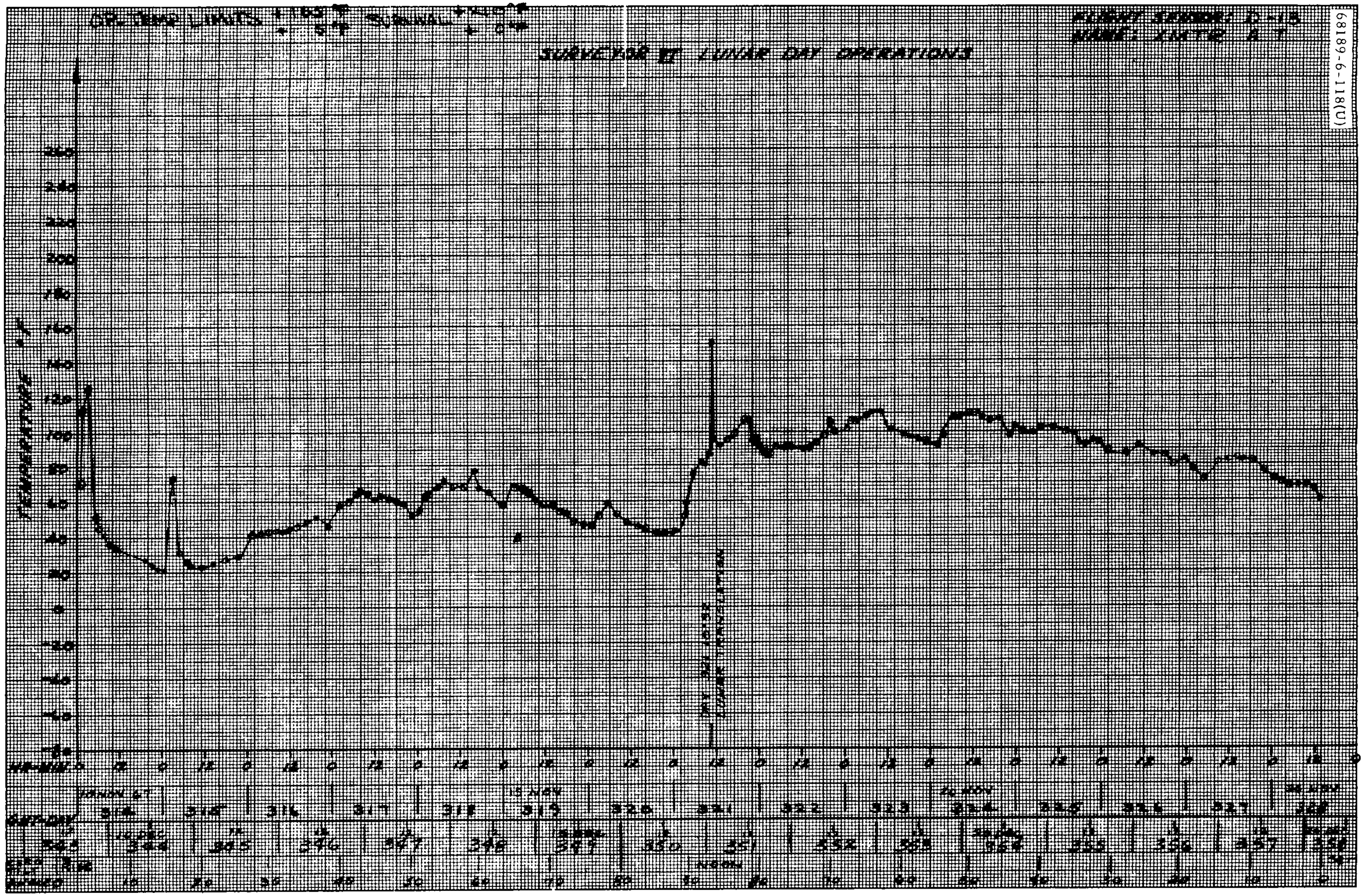

Figure 5.1-B3. Sensor D-13: Transmitter A

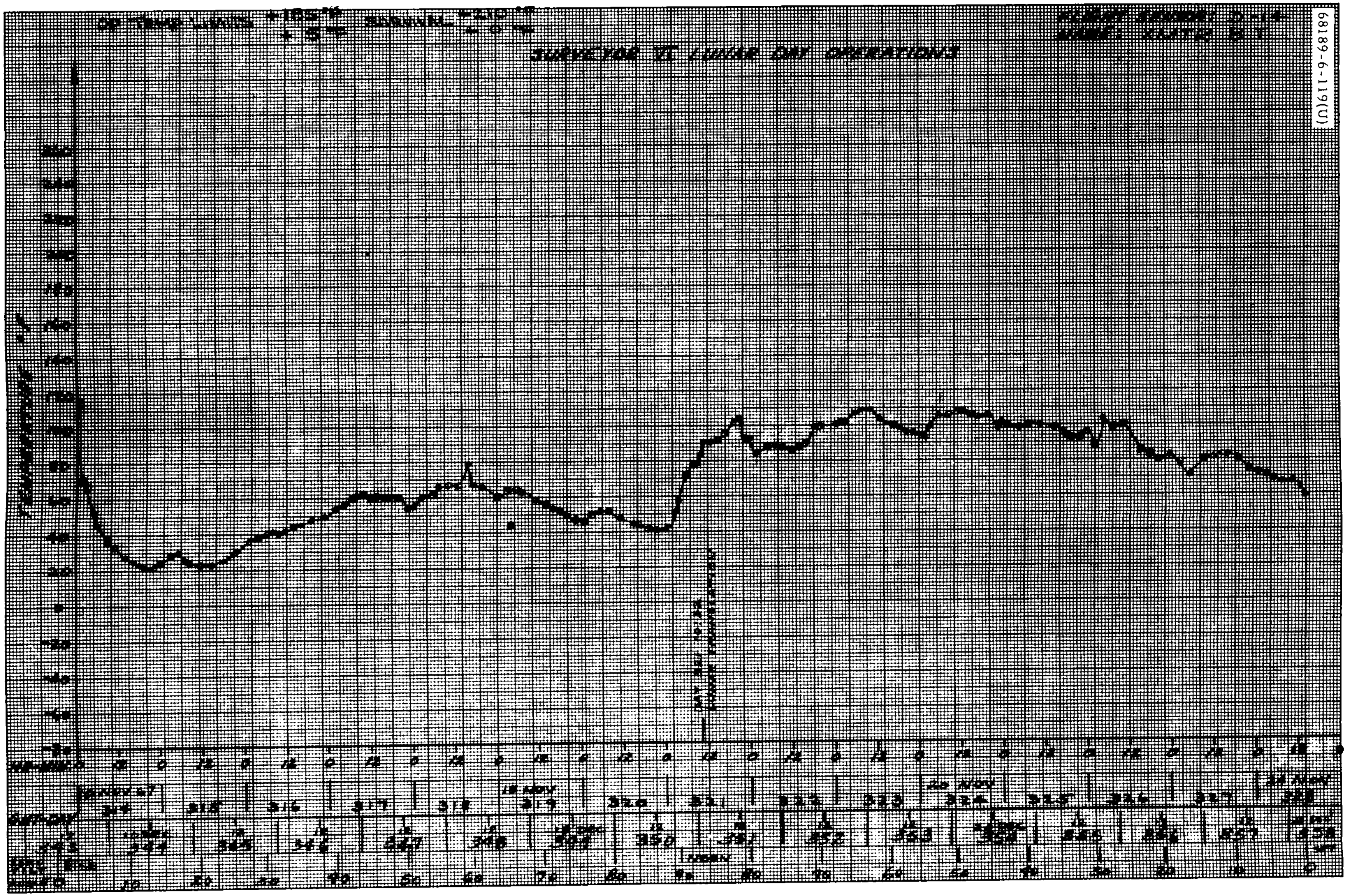

Figure 5.1-B4. Sensor D-14: Transmitter B

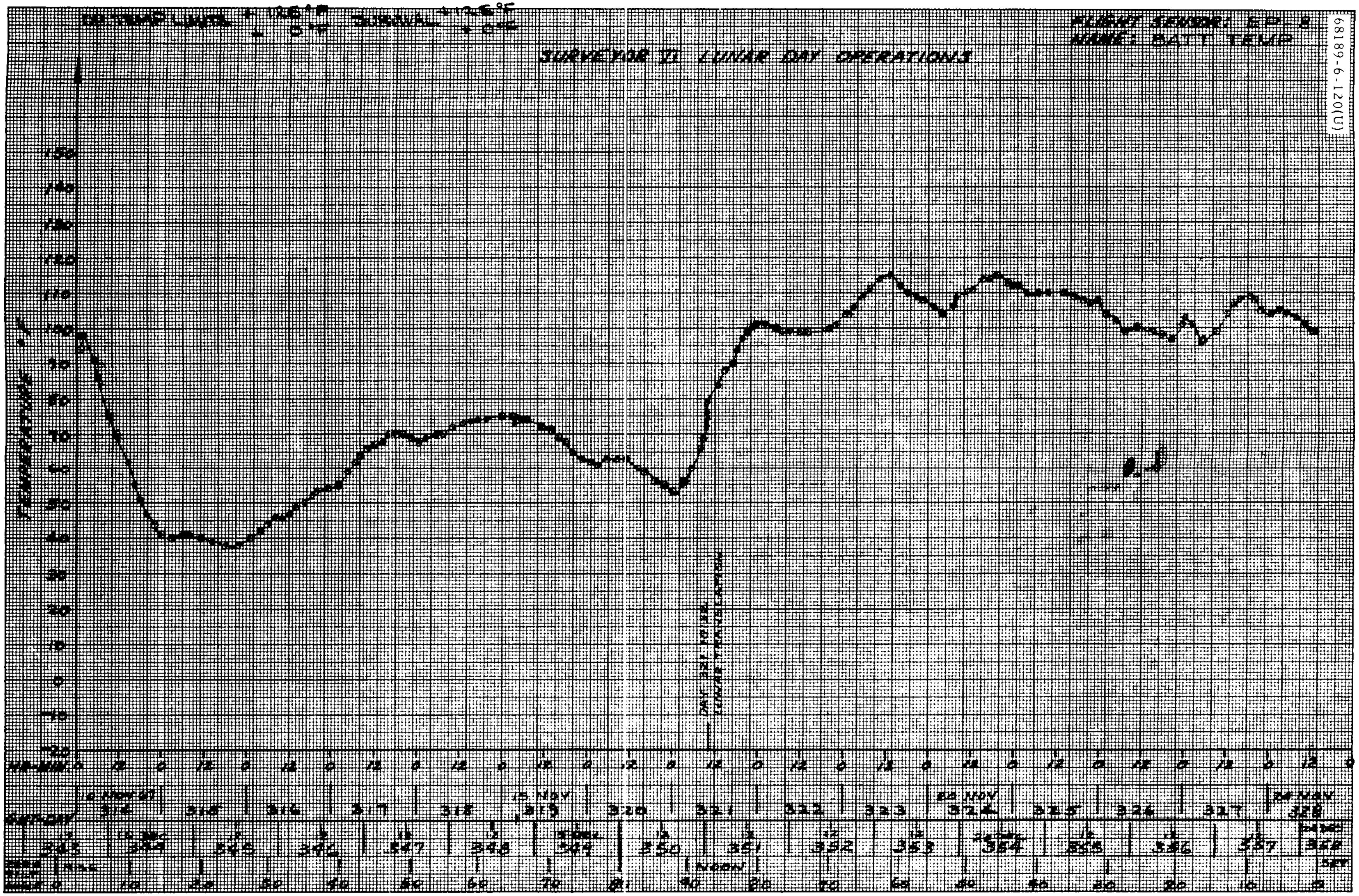

Figure 5.1-B5. Sensor EP-8: Main Battery

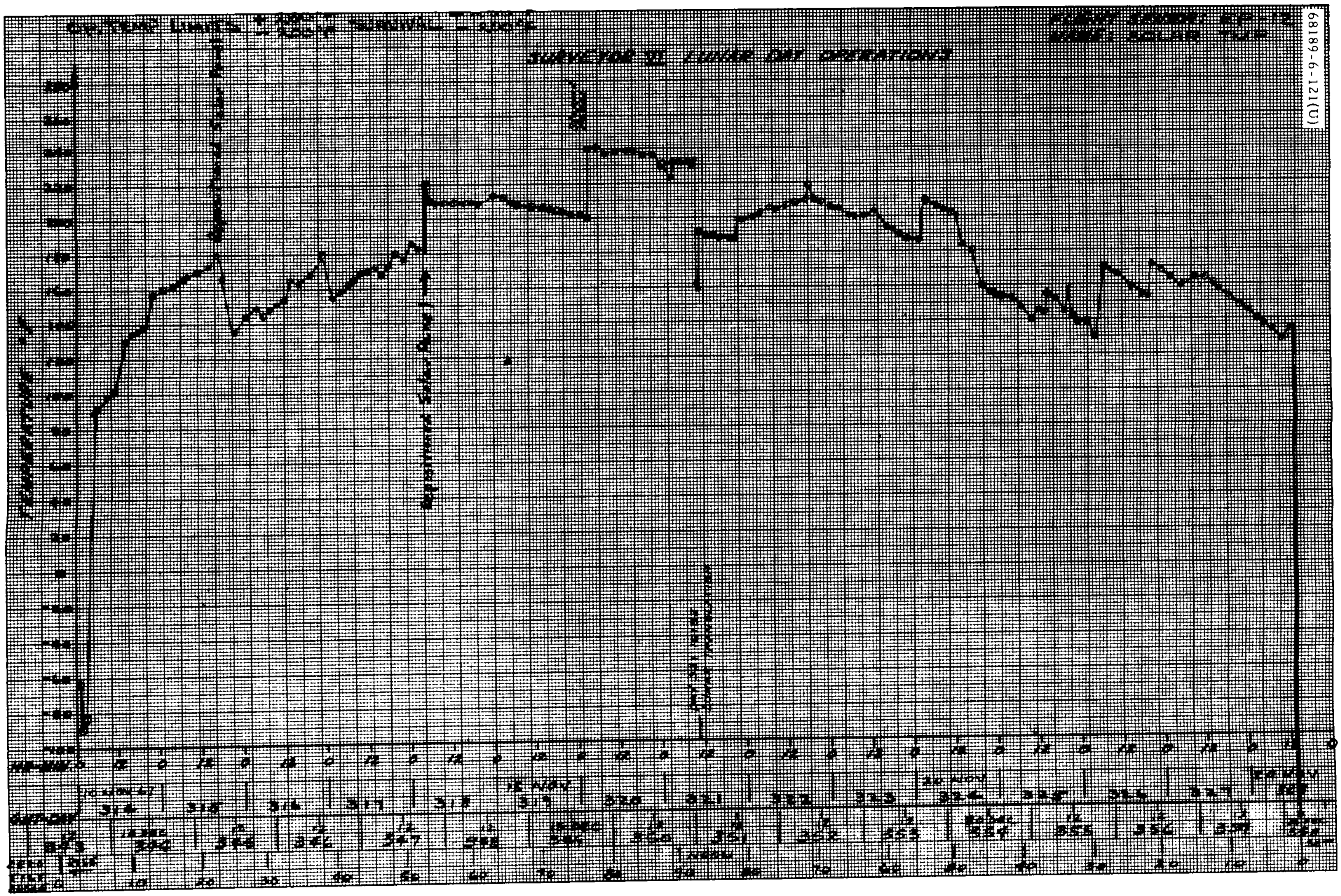

Figure 5.1-B6. Sensor EP-12: Solar Array

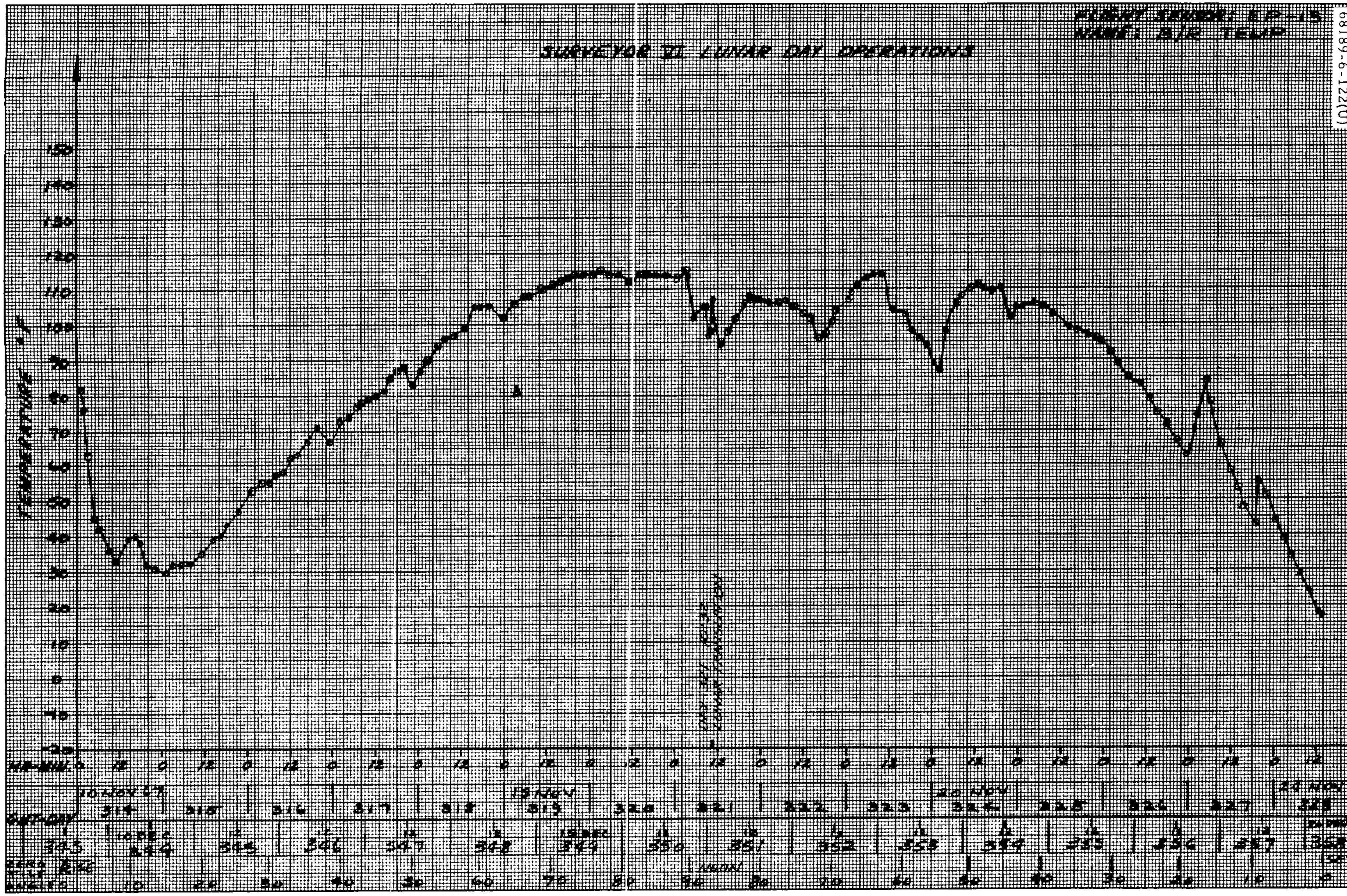

Figure 5.1-B7. Sensor EP-13: Boost Regulator

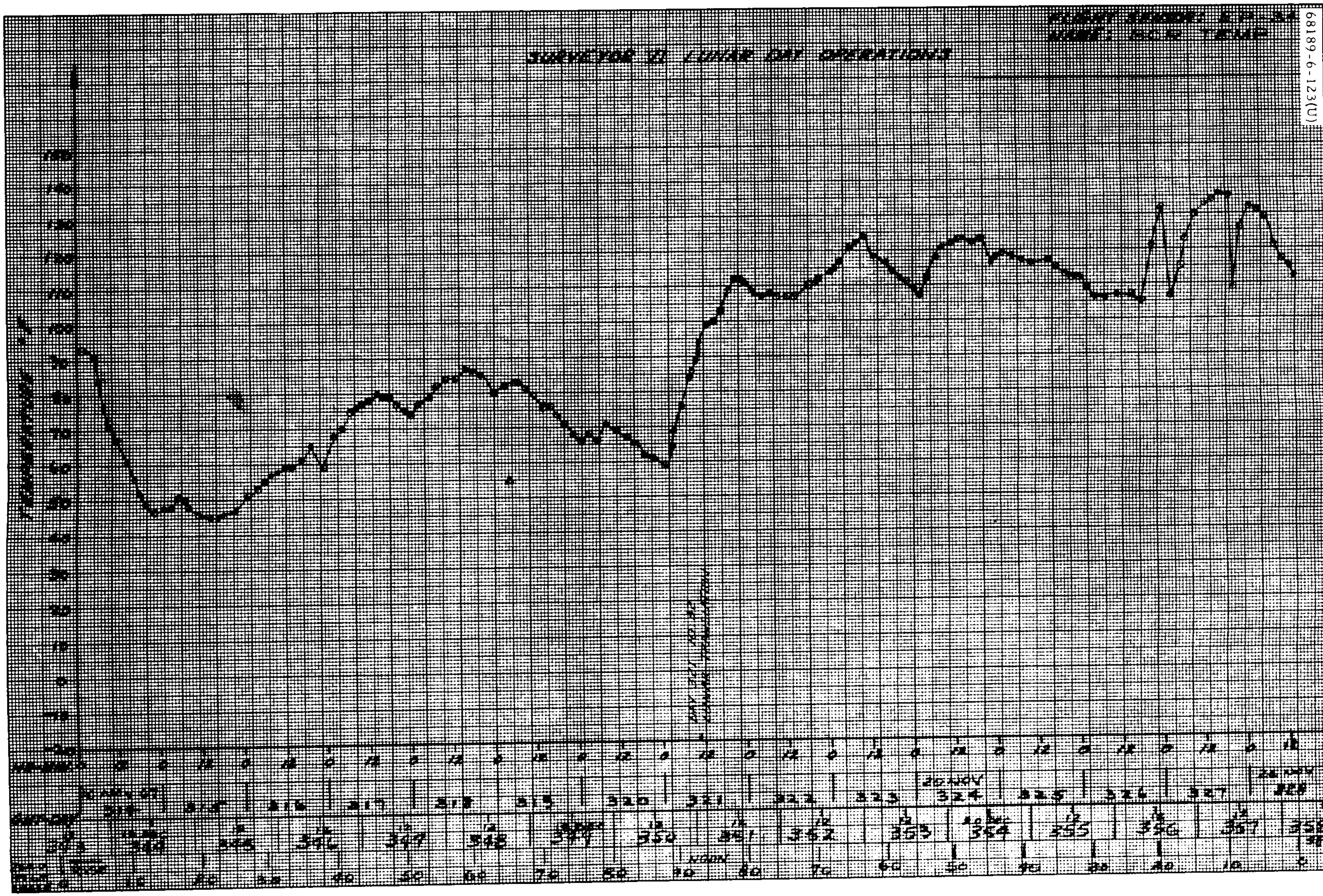

Figure 5.1-B8. Sensor EP-34: Battery Charge Regulator

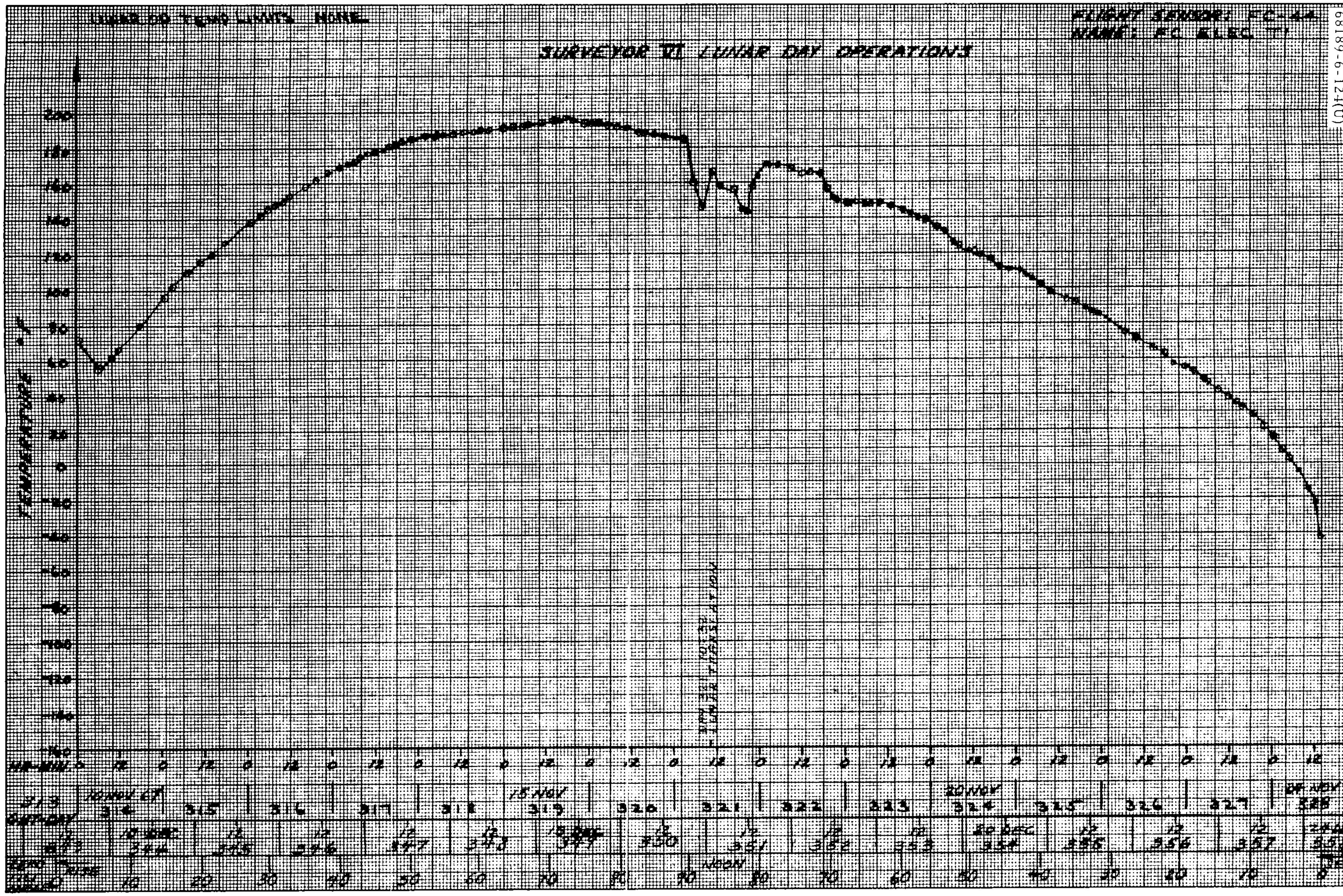

Figure 5.1-B9. Sensor FC-44: Flight Control Electronics (1)

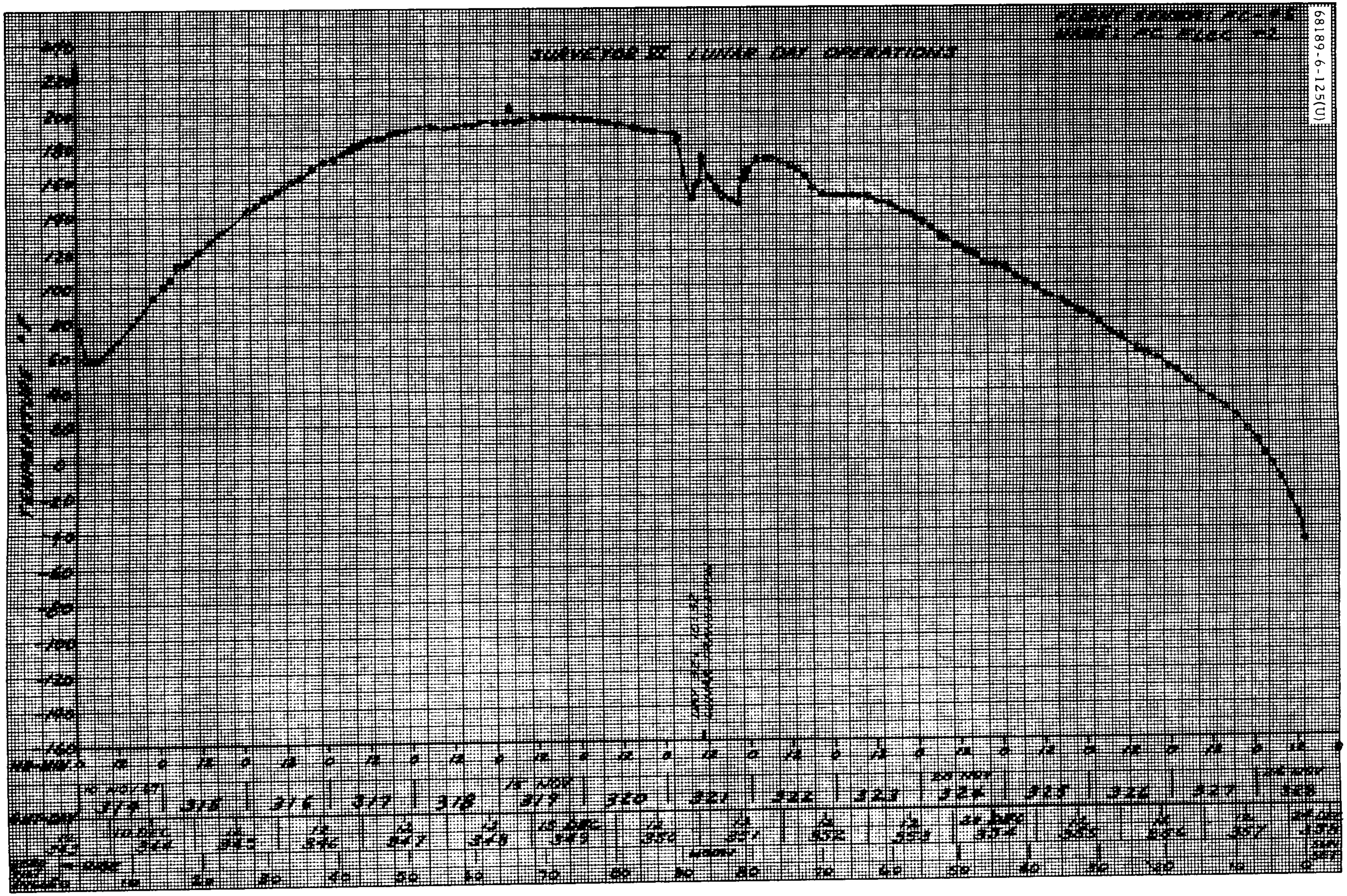

Figure 5. 1-B10. Sensor FC-45: Flight Control Electronics (2)

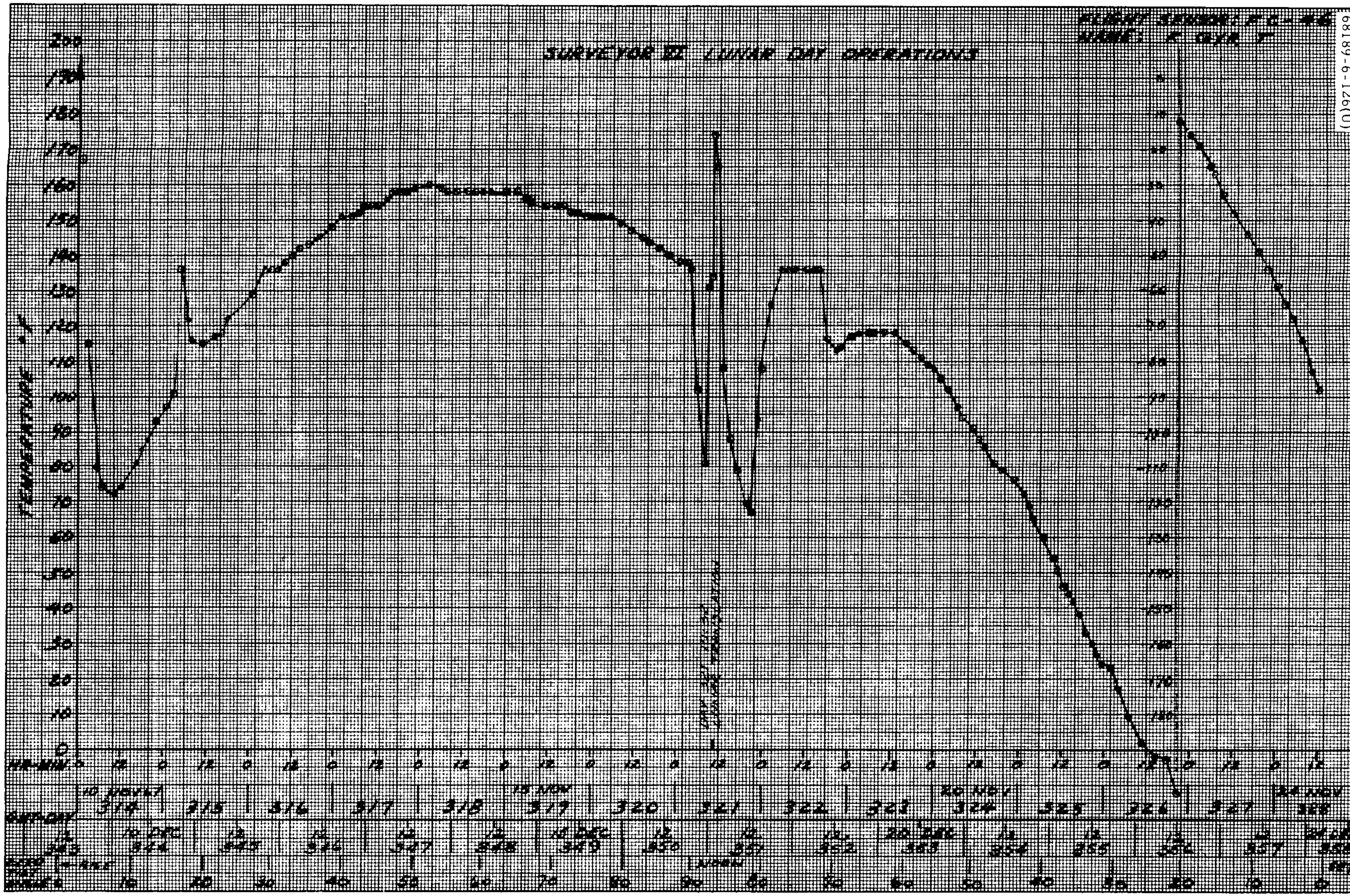

Figure 5.1-B11. Sensor FC-46: Roll Gyro

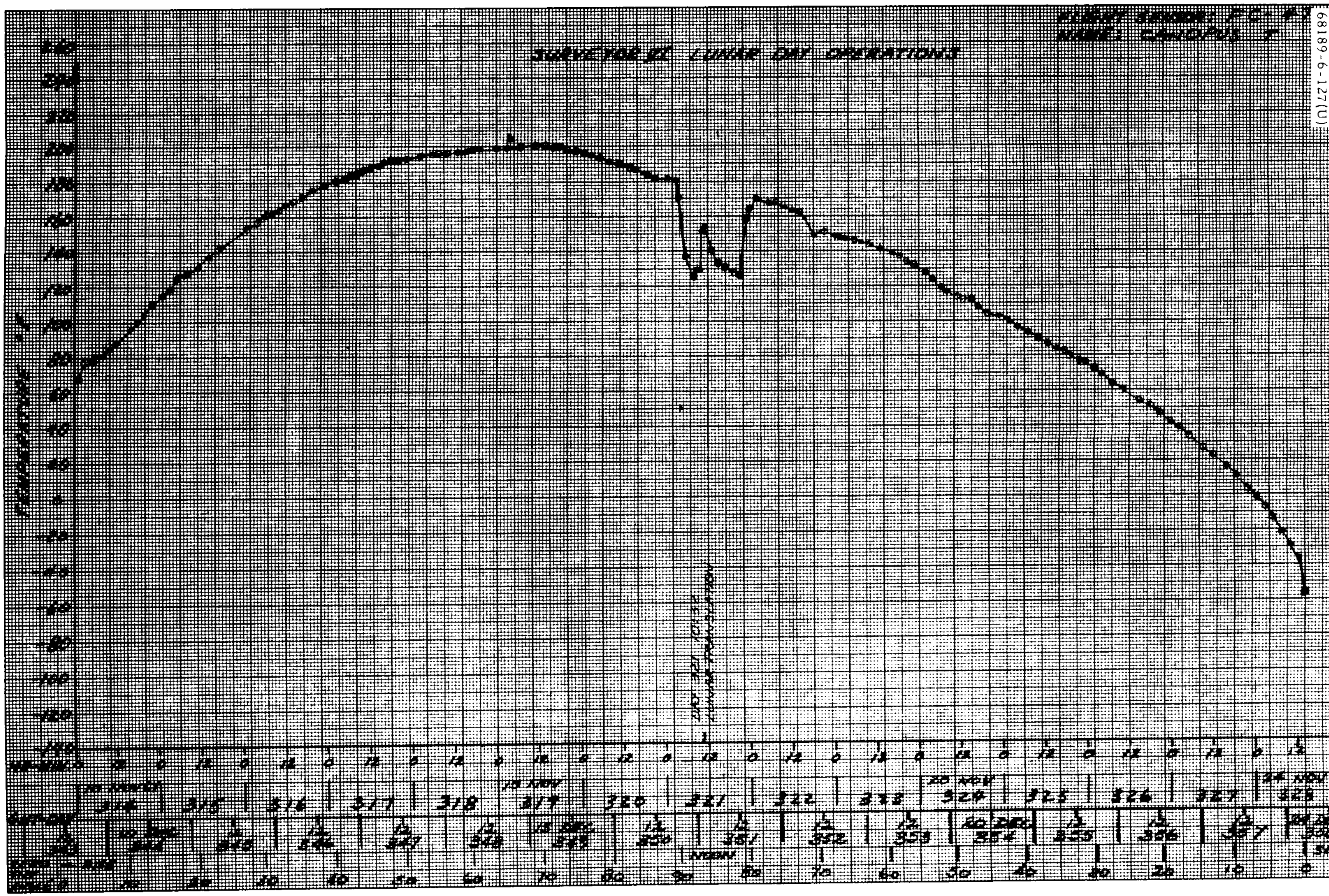

Figure 5.1-B12. Sensor FC-47: Canopus Sensor

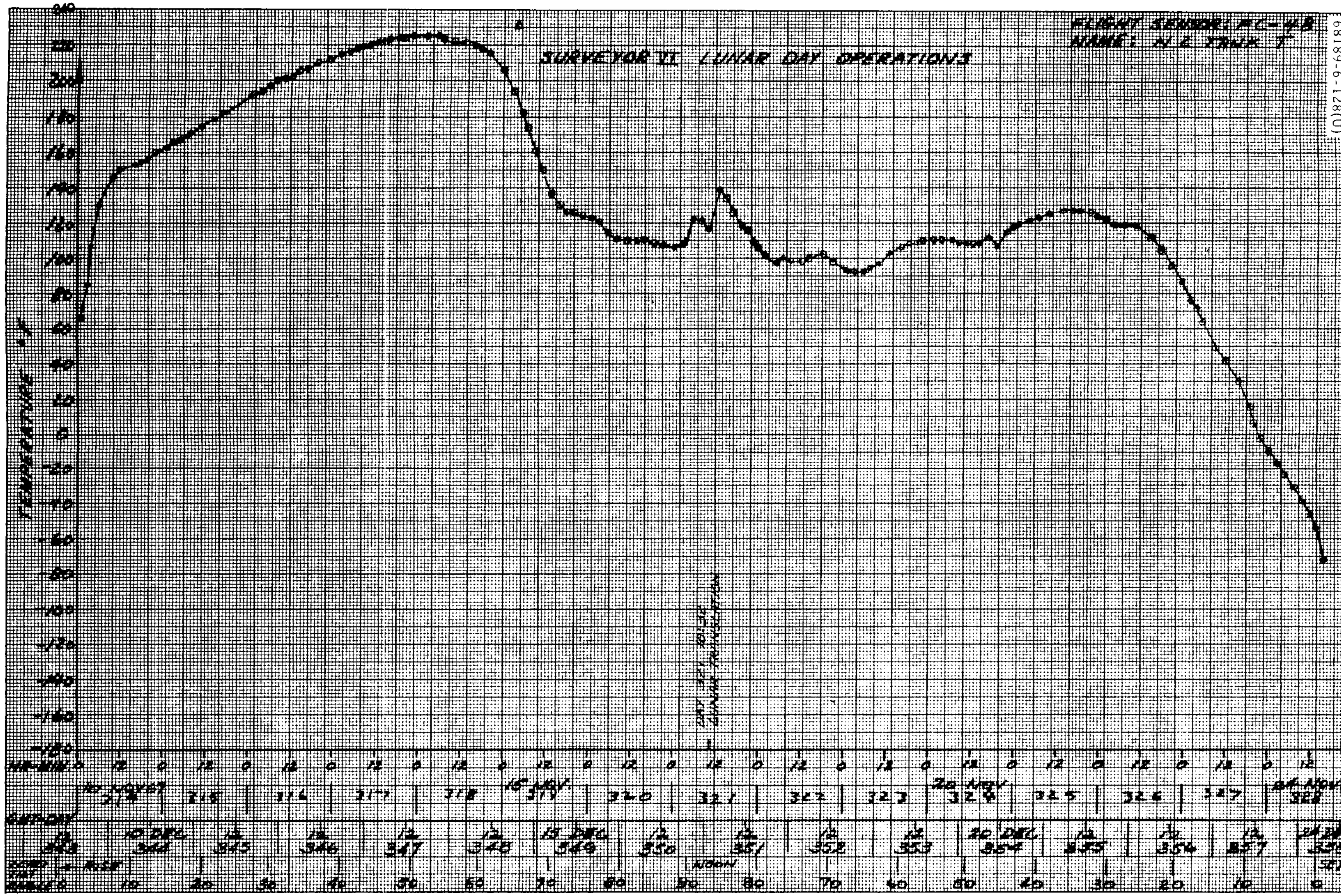

Figure 5.1-B13. Sensor FC-48: Nitrogen Gas Tank

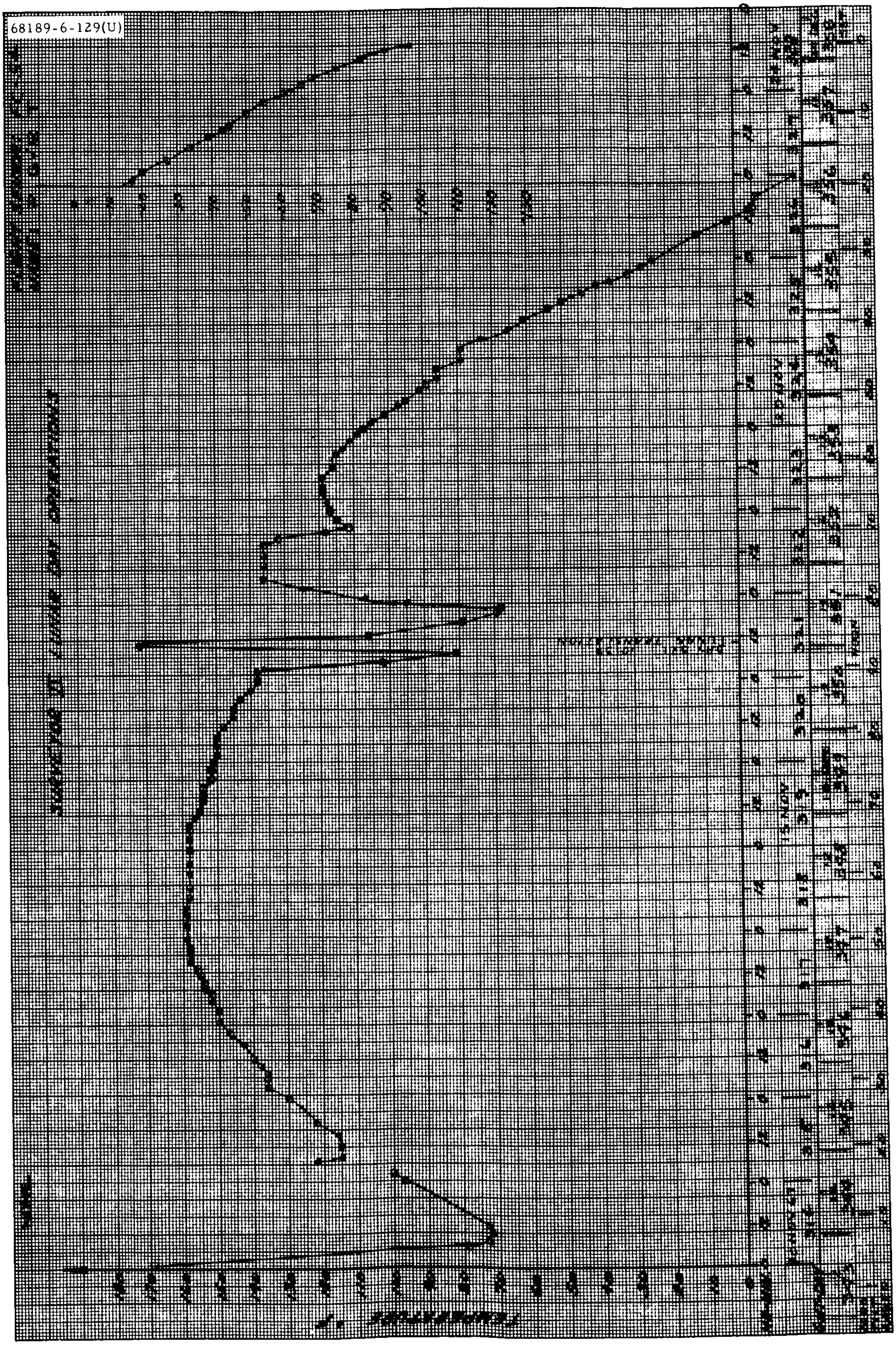

Figure 5.1-B14. Sensor FC-54: Pitch Gyro

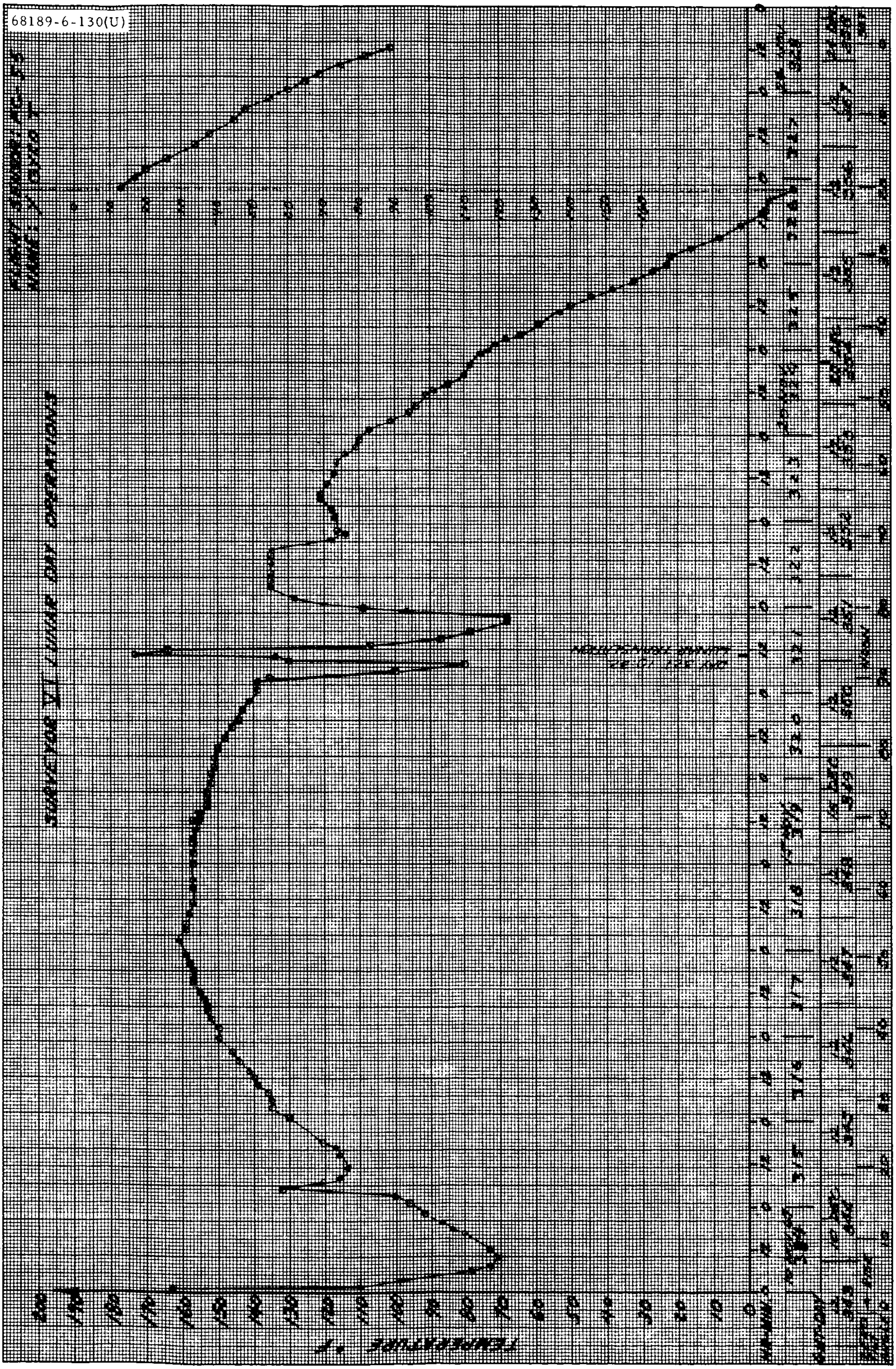

Figure 5.1-B15. Sensor FC-55: Yaw Gyro

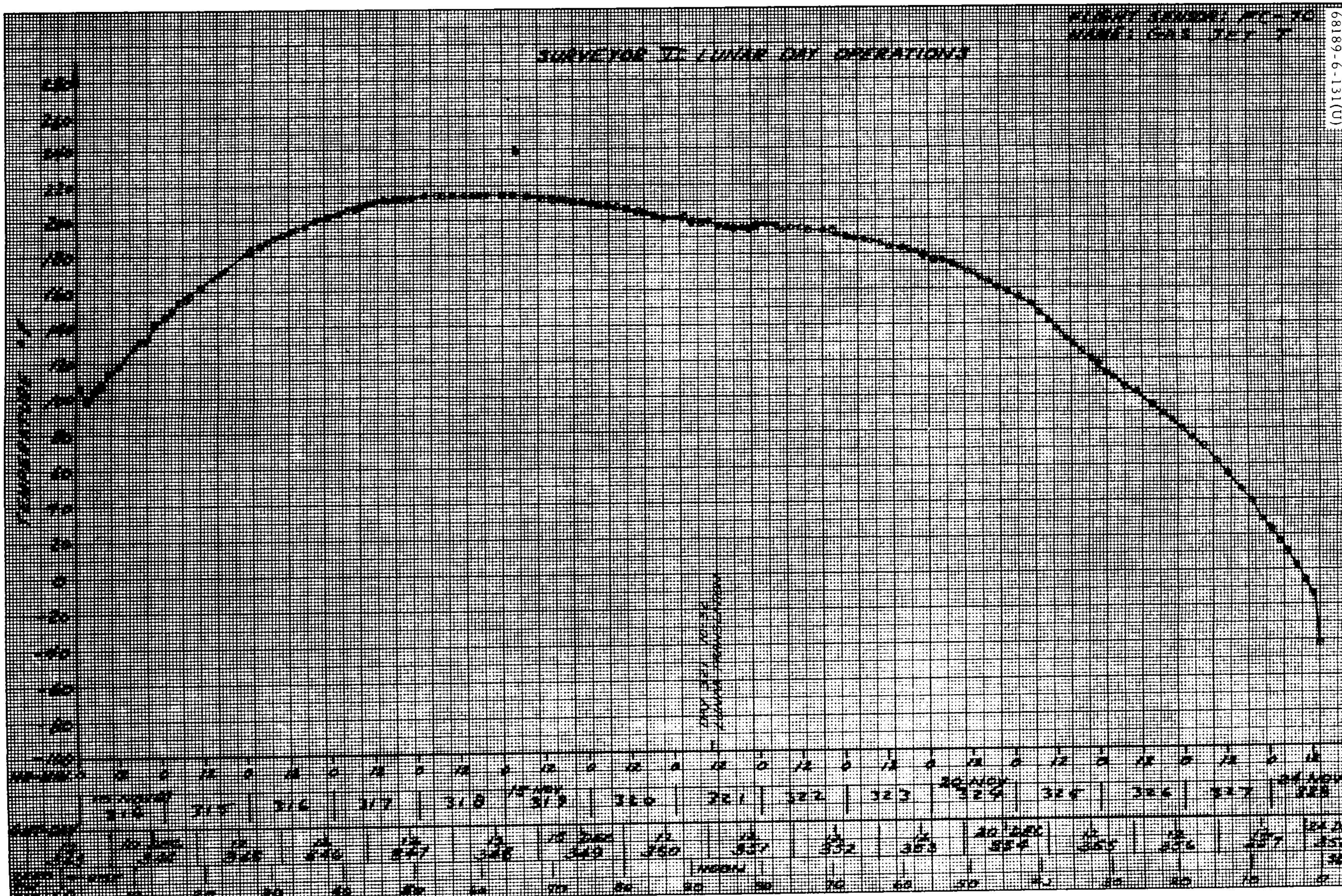

Figure 5.1-B16. Sensor FC-70: Attitude Gas Jet 2

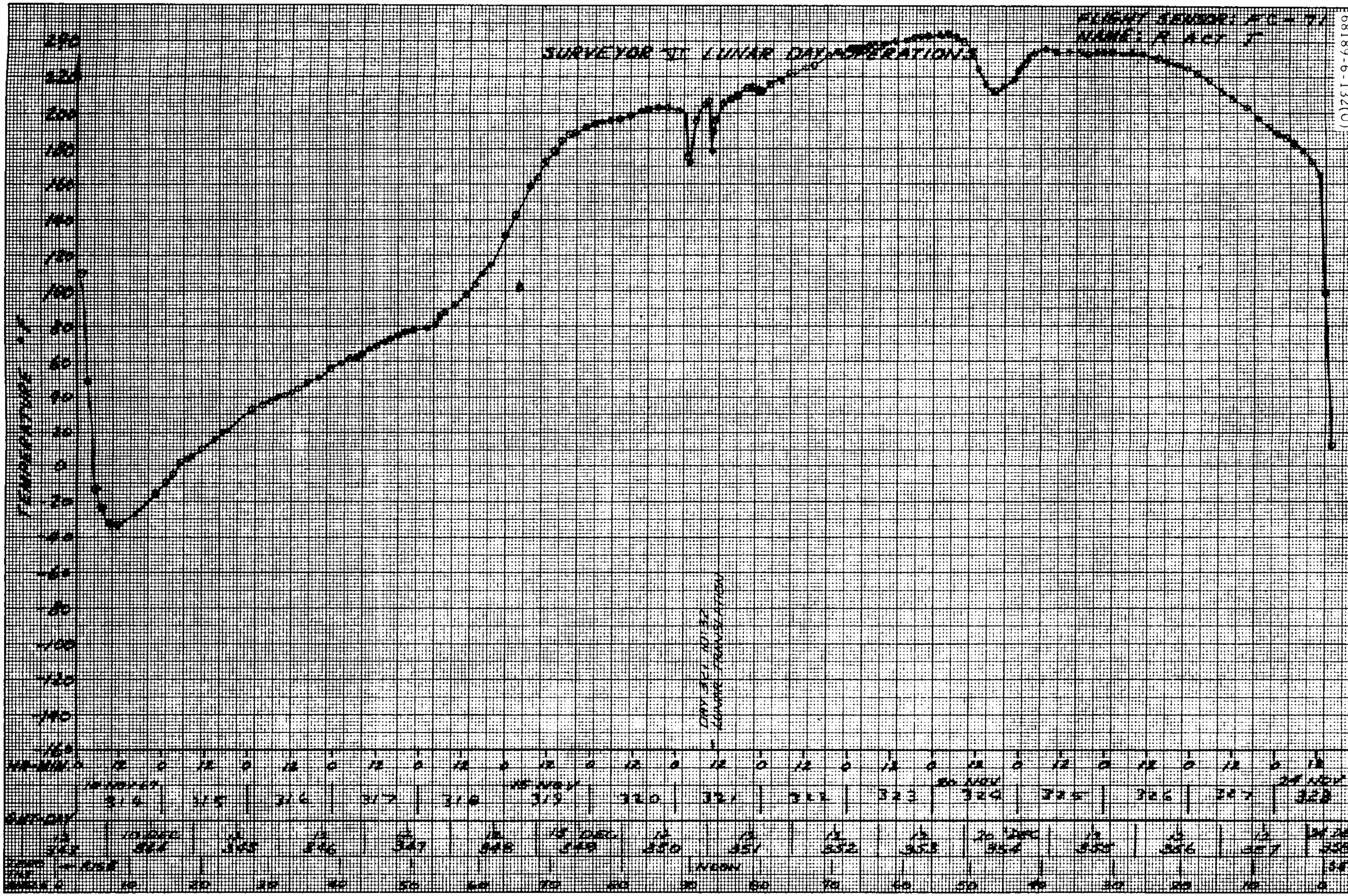

Figure 5.1-B17. Sensor FC-71: Roll Actuator

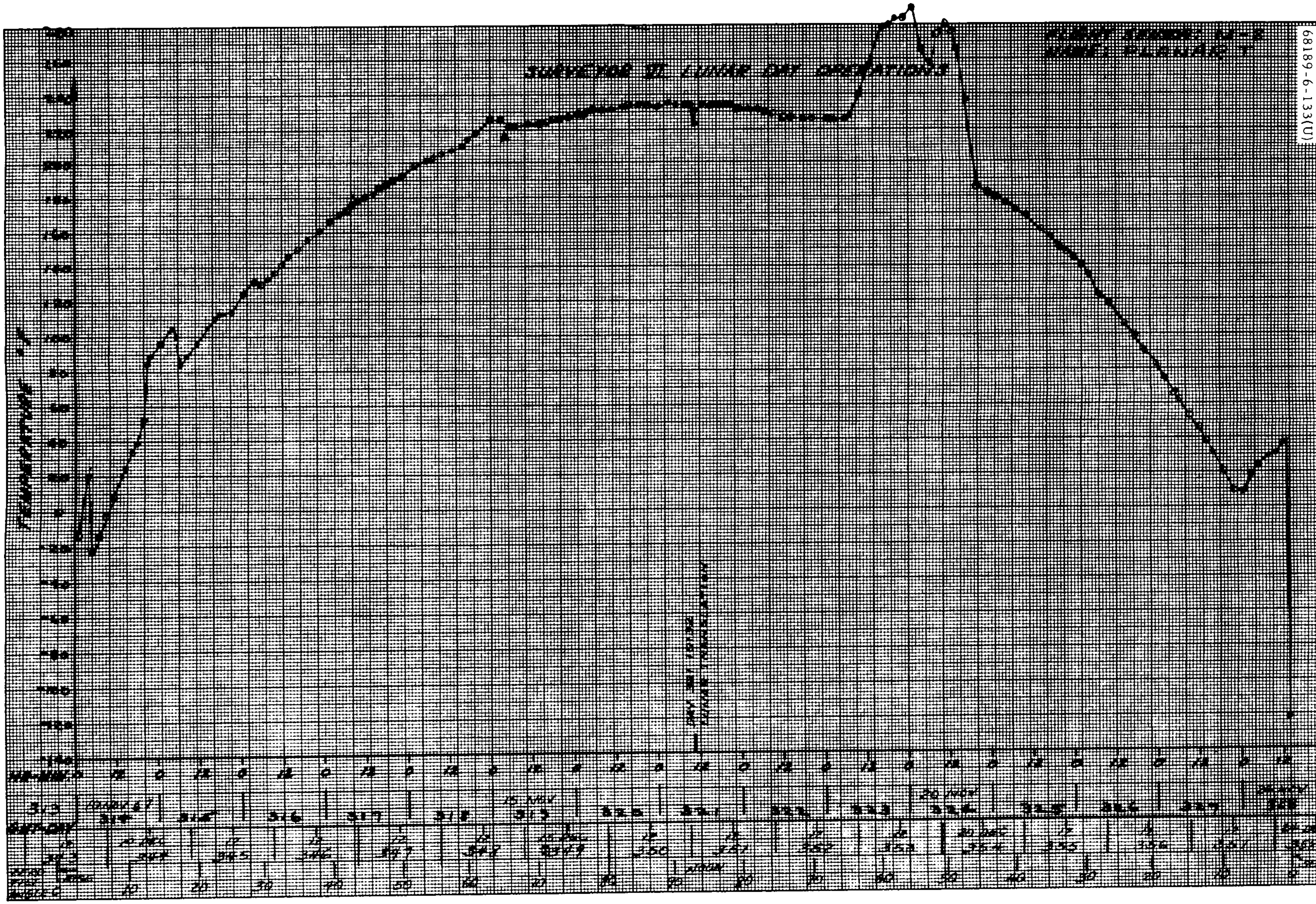

Figure 5.1-B18. Sensor M-8: Planar Array

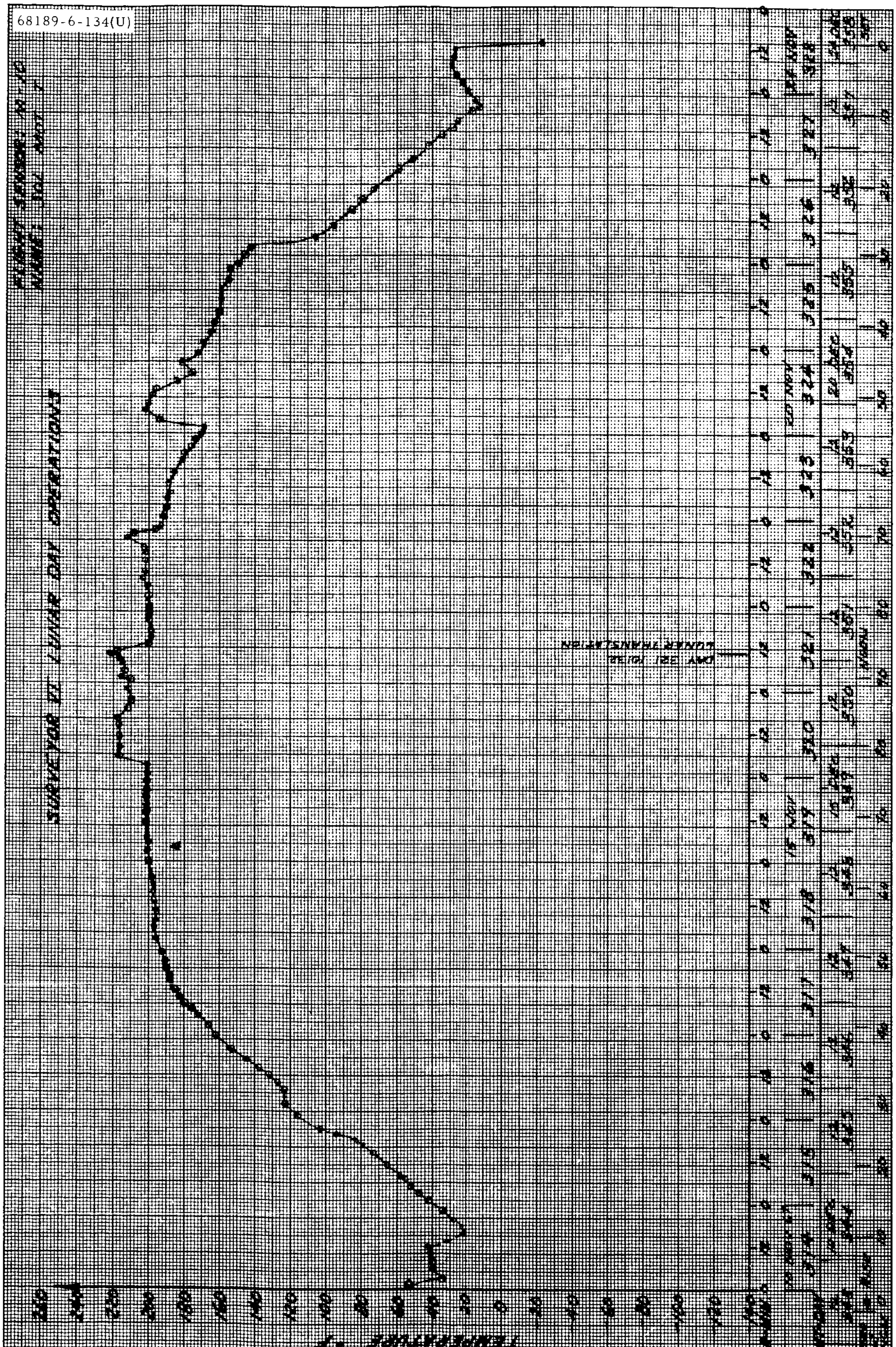

Figure 5.1-B19. Sensor M-10: Solar Panel Stepping Motor

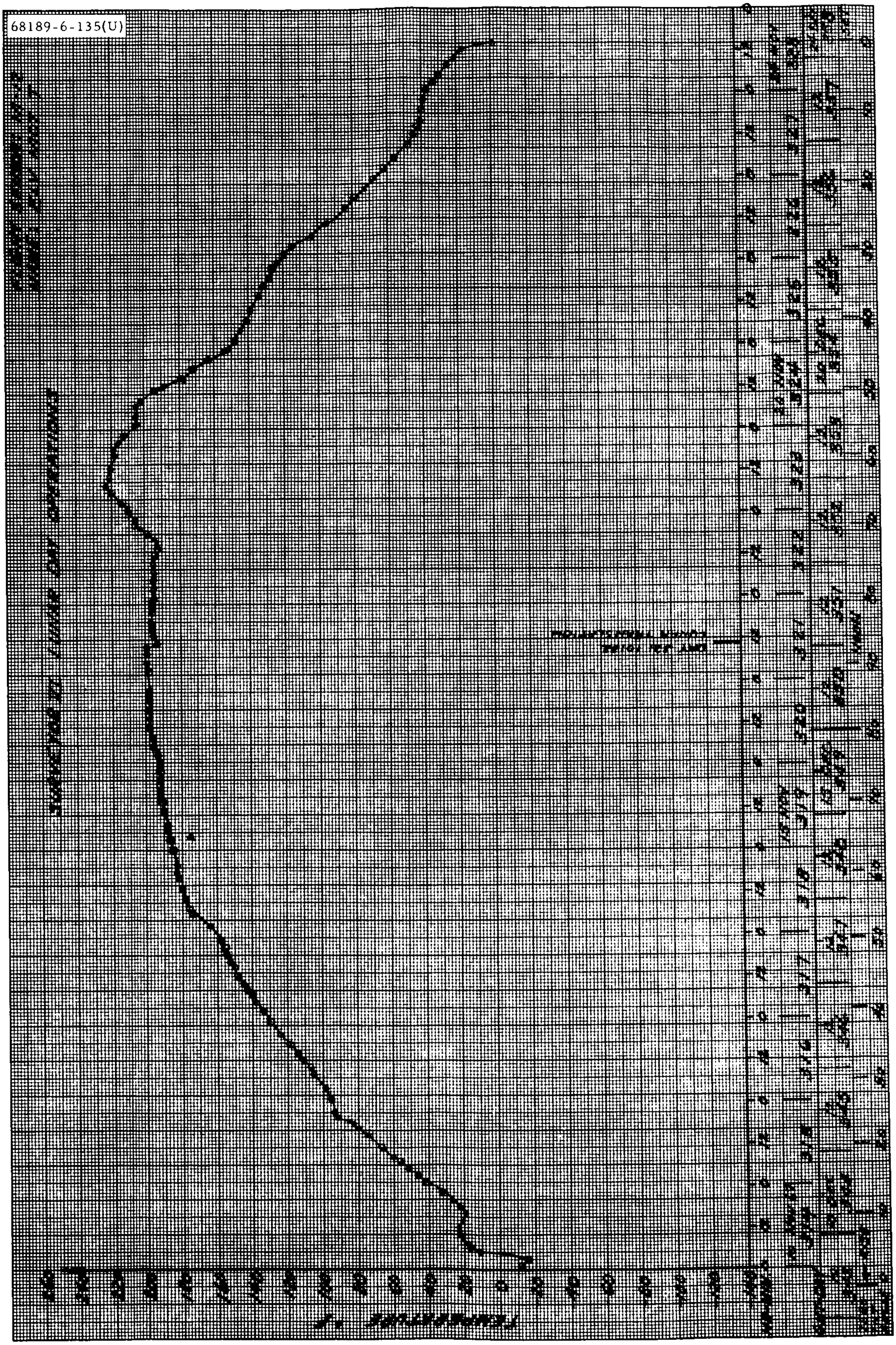

Figure 5. 1-B20. Sensor M-12: Elevation Axis Stepping Motor

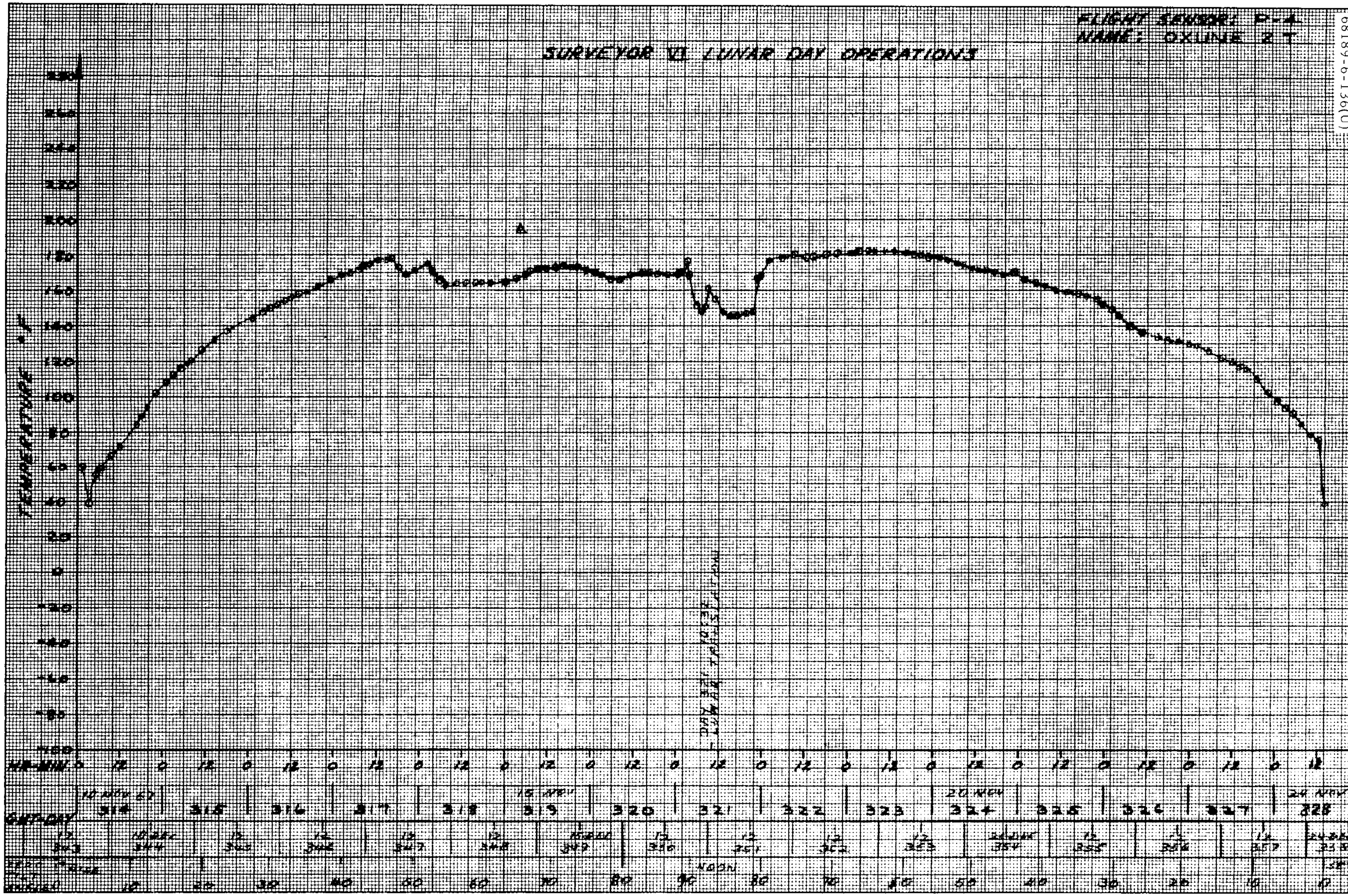

Figure 5.1-B21. Sensor P-4: Vernier Lines 2

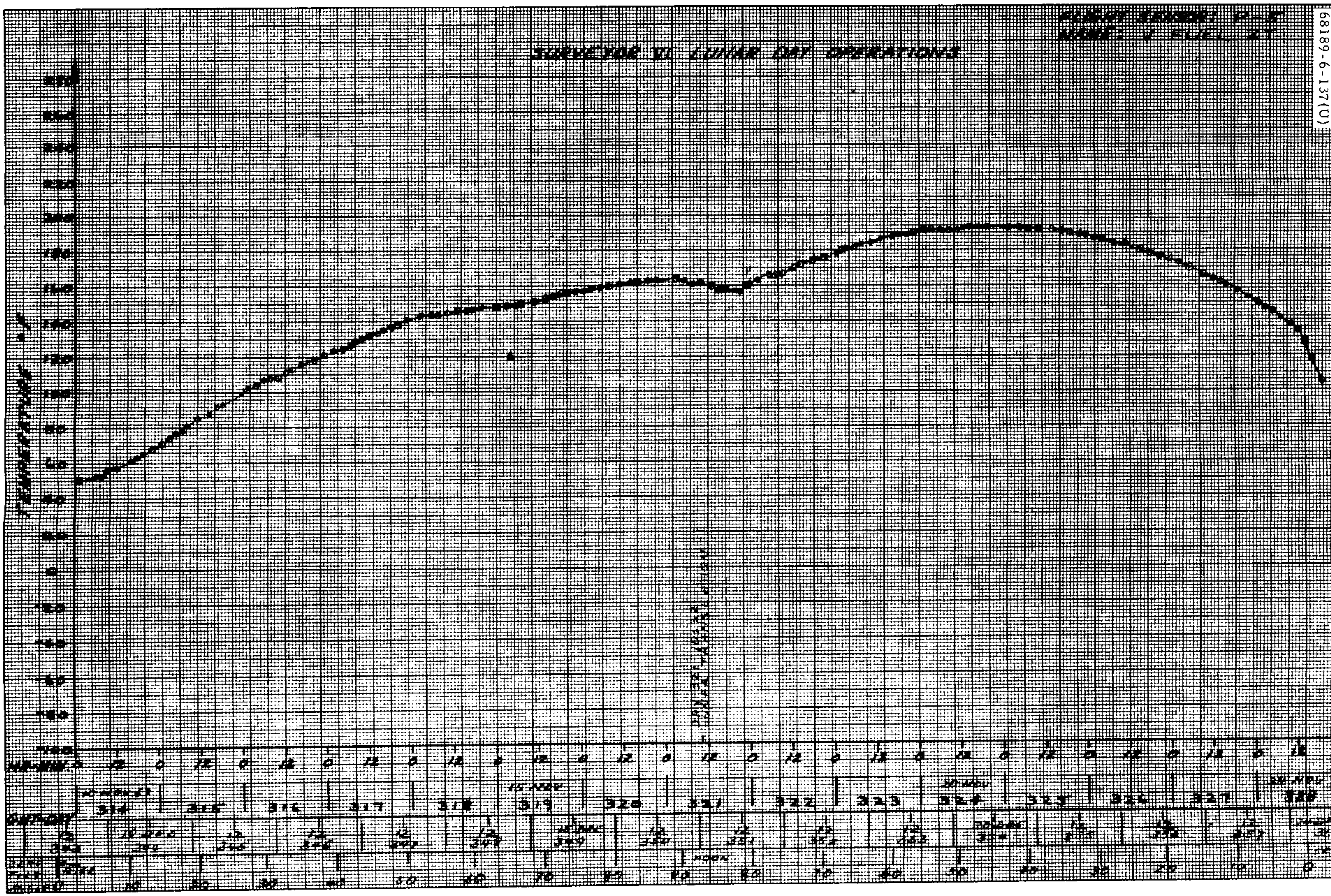

Figure 5.1-B22. Sensor P-5: Vernier Fuel Tank 2

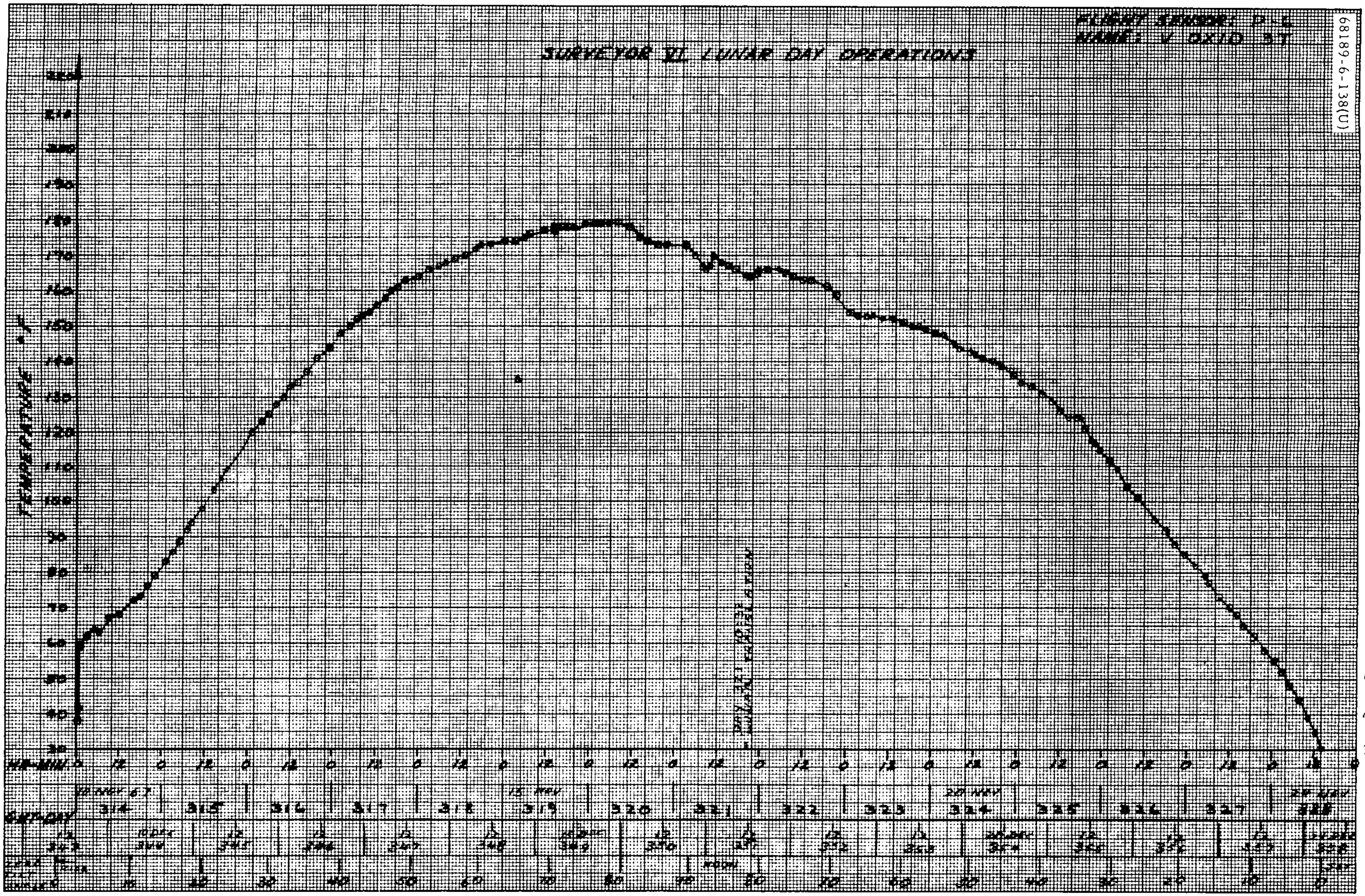

Figure 5.1-B23. Sensor P-6: Vernier Oxidizer Tank 3

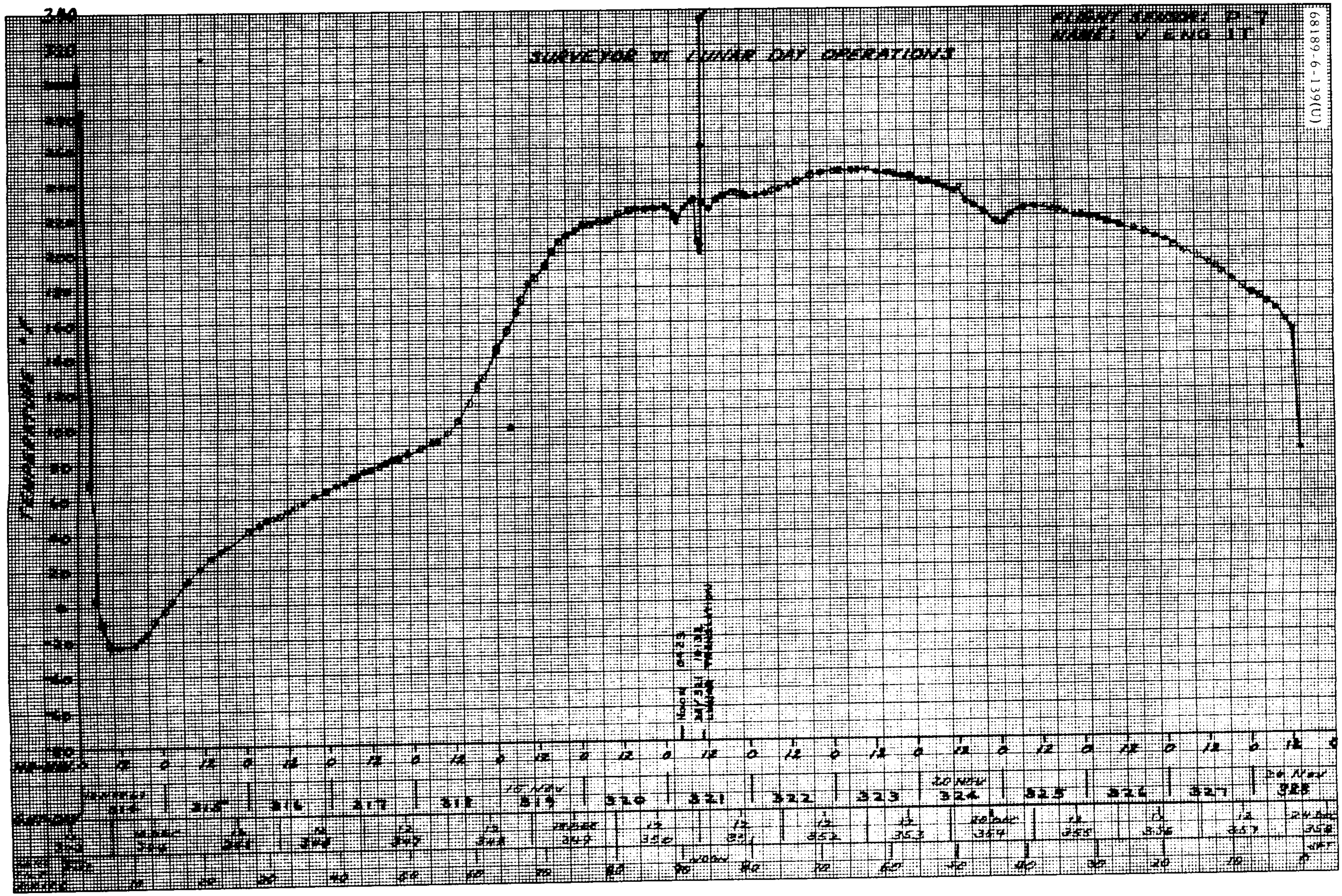

Figure 5.1-B24. Sensor P-7: Vernier Engine 1

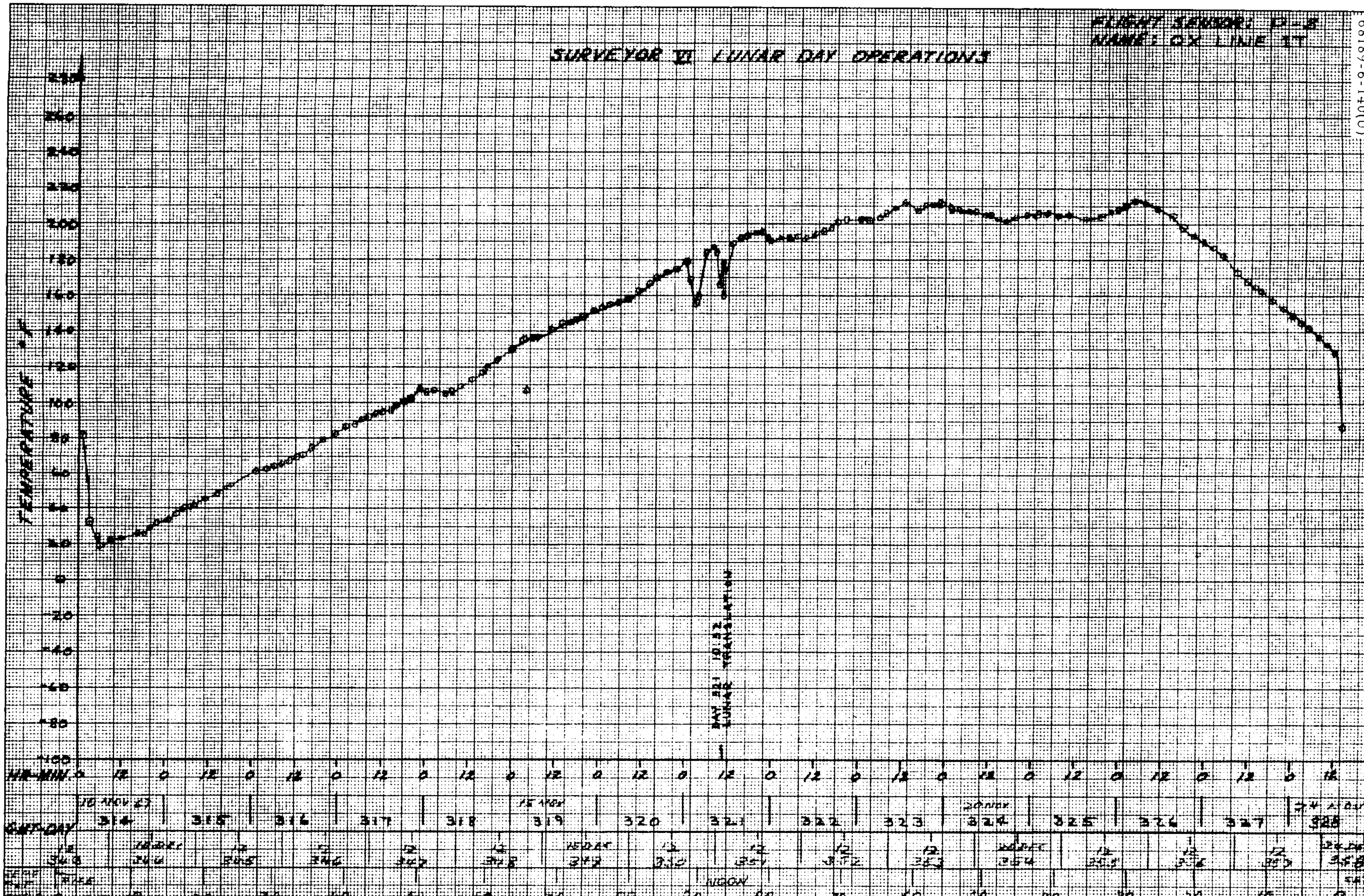

Figure 5.1-B25. Sensor P-8: Vernier Lines 1

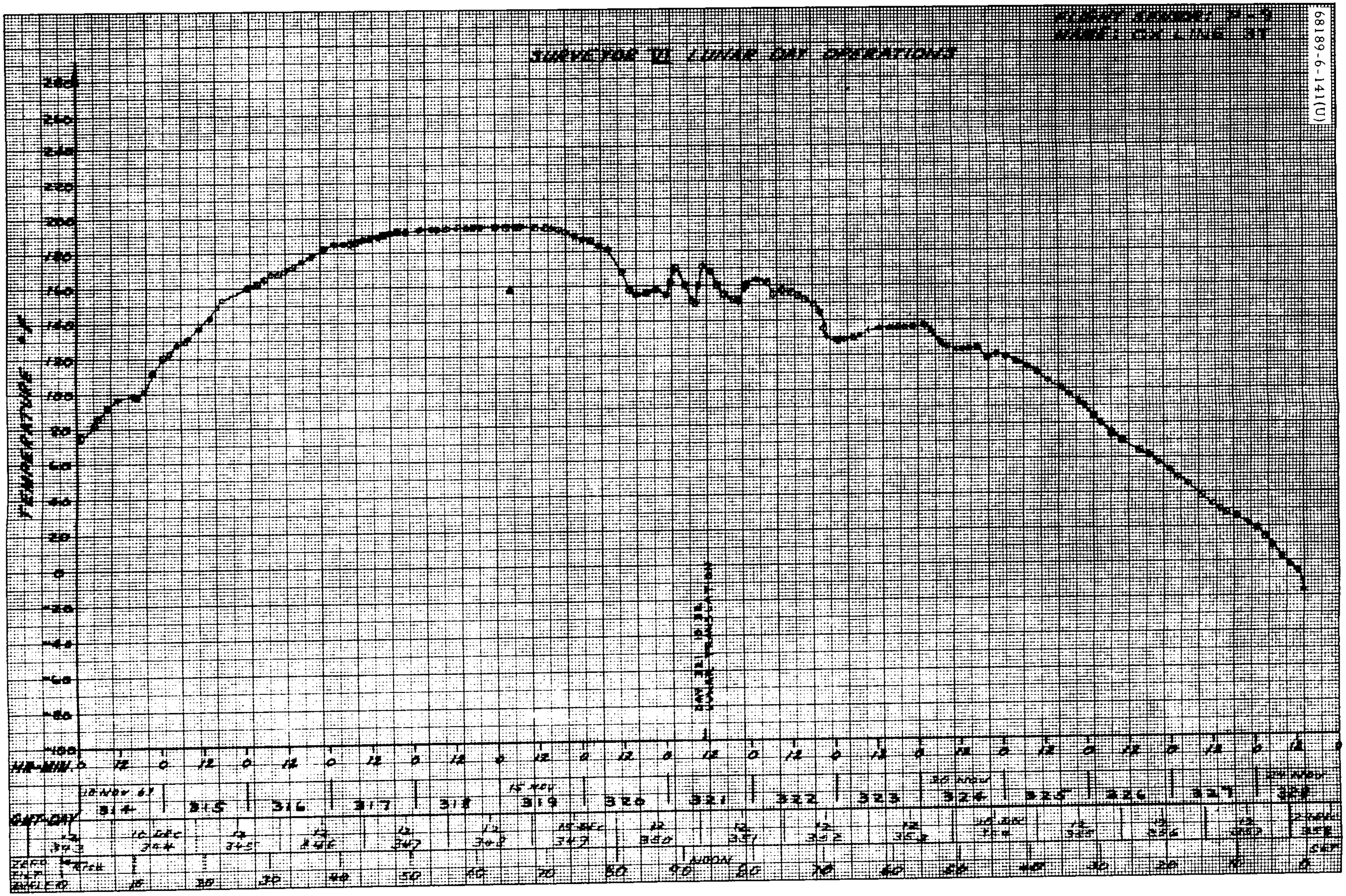

Figure 5.1-B26. Sensor P-9: Vernier Lines 3

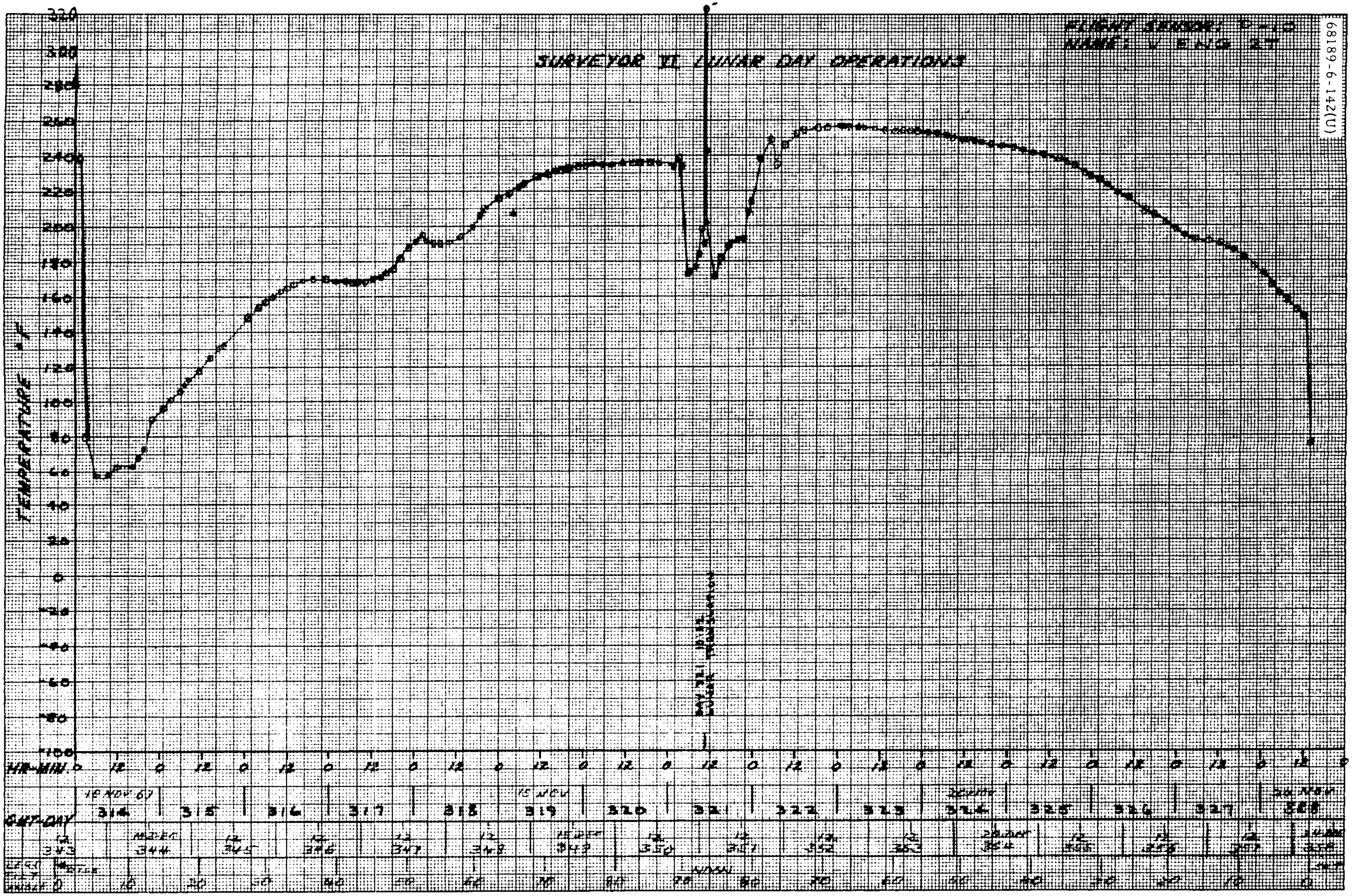

Figure 5.1-B27. Sensor P-10: Vernier Engine 2

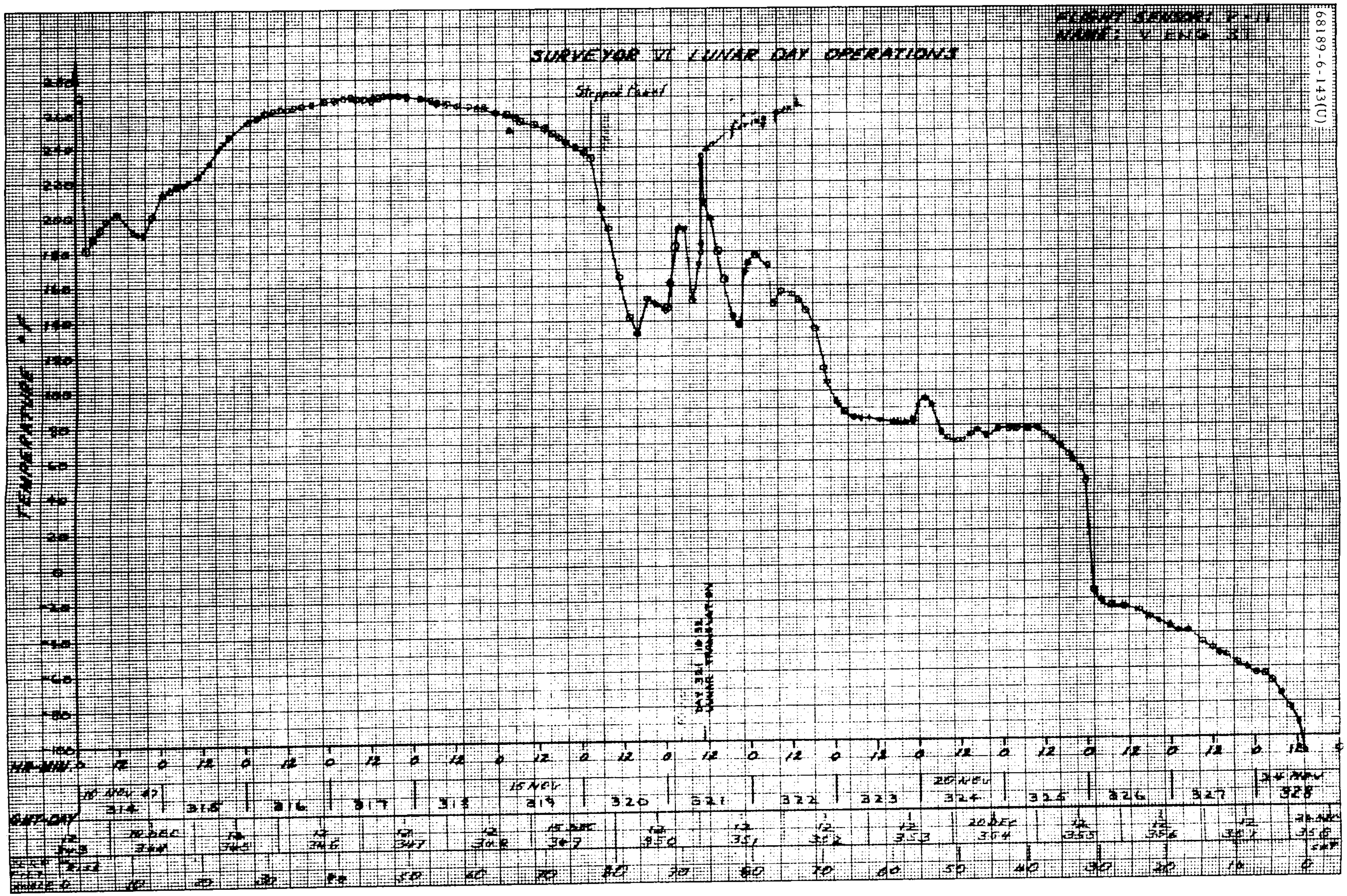

Figure 5.1-B28. Sensor P-11: Vernier Engine 3

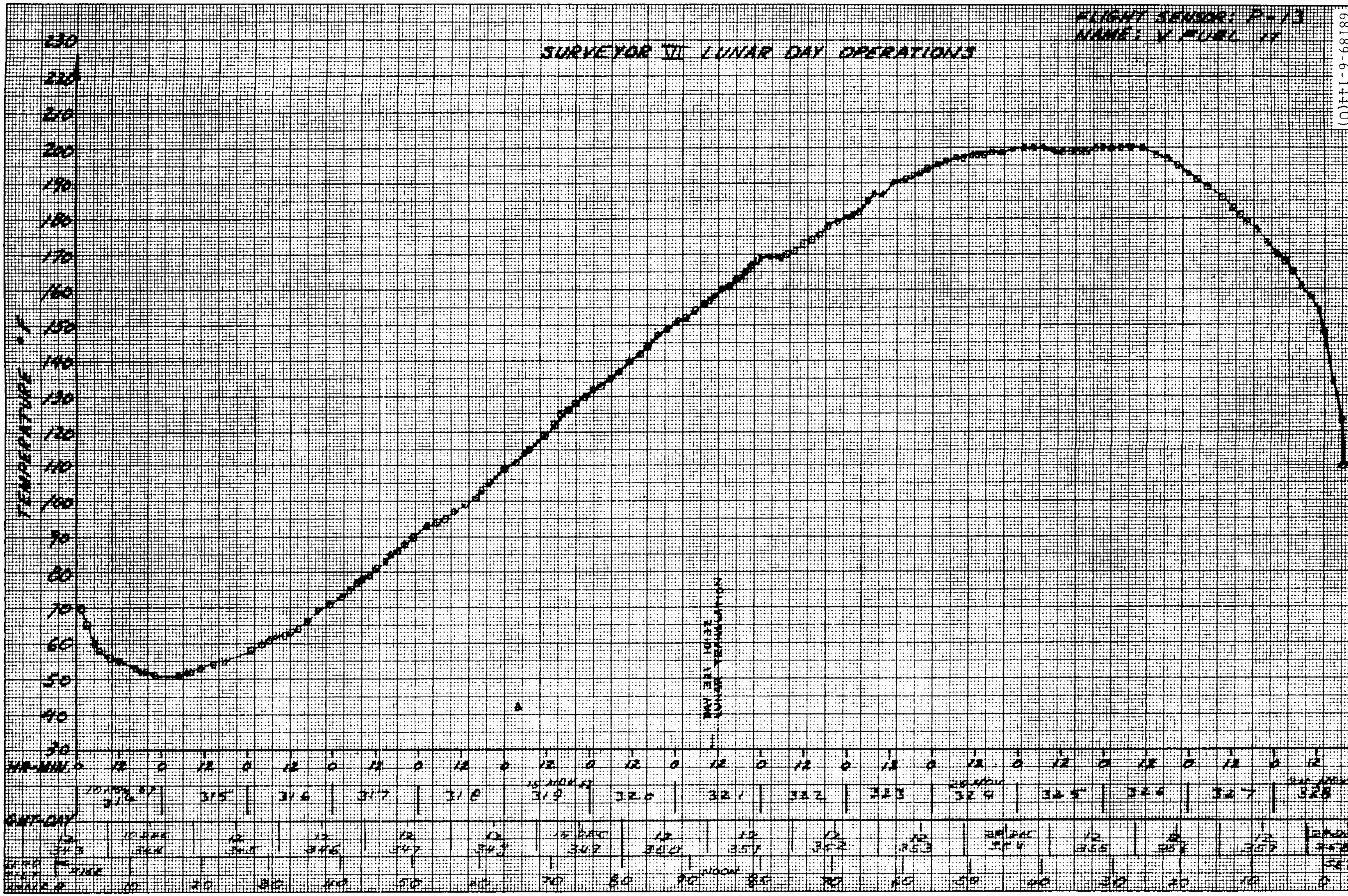

Figure 5.1-B29. Sensor P-13: Vernier Fuel Tank 1

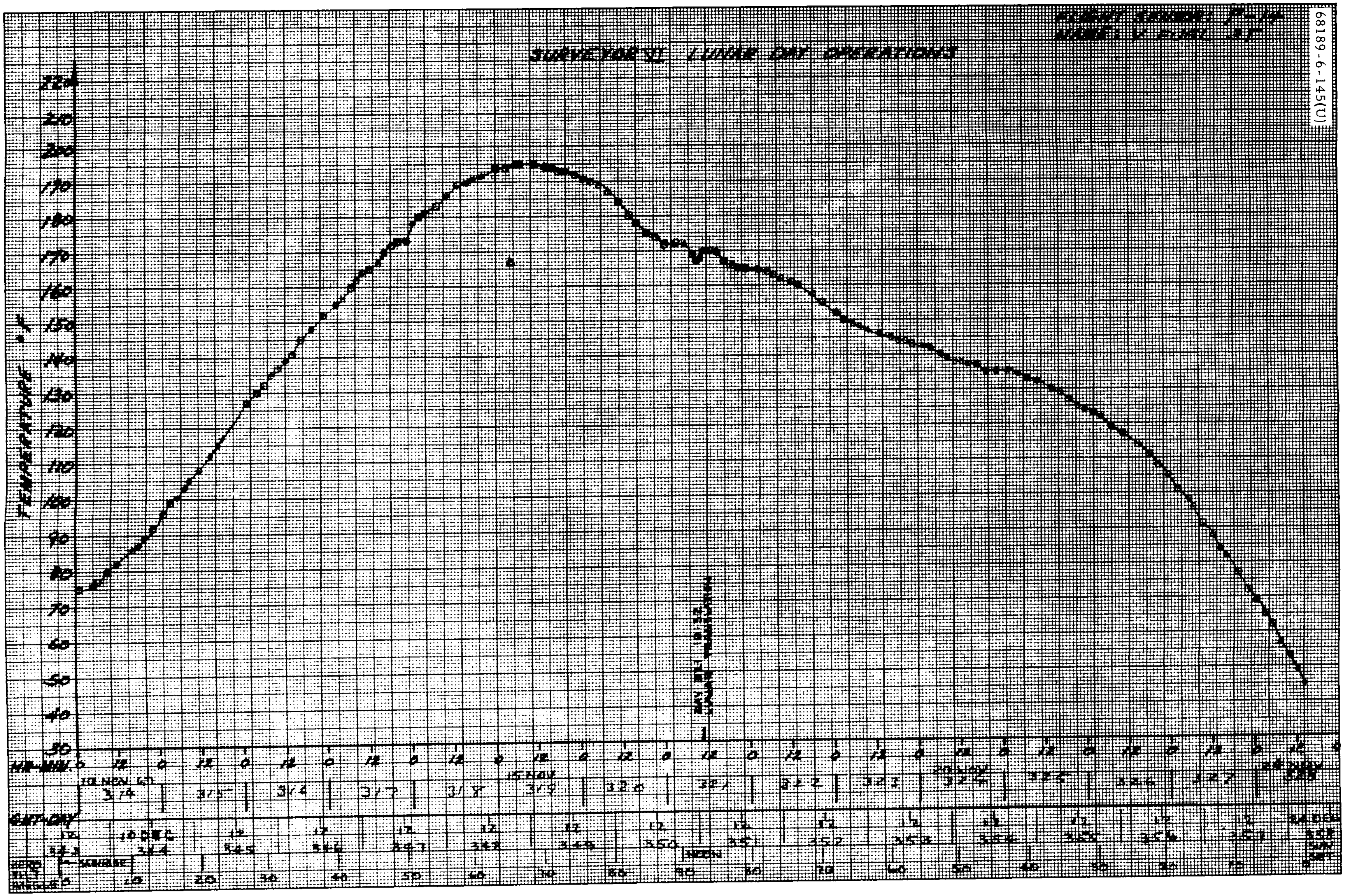

Figure 5.1-B30. Sensor P-14: Vernier Fuel Tank 3

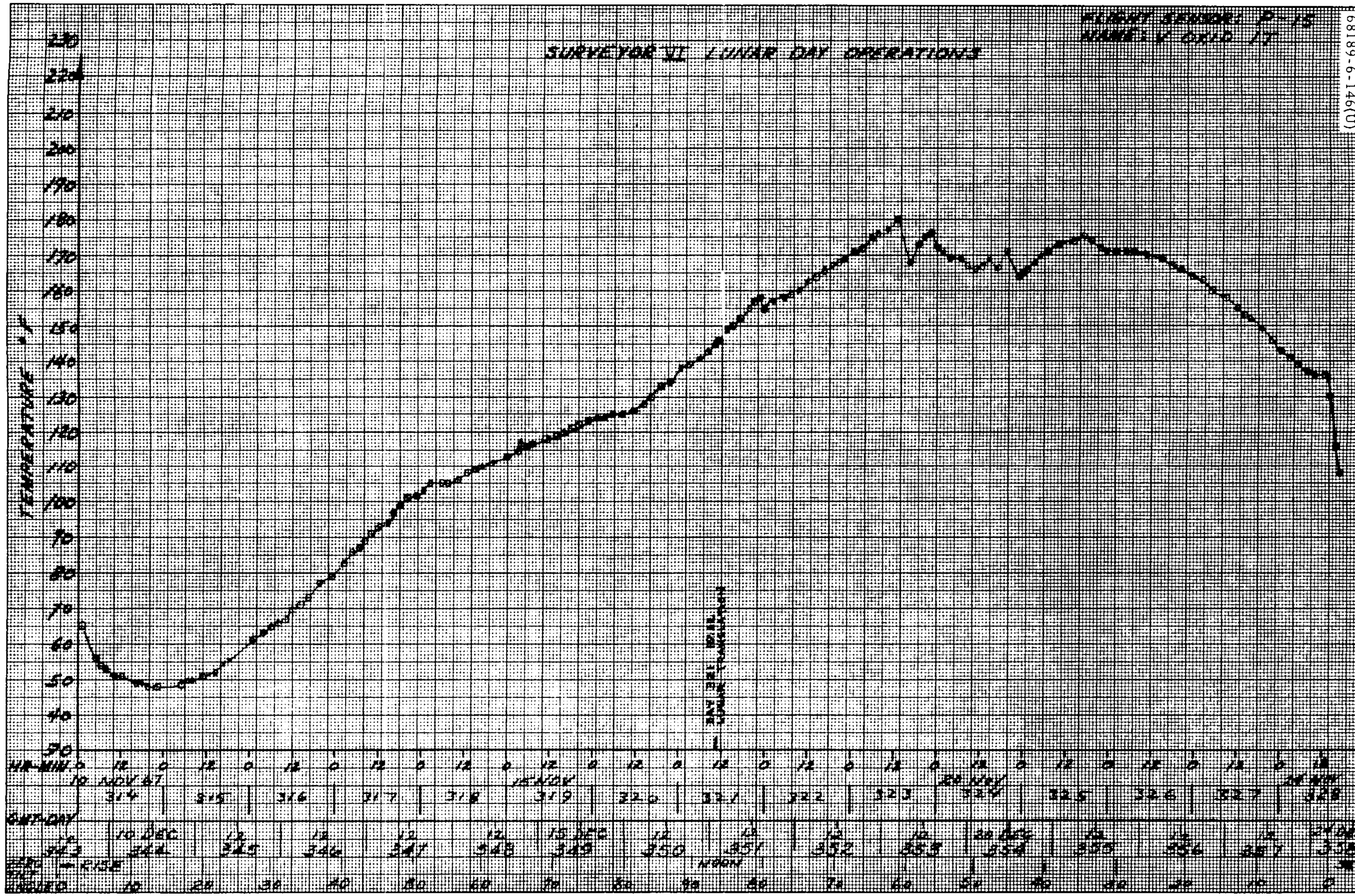

Figure 5.1-B31. Sensor P-15: Vernier Oxidizer Tank 1

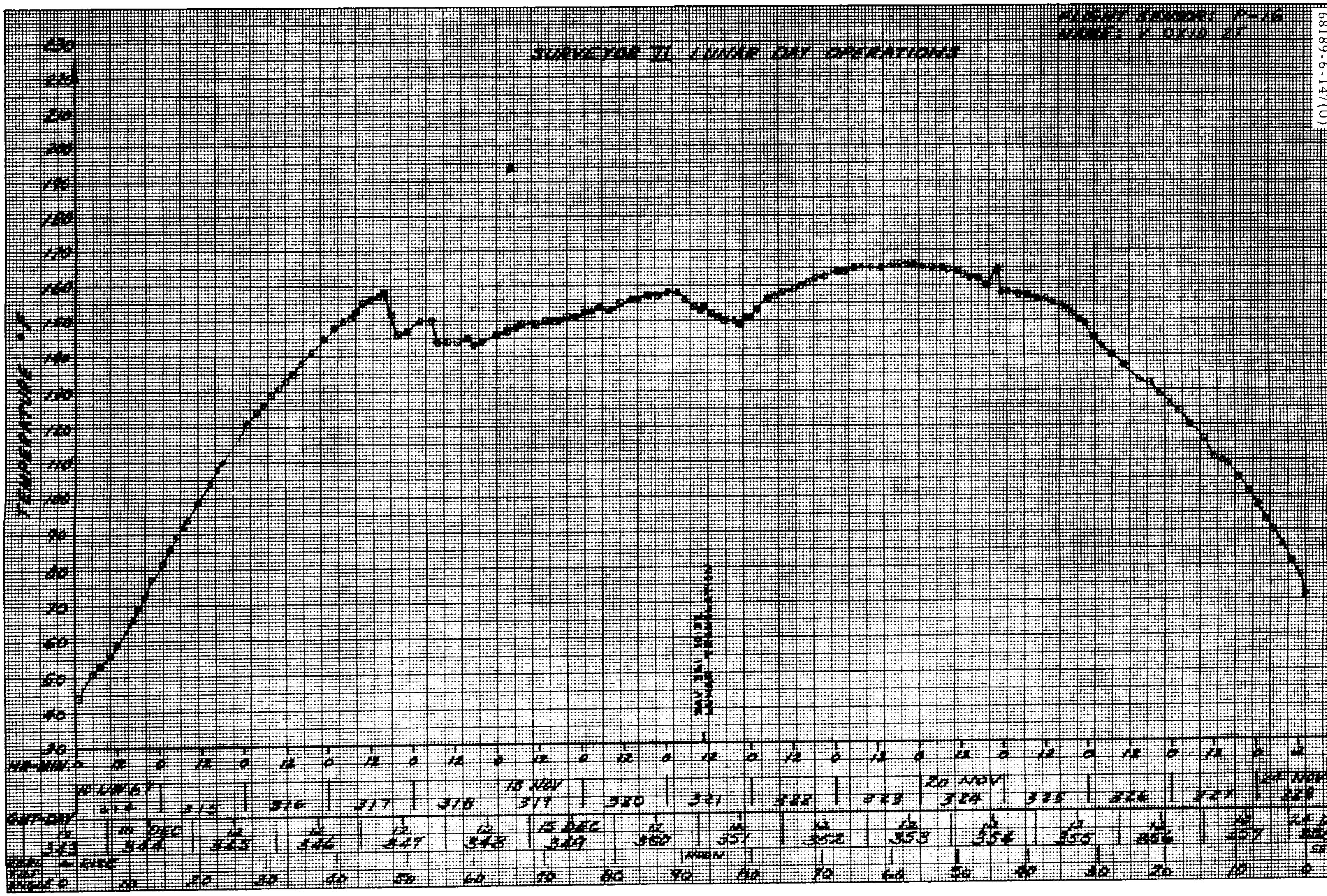

Figure 5.1-B32. Sensor P-16: Vernier Oxidizer Tank 2

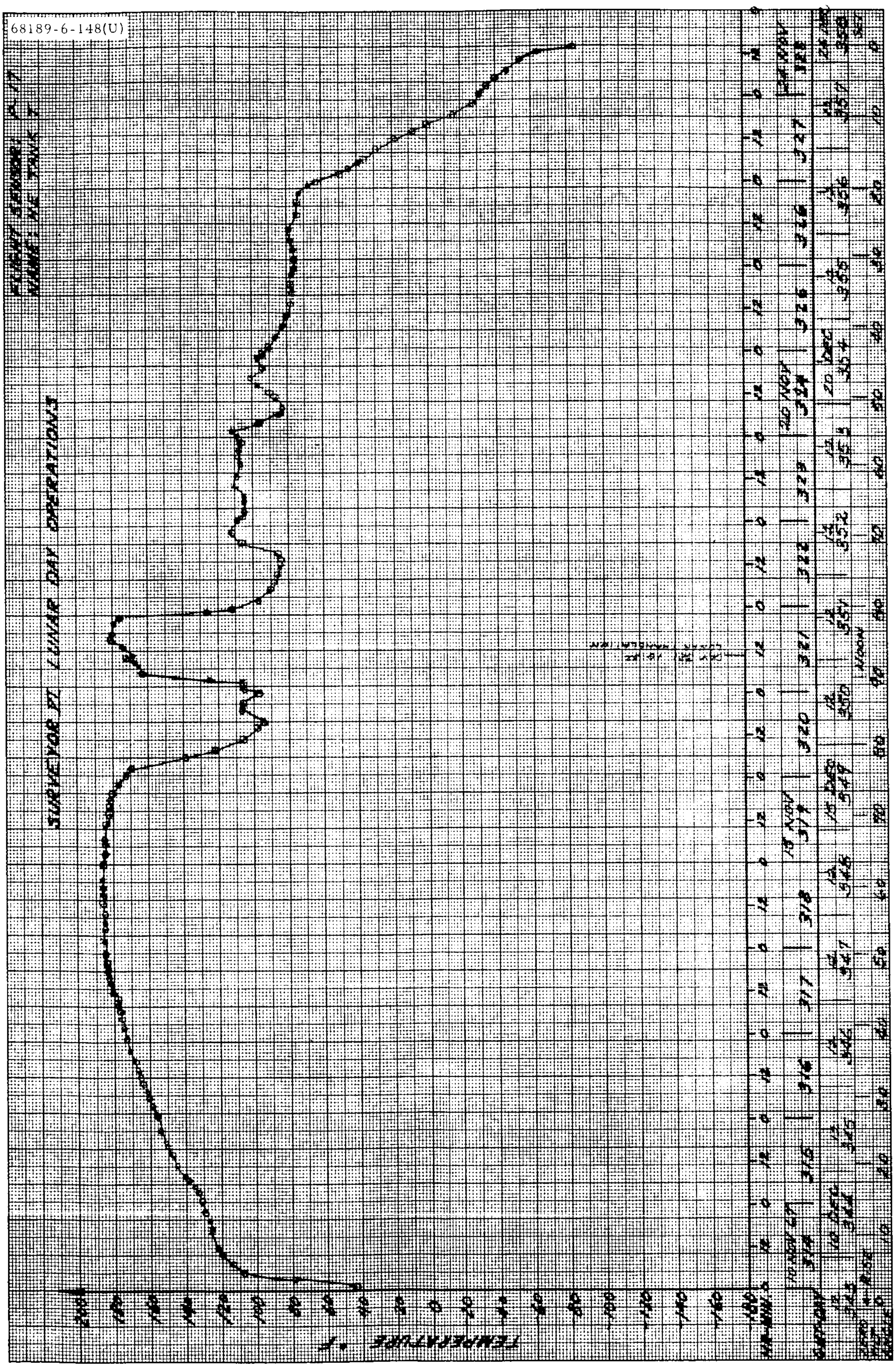

Figure 5.1-B33. Sensor P-17: Helium Tank

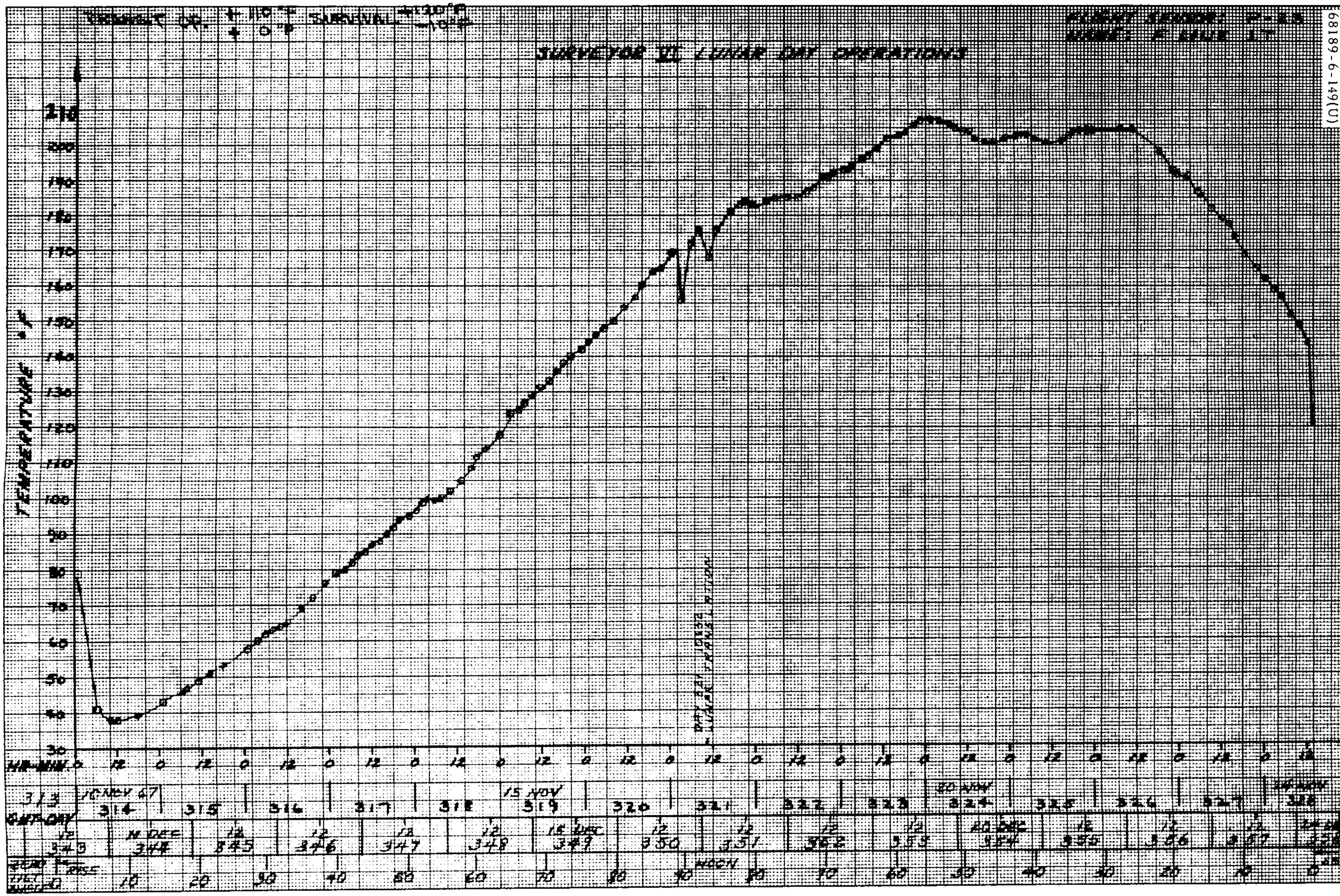

Figure 5.1-B34. Sensor P-23: Vernier Fuel Line 1

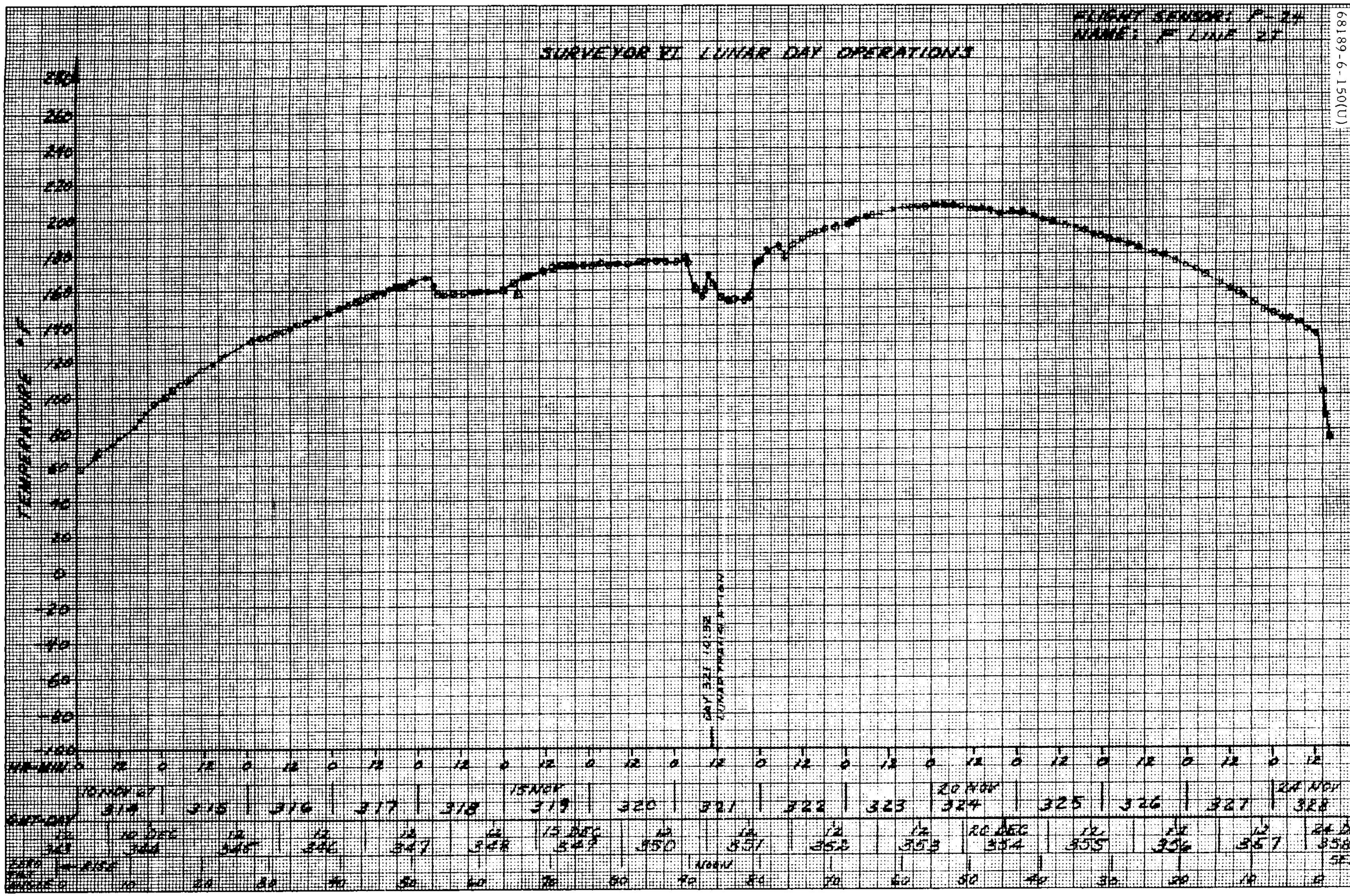

Figure 5.1-B35. Sensor P-24: Vernier Fuel Line 2

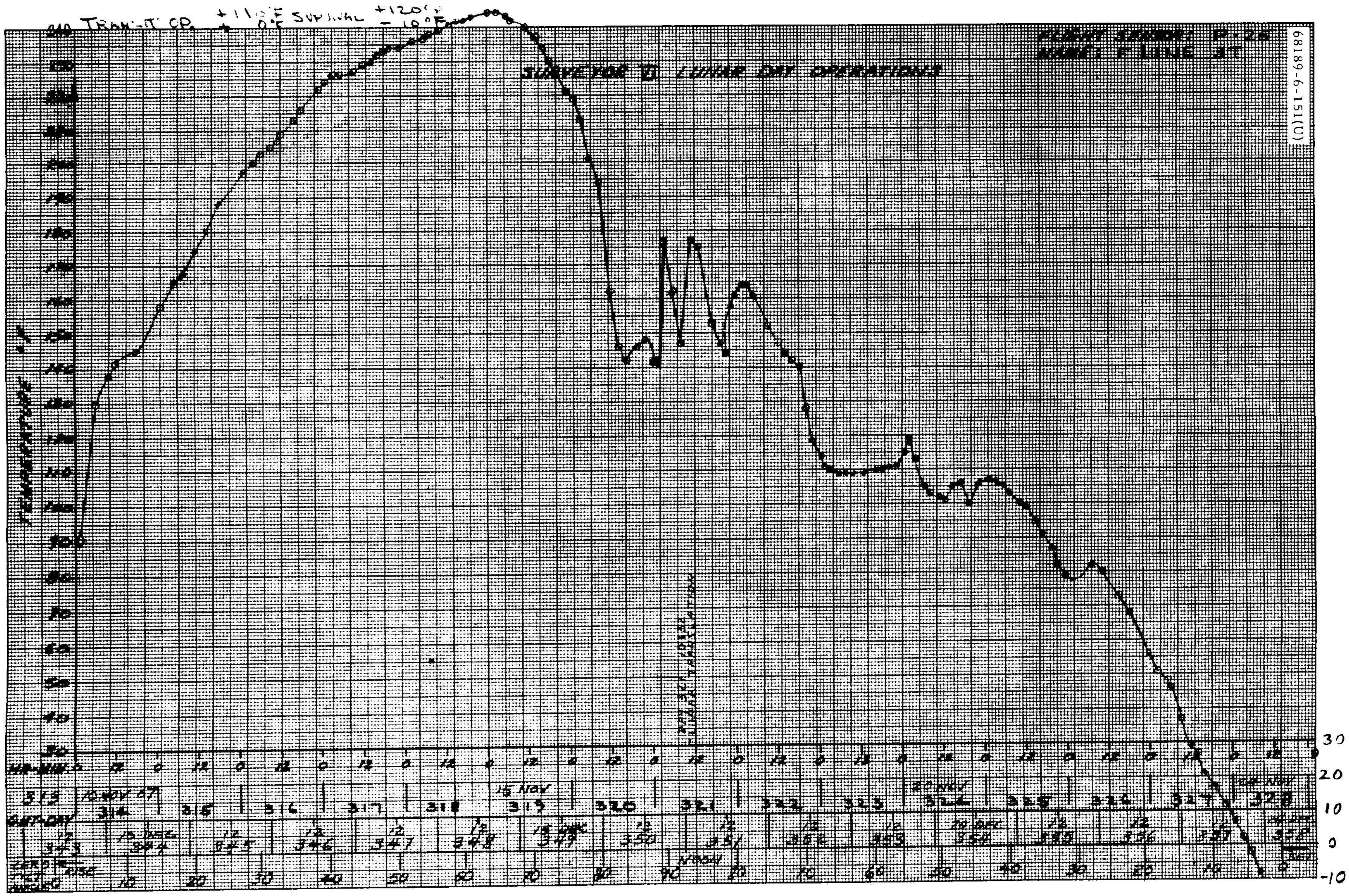

Figure 5.1-B36. Sensor P-25: Vernier Fuel Line 3

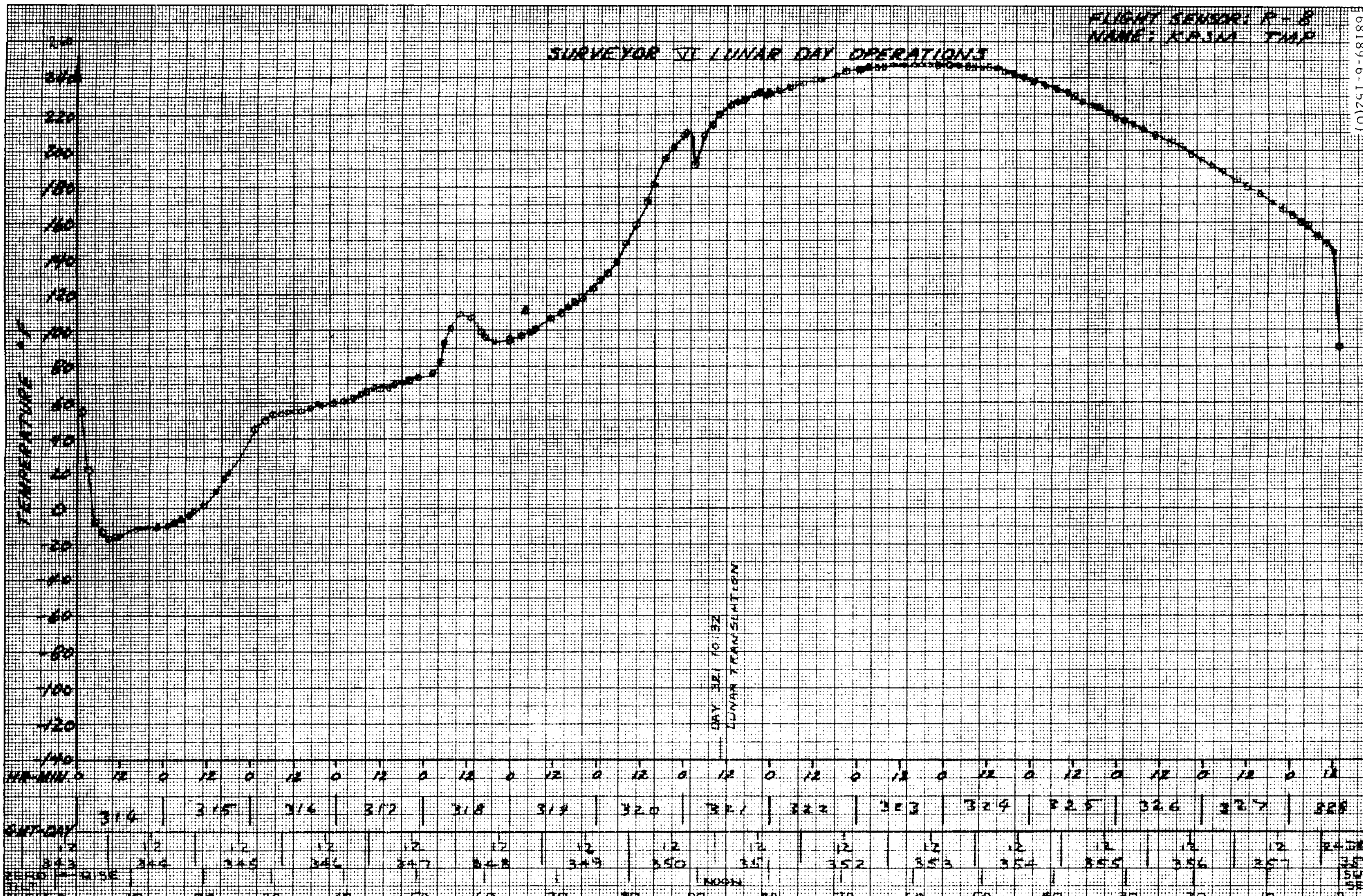

Figure 5.1-B37. Sensor R-8: RADVS (Klystron) Unit

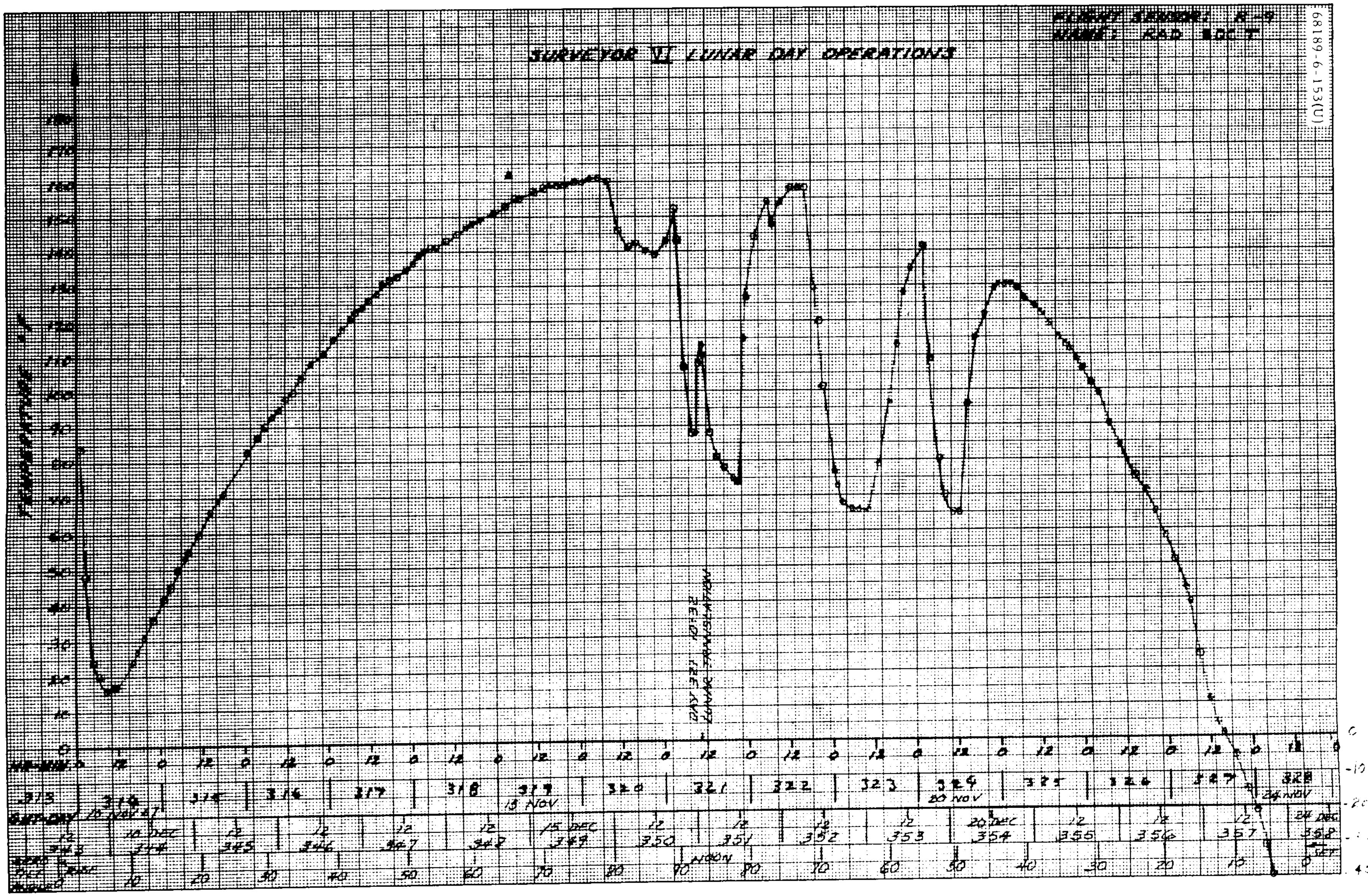

Figure 5.1-B38. Sensor R-9: RADVS Signal Data Converter

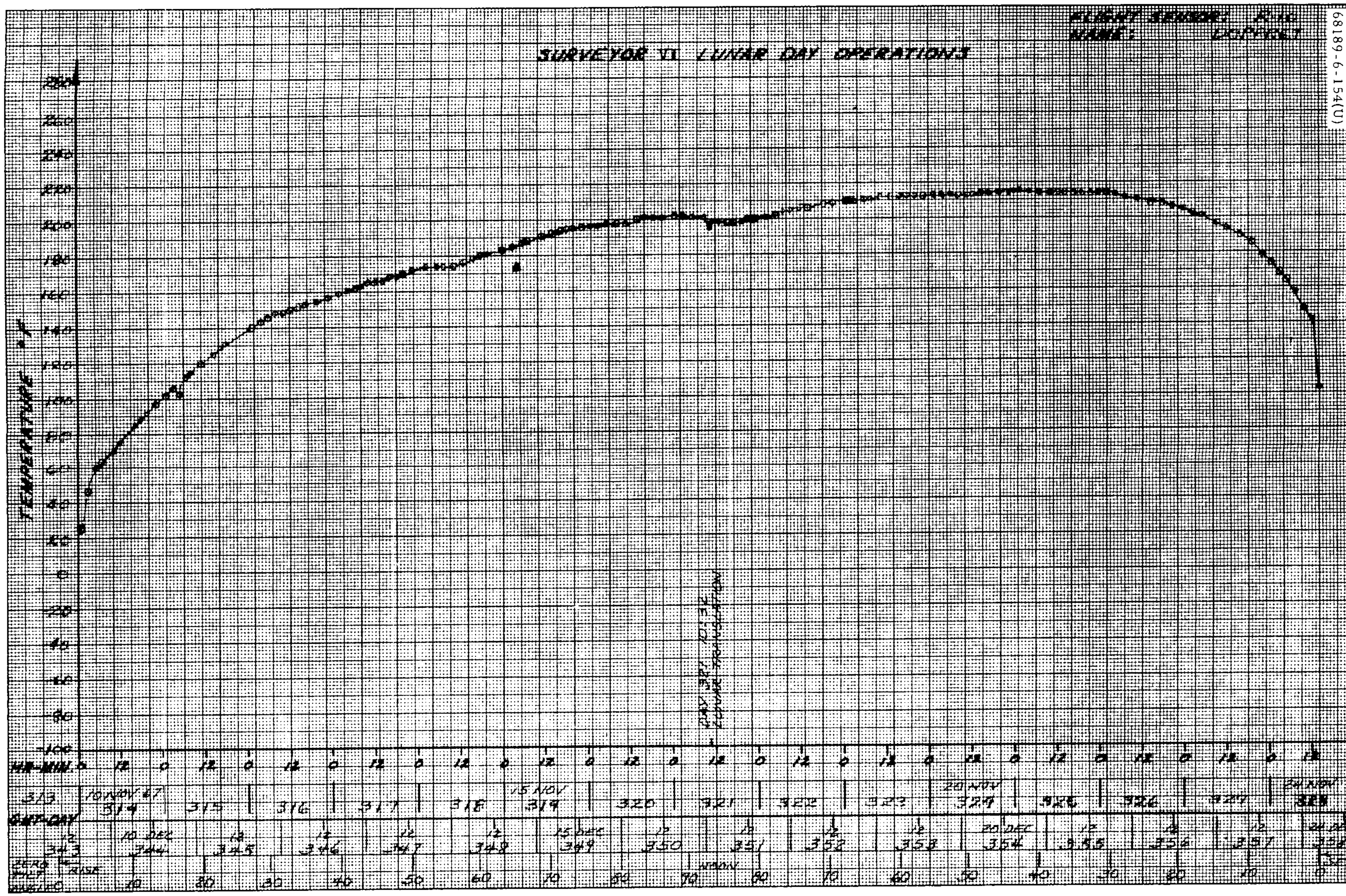

Figure 5.1-B39. Sensor R-10: Doppler Radar Sensor

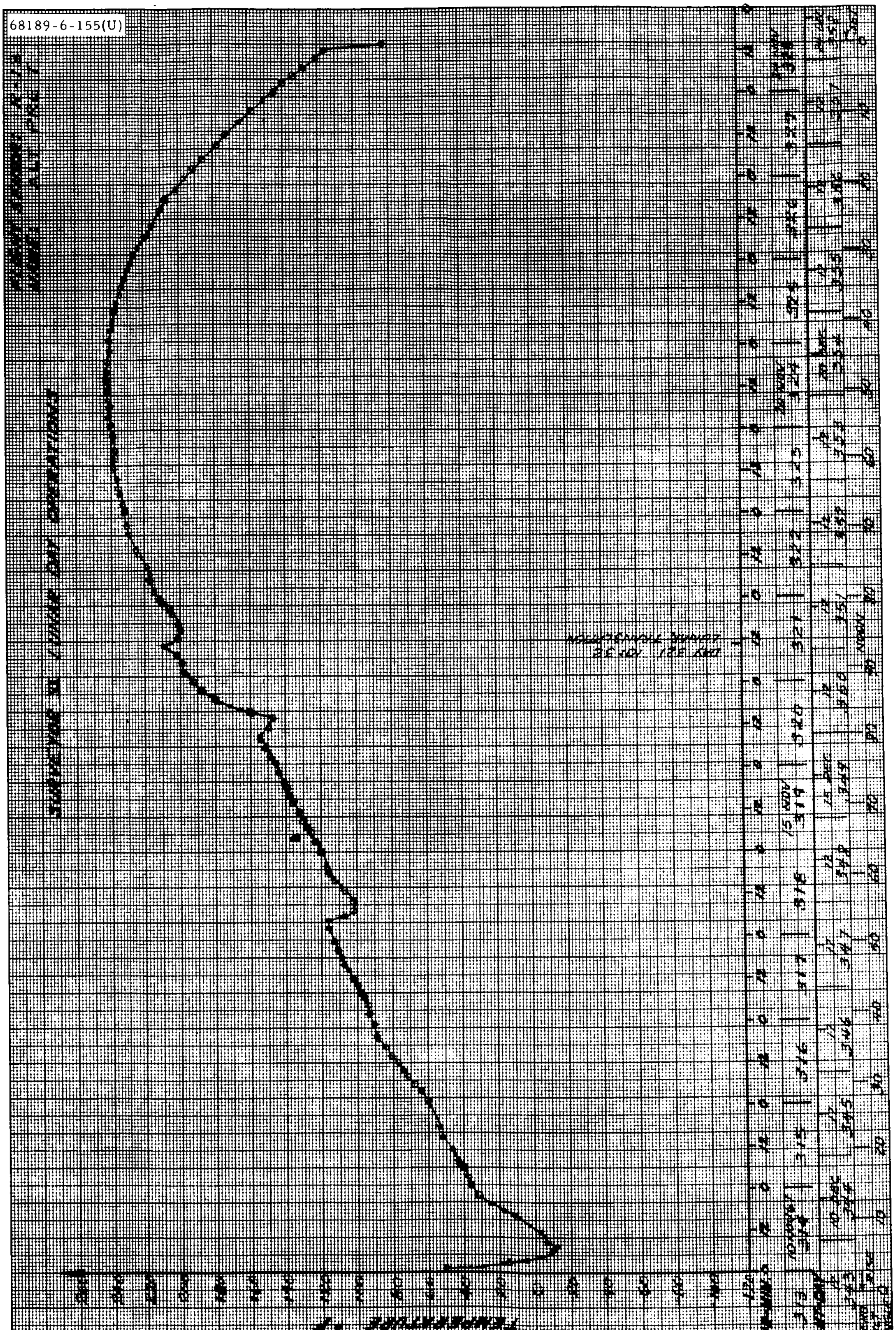

Figure 5.1-B40. Sensor R-13: Altimeter Radar Sensor

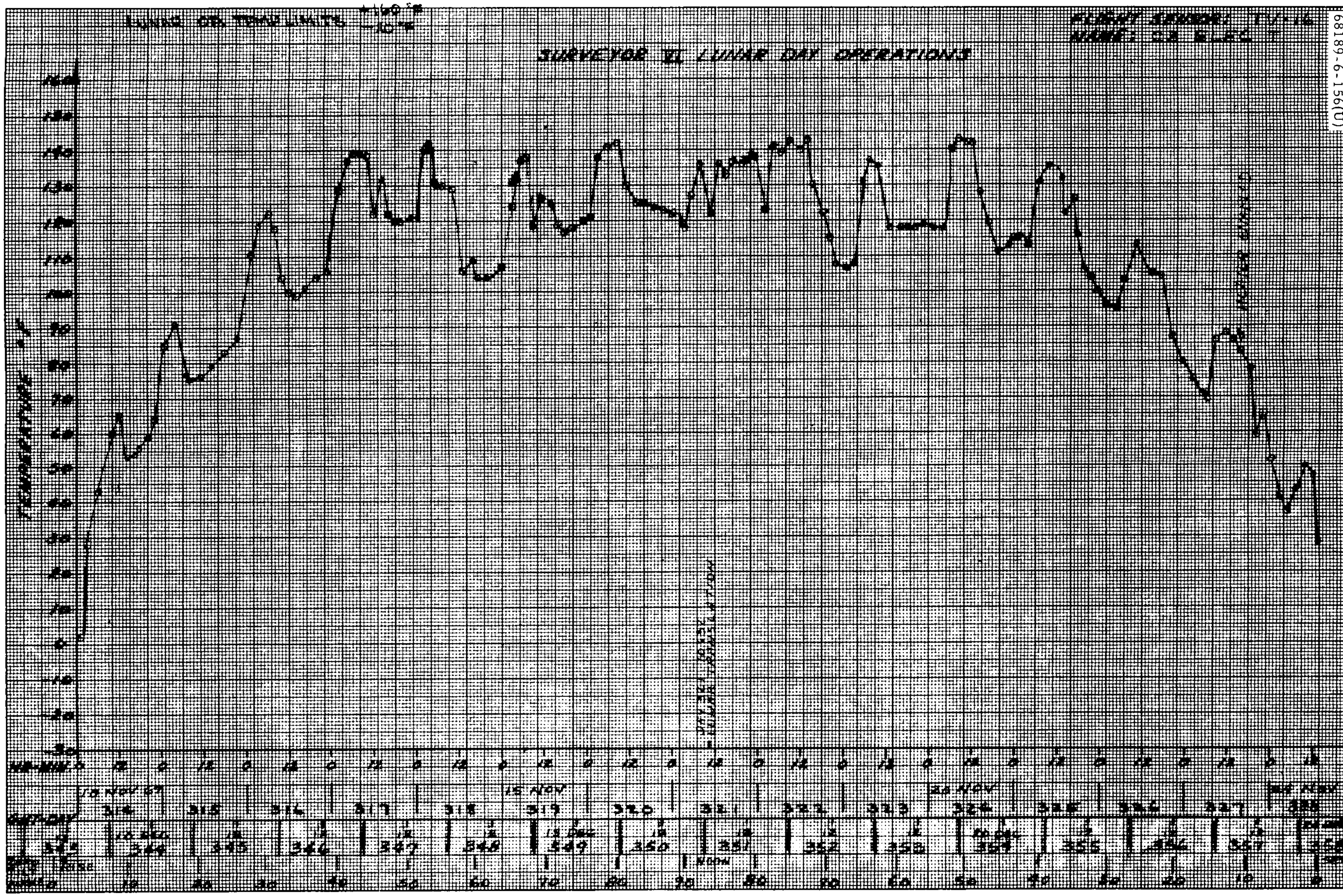

Figure 5.1-B41. Sensor TV-16: Surveyor Camera Electronics

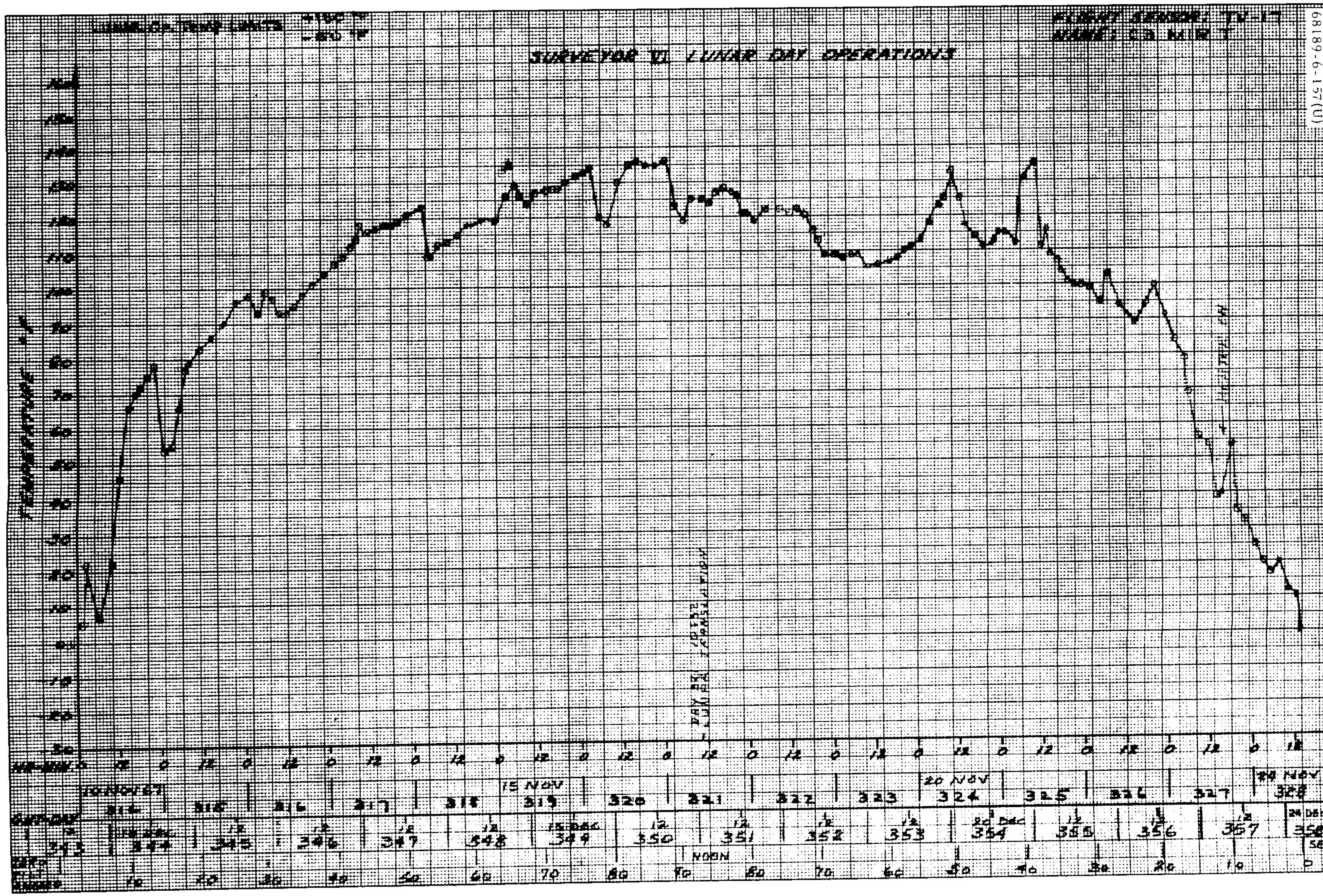

Figure 5.1-B42. Sensor TV-17: Surveyor Camera Mirror Assembly

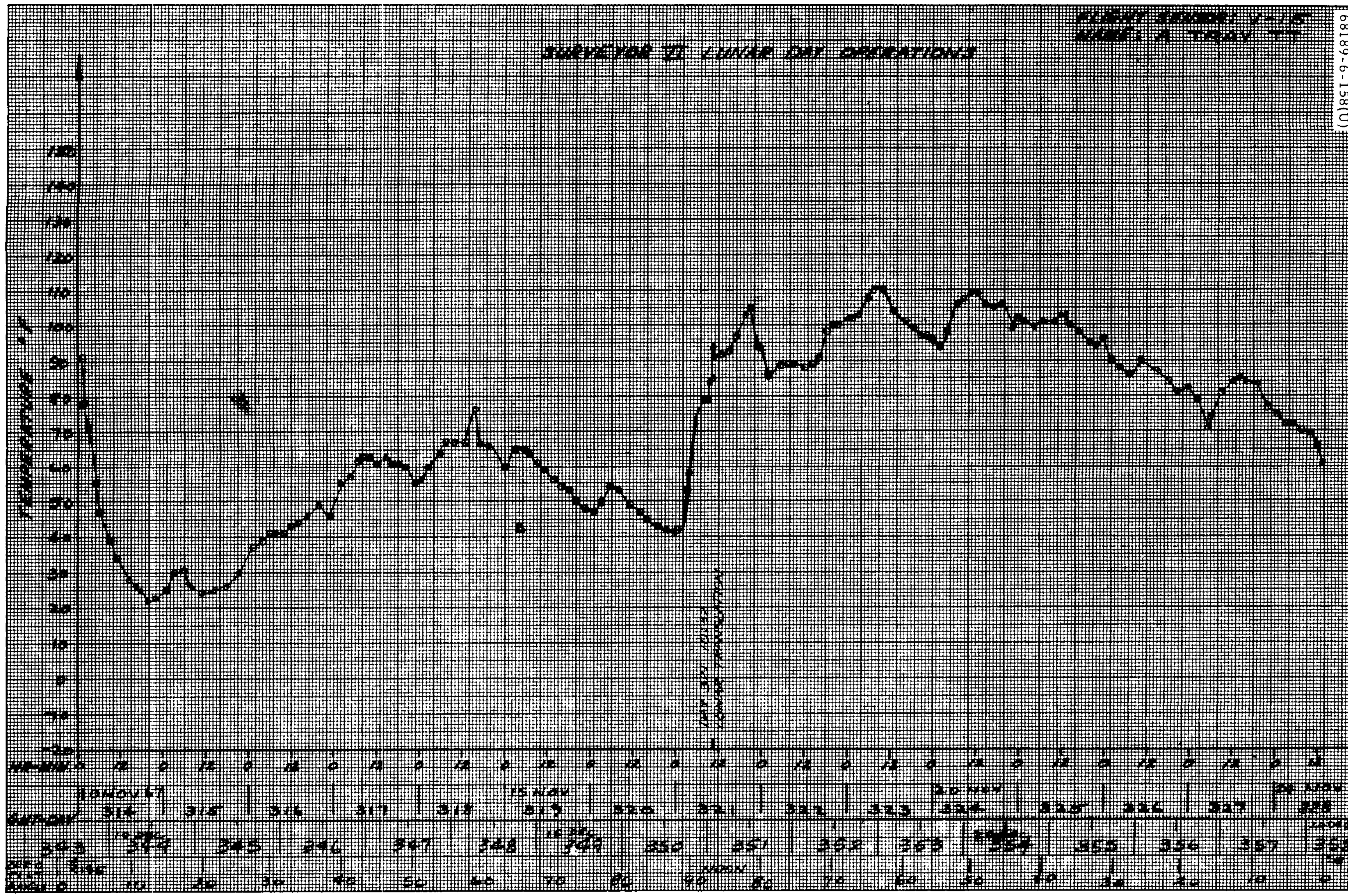

Figure 5.1-B43. Sensor V-15: Compartment A Thermal Tray

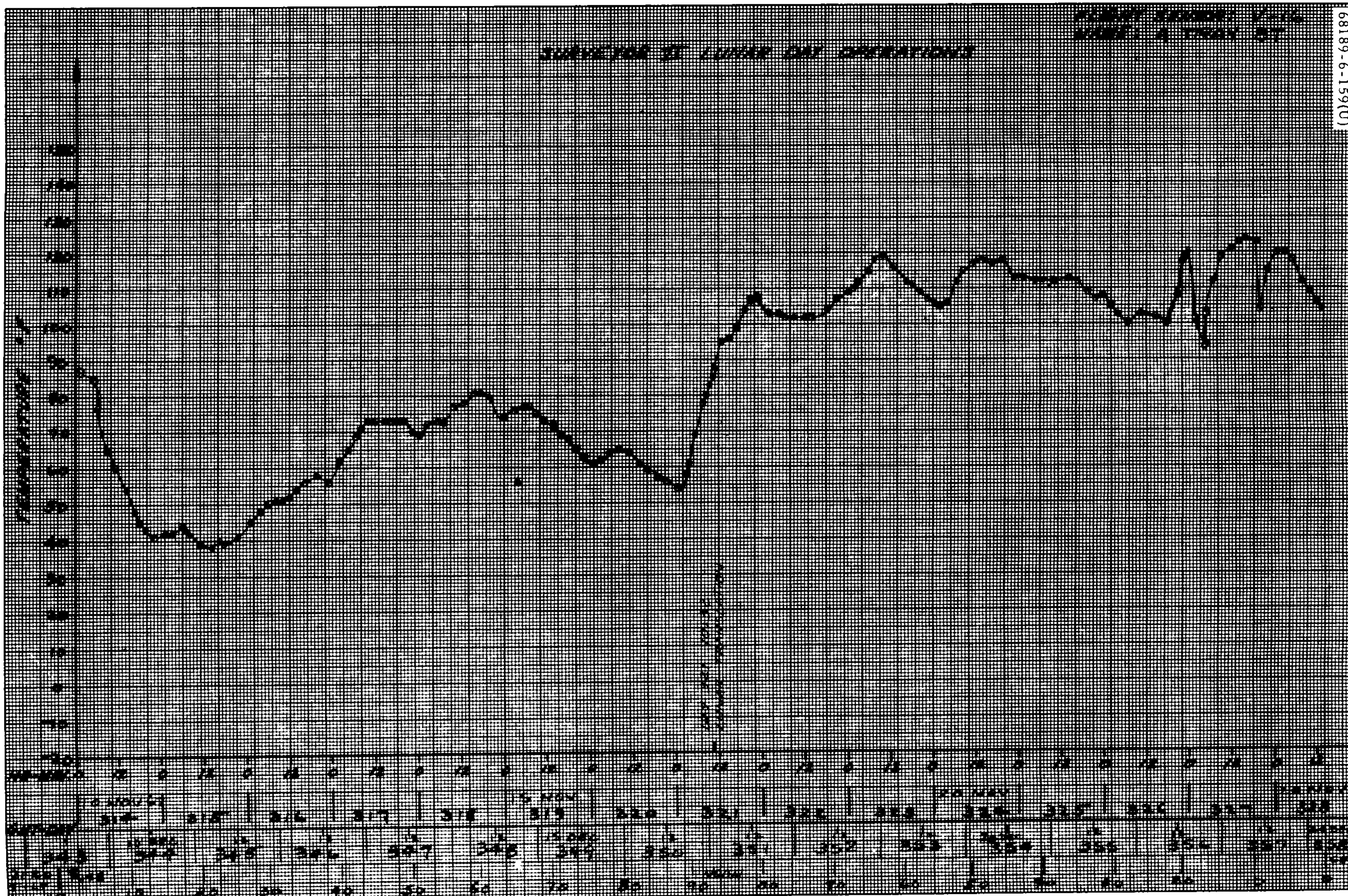

Figure 5.1-B44. Sensor V-16: Compartment A Lower Support

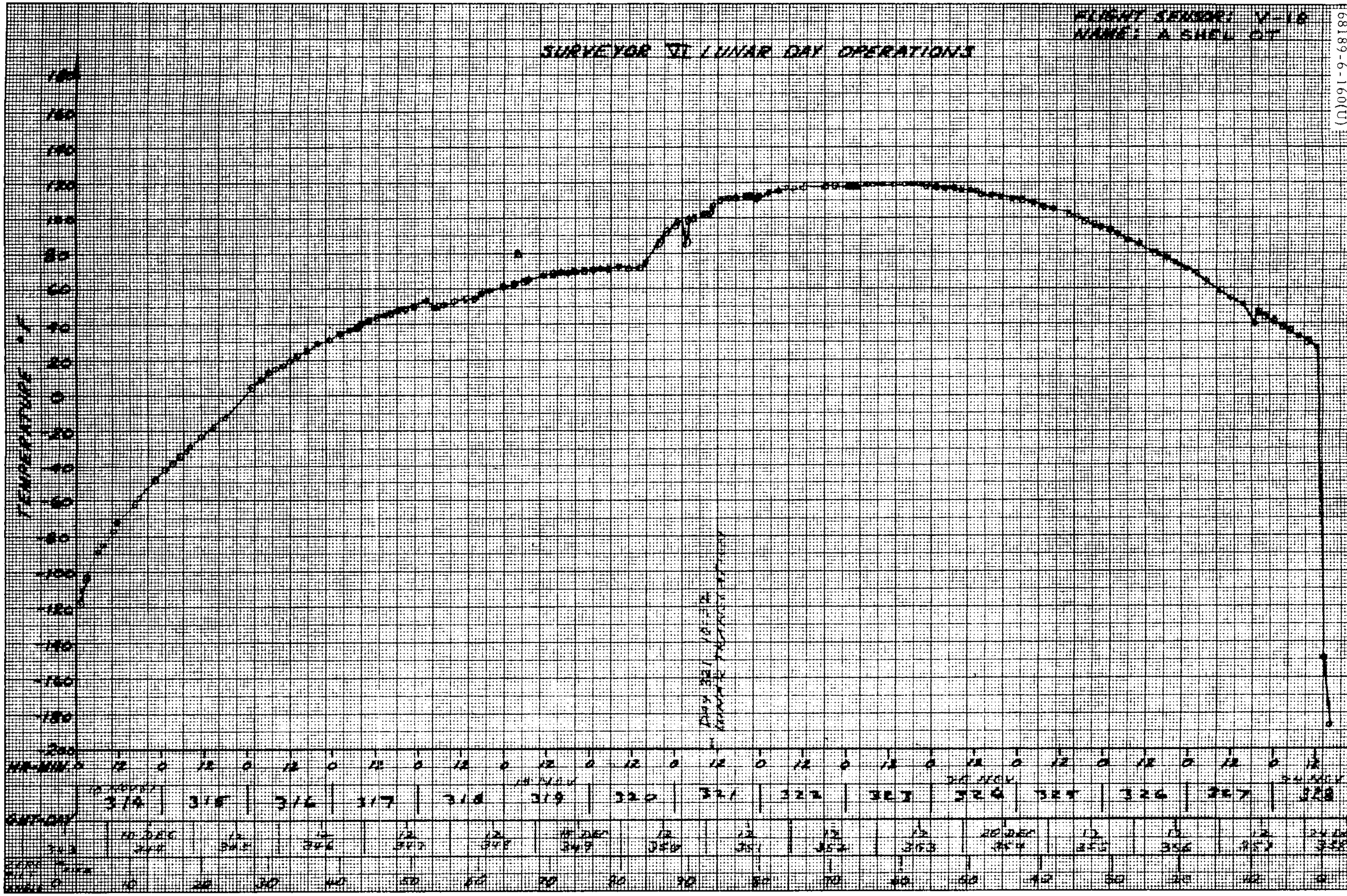

Figure 5.1-B45. Sensor V-18: Compartment A Canister

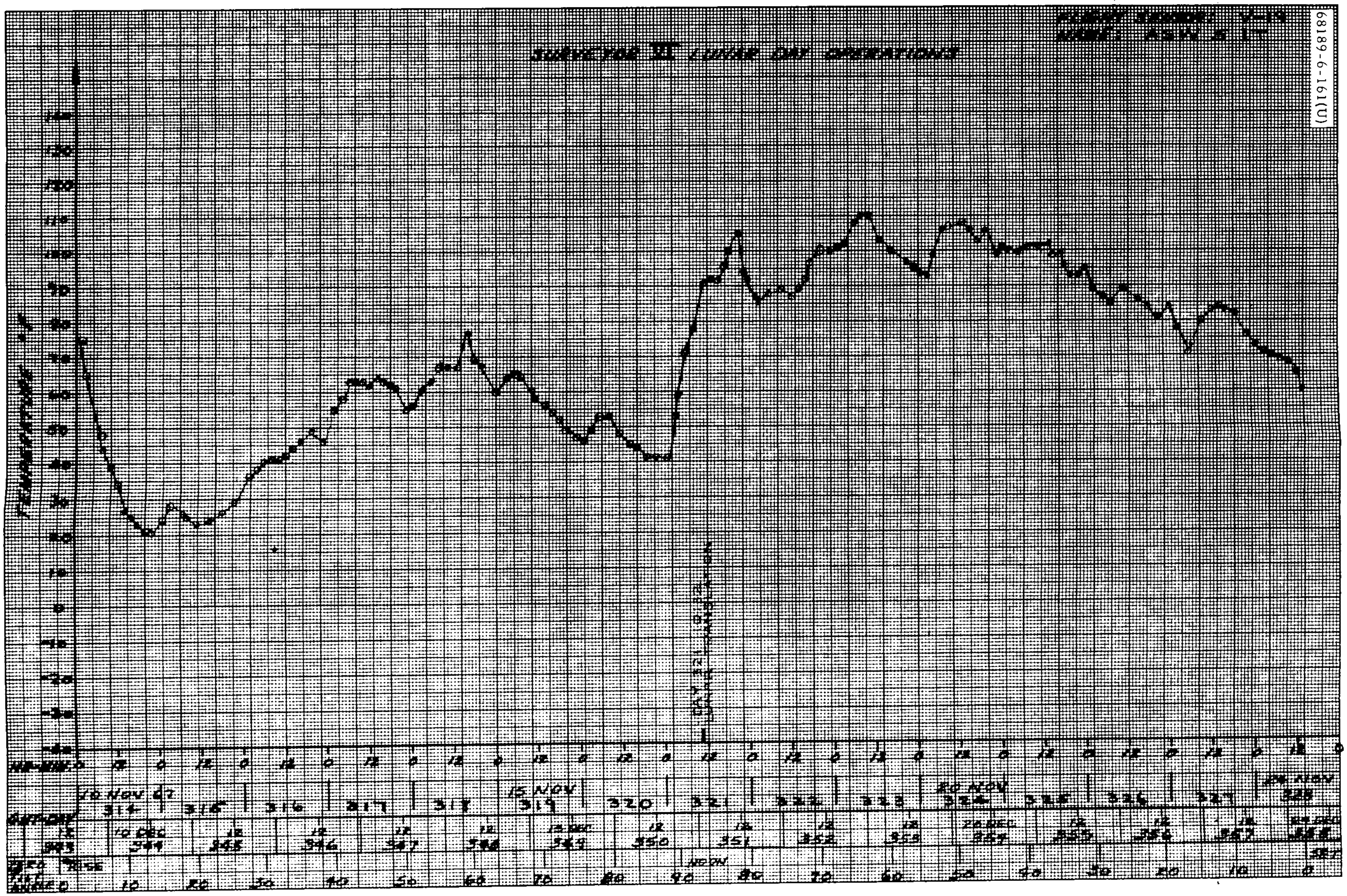

Figure 5. 1-B46. Sensor V-19: Compartment A Switch 5 Base

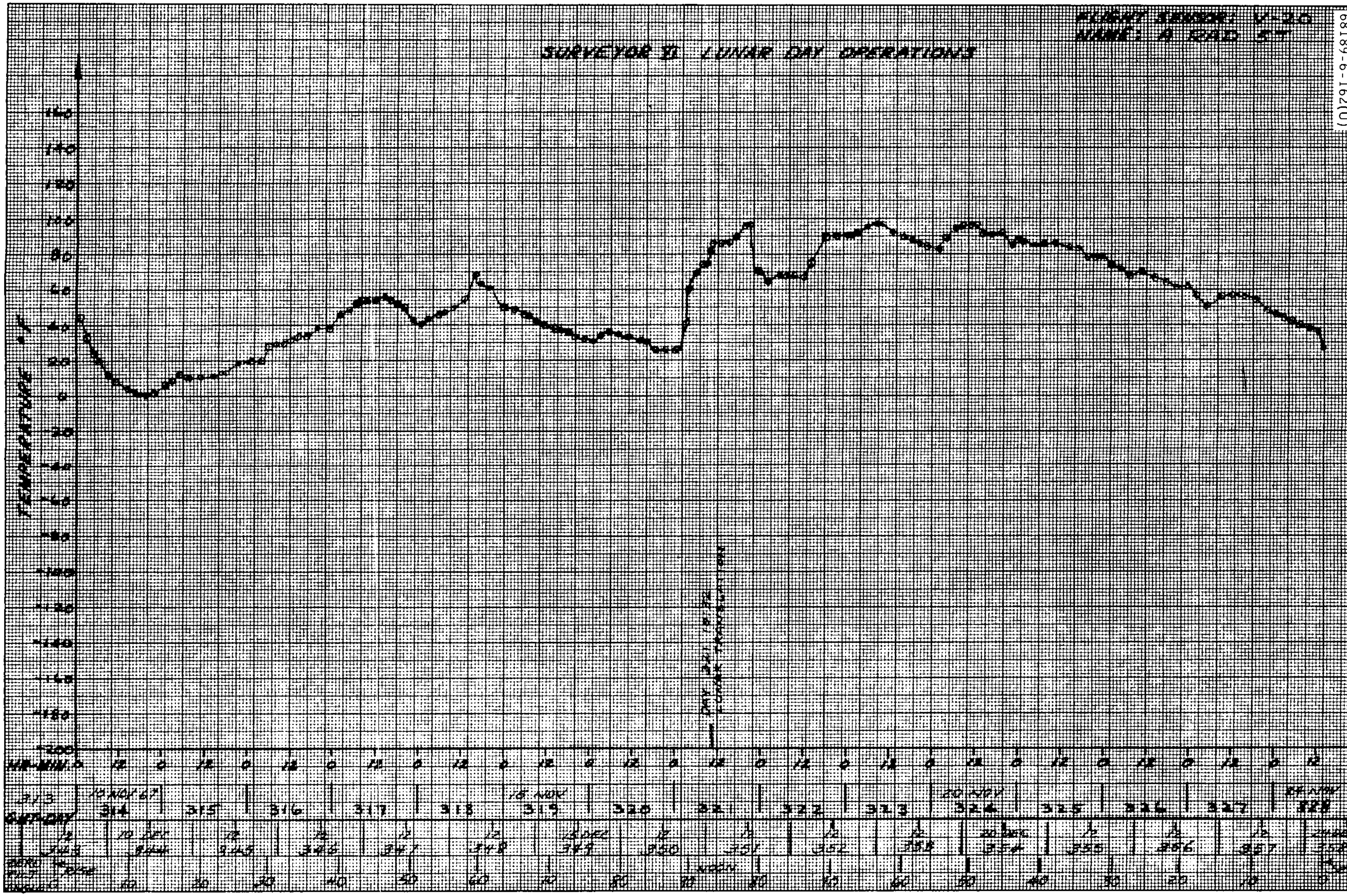

Figure 5.1-B47. Sensor V-20: Compartment A Switch 5 in Face Radiator

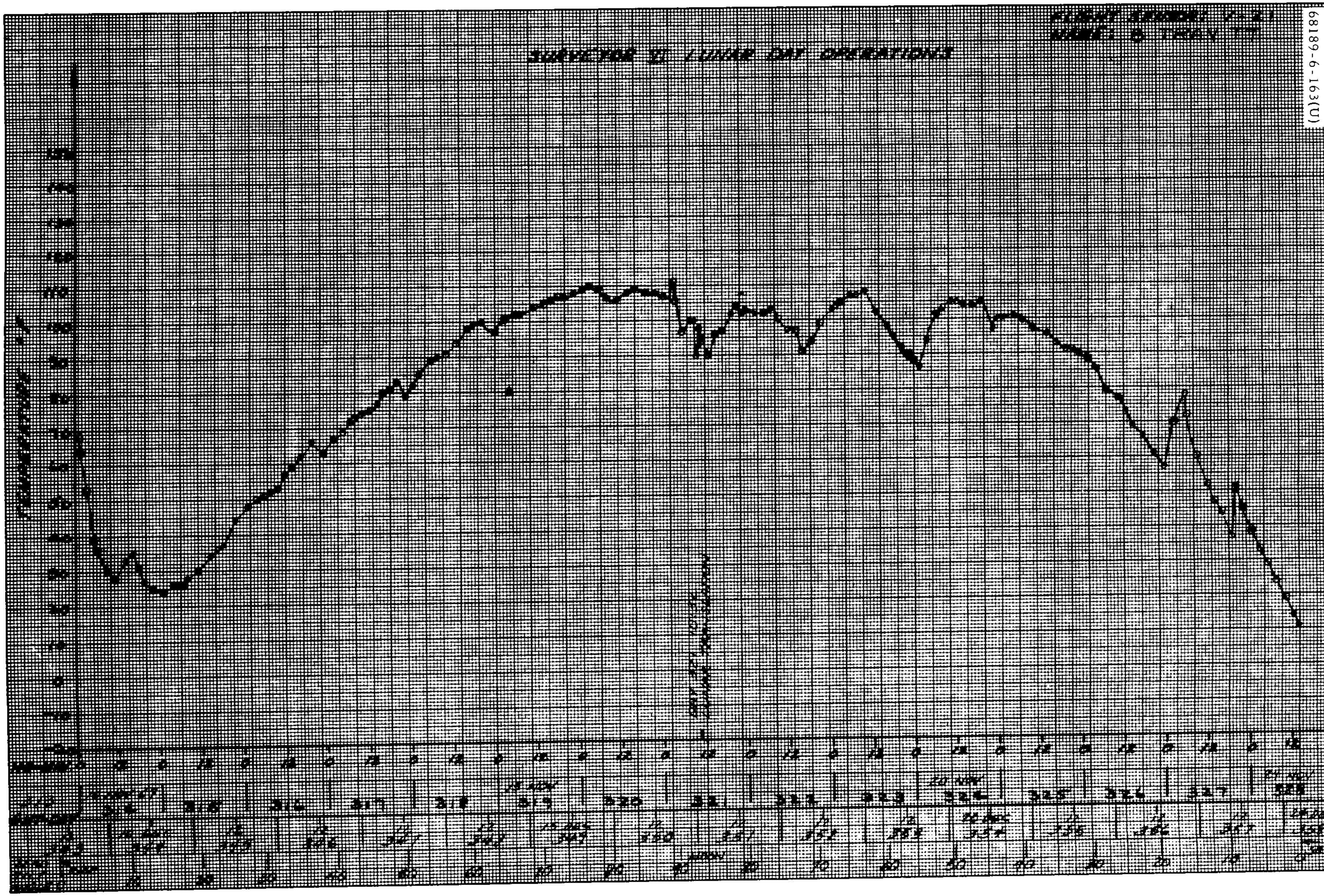

Figure 5.1-B48. Sensor V-21: Compartment B Tray Top Center

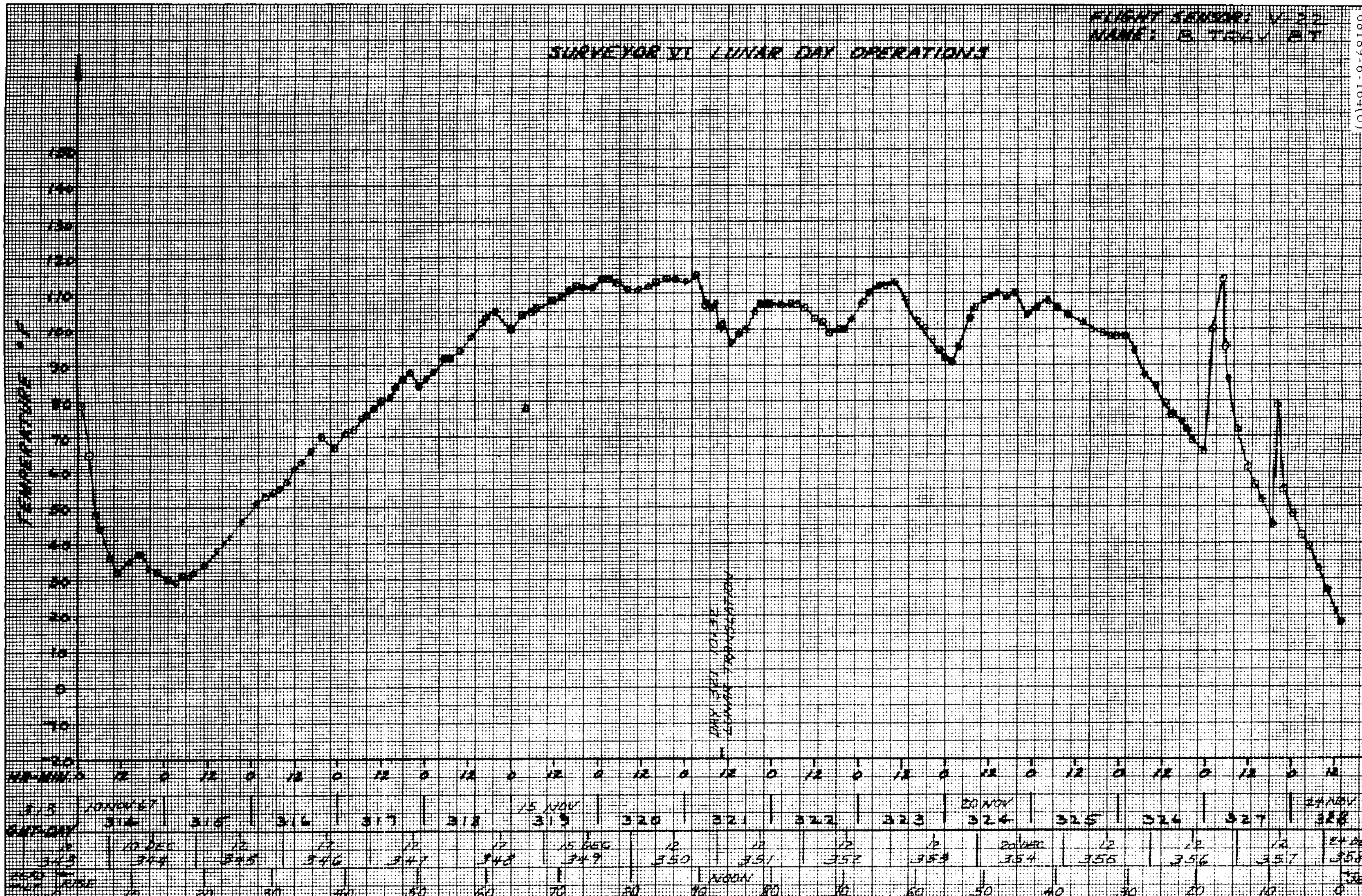

Figure 5.1-B49. Sensor V-22: Compartment B Lower Support

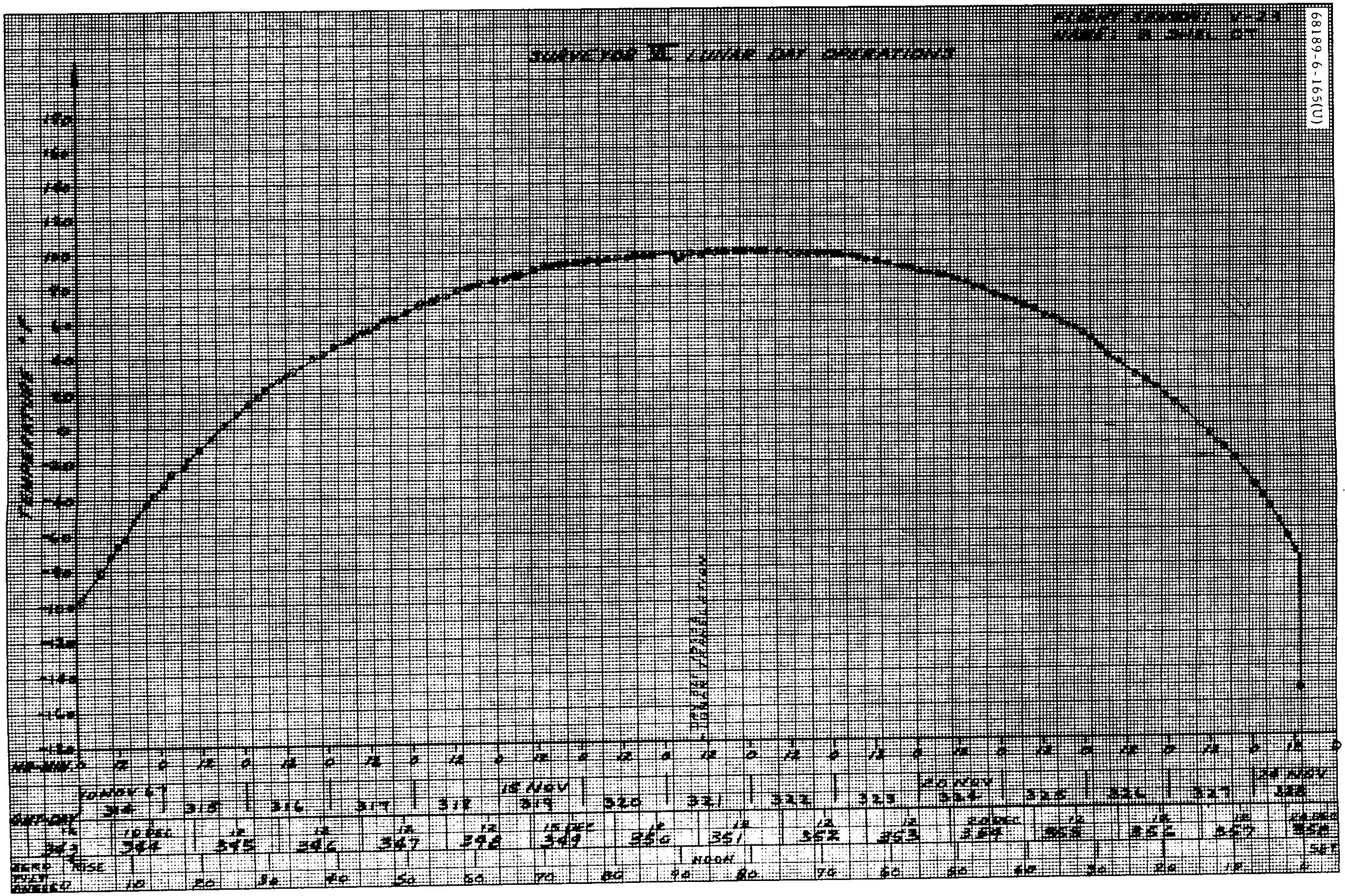

Figure 5.1-B50. Sensor V-23: Compartment B Canister

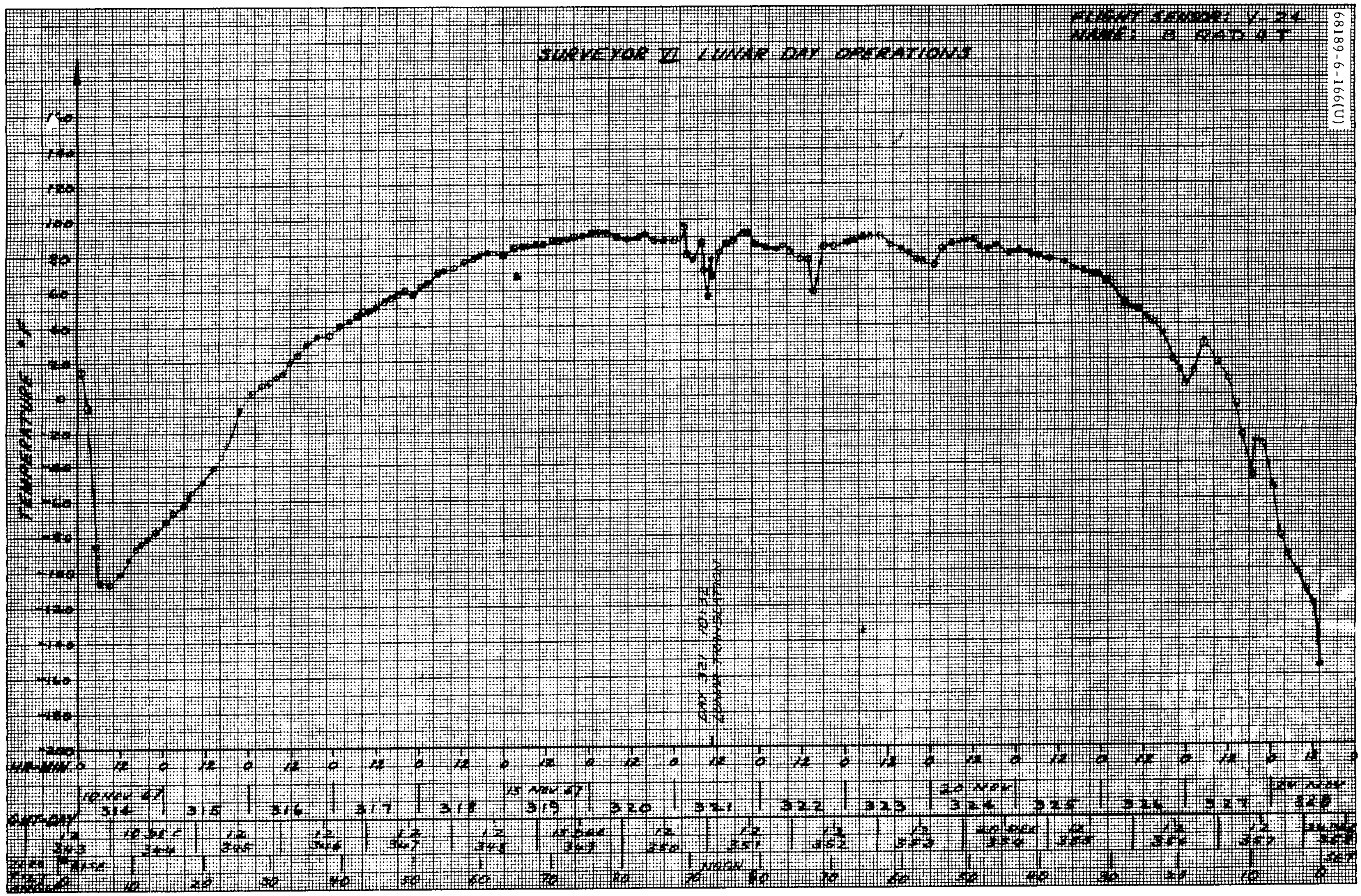

Figure 5.1-B51. Sensor V-24: Compartment B Switch 4 in Face Radiator

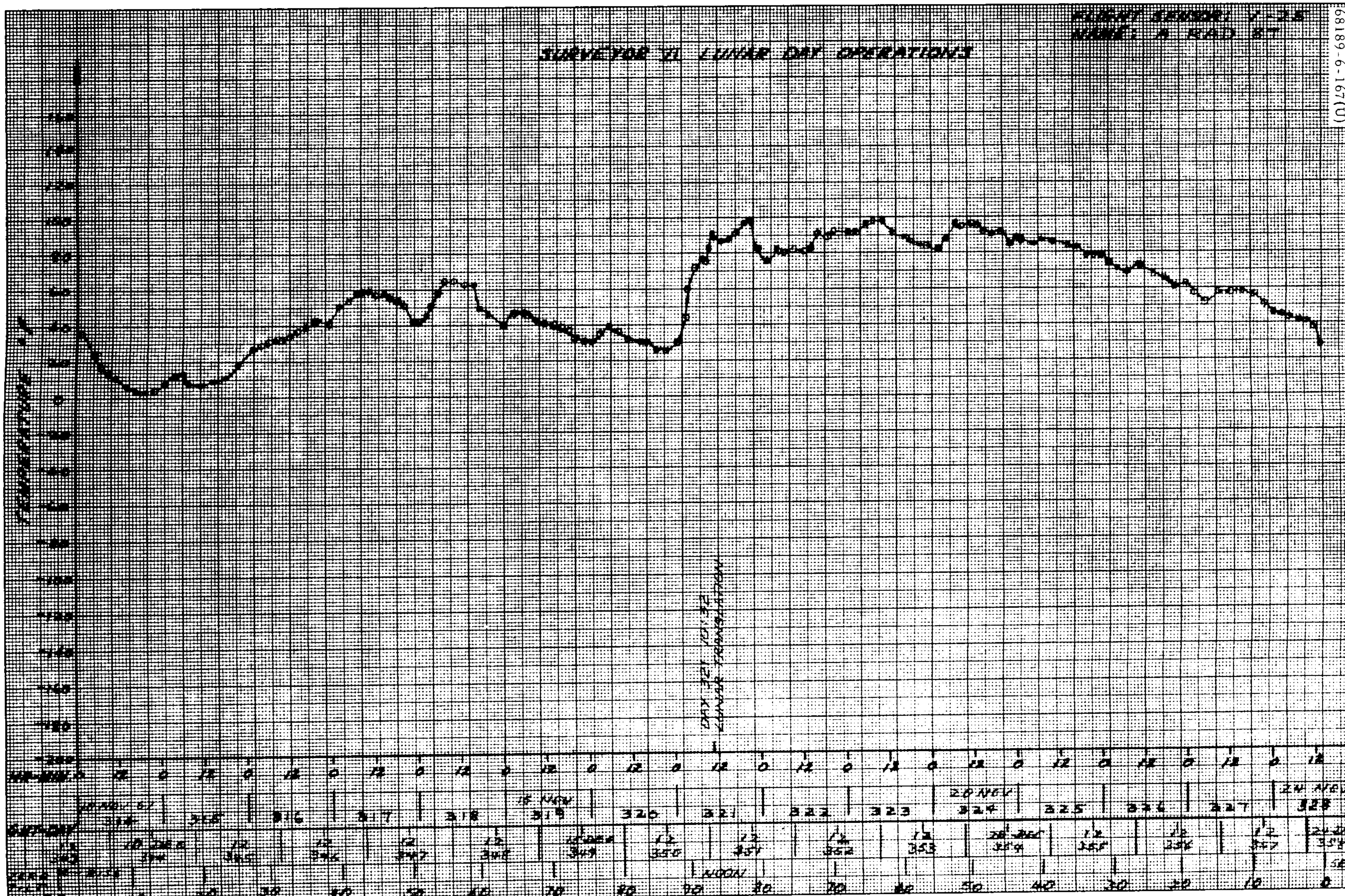

Figure 5.1-B52. Sensor V-25: Compartment A Switch 8 in Face Radiator

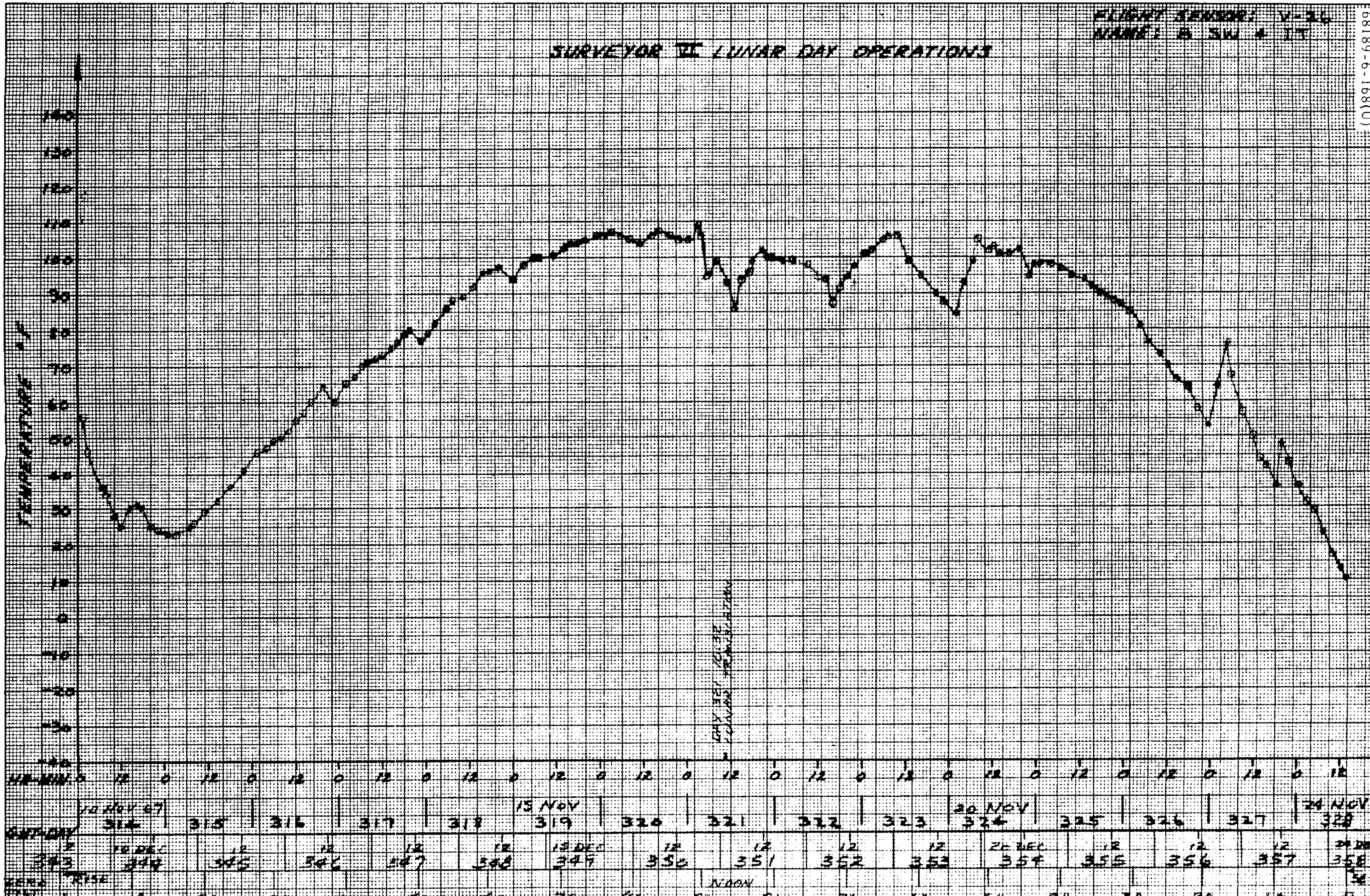

Figure 5.1-B53. Sensor V-26: Compartment B Switch 4 Base

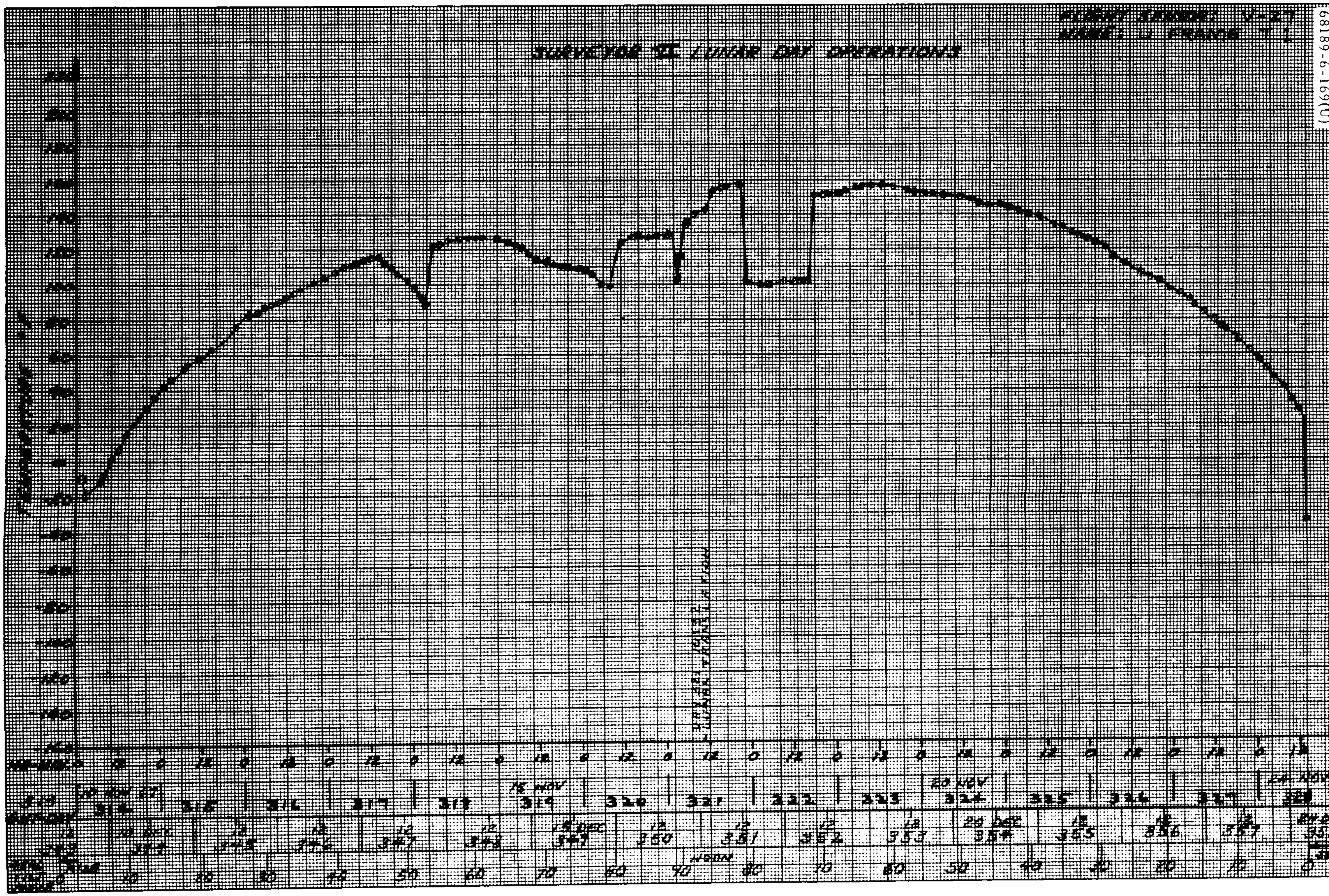

Figure 5.1-B54. Sensor V-27: Upper Spaceframe 1

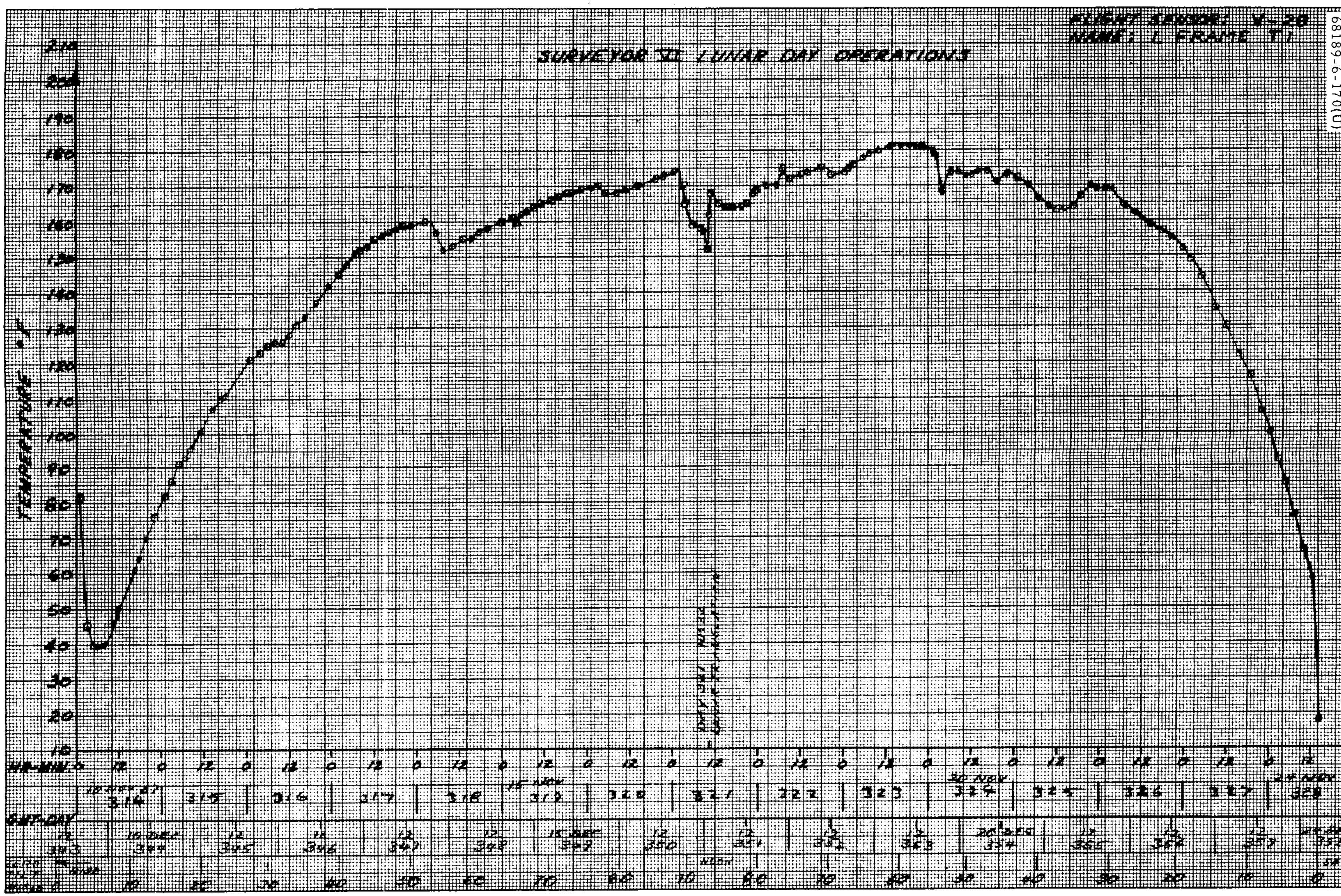

Figure 5.1-B55. Sensor V-28: Spaceframe Temperature Under Compartment A

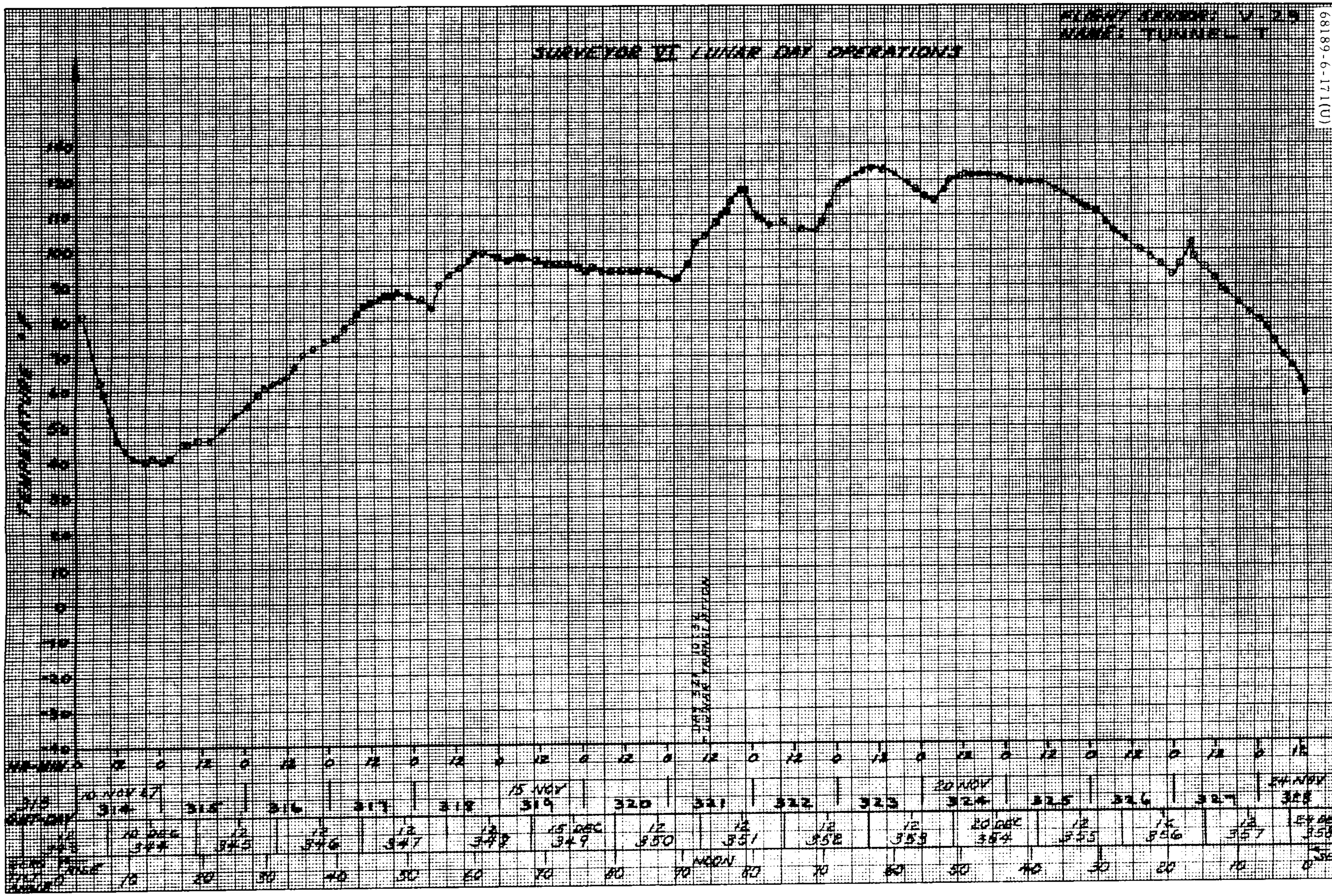

Figure 5.1-B56. Sensor V-29: Wire Harness Temperature Thermal Tunnel

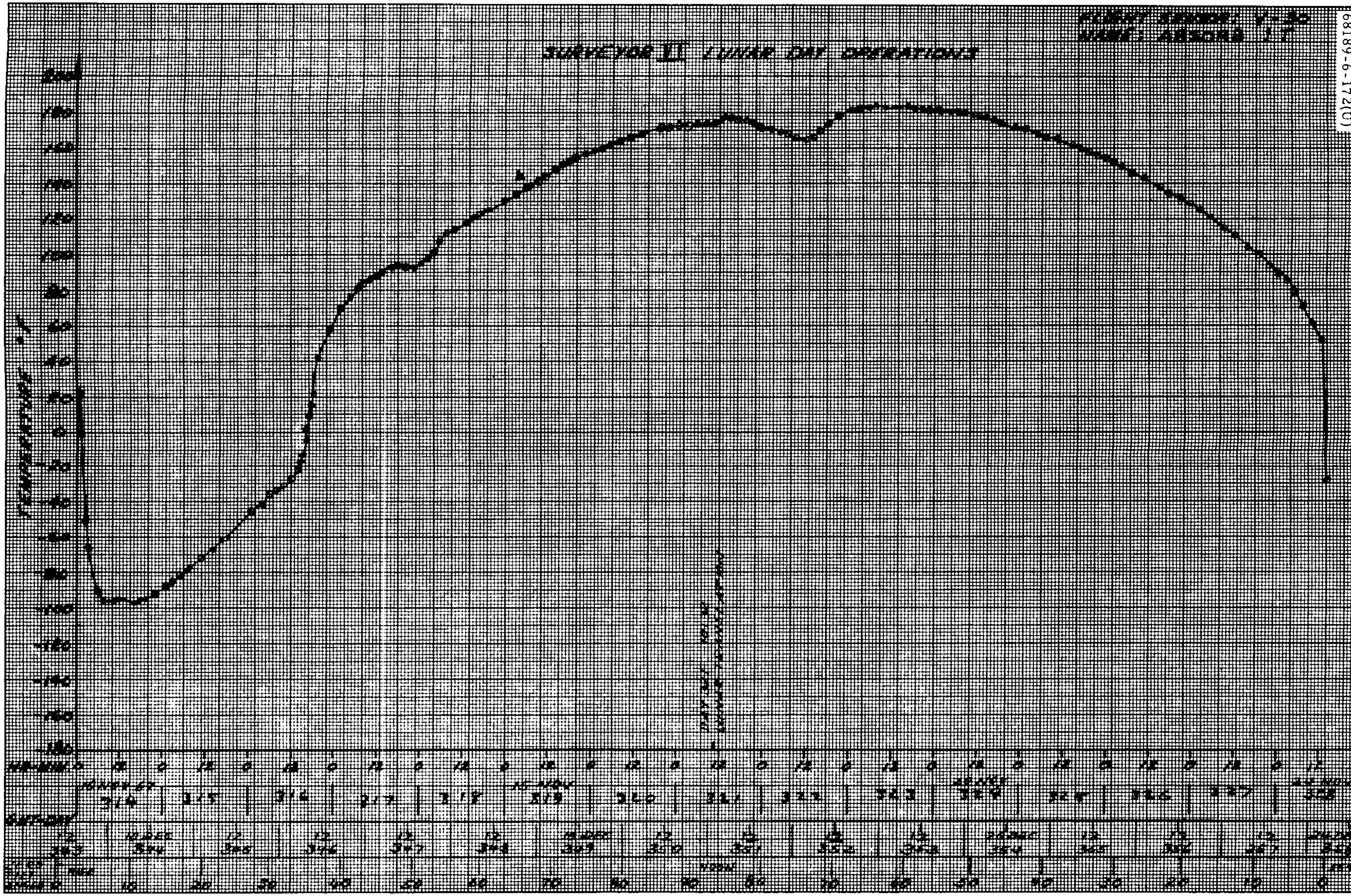

Figure 5. 1-B57. Sensor V-30: Shock Absorber 1

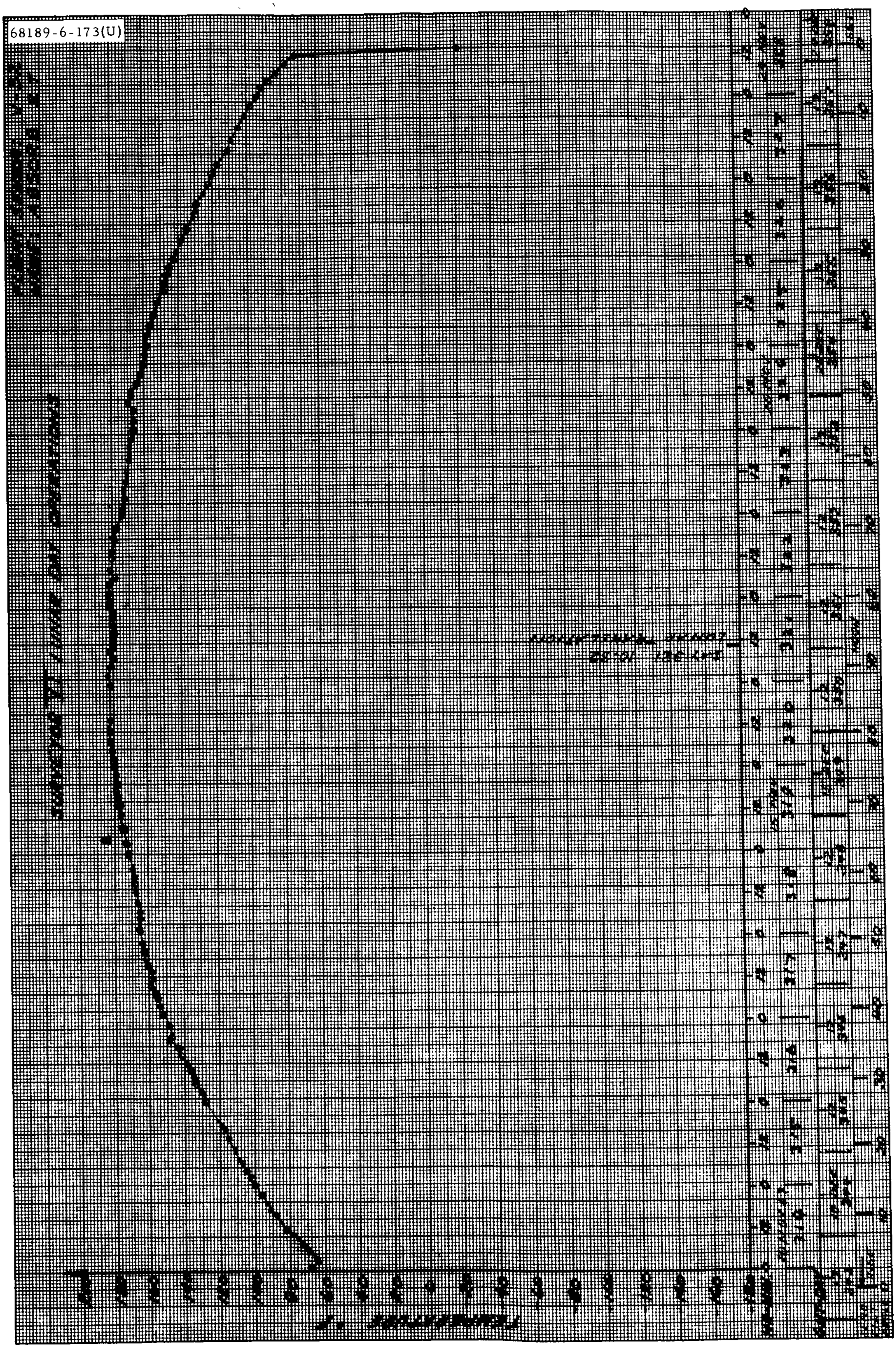

Figure 5.1-B58. Sensor V-32: Shock Absorber 2

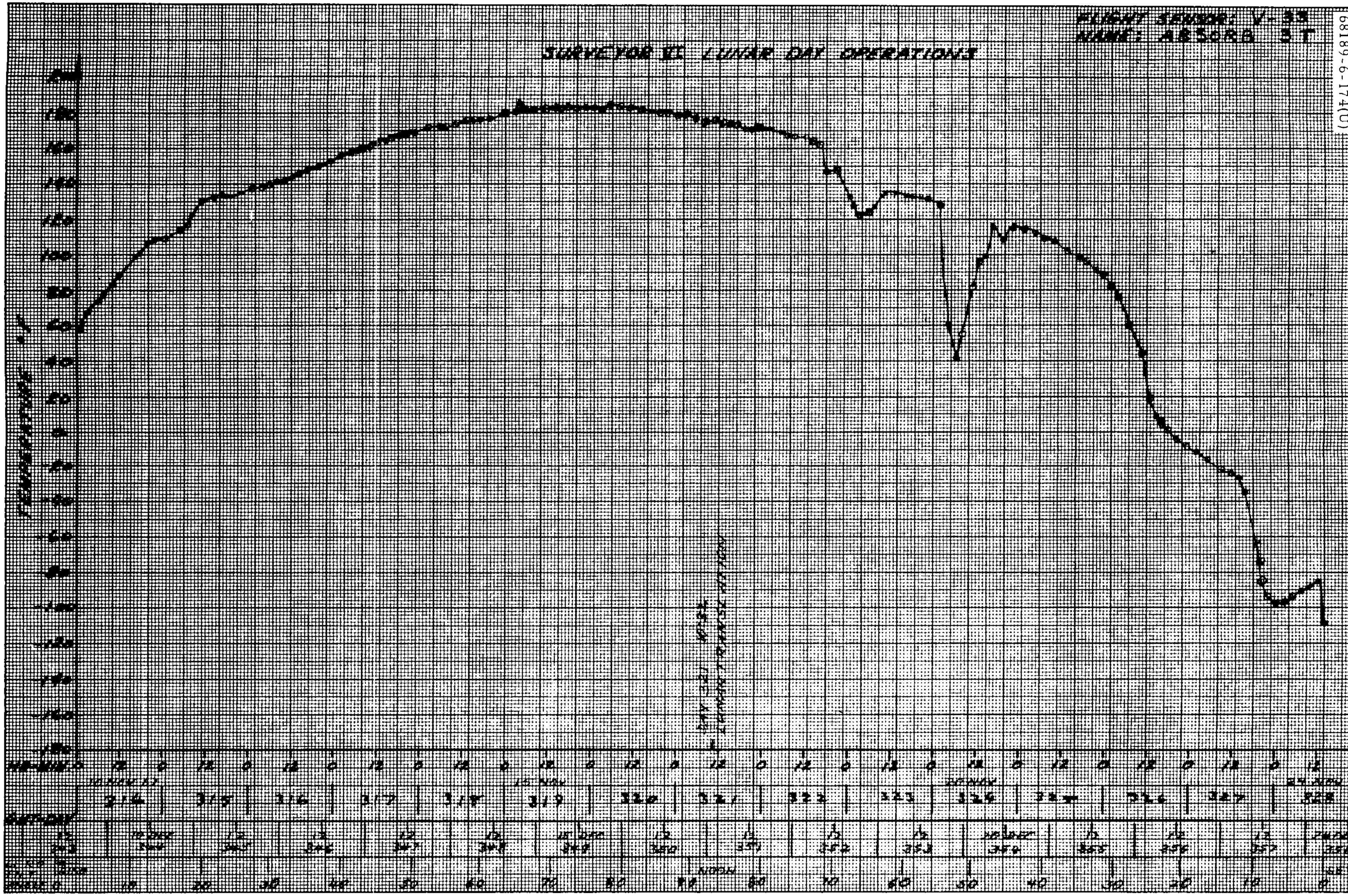

Figure 5. 1-B59. Sensor V-33: Shock Absorber 3

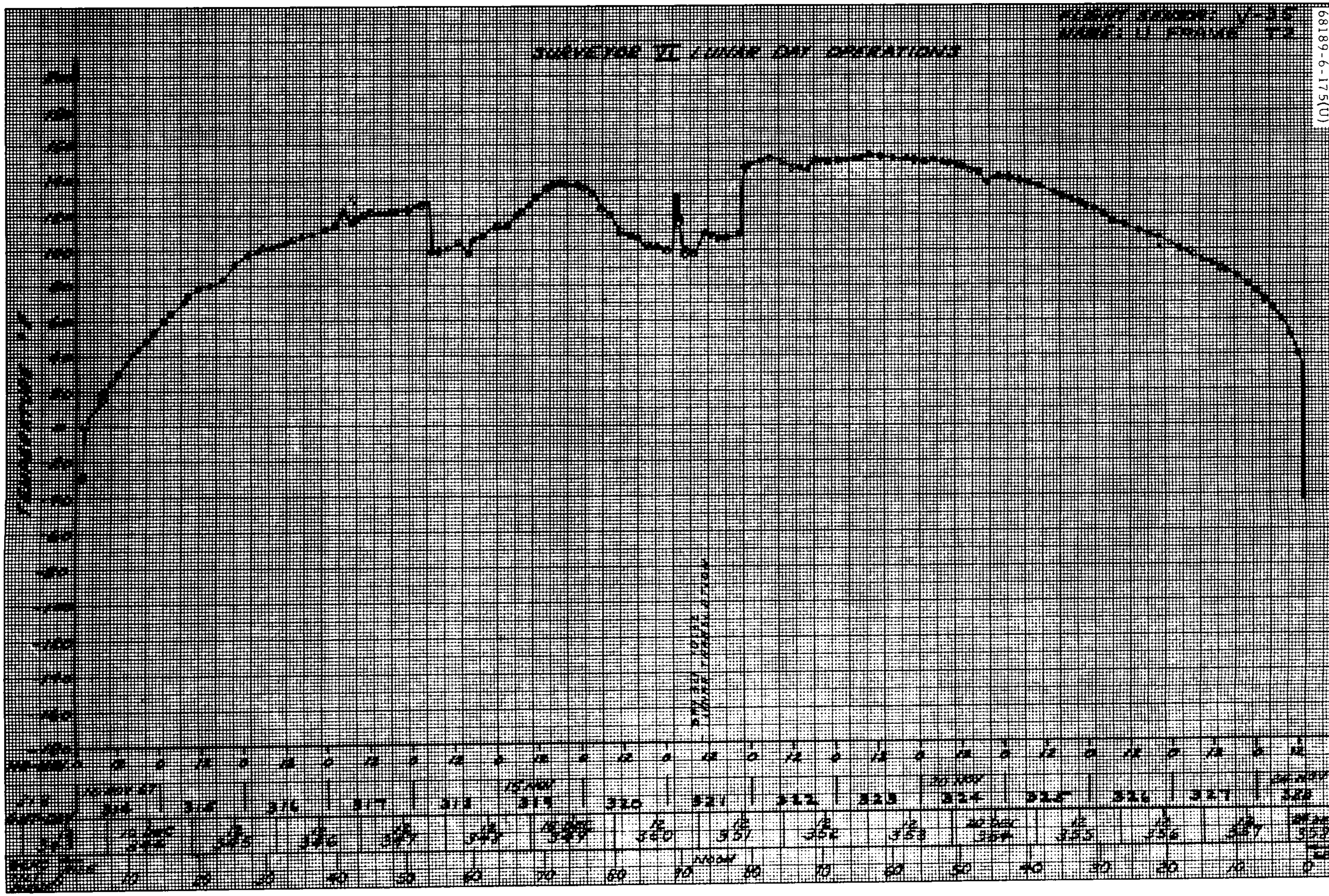

Figure 5.1-B60. Sensor V-35: Upper Spaceframe 2

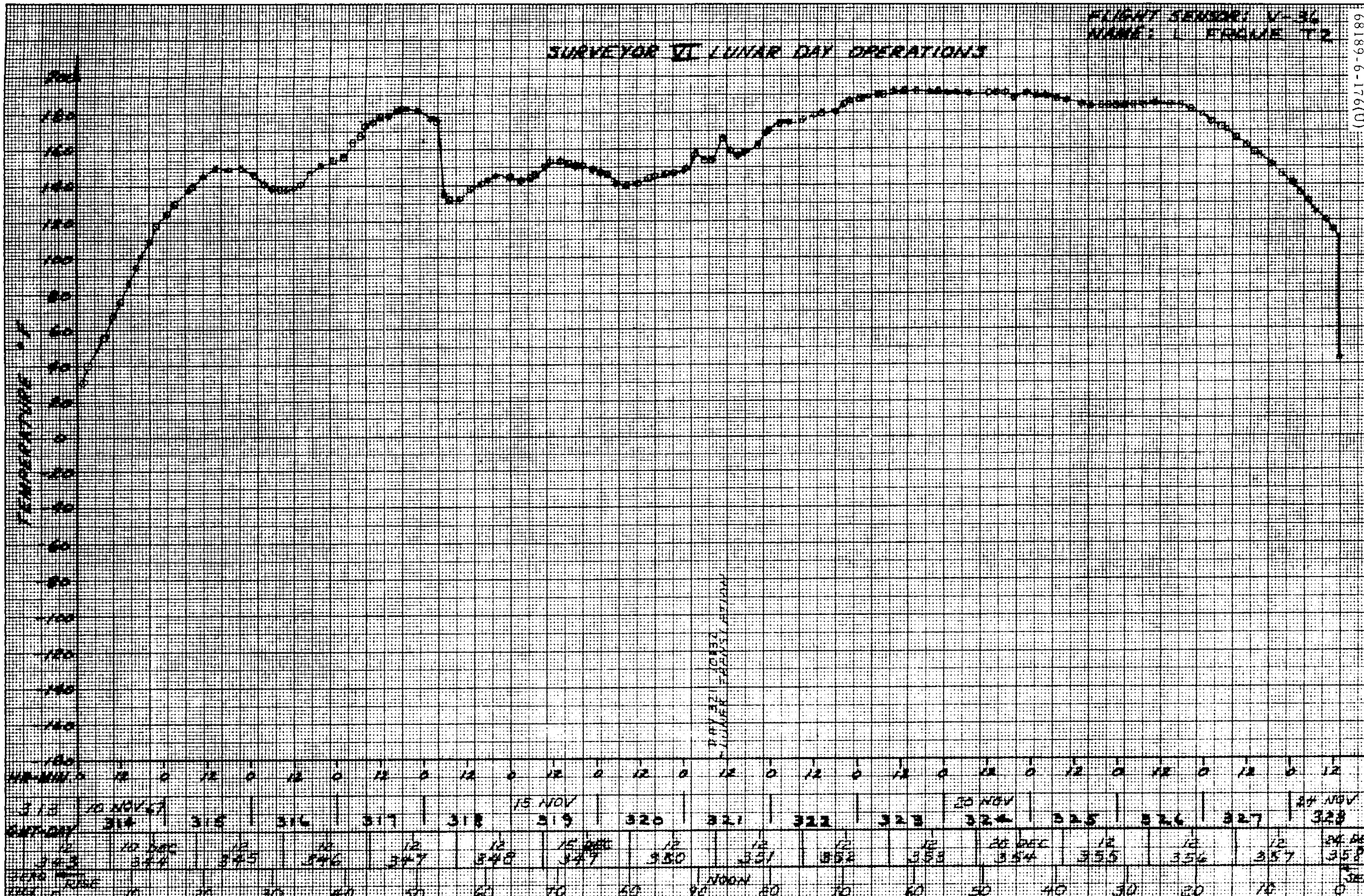

Figure 5.1-B61. Sensor V-36: Spaceframe Temperature Under Compartment 3

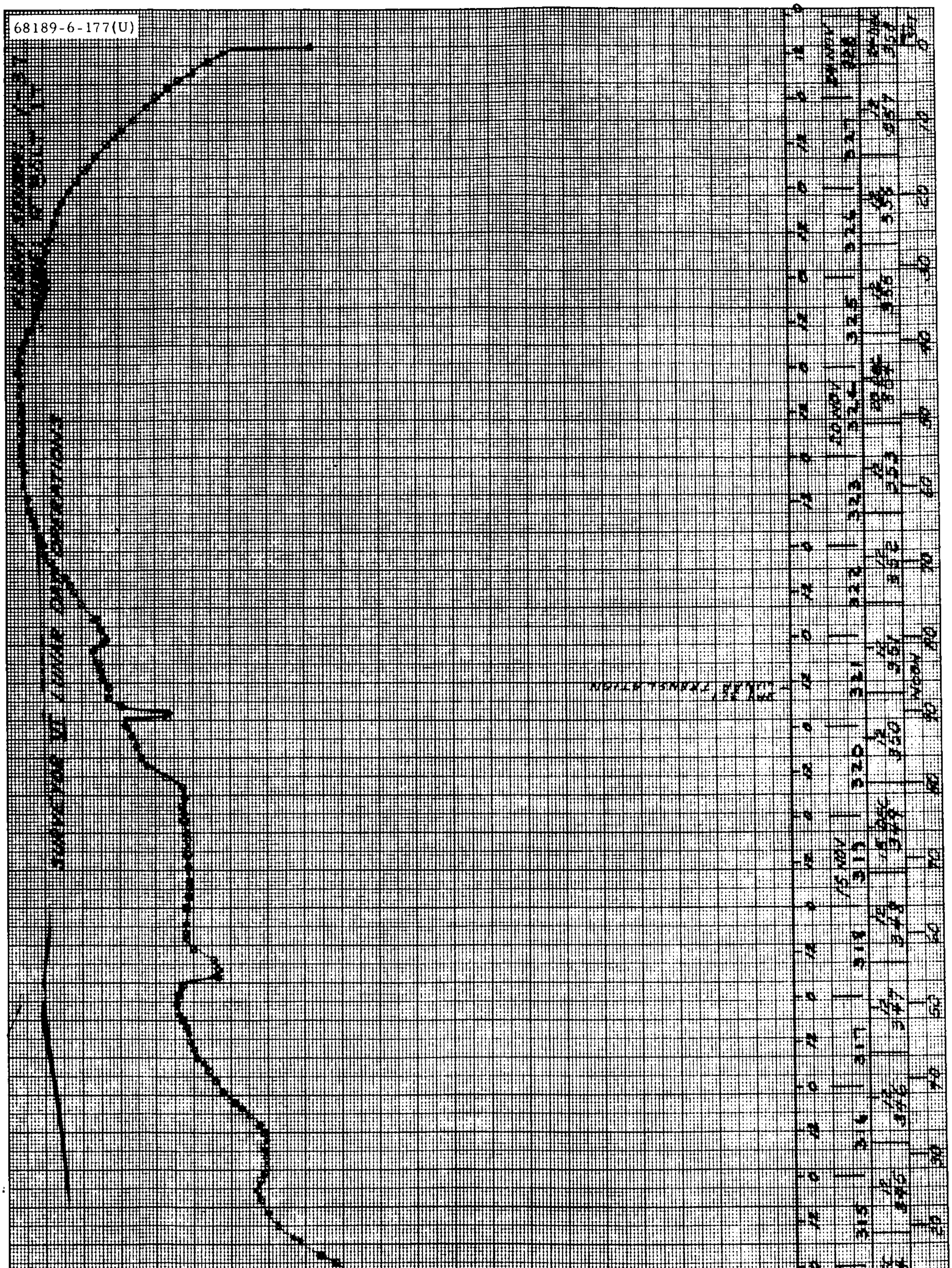

Figure 5.1-B62. Sensor V-37: Retro Attach Point 1

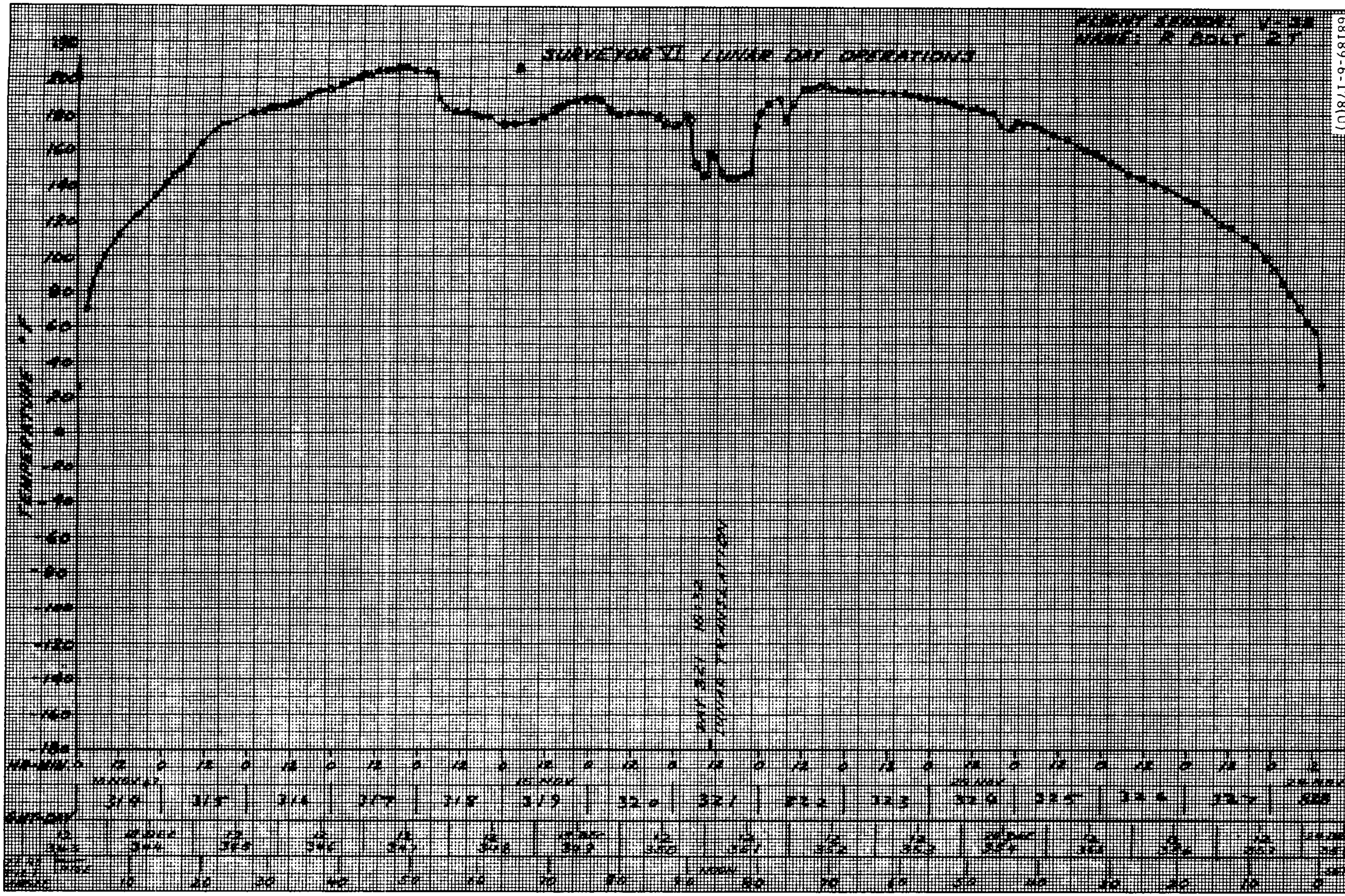

Figure 5.1-B63. Sensor V-38: Retro Attach Point 2

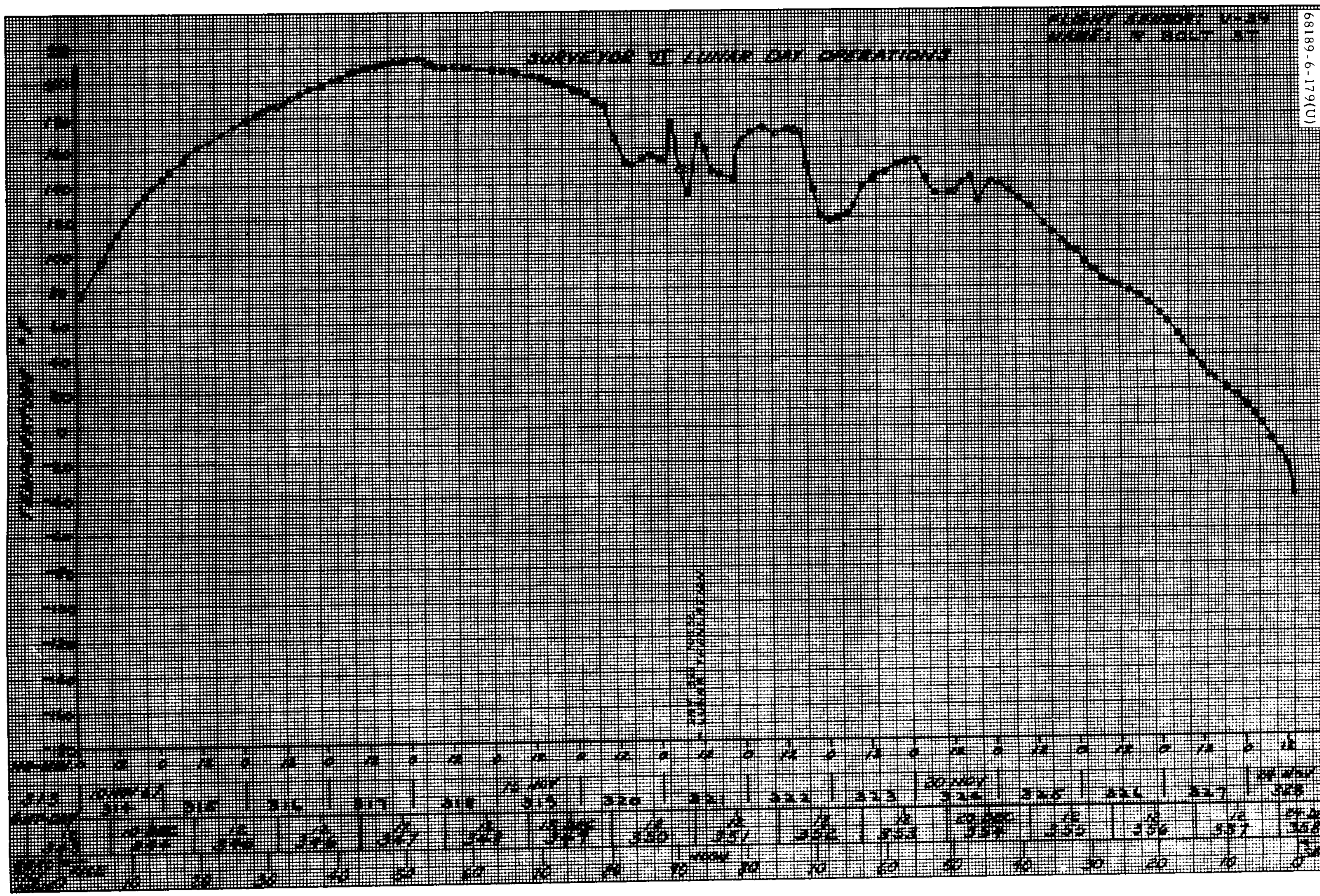

Figure 5.1-B64. Sensor V-39: Retro Attach Point 3

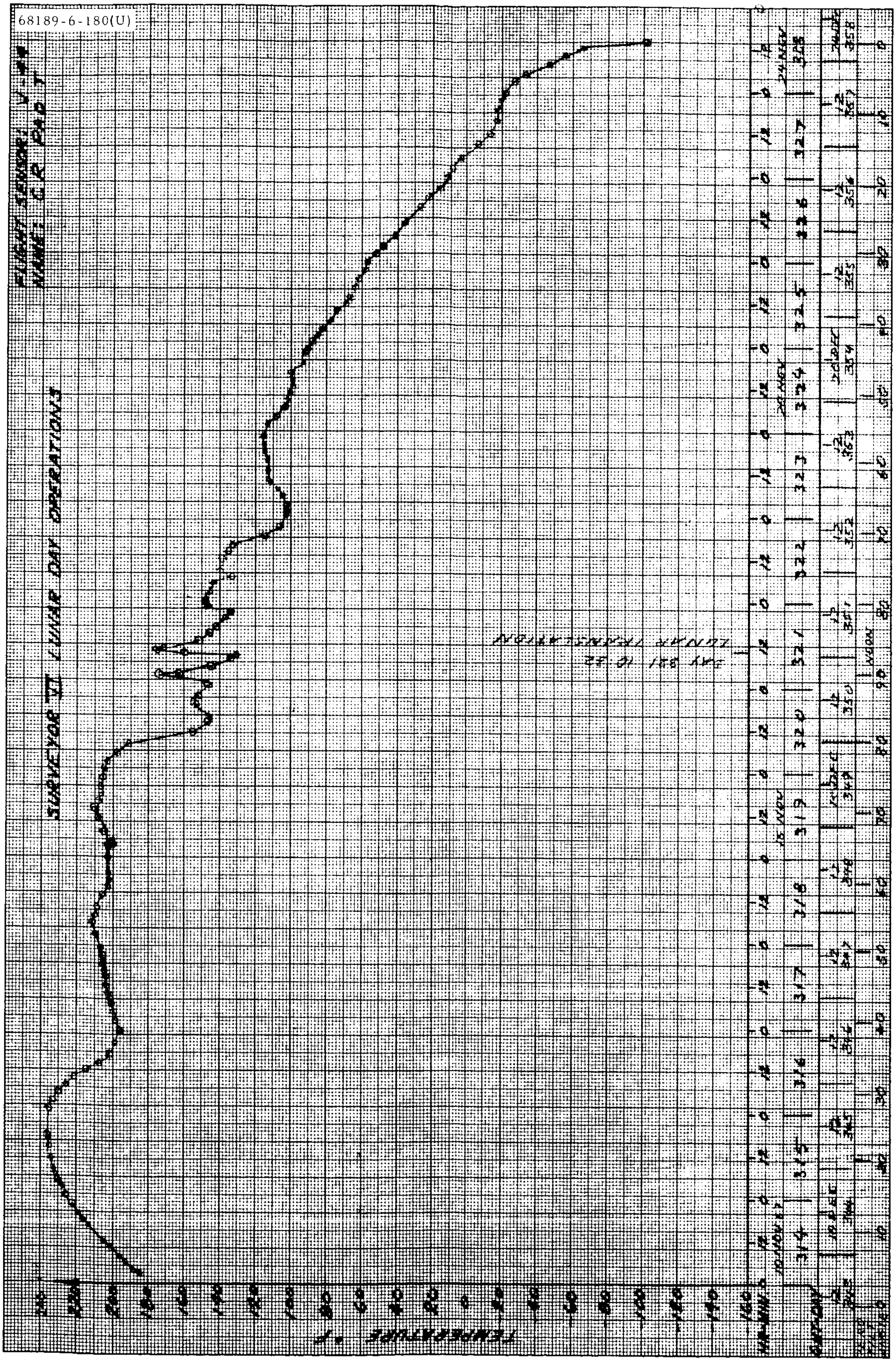

Figure 5.1-B65. Sensor V-44: Crushable Block

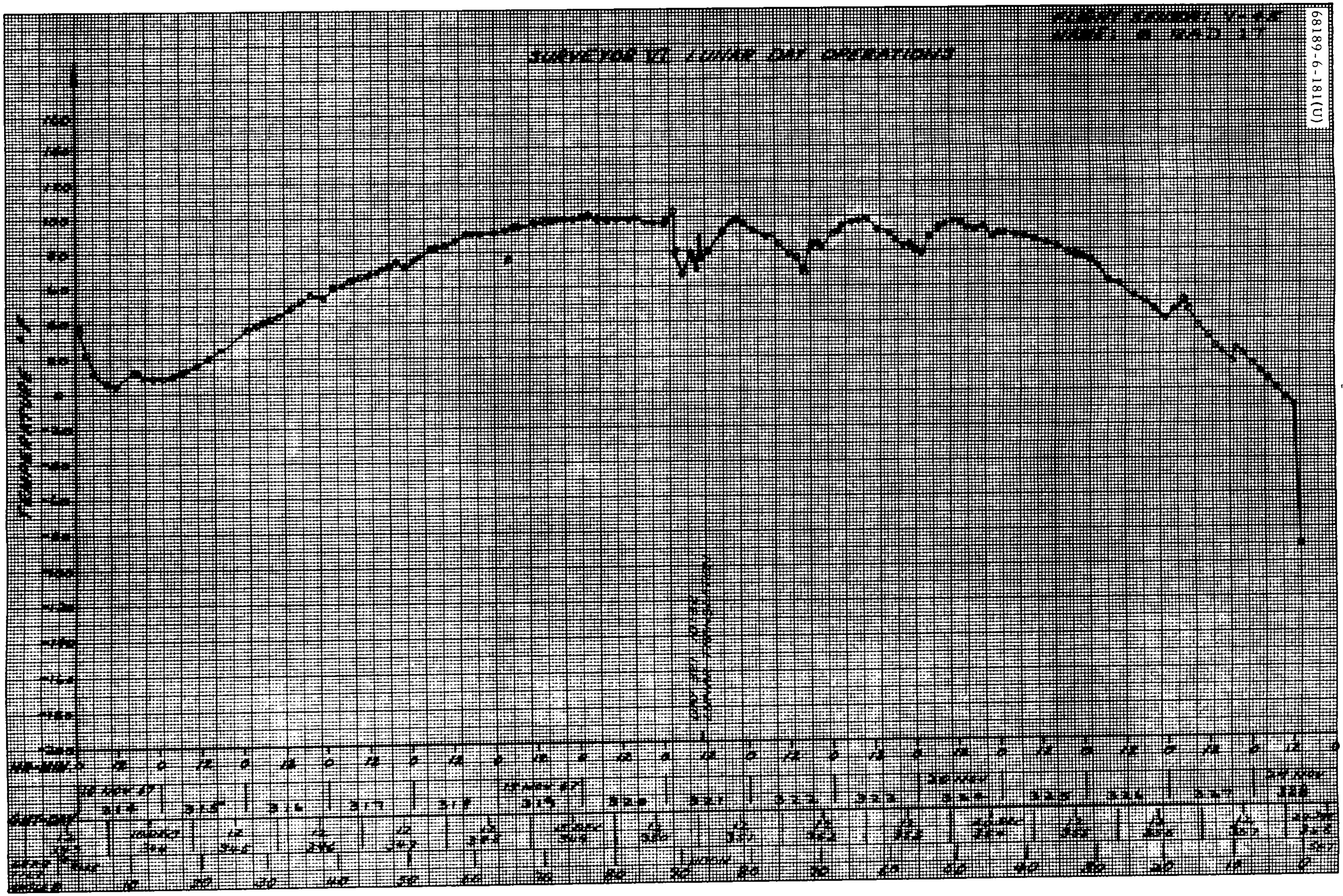

Figure 5.1-B66. Sensor V-45: Compartment B Switch 1 in Face Radiator

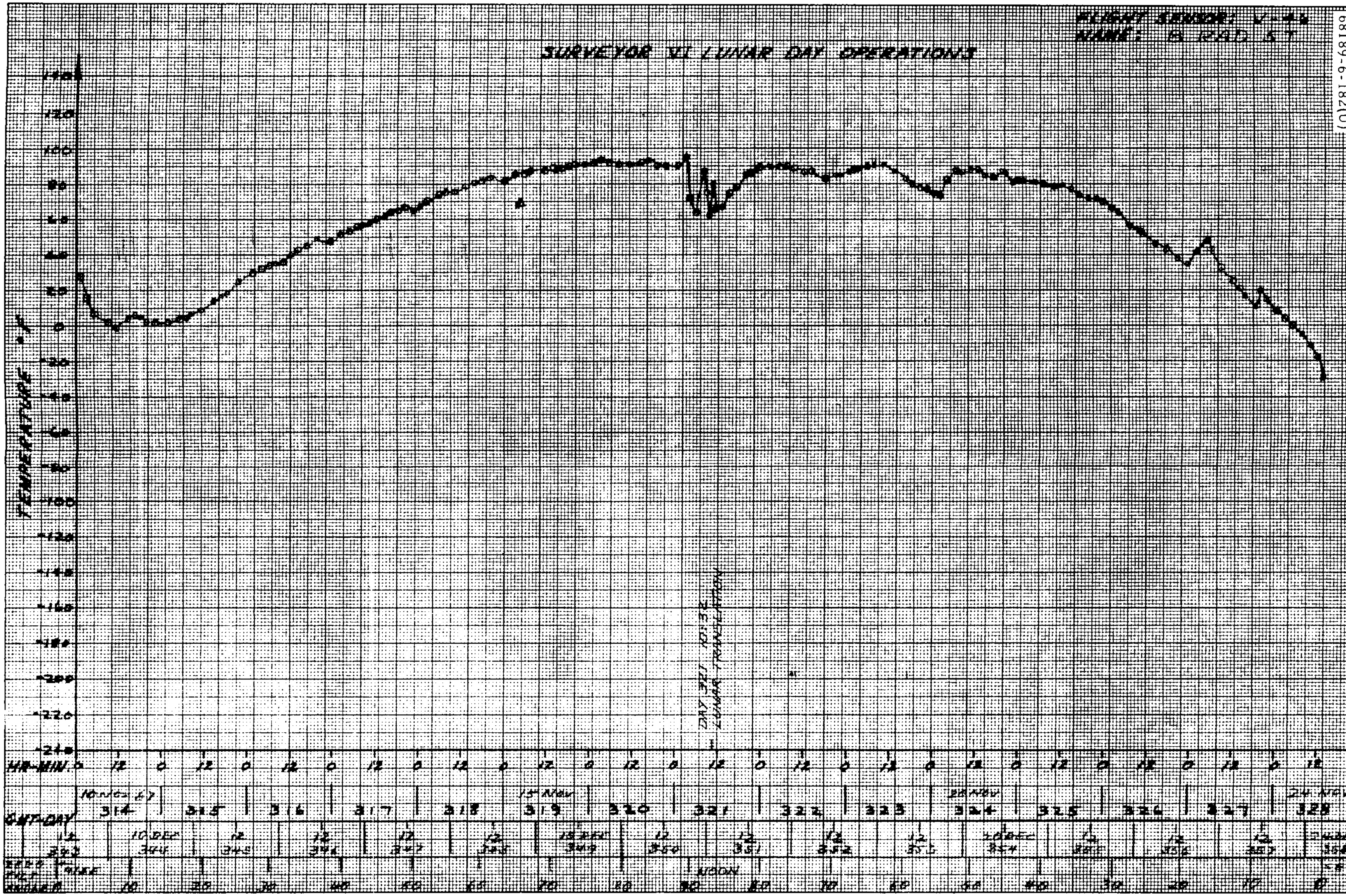

Figure 5. 1-B67. Sensor V-46: Compartment B Switch 5 in Face Radiator

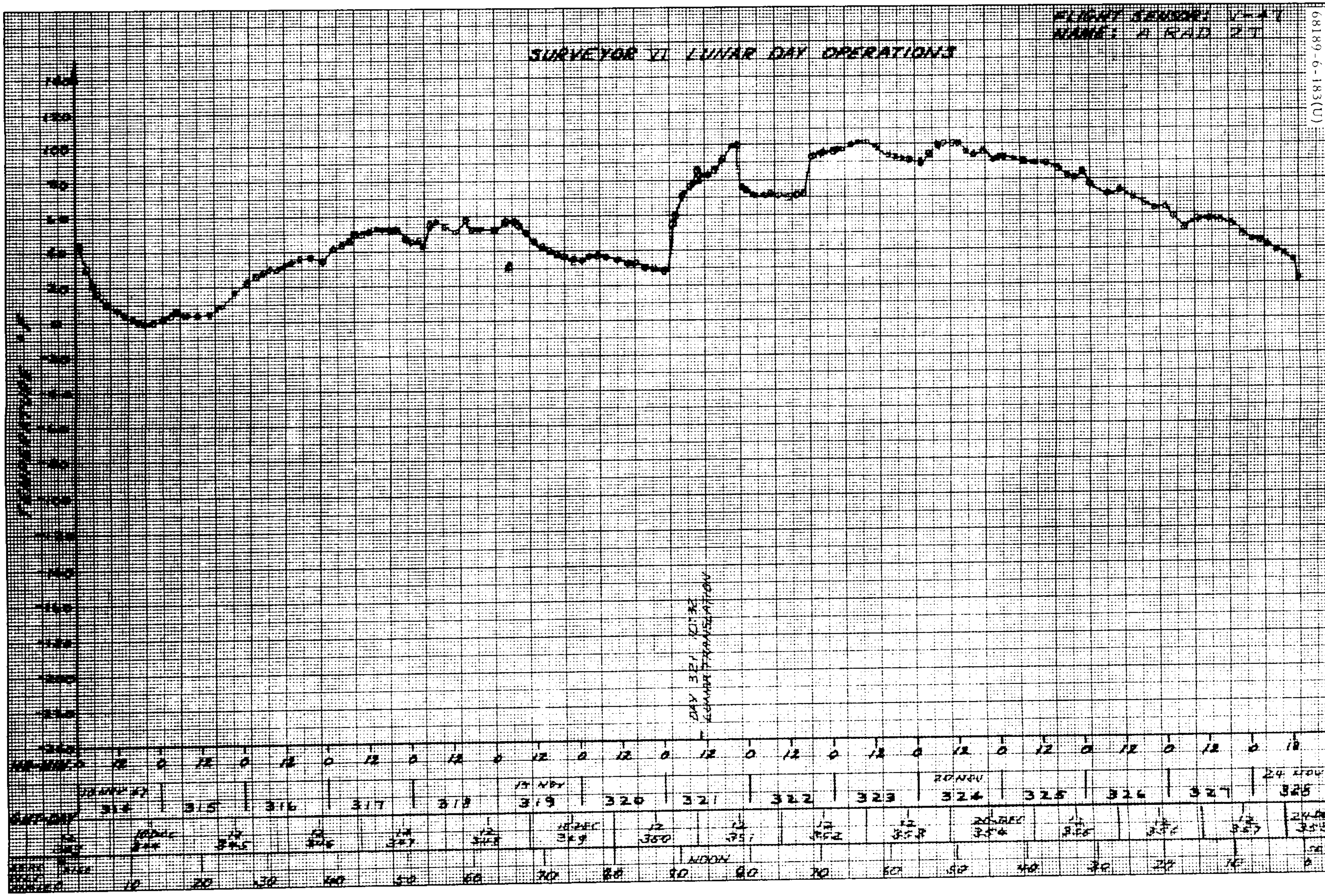

Figure 5.1-B68. Sensor V-47: Compartment A Switch 2 in Face Radiator

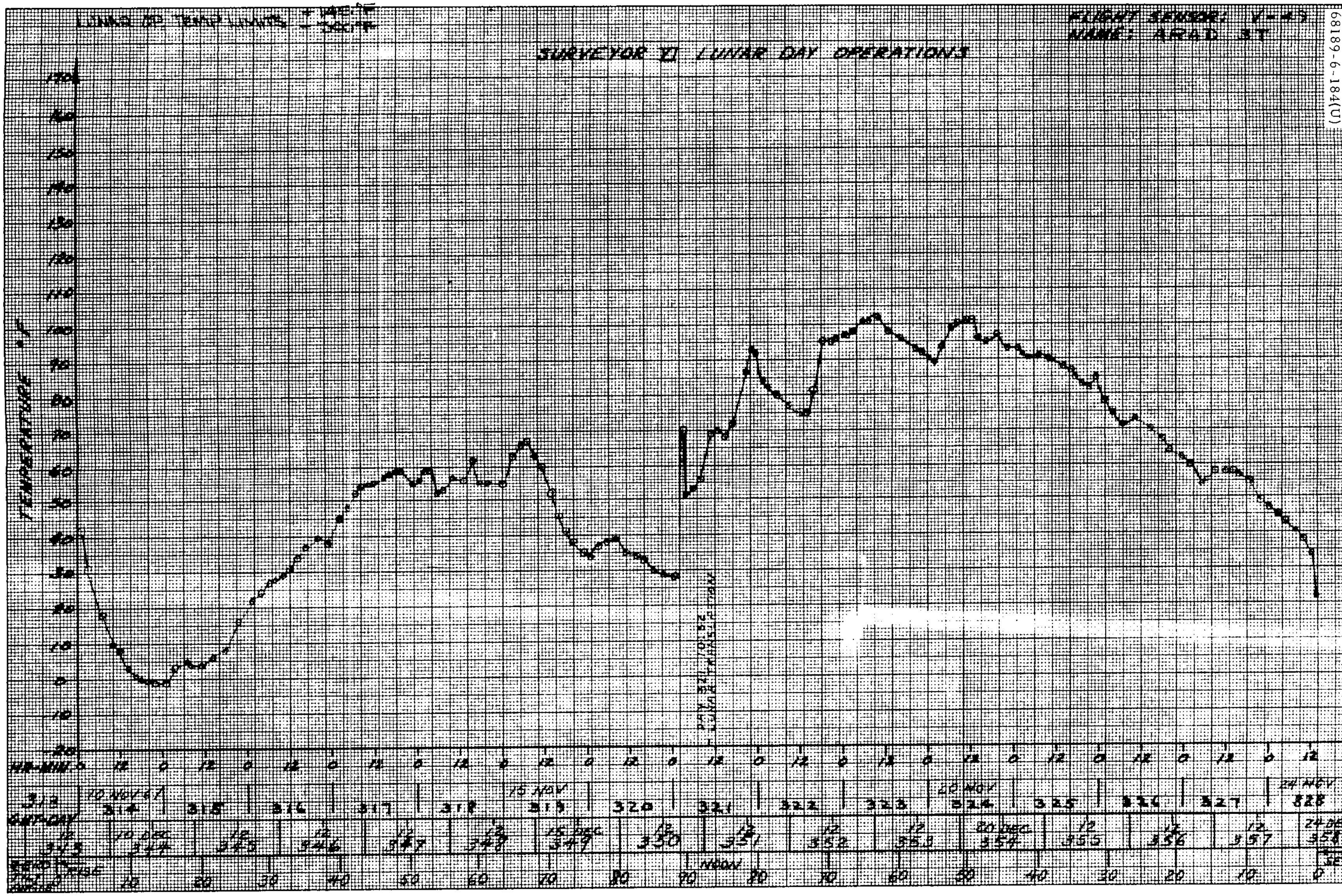

Figure 5. 1-B69. Sensor V-49: Compartment A Switch 3 in Face Radiator

5.2 ELECTRICAL POWER SUBSYSTEM

5.2.1 INTRODUCTION

The electrical power (EP) subsystem generates, stores, and controls electrical energy for distribution to other spacecraft subsystems. There are two sources for this energy: a storage battery, and radiant energy converted directly to electrical energy for system loads or battery charging. During transit, the primary source of power is radiant energy via the solar panels. Figure 5.2-1 shows associated equipment groupings.

Performance of the EP subsystem during the Surveyor VI flight and first lunar day operation was entirely nominal as compared to test data and simulation analysis predictions. Solar panel output power was approximately 4 percent above nominal, and can be in part attributed to the greater than nominal solar intensity characteristic for a September launch window.

With this increased solar panel output, battery power utilized for the mission was slightly below the prediction of 81 amp-hr. In all, 58 amp-hr were required from the battery for the transit portion of the mission.

The power subsystem responded properly to all earth commands and performed as anticipated.

In anticipation of the lunar translation experiment, at approximately 08:00 GMT on day 321 flight control power was commanded on to determine if the flight control unit was still operable. After approximately 35 minutes of operation, it was determined that the unit was capable of supporting the translation experiment, and flight control power was then removed. Flight control was again turned on at approximately 09:46 GMT. A/SPP stepping was initiated to stow the solar panel, at which time all solar power was lost. The spacecraft was then configured for the translation which occurred at approximately 10:32 GMT of day 321. Throughout the experiment, the power subsystem once again performed nominally. Minimum battery voltage was 21.01 volts for a maximum load current of 12.84 amperes.

Flight data were used to calculate solar panel power and regulator efficiencies. Analysis of specific loads, comparison to prediction, and an explanation of discrepancies will be made.

68189-6-40(U)

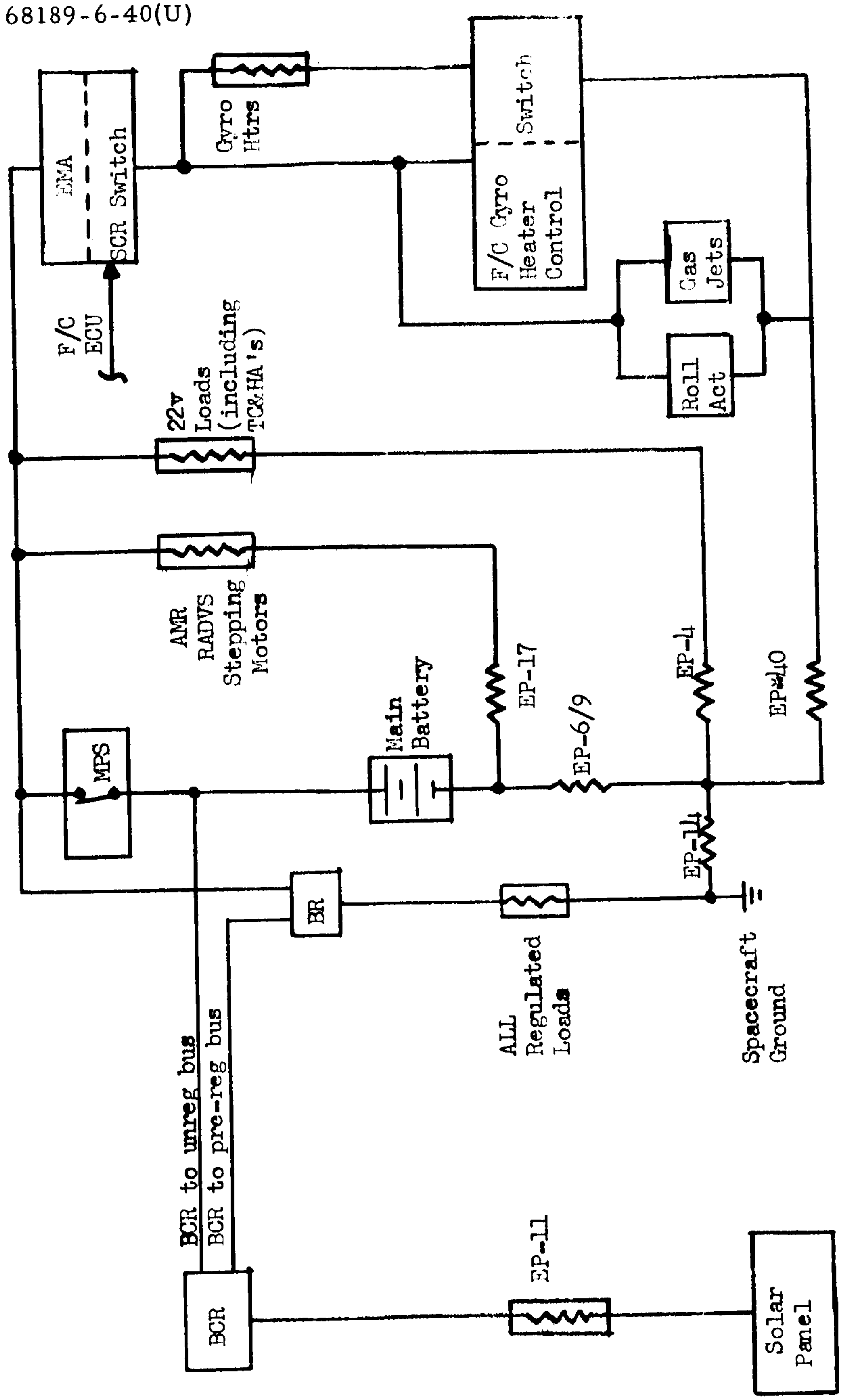

Figure 5.2-1. Power System Block Diagram, Flight Configuration

In Table 5.2-1, major events are presented in GMT. In general, the division of this table corresponds to flight phases of importance to the EP subsystem and may not correspond to flight phases in other subsections. The flight is divided into times corresponding to significant changes in electrical loads. Load changes corresponding to these flight phases are partially illustrated by the regulated current (EP-14) and more completely by the battery discharge current (EP-9).

TABLE 5.2-1. ELECTRICAL POWER EVENTS AND TIMES

GMT day:hr:min:sec		Comments
From	To	
311:07:39:02	311:08:04:20	Launch and separation
311:08:04:20	311:08:19:32	Transmitter high power
311:08:19:32	311:15:44:28	Coast
311:15:44:28	311:16:37:37	Coast, transmitter high power
311:16:37:37	312:01:51:32	Coast
312:01:51:32	312:02:17:15	Transmitter high power
312:02:17:15	312:02:20:00	Midcourse maneuver, transmitter high power, and flight control thrust phase power on
312:02:20:00	312:02:20:10	Vernier engine burn period, transmitter in high power
312:02:20:10	313:11:04:08	Coast
313:11:04:08	313:23:13:13	Coast, compartment A heater on
313:23:13:13	314:00:07:31	Compartment A heater off, coast
314:00:07:31	314:00:53:17	Transmitter high power, preretro maneuvers
314:00:53:17	314:01:06	Transmitter high power, AMR on, thrust phase power on, RADVS on, terminal descent, and touchdown

5.2.2 ANOMALY DESCRIPTION

No anomalies were detected in the electrical power subsystem during the transit or the first lunar day.

5.2.3 SUMMARY

5.2.3.1 Transit

The transit portion of the Surveyor VI mission was entirely nominal. The solar panel switch tripped six times during coast phase I. This is due to the fact that when all three IRU gyros are off, solar panel energy is sufficient to supply all spacecraft loads and also provides approximately 0.5 ampere of charge current. This current is cyclic in nature and, if fed to a battery that is on its upper plateau of charge (approximately 90 to 100 percent charged), then the unregulated lines will vary several volts due to the high internal impedance of the battery. When the battery voltage reaches 27.23 ± 0.07 volts, the solar panel switch will turn off. This phenomenon is normal and was predicted to occur during the early part of the mission. Minimum bus voltage during the mission was 19.16 volts with spacecraft loads at 42.65 amperes. This bus voltage is above the minimum requirement of 17.75 volts. Table 5.2-2 presents a summary of flight data for Surveyor VI compared to test data for the electrical power subsystem. Table 5.2-3 represents typical transit data.

5.2.3.2 Lunar

Lunar operation of the power subsystem was nominal and followed the pattern of previously landed spacecraft. With approximately 67 percent charge remaining in the battery at touchdown, the solar panel was not positioned directly on the sun until the last 24 hours of the lunar day. The solar panel was positioned at all times from approximately 15 to 45 degrees ahead of the sun to prevent solar current exceeding the desired battery charge rate.

No problems were encountered during the lunar translation experiment. During the experiment, the battery was the sole source of power and performed as anticipated. From all indications, it did not degrade at all as compared to the transit mission performance. Table 5.2-4 represents typical first lunar day data.

5.2.4 ANALYSIS

The analysis considers five areas: mission telemetry plots, lunar translation plots, power loads and sources budget, comparison of flight loads and flight acceptance test loads, and cyclic loads.

TABLE 5.2-2. ELECTRICAL POWER SUMMARY

Item	Flight Data	Predicted or Specification
Boost regulator efficiency, transmitter low power, percent	80.5	77 (minimum)
Boost regulator efficiency, transmitter high power, percent	87	82 (minimum)
Battery charge regulator efficiency	95.3	93.3 (minimum)
Battery charge regulator output energy, w-hr	5444	5171
Solar panel output power, watts	86.0	81 (minimum)
Battery energy used, w-hr	1276	1804
Total energy used, w-hr	6720	6975
<u>Selected loads:</u>		
Transmitter B high pwer, watts	58.7	58.0
Transmitter B filament power, watts	2.9	2.9
Flight control thrust phase power on		
Regulated, watts	33.7	35.09
Unregulated, watts	7.85	10.56
AMR on, watts	41.36	41.53
AMR enable, watts	31.02	31.60
RADVS power on, watts	532	551
Vernier ignition		
Midcourse, watts	34.03	39.6
Terminal descent, watts	32.34	39.6
Lunar translation, watts	30.88	34.98
Vernier line 2 heater, watts (32 percent duty cycle)	2.11	6.6 (maximum)
Altitude marking radar heater, watts (54 percent duty cycle)	2.86	5.04 (maximum)
Gyro heater, watts (30 percent duty cycle)	10.45	33.0 (maximum)

TABLE 5.2-3. TYPICAL COAST PHASE II DATA

Day 312, GMT hr:min:sec	Regulated Bus, volts (EP-1)	Unregulated Bus, volts (EP-2)	Battery Pressure, psi (EP-3)	Unregulated Current, amperes (EP-4)	Discharge Current, amperes (EP-6/9)	Difference Current, amperes (EP-7)	Solar Voltage, volts (EP-10)	Solar Current, amperes (EP-11)	Solar Temperature, °F (EP-12)	Regulated Current, amperes (EP-14)	Preregulated Bus, volts (EP-30)	FC Unregulated Current, amperes (EP-40)
00:09:00	28.99	22.42	14.7	0.650	1.130	0.184	30.2	2.879	126.5	1.805	29.97	0.723
01:03:00	28.99	22.48	14.7	0.350	0.910	0.184	30.2	2.874	126.5	1.805	29.97	1.215
01:29:00	28.99	25.15	14.7	0.110	0.670	0.208	30.2	2.879	126.5	1.805	29.97	0.793
02:34:00	28.94	21.71	14.7	0.330	2.55	0.776	30.6	2.827	126.5	3.897	29.87	0.155
03:55:09	28.99	22.51	14.7	0.110	-0.028	0.184	30.2	2.868	126.5	1.805	29.97	0.793
04:40:40	28.99	22.01	14.7	0.650	0.708	0.185	30.2	2.868	126.5	1.772	29.97	0.601
05:26:08	28.99	22.28	14.7	0.350	0.125	0.184	30.2	2.868	126.5	1.772	29.97	0.656
06:03:11	28.99	22.52	14.7	0.110	-0.080	0.184	30.2	2.879	126.5	1.805	29.97	0.711
06:40:03	28.99	22.47	14.7	0.110	-0.193	0.184	30.2	2.879	126.5	1.805	29.97	0.564
07:10:03	28.99	22.37	14.7	0.350	0.198	0.184	30.2	2.879	126.5	1.805	29.97	0.739
07:40:03	28.99	22.15	14.7	0.419	0.244	0.185	30.2	2.874	126.5	1.805	29.97	0.612
08:18:23	28.94	22.27	14.7	0.360	0.195	0.185	30.2	2.879	126.5	1.813	29.97	0.501

TABLE 5.2-4. TYPICAL LUNAR DAY DATA

Day 319, GMT hr:min:sec	Regulated Bus, volts (EP-1)	Unregulated Bus, volts (EP-2)	Battery Pressure, psi (EP-3)	Unregulated Current, amperes (EP-4)	Discharge Current, amperes (EP-6/9)	Difference Current, amperes (EP-7)	Solar Voltage, volts (EP-10)	Solar Current, amperes (EP-11)	Solar Temperature, °F (EP-12)	Regulated Current, amperes (EP-14)	Preregulated Bus, volts (EP-30)	FC Unregulated Current, amperes (EP-40)
00:21:12	28.94	27.21	15.1	-	-0.76	0.325	27.2	1.754	212.5	0.767	29.97	-
02:57:13	28.94	27.00	15.3	-	-0.67	0.342	27.0	1.766	211.6	0.825	29.97	-
05:34:05	28.94	26.82	15.1	-	-0.67	0.348	26.8	1.766	208.8	0.825	29.97	-
07:07:30	28.94	26.77	15.1	-	-0.62	0.348	26.8	1.760	207.9	0.859	29.97	-
08:22:50	28.94	27.03	15.1	-	-0.57	0.348	27.1	1.708	207.9	0.859	29.97	-
09:25:15	28.94	27.15	15.3	-	-0.57	0.336	27.2	1.672	207.9	0.859	29.97	-
11:04:09	28.94	26.79	15.1	-	-0.59	0.348	26.8	1.725	207.9	0.859	29.97	-
12:21:00	28.94	27.12	15.1	-	-0.54	0.336	27.2	1.637	207.0	0.859	29.97	-
13:50:00	28.94	27.06	15.1	-	-0.54	0.348	27.1	1.637	206.1	0.859	29.97	-
16:15:00	28.94	27.15	15.1	-	-0.50	0.336	27.2	1.649	205.2	0.859	29.97	-
18:14:00	28.94	27.15	15.1	-	-0.47	0.336	27.2	1.614	204.3	0.859	29.97	-
19:20:00	28.94	27.18	15.1	-	-0.59	0.325	27.2	1.590	203.4	0.767	29.97	-

5.2.4.1 Mission Telemetry Plots

Figures 5.2-2 through 5.2-7 are plots for approximately the last 4 hours of the transit mission, which are pertinent to the EP subsystem. They represent line plots of the analog signals averaged at 1-minute intervals. With the scales used, and the averaging, these plots provide a good indication of spacecraft trends, and allow identification of pertinent spacecraft functions. Many annotations have been made on these plots identifying spacecraft responses to ground and on-board commands. Figure 5.2-8 gives radar loads during the terminal phase. Identified on the plot is AMR power on and AMR enabled, AMR off prior to RADVS turn-on, and RADVS time in.

5.2.4.2 Power Loads and Sources Budget

Energy Used

Table 5.2-2 contains a summary of energy expended as calculated from flight telemetry data. Solar panel output power was approximately 2.4 percent greater than for Surveyor V due to an increase in solar intensity (142 instead of 138 mv/cm^2). Energy supplied by the battery was therefore below the 81 amp-hr predicted.

Power Data

Figures 5.2-9 through 5.2-12 represent various power parameter plots for approximately the last 4 hours prior to and including touchdown. Changes in power can be identified with changes in current level in the telemetry plots.

Efficiency calculations were made using the following formulas (Table 5.2-2):

1) BCR Efficiency

$$\mathrm{Eff}_{BCR} = \frac{(EP\text{-}30)\,(EP\text{-}11 - 0.125)}{(EP\text{-}10)\,(EP\text{-}11)} \times 100$$

where (EP-11 - 0.125) is the output of the BCR. EP-11 represents solar panel output current, with 0.125 amp assumed loss in the BCR. No shunt is provided to measure actual BCR output current.

2) BR Efficiency

a) For EP-14 less than the BCR output:

$$\mathrm{Eff}_{BR} = \frac{(EP\text{-}1)(EP\text{-}14) + (EP\text{-}2)(EP\text{-}11 - 0.125 - EP\text{-}14/0.92)}{(EP\text{-}30)(EP\text{-}11 - 0.125) + (EP\text{-}2)(EP\text{-}7)} \times 100$$

where EP-14/0.92 represents input to the postregulator (postregulator efficiency is estimated at 92 percent).

b) For EP-14 greater than the BCR output:

$$Eff_{BR} = \frac{(EP\text{-}1)\ (EP\text{-}14)}{(EP\text{-}30)(EP\text{-}11 - 0.125) + (EP\text{-}2)[EP\text{-}7 + EP\text{-}14/0.92 - (EP\text{-}11 - 0.125)]}$$

5.2.4.3 Comparison of Flight Loads and Flight Acceptance Test Loads

Comparison of telemetry-measured and flight acceptance test measured loads (Reference 1) are listed in Table 5.2-5. It can be seen that flight data compare quite closely with FAT data. For unregulated loads, FAT data represents currents obtained when the bus voltage was set at 22 volts, but in flight the unregulated bus voltage depends on mission phase and is usually slightly less than 22 volts.

5.2.4.4 Cyclic Loads

Gyro Heater

The periodic changes that occur in EP-40 are due to gyro heater cycling. The gyro heaters have a short on-off cycle compared to the altitude marking radar (AMR) and vernier line heaters (EP-4). All three gyro heater loads were determined to be 0.48 ampere, comparing favorably with the flight acceptance test data.

AMR, Vernier Lines, TV, and Compartment C Heaters

Figure 5.2-13 is a plot of unregulated current. The cyclic load effects of the vernier line 2 heater are apparent. Also, cycling in the 50-minute plot are AMR heater, TV mirror assembly, and compartment C heaters. Approximate current levels for each heater are noted on the plot. Although not a cyclic load, compartment A heater turn-off has also been noted on the plot.

5.2.4.5 Lunar Translation Plots

Figures 5.2-14 through 5.2-16 represent plots for the burn period of the translation experiment. These plots show all data points obtained and, in the case of battery discharge current (EP-9), provide a rough approximation of cyclic loads with the solenoid current clearly identified.

TABLE 5.2-5. SELECTED EQUIPMENT LOADS

Spacecraft Load Change*	Command Time, GMT, day:hr:min:sec	Current, milliamperes		Power, watts	
		Flight	Specification (Reference 1)	Flight	Specification (Reference 1)
Flight control thrust phase power on					
R	Midcourse	1162	1210	33.7	35.09
U	312:02:17:17	383	480	7.9	10.56
R	Terminal	1162	1210	33.7	35.09
U	314:00:54:17	447	480	9.39	10.56
Transmitter B high voltage on	312:01:51:19				
R		2025	2000	58.7	58.0
Filament B power on	312:01:49:27				
R		100	100	2.9	2.9
Vernier ignition					
U	Midcourse 312:02:20:02	1660	1800	34.03	39.6
U	Terminal 314:00:57:52	1680	1800	32.34	39.6
AMR on	314:00:53:17				
U		2000	1886	41.36	41.53
AMR enable	314:00:56:17				
U		1500	1439	31.02	31.60
RADVS power on	314:00:58:16				
U		27700	29000	532	551

*R = regulated; U = unregulated.

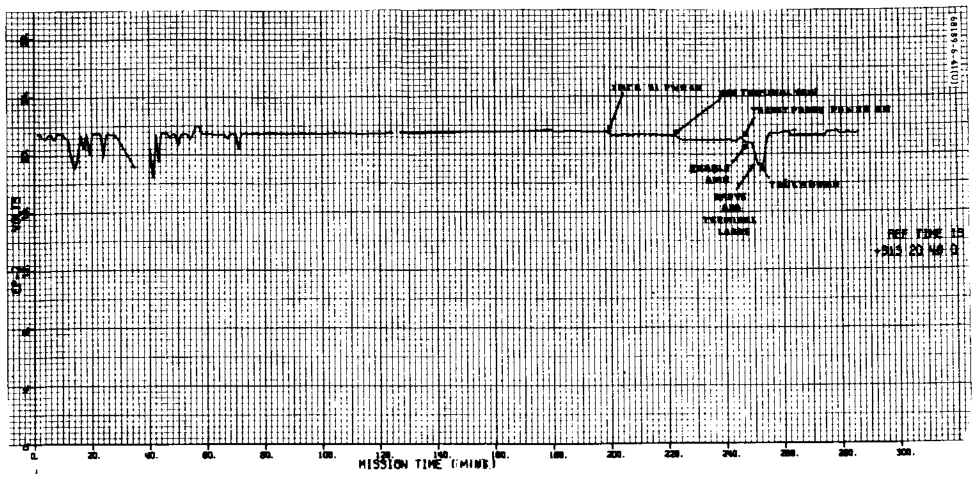

Figure 5.2-2. Sensor EP-2: Unregulated Bus Voltage

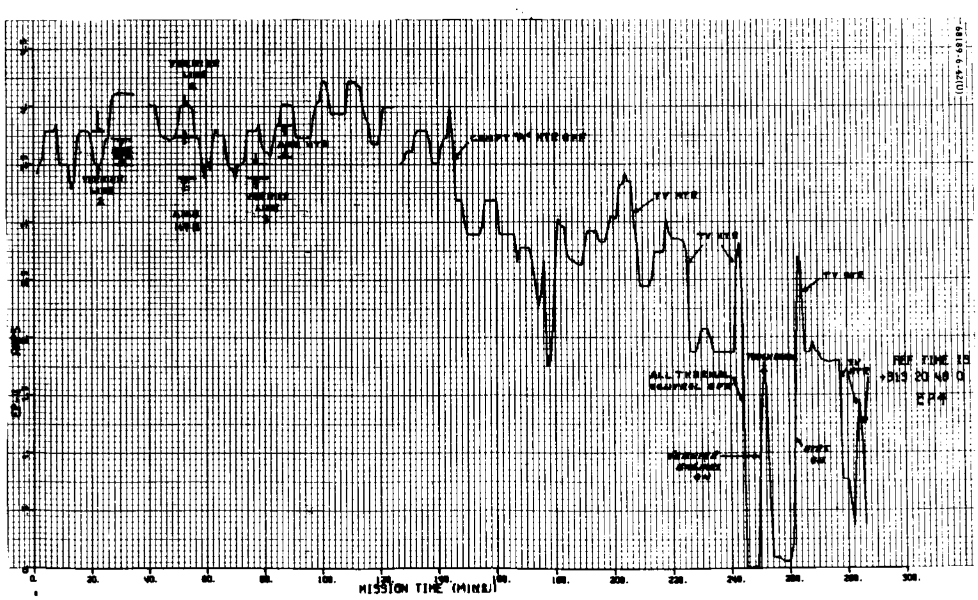

Figure 5.2-3. Sensor EP-4: Unregulated Output Current

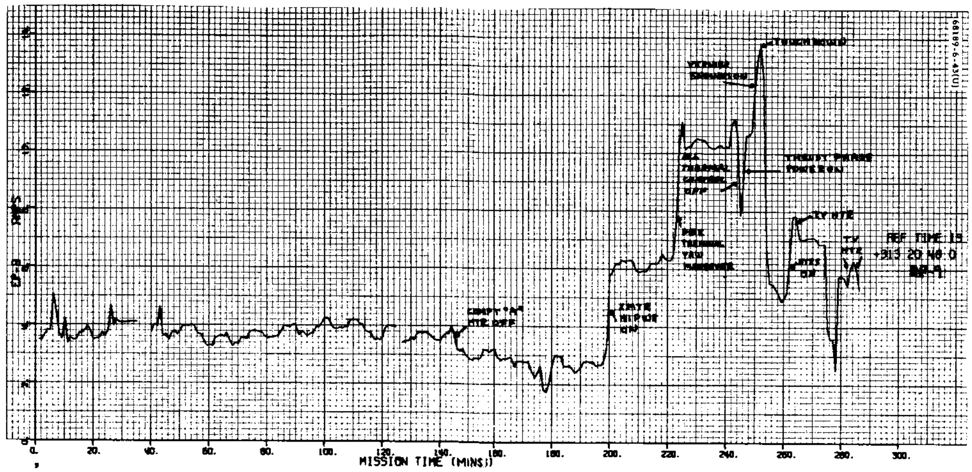

Figure 5.2-4. Sensor EP-9: Battery Discharge Current

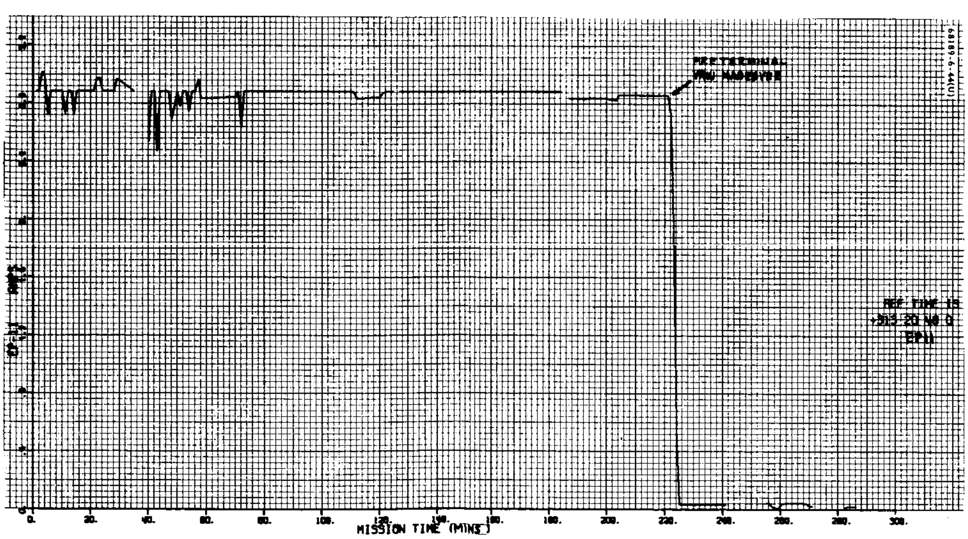

Figure 5.2-5. Sensor EP-11: Solar Cell Array Current

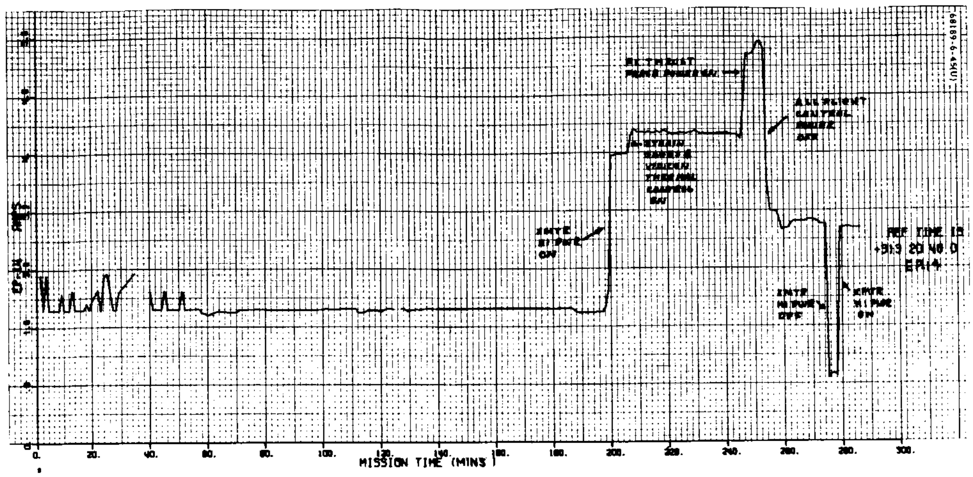

Figure 5. 2-6. Sensor EP-14: Regulated Output Current

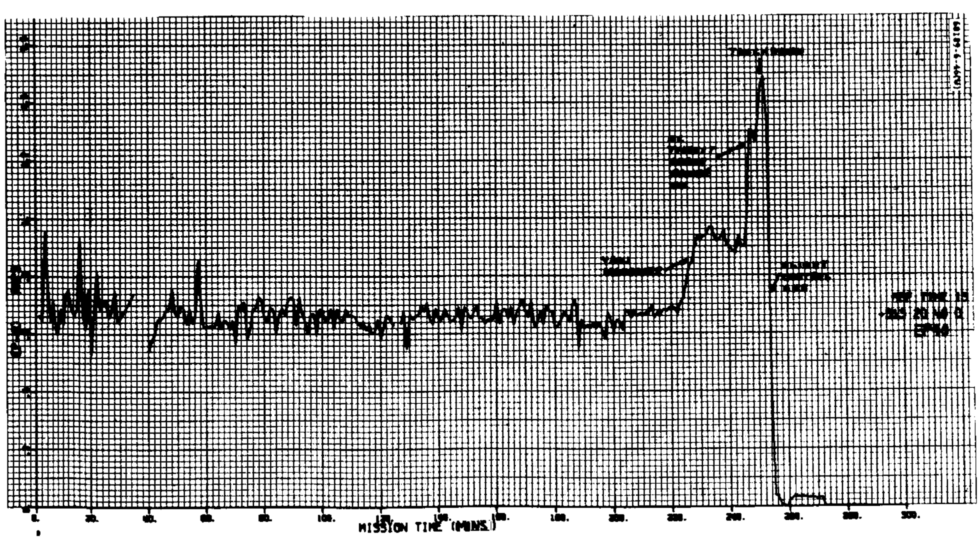

Figure 5. 2-7. Sensor EP-40: Flight Control Unregulated Current

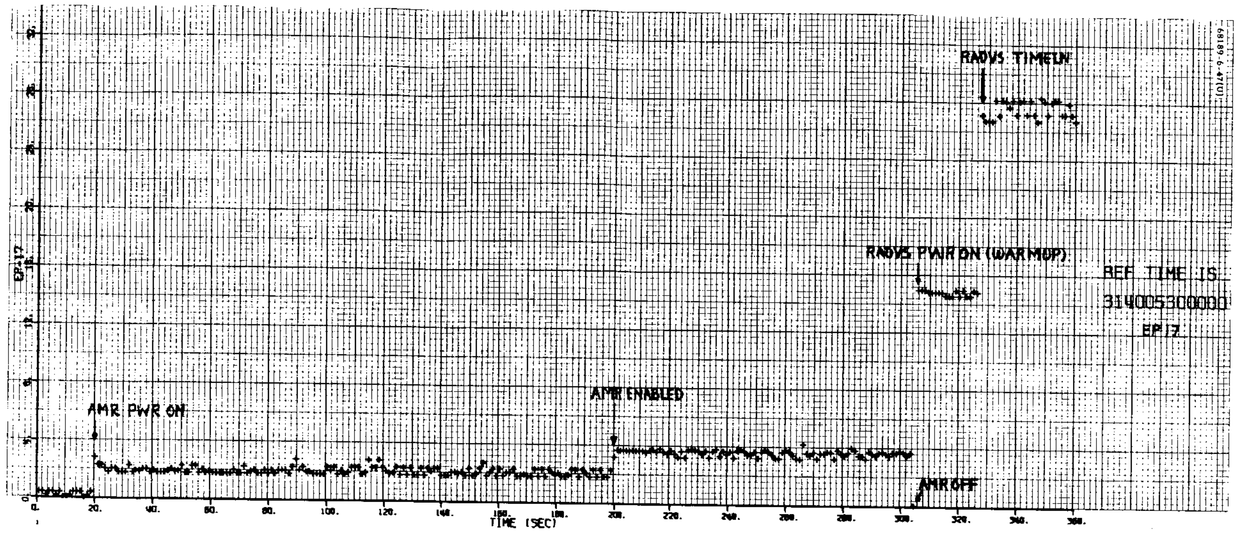

Figure 5.2-8. Radar and Squib Current On (RADVS Power On)

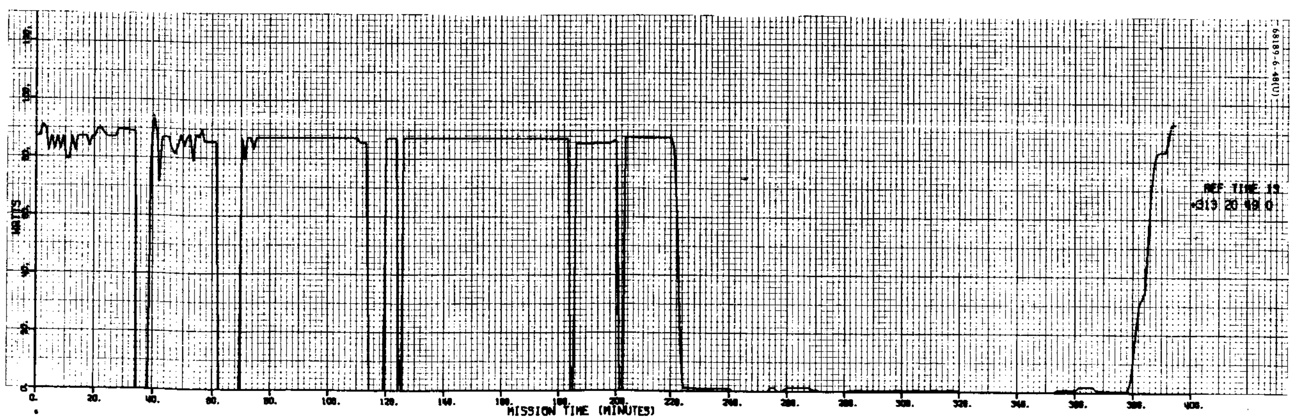

Figure 5.2-9. Solar Panel Power

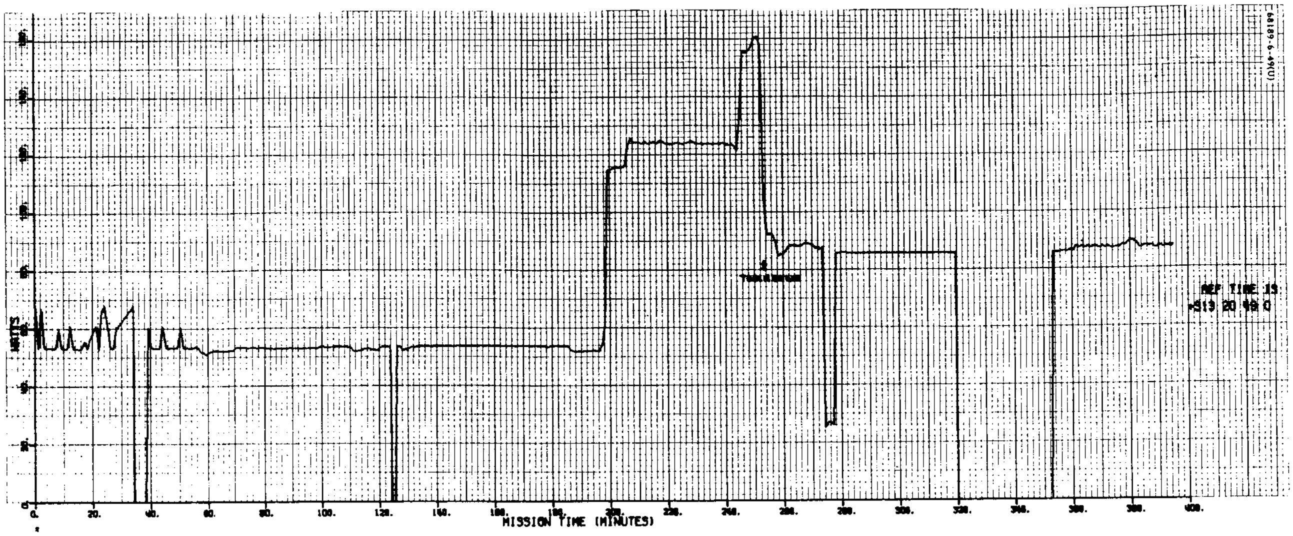

Figure 5.2-10. Regulated Power

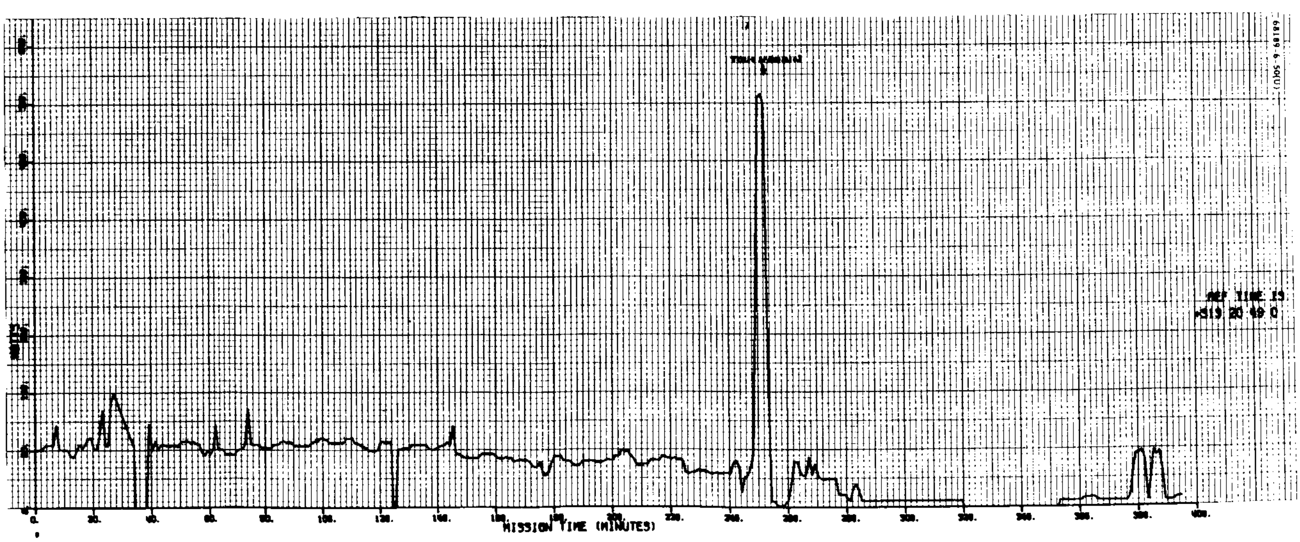

Figure 5.2-11. Unregulated Power

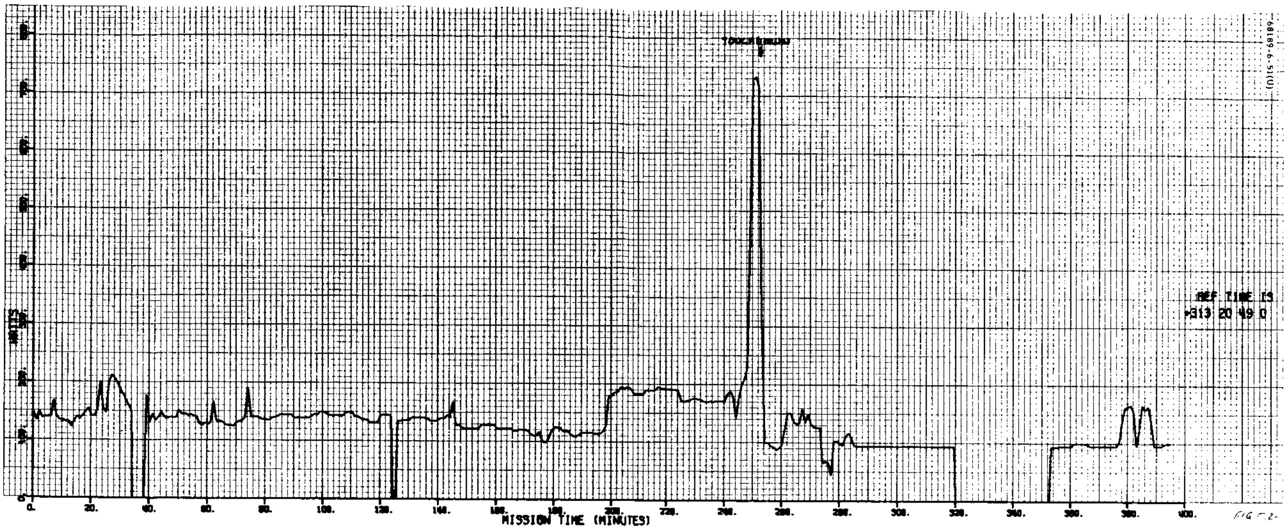

Figure 5. 2-12. Total Power

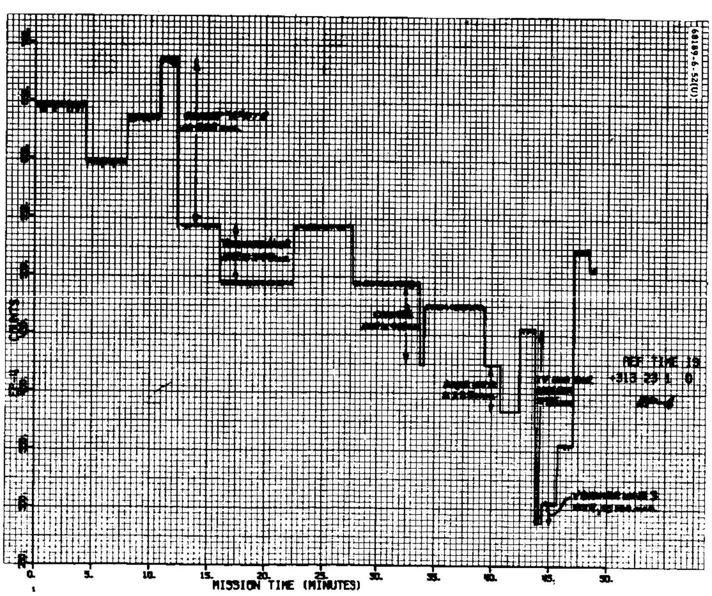

Figure 5. 2-13. Unregulated Output Current – Coast Phase II

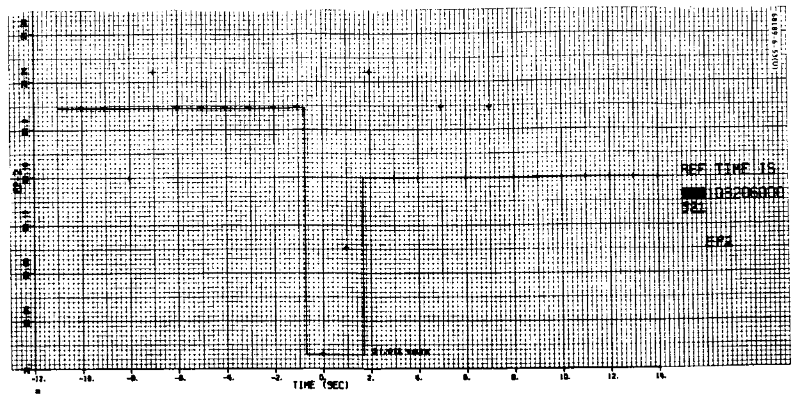

Figure 5.2-14. Unregulated Bus Voltage (EP-2) at Lunar Translation

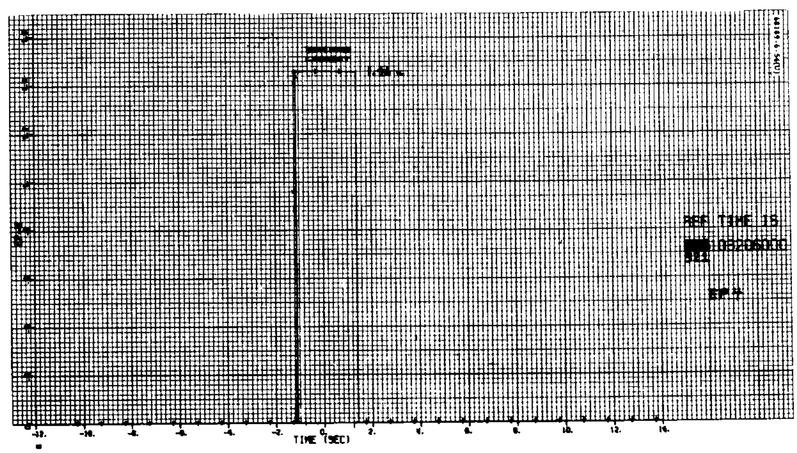

Figure 5.2-15. Unregulated Current (EP-4) at Lunar Translation

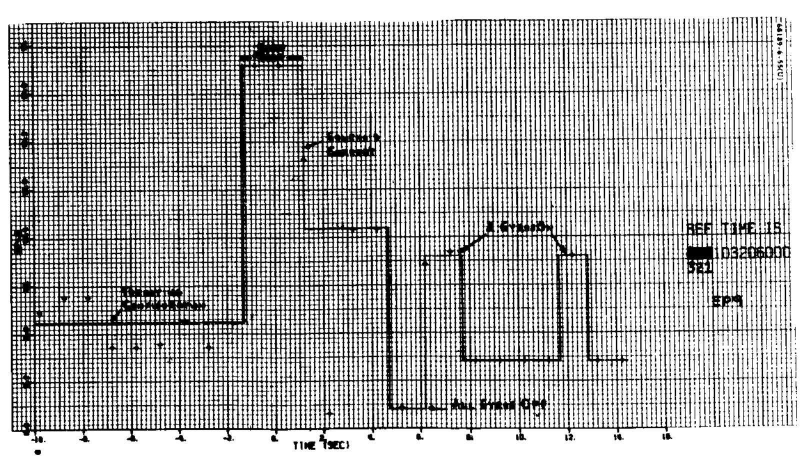

Figure 5.2-16. Battery Discharge Current (EP-9) at Lunar Translation

5.2.5 REFERENCE

1) J. E. Mundy, "System Specification Power Management Data Summary SC-6 Spacecraft," Hughes Aircraft Company No. 302393, Revision A, 25 August 1967.

5.2.6 ACKNOWLEDGMENT

N. J. Kaman, technical coordinator and author.

5.3 RF DATA LINK SUBSYSTEM

5.3.1 INTRODUCTION

This section contains a summary and analysis of the performance of the data link subsystem during Surveyor Mission F.

The data link subsystem consists of the transmitters, transponders, receivers, command decoders, and antennas. It is the function of this subsystem to: 1) provide engineering data transmission from the spacecraft at bit rates compatible with specific mission phases, 2) provide analog data, such as that from television and strain gages, at signal levels high enough for proper discrimination, 3) provide phase coherent two-way doppler for tracking and orbit determination, and 4) provide command reception capability throughout the mission to allow for complete control of the spacecraft from the ground. A simplified block diagram of the communications subsystem is shown in Figure 5.3-1.

The pertinent subsystem units on the spacecraft during the mission are as follows:

Unit	Part Number	Serial Number
Receiver A	231900-3	18
Receiver B	231900-3	26
Transmitter A	3024400-1	17
Transmitter B	3024400-1	19
Command decoder unit	232000-5	7

Unlike most subsystems, individual data link subsystem parameters, such as losses, threshold sensitivity, modulation index, etc., are not measured or individually determined from mission data. The composite effect of these parameters on the performance is measured as received signal power at the spacecraft and the tracking station (DSS) and as telemetry and command error rates. Consequently, it is impossible to compare individual link parameters to specified performance criteria. The best that can be done is to compare measured signal levels to predicted levels, and telemetry quality and command capability to predicted capabilities. To further cloud the analysis, omnidirectional antenna gain is a major contributor to the uncertainty in received signal levels. Accurate omnidirectional antenna gain measurements are difficult to achieve and, in most cases, deviations

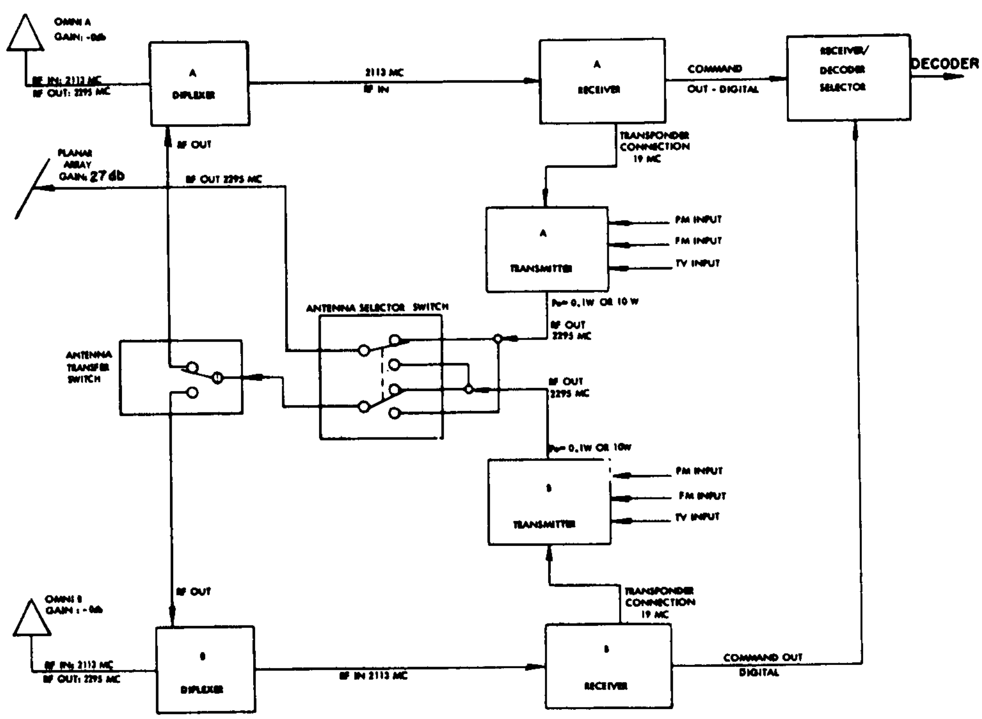

68189-2-134

Figure 5.3-1. Communications Subsystem Block Diagram from predictions can most likely be attributed to antenna gain uncertainty. Because of the problems outlined above, analysis of the data link subsystem performance will, in general, be a qualitative analysis of the performance of the entire subsystem rather than a quantitative assessment of the performance of the individual subsystem parameters. Equally as important as subsystem performance evaluation is the qualitative assessment of the premission and real-time prediction techniques used during the mission, since future missions must rely on these techniques as guidelines during the real-time operation.

In general, the RF data link subsystem performed as expected with two exceptions. Two-way lock was lost during Canopus acquisition, and a transmitted command was not accepted at the spacecraft during the lunar operations liftoff and translation experiment. All subsystem units, however, performed close to nominal predictions.

The data contained in this report consist of spacecraft telemetered, DSS, and mission event time data. Where meaningful, the data are correlated to and compared with equipment specifications, previous test data, preflight predictions, and in-flight analysis predictions. Specifically, this section contains the following discussions which are shown with the appropriate subsection notation:

Anomaly Discussion (subsection 5.3.2) — This subsection contains a discussion of three topics:

1) Loss of two-way lock during Canopus acquisition

2) Ground receiver signal levels being, in general, stronger than predicted nominal

3) Spacecraft not accepting a ground transmitted command during liftoff and translation experiment

Summary and Conclusions (subsection 5.3.3) — This subsection contains a summary of subsystem performance with conclusions relative to performance and postflight analysis.

Subsystem Performance Analysis (subsection 5.3.4) — This subsection contains the following items:

1) General discussion of data, equations used, and path of the earth vector relative to omnidirectional antenna gain contours

2) Discussion of subsystem performance during specific mission phases

3) Discussion of pertinent subsystem telemetry signals plotted as a function of time from launch

The major mission event times relative to the RF data link subsystem are tabulated in Tables 5.3-1 and 5.3-2. Table 5.3-1 contains telemetry mode and bit rate, primary tracking station number, and station automatic gain control values as a function of time. Table 5.3-2 contains a tabulation of the subsystem configuration as a function of time. Both tables cover the mission from launch to the time of loss of signal during retro engine firing at terminal descent. Also, in some cases, the times in these tables are accurate only to the nearest minute.

5.3.2 ANOMALY DISCUSSION

The three events discussed in this section are not considered to have resulted from spacecraft data subsystem anomalies, but rather as deviations from the expected or predicted performance. No known spacecraft RF subsystem anomaly existed.

5.3.2.1 Loss of Two-Way Lock During Canopus Acquisition

The premaneuver analysis associated with the roll maneuver required for the Canopus acquisition phase of the mission indicated that the earth vector would pass through the deep null region of both the up and down links of omnidirectional antennas A and B. Investigation of the up link patterns of omnidirectional antenna B in the vicinity of the earth vector trace showed that the minimum expected antenna gain would be -36 db. Applying the ±10 db tolerance in the worst case to this gain yielded a 0.0 db two-way carrier tracking margin (signal-to-noise ratio = 12 db). The two-way tracking configuration (transponder B) was recommended; however, receiver B phase lock was lost during the maneuver. The frequency shift associated with the spacecraft reverting to the NBVCXO resulted in loss of the ground receiver lock. A delay in the sequence resulted since it was necessary to reconfigure the spacecraft in the one-way mode. The sequence was then continued and Canopus lock subsequently established.

The reaction of the spacecraft and ground system to this situation was normal. Comparisons of the actual antenna gain seen during the maneuver to the predicted gains (Figure 5.6-6d) shows that the receiver lost lock while the earth vector was in the null region of omnidirectional antenna B. The null apparently was greater than -50 db, which is much deeper than the measured antenna pattern data indicates. Omnidirectional antenna patterns, however, are difficult to measure accurately, and low gains are especially difficult to define.

Because of the experience discussed in the preceding paragraphs, it is recommended that two-way tracking not be attempted if the antenna null region will be encountered, regardless of gain values indicated in the antenna pattern data.

5.3.2.2 Down Link Signal Levels Larger Than Expected

Figure 5.3-4 shows that the ground received signal levels for the coast phases fall within the predicted tolerance region but are, in general,

TABLE 5.3-1. TELEMETRY MODE SUMMARY

Time, hr:min:sec	Mode	Bit Rate	DSIF Station	DSIF AGC, dbm	Telemetry Margin, db	Comments
			Day 311			
07:39:01.075	5	550				Liftoff (low mod index SCO)
08:08:50			51			Receivers 1 and 2 in lock
08:09:00			51			Decom in lock
08:10:16						Auto track on SAA
08:10:41				-115.0		Auto track on SCM
08:12:00						Ground transmitter on
08:12:06						Signal in passband spacecraft receiver A
08:13:04						Ground receivers out of lock
08:13:25						Ground receivers 1 and 2 in lock
08:13:27						Two-way verified — auto SCM
08:13:30						Decom in lock
08:13:40						Confirm receiver B phase lock at SFOF
08:14:30						Command mod on
08:15:00			51	-83.0		
08:18:30				-84.0		
08:19:33						Spacecraft transmitter high voltage off
08:20:35				-102.0		Transmitter B low power
08:25:31	1					
08:25:33		1100		-107.0	+31.6	
08:27:00				-107.0	+31.6	
08:30:27	4					
08:32:00				-109.0	+29.6	
08:32:00			42	-146.0		
08:33:18	2					
08:38:25	5					
08:40:00			51	-110.5		
08:40:18			51			Command mod off
08:42:05			51			DSS tuned to track syn frequency
08:44:00			51			Command mod on
08:50:00			51	-114.0		
08:50:00			42	-111.0		
09:11:58			51	-115.0		
09:17:43			51	-116.2		
09:30:00			51	-117.6		
09:44:00			51	-118.6	+20.0	

Table 5.3-1 (continued)

Time, hr:min:sec	Mode	Bit Rate	DSIF Station	DSIF AGC, dbm	Telemetry Margin, db	Comments
10:00:00			51	-119.3		
10:00:00			42	-121.5		
10:04:00			51			Command mod off — transfer to 42
10:10:00			42			Transmitter on
10:10:02			51			Transmitter off — three-way with 42
10:13:06			42			Command mod on
10:30:00			51	-120.5		
10:33:00			42	-120.2		
11:00:00			51	-122.3		
11:05:00			42	-122.5		
11:35:42			42	-123.5		
12:00:00			42	-125.0		
12:00:00			51	-123.6		
12:03:51			42			Command mod off for transfer to 51
12:10:15			51			Two-way confirmed
12:11:11			51			Transmitter at track syn frequency
12:12:20			51			Command mod on
12:14:47	4					
12:20:30	2					
12:25:02	1					
12:28:12	5					
12:30:00			51	-124.6		
13:00:00			51	-125.2		
13:03:00			42	-126.2		
13:30:00			51	-125.9		
14:00:00			51	-126.2		
14:25:26						Data outage SPAC
14:30:00			51	-126.3		
14:30:24						Resume data at SPAC
14:31:00			61	-129.5		
14:39:00			51			Command mod off for transfer to 61
14:45:00			61			Transmitter on
14:45:10			61			Two-way confirmed
14:47:20			61			Command mod on
15:02:00			61	-128.2		
15:30:01	4					
15:34:00			61	-128.6		
15:36:07	2					
15:39:25	1					
15:42:36						Transmitter B filament on

Table 5.3-1 (continued)

Time, hr:min:sec	Mode	Bit Rate	DSIF Station	DSIF AGC, dbm	Telemetry Margin, db	Comments
15:44:21			61	-112.7		Transmitter B high power
15:45:00		4400	61	-117.8		
15:46:31			61	-127.4		Omniantenna A
15:50:22						Start roll-star map
15:55:09						Loss of ground receiver lock
15:56:40						Select omniantenna B
15:58:44						Sun mode on
16:00:23						Resume data
16:04:39						Transponder power off
16:05:04			61	-119.6		
16:06:52	4					
16:09:21			61	-119.6		
16:12:12	1					
16:14:23						Sun and roll
16:25:28						Sun and star mode on
16:27:55						Canopus lock
16:28:40			61	-119.0		
16:29:12						Cruise mode on
16:30:11	5					
16:32:08						Transponder B power on
16:33:44						Two-way lock confirmed
16:35:45				-119.4		
16:36:19		1100				
16:36:58				-114.4		
16:37:29				-130.8		Low power; $\Delta P = 16.4$ db
16:43:05						Inertial mode on
17:01:40			61	-131.0		
17:03:40			51	-129.0		
17:24:05			61			Command mod off for transfer to 51
17:30:00			51			Transmitter on
17:32:02			51			Command mod on
17:35:00			51	-129.2		
18:00:00			51	-129.3		
18:04:11						Cruise mode on
18:18:22						Inertial mode on
18:21:00			51	-129.3		
18:30:00			51	-129.5		
19:00:00			51	-129.8		
19:22:32						Cruise mode on
19:24:25						Inertial mode on
19:30:00			51	-129.7		
19:45:48			51	-129.8		

Table 5.3-1 (continued)

Time, hr:min:sec	Mode	Bit Rate	DSIF Station	DSIF AGC, dbm	Telemetry Margin, db	Comments
20:00:00			51	-129.9		
20:30:00			51	-130.0		
20:38:58						Cruise mode on
20:44:53						Inertial mode on
21:00:00			51	-130.1		
21:30:00			51	-130.7		
22:00:00			51	-131.2		
22:03:03						Cruise mode on
22:03:22			11	-132.3		
22:05:00			51			Command mod off — transfer to 11
22:10:00			11			Transmitter on
22:10:25			11			Two-way lock confirmed
22:11:43			11			Command mod on
22:16:24	4					
22:17:28			11	-132.6		
22:20:01		137.5				
22:21:56				-132.6		
22:23:33		1100				
22:25:34	2					
22:29:02	1					
22:32:09	5					
22:02:15			11	-132.5		
			Day 312			
00:01:40			11	-132.6		
00:03:29			14	-122.0		
00:12:15	4					
00:14:26	2					
00:16:25	1					
00:18:44	5					
00:19:15			11	-132.7		
00:24:43	None	—				A/D SCOs off
00:24:46	None	—				Gyro speed SCOs on
00:31:35	None	—				Gyro speed SCOs off
00:31:45	5	1100				
00:32:50			11	-132.7		
01:21:40			11	-132.9		
01:36:58	4					
01:39:21	2					
01:42:49	1					
01:49:27						Transmitter B filament on
01:51:19						Transmitter B high power
01:51:30				-117.0		

Table 5.3-1 (continued)

Time, hr:min:sec	Mode	Bit Rate	DSIF Station	DSIF AGC, dbm	Telemetry Margin, db	Comments
01:52:05		4400				
01:52:44				-122.1		
02:03:00						Start positive roll 183.8 seconds, 91.9 degrees
02:06:04				-126.0		End roll (-126 to -127 dbm)
02:09:08						Start positive yaw 254.6 seconds, 127.3 seconds
02:13:23				-124.8		End yaw
02:20:02						Midcourse thrust (10.25 seconds)
02:22:18	5					
02:26:07						Start postmidcourse yaw
02:30:21				-124.9		End yaw
02:32:57						Start postmidcourse roll
02:36:01				-122.6		End roll
02:37:39						Cruise mode on
02:38:24	2					
02:42:07	4					
02:45:10	5					
02:46:09		1100				
02:46:31			11	-117.3		
02:47:09						Transmitter B low power
02:47:20				-133.8		ΔP = 16.5 db
03:11:00				-133.9		
03:11:00			14	-124.1		Start special test
03:12:43						1100 bits/sec + touch-down strain gages
03:13:00			11	-136.4		
03:13:00			14	-126.8		
03:28:35						Touchdown strain gage off
03:28:50			11	-133.9		
03:28:50			14	-124.1		End special test
03:32:24			11			Command mod off — transfer to 42
03:40:00			42	-134.5		Two-way
03:43:05			42	-134.3		Command mod on
04:22:47	4		42	-134.0		
04:28:50	2					
04:33:39	1					
04:36:19	5					

Table 5.3-1 (continued)

Time, hr:min:sec	Mode	Bit Rate	DSIF Station	DSIF AGC, dbm	Telemetry Margin, db	Comments
04:37:43						Inertial mode on
04:40:00			42	-134.0		
05:01:37			42	-133.9		
05:35:14			42	-133.8		
05:42:51						Cruise mode on
05:43:36			42	-134.1		
06:00:00			42	-134.2		
06:31:00			42	-134.3		
07:01:00			42	-134.3		
07:30:00			42	-134.5		
08:00:00			42	-134.6		
08:32:00			42	-134.6		
08:32:27						Sun mode on
09:00:00			42	-135.0		
09:30:00			42	-134.7		
10:00:00			42	-135.0		
11:00:00			42	-135.4		
11:30:00			42	-135.4		
12:00:00			42	-135.6		
12:17:20			42	-135.6		
12:25:28	4					
12:29:16	2		42	-135.8		
12:32:01	1					
12:36:33	5					
12:37:00			42	-136.0		
12:46:29						Cruise mode on
12:47:07				-136.1		
13:00:00			42	-136.1	+2.7	
13:00:00			51	-134.8	+4.0	
13:24:34			42			Command mod off — transfer to 51
13:30:00			51			Transmitter on
13:33:00			51			Command mod on
13:35:00			51	-135.0		
14:00:00			51	-134.9		
14:30:00			51	-135.1		
14:30:00			42	-136.3		
15:00:00			51	-135.1		
15:00:00			42	-136.7		
15:00:00			61	-134.9		
15:30:00			51	-135.1		
16:00:00			51	-135.2		
16:00:00			61	-134.9		
16:18:40						Inertial mode on

Table 5.3-1 (continued)

Time, hr:min:sec	Mode	Bit Rate	DSIF Station	DSIF AGC, dbm	Telemetry Margin, db	Comments
17:00:00			51	-135.4		
17:15:02	4					
17:23:33	2					
17:27:47	1					
17:32:22	5		51	-135.5		
17:35:00			61	-135.8		
17:53:41						Cruise mode on
18:00:00			51	-135.5		
18:10:00			61	-134.9		
18:30:00			51	-135.6		
18:59:39						Sun mode on
19:00:00			51	-135.6		
19:30:00			51	-135.5		
19:33:00			61	-135.4		
19:50:00			51			Command mod off — nonstandard transfer
19:54:00			51			Exciter on 1955Z XA
19:54:30			51			Reducing transmitter power
19:55:10			51			Transmitter 1 kw
20:00:00			51	-135.6		
20:12:15						Increasing transmitter power
20:12:35						Transmitter power 10 kw
20:12:35						No high-speed data
20:14:50			51			Command mod on
20:30:00			51	-135.5		
20:35:00			51			Command mod off — nonstandard transfer
20:37:30			51			Exciter on XA
20:38:30			51			Transmitter at 1 kw
20:43:30			51			Transmitter off
20:43:30			61			Transmitter on
20:53:00			61	-135.7		
21:00:14						Resume high speed data
21:16:44	4					
21:19:56	2					
21:24:55	5					
21:27:13			61	-135.4		
21:31:55			61	-136.3		
21:37:14	1					
21:42:04	5					
21:42:26						Cruise mode on
21:45:30			61	-134.5		Signal level varied from -138.0 to -134.5 dbm in few seconds

Table 5.3-1 (continued)

Time, hr:min:sec	Mode	Bit Rate	DSIF Station	DSIF AGC, dbm	Telemetry Margin, db	Comments
22:09:07			61			Command mod off — transfer to 11
22:19:49			11	-136.8		Command mod on
22:21:50			61	-135.7		
22:30:00			11	-137.0		
22:45:02						Inertial mode on
22:50:00			11	-136.6		Bit error rate (BER) $= 1.4 \times 10^{-3}$
23:05:00			11	-136.4		
23:37:00			11	-136.7		
			Day 313			
00:00:00			11	-137.0		
00:11:18			11	-136.7		Cruise mode on
00:30:00			11	-136.7		
01:00:00			11	-136.7		
01:11:25						Inertial mode on
01:30:00			11	-136.7		
01:50:40	4					
01:53:03	2					
01:54:48	1					
01:57:40	5					
02:00:00			11	-137.0		
02:25:37			11	-136.8		Cruise mode on
03:00:00			11	-137.0		
03:29:52						Inertial mode on
03:30:00			11	-137.0		
04:00:00			11	-137.4		
04:00:00			42	-137.2		
04:30:00			11	-137.5		
04:49:00			11	-137.8		
04:49:10			11	-137.3		Cruise mode on
05:00:00			11	-137.4		
05:30:00			11	-137.5		
05:30:00			42	-137.3		
05:30:59			11			Command mod off — transfer to 42
05:41:26			42			Command mod on
06:00:00			42	-137.5		
06:14:05	4					
06:19:52	2					
06:23:06	1					
06:25:08	5					
06:25:57						Inertial mode on

Table 5.3-1 (continued)

Time, hr:min:sec	Mode	Bit Rate	DSIF Station	DSIF AGC, dbm	Telemetry Margin, db	Comments
06:28:00			42	-137.4	+1.2	
06:35:37			42			Ground transmitter failure
06:35:40			42			Ground receivers out of lock
06:36:57			42			Ground receivers in lock-data
06:40:00			42			Ground transmitter on
06:40:05						Signal in passband both spacecraft receivers
06:41:47						Receiver B phase locked
06:43:43			42			On track syn frequency
06:44:47			42			Command mod on
06:56:14			42	-137.5	+1.1	
07:30:00			42	-137.4	+1.2	
07:38:33			42	-137.4	+1.2	Cruise mode on
08:00:00			42	-137.5	+1.1	
08:30:00			42	-137.5		
09:00:00			42	-137.5		
09:04:08						Inertial mode on
09:30:00			42	-137.5		
10:30:00			42	-137.5		
10:42:29						Cruise mode on
10:46:52	4					
10:50:36	2					
10:53:25	1					
10:57:53	5					
11:01:22						Sun mode on
11:30:00			42	-138.0	+0.6	
11:49:00			42	-138.0	+0.6	BER = 2.94×10^{-3}
12:00:00			42	-138.0	+0.6	
12:30:00			42	-138.0	+0.6	
13:00:00			42	-137.9	+0.7	
13:24:08			42			Command mod off — transfer to 51
13:30:00			51			Transmitter on
13:30:20			51			Two-way confirmed
13:31:30			51			Command mod on
13:42:40			51	-138.0	+0.6	
13:53:04	4					
13:56:55	2					
14:00:01	1					
14:02:42	5					

Table 5.3-1 (continued)

Time, hr:min:sec	Mode	Bit Rate	DSIF Station	DSIF AGC, dbm	Telemetry Margin, db	Comments
14:05:00			51	-138.1	+0.5	
14:30:00			51	-138.4	+0.2	
14:40:00			51	-138.5	+0.1	BER = 2.42×10^{-3}
15:00:00			51	-138.5		
15:19:00			51	-138.4	+0.2	BER = 3.02×10^{-3}
15:26:56						Cruise mode on
15:31:00			51	-139.0	-0.4	BER = 1.31×10^{-3}
15:52:00			61	-138.5	+0.1	BER = 5.2×10^{-3}
16:05:00			51	-138.0	+0.6	
16:30:00			51	-137.6	+1.0	
16:40:00			61	-138.6	+0.0	
17:00:00			51	-138.0	+0.6	
17:30:00			51	-138.0	+0.6	
17:30:00			61	-138.6		
17:58:24	4					
18:01:52	2		51	-138.0		
18:05:00	1					
18:07:15	5					
18:09:04		550				
18:10:00			51	-139.5	+4.2	
18:30:00			51	-139.4	+4.3	
19:00:00			51	-139.4		
19:00:00			61	-139.7		
19:30:00			51	-139.4		
20:00:00			51	-139.5		
20:00:00			61	-140.1		
20:30:00			51	-139.6		
20:37:22	4					
20:43:18	5					
21:00:00			51	-139.6		
21:30:00			51	-139.7		
21:35:56	4					
21:50:09	2					
21:53:04	1					
21:58:35	5					
22:00:00			51	-139.7		
22:09:00			51			Command mod off — transfer to 11
22:15:00			11			Transmitter on
22:17:43			11			Command mod on
22:28:20			11	-141.4		
22:29:00			14	-131.8		
22:39:33	4					
22:42:10	2					
22:46:04	1					
22:49:00	5					

Table 5.3-1 (continued)

Time, hr:min:sec	Mode	Bit Rate	DSIF Station	DSIF AGC, dbm	Telemetry Margin, db	Comments
22:51:23	None	—				A/D SCOs off
22:51:29	—	—				Gyro speed SCO on
22:54:51	5	550				
22:56:43						Transponder power off
22:58:04						Transponder B power off
22:58:27			11			Command mod off
22:59:34						Receiver B phase locked
22:59:40			11	-141.3		Two-way confirmed
23:01:46			11			Command mod on
23:04:25			11	-141.5		
23:44:56			11			Command mod off — touchdown frequency offset
23:48:46			11			Command mod on
23:52:11	6					
23:55:07	4					
Day 314						
00:05:52						Transmitter B filament on
00:06:55			11	-141.3		
00:07:33			11	-125.1		Transmitter B high power
00:08:20		1100	11	-124.0		
00:08:20			14	-116.0		
00:09:21	2					
00:09:38			11	-124.0		
00:11:45	5					
00:15:01						Touchdown strain gage power on
00:15:01						Touchdown signal data channels on
00:16:59						Transponder power off
00:17:30			11	-123.7		Ground receivers in lock
00:25:20						Preterminal roll 163.4 seconds, 81.7 degrees
00:28:04			11	-126.1		End roll
00:29:38						Start yaw 223.4 seconds, 111.7 degrees
00:33:22			11	-126.9		End yaw

Table 5.3-1 (continued)

Time, hr:min:sec	Mode	Bit Rate	DSIF Station	DSIF AGC, dbm	Telemetry Margin, db	Comments
00:34:56						Start roll 241 seconds, 120.5 degrees
00:38:57			11	-122.0		End roll
00:39:30			14	-114.1		
00:40:03						Pre-sum amplifier on (strain gages on)
00:40:30			11	-124.8		
00:41:42						Retro delay quantity 5.9 seconds
00:48:58	6					
01:01:25			11	-126.9		Touchdown
01:02:45	5					
01:05:07	2					
01:06:10						Touchdown strain gage power off
01:08:04	5					
01:13:49						A/D converter 2
01:17:00			11	-125.5		
01:19:40	4					
01:21:22		137.5	11	-129.4		
01:22:21				-146.2		Transmitter B low power
01:24:57						Transmitter A low power/omni B
01:25:40			11	-146.0		Signal level increasing
01:26:00			11	-144.7		Transmitter A low power steady
01:26:39			11	-128.0		Transmitter A high power; $\Delta = 16.7$ db
01:27:18		1100	11	-124.5		
01:32:00			11	-124.8		
01:32:24			11	-127.5		Select omni A
01:32:58			11	-125.7		Select omni B
01:35:24						Eng comm off/camera power on
01:44:27						Survey camera power off
01:44:40			11	-124.7		
01:44:44						Sum amps off
01:45:01			11	-122.9		
01:49:00						Start 200-line TV

TABLE 5.3-2. SPACECRAFT CONFIGURATION SHEET

hr:min:sec	Major Sequence Title	Transmitter A/B	Transmitter Power H/L*	Omni-directional Antenna A/B	Analog to Digital Converter 1/2	Receiver A φL/AFC**	Receiver A Transponder A	Receiver B φL/AFC**	Receiver B Transponder B	Command Decoder A/B	Comments
DAY 311											
07:39:01.075	Liftoff	B	L	B	1		Off		On	A	
08:04:20			H								
08:13:40						AFC		φL			
08:19:41			L								
08:40:18											DSS-51 command mod off
08:44:00											DSS-51 command mod on
10:04:00										B	DSS-51 command mod off — transfer to DSS-42
10:13:06											DSS-42 command mod on
12:03:51											DSS-42 command mod off — transfer to 51
12:12:20											DSS-42 command mod on
14:25:26											Data outage
14:30:24											Resume data
14:39:00										A	DSS-42 command mod off — transfer to 61
14:47:20											DSS-61 command mod on
15:44:21	Star acquisition		H								
15:46:31				A							
15:55:09											Loss of data
15:56:40				B							
16:00:23										B	Resume data
16:04:39								AFC	Off		
16:32:08									On		
16:32:36											DSS-61 — command mod off to reacquire up link
16:35:13								φL		A	
16:37:29			L								

Table 5.3-2 (continued)

Time, hr:min:sec	Major Sequence Title	Transmitter		Omni-directional Antenna A/B	Analog to Digital Converter 1/2	Receiver A		Receiver B		Command Decoder A/B	Comments
		A/B	Power H/L*			φL/AFC**	Transponder A	φL/AFC**	Transponder B		
17:24:05											DSS-61 – command mod off – transfer to 51
17:32:02											DSS-51 – command mod on
22:05:00										B	DSS-51 – command mod off – transfer to 11
22:11:43											DSS-11 – command mod on
DAY 312											
01:51:19	Midcourse		H								
02:47:09			L								
03:32:24											DSS-11 – command mod off – transfer to 42
03:43:05											DSS-42 command mod on
13:24:34										A	DSS-42 – command mod off – transfer to 51
13:33:00											DSS-51 – command mod on
19:50:00											DSS-51 – command mod off
20:12:35											Data outage
20:14:50											DSS-51 – command mod on
20:35:00											DSS-51 – command mod off – transfer to 61
21:00:14										B	Resume data
22:09:07											DSS-61 – command mod off – transfer to 11
22:19:49											DSS-11 – command mod on

Table 5.3-2 (continued)

Time, hr:min:sec	Major Sequence Title	Transmitter		Omni-directional Antenna A/B	Analog to Digital Converter 1/2	Receiver A		Receiver B		Command Decoder A/B	Comments
		A/B	Power H/L*			φL/AFC**	Transponder A	φL/AFC**	Transponder B		
DAY 313											
05:30:59										A	DSS-11 – command mod off – transfer to 42
05:41:26											DSS-42 – command mod on
06:35:37						Out of lock		Out of lock			DSS-42 transmitter failure
06:41:47						AFC		φL			Command mod off
06:44:47											DSS-42 – command mod on
13:24:08										B	DSS-42 – command mod off – transfer to 51
13:31:41											DSS-51 – command mod on
22:09:00											DSS-51 – command mod off – transfer to 11
22:17:43											DSS-11 – command mod on
22:56:43								AFC	Off		
22:58:04									On		
22:58:27											DSS-11 – command mod off to reacquire receiver B
22:59:34								φL			
23:01:46											DSS-11 – command mod on
23:44:56											DSS-11 – command mod off touchdown frequency offset
23:48:46											DSS-11 – command mod on

Table 5.3-2 (continued)

Time, hr:min:sec	Major Sequence Title	Transmitter		Omni-directional Antenna A/B	Analog to Digital Converter 1/2	Receiver A		Receiver B		Command Decoder A/B	Comments
		A/B	Power H/L*			ΦL/AFC**	Transponder A	ΦL/AFC**	Transponder B		
DAY 314											
00:07:33	Terminal descent		H								
00:16:59								AFC	Off		
01:13:49					2						
01:22:21			L								
01:24:57		A									
01:26:39			H								
01:32:24				A							
01:32:58				B							
01:49:00						AFC	Off			B	Start 200-line TV

*High/low.

**Phase lock/automatic frequency control.

Table 5.3-2 (continued)

Time, hr:min:sec	Major Sequence Title	Transmitter		Omni-directional Antenna A/B	Analog to Digital Converter 1/2	Receiver A		Receiver B		Command Decoder A/B	Comments
		A/B	Power H/L*			φL/AFC**	Transponder A	φL/AFC**	Transponder B		
DAY 313											
05:30:59										A	DSS-11 – command mod off – transfer to 42
05:41:26											DSS-42 – command mod on
06:35:37						Cut of lock		Out of lock			DSS-42 transmitter failure
06:41:47						AFC		φL			Command mod off
06:44:47											DSS-42 – command mod on
13:24:08										B	DSS-42 – command mod off – transfer to 51
13:31:41											DSS-51 – command mod on
22:09:00											DSS-51 – command mod off – transfer to 11
22:17:43											DSS-11 – command mod on
22:56:43								AFC	Off		
22:58:04									On		
22:58:27											DSS-11 – command mod off to reacquire receiver B
22:59:34								φL			
23:01:46											DSS-11 – command mod on
23:44:56											DSS-11 – command mod off touchdown frequency offset
23:48:46											DSS-11 – command mod on

Table 5.3-2 (continued)

Time, hr:min:sec	Major Sequence Title	Transmitter		Omni-directional Antenna A/B	Analog to Digital Converter 1/2	Receiver A		Receiver B		Command Decoder A/B	Comments
		A/B	Power H/L*			ΦL/AFC**	Transponder A	ΦL/AFC**	Transponder B		
DAY 314											
00:07:33	Terminal descent		H								
00:16:59								AFC	Off		
01:13:49					2						
01:22:21			L								
01:24:57		A									
01:26:39			H								
01:32:24				A							
01:32:58				B							
01:49:00						AFC	Off			B	Start 200-line TV

*High/low.

**Phase lock/automatic frequency control.

approximately 2-1/2 db above the nominal predicted values. Also, ground received signal levels obtained during the Canopus acquisition sequence were normalized to antenna gain and compared to predicted antenna gains for both omnidirectional antennas A and B (Figure 5.3-6a and b). These comparisons both show that the measured gains lie below the predicted gains by approximately 2 db. It is unlikely that both antenna patterns are biased by the same amount. Omnidirectional antenna B down link gains have been very predictable on previous spacecraft.

The above conditions imply that either the transmitter B output power was larger than nominal, or the circuit losses common to both antennas were less than nominal, or both. The high power output of the transmitter remains relatively constant for variations in the low power driver output since the TWT is driven in high saturation. The observed signal level increases when going to high power indicate that the low power output was higher than nominal. In general, the signal increased by 16.0 db where 16.9 db was nominally expected. This, however, does not explain the bias during the Canopus phase, since the spacecraft operates in high power during this sequence. Compartment A temperatures were running lower than that where nominal transmitter power output was defined and can partially explain the increased low power output. However, the high power output is not so sensitive to temperature variations. Also, if the cable common to both antennas was the only cause for the observed high signal levels, it must have a positive gain associated with it.

No single cause can be established for the situation discussed in the preceding paragraph. It could be the case that several parameter tolerances added to give the deviations seen; however, the signal levels in all cases were within the predicted tolerance region.

5.3.2.3 Spacecraft Not Reacting to Transmitted Command

Two back-to-back commands were transmitted to the spacecraft to terminate vernier engine thrusting during the liftoff and translation experiment (day 321). Spacecraft telemetry indicated that only one command was accepted, and the timing of the hop also indicated that the command that terminated thrusting was the second transmitted command. Telemetry data (1100 bits/sec) also indicated that the signal level in both receivers was above the command threshold value and changed very slightly during the sequence.

The performance of the ground system was investigated, and it was found that both commands were transmitted correctly. A receiver at the ground station samples the radiated RF and processes the command information for comparison with the command SCO output. A positive comparison was made for both commands. A record of the command SCO output showed that both commands were properly modulated on the subcarrier.

The most probable cause for the rejection is an RF multipath null that existed for so short a time that the AGC time constant did not allow the associated low signal level to be indicated in spacecraft telemetry. Another possibility is an extremely rare statistical event. However, it would be quite a coincidence if the first known rejected command occurred during a highly dynamic period such as this experiment.

Based on the performance during the experiment, it is recommended that time-critical commands be sent a minimum of three times for future liftoff and translation experiments. Two adjacent commands could conceivably be rejected if the multipath null extended over part of the time period of either command. Since it is felt that a null would be of relatively short duration and that nulls would not occur frequently, sending three commands would minimize the possibility of command reject. Also, in order to evaluate the sensitivity of the antenna patterns, it is recommended that the antenna solar panel positioner be stepped ±5 degrees in polar, elevation, and roll after final positioning.

5.3.3 SUMMARY AND CONCLUSIONS

Table 5.3-3 contains a summary of the measurable performance parameters compared with applicable requirements and premission predictions. Most subsystem parameters are not directly measurable, and those that are measurable are difficult to summarize due to time variability.

Received signal level, for example, is a function of time and spacecraft attitude. The summary for these parameters reflects wide tolerances, with corresponding wide variations in actual performance in cases when the earth vector was in the omnidirectional antenna null. Performance and predictions outside the null are much more closely bounded. More detailed information is found in the subsections dealing with each mission phase.

The following conclusions can be drawn as a result of the foregoing analysis:

1) The RF subsystem performed within the predicted tolerance region for both the up and down links.

2) RF subsystem premission and real-time analysis techniques used during Mission F were relatively accurate with the exception of that associated with two-way tracking during Canopus acquisition.

3) The loss of two-way lock during Canopus acquisition was due to a deep null in the omnidirectional antenna B up link gain pattern and was not associated with the ground system or spacecraft hardware.

4) Mission F data again verified the bias in the omnidirectional antenna B up link antenna gain pattern. This measured gain pattern had been adjusted by 2 db for all predictions and analysis as a result of postmission analysis on Mission E.

Table 5.3-3 (continued)

Parameter	Predicted Value	Requirement	Actual Performance
Receiver B signal levels during terminal maneuver	Time variable predictions. Predictions are some nominal value ±5.7 db.	>-114 dbm**	Level variations of 11.6 db and >-106.1 dbm (predicted variations of 11.0 db)
DSS signal levels during coast phases*	Time variable predictions. Predictions are some nominal value ±5 db.	>-157.4 dbm (carrier power) (17.2 bits/sec threshold)	Level between +3.5 and -1.5 db of nominal and >-141 dbm at 550 bits/sec
DSS signal levels during star maneuver	Time variable predictions. Predictions are some nominal value ±10 db.	None	Level between +2.0 and -7 db of expected and ≥-153.4 dbm (carrier power at 4400 bits/sec)
DSS signal levels during midcourse maneuvers	Time variable predictions. Predictions are some nominal value ±2.9 db.	>-136.1 dbm (carrier power at 4400 bits/sec/ high power)	Level variations of 5.6 db and ≥-126.9 dbm carrier power at 4400 bits/sec (predicted variations of 5.8 db)
DSS signal levels during terminal maneuver	Time variable predictions. Predictions are some nominal value ±2.9 db.	>-130.4 dbm (carrier power at 1100 bits/sec/ high power)	Level variations of 5.9 db and ≥-127.2 dbm carrier power at 1100 bits/sec (predicted variations of 5.6 db)
DSS signal levels during descent and touchdown	Time variable predictions. Predictions are some nominal value ±3.0 db.	>-129.8 dbm (carrier power at 1100 bits/sec and strain gages)	Level variations of 2.7 db and ≥-127.5 dbm carrier power at 1100 bits/sec and strain gages on 85-foot antenna (predicted variations of 2.0 db)

Table 5. 3-3 (continued)

Parameter	Predicted Value	Requirement	Actual Performance
Transmitter A high power output	41.2 dbm ± 0.2 db	>39. 6 dbm	Output between 40. 9 and 41. 1 dbm
Transmitter A low power output	23.25 dbm $^{+0.5}_{-0.3}$ db	>20. 0 dbm	Output between 23. 7 and 24. 7 dbm
Transmitter B high power output	40.86 dbm ± 0.2 db	>39. 6 dbm	Output between 40. 5 and 40. 7 dbm
Transmitter B low power output	24.05 dbm $^{+0.0}_{-1.1}$ db	>20. 0 dbm	Output between 23. 7 and 25. 0 dbm
Command reject rate	<1/2000	≤1/2000 at signal level > -114 dbm	One command not processed (liftoff and translation experiment — lunar) at signal levels greater than -100 dbm.
Telemetry bit error rate	<3/1000	≤3/1000 at input SNR ≥10 db	BER = 3×10^{-3} at input SNR ≈ 8. 89 ± 1. 5 db. (Maximum error rate noted of 5.2×10^{-3})

*Gyro drift checks during coast phases caused antenna gain variations not taken into account in the predicted signal levels.

**Threshold value applies to command threshold and, as such, only requires one of the two receivers to be above -114 dbm at any one time.

5) Only one of the two commands to terminate vernier engine thrusting during the liftoff and translation experiment was accepted by the spacecraft. The most probable cause for the rejection is an RF multipath null that existed for too short a time to be indicated in spacecraft telemetry.

5.3.4 SUBSYSTEM PERFORMANCE ANALYSIS

5.3.4.1 General Discussion

Before specific phases are discussed, a general treatment of the mission will be undertaken. Information applicable to all mission phases is included in this subsection.

Subsystem Parameters

Most quantitative estimates of performance are based on received signal levels which, in turn, are determined from individual link parameters. Those parameters used in the performance predictions and the subsystem analyses are tabulated in Table 5.3-4. Equations using these data are derived here; parameters discussed in later portions can be evaluated from these data. Tables 5.3-4 and 5.3-5 consist of measured data taken from flight acceptance (FAT), solar thermal vacuum (STV), and command and data handling console (CDC) tests or specification values where measurements were not available.

Computations Used

In this subsection, reference is made to received signal levels and quantities computed from these levels. The equations used are listed below and will not be derived again:

1) Spacecraft transmitter high power output is

$$P_{xmtr}(\text{dbm}) = 10 \log (P_{tm} \times 10^3) + L$$

where

P_{xmtr} = transmitter power (dbm) = P_{high}

P_{tm} = telemetered power output (watts)

L = loss from transmitter to power monitor. (Value for transmitter B/omnidirectional antenna B ≃ as determined from STV calibration data.)

TABLE 5.3-4. UPLINK PARAMETERS FROM FAT, STV, AND CDC TESTS

Description	Value
Transmitting system (DDS)	
RF power	$70.0^{+0.5}_{-0.0}$ dbm
Antenna gain	
SAA	20.0 ± 2.0 db
SCM	51.0 (+1.0, -0.5) db
Circuit loss	
SAA	-0.5 ± 0.0 db
SCM	-0.4 ± 0.1 db
Receiving system (Surveyor VI)	
Circuit loss	
Receiver A	-3.7 ± 0.5 db
Receiver B	-4.3 ± 0.5 db
Up link carrier tracking loop	
Equivalent noise	
Bandwidth	240 ± 24 Hz
Threshold SNR	12 db
Up link channel	
Threshold SNR	9 db
System noise	
Temperature	2700° K
Equivalent noise	
Bandwidth (predetection)	13430 Hz
Data/subcarrier modulation index	7.2
Subcarrier/carrier modulation index	1.6 ± 0.16

TABLE 5.3-5. DOWN LINK PARAMETERS FROM FAT, STV, AND CDC TESTS

Description	Value
Transmitting system (Surveyor VI)	
RF power	
Transmitter A (low power)	23.25 (+0.5, -0.3) dbm
Transmitter B (low power)	24.05 (+0.0, -1.1) dbm
Transmitter A (high power)	41.2 (±0.2) dbm
Transmitter B (high power)	40.86 (±0.2) dbm
Planar array gain	27.0 ± 0.5 db
Circuit loss	
Transmitter A Omnidirectional antenna A	-3.16 (±0.5) db
Transmitter B Omnidirectional antenna A	-3.8 (±0.5) db
Transmitter A Omnidirectional antenna B	-3.21 (±0.5) db
Transmitter B Omnidirectional antenna B	-3.8 (±0.5) db
Planar array	-2.3 (+0.0, -0.22) db
Carrier frequency	2295 MHz
Receiving system (DSS)	
Antenna gain	
SAA (acquisition aid antenna)	21.0 ± 1.0 db
SCM (85-foot antenna)	53.0 (+1.0, -0.5) db

Table 5.3-5 (continued)

Description	Value
Circuit loss	
SAA	-0.5 ± 0.0 db
SCM	-0.18 ± 0.05 db
Effective noise temperature	
Maser	55 ± 10° K
Parametric amplifier (SAA antenna)	
All DSS except Johannesburg	270 ± 50°K
Johannesburg	320 ± 50°K
Lunar temperature	110 ± 25° K
Carrier channel	
Equivalent noise bandwidth for maneuvers (at threshold)	152 Hz
Equivalent noise bandwidth for coast mode (at threshold)	12 Hz
Threshold SNR	
Acquisition	9.0 db
Maneuvers	14.0 ± 1.0 db
Coast mode	11.4 db
Subcarrier oscillator	
Equivalent predetection noise bandwidth, Hz ± 10 percent	
4400 bits/sec	5160
1100 bits/sec	1290
550 bits/sec	685
137.5 bits/sec	169
17.2 bits/sec	26.7
Strain gauge 1	169
Strain gauge 2	169
Strain gauge 3	169
Reject/enable	405
Gyro speed	948
Alpha counts	11400
Proton counts	948

Table 5.3-5 (continued)

Description	Value
Subcarrier oscillator center frequencies, kHz	
4400 bits/sec	33.0
1100 bits/sec	7.35
550 bits/sec	3.90
137.5 bits/sec	0.96
17.2 bits/sec	0.56
Strain gauge 1	0.96
Strain gauge 2	1.30
Strain gauge 3	1.70
Reject/enable	2.3
Gyro speed	5.4
Alpha counts	70.0
Proton counts	5.4
Threshold signal-to-noise ratio for telemetry data, ±1.0 db	
4400 bits/sec	9.0
1100 bits/sec	9.0
550 bits/sec	9.0
137.5 bits/sec	9.0
17.2 bits/sec	9.0
Strain gauge 1	7.0
Strain gauge 2	7.0
Strain gauge 3	7.0
Reject/enable	10.0
Gyro speed	10.0
Alpha counts	11.0
Proton counts	10.0
Subcarrier oscillator modulation indices, ±10 percent	
4400 bits/sec	1.6
1100 bits/sec	0.935
550 bits/sec (acquisition)	0.3
550 bits/sec	1.15
137.5 bits/sec	1.45
17.2 bits/sec	1.45
Strain gauge 1	0.65
Strain gauge 2	0.65
Strain gauge 3	0.65
Reject/enable	0.655
Gyro speed	1.600
Alpha counts	1.40
Proton counts	0.60

2) Spacecraft transmitter low power output is

$$P_{low} = P_{high} - P_{DSS_H} + P_{DSS_L} \text{ (dbm)}$$

where

P_{low} = transmitter low power output

P_{high} = telemetered transmitter high power output

P_{DSS_H} = DSS received signal level at high power

P_{DSS_L} = DSS received signal level at low power

3) Spacecraft omnidirectional antenna gain (up-link) is

$$G_R = \frac{P_R}{P_T G_T \left(\frac{\lambda}{4\pi R}\right)^2 L}$$

where

G_R = received omnidirectional antenna gain (up-link gain)

P_R = received signal level (determined from spacecraft AGC)

P_T = DSS nominal transmitter power

G_T = DSS nominal antenna gain

λ = wavelength of up link signal

R = slant range at time of computation

L = nominal spacecraft and DSS losses

(Note: For down link gain, appropriate down link parameters are inserted in a similar equation.)

4) Signal-to-noise ratio (SNR) for any subcarrier is

$$SNR = \frac{P_S}{P_N} = \frac{MP_R}{KT_{eff}BW_{sc}}$$

where

P_S = signal power in predetection noise bandwidth

P_N = total noise power in predetection noise bandwidth

M = carrier to subcarrier modulation loss adjustment constant based on subcarrier oscillator modulation index on the carrier

P_R = received carrier power reported by the DSS

K = Boltzmann's constant

T_{eff} = DSS system temperature reported by the DSS

BW_{sc} = subcarrier equivalent predetection noise bandwidth

When using these equations, attention must be given to the desired accuracy of the answer. Since several parameters not measurable in flight, spacecraft telemetry, and DSS station reports are used, computed parameters have potentially large errors. Their validity is thus weighed against similar test data and/or is judged quite subjectively based on past experience. These equations are not used so much for their numerical results as for the total picture of subsystem performance generated. Any gross subsystem problems or computation errors will tend to be uncovered in this analysis, but subtle errors will not.

Bit Error Rate Calculations

One subsystem parameter of interest is the telemetry bit error rate (BER). This parameter serves as an example of the problems encountered when attempting to evaluate postmission data. BER is required to be less than 3×10^{-3} at input SNR ratios of 9 ± 1 db. BER cannot be measured in flight, but word error rate can. On day 313 at approximately 11-1/2 hours GMT, DSS-42 began counting parity errors. Based on the assumption that a bad parity word represented a single bit error, a BER of 2.94×10^{-3} was observed at a reported -138.0 dbm ground station received carrier power (11 hours 49 minutes).

The SNR at this time of the observed 2.94 x 10^{-3} BER was computed as shown below:

DSS AGC/1100 bits/sec = -138.0 dbm

System noise temperature = 64.0° K = 18.06 db
(DSS-42 post-track)

Boltzmann's constant = -198.6 dbm/deg/cps

Bandwidth = 1290 Hz ± 10 percent = 31.1 (+0.41, -0.46) db

Noise power = -149.44 (+0.41, -0.46) dbm

Modulation loss

Carrier	-2.01 (+0.40, -0.46) db
Subcarrier	-4.56 (+0.62, -0.73) db

Δ modulation loss = -2.55(+ 1.08, -1.13) db

Subcarrier power = -140.55 (+1.08, -1.13) dbm

SNR = subcarrier power − noise power = +8.89 (+1.54, -1.54)

The tolerance in this computation is only approximate and is probably greater. Based on the SNR requirement of 9 ± 1.0 db, the measured parameter (BER) meets the specification.

Omnidirectional Antenna Gain Maps

In order to better visualize and interpret the significance of the signal level data, traces of the earth vector on the omnidirectional antenna gain contour maps are presented. Figures 5.3-2 and 5.3-3 show the antenna up and down links. Since signal level variations are, for the most part, the result of increasing range (i.e., more space loss) and changing omnidirectional gain, these plots allow visualization of the expected signal level changes for comparison with plots of up link and down link signal levels versus time.

5.3.4.2 Mission Phase 1: Prelaunch to Spacecraft Acquisition

Subsystem performance is assessed during the launch pad systems readiness test and prelaunch countdown test. Next to assuring normal system performance prior to launch, the most important subsystem data taken during this phase are transmitter and receiver frequency data. Frequency data are used to predict the frequencies at initial acquisition and are transmitted from the Cape prior to launch. The DSS, in turn, uses these data to tune the DSS receiver for one-way lock and the DSS transmitter for eventual two-way lock.

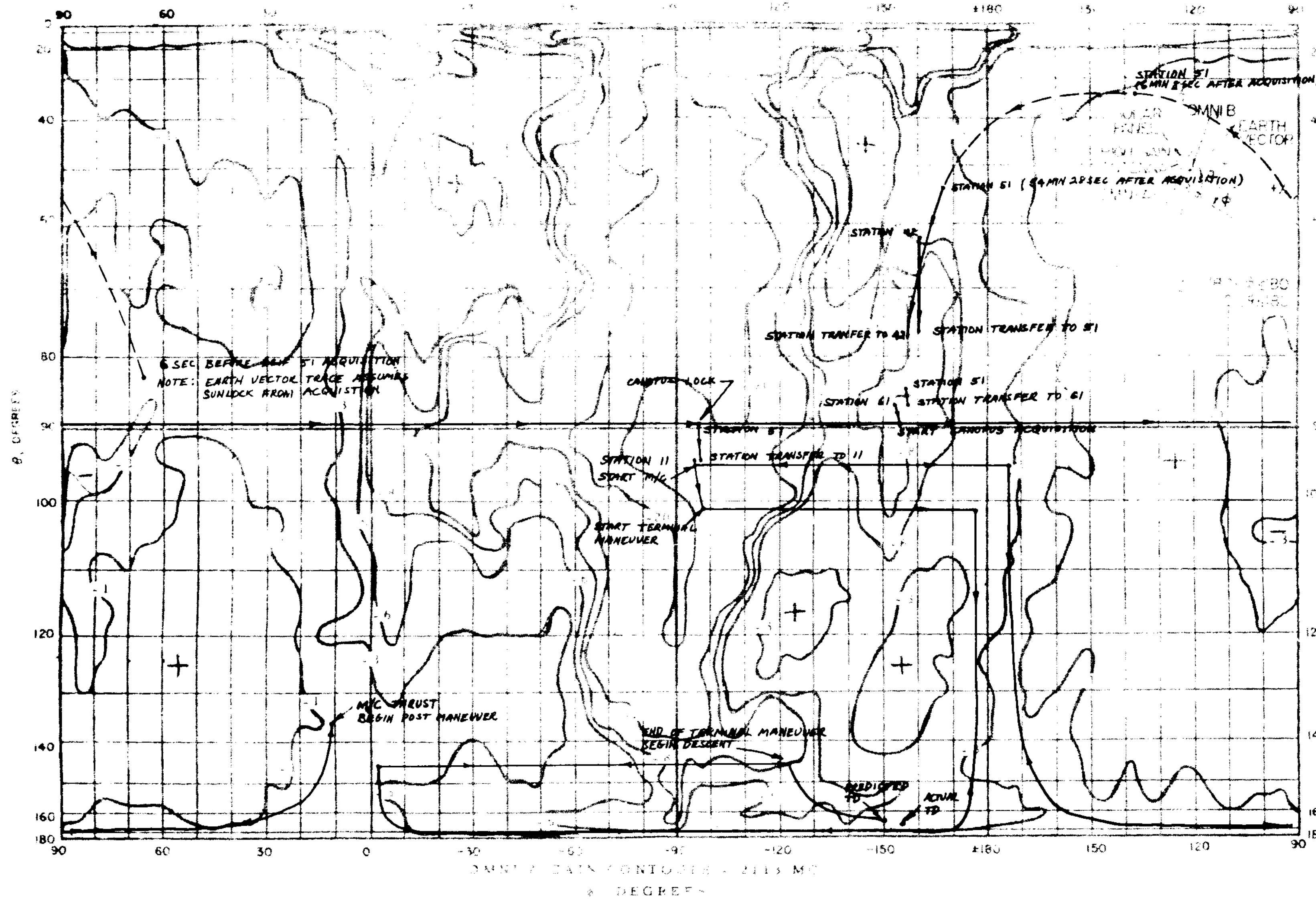

a) Antenna A Gain Contours

Figure 5. 3-2. Up Link (2113 MHz) Omnidirectional Antenna Gain Map

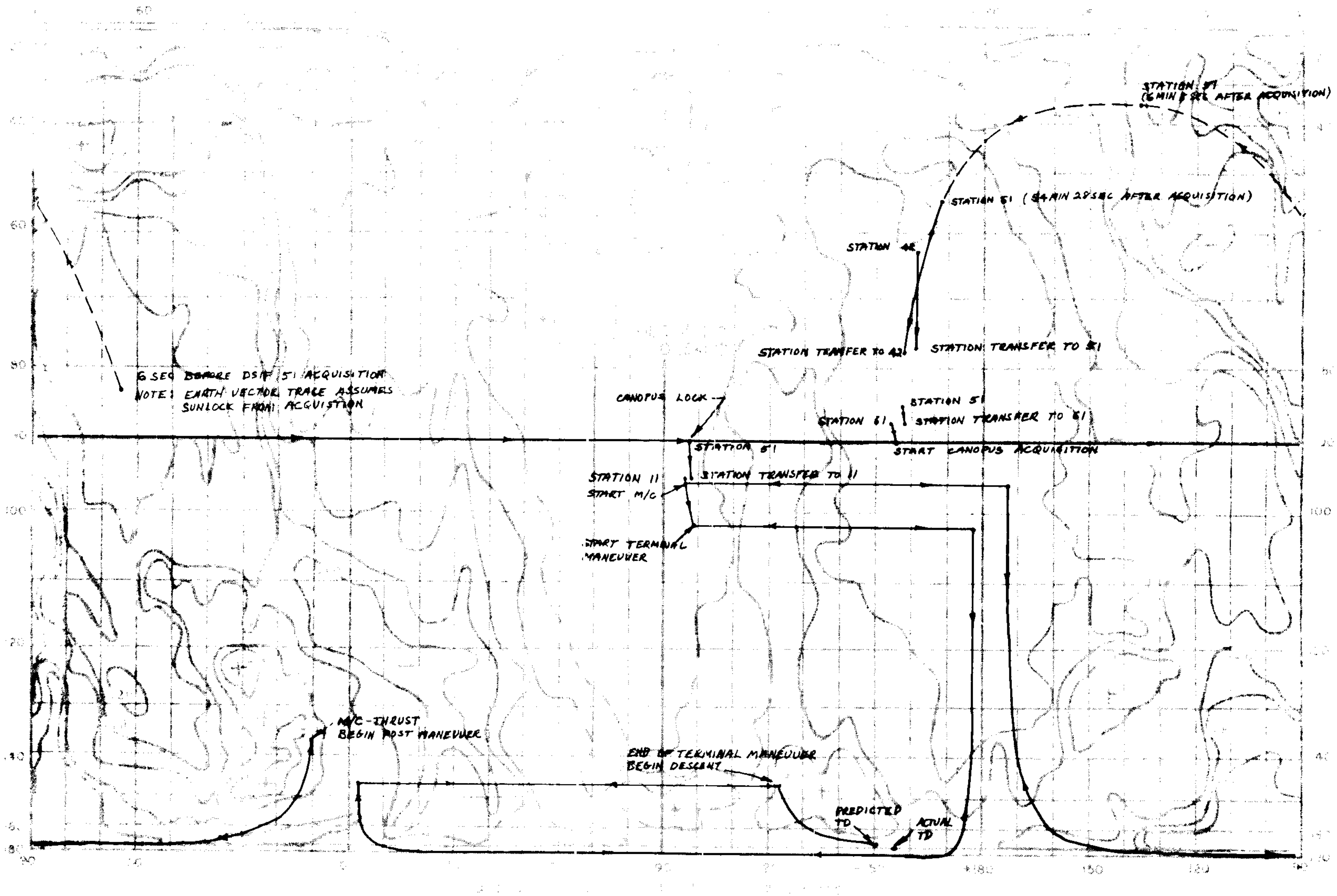

b) Antenna B Gain Contours

Figure 5.3-2 (continued). Up Link (2113 MHz) Omnidirectional Antenna Gain Map

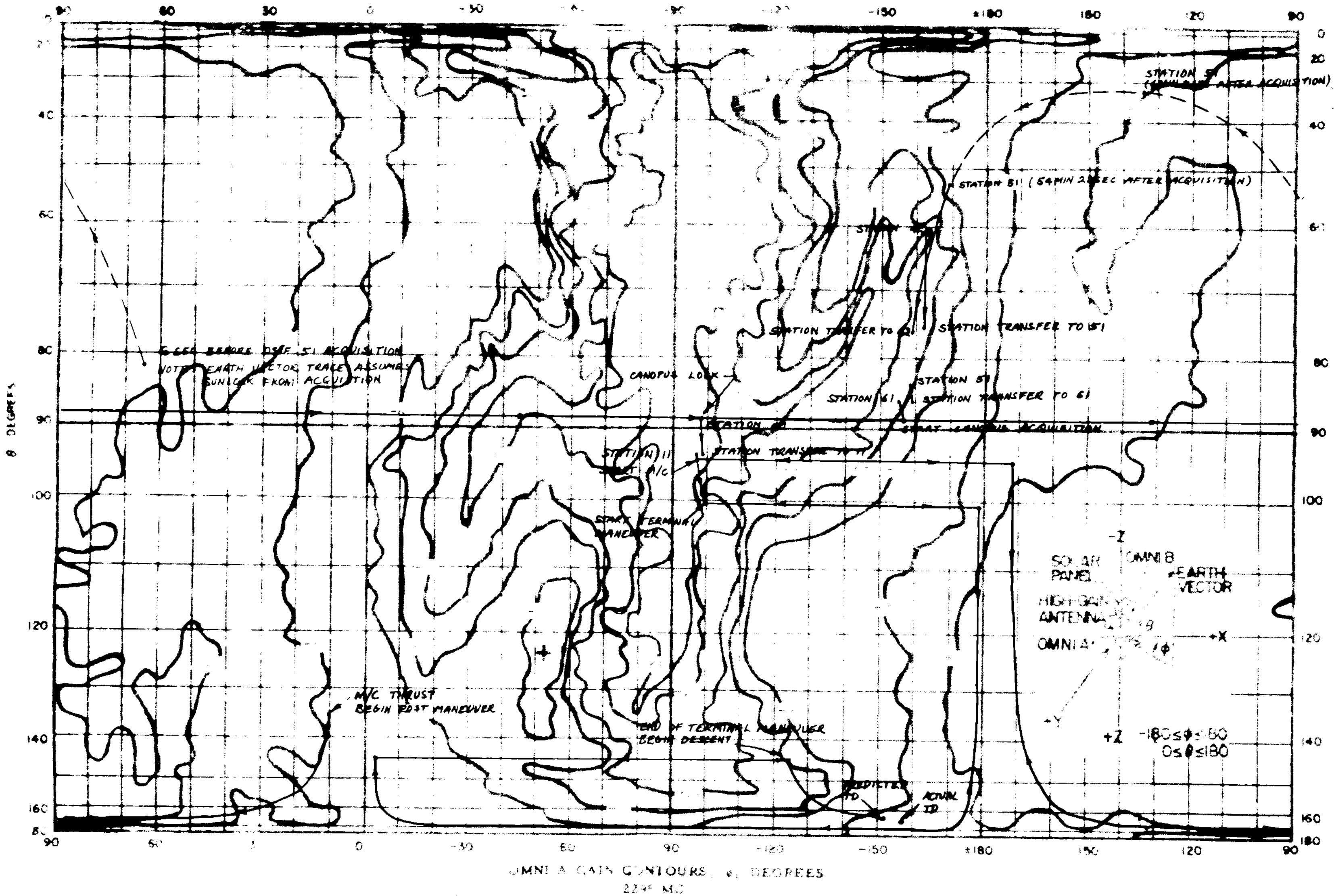

a) Antenna A Gain Contours

Figure 5.3-3. Down Link (2295 MHz) Omnidirectional Antenna Gain Map

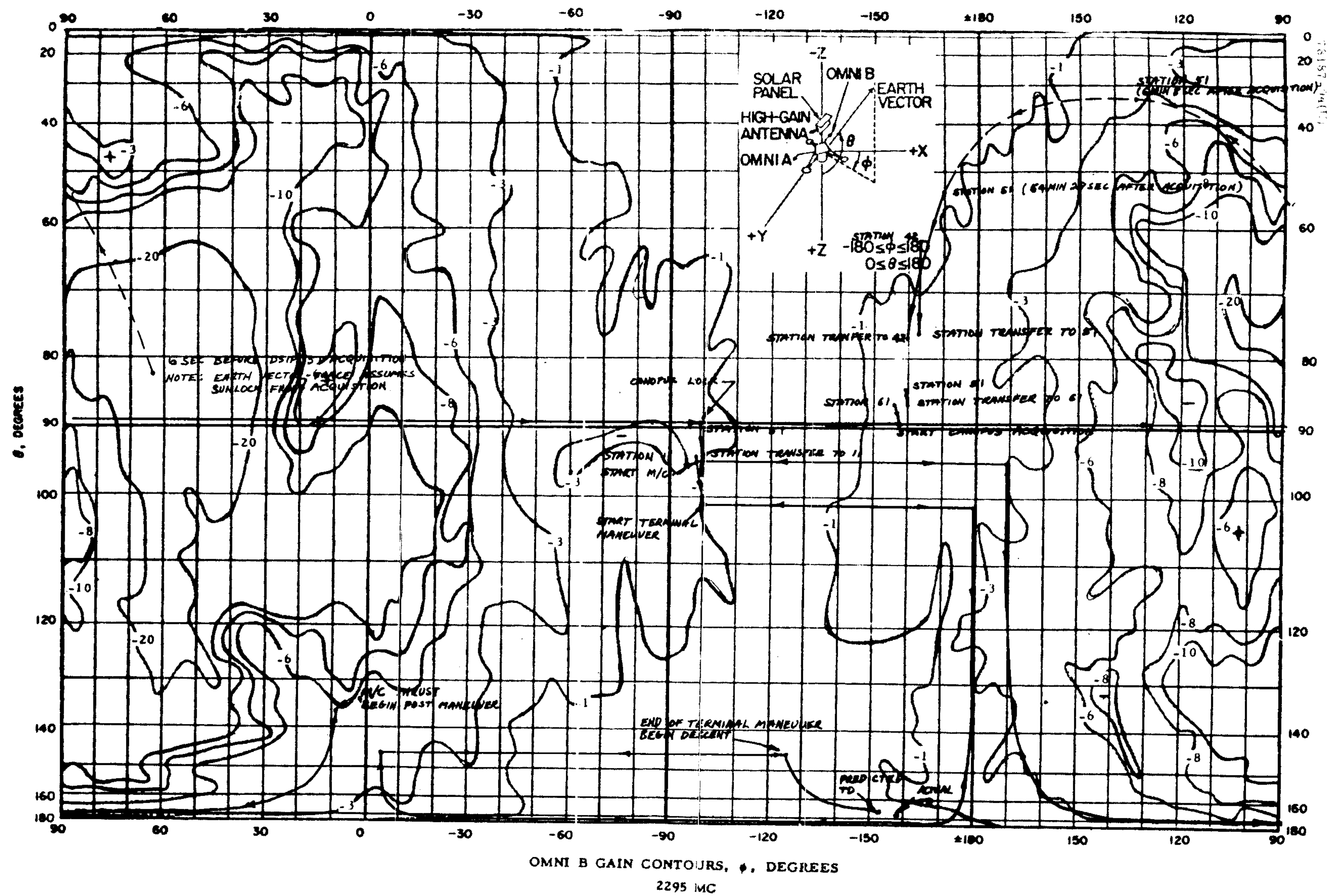

b) Antenna B Gain Contours

Figure 5. 3-3 (continued). Down Link (2295 MHz) Omnidirectional Antenna Gain Map

The measured transmitter and receiver frequency data are tabulated in Table 5.3-6. Compartment temperature during the prelaunch period was increasing, thus causing a transmitter frequency decrease and a receiver frequency increase, as expected. The temperature directly affecting the frequency is not actually measured since the telemetered sensor is in the thermal tray and not at the voltage controlled crystal oscillator. Relative temperature versus frequency information is thus considered to be most reliable. Based on this judgment, the measured frequency data were consistent with previous Surveyor VI test data.

Acquisition frequencies are determined by extrapolating the measured values by essentially predicting the compartment temperature increase due to the high-power operation from just prior to Centaur/Surveyor separation to the time of initial spacecraft acquisition. The measured frequencies were biased by -0.5 kHz as determined from data obtained from Reference 5 and assuming 10 minutes of high power operation from injection to initial DSS-51 acquisition.

The actual frequencies at initial DSS-51 acquisition were:

Transmitter (one-way) = 2294.987892 MHz

Receiver (two-way) = 2113.320576 MHz

The difference between final predicted (T-306 report) and actual frequencies were:

Transmitter = 1489 Hz

Receiver = 2012 Hz

Table 5.3-7 is a summary of the significant events during initial RF acquisition at DSS-51 (Johannesburg). One-way acquisition was accomplished 73 seconds before the predicted first visibility, and good two-way lock was accomplished 5 minutes and 24 seconds later. The spacecraft received signal levels for both receivers A and B were greater than -80 dbm during the initial acquisition phase. Telemetry data also indicated a signal in the passband of both spacecraft receivers at DSS transmitter turn on.

No problems were encountered during initial spacecraft acquisition. The spacecraft high power transmitter was turned off 15 minutes and 13 seconds after being commanded to high power by the Centaur. The maximum allowable time to accomplish turn off is 1 hour.

5.3.4.3 Mission Phase 2: Coast

The coast phases consist of the following:

1) Pre-Canopus acquisition — Period from initial spacecraft acquisition until Canopus acquisition. During this time, the spacecraft attitude is uncertain in roll, and the spacecraft -Z axis is pointed toward the sun.

TABLE 5-3.6. PRELAUNCH FREQUENCY SUMMARY*

Frequency Message Time, minutes	Measured Frequencies, MHz		Predicted Acquisition Frequencies, MHz		Lower Tray Temperature, °F
	One-Way NBVCXO	Best Lock	One-Way NBVCXO	Best Lock	
T-669 (Transmitter A)	2295.000430	2113.318496	—	—	72
T-565 (Transmitter B)	2294.997929	2113.317480	2294.997439	2113.316980	73
T-326 (Transmitter A)	2294.997337	2113.316360	—	—	78
T-50 (Transmitter B)	2294.998430	2113.317344	2294.997930	2113.316844	73
T-30a (Transmitter B)	2294.990617	2113.318512	2294.990117	2113.318012	77
T-30b (Transmitter B)	2294.989881	2113.319064	2294.989381	2113.318564	80

*Frequencies used by FPAC for initial DSS-51 acquisition were those contained in the T-30a Report.

TABLE 5.3-7. ACQUISITION EVENTS

Events	GMT (Day 311), hr:min:sec	Comments
Transmitter B high power on	08:04:20	Spacecraft commanded to high power by Centaur
DSS 51 acquires spacecraft one-way on SAA (acquisition aid antenna)	08:08:51	Predicted rise was 08:10:04 .
DSS 51 auto tracking on SAA/paramplifier	08:10:16	
DSS 51 switch from SAA to SCM/maser (85 foot antenna)	08:10:45	
DSS 51 transmitter turn on	08:12:00	
Signal in passband of spacecraft receivers	08:12:06	(From telemetry.) Receiver A in AFC capture. Receiver B pulling in, not phase locked
Phase lock receiver B	08:13:25	DSS receiver dropped phase lock, indicating phase lock on receiver B
DSS 51 reports good two-way data	08:14:15	Good two-way acquisition 35 minutes and 14 seconds after launch
DSS 51 command modulation on	08:14:30	
Transmitter B high power off	08:19:33	Spacecraft was in high power for 15 minutes and 13 seconds for initial acquisition phase (a maximum time of 1 hour is allowed)

2) Premidcourse — Period from Canopus acquisition until midcourse maneuvers.

3) Postmidcourse — Period from completion of midcourse maneuvers until terminal maneuvers.

Figures 5.3-4 and 5.3-5 are plots of DSS, receiver A, and receiver B signal levels from launch to touchdown. The premission predicted signal level after Canopus acquisition is shown in each figure. Since the spacecraft attitude in roll is uncertain to ±60 degrees about an estimated reference point prior to Canopus acquisition, no premission predictions are made for this period.

Referring to Figures 5.3-3 and 5.3-4, which show traces of the earth vector relative to omnidirectional antenna B down link and omnidirectional antennas A and B up-link gain contours, it can be noted that changes in signal levels during the pre-Canopus acquisition phase and right at Canopus acquisition are in complete agreement with the antenna gain contour maps. The approximate antenna gains during the pre-Canopus phase are noted in Table 5.3-8.

Figures 5.3-4 and 5.3-5 indicate that, during the premidcourse and postmidcourse coast periods, received signal levels deviated from the predicted values in both the up and down links. Gyro drift checks performed during these two periods account for earth vector variations not taken into consideration when generating the predictions. As pointed out in Reference 7, these minor look angle variations can cause the observed signal level variations. However, the data indicate that the tolerances on the nominal predicted signal level, which also includes antenna gain variations, bound those values seen in the mission data.

During Mission E, severe degradation of the 1100 bits/second data occurred at DSS-14 (210-foot antenna) when the touchdown strain gage SCOs were multiplied with the 7.35 kHz PCM SCO. Data at DSS 11 indicated nominal spacecraft performance. Prior to Mission F the DSS 14 receivers were modified from the MSFN to the standard DSN configuration. The MSFN configuration has wider tracking loop bandwidths than the standard configuration and had been used previously to enhance the tracking capability at touchdown. Details of tests performed at DSS 14 subsequent to this modification are contained in Reference 8.

After completion of the midcourse correction, a special test was performed with DSS 11 and DSS 14. The purpose of the test was to verify analytical and premission test results of the ground station data handling performance with the spacecraft data system in a lunar landing configuration. The touchdown strain gage SCOs were multiplexed with the 7.35 kHz SCO (1100 bits/sec data), resulting in a received carrier power at DSS 11 of -136.4 dbm with a corresponding bit error rate of 1.1×10^{-3}. The received signal level at DSS 14 was reduced by moving the 210-foot antenna off the spacecraft/station vector. When the carrier power at DSS 14 reached -135.0 dbm it was determined by visual comparison of the two data streams

TABLE 5.3-8. PRE-CANOPUS ANTENNA GAIN VARIATIONS

Omnidirectional Antennas	Gain Variations (Coast), db		Pre-Canopus Gain, db		Gain at Canopus, db	
	Predicted	Actual	Predicted	Actual	Predicted	Actual
B down link	-1.0 to -2.0	0.0 to -3.4	-2.1	-3.2	-1.6	-3.4
A up link	-3.0 to -9.0	-3.0 to -6.0	-8.9	-6.0	-12.7	-9.7
B up link	+0.0 to -3.0	+2.0 to -1.2	-1.8	-1.2	+0.6	+1.2

that the PCM data at both DSS 14 and DSS 11 were equivalent. As a result of this check, it was concluded that nominal theoretical PCM threshold performance at DSS 14 could be expected with the spacecraft in the 1100 bits/second and touchdown strain gage data multiplier mode during terminal descent and touchdown.

At approximately L + 58-1/2 hours, the spacecraft data rate was reduced to 550 bits/sec. At 1100 bits/sec data, the received carrier power at DSS 61 had been running approximately -138.5 dbm with a nominal telemetry margin of +0.1 db. Excessive errors in the data were not noted; however, the ground system was experiencing some data processing difficulties. An error rate count at the station indicated a bit error rate of approximately 5.2×10^{-3} at this time. The 550 bits/sec data rate continued to be the data mode for the remainder of the coast phase.

5.3.4.4 Mission Phase 3: Canopus Acquisition Maneuver

At approximately L+8 hours, the star acquisition maneuver was initiated. A total roll of 657.5 degrees about the Z axis was required to make a star map, to adequately identify Canopus, and to finally acquire the star.

Real-time analysis indicated that the roll maneuver would take the earth vector through deep antenna nulls on both the up and down links of both omnidirectional antennas A and B. However, predicted signal level values during the maneuver, even considering worst-case tolerances, would not exceed the two-way tracking threshold. The transponder mode was therefore recommended for the acquisition sequence. Also, the analysis indicated that, in order to map all expected stars with only one roll at a data rate of 4400 bits/sec, it would be necessary to switch antennas during the roll. The sequence was designed to start the roll with data transmission via omni A and switch to omni B when either the moon was seen in the Canopus sensor or

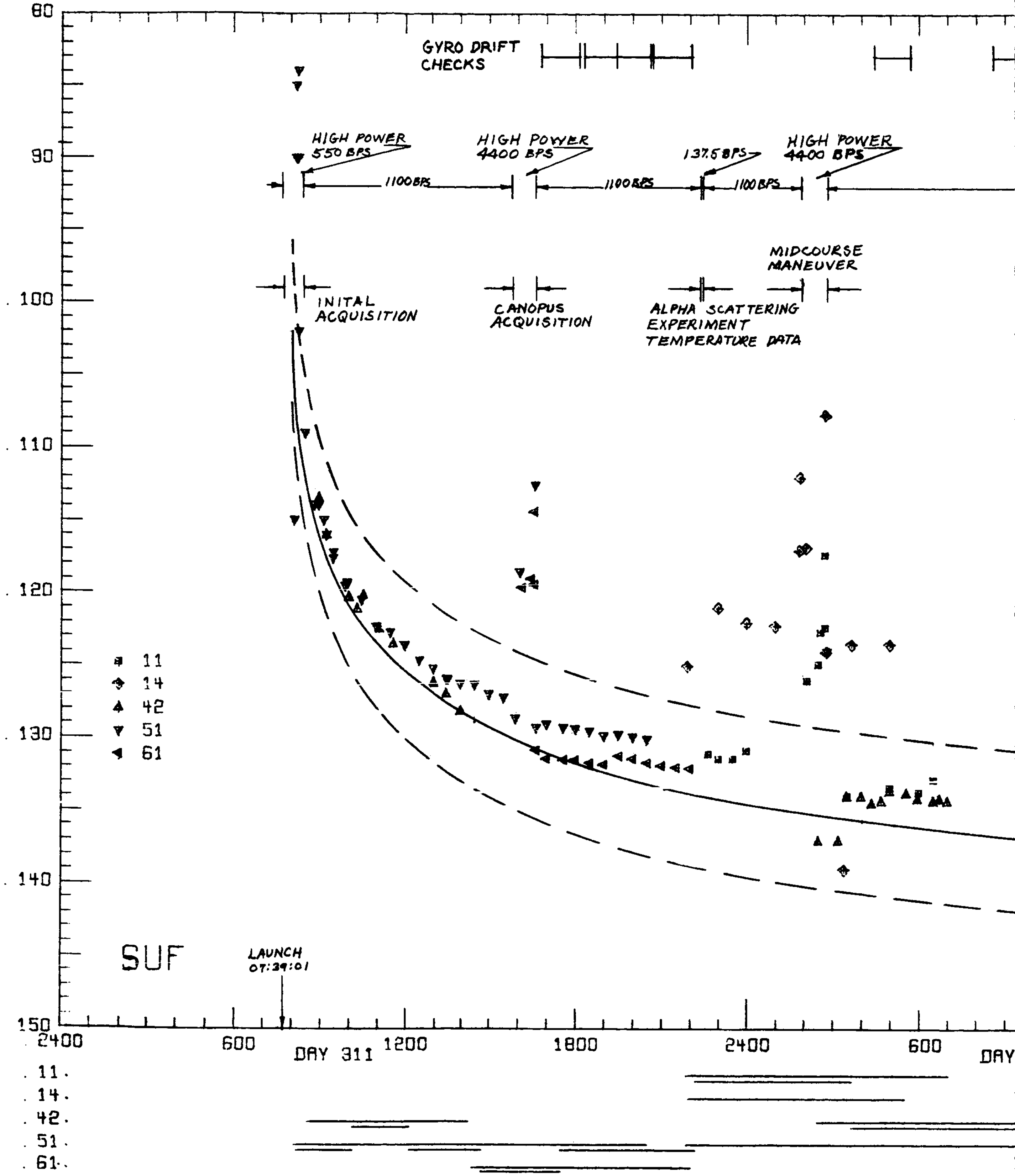

Figure 5.3-4. DSS-Received Carrier Power (dbm)

FOLDOUT FRAME

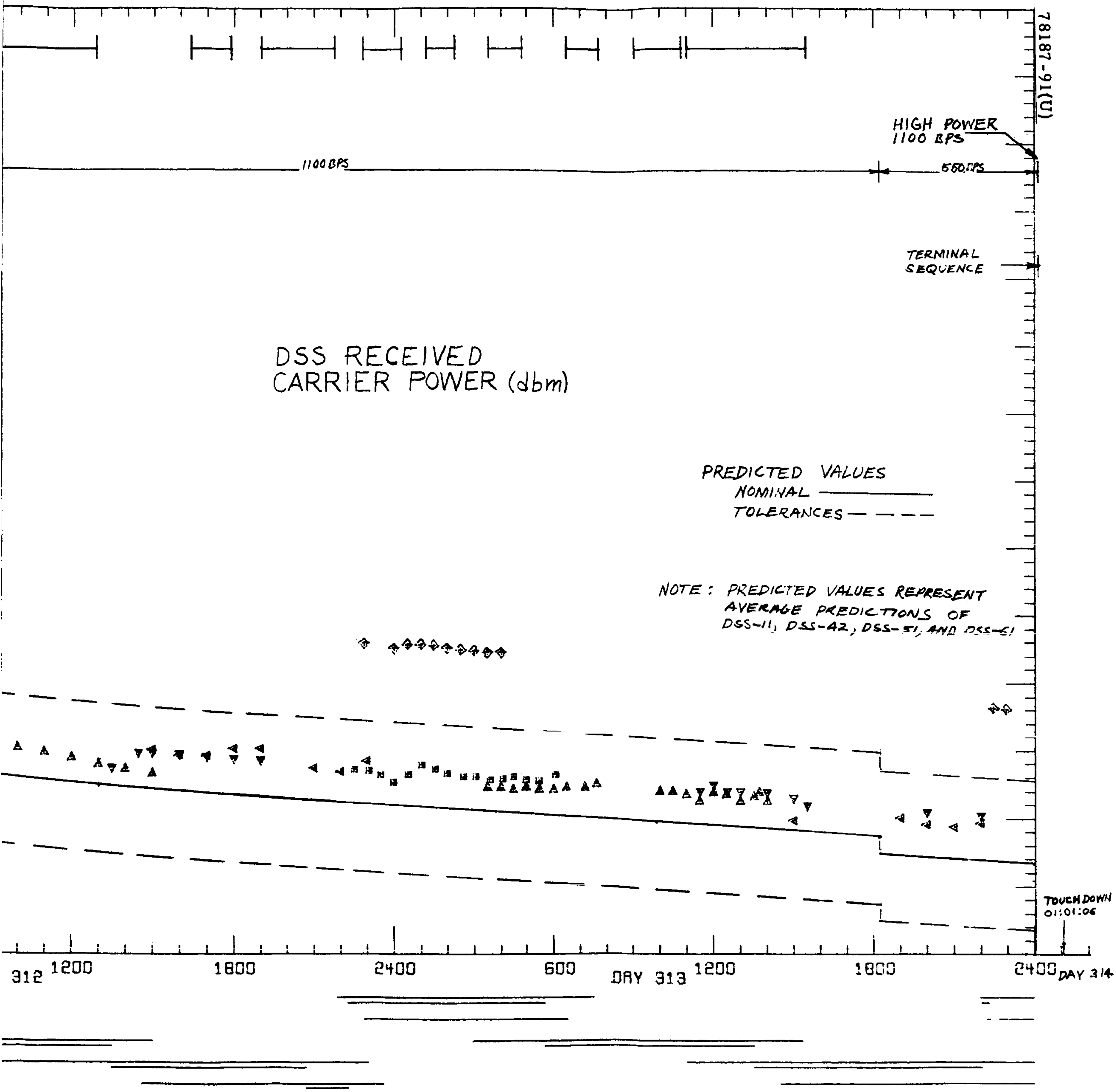

FOLDOUT FRAME

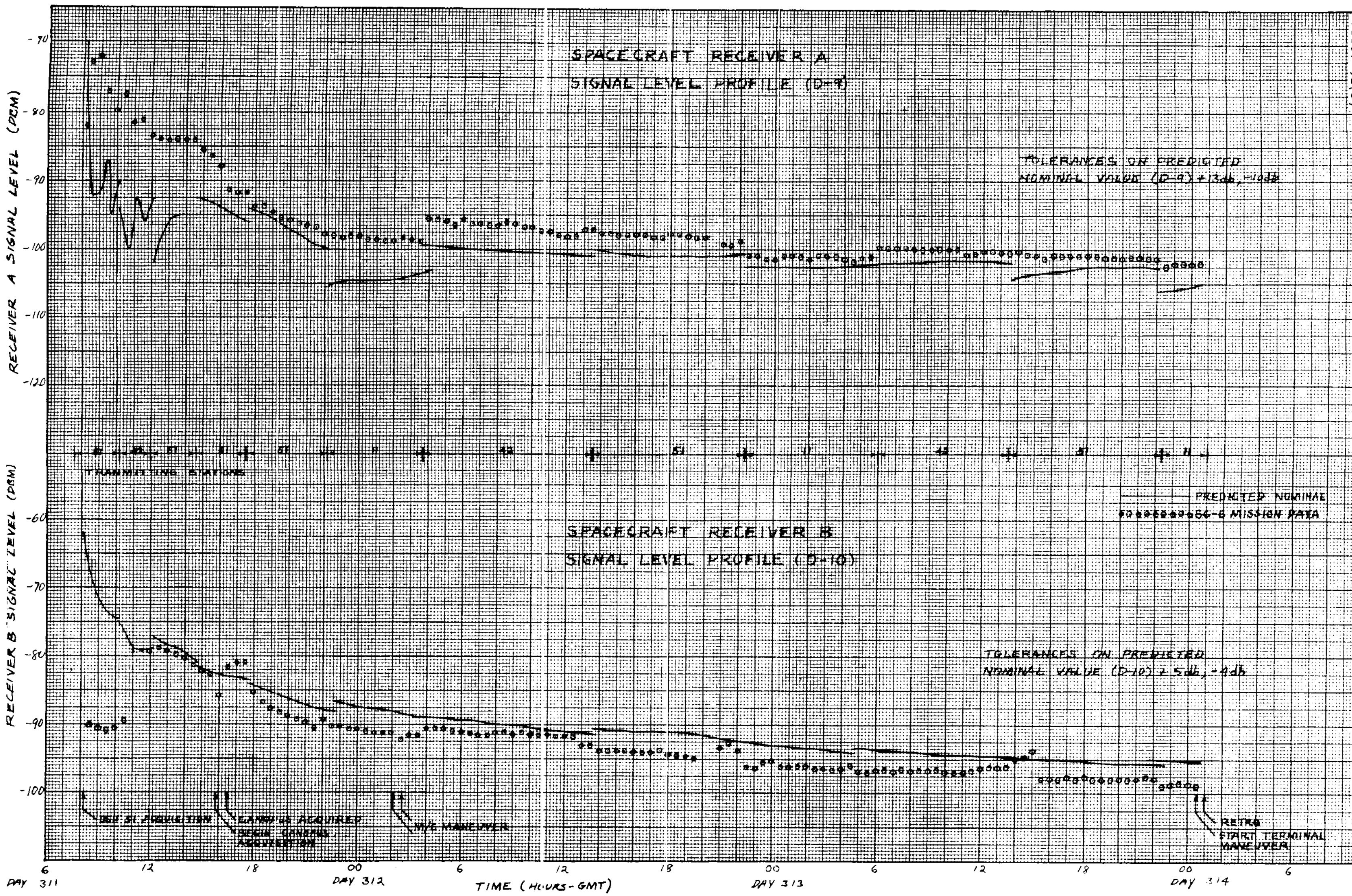

Figure 5.3-5. Spacecraft Receiver A Signal Level Profile

when the spacecraft had rolled 180 degrees, whichever occurred first. Omni B would be the transmitting antenna for the remainder of the first roll and for that portion of a second roll that would be necessary to lock on to Canopus.

At 15:44:21 GMT, transmitter B was commanded to high power with the ground received signal indicating an increase of 15.9 db. Omnidirectional antenna A was selected at 15:46:31 GMT, and star mapping was initiated at 15:50:22 GMT from DSS 61 with the spacecraft operating in the transponder B mode and transmitting data at 4400 bits/sec in mode 1.

At 15:55:25 GMT, after approximately 151 degrees of roll, the ground receiver lost phase lock. Since a strong signal was being received at DSS 61 just prior to the loss of lock, the cause was attributed to the spacecraft. Omnidirectional antenna B was selected at 15:56:39 GMT after the spacecraft had rolled approximately 188 degrees, which was in accordance with the original plan. DSS 61 was then instructed to tune their receiver in an attempt to recognize the spacecraft signal. The roll maneuver was stopped at 15:58:44 GMT after the spacecraft had rolled approximately 251 degrees, of which 100 degrees were after the loss of ground receiver lock. A signal in the DSS 61 receiver indicated that the spacecraft may have been trying to phase lock to a sideband resulting from the presence of command modulation on the up link carrier. Transponder B was commanded off and solid ground station receiver lock was established. The roll maneuver was continued at 16:14:22 GMT after an assessment indicated that the spacecraft was operating normally. The spacecraft was then operating in the one-way mode and transmitting data via omni B. Down link signal variations of approximately 36 db were noted which agreed with the predictions for a 360-degree roll in omnidirectional antenna B. Intermittent decommutator lock occurred within the null region; however, down link carrier lock was maintained. Canopus lockon was verified at 16:28:30 GMT.

Transmitter B high power was commanded off at 16:37:16 GMT which resulted in 52 minutes and 55 seconds of high-power operation for star acquisition. DSS 61 receiver carrier power for low-power operation was -130.8 dbm which was a 16.4 db decrease from high power and resulted in a 7.8 db nominal telemetry margin for 1100 bits/sec data.

Variations in antenna gain seen in the data are compared to predicted variations for both the up and down links and are illustrated in Figure 5.3-6. Both omnidirectional antennas A and B up link variations agree well with the predicted variations except in the null regions of omnidirectional antenna B. The data show that a portion of this null is much deeper than expected. The low signal level that resulted caused receiver B to drop phase lock during the maneuver sequence. The spacecraft transmitter then reverted to the NBVCXO for its frequency control, and thus a shift in the down-link frequency resulted which subsequently also caused the ground receiver to lose phase lock.

The comparison of both down links shows the predicted gains to be higher than the gains determined from the mission data. The deviation from

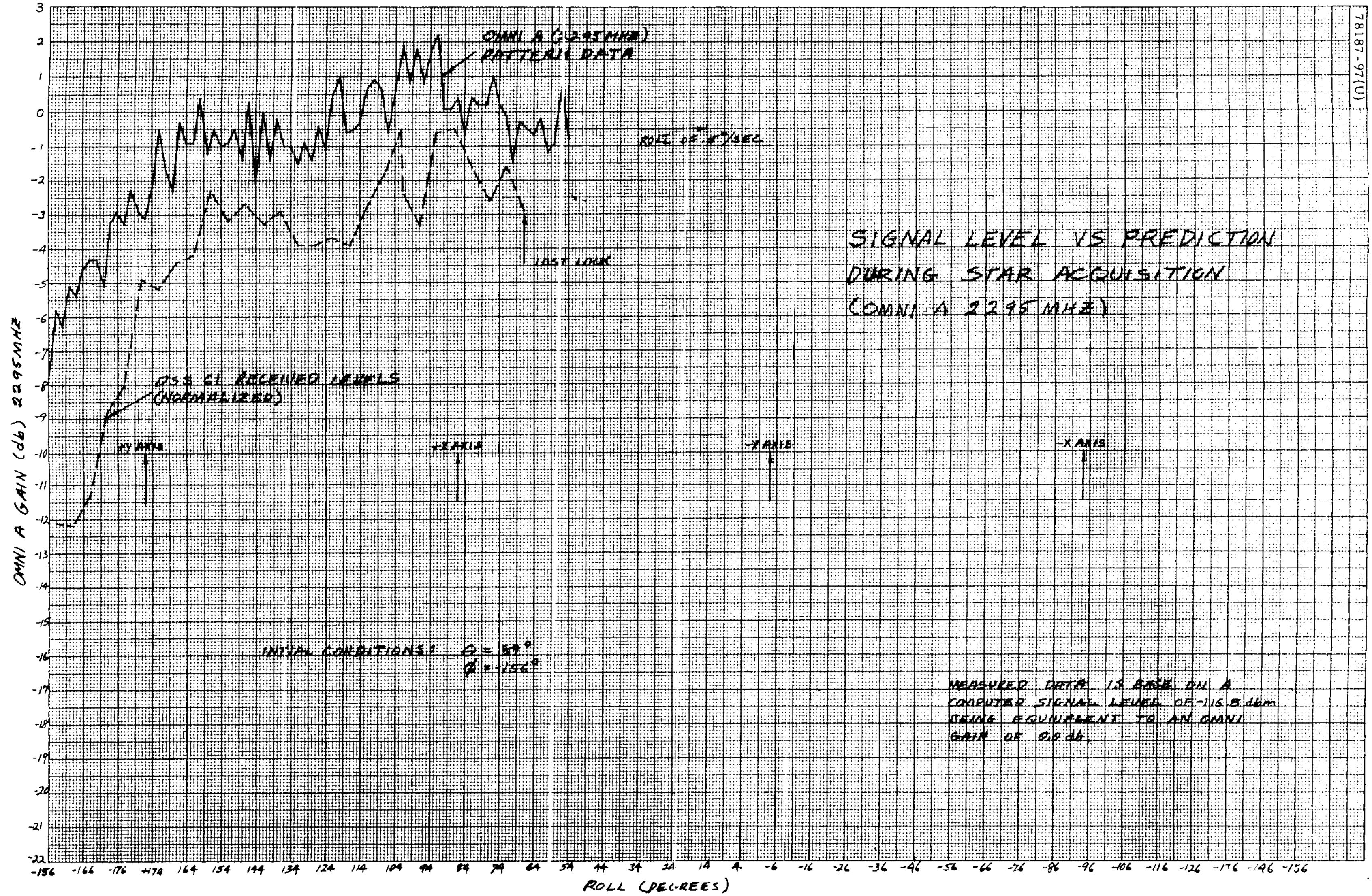

a) Omnidirectional Antenna A Down Link (2295 MHz)

Figure 5.3-6. Signal Level Versus Predictions During Star Acquisition

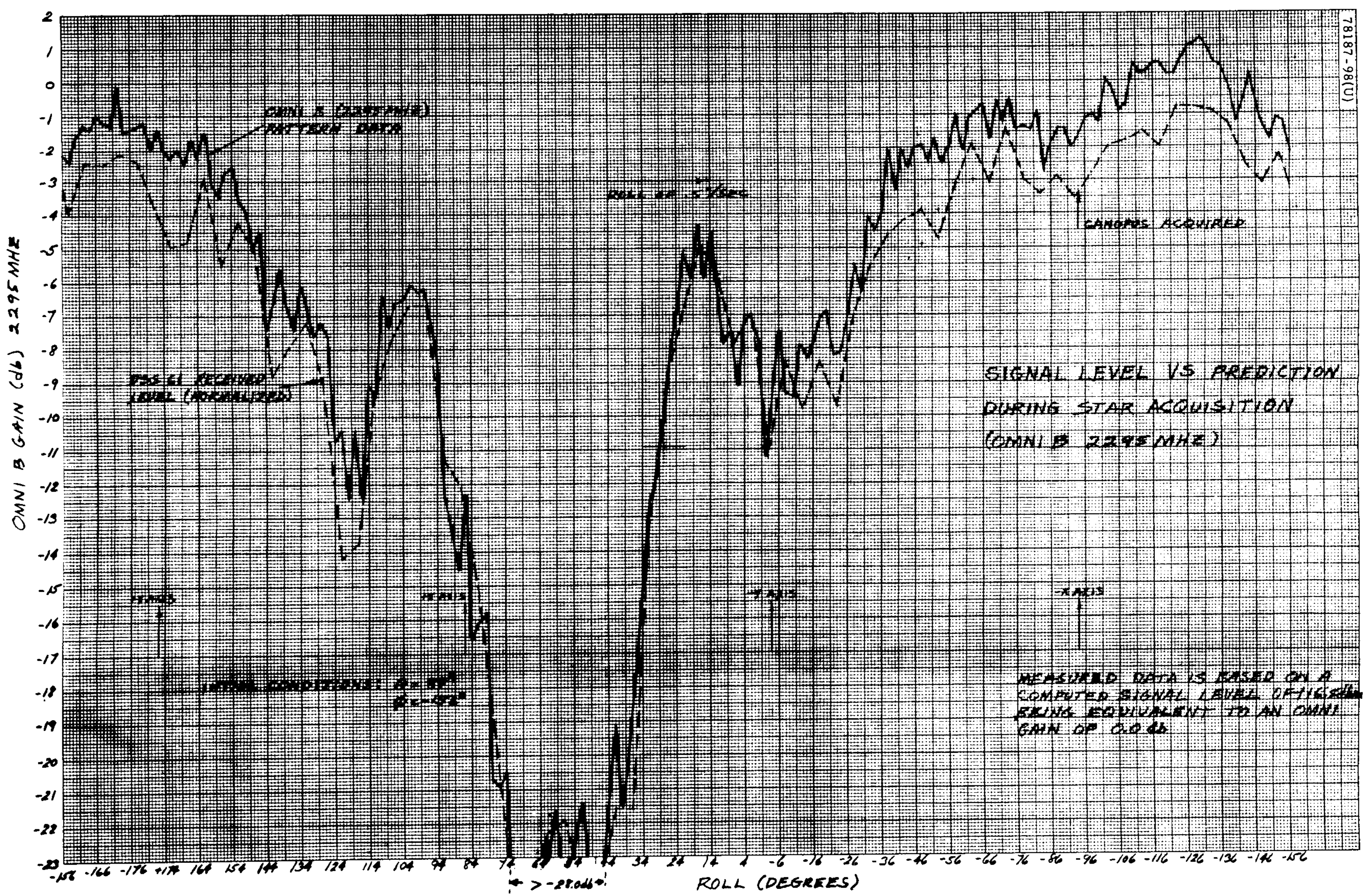

b) Omnidirectional Antenna B Down Link (2295 MHz)

Figure 5.3-6 (continued). Signal Level Versus Predictions During Star Acquisition

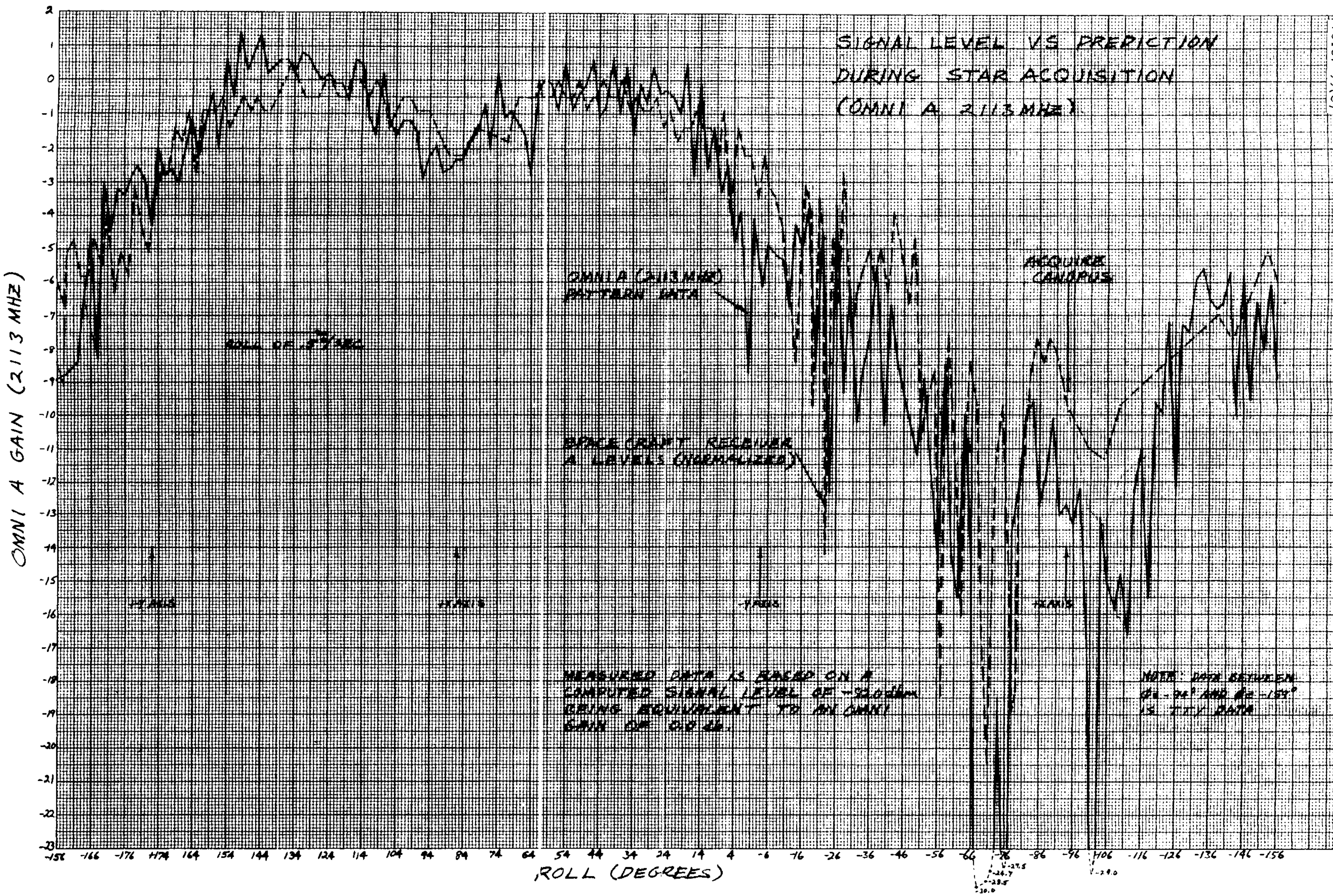

c) Omnidirectional Antenna A Up Link (2113MHz)

Figure 5.3-6 (continued). Signal Level Versus Predictions During Star Acquisition

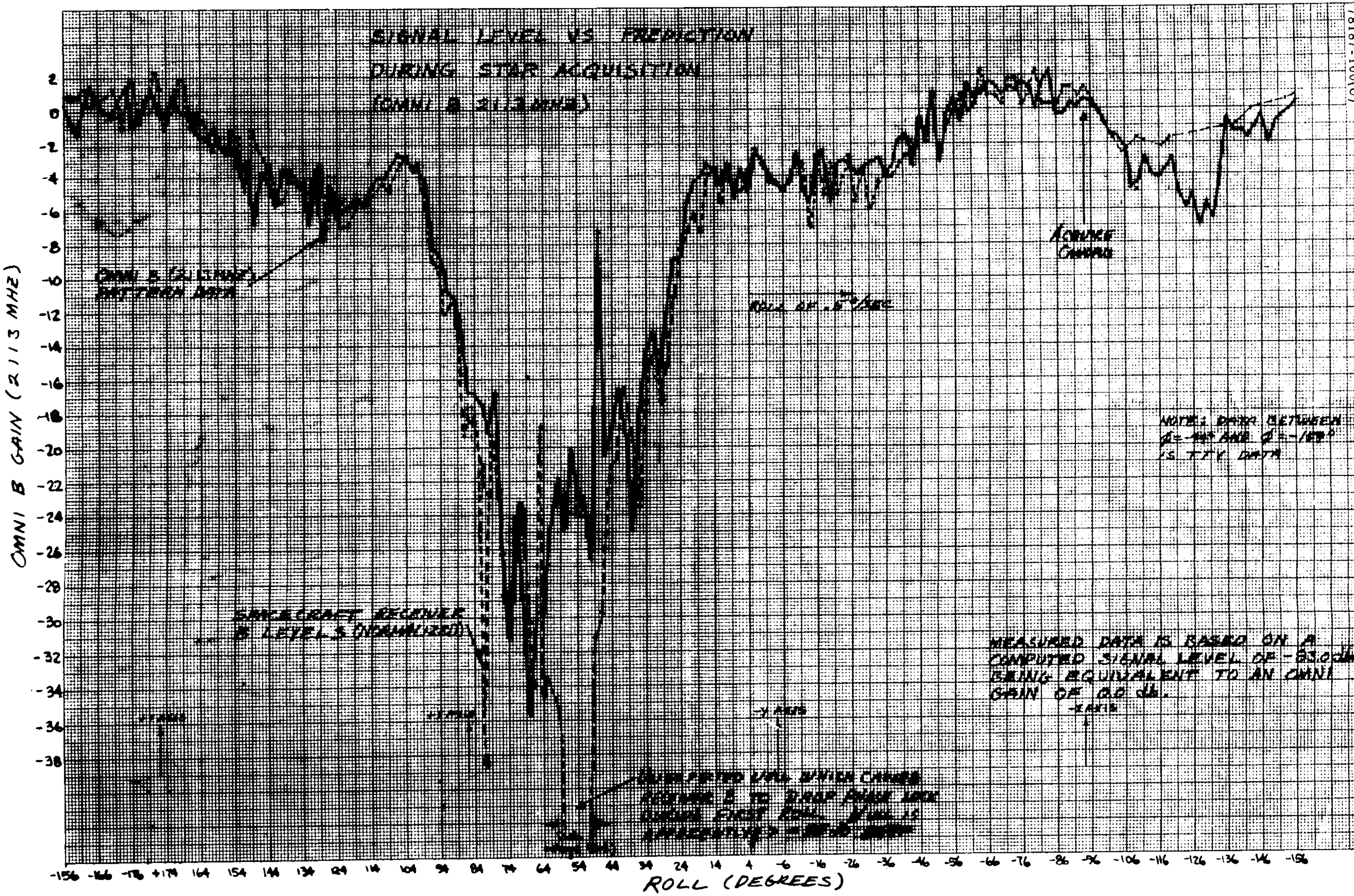

d) Omnidirectional Antenna B Up Link (2113 MHz)

Figure 5.3-6 (continued). Signal Level Versus Predictions During Star Acquisition

predicted seems to be, in general, the same for both omnidirectional antennas A and B. It is unlikely that both antennas would be biased by the same amount. Therefore, these data indicate that the transmitter power may be higher than expected or that the transmitting circuit losses common to both antennas may be lower than expected.

5.3.4.5 Mission Phase 4: Midcourse Maneuvers

The L+18 hours optional roll-yaw was selected from 16 possibilities as the midcourse maneuver. Real-time analysis predicted the following variations in nominal omnidirectional antenna gain during the maneuver:

1) Omnidirectional antenna B down link: $-4.6 < G < +1.2$ db

2) Omnidirectional antenna A up link: $-20.2 < G < +0.1$ db

3) Omnidirectional antenna B up link: $-12.6 < G < +1.6$ db

Predicted minimum margins were 12.9 db for 4400 bits/sec telemetry, 5.8 db on receiver A, and 13.4 db on receiver B command links. Two-way (transponder) mode was recommended.

At 312:01:51:19 GMT, the spacecraft was commanded to high power and, at 312:01:52:05 GMT, the 4400 bit/sec data rate was selected. The ground received signal increased by 15.9 db when the spacecraft was commanded from lower power to high power, with DSS 11 reporting a received carrier power of -122.0 dbm prior to maneuvering. Maneuver initiation times were 312:02:02:59 GMT for the roll and 312:02:09:08 GMT for the yaw. The DSS 11 received carrier power at the end of the premidcourse maneuver was reading -124.7 dbm and had indicated approximately a 4.9 db variation during the maneuver, as opposed to predicted variations of 5.8 db. Spacecraft receiver signal level variations were approximately 17.1 db for receiver A and 12.1 db for receiver B, as opposed to predicted variations of 22 db and 14.2 db for receivers A and B, respectively.

At 312:02:20:02 GMT, midcourse thrust was executed. DSS 11 received carrier power was steady with reported 0.4 db variations during the thrusting period.

At 312:02:22:18 GMT, mode 5 data were selected in preparation for the postmidcourse maneuver. Maneuver initiation times were 312:02:26:07 GMT for the yaw and 312:02:32:57 GMT for the roll. The postmidcourse maneuver ended at approximately 312:02:36:05 GMT with both the up-link and down-link signal levels essentially retracing those seen in the premidcourse maneuver.

Canopus lockon was indicated at 312:02:35:53 GMT, and preparations were made to return the spacecraft to its cruise configuration. At the end of the midcourse sequence, the DSS 11 received carrier power (-122.3 dbm) indicated that a nominal positive telemetry margin should exist with the spacecraft at 1100 bits/sec in low power. At 312:02:46:09 GMT, the

1100 bits/sec data rate was selected and, at 312:02:46:08, the spacecraft was returned to low power. The spacecraft operated in high power for 54 minutes and 49 seconds during the midcourse maneuver sequence. Approximately a 16.5 db decrease from high to low power was noted. The resulting -133.8 dbm received carrier level produced a 4.8 db telemetry margin for 1100 bits/sec data.

5.3.4.6 Mission Phase 5: Terminal Maneuver

The roll-yaw-roll standard maneuver was selected from eight possibilities as the terminal maneuver, and was optimum for the communications link. Real-time analysis predicted the following variations in nominal omnidirectional antenna gains during the maneuver:

1) Omnidirectional antenna B down link: $-3.7 < G < +1.9$ db

2) Omnidirectional antenna A up link: $-14.1 < G < +0.5$ db

3) Omnidirectional antenna B up link: $-10.1 < G < +0.9$ db

Predicted minimum margins were 4.8 db for 1100 bits/sec telemetry, 5.0 db on receiver A, and 9.0 db on receiver B command links. One-way mode was recommended even though adequate margins were available for the transponder operation. This recommendation was made since one-way configuration was desired for the terminal descent sequence and, operationally, it was safer to establish before the terminal maneuver.

The spacecraft was commanded to high power at 00:07:32 GMT of day 314, and 1100 bits/sec data was selected at 00:08:20 GMT. The resulting -124.0 dbm carrier level indicated an increase of 16.4 db over low power operation. Transponder B was turned off at 00:16:59 GMT, establishing the spacecraft configuration for the terminal sequence. Maneuver initiation times were 00:25:20 for the first roll, 00:29:38 for the yaw, and 00:34:56 GMT for the second roll. The received carrier power at DSS 11 of -122.0 dbm at the end of the terminal maneuvers was in complete agreement with the predicted nominal expected value. Signal level variations during the maneuvers are shown in Table 5.3-9.

TABLE 5.3-9. SIGNAL LEVEL DURING TERMINAL MANEUVERS

Attitude Rotation, degrees	Signal Level Variations, db					
	Spacecraft to Earth (Omnidirectional Antenna B)		Earth to Spacecraft			
			Receiver A		Receiver B	
	Predicted	Observed	Predicted	Observed	Predicted	Observed
Roll + 82.0	3.3	3.1	12	10.2	5.9	8.3
Yaw + 111.8	2.8	4.7	2.6	4.4	11.0	10.1
Roll + 120.5	5.6	5.8	9.5	9.9	7.9	7.2

5.3.4.7 Mission Phase 6: Descent and Touchdown

A preterminal maneuver analysis was performed to evaluate the expected data link performance during the descent and touchdown phase with the touchdown strain gages on prior to retro ignition. Best estimates of spacecraft worst-case performance during this phase indicated that, with strain gages on, 1100 bits/sec data would be obtained at a bit error rate less than 3×10^{-3} at both DSS 14 (210-foot antenna) and DSS 11 (85-foot antenna) with the spacecraft transmitting on omnidirectional antenna B.

The touchdown strain gages were turned on at 00:40:03 GMT. The DSS 11 received carrier power was -124.8 dbm prior to retro ignition which was in agreement with the predicted nominal value used for the preterminal strain gage feasibility analysis.

Retro burn was initiated at approximately 00:58:04 GMT, and the signal level at DSS 11 remained steady with approximately a 0.7-db variation during the burn period. Burnout occurred at approximately 00:58:44 GMT, and the spacecraft began the steering phase of descent. Signal level variations of 2.7-db were noted during descent with the minimum signal level being -127.5 dbm which agreed with nominal predictions.

Touchdown occurred at 314:01:01:05.5 GMT with the carrier power at DSS 11 reported as -126.9 dbm. Good PCM data and touchdown strain gage data were obtained, and ground receiver lock was retained through touchdown.

5.3.4.8 Mission Phase 7: Lunar

The data relative to the lunar phase consist of several disjointed topics. The topics applying to the RF subsystem will be summarized in the following text.

Post-Touchdown Spacecraft Assessment (Day 314)

Transmitter B high voltage was commanded off at 01:22:14 GMT after having been in high power for 1 hour 14 minutes and 42 seconds during the terminal phase of the mission. A 16.8-db decrease from high to low power was observed. Transmitter A was turned on for the first time since the prelaunch countdown approximately 1/2 hour after touchdown. DSS 11 receiver carrier power was reported to be -124.5 dbm with the spacecraft at 1100 bits/sec data with transmitter A in high power on omnidirectional antenna B. Omnidirectional antenna A was selected with a resulting 1.2-db decrease in the ground received signal. Omnidirectional antenna B was then reselected since it was obviously the favorable transmitting omnidirectional antenna.

TV Performance

The first 200-line television picture was transmitted approximately 1 hour after touchdown. Based on reported DSS 11 signal levels, the computed nominal SNR for the first picture was 13.0 ± 1.0 db.

The first 600-line television picture was transmitted approximately 3 hours after touchdown, shortly after the planar array was roughly aligned with the earth. Based on reported DSS signal levels, the computed nominal SNR for the first picture was 16.2 ± 1.0 db.

In both cases, the SNR was high enough to provide good quality detected video data which is apparent in the quality and resolution of the pictures.

Alpha Scattering Performance

The alpha scattering experiment was performed during much of the first lunar day. The total power at the ground station, with the planar array pointed toward the earth, was reported to be, in general, -111.6 dbm (spacecraft transmitter A). This signal level for the 1100 bits/sec/alpha scattering multiplex mode resulted in nominal SNRs of 23.3 db for the 1100 bits/sec data, and 20.2 and 19.1 db for the two alpha scattering channels. Good quality data, therefore, was expected and received for this experiment.

RF Assessment

Two spacecraft RF performance assessments were made during the first lunar day. DSS 42 provided ground support on day 318 with DSS 61 handling the assessment on day 325. This assessment essentially exercises the subsystem in all possible transmitting and command receiving configurations. It was clearly evident from this assessment that all aspects of the subsystem were performing in a nominal manner.

Liftoff and Translation Experiment

A liftoff and translation experiment was performed on day 321. The spacecraft configuration and initial conditions were as follows:

1) Receiver A AGC = -96 dbm (command margin of +18 db)
   Receiver B AGC = -107.4 dbm
   (after A/SPP positioning for the experiment)

2) Spacecraft earth vector in MTGS coordinates was θ = 177.1 degrees, φ = -23.8 degrees.

3) Data transmission on omni antenna A with transmitter A in high power.

4) Receiver A was selected.

The telecommunications performance during the experiment was as follows:

1) No plume effects were evident during the experiment.

2) The spacecraft earth vector was such that there was no line of sight interference from the solar panel and planar array.

3) Vernier engine thrusting during the hop was terminated by two turn-off commands, with the second command immediately following the first. The first turn-off command was rejected by the receiver for unknown reasons. However, the following items have been determined to not have been the cause:

   a) Improper command

   b) Fault in ground equipment

   c) Faulty spacecraft receivers

The most probable cause for the command rejection is an RF multipath null or an extremely rare statistical event.

Based on the performance during the experiment, it is recommended that time critical commands be sent a minimum of three times for future lift-off and translation experiments. Two adjacent commands could conceivably be rejected if the multipath null extended over part of the time period of either command. Since it is felt that a null would be of relatively short duration and that nulls would not occur frequently, sending three commands would minimize the possibility of a command reject.

In order to evaluate the sensitivity of the antenna patterns it is also recommended that the A/SPP be stepped ±5 degrees in polar, elevation, and roll after final positioning.

5.3.4.9 Mission Data Plots

Transmitter B Traveling-Wave Tube Temperature (D-14) (Figure 5.1-A1) — These data represent the temperature of the traveling-wave tube used for high-power transmitter operation during transit.

5.3.5 REFERENCES

1. "Surveyor Mission F Space Flight Operations Report," Hughes Aircraft Company, SSD 78187, December 1967.

2. "Surveyor Mission F Telecommunication Subsystem Prediction and Performance Summary Document," Hughes Aircraft Company, SSD 74118, 19 September 1967.

3. B. M. Ross, "Telemetry Calibration Data for SC-6," Hughes Aircraft Company, IDC 2294.2/155.

4. B. M. Ross, "S/C RCVRA S/N 18 and RCVR B S/N 26 Space-environment Calibration Data," Hughes Aircraft Company, IDC 2294.2/172.

5. "Final Report, Surveyor Spacecraft 6 Mission Operations System Compatibility Test (Conducted at AFETR)," Jet Propulsion Laboratory, October 1967.

6. "Surveyor V Flight Performance Final Report," Hughes Aircraft Company, SSD 68189-5, November 1967.

7. "Surveyor III Flight Performance Final Report," Hughes Aircraft Company, SSD 68189-3, July 1967.

8. R. L. Chafin, "700 Hz Tracking Loop Bandwidth Operation at DSS-14," Jet Propulsion Laboratory, 10M 337F-67-419, 6 November 1967.

5.3.6 ACKNOWLEDGMENTS

1) J.O. Votaw was the coordinator and author of this section.

2) Q.D. Howard, and W. Mitchell for their assistance in reducing, formatting, and analyzing much of the data contained in this section.

3) The DSS tracking advisors at JPL for supplying ground station data.

4) The Spacecraft Performance/Analysis/Command Telecommunications Team, consisting of V.S. Amstadter, W. Mitchell, W.G. Moore, Q.D. Howard, and M.R. Weiner, for maintaining accurate mission records and logs.

5) F.K. Rickman who, although not officially a member of the Spacecraft Performance/Analysis/Command Telecommunications Team, significantly contributed to the real-time operational support of the subsystem.

5.4 SIGNAL PROCESSING

5.4.1 INTRODUCTION

The signal processing subsystem is composed of the following units:

1) Engineering signal processor (ESP)
2) Auxiliary engineering signal processor (AESP)
3) Central signal processor (CSP)
4) Signal processing auxiliary (SPA)
5) Low data rate auxiliary (LDRA)

These units, ~~containing~~ containing two electronic commutators with 6 operational modes, 2 analog-to-digital converters that have available 5 digital bit rates, 17 subcarrier oscillators for transmission of pulse coded modulation data and continuous real-time data, 9 summing amplifiers, and a signal conditioning subsystem, performed normally throughout the mission.

A summary of test and flight values for signal processing telemetry can be found in Table 5.4-1. Values for the Surveyor I, 2, III, 4, and V flights have been included for comparison.

5.4.2 ANOMALIES

There were no anomalies in the signal processing subsystem throughout the transit flight.

5.4.3 SUMMARY

The signal processing subsystem performed properly throughout the transit flight. A thorough analysis of the touchdown strain gages was performed in which computerized signal processing techniques were used, such as diversity combining and digital filtering. An alpha scattering bit error rate of 10^{-6} was determined from the received data.

TABLE 5.4-1. COMPARISON OF SIGNAL PROCESSING VALUES FROM TEST AND FLIGHT

Telemetry Signal	Surveyor VI STV-A1 Retest Values	Surveyor VI Flight Values	Surveyor V Flight Values, Day 251	Surveyor 4 STV Retest Values	Surveyor 4 Flight Values, Day 197	Surveyor III STV-C4 Retest Values	Surveyor III Flight Values, Day 107	Surveyor 2 Flight Values	Surveyor I Flight Values
S-1 reference voltage, volts*	4.895	4.89	4.90	4.88	4.875	4.86 to -4.9	4.86	4.9	4.88
S-2 reference return, volts*	0.00244	0.0024	0.0024	0	0	0	0	0.003	0.0024 to 0.0072
S-5 ESP commutator unbalance current, microamperes*	0.32	0.32	-0.7649	-1.7	-1.714	-2.2 to -2.6	-2.1	-1.4	-3.1
S-7 AESP commutator unbalance current, microamperes**	-0.9669	-0.7618	-2.062	-3.0	-2.813	-1.0 to -1.2	-1.3	-1.7	-2.8
S-8 AESP reference voltage, volts***	4.958	4.948	4.95		4.938		4.94	4.94	4.938

*Mode 4.
**Mode 5.
***Mode 5; values before Surveyor V are computed.

5.4.4 SIGNAL PROCESSING ANALYSIS

5.4.4.1 Unbalance Current Corrections

In each telemetry commutator, transistor switches connect each analog output voltage (representing a spacecraft voltage, current, or temperature) with a common commutator line connected to the input of one of two analog-to-digital converters. A bootstrap unloader circuit is connected to this common line to reduce the stray capacitance, equalize the load impedance, and provide bias currents for the commutator and master switches. Since these bias currents are not exactly equal, a difference or unbalance current exists. The telemetry circuit being sampled must supply this current, causing an error in the measured voltage proportional to the output impedance of the circuit.

The unbalance current for a specific telemetry channel in each commutator (S-5 for ESP and S-7 for AESP) is measured in telemetry modes 2, 4, and 5, with typical values given in Table 5.4-1.

5.4.4.2 Potentiometer Reference Voltage Corrections

The nominally 4.85 reference voltage is supplied by either the ESP or AESP units to the landing gear and solar panel position potentiometers, to the propulsion pressure transducers, and to the secondary sun sensors. This reference voltage, derived from the 29-volt nonessential bus, varies due to load and input supply voltage changes. The ESP voltage is telemetered in modes 2 and 4, and can be used to correct the affected signals, whose calibrations are based on a reference voltage of exactly 4.85 volts. The AESP voltage was not telemetered before Surveyor V; therefore, the values given in Table 5.4-1 for earlier spacecraft were obtained by computation.

5.4.4.3 Current Calibration Signals

Current measurements are accomplished by measuring the voltage drop across a low resistance shunt which is in series with the power line being monitored. This measurement is in the range of 0 to 100 millivolts. Since this voltage is not referenced to ground and is not scaled to the 0- to 5-volt telemetry input level range, it is necessary to amplify it with a differential amplifier. The nominal gain of this amplifier is 50, but its actual gain linearity and stability are not specified to a tight tolerance. To determine the current amplifier parameters and thereby increase the accuracy of current measurements, three calibration signals (with 0.2-percent stability) are amplified and telemetered in each commutator. These signals can thus be used by postmission processing for a continual in-flight calibration of the current amplifier.

Only the AESP current calibration signals were investigated. Table 5.4-2 shows that these signals have changed by no more than 0.5 percent since being initially set at the unit flight acceptance test. It is also seen that the gain of the AESP current amplifier was reasonably constant over the mission.

TABLE 5.4-2. SUMMARY OF CURRENT CALIBRATION SIGNAL DATA IN AESP

Signal	Nominal Percent of Full Scale	Flight Data, percent change	Remarks
EP-27	90	0.1745	Before midcourse
		0.2	After midcourse
EP-28	50	0.182	Before midcourse
		0.0	After midcourse
EP-29	10	0.445	Before midcourse
		0.15	After midcourse

5.4.4.4 Touchdown Strain Gage Data

Magnetic tape data were obtained from two DSIF stations via the 85-foot diameter antenna at the Pioneer site and the 210-foot diameter antenna at the Mars site. These two independent signal paths allow the technique of space diversity combining (References 1 and 2) to be used on the two sets of touchdown strain gage (TSG) data, resulting in a signal trace with improved signal-to-noise ratio. A set of waveforms from the 85-foot diameter antenna was also obtained on the Surveyor hop.

Footpad impact times were as follows:

Leg 1: 314:01:01:05.467 ± 0.003

Leg 2: 314:01:01:05.490 ± 0.003

Leg 3: 314:01:01:05.506 ± 0.003

The original data were recorded with a cutoff frequency of 100 Hz. They were then low-pass filtered (by means of digital filtering on a computer) at 50-, 30-, and 15-Hz (-3 db) bandwidths before being diversity combined. This method provided better signal-to-noise ratios on the waveforms that were filtered by the 30- and 15-Hz bandwidths, because of intermodulation distortion (IMD) components at approximately 45 to 50 Hz. This can be seen by comparing Figure 5.4-1 (50-Hz bandwidth) with Figure 5.4-2 (30-Hz bandwidth).

Figure 5.4-1 shows strain gages 1, 2, and 3 filtered by a sixth order Butterworth filter with a 50-Hz bandwidth. Figures 5.4-2 and 5.4-3 are similar with filter bandwidths of 30 and 15 Hz, respectively.

The signal-to-noise ratio listed on each plot is a mean power ratio of the signal from an assumed initial zero deflection point to an assumed final zero deflection point with respect to the noise defined over some interval prior to touchdown. This analysis assumes that the noise variance is unchanged prior to and during the signal duration.

5.4.5 DOCUMENTATION

1) A. W. Dittmer, "The Use of Diversity Receiving Techniques to Enhance Surveyor SC-1 Strain Gage Signals," Hughes IDC 2292/188, 10 January 1967.

2) A. W. Dittmer, "Computer Analysis and Prediction of Surveyor Spacecraft (SC-1) Strain Gage Signals," Hughes IDC 2292/85, 1966.

3) R. J. Rechter, "Computer Analysis of SC-3 through SC-7 TSG Multiplex Intermodulation Distortion and Other Factors," Hughes IDC 2292/223, Revision 1, March 1967.

4) M. Fashano and R. J. Rechter, "DTRB-21 Test Procedures, Results and Summary (TSG Multiplex)," Hughes IDC 2292/267, 5 May 1967.

5.4.6 ACKNOWLEDGMENTS

This section was coordinated by A. W. Dittmer. The touchdown strain gage diversity combining and filtering was done by W. W. Mayfield.

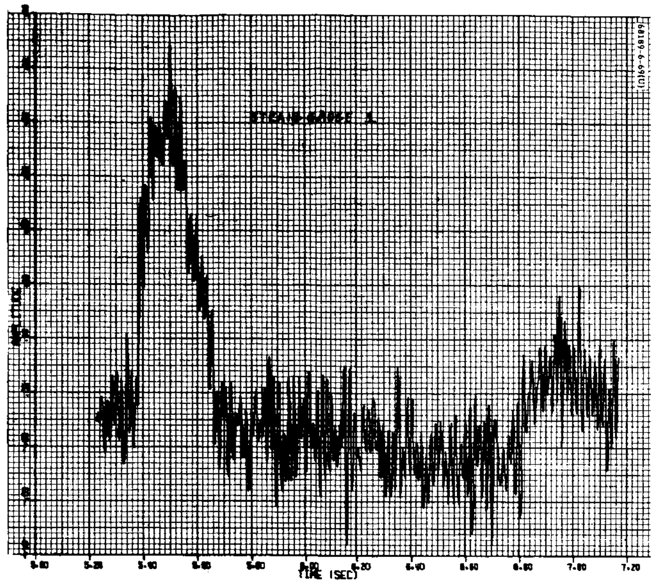

a) Strain Gage 1

SNR = 4. 5 db

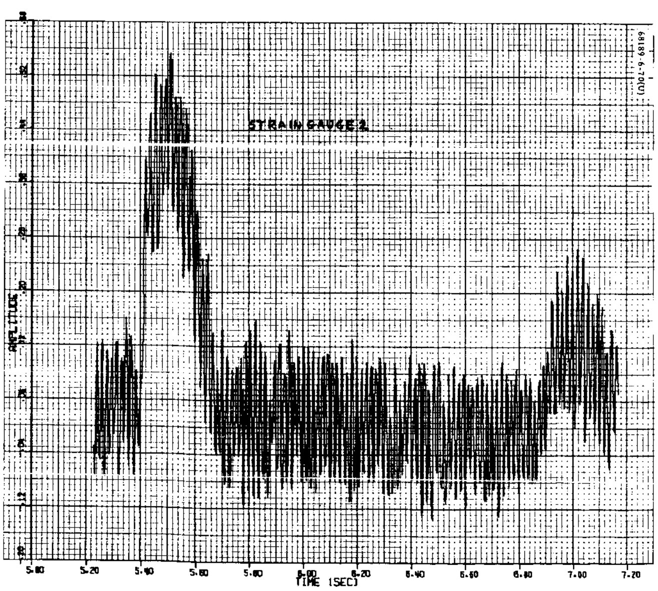

b) Strain Gage 2

SNR = 5. 5 db

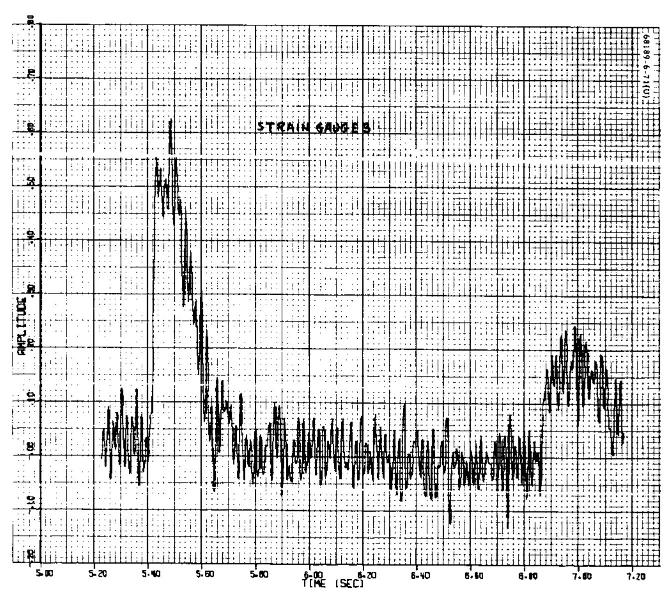

c) Strain Gage 3

SNR = 11. 1 db

Figure 5. 4-1. Diversity Combined
50-Hz Bandwidth

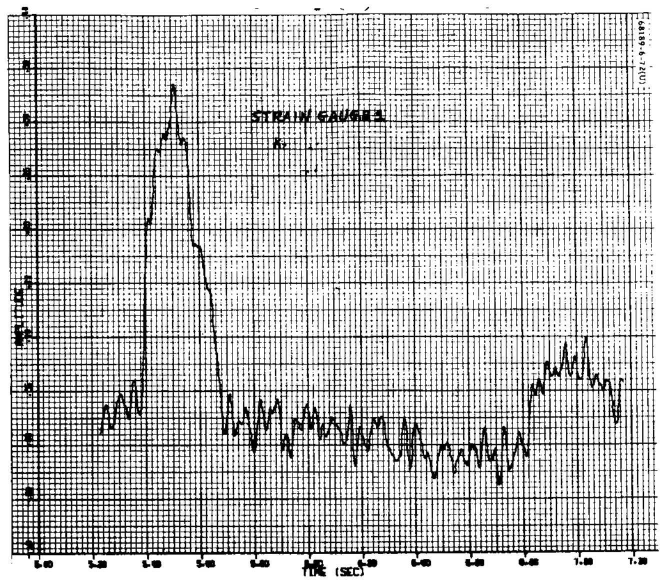

a) Strain Gage 1

SNR = 3.0 db

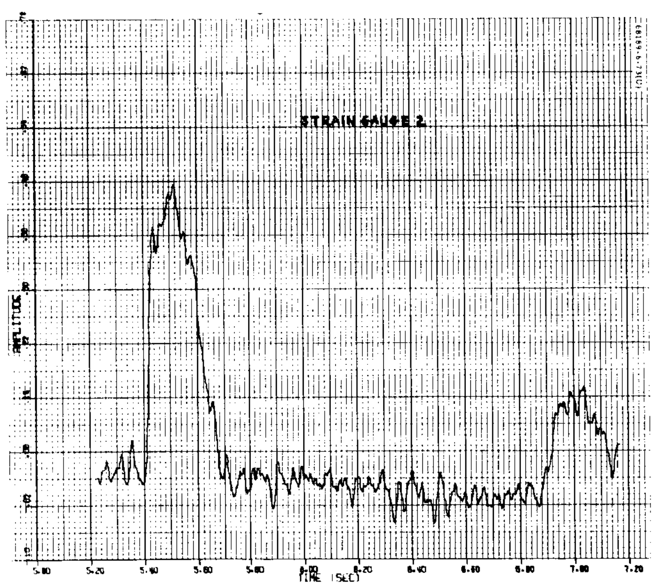

b) Strain Gage 2

SNR = 9.5 db

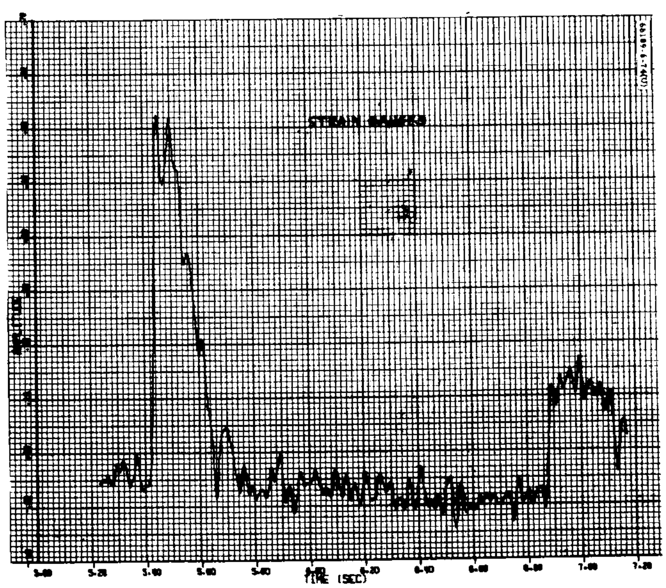

c) Strain Gage 3

SNR = 16.0 db

Figure 5.4-2. Diversity Combined
30-Hz Filter Bandwidth

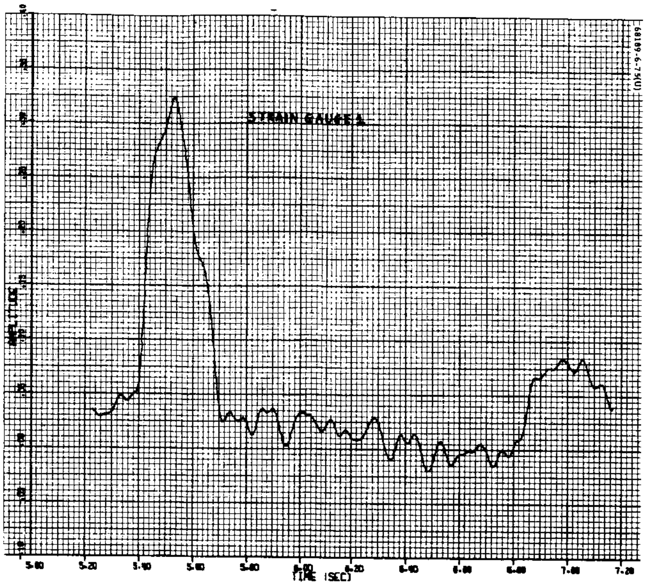

a) Strain Gage 1

SNR = 1.0 db

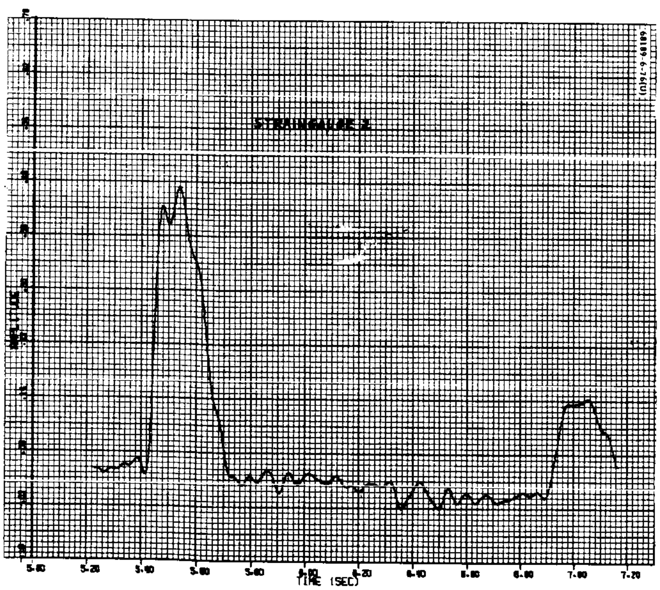

b) Strain Gage 2

SNR = 7.3 db

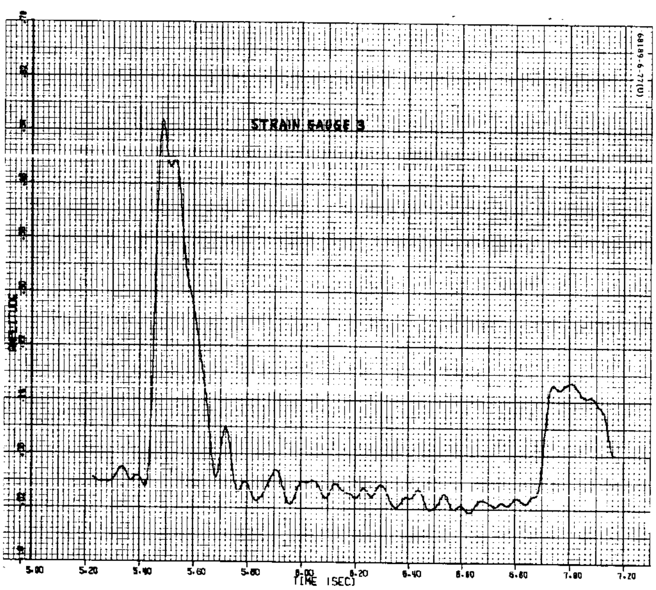

c) Strain Gage 3

SNR = 19.6 db

Figure 5.4-3. Diversity Combined
15-Hz Filter Bandwidth

5.5 FLIGHT CONTROL

5.5.1 INTRODUCTION

The principal requirements of the Surveyor flight control system are attitude control, accurate angular maneuvers, precision velocity corrections, and a soft lunar landing. In order to accomplish these functions, the control system utilizes such hardware as gyros, gas jets, a solid fuel engine, liquid fuel engines, optical sensors, timing devices, radars, and acceleration sensing mechanisms.

5.5.1.1 Attitude Control

Attitude control is accomplished by two basic types of active control systems. During coast phase, a bang-bang type of attitude gas jet system is employed which utilizes artificial rate feedback for loop stabilization. During periods of potentially large moment disturbances, such as the main retro phase, the throttle-controlled vernier engine system is used. The error signals required for controlling the propulsion systems are derived from optical sensors or rate integrating gyros which are mounted on the spacecraft in such a way as to provide a three-axis control system. During coast phase, when the gas jet system is used, two modes of operation are available. One is the celestial referenced mode using the sun and Canopus, and the second is self-contained inertial referencing (gyros). The first mode is used to establish accurate spatial attitude, and the second mode is generally used when momentary inertial reference is desired; such an instance occurs during an attitude maneuver.

5.5.1.2 Angular Maneuvers

The rate integrating gyros are also used for accurate angular maneuvers, accomplished by precessing the gyros at precise rates for given time intervals and slaving the spacecraft to the gyros through the gas jet system.

5.5.1.3 Velocity Correction

A midcourse velocity correction capability is provided by a system consisting of three vernier engines, a precision timer, and an accurate acceleration sensing device. The difference between the commanded acceleration level and the output from an accelerometer provides the error signal that commands the vernier engines to the required thrust levels. The constant acceleration and variable time concept used by the Surveyor flight control system provides the flexibility of choosing velocity corrections from 2.0 to 100 m/sec.

5.5.1.4 Soft Landing

Surveyor's soft landing capability is provided by a sophisticated technique utilizing radars to compute velocities and range. The range information is then used by an on-board computer to provide vertical velocity commands to the vernier engine system according to an approximate, constant acceleration, V^2/R function. The velocity information is used by the vernier engine attitude control loop to produce a near-gravity turn descent by aligning the spacecraft thrust axis to the true velocity vector. The velocity information is also used, along with velocity commands, to generate error signals for the velocity control loop.

To provide the required condition of low velocity for the soft landing phase, a large amount of approach velocity is removed by a solid fuel rocket engine during the initial portion of the terminal descent phase. Spacecraft attitude during this phase is inertially stabilized by the gyro vernier engine control system.

5.5.1.5 Mission Performance

During the Surveyor VI mission, each of the above mentioned tasks was performed satisfactorily.

5.5.1.6 Analysis

Subsection 5.5.4 contains the analysis effort. The analysis items are categorized under major mission phases for easier identification and performance evaluation. A log of time and events is presented in Table 5.5-1, and a table of results (Table 5.5-2) is given in subsection 5.5.3.

5.5.2 ANOMALY DESCRIPTION

No flight control anomalies occurred during the mission.

5.5.3 SUMMARY

A summary of flight control performance is presented in Table 5.5-2.

TABLE 5.5-1. SURVEYOR VI TIME AND EVENTS LOG

Event	Date, GMT	Mission Time	
		GMT, hr:min:sec	From Launch
Launch	7 November 1967	07:39:01	0
Injection		08:03:30	24M29S
Separation			
Electrical		08:04:24	25M23S
Mechanical		08:04:30	25M29S
Automatic sun acquisition			
Start		08:05:18	26M17S
Completed		08:14:50	39M49S
Canopus verification, started		15:50:23	8H11M22S
Canopus acquisition, completed		16:27:49	8H48M48S
Gyro drift check No. 1			
Start		16:43:04	9H04M03S
Stop		18:04:10	10H25M09S
Gyro drift check No. 2			
Start		18:18:21	10H39M20S
Stop		19:22:31	11H43M30S
Gyro drift check No. 3, roll only			
Start		19:24:24	11H45M23S
Stop		20:38:56	12H59M55S
Gyro drift check No. 4			
Start		20:44:50	13H05M49S
Stop		22:03:03	14H24M02S
Premidcourse (+) roll, 91.9 degrees	8 November 1967		
Start		02:03:00	18H23M59S
Stop		02:06:04	18H27M03S

Table 5.5-1 (continued)

Event	Date, GMT	Mission Time	
		GMT, hr:min:sec	From Launch
Premidcourse (+) yaw, 127.3 degrees			
Start		02:09:09	18H30M08S
Stop		02:13:24	18H34M23S
Midcourse thrust executed		02:20:03	18H41M02S
Sun reacquired		02:31:44	18H52M43S
Canopus reacquired		02:35:53	18H56M52S
Gyro drift check No. 5			
Start		04:37:49	20H58M48S
Stop		05:42:50	22H03M49S
Gyro drift check No. 6 (roll only)			
Start		08:32:26	24H53M25S
Stop		12:46:28	28H59M27S
Gyro drift check No. 7			
Start		16:18:38	32H39M37S
Stop		17:53:41	34H14M40S
Gyro drift check No. 8, (roll only)			
Start		18:59:38	35H20M37S
Stop		21:42:26	38H03M25S
Gyro drift check No. 9			
Start		22:44:59	39H05M58S
Stop	9 November 1967	00:11:16	40H32M15S
Gyro drift check No. 10			
Start		01:11:23	41H32M22S
Stop		02:25:34	42H46M33S
Gyro drift check No. 11			
Start		03:29:50	43H50M49S
Stop		04:49:08	45H10M07S

Table 5.5-1 (continued)

Event	Date, GMT	Mission Time	
		GMT, hr:min:sec	From Launch
Gyro drift check No. 12			
Start		06:25:57	46H46M56S
Stop		07:38:32	47H59M31S
Gyro drift check No. 13			
Start		09:04:07	49H25M06S
Stop		10:42:27	51H03M26S
Gyro drift check No. 14, (roll only)			
Start		11:01:22	51H22M21S
Stop		15:26:55	55H47M54S
Preretro (+) roll, 81.7 degrees	10 November 1967		
Start		00:25:20	64H46M19S
Stop		00:28:04	64H49M03S
Preretro (+) yaw, 111.7 degrees			
Start		00:29:38	64H50M37S
Stop		00:33:22	64H54M21S
Preretro (+) roll, 120.5 degrees			
Start		00:34:56	64H55M55S
Stop		00:38:57	64H59M56S
AMR mark		00:57:57	65H18M56S
Vernier ignition		00:58:03	65H19M02S
Retro eject		00:58:56	65H19M55S
1000-foot mark		01:00:41	65H21M40S
14-foot mark		01:01:04	65H22M03S
Touchdown		01:01:05	65H22M04S

TABLE 5.5-2. FLIGHT CONTROL RESULTS

	Controlling Specification	Specification Value	Results	Comments
Prelaunch				
Proper gyro temperature control			Roll 168.6 °F Pitch 163.0 °F Yaw 162.5 °F	Time was 311:07:39 GMT
Verification of N_2 loading	224832A	4.57 pounds	4.56 pounds	(FC-4) = 4686 psi (FC-48) = 80.4°F
Centaur separation	(3.5.2.1)			
Time required to null rates to less than 0.1 deg/sec		<0.1 deg/sec within 50 seconds	<17 seconds	
Magnitude of angular rate at separation		≤3.0 deg/sec	≈0.0 deg/sec	
Sun acquisition				
Proper sun acquisition	(7.3.3.3.4)	Minus roll maneuver until activation of acquisition sun sensor and then a plus yaw maneuver until primary sun sensor illumination		
Roll			264 degrees of roll	
Yaw			22 degrees of yaw	
Total time			572 seconds	
N_2 gas used	Design	0.054 pound (average)	<0.1 pound	
Star acquisition	(7.3.3.3.5)	Positive roll maneuver sufficient to produce an adequate star map for Canopus verification. Provide a lockon signal when Canopus appears in the sensor field of view		
Proper acquisition and verification of Canopus			Automatic lockon	
Roll angle from beginning of maneuver to Canopus			298 degrees	
Objects identified			Deneb, Canopus, earth	
Mean roll rate during star map phase		0.5 deg/sec	0.5009 deg/sec	
Effective gain (relative to nominal Canopus) of Canopus sensor			1.10 x Canopus	
N_2 gas used	Design	0.048 pound (average)	<0.1 pound	
Coast mode	(7.3.3.3.6)	Roll axis shall be held to within 0.20 degree of sun-spacecraft line, plus a ±0.30 degree limit cycle Same magnitude as above for Canopus-spacecraft line		Sun and star error signal noise level were low enough to have no effect on the limit cycle performance
Limit cycle (gas jet system)	(7.3.3.3.3)			
Optical mode/inertial mode	(7.3.3.3.5)	±0.30 degree		Values are that of the total deadband. Predicted values were:
Average amplitude—roll			0.41/0.48 degree	0.44/0.44 degree
Average amplitude—pitch			0.52/0.37 degree	0.44/0.44 degree
Average amplitude—yaw			0.52/0.30 degree	0.44/0.44 degree
Gyro drift	(7.3.3.3.3C)	<1 deg/hr		
Roll			Roll -0.64 deg/hr	
Pitch			Pitch ≈0 deg/hr	
Yaw			Yaw +1.4 deg/hr	
Gas jet thrust level		>0.052 pound	0.064 pound (roll)	Design value is 0.057 pound

Table 5. 5-2 (continued)

	Controlling Specification	Specification Value	Results	Comments
Premidcourse maneuvers				
Maneuver angles	(7.3.3.3.7)	Rates shall be controlled to be 0.5 ±0.0011 deg/sec		Assuming a precession level of 0.5000 deg/sec
Roll + 91.9 degrees			+91.815 degrees	
Yaw + 127.3 degrees			+127.35 degrees	
Precession command times		0.2 second plus 0.02 percent of command interval magnitude		These times were obtained from the gyro error signal response profile
Roll 183.8 seconds			183.63 seconds	
Yaw 254.6 seconds			254.7 seconds	
Attitude maneuver accuracy (includes drift, initial attitude errors, and limit cycle)			0.16 degree with 0.24 degree 3σ uncertainty	Calculated using actual data of drift, attitude errors, and execution errors
Maximum midcourse acceleration error	224832A	ΔV error <±1.3 ft/sec	-0.132 fps	
Expected ΔV/tracking ΔV			10.064 m/sec 10.122 m/sec	
Shutdown impulse (No. 1 burn)	(8.3.1.3.2.4.1)	<5 lb-sec/engine Δ impulse <0.66 lb/sec		
Engine 1			+0.085 lb-sec	
Engine 2			-0.09 lb-sec	
Engine 3			+0.015 lb-sec	
Preretro maneuvers				
Manuever angles	(7.3.3.3.7)	Rates shall be controlled to be 0.5±0.0011 deg/sec		Values only include execution error. The desired values were:
Roll			+81.82 degrees	Roll (+)81.7 degrees
Yaw			+111.71 degrees	Yaw (+)111.7 degrees
Roll			+120.55 degrees	Roll (+)120.5 degrees
Precession command times		0.2 second plus 0.02 percent of the command interval magnitude		The command values were:
Roll			163.64 seconds	163.4 seconds
Yaw			223.42 seconds	223.4 seconds
Roll			241.09 seconds	241.0 seconds
Pointing accuracy (includes drift, initial attitude errors, and limit cycle)		Within ±1 degree	0.26 degree with 0.21 3σ uncertainty	
Gyro drift compensation values				
Roll			-0.64 deg/hr	
Pitch			0 deg/hr	
Yaw			+1.4 deg/hr	
Terminal descent				
Main retro				
Burn time (from ignition to 3.5 g switch)	(7.3.3.3.9)	Approximately 39 seconds	39.56 seconds	
Maximum retro thrust		<10,000 pounds	9550 pounds	Computed using retro accelerometer data
Peak attitude transient at vernier ignite – retro ignite	(7.3.3.3.10)			
Roll			-0.77 degree	
Pitch			-0.17 degree	
Yaw			-0.08 degree	

Table 5.5-2 (continued)

	Controlling Specification	Specification Value	Results	Comments
Main retro thrust vector to spacecraft center of gravity	(8.3.5.3.2.8)	<0.18 inch	0.04 inch	
Thrust vector pointing accuracy during retro burn	(8.3.5.3.2.9)	Within ±1 degree	0.8 degree	Based on estimated versus actual burn-out conditions
Main attitude error during burn				
Roll			-0.15 degree	
Pitch			+0.08 degree	
Yaw			-0.03 degree	
Roll actuator position				
Peak at retro ignition			+1.08 degrees	
Mean value during burn			+0.125 degree	
Time between major events	(7.3.3.3.9)			
AMR mark and vernier ignition		5.875 seconds expected	5.9 seconds	
Vernier and retro ignition		1.1 ± 0.1 seconds	1.1 seconds	
Retro ignition and RADVS pyro switch on		0.55 ± 0.1 second	$0.36^{+0.6}_{-0.36}$ second	
Retro ignition and retro burnout (inertia switch closes)		39.6 seconds expected	39.56 seconds	
Retro burnout and high thrust		10.0 seconds expected	9.65 seconds	
High thrust and retro eject		2.0 seconds expected	2.3 seconds	
Retro eject and start of RADVS-controlled descent		2.15 seconds expected	2.10 seconds	
Retro burnout conditions				
Attitude			36,625 feet	
Total velocity			515 fps	
Angle between thrust vector and velocity vector			26 degrees	$V_x \approx +0.0$ fps $V_y = +225$ fps
Time to align Z-axis to velocity vector		9 seconds maximum	<6 seconds	
Descent segment intercept conditions			24,730 feet 522 fps	
Touchdown conditions				
Vertical velocity		<15 fps	≈12 fps	
Lateral velocity		<5.0 fps	≈ 0 fps	
Additional information				
Total nitrogen gas used	Design	0.64 ± 0.22 pound	0.44 pound	See coast mode gas consumption
Gyro speeds	235159	Telemetry value = 50 cps for all three gyros		
Roll gyro			Roll = 50 Hz (average)	
Pitch gyro			Pitch = 50 Hz(average)	
Yaw gyro			Yaw = 50 Hz (average)	
Gyro heater duty cycle				
Roll			Roll = 20 percent (on)	
Pitch			Pitch = 43 percent (on)	
Yaw			Yaw = 27 percent (on)	

*Seen as composite signal.

5.5.4. SUBSYSTEM PERFORMANCE ANALYSIS

5.5.4.1 Prelaunch

Gyro Temperatures

The gyro temperatures at 06:39 GMT just prior to launch were as follows:

Roll = 168.6°F

Pitch = 163.0°F

Yaw = 162.5°F

Nitrogen Weight

The estimated on-board nitrogen weight at launch was 4.56 pounds based on a telemetered tank pressure of 4686 psi at a tank temperature of 80.4°F. This agreed closely with the best estimate of 4.6 pounds of nitrogen loaded.

5.5.4.2 Launch Through Separation From Centaur

After extending its landing legs, Surveyor is separated from the Centaur booster. When the three legs-down signals and the separation signal have been generated, the programmer removes the logic signal which has been inhibiting operation of the gas jet amplifiers. At this same instant, the magnitude register begins to count down 1024 counts for a 51-second interval; the start of sun acquisition is inhibited for this interval to give the cold gas attitude control system opportunity to rate stabilize the spacecraft. Table 5.5-1 presents these events in time reference.

Rate stabilization is accomplished by using the three-axis attitude control system to torque the spacecraft and drive the caged integrating rate gyros error signals to within the deadband of each gas jet amplifier. Thus, at the end of a nominal rate stabilization maneuver, the spacecraft has achieved a low angular velocity at a random orientation in inertial space. The system response is dependent upon the magnitude and direction of the initial velocity vector and the gas jet thrust levels, and is essentially deadbeat in nature.

Flight control system performance just after Centaur separation was evaluated for proper nulling of the separation rates, the time required to null rates to less than 0.1 deg/sec, the total angular excursion, and magnitude of angular rates due to separation.

Separation transients are plotted in Figure 5.5-1. The transients about all three axes appear normal and indicate that any separation-induced rates were essentially zero.

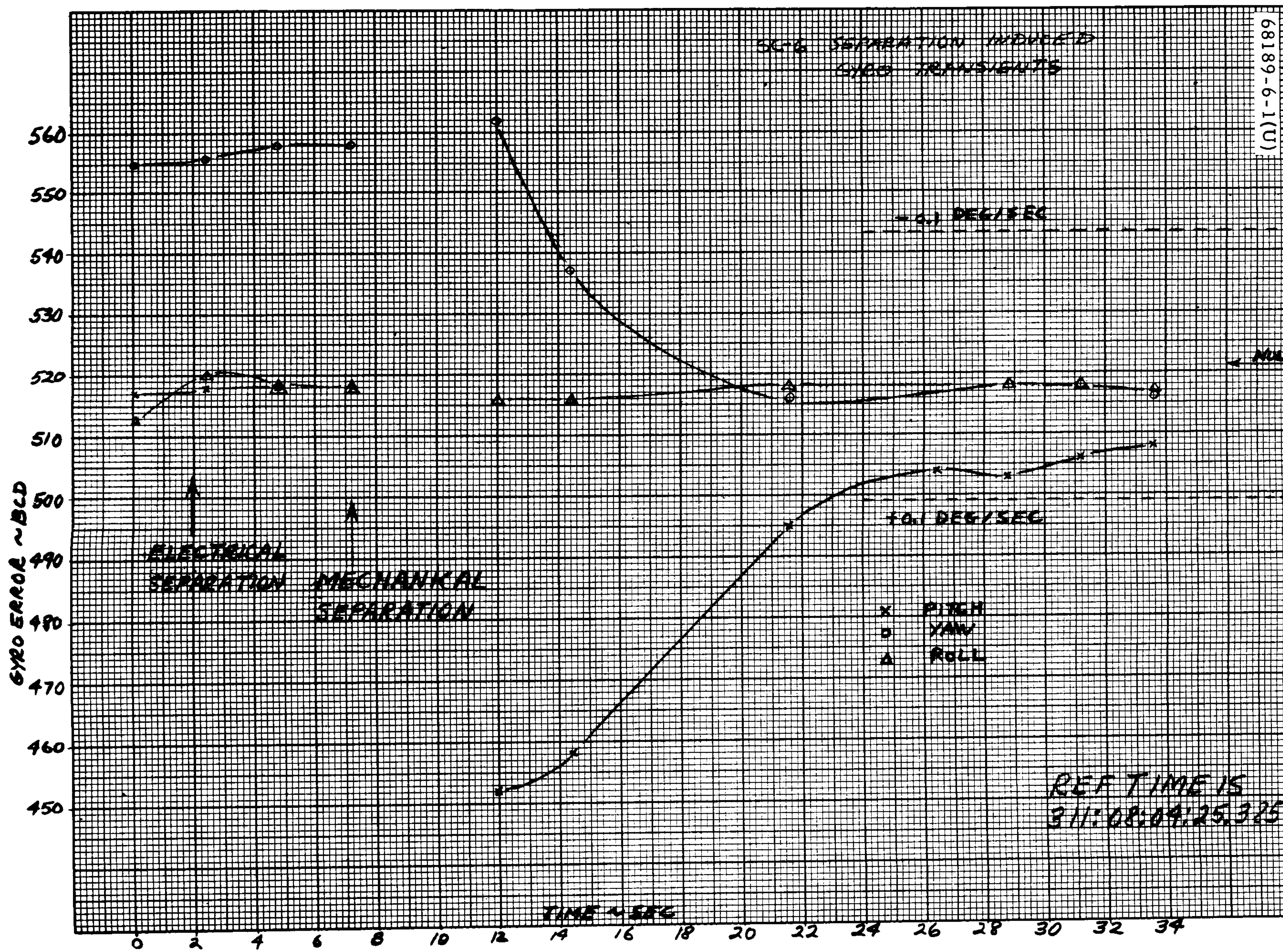

Figure 5.5-1. Separation-Induced Gyro Transients

All three body rates were reduced to ≤0.1 deg/sec in less than 20 seconds. The total attitude change of the spacecraft from the time of mechanical separation until each body rate was less than 0.1 deg/sec is simply the time integral of the plots in Figure 5.5-1 over the applicable time range. Graphical integration provided the following results:

Roll: 0 degree

Pitch: +2.0 degrees

Yaw: +0.36 degree

The expected nitrogen usage for rate dissipation is small. A typical rate dissipation transient will require the use of 0.040 pound of nitrogen. Because the measurement uncertainties are large compared to the usage, no quantitative measurement of nitrogen gas consumption during rate dissipation was attempted.

5.5.4.3 Sun Acquisition

Fifty-one seconds after electrical separation, sun acquisition is initiated by a command from the flight control programmer which causes a vehicle roll maneuver of -0.5 deg/sec and continues until the sun comes into the acquisition sun sensor field of view which is aligned approximately to the spacecraft roll-pitch plane. When this occurs, the roll command is removed and a plus yaw maneuver is initiated to point the primary sun sensor line of sight toward the sun. When the sun falls into the primary sun sensor field of view, a lockon signal is generated. This signal switches vehicle attitude control to the primary sun sensor and also serves to indicate (via telemetry) the completion of sun acquisition.

The automatic sun acquisition mode was initiated at 08:05:18.228 GMT as indicated by the countdown of the programmer clock. The estimated magnitude of the roll maneuver based on a constant gyro precession rate of 0.5 deg/sec was 264 degrees, while the yaw maneuver was estimated to be 10.0 degrees based on real time flight data. The sun acquisition phase is depicted in Figure 5.5-2.

Nitrogen Utilization

Following sun acquisition, the remaining nitrogen was estimated at 4.52 pounds, indicating that 0.04 pound was consumed during the separation rate dissipation and sun acqusition maneuvers. The expected nominal value is 0.094 pound.

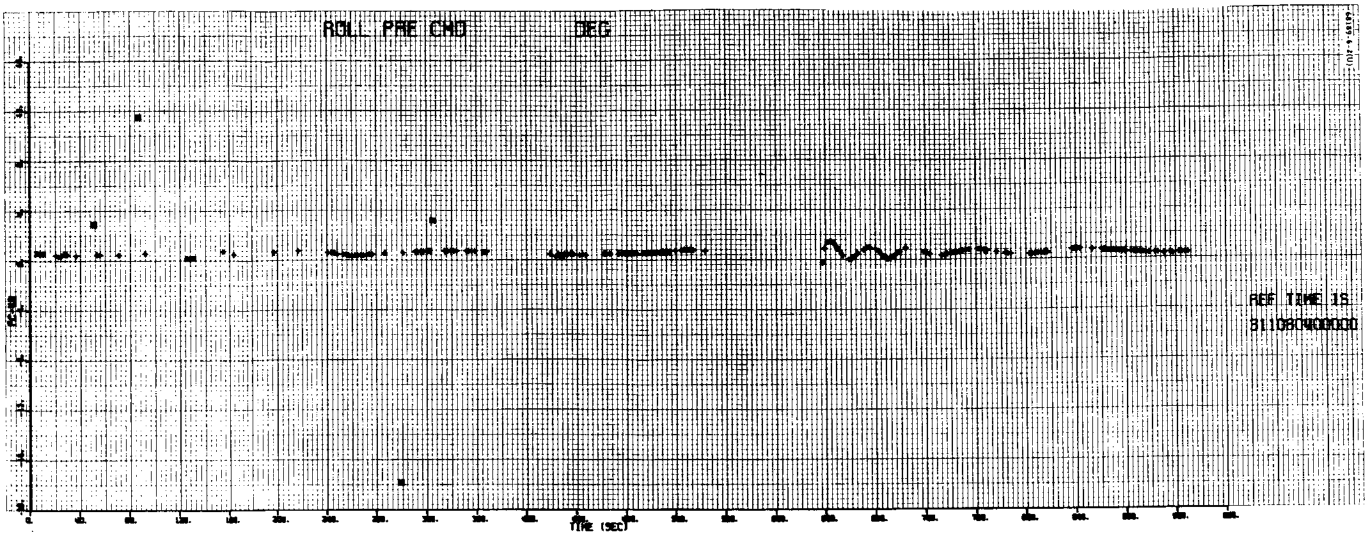

a) Roll Precession Command

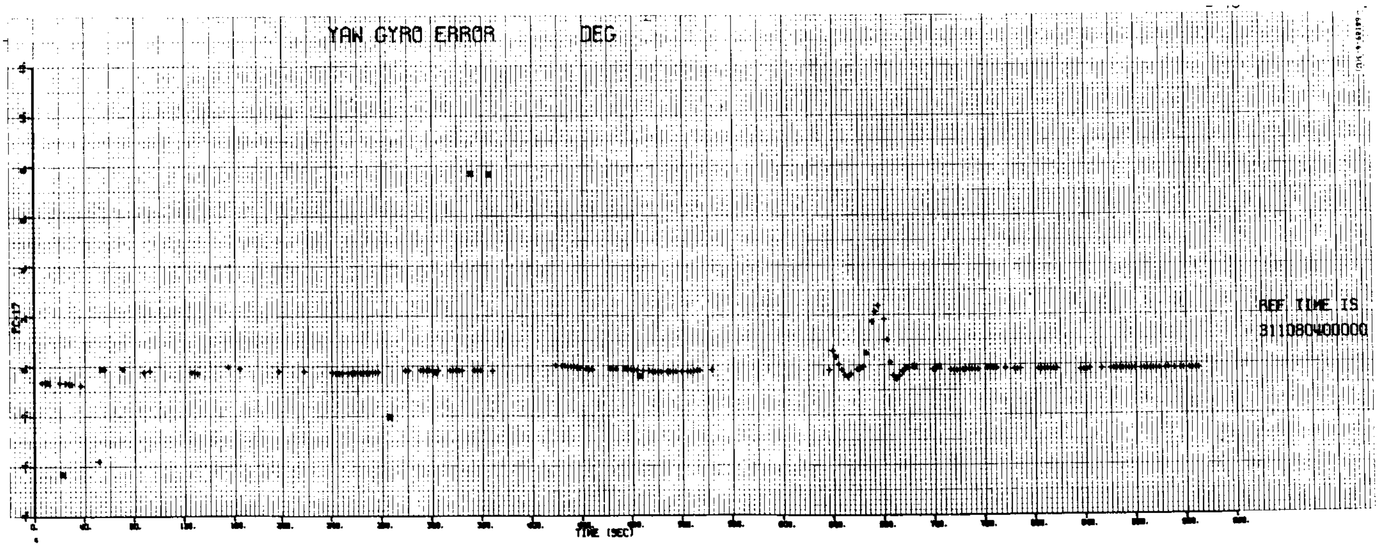

b) Yaw Gyro Error

Figure 5. 5-2. Sun Acquisition Phase

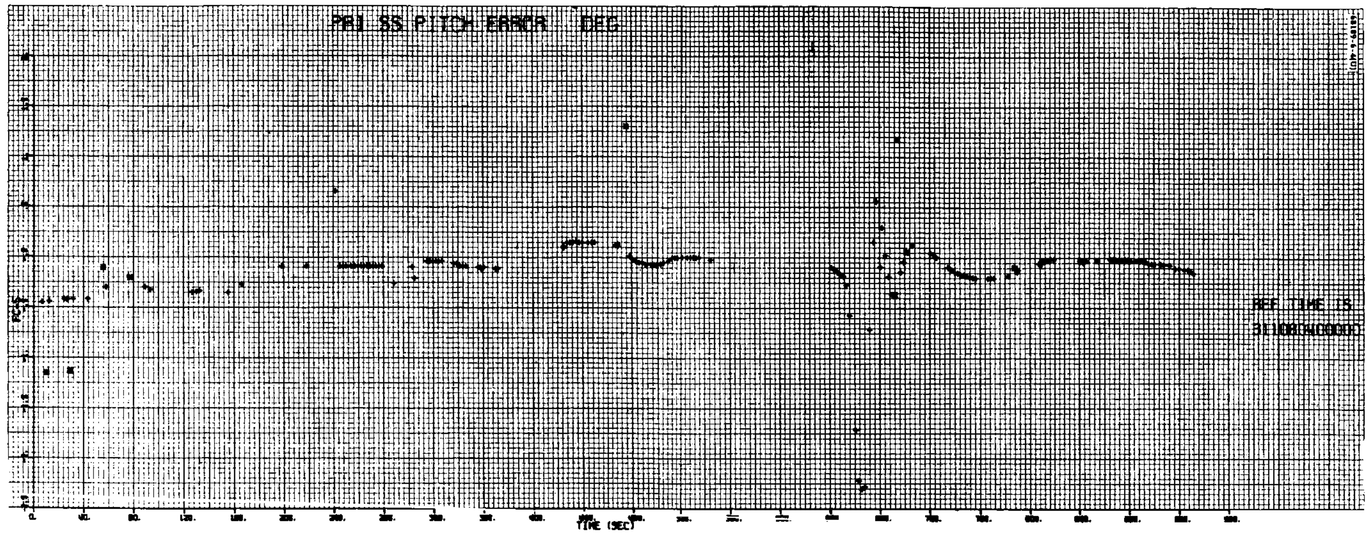

c) Primary Sun Sensor Pitch Error

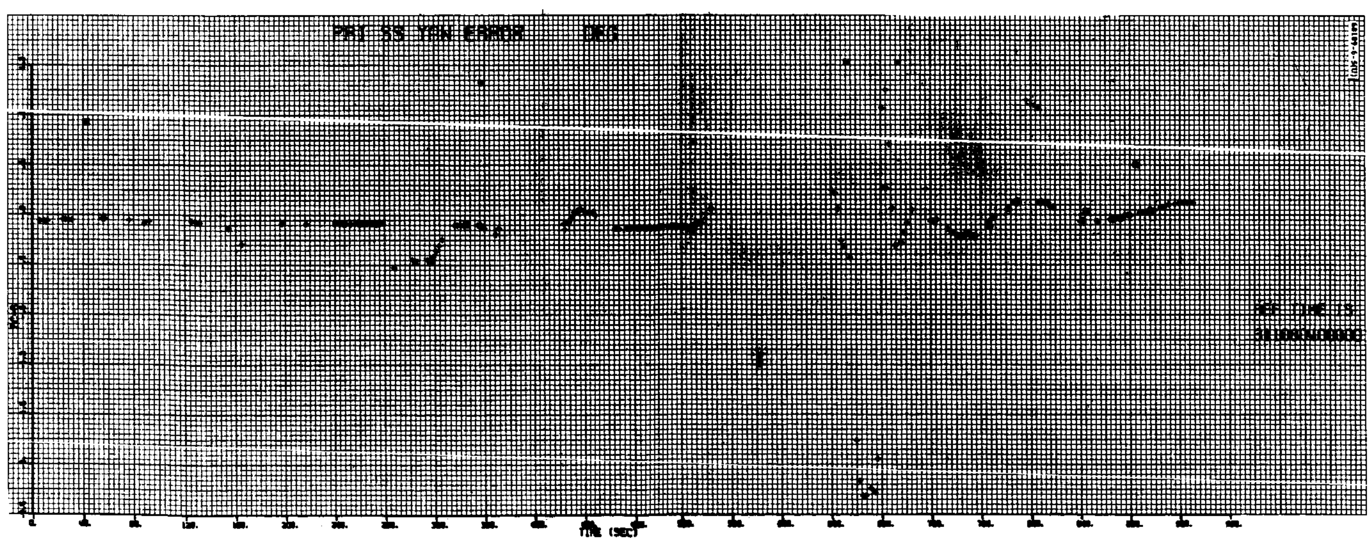

d) Primary Sun Sensor Yaw Error

Figure 5.5-2 (continued). Sun Acquisition Phase

5.5.4.4 Canopus (Star Acquisition)

As defined in Reference 1 (Model A-21 Equipment Specification 224832), paragraphs 7.1.2.7 and 7.1.2.7.1:

> "... a star map shall... be obtained by rotating the spacecraft about the Z-axis [Ed. note: initiated by receipt of a sun and roll command 0714] and recording the Canopus sensor output intensity signal as a function of time. Canopus shall be identified by position and magnitude relative to other stars [Ed. note: and celestial objects] passing in the field of view of the sensor...... The star acquisition mode shall be initiated when the flight control subsystem receives the Sun and Star... command 0703.... The spacecraft shall rotate about the Z-axis in the positive direction until the star Canopus appears within the... sensor field of view. Illumination of the ... sensor [Ed. note: by the star Canopus] shall effect star acquisition, star lock and star track about the spacecraft Z-axis."

During Mission F, the spacecraft was commanded to roll at +0.5 deg/sec at 311:15:50:21.9 GMT. Telemetered confirmation occurred at the received time of 311:15:50:22.645 GMT, corresponding to L + 8:11:20.8. During the ensuing roll, a star map was generated by recording the telemetered analog signals star intensity (FC-14) (i.e., output intensity signal) and star angle or roll error (FC-12) on a strip chart recorder. From this map, Canopus was positively identified during the first 360 degrees of roll by comparing the angular spacing and star intensity signal magnitudes of three celestial objects passing through the field of view. Since the Canopus lockon signal occurred when Canopus was in the field of view during the first roll resolution, it was decided to continue rolling and acquire Canopus by employing sun and star command 0703. The spacecraft was commanded to the sun and star mode at 311:16:25:27..6, and telemetered confirmation occurred at the received time of 311:16:25:28.151. Canopus lockon telemetry was received at 311:16:27:47.238, after which it required approximately 50 seconds for the roll error signal to stabilize to the deadband limit.

Star Map

At this point in time, the spacecraft, moon, sun, and earth relationships in the ecliptic plane are as shown in Figure 5.5-3a. The center of the moon would pass approximately 26 degrees outside the field of view in a plus yaw direction, and the center of the earth would pass approximately 2 degrees outside the field of view in a minus yaw direction. As shown in Figure 5.5-3a, the spacecraft is behind the moon and would therefore "see" less than a half moon. However, the dark side of the earth would appear in the minus yaw half of the field of view, and the large bright side of the earth would be just outside the field of view in a minus yaw direction. Figure 5.5-3b depicts the relationship of the sensor field of view and the earth as the spacecraft's -X axis points toward the earth during spacecraft roll.

Since large area bright objects within approximately 35 degrees of the sensor's line of sight will reflect light into the sensor from baffles in the sensor's light shield, it was expected that a sizeable star intensity signal would result when the sensor was rolling past the earth and very little, if any, signal would result when rolling past the moon. In addition 22 stars with intensities greater than 0.37×10^{-14} w/cm^2 come within the field of view during a complete roll revolution. Based on laboratory measurements of star intensity telemetry signals versus star intensity on this particular sensor (S/N 7) it was predicted that three stars might be observed. Figure 5.5-3c depicts the preflight calculated angular (roll angle) spacing of the moon, earth, Canopus, and the other expected stars.

The telecommunications subsystem was in mode 1 at 4400 bits/sec, resulting in transmission of a 100-word commutator word frame each 0.25 second. Star angle and star intensity signals, plus digital word 3, are read out each 0.05 second during each frame (equivalent to each 0.025 degree of spacecraft roll at the commanded roll rate of 0.5 deg/sec) and digital words 1 and 9 are read out once per frame (equivalent to each 0.125 degree of spacecraft roll).

During the mission, spacecraft telemetry was transmitted to the SFOF from Madrid (DSS-61) at 1100 bits/sec, resulting in the transmission of a 100 word commutator word frame each second. Thus, during the star mapping portion of the mission in real time at the SFOF, only one-fourth of the total data was available for star identification. From the real-time SFOF analog recorder traces of star angle and star intensity, it was possible to distinguish two stars plus a 43-degree-wide high star intensity signal. The angular spacing and magnitude of these signals was compared with preflight calculated star and earth angles and intensities, thus permitting positive identification of Canopus and Deneb, plus the earth. Postmission analysis of the total data, containing all commutator frames versus every fourth frame received in real time, revealed no other celestial bodies.

Figure 5.5-4 depicts analog traces of primary sun sensor pitch angular error (FC-5), primary sun sensor yaw angular error (FC-6), roll gyro error (FC-49), star angle, star intensity, digital word 1, and digital word 9 from the start of roll through Canopus acquisition.

Table 5.5-3 indicates the responses received versus predicted responses. The roll angles listed are calculated from the times when the star intensity signals reach their peak values. Although star intensity readings are commutated every 0.025 degree, the ability of the analyst to actually determine where the peak value of intensity occurs is probably limited to at least ±0.3 degree. This is due to the unknown effect of circuit time constants on the lag at peak intensities and the lack of any well defined peak on stars of low intensity. As noted in Table 5.5-3, the correlation between the post- and preflight calculated angle from Canopus for Deneb is +0.2 degree and for the earth, -2.7 degrees, which is within the accuracy of determining the center of a widely varying high intensity signal.

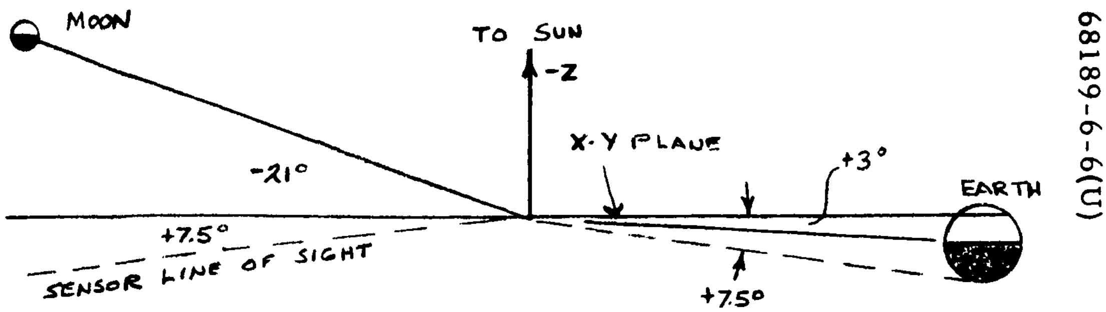

a) Ecliptic Plane Relationships

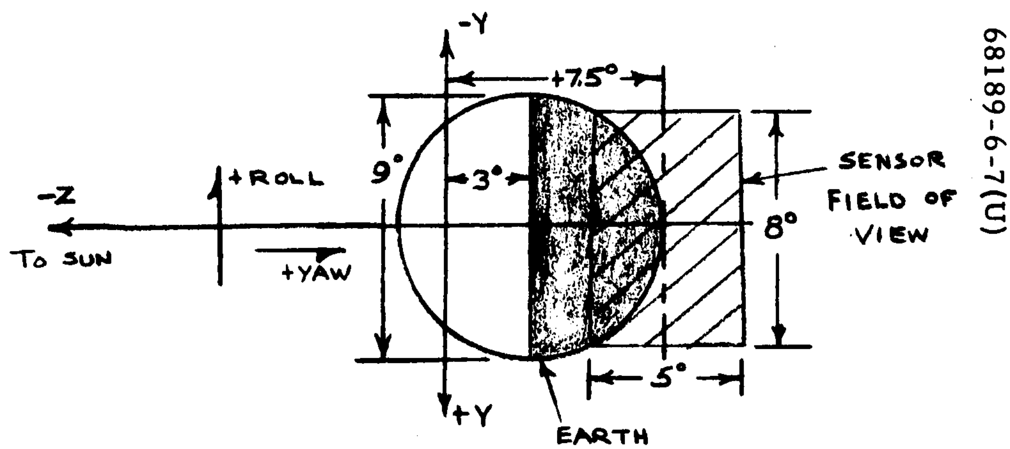

b) Sensor Field of View With Respect to Earth

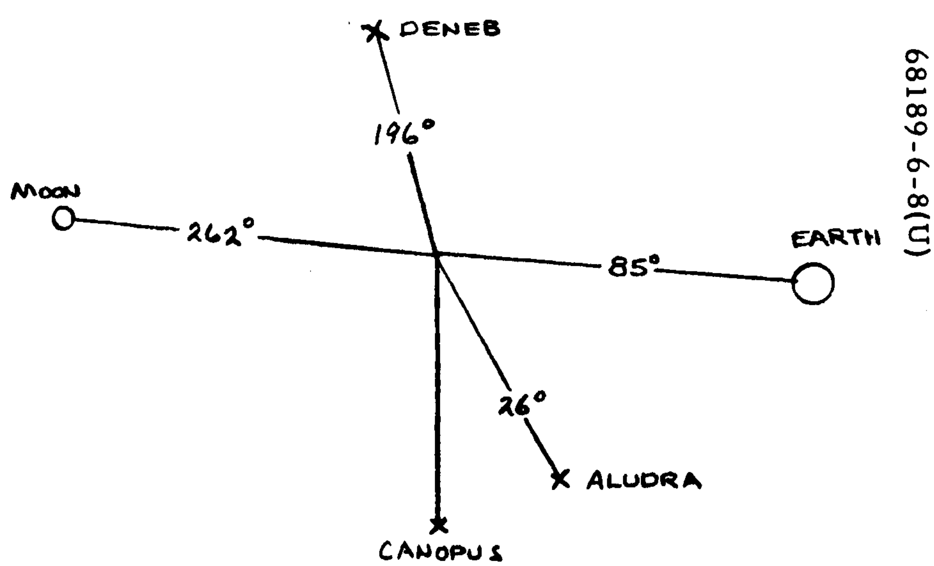

c) Angular Spacing (in Roll) of Observed Objects

Figure 5.5-3. Canopus Sensor Relationships to Observed Objects

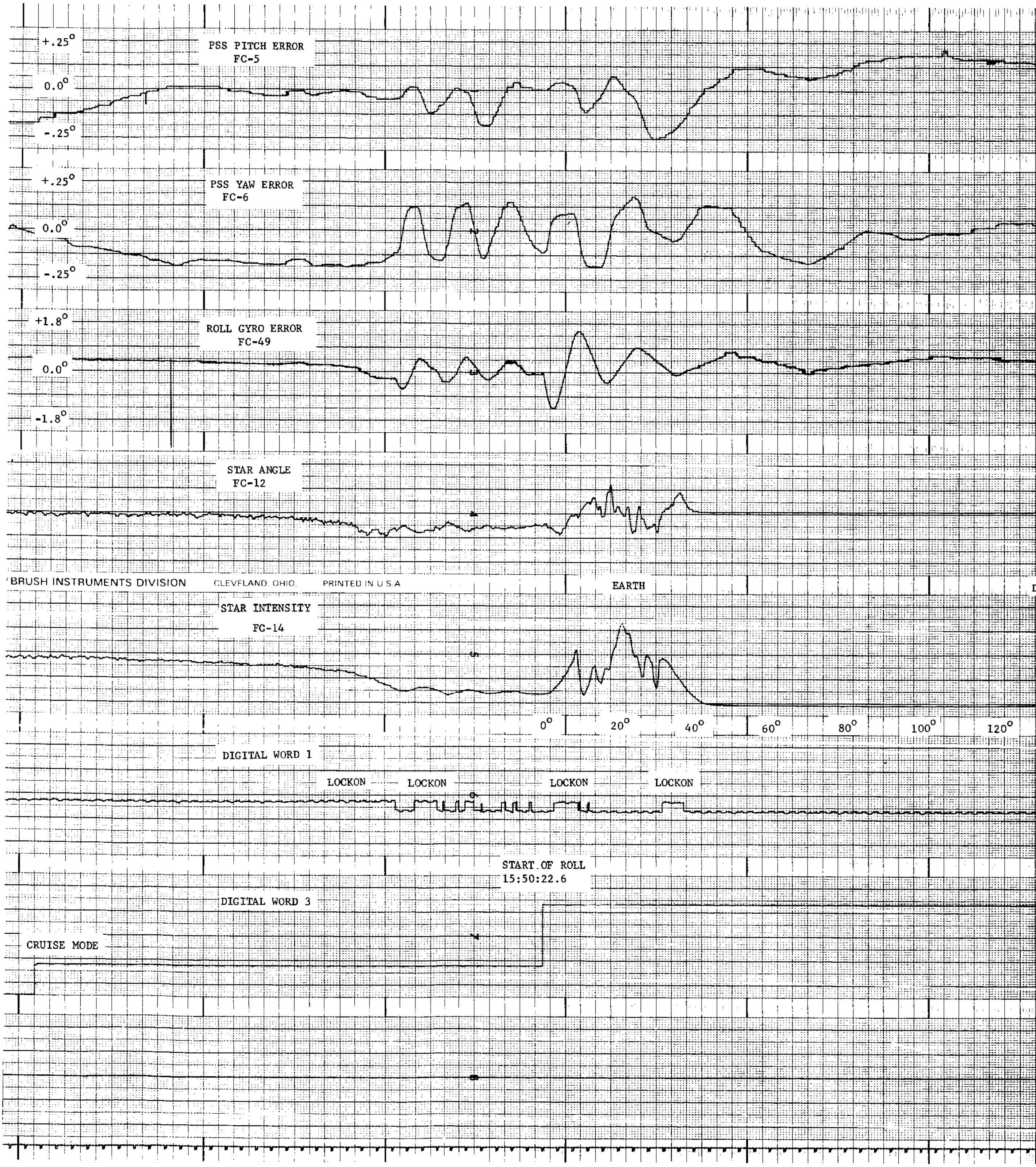

Figure 5.5-4. Analog Plot of Canopus Acquisition

FOLDOUT FRAME

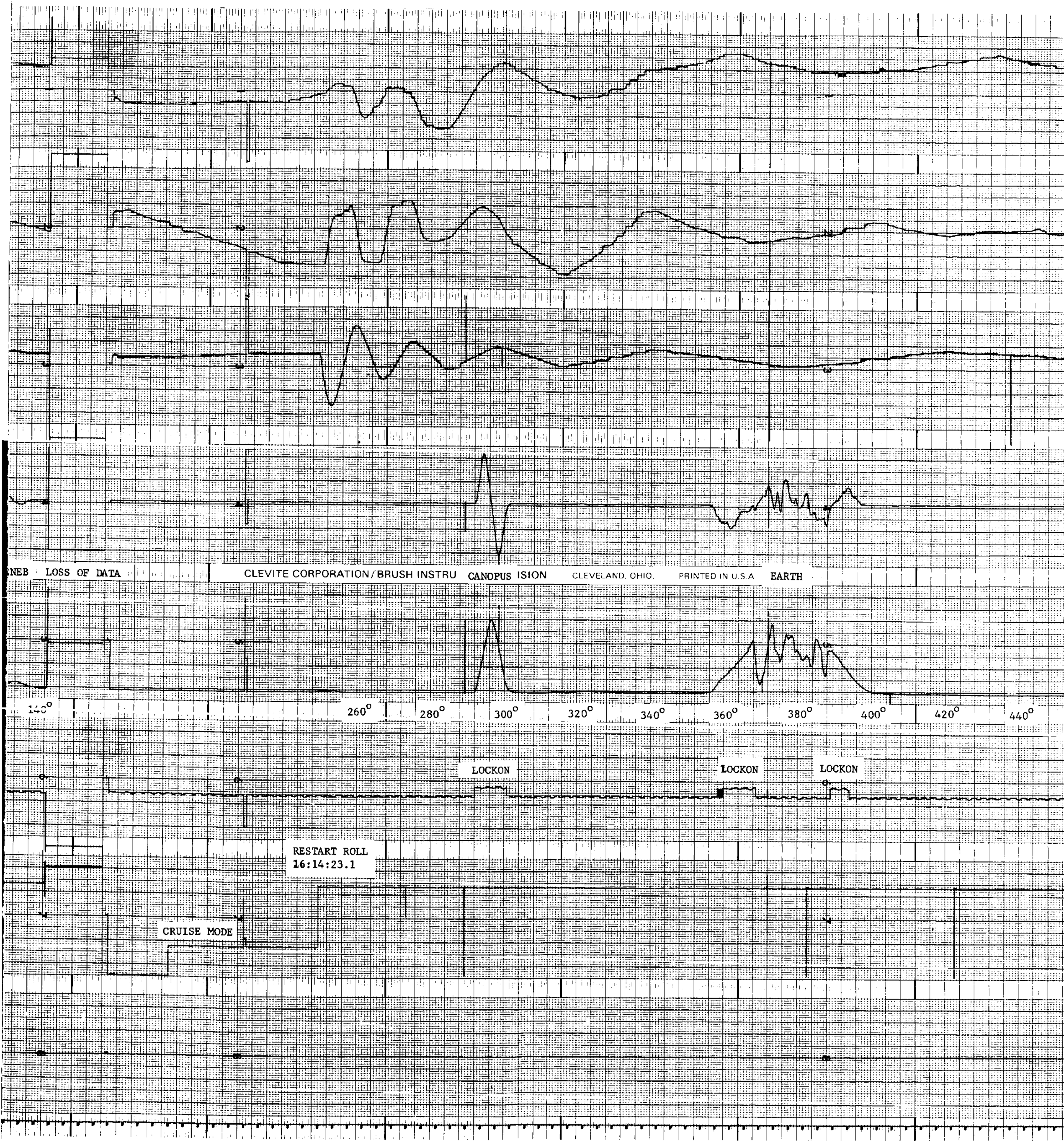

FOLDOUT FRAME

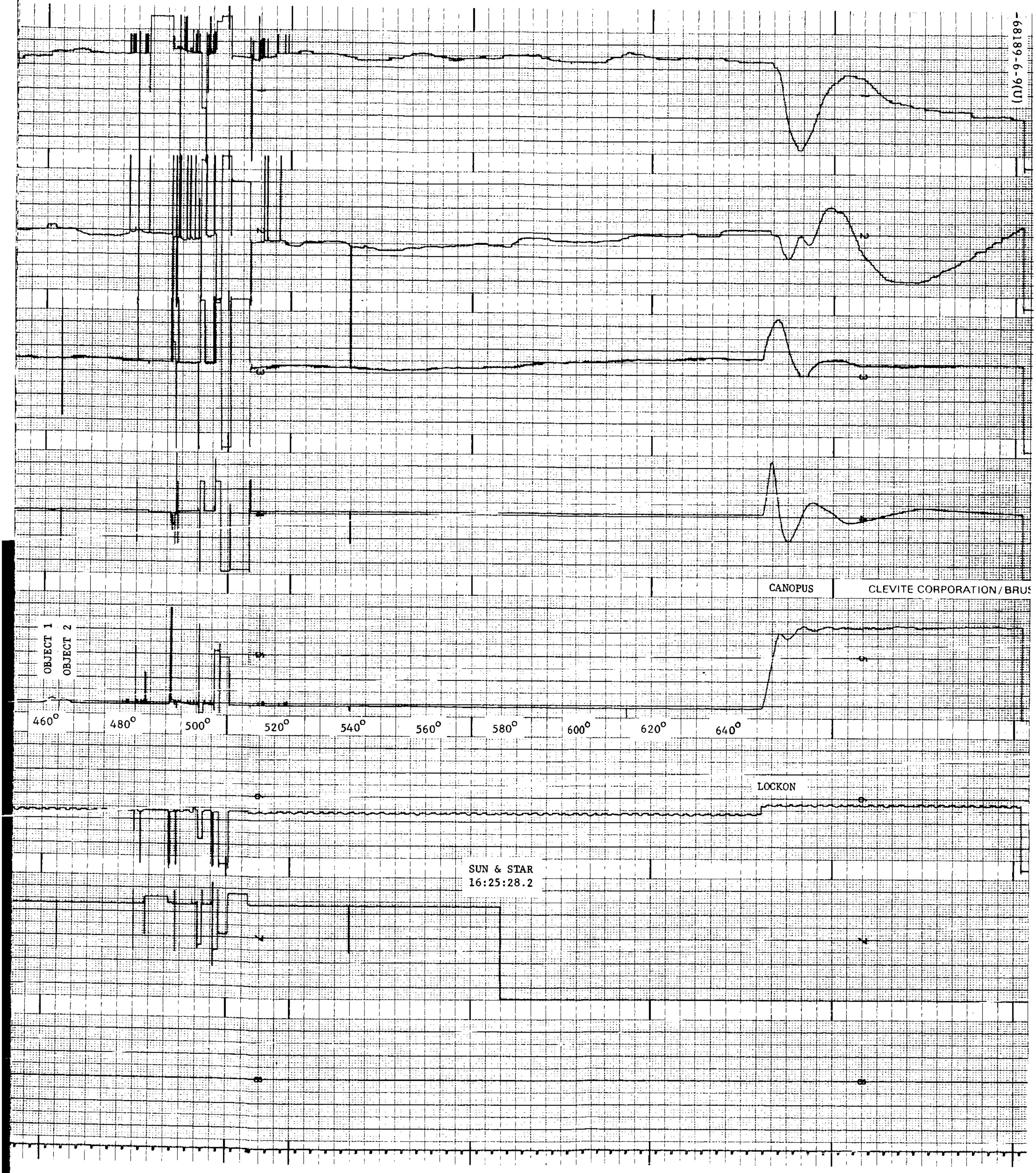

FOLDOUT FRAME

5.5-18A

TABLE 5.5-3. SURVEYOR VI STAR MAP – RECEIVED VERSUS PREDICTED RESPONSES

GMT, hr:min:sec	Postflight Calculated Roll Angle, degrees = Δt × 0.5009 deg/sec	Object (or Event)	Postflight Calculated Angle From Canopus, degrees	Prelight Calculated Angle From Canopus, degrees	Measured Peak Intensity During Roll, telemetry volts	Predicted Peak Intensity During Roll, telemetry volts	Measured Peak Intensity at 0 Roll Rate, telemetry volts	Predicted Peak Intensity at 0 Roll Rate, telemetry volts	Occurrence of Canopus Lockon, Digital Word 1
15:50:22.65	0	(Start of roll)	-298.5	–	–	–	–	–	–
15:54:51.75	134.8	Deneb	-163.7	-163.9	–	–	–	–	No
15:55:09.40	143.6	(Loss of data)	-154.9	–	–	–	–	–	–
15:58:44.0	251.5	(Stop roll)	-47.0	–	–	–	–	–	–
16:14:23.11	251.5	(Restart roll)	-47.0	–	–	–	–	–	–
16:15:48.50	294.3	Canopus lockon	-4.2	–	–	–	–	–	Yes
16:15:56.93	298.5	Canopus	0	0	3.49	4.01	–	–	Yes
16:18:41.32	380.8	Earth	+82.3	85	3.35	4.80	–	–	Yes
16:21:30.77	465.7	Object 1	+167.2	–	0.66	–	–	–	No
16:21:37.02	468.8	Object 2	+170.3	–	0.61	–	–	–	No
16:22:20.72	490.7	(Loss of data)	+192.2	–	–	–	–	–	–
16:22:32.97	496.9	(Return of data)	+198.4	–	–	–	–	–	–
16:25:28.15	584.6	(Sun and star command)	+286.1	–	–	–	–	–	–
16:27:47.24	654.3	Canopus lockon	+355.8	–	–	–	–	–	Yes
		Canopus					3.81	4.33	
		No star					0.42	0.46	

Spacecraft rolling during generation of the star map was interrupted because of a loss of data due to rolling into an antenna null. Rolling was resumed after regaining data in a new telecommunications mode. A second short-term loss of data occurred later which caused the loss of all but the last third of the data when Deneb was in the field of view for the second time. Two objects appeared in the field of view during the second revolution (at 464.8 and 468.0 degrees) which were not seen during the first revolution. The shapes of the responses of these objects could be caused by area type (rather than point type) bright objects moving across the field of view one and a half to two times faster than the image of a stationary celestial body. Therefore, it is concluded that these were not celestial bodies but rather objects of unknown size, shape, or distance.

The mean roll rate, as determined from the incremental time between the first and second Canopus lockon signals, is 360/(16:27:47.238-16:15:48.502) = 360/718.736 = 0.5009 deg/sec. The error due to sampling timing is ±0.25 second or ±0.00003 deg/sec, and the error due to roll gyro limit cycling is ±0.2 degree or ±0.0003 deg/sec.

Star Sensor Performance

The star sensor provides three telemetry outputs: star angle or roll error, Canopus lockon, and star intensity. A comparison of inflight and preflight measurements is used to determine how well the sensor performed in flight.

The star angle telemetry signal is designed to increase from a quiescent level, close to 512 BCD when no star is in the field of view, to a maximum of close to 1023 BCD, when Canopus is approximately +2 degrees from the X-Z plane. It returns to its quiescent level when Canopus is in the X-Z plane, then to a minimum, close to 0 BCD when Canopus is approximately -2 degrees from the X-Z plane, and finally increases to its quiescent level as Canopus leaves the field of view.

The star intensity telemetry signal is designed to increase from a quiescent level when no star is in the field of view to a maximum when Canopus is in the X-Z plane. It then decreases to its quiescent level as Canopus leaves the field of view. No star and maximum intensity telemetry values are listed in Table 5.5-3.

Figure 5.5-4 depicts the star angle and star intensity signals for all objects observed during the star map. From this figure, it can be seen that the star angle and star intensity telemetry signals perform as designed.

Inflight star intensity telemetry values are compared with preflight star intensity values to calculate the effective gain of the sensor. The gain of a sensor is a function of the photomultiplier tube scale factor which is controlled by the intensity of the sunlight actually reaching the tube through a sun filter in the sun channel optics. All preflight star sensor measurements are made with a unit sun intensity illuminating the sun channel. For flight, a flight filter is installed with a transmission factor that will admit more, equal, or less than a unit sun into the sensor.

Following are the sun filter transmission factors and calculated effective gains for Missions A through E:

	A	B	C	D	E
Filter factor	1.5	1.17	0.80	0.80	0.80
Effective gain	1.5+	1.5+	1.17	1.24	1.32

It was decided to install a 0.8 x Canopus sun filter for Mission F which was expected to result in an effective gain in the range of 1.17 to 1.32.

The actual observed peak star intensity telemetry value of Canopus is 3.81 volts, and the average preflight 1.0 x Canopus measurement is 3.46 based on 19 intensity measurements. Thus, the calculated effective gain for Mission F is 3.81/3.46 or 1.10 x Canopus. The differences in calculated effective gains of Missions C through F, all will nominally the same filter factor, are attributed to inaccuracies inherent in preflight sensor intensity measurements and in sun filter transmission measurements.

The third sensor output, Canopus lockon, is shown in Figure 5.5-4 as part of digital word 1 and appears not only when Canopus is in the field of view but also during the time reflected light from the earth is entering the sensor. Since this earth light was of sufficient magnitude to result in a Canopus lockon signal, it was decided to send the sun and star command, and to initiate automatic star acquisition after the spacecraft had rolled past the earth the second time.

Canopus Acquisition

Figure 5.5-4 depicts the response of the star intensity signal after receipt of the Canopus lockon signal has put the spacecraft in a closed-loop roll error controlled mode. When lockon occurs, the spacecraft is rolling at +0.5 deg/sec, and the roll error signal is increasing to a maximum which commands the spacecraft to roll positive to obtain a nulled roll error signal. Thus, the positive command causes the plus roll rate to increase, which results in a steeper slope of the star intensity signal and a lower amplitude peak due to the effect of filtering on the faster changing signal. As the star intensity signal crosses its peak, the roll error signal is going negative, causing the plus roll rate to decrease to zero and become negative to swing the -X axis back negative to alignment with Canopus. As the star intensity signal crosses its valley, the roll rate is zero and, as the star intensity signal crosses the next peak, the roll error signal is going positive, causing the negative roll rate to increase to zero and become positive to swing the -X axis back positive to alignment with Canopus. After several such cycles, the spacecraft settles down to a slow roll oscillation which causes the star intensity signal to oscillate on either side of its peak amplitude while the roll error signal oscillates above and below its null position. This oscillation is bounded, and the bounds are referred to as the roll optical limit cycle.

As noted in Figure 5.5-4, the star intensity peak amplitudes increase as the limit cycle is approached since there is less attenuation due to filtering as roll rate decreases to almost zero.

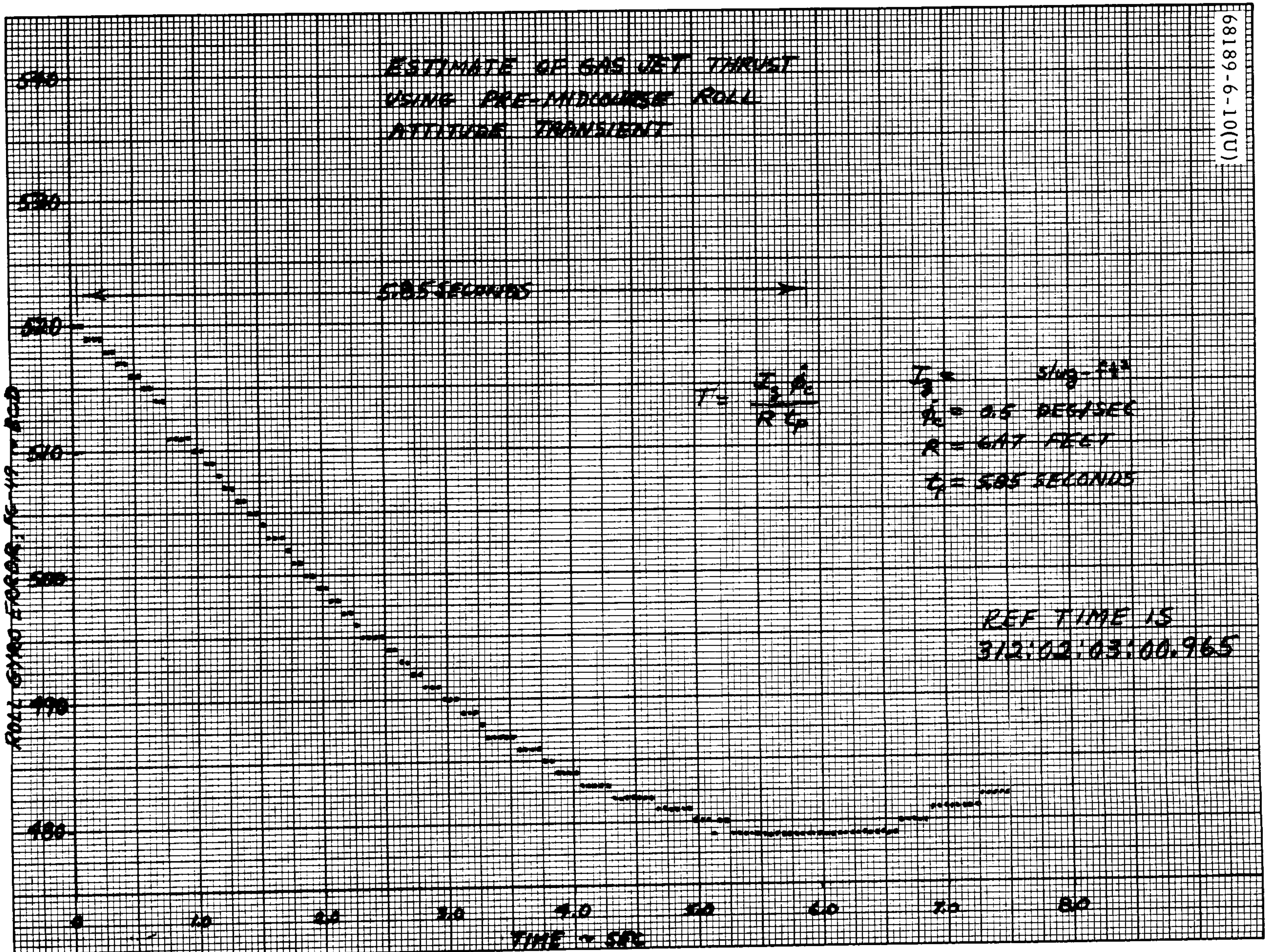

Figure 5. 5-5. Gas Jet Thrust Level Determination of Firing

Conclusions

The Canopus sensor performedas designed without malfunction. The star intensity signal, with Canopus in the field of view, was lower than predicted, but within the accuracy of the preflight measurements. The automatic star acquisition capability was successfully utilized.

5.5.4.5 Coast Phase Attitude Control

Gas Jet Thrust Level

Reference 2 developed the following expression for the gas jet thrust level:

$$\text{thrust} = T = \frac{I_z \dot{\varphi}_c}{R t_p}$$

where

I_z = roll inertia -213 slug-ft^2

$\dot{\varphi}_c$ = commanded precession rate = 0.5 deg/sec

R = gas jet movement arm = 6.47 feet

t_p = thrusting time of the gas jet from initiation of precession command to point at which $\dot{\varphi}_{gyro}$ = 0

This equation was used to determine the thrust level.

Using the premidcourse roll attitude maneuver data (Figure 5.5-5) the time from command initiation until $\dot{\varphi}_{gyro}$ = 0 was 5.25 seconds. Since the No. 1 gas jet amplifier is off 1.32 seconds of this time (Reference 3), t_p = 5.85 seconds -1.32 seconds = 4.52 seconds.

$$\text{thrust} = \frac{I_z \dot{\varphi}_c}{R\, t_p} = \frac{(213 \text{ slug-ft}^2)(0.5 \text{ deg/sec})}{(6.47 \text{ feet})(4.52 \text{ seconds})} = 0.064 \text{ pound}$$

Nitrogen Consumption

Nitrogen consumption for the period from launch to preretro maneuvers was 0.44 pound. This number compares favorably with predicted usage when measurement uncertainties and postgyro drift lockon transients are taken into account. Mission nitrogen usage was obtained from pressure and temperature information telemetered on flight control signals FC-4 and FC-48.

The predicted nitrogen usage for each maneuver was determined from the simulation defined in Reference 4; a detailed breakdown of the predicted impulse and weight expenditures is documented in Reference 5.

For the number and sequence of Mission F maneuvers, Attachment 1 of Reference 5 yields the following nominal impulse consumption budget:

	lb-sec
Vernier phase of midcourse maneuver	2.00
Limit cycle operation	4.50
Sun acquisition	3.25
Inertial roll maneuvers (3)	4.50
Star verification	1.50
Star acquisition	1.40
Inertial yaw maneuvers (2)	2.50
Rate dissipation	2.75
Postmidcourse rate dissipation	1.00
Total =	26.80

Assuming an average I_{sp} of 60 seconds yields a nominal nitrogen usage prior to the preretro maneuvers of approximately 0.45 pound. Reference 5 also predicts a 3σ usage uncertainty of 0.22 pound for this particular mission profile.

The fuel consumption due to postgyro drift check lockon transients was determined using the final angular attitude positions of each drift check as initial conditions to the simulation documented in Reference 4 with the following results:

1) The average impulse expenditure for one of the post-three-axis drift transients was 0.70 lb-sec.

2) The average impulse expenditure for one of the post-roll-axis-only drift transients was 0.55 lb-sec.

So there is an increase in the nitrogen consumption prediction of

$$\frac{3(0.55)\ \text{lb-sec} + 11(0.90)\ \text{lb-sec}}{60\ \text{seconds}} = 0.19\ \text{pound}$$

The net prediction would be

$$(0.45 + 0.19) \pm 0.22 = 0.64\ \text{pound} \pm 0.22\ \text{pound}$$

It was concluded that the measured nitrogen usage of 0.44 pound was within anticipated limits.

5.5.4.6 Premidcourse Attitude Maneuvers

In order to orient the spacecraft thrust axis properly prior to vernier engine ignition, a positive roll maneuver of 91.9 degrees and a positive yaw maneuver of 127.3 degrees were commanded. Although these were the values entered into the magnitude register, the desired maneuvers per the midcourse and terminal guidance system calculations were 91.7054 degrees of roll and 127.4787 degrees of yaw. These magnitudes were corrected for gyro drift by adding 0.1 degree to the roll magnitude and subtracting 0.17 degree from the yaw magnitude. It was estimated that the roll and yaw attitude control loops would be in the inertial (drift) mode for 0.17 and 0.14 hour, respectively. The drift values used were as follows:

Pitch = 0 deg/hr

Yaw = +1.2

Roll = -0.55 deg/hr

Several variables affect the accuracy of an angular maneuver: precession rate accuracy, precession command time, gyro drift, and initial attitude errors due to biases and limit cycle. When several maneuvers are performed with large time intervals between them, attitude errors due to gyro drift must be included. A list of all parameters affecting the midcourse attitude maneuver accuracy is presented in Table 5.5-4 along with their allowable 3σ values and actual performance values wherever possible.

As in Missions D and E, an attempt was made to initiate the maneuvers at the optical mode limit cycle null point. The roll maneuver was started within -0.048 degree of null, while the pitch and yaw optical errors at the start of the yaw maneuver were -0.03 and 0 degree, respectively.

Determination of Precession Times

The register was loaded with 460 bits for roll and 637 bits for yaw. For a clock rate of 2.5 cps, the respective times are 183.8 and 254.6 seconds with a maximum error of 0.20 second ±0.02 percent.

The telemetered gyro error signal data were used in determining the actual precession time. The sampling rate during the maneuvers was 20 times/sec, giving a resolution of 0.05 second. The results are as follows (Figure 5.5-6):

T = 183.631 seconds, or 91.815 degrees of roll

T = 254.705 seconds, or 127.352 degrees of yaw

Precession Rates. The precession rate obtained during the star mapping phase indicated that the positive precession rate was 0.5009 deg/sec.

Attitude Maneuver Error

Reference 6 develops two orthogonal equations that specify the spacecraft thrust axis pointing error during midcourse thrusting. The equations were derived for the roll-yaw rotation sequence which applies here.

Neglecting error sources that are present only after engine ignition results in the following equations:

TABLE 5. 5-4. PREMIDCOURSE ATTITUDE ERROR SUMMARY

Parameter	3σ Requirement	Reference Number	Measured Value	Comments
Primary sun sensor null with respect to FCSG roll axis	0. 2 degree	2 (paragraph 4. 3. 1. 1)	Pitch = -0. 04 degree Yaw = -0. 05 degree	
Canopus sensor null with respect to FCSC roll/pitch plane	0. 2 degree	2 (paragraph 4. 3. 1. 2)	+0. 09 degree	
Pitch/yaw limit cycle	0. 3 degree	2 (paragraph 4. 3. 1. 1)	-0. 03/0 degree	Based on sun sensor error signals at start of yaw
Roll limit cycle	0. 3 degree	2 (paragraph 4. 3. 1. 2)	-0. 048 degree	Based on Canopus error signal at start of roll
Gyro torquer scale factor	0. 15 percent	12 (paragraph 3. 2. 5. 1. 3)		
Precession current source accuracy	0. 13 percent		0. 2 percent	
Precession current source drift	0. 1 percent			
Timing source accuracy	0. 2 second ±0. 02 percent		Roll = +0. 01 degree Pitch = +0. 044 degree	Based on timing errors determined in subsection 5. 5. 4. 6
Gyro alignment to FCSC roll axis	0. 14 degree	12 (paragraph 3. 2. 5. 1. 4)	Pitch = +0. 12 degree Yaw = +0. 065 degree	
FCSG/spacecraft roll axis alignment	0. 1 degree	2 (paragraph 4. 1. 3. 7. 1)		
Gyro non-g sensitive drift	1. 0 deg/hr	2 (paragraph 4. 3. 1. 5)	Roll = +0. 023 degree Yaw = +0, 05 degree Pitch = +0 degree	Based on measured -0. 55 deg/hr in roll for 0. 03 hour less than estimated, +1. 2 deg/hr in yaw for 0. 04 hour more than estimated.
Total attitude error prior to ignition			0. 16 degree with 0. 24-degree 3σ uncertainty	

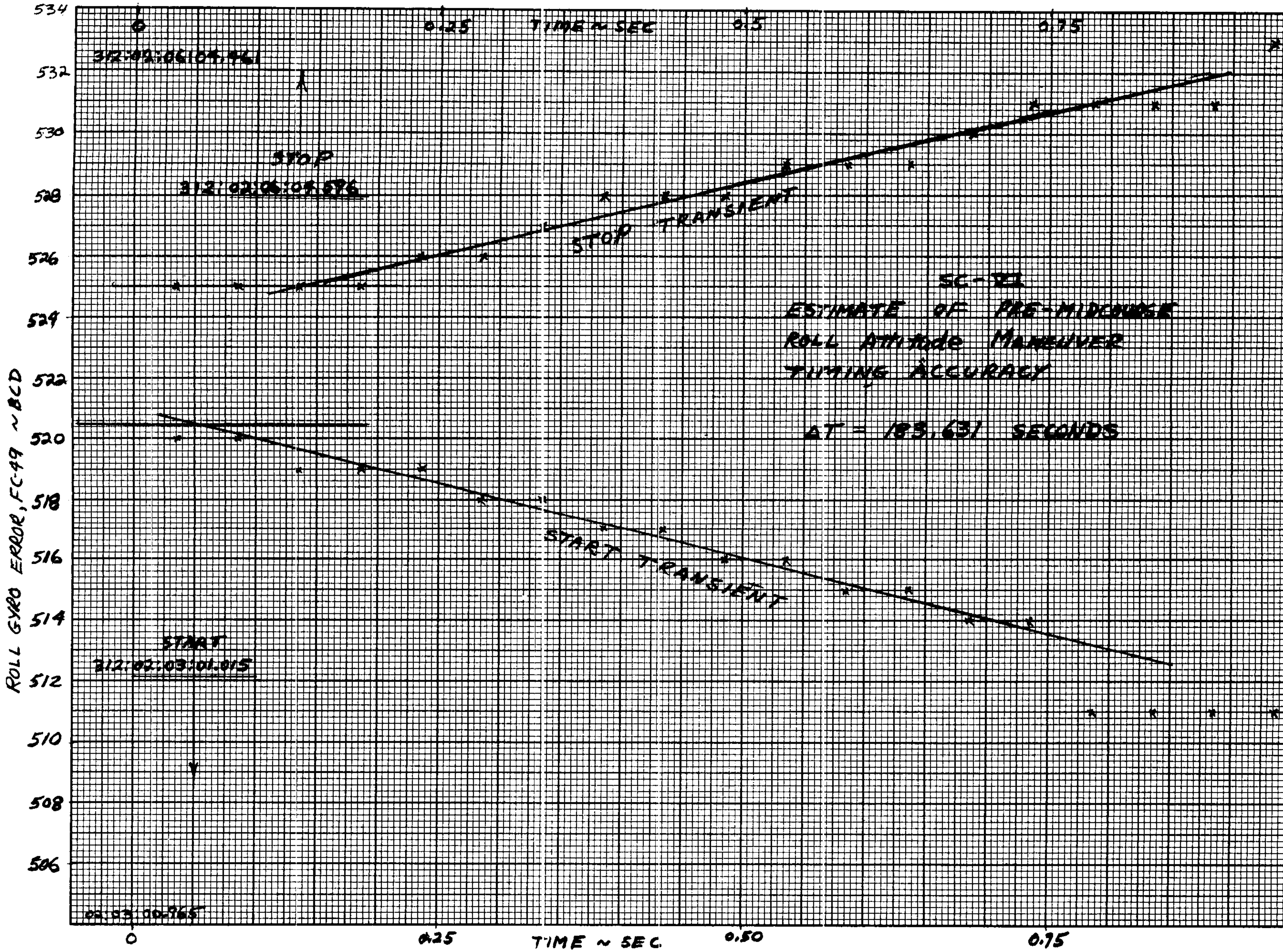

a) Roll Attitude Maneuver

Figure 5.5-6. Premidcourse Maneuver Timing Accuracy

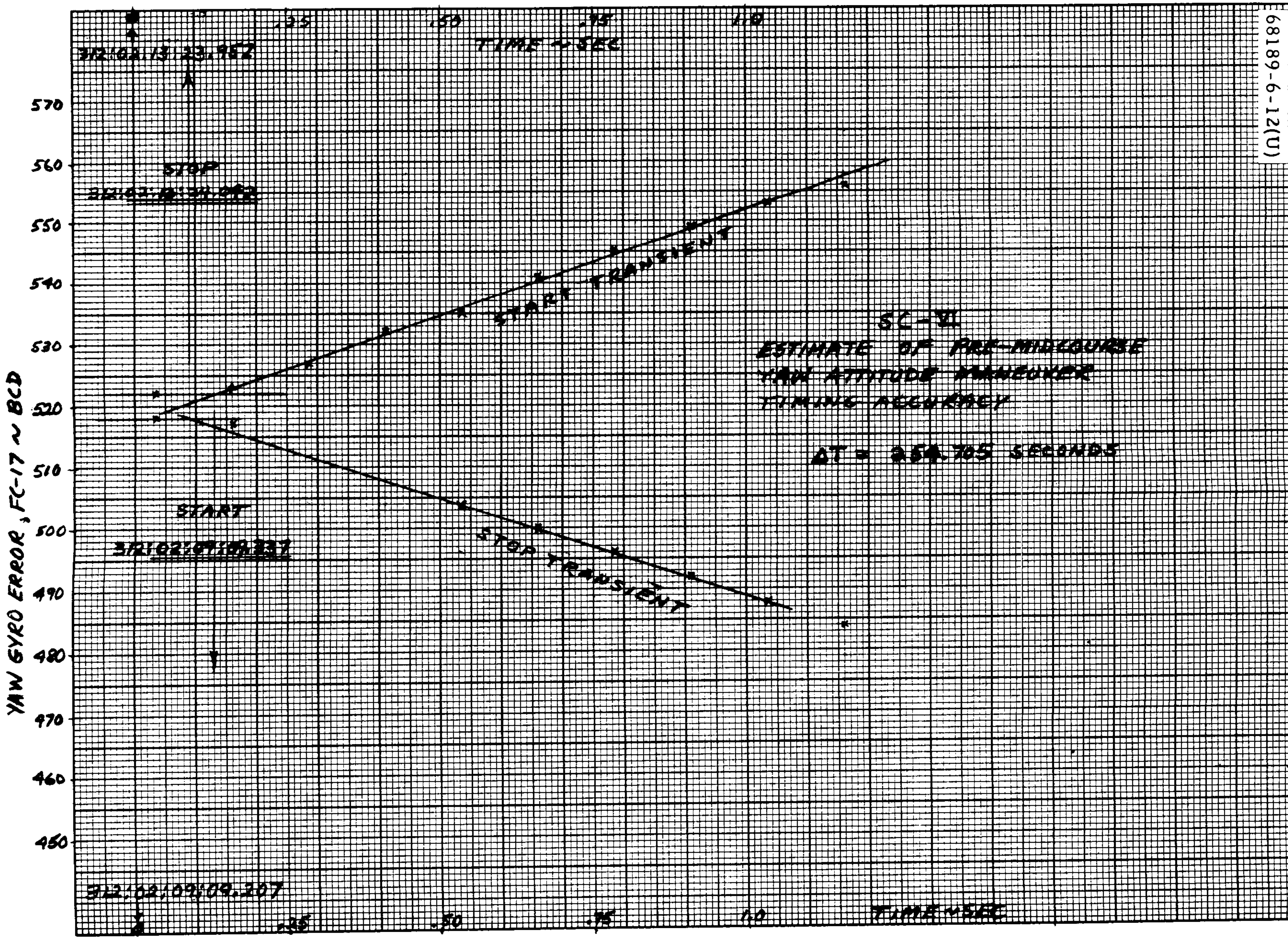

b) Yaw Attitude Maneuver

Figure 5.5-6 (continued). Premidcourse Maneuver Timing Accuracy

$$\text{Error about yaw axis} = -\psi_{R_E} - \psi_{A_E} \cos\varphi - \theta_{A_E} \sin\varphi$$

$$\text{Error about pitch axis} = \left(\varphi_{A_E} + \varphi_{R_E}\right) \sin\varphi + \theta_{A_E} \cos\psi \cos\varphi$$

$$- \psi_{A_E} \sin\varphi \cos\psi$$

where

$(\varphi, \theta, \psi)_{A_E}$ = spacecraft inertial reference alignment errors

$(\psi, \varphi) R_E$ = rotation errors

Use of φ = 91.9 degrees, ψ = 127.3 degrees, and the errors listed in the summary chart results in an 0.16-degree attitude error. The resultant pointing error has a 99-percent circular probable uncertainty of 0.24 degree.

5.5.4.7 Postmidcourse Attitude Maneuvers

The postmidcourse attitude maneuvers are used to realign the spacecraft to the celestial reference after performing a midcourse velocity correction. To accomplish this, two reacquisition schemes are available. One method is to perform the premidcourse attitude maneuvers in reverse, and the other is to perform another automatic sun acquisition sequence. The first method is more desirable since real-time monitoring of optical sensor signals provides a good indication of premidcourse maneuver accuracy and attitude control during the thrust period. If reacquisition of the sun and Canopus is not achieved to within a fair degree of accuracy, one or more of the following conditions must have existed:

1) Nonsymmetrical precession commands

2) Spacecraft attitude change occurred between maneuver periods

3) Premidcourse maneuvers were not accurate

4) Postmidcourse maneuvers were not accurate

5) Vernier engine shutoff transients excessive

The first method was chosen for the Surveyor VI mission, and the celestial reference was successfully reacquired.

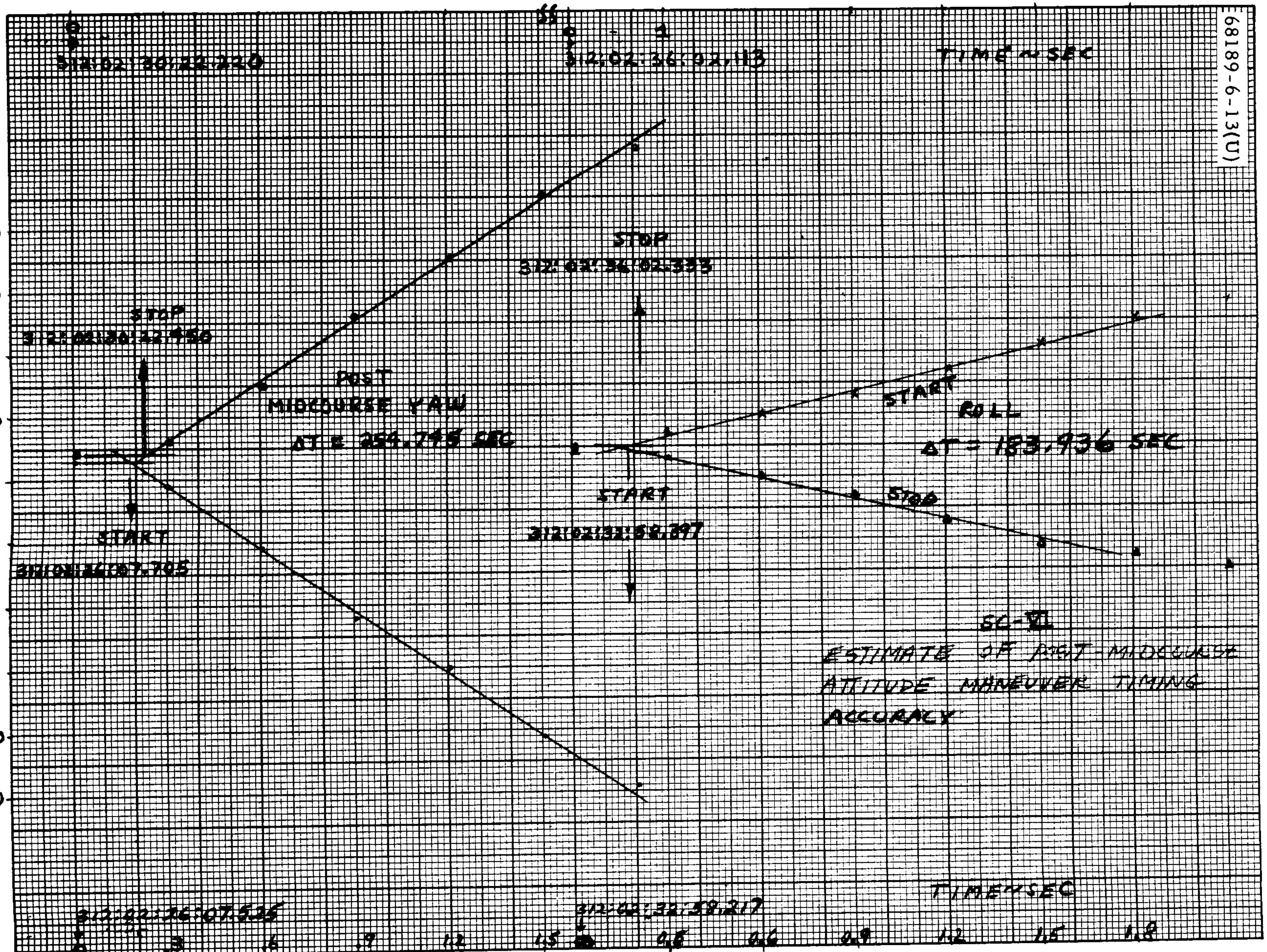

Figure 5.5-7. Postmidcourse Timing Accuracy

Determination of Precession Times

For the postmidcourse attitude maneuvers, the magnitude register was loaded with 637 bits for yaw and 460 bits for roll. This corresponds to 254.6 and 183.8 seconds, respectively.

The precession times, using gyro error signal data (Figure 5.5-7) were found to be as follows:

$T = 254.745$ seconds (yaw)

$T = 183.936$ seconds (roll)

The postmidcourse maneuvers were performed using the coast mode commutator at 4400 bits/sec, thereby increasing the data granularity to 0.3 second from the 0.05 second obtained for the premidcourse attitude maneuvers which were performed using the mode 1 commutator at 4400 bit/sec.

5.5.4.8 Midcourse Velocity Correction

The midcourse velocity correction was successfully executed starting at 02:20:03.263 GMT on 8 November. From orbit determination, the actual magnitude of the velocity change was estimated to be 10.1217 m/sec compared to the commanded value of 10.06 m/sec. This constitutes a ΔV execution error of 0.0579 m/sec. Using prelaunch alignment information and inflight data, the preignition pointing error was calculated to be 0.16 degree in subsection 5.5.4.6.

Midcourse Engine Ignition Characteristics

The midcourse velocity correction was characterized by a smooth vernier ignition followed by a nominal, uneventful thrusting phase (Figure 5.5-8). Peak pitch and yaw gyro errors were 0.17 degree or less during the ignition transient and less than 0.13 degree thereafter until engine cutoff.

Prior to vernier ignition, pitch and yaw gyro errors were maintained within the inertial deadband of ±0.22 degree by the gas jet system. The transient at ignition was reduced to zero in approximately 2 seconds. The yaw error transient overshoot was 0.04 degree, while the pitch error overshoot was essentially zero. The transient behavior was dominated by the 1.0-second time constant of the attitude control loops.

Based on the acceleration error telemetry signal (FC-15) (Figure 5.5-9), it was concluded that all three engines were producing controlled thrust within about 0.150 second of the ignition command signal. Therefore, acceleration signal amplifier saturation, which requires a startup delay of 0.26 second, did not occur, and no ΔV error information was lost.

Midcourse Engine Shutdown Dispersions

A summary of the peak spacecraft angles and angular rates and computed vernier engine shutdown impulse dispersions are given in Table 5.5-5.

It should be noted that peak gyro angles were less than 1.0 degree and well within the required travel range of ±10 degrees. Inertial reference was therefore retained, and reacquisition of the sun and Canopus was accomplished via the reverse maneuver sequence.

Vernier engine shutdown impulse dispersions (relative to mean impulse of the three engines), calculated from pitch and yaw angular rate data as per the procedure outlined in Reference 10, were well within the specification limit of ±0.63 lb-sec (Reference 7).

Midcourse Velocity Determination

The general concept of midcourse correction capability employed by Surveyor is to apply a constant acceleration for a finite period of time. Thus, in theory, once the magnitude of the velocity correction is known, the exact duration of the constant acceleration phase can be determined. In practice, this approach is slightly altered to account for such error sources as engine ignition transients, shutdown impulse, and hysteresis. Thus, the actual command time ΔT is slightly higher.

The desired values used during flight were as follows:

1) Desired ΔV = 10.064 m/sec (33.02 fps)

2) Desired ΔT = 10.281 seconds

Duration of Burn Time. The acceleration error signal data were used in an attempt to determine the actual burn time. The results (Figure 5.5-10) indicated that the burn time was 10.242 seconds for a timing error of 0.04 second (the magnitude register was loaded with 103 counts or ΔT = 10.25 seconds).

Estimate of ΔV. Assuming that acceleration command remained at the design value of 3.225 ft/sec^2, the actual acceleration level was determined by subtracting the acceleration error value (ϵ_A = 0.014 ft/sec^2) from the design value. The acceleration error signal remained essentially constant during the burn period. Therefore, the actual acceleration level was 3.211 ft/sec^2, and the midcourse ΔV was 3.211 × 10.242 = 32.887 fps for an error of -0.132 fps. From orbit determination, it was concluded that the actual midcourse ΔV was 10.1217 m/sec (33.2092 fps).

A list of parameters affecting the accuracy of the velocity correction is presented in Table 5.5-6 along with the values of maximum allowable errors. Actual performance values were used wherever possible.

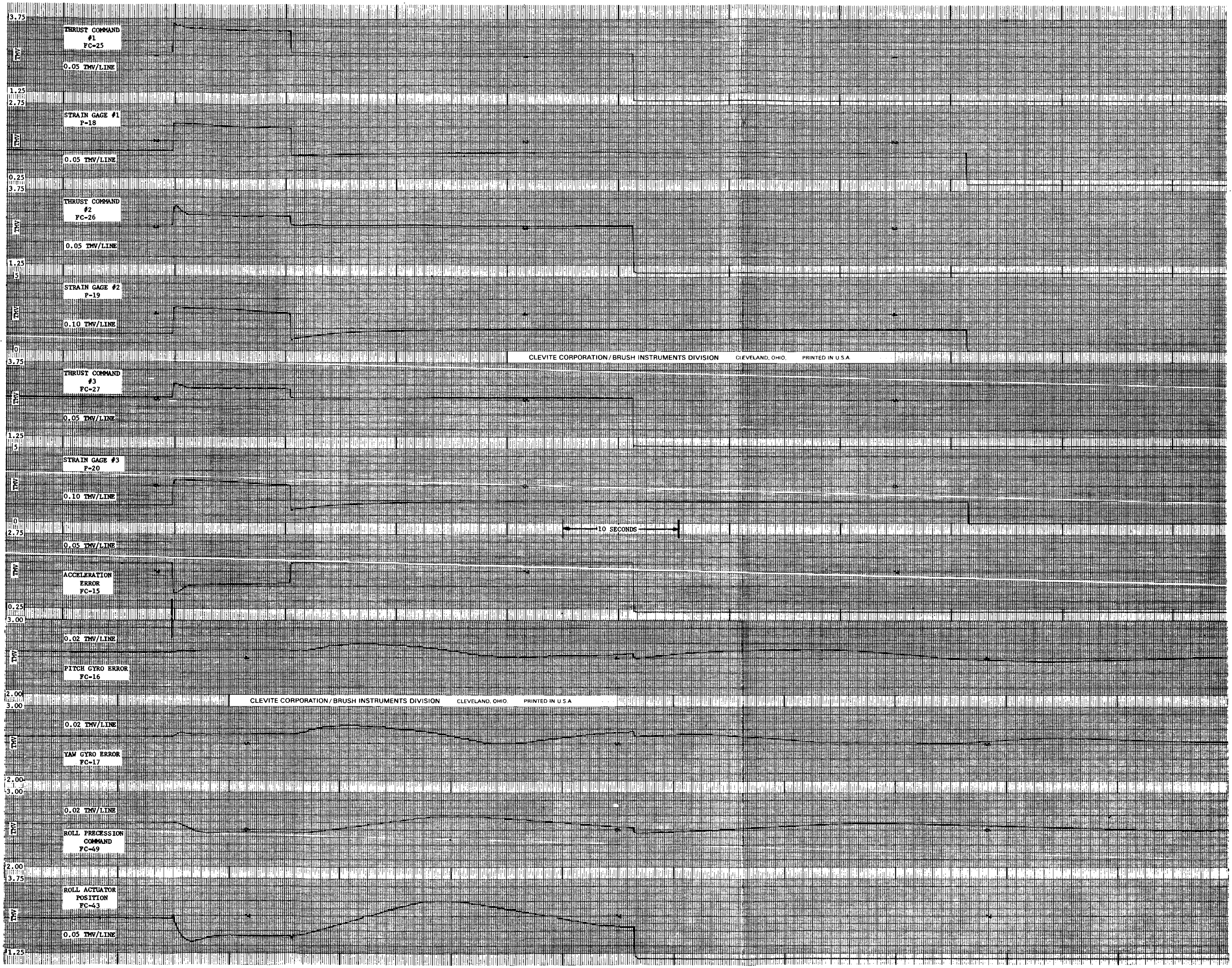

Figure 5.5-8. Midcourse Velocity Correction

FOLDOUT FRAME

FOLDOUT FRAME

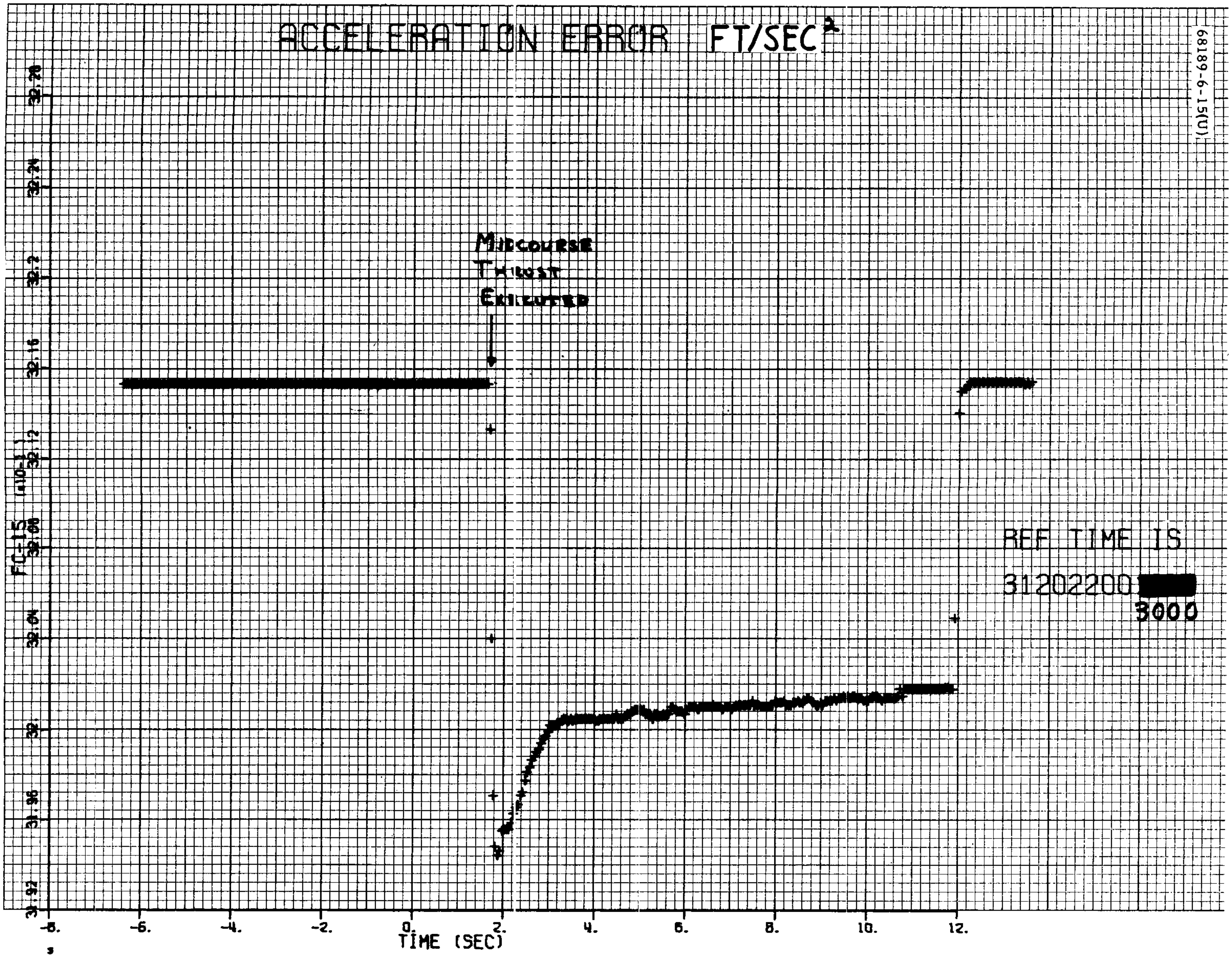

Figure 5.5-9. Acceleration Error

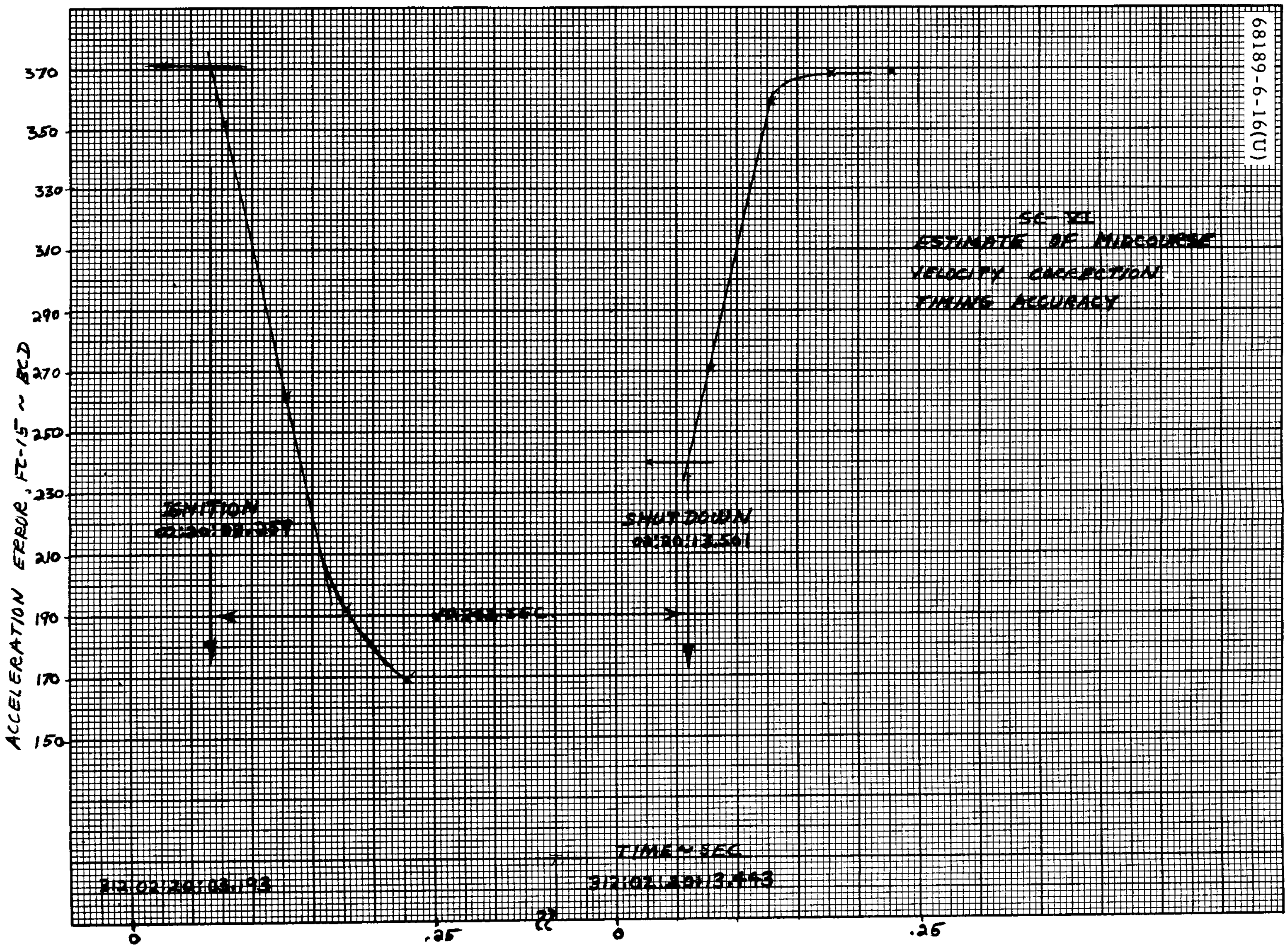

Figure 5. 5-10. Estimate of Midcourse Velocity Correction Timing Accuracy

TABLE 5.5-5. MIDCOURSE SHUTDOWN SUMMARY

Peak angular errors, degrees:		
Pitch	=	-0.33
Yaw	=	-0.47
Roll	=	+0.77
Roll act	=	-0.77
Peak angular rates, deg/sec:		
Pitch	=	-0.08
Yaw	=	-0.1
Vernier shutdown impulse dispersions, lb-sec:		
Leg		
1		+0.085
2		-0.09
3		+0.005

Telemetered Thrust Levels

The approximate steady-state vernier engine thrust levels during the midcourse velocity correction were as follows:

Engine		Pounds
1	=	80.0
2	=	73.0
3	=	72.0

Based on a spacecraft weight at injection of 2220.79 pounds and an estimated constant acceleration of 3.211 ft/sec^2, the expected total thrust is 222 which compares favorably with the total thrust of 225 pounds obtained from the telemetered vernier engine thrust commands.

5.5.4.9 Preretro Maneuvers

Before retro ignition, it is required that the spacecraft thrust axis (roll axis) be aligned to the translational velocity vector of the spacecraft as

TABLE 5.5-6. SC-6 MIDCOURSE VELOCITY CORRECTION ACCURACY

Item	Parameter	Requirement 3σ or Limit	Limit, fps	Specification	Performance Value, fps	Comments
1	Errors proportional to maneuvers magnitude					Much of the error was anticipated and was included in the calculation of the desired burn time
	Accelerometer accuracy	1.1 percent	0.15	234632C		
	Reference signal	0.5 percent	0.068	234600E		
	Flight control electronics null	0.15 percent	0.02	234600E		
	Thrust bias variation	0.09 percent	0.01	287105	0.17	
	Control channel gain variation	0.07 percent	0.009	234600E		
	Accelerometer misalignment	0.06 percent	0.008	234600E		
	Total proportional errors (RSS)	1.22 percent	0.17			
2	Errors independent of maneuver magnitude					
	Shutdown impulse dispersion	±0.63 lb-sec	0.016	287015	-0.002	
	Hysteresis limit cycle	3 milliamperes	0.035	287105	0	
	Ignition transient	–	0.47	–	0	
	Timing granularity	±0.1 second	0.32	224832 7.2.1.9	-0.13	
	Total independent errors (RSS)		0.568		0.13	
3	Total magnitude errors (RSS)		0.782		0.21	

part of the gravity turn terminal descent phase guidance. The alignment is performed by means of two sequential rotations about the spacecraft body (gyro) axes. A third roll rotation may be required to satisfy a RADVS sidelobe constraint (Reference 8).

These maneuvers are accomplished by using the cold gas attitude control system, with the body-fixed integrating rate gyros as inertial references. To accomplish a rotation, the appropriate gyro torquer winding is driven by a constant current source for a precise length of time; the spacecraft is slaved to this changing reference at a constant rate of 0.5 deg/sec.

The major events and times associated with the positive roll, yaw, roll preretro maneuver combinations selected for Surveyor VI are given in Table 5.5-7.

TABLE 5.5-7. MAJOR EVENTS AND TIMES (DAY 314) FOR PRERETRO MANEUVERS

Event	Command	GMT, min:sec (00 hr)
Begin roll	0714	25:22.472
End roll		28:06.107
Begin yaw	0713	29:40.785
End yaw		33:24.200
Begin roll	0711	34:58.498
End roll		38:59.592
Retro ignition		58:04.087

The preretro maneuvers were analyzed in terms of the following:

1) The gyro precession times were determined from gyro error signals and precession logic signals and compared to commanded times.

2) Using these attitude errors and the initial sun and Canopus error signals, the preignition terminal pointing accuracy was determined.

The first attitude maneuver (roll) was initiated 32 minutes and 41.6 seconds before retro ignition. The time constraint on break of optical lock is 33 minutes based on an allowable 1 deg/hr gyro drift contribution to the pointing error (Reference 8). An attempt was made to reduce the optical mode limit cycle contribution to the pointing error by initiating the roll and yaw attitude maneuvers at the limit cycle null point. The degree of success is illustrated by the following data which indicates the limit cycle errors which existed at the start of each maneuver.

Maneuver	Limit Cycle Error, degree
Roll	-0.06
Yaw	+0.2 (yaw)
	0 (pitch)

Gyro Precession Times

The attitude maneuvers entered into the flight control programmer magnitude register are as follows:

Maneuvers	Degrees	Bits
+ Roll	81.7	409
+ Yaw	111.7	559
+ Roll	120.5	603

Table 5.5-8 presents the estimated gyro precession times.

TABLE 5.5-8. ESTIMATED GYRO PRECESSION TIMES

Attitude Maneuver	Commanded Time, seconds	Observed Time, seconds	ΔT, seconds	Rotation Error, degrees
Roll	163.4	163.635	+0.235	$\Delta\varphi = +0.12$
Yaw	223.4	223.415	+0.015	$\Delta\psi = +0.007$
Roll	241	241.094	+0.094	$\Delta\varphi = +0.05$

Since the gyro error signals are only sampled once every 1.2 seconds (coast mode at 1100 bits/sec) during the preretro maneuvers, it was assumed that the shapes of roll and pitch gyro transients were the same as those observed during the premidcourse attitude maneuvers when the gyro error signals were sampled once every 0.05 second. The precession times were then estimated graphically based upon the intersection points of the start and stop transients with the steady-state gyro error values (Figure 5.5-11).

Gyro Drift Compensation

Eleven three-axis gyro drift checks were made during the mission, four of them prior to the midcourse velocity correction. Three roll-axis-only drift checks were also made. A summary of gyro drift measurements is presented in Table 5.5-9. Two techniques were used to measure the drift rates. The first was based on average slopes of the optical error signals obtained from analog Brush recorder and Milgo plots. In the second technique, iterated calculations were made as described in Reference 9.

68189-6-17(U)

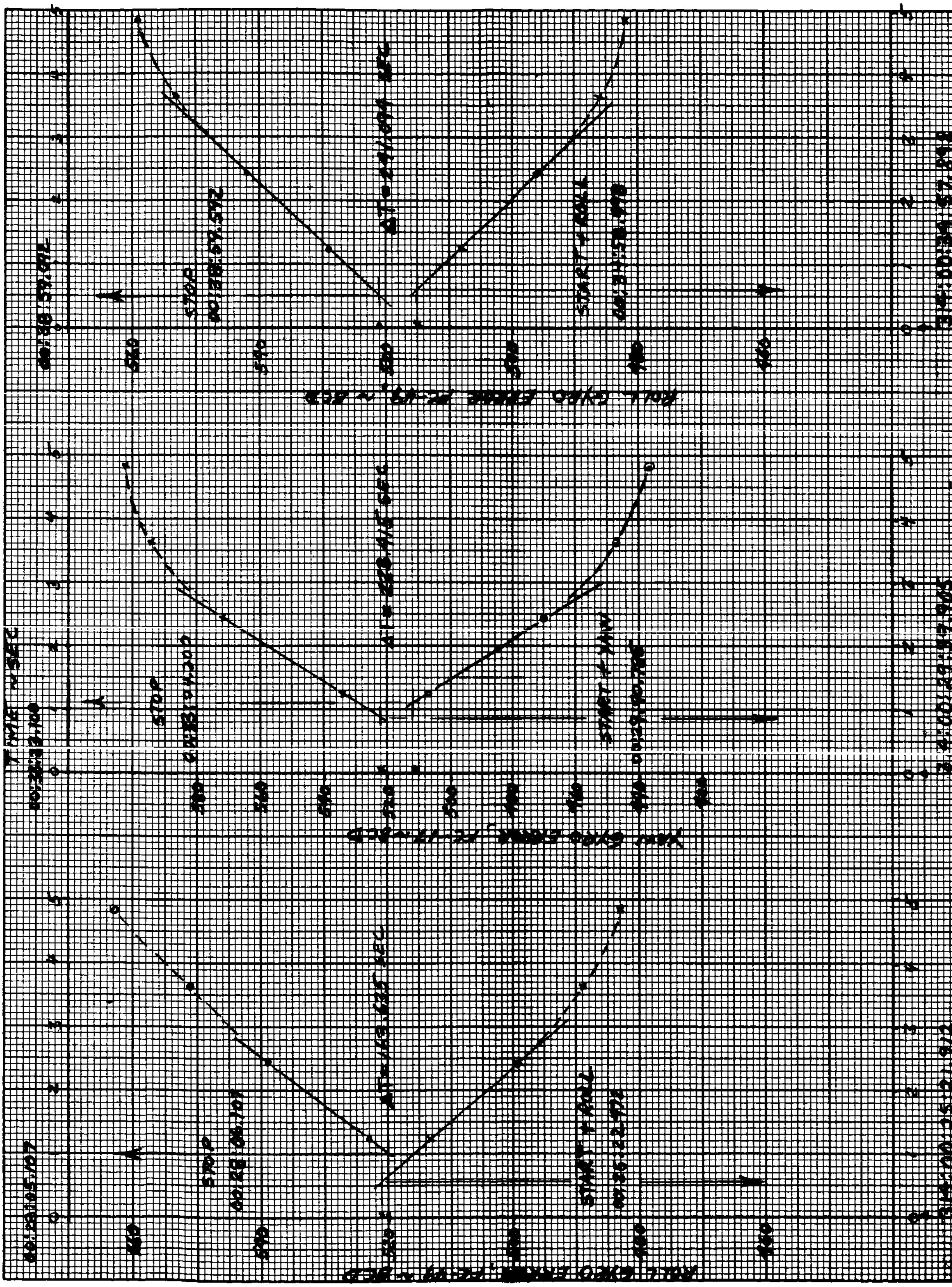

Figure 5.5-11. Gyro Error Signals

TABLE 5.5-9. GYRO DRIFT SUMMARY

Number	Type	Start Time, hr:min:sec	Stop Time, hr:min:sec	Δ Time, hr:min:sec	Drift Rate, deg/hr Roll	Pitch	Yaw
1	3 axis	16:43:04	18:04:10	1:21:06	-0.57	0.0	+1.22
					(-0.56)		(+1.34)
					-0.52	+0.18	+1.16 (bulk)
2	3 axis	18:18:21	19:22:31	1:04:10	-0.59	+0.13	+1.2
					(-0.606)	–	(+1.18)
3	3 axis	19:24:24	20:38:56	1:14:32	-0.53	+0.10	+1.22
					(-0.55)	–	(+1.13)
4	3 axis	20:44:50	22:03:00	1:18:10	-0.59	+0.03	+1.28
					(-0.52)	–	(+1.08)
5	3 axis	04:37:41	05:42:50	1:05:09	-0.58	+0.21	+1.21
6	Roll	08:32:26	12:46:28	4:14:02	-0.71	–	–
7	3 axis	16:18:39	17:53:31	1:34:52	-0.58	0	+1.22 Analog
					-0.543	+0.2	+1.49 Bulk
					-0.49	-0.02	+1.64 Milgo
8	Roll	18:59:38	21:42:27.6	2:42:50	-0.64	–	– Milgo
					-0.667	–	– Analog
9	3 axis	22:44:59	00:11:16	1:26:17	-0.644	0	+1.42 Analog
					-0.67	0	+1.21 Milgo
10	3 axis	01:11:23	02:25:34	1:14:11	-0.613	0	+1.37 Analog
11	3 axis	03:29:50	04:49:08	1:19:18	-0.617	0	+1.40 Analog
					-0.61	0	+1.35 Milgo
					-0.605	0	+1.38 SCCF
12	3 axis	06:25:57	07:38:32	1:12:35	-0.68	0	1.29 Analog
13	3 axis	09:04:07	10:42:27	1:38:20	-0.672	0	1.41 Analog
14	Roll	11:01:22	15:26:55	4:25:33	-0.68	–	– Analog

Note: TFAG estimates indicated in ( ).

The preterminal attitude maneuver magnitudes were compensated for the following gyro drift rates:

Roll = -0.64 deg/hr

Pitch = 0 deg/hr

Yaw = +1.4 deg/hr

The drift values selected for preterminal maneuver compensation were based essentially upon an average of all measurements made during the mission.

Preretro Pointing Error

The technique described in subsection 5.5.4.6 was used to determine the preretro attitude pointing error of 0.26 degree with a 3σ uncertainty of 0.21 degree.

5.5.4.10 Main Retro Phase

Main retro phase began at 314:00:57:57.038 GMT with the indication of altitude marking radar mark and successfully ended at 00:58:55.637 with verification of retro eject. At the start of the RADVS-controlled descent phase, the longitudinal velocity was reduced to approximately 463 fps at an altitude of 36,625 feet. The predicted values for burnout conditions were 482 fps at an altitude of 37,005 feet.

During this phase, the function of the flight control system is to maintain the attitude of the spacecraft inertially fixed and to provide and execute a fixed sequence of commands to establish the necessary initial conditions for the vernier descent phase. The following analysis reveals that these functions were performed satisfactorily.

A list of retro phase events and their corresponding time of occurrence is given in Table 5.5-10 along with expected time intervals. These results confirm the performance of the magnitude register and programmer.

Ignition of the vernier engines during the main retro phase was executed smoothly.

Retro Phase Attitude Control

During the main retro phase, extending from vernier ignition through case separation, spacecraft attitude motion was small in all three axes (Figure 5.5-12). Peak pitch and yaw inertial attitude motion, as read directly from gyro error telemetry data (FC-16 and FC-17), occurred at vernier ignition and amounted to -0.17 degree in pitch and -0.08 degree in

TABLE 5.5-10. TIME AND EVENTS LOG, RETRO PHASE

Main Retro Phase Event	Time of Occurrence, Day 314 GMT, hr:min:sec	Time Between Events, seconds	Expected Time Intervals, seconds
Altitude marking radar signal (FC-64)	00:57:57.038		
Vernier ignition (FC-28)	00:58:02.938	5.90	5.875
Retro ignition (FC-29)	00:58:04.038	1.100	1.1
RADVS on (R-28)	00:58:05.798	1.760	0.55
Retro burnout (FC-30) 3.5 g switch	00:58:43.647	39.560	39.6 (retro burn)
High thrust (FC-78)	00:58:53.297	9.65	10.0
Retro eject (FC-31)	00:58:55.637	2.340	2.0
Start RADVS-controlled descent (FC-42)	00:58:57.737	2.10	2.15

yaw. Following ignition, static attitude error was virtually zero in both pitch and yaw axes. Roll inertial attitude error was less than 0.2 degree throughout the main retro phase (less than 1.0 degree is required).

Since all gyro error signals were maintained to within ±1.0 degree (during retro burn), each gyro was exercised less than 10 percent of the available travel range of more than ±10 degrees. A summary of pitch and yaw inertial attitude angles produced at various points in the retro phase is given in Table 5.5-11. No attitude disturbance was noted at retro eject, indicating a clean case separation.

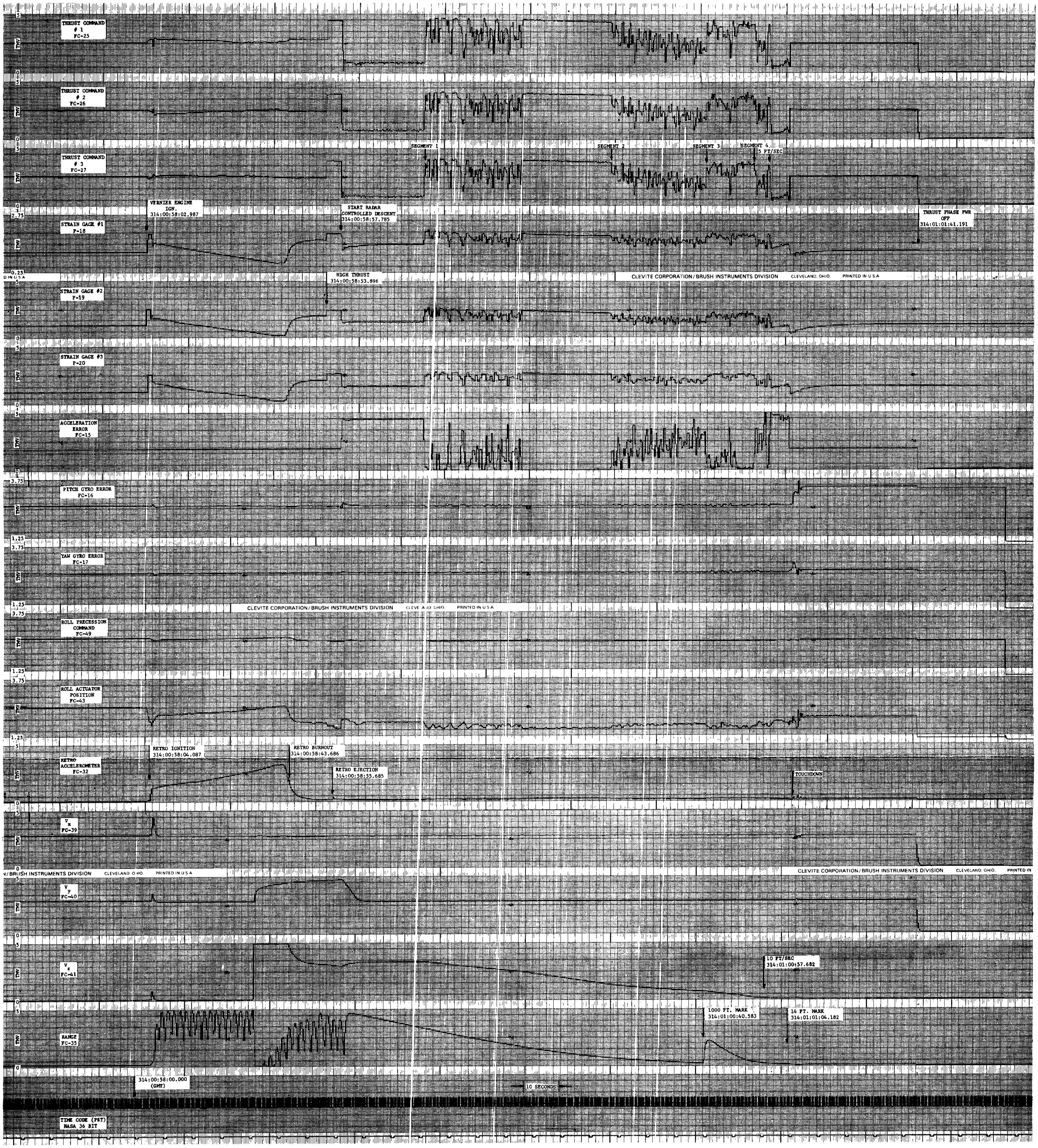

Figure 5.5-12. Surveyor VI Terminal Descent

FOLDOUT FRAME

FOLDOUT FRAME

5.5-46

TABLE 5.5-11. RETRO PHASE ATTITUDE CONTROL SUMMARY

Peak attitude motion, degrees

Event	Pitch	Yaw
Vernier ignition	+0.08	-0.08
Retro ignition	-0.17	0
Retro burnout	+0.18	+0.06
Start RADVS-controlled descent	-0.26	-0.14

Pitch and yaw control moments generated by the vernier engines were estimated by means of the following equations:

$$L_x = -2.969\ T_1 + 0.5723\ T_2 + 2.397\ T_3$$

$$L_y = -1.053\ T_1 + 3.098\ T_2 - 2.045\ T_3$$

where L_x and L_y are pitch and yaw control torques (ft-lb), respectively, and T_1, T_2, and T_3 are thrusts (pounds) generated by engines 1, 2, and 3, respectively. Values for T_1, T_2 and T_3 were estimated from the thrust command telemetry signals (FC-25, FC-26, and FC-27) (Figure 5.5-12). As indicated by the telemetry data, very little throttling of the engines occurred during the retro period. Shortly after retro ignition, differential throttling equivalent to approximately 38.0 ft-lb of control torque were produced. At all other times during the retro burn period, there was essentially no differential engine throttling.

The maximum thrust vector to center of gravity offset can be estimated using this maximum control torque magnitude of 38 ft-lb. Assuming a 9550-pound retro thrust, the offset was estimated as

$$\text{Maximum center of gravity offset} = \frac{38.0\ \text{ft-lb}}{9550\ \text{pounds}} \times \frac{12\ \text{inch}}{\text{feet}}$$

$$= 0.04\ \text{inch}$$

This compares to the required value of 0.18 inch.

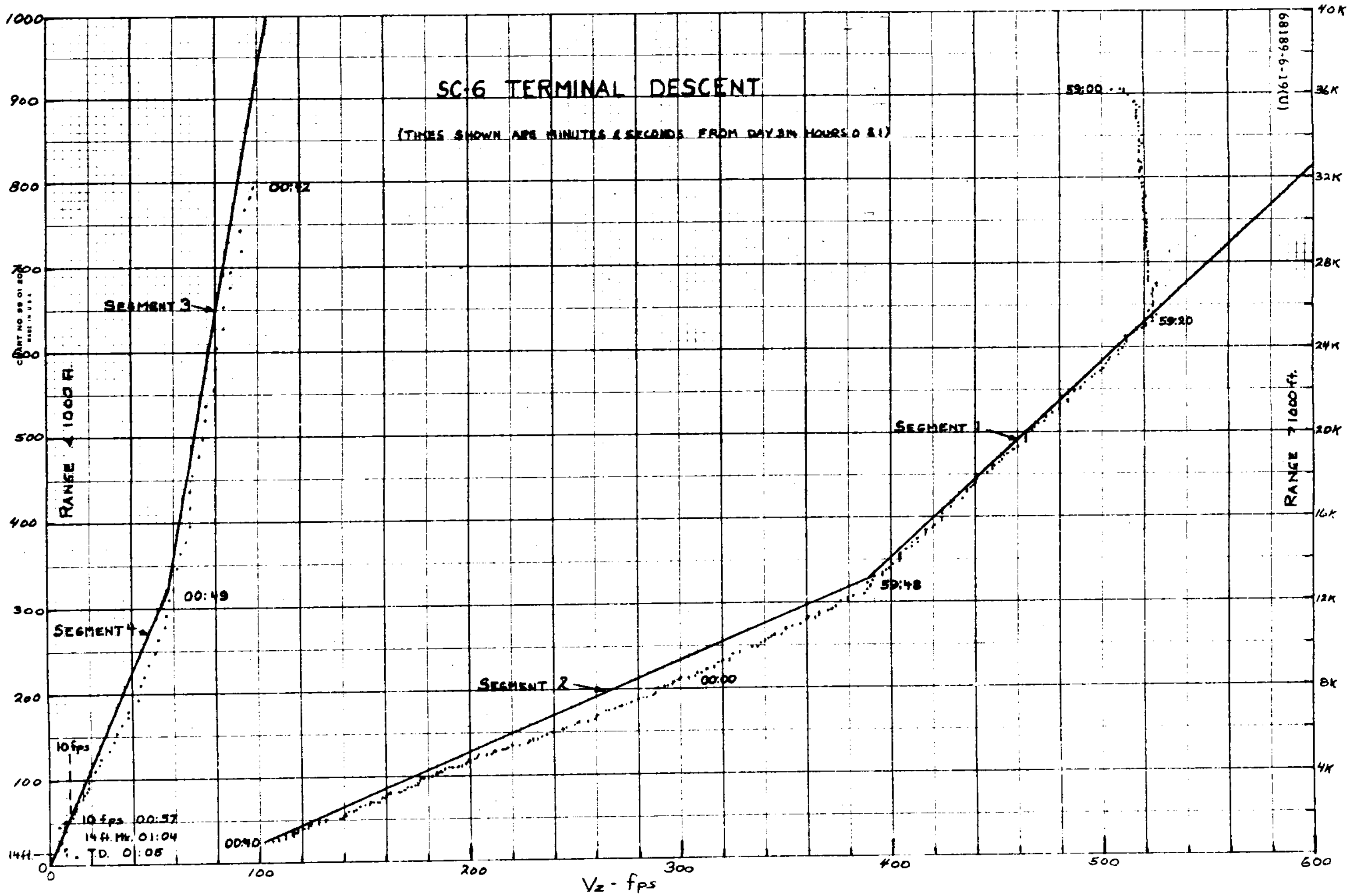

Figure 5. 5-13. Range Versus V_z

The maximum attitude error produced by the retro disturbance torques was also determined from the maximum torque magnitude of 38 ft-lb. Since the static gain (stiffness) of the pitch and yaw attitude control loops is

$$\text{static gain} = 1200 \text{ ft-lb/deg}$$

the maximum static attitude error is estimated to be

$$\text{maximum static error} = \frac{38}{1200} = 0.032 \text{ degree}$$

which is less than the allowable value of 0.12 degree.

5.5.4.11 Terminal Descent Phase

The RADVS-controlled terminal descent phase began at 314:00:58:57.737 GMT with initiation of the minimum acceleration (4.85 ft/sec^2) mode and a spacecraft attitude maneuver to null lateral velocities and align the thrust axis with the total velocity vector. The initial conditions at this time included a vertical velocity of 463 fps and an altitude of 36,625 feet. The lateral velocities ($V_x \approx +0.0$ fps, $V_y = +225$ fps) were nulled within 6 seconds (9 seconds allowed) and remained essentially at zero to touchdown. It was estimated that the spacecraft roll axis was maneuvered through a total angle of 26 degrees.

Intercept of the descent line segments occurred at approximately a vertical velocity of 522 fps and a slant range of 24,730 feet. The descent segment tracking performance of the flight control system (Figure 5.5-13) was normal.

A list of pertinent terminal descent events and times of occurrence are presented in Table 5.5-12.

Vernier Descent Attitude Control

Spacecraft attitude motions determined from gyro error telemetry signals (FC-16, -17, and -49) were maintained to less than ±1.0 degree in each axis during the vernier descent phase.

Following generation of the "RODVS" signal and the "Start RADVS-Controlled Descent" signal, the spacecraft initiated an attitude maneuver to align the thrust axis with the total velocity vector. Initial velocity conditions preceding the maneuver were as follows (taken from RADVS telemetry data, FC-39, FC-40, and FC-41) (see Figure 5.5-12).

TABLE 5.5-12. TERMINAL DESCENT PHASE LOG OF EVENTS, DAY 314

Event	GMT, hr:min:sec
RODVS	00:58:34.098
Start of RADVS-controlled descent (minimum acceleration)	00:58:57.737
RORA on	00:58:59.297
Segment intercept	00:59:21.276
1000-foot mark	01:00:40.534
10-fps mark	01:00:57.634
14-foot mark	01:01:04.133
Touchdown (first "glitch" on retro accelerometer)	01:01:05.832
Thrust phase power off	01:01:41.191
Flight control power off	01:02:05.580

Premaneuver velocity conditions were as follows:

$V_x = +0.0$ fps

$V_y = +225$ fps

$V_z = 463$ fps

The alignment maneuver was completed in less than 6 seconds (9 seconds allowed), after which time V_x and V_y were held essentially at zero and V_z became equal to the total velocity of 515 fps. The attitude maneuver magnitudes were computed as follows:

$$\text{Pitch maneuver: } \Delta\theta_x = \tan^{-1}\frac{V_y}{V_z} = 26.0 \text{ degrees}$$

$$\text{Yaw maneuver: } \Delta\theta_y = \tan^{-1}\frac{V_x}{V_z} = 0 \text{ degree}$$

The spacecraft Z-axis was therefore maneuvered through approximately 26.0 degrees.

At touchdown, changes in gyro gimbal errors of -2.3 degrees in pitch, -0.21 in yaw and +0.31 in roll were observed.

5.5.5 REFERENCES

1. "Surveyor Spacecraft Equipment," Hughes Specification 224832.

2. K. Kobayashi, "A Method for Determining Gas Jet Thrust Level – Post Mission Analysis," Hughes Aircraft Company IDC 2253.4/25, 1 March 1966.

3. "Surveyor III Flight Performance Final Report," Hughes Aircraft Company, SSD 68189-3, July 1967.

4. R.H. Bernard, "Restoration and Updating of Surveyor Coast Phase Analog Computer Mechanization," Hughes Aircraft Company IDC 2223/77, 29 July 1964.

5. R.H. Bernard, "Revised Gas Jet Fuel Consumption for 66-hour Mission," Hughes Aircraft Company IDC 2223/843, 19 February 1965.

6. E.I. Axelband, "Analysis of Inertial Pointing Accuracy of Surveyor Midcourse Thrust Vector," Hughes Aircraft Company IDC 2242/2706, 17 June 1963.

7. "Interface Document, Surveyor Vernier Propulsion Thrust Chamber Assembly," Hughes Specification 287015.

8. "Standard Transit Sequence of Spacecraft Operations," Hughes Specification 224550.

9. "Flight Control SPAC Handbook," Hughes Aircraft Company.

10. H.D. Marbach, "Angular Rates at Midcourse Shutdown," IDC 2223/731, 3 February 1965.

5.5.6 ACKNOWLEDGMENTS

J. Angerman, Technical Coordinator

B.N. Smith

L.R. Stumpf

R.H. Bernard

P.L. Welton

M.R. Buehner

5.6 VERNIER PROPULSION

5.6.1 INTRODUCTION

5.6.1.1 Description

The Surveyor vernier propulsion system (VPS) (Figure 5.6-1) is a bipropellant, variable thrust, liquid rocket system utilizing an oxidizer composed of 90 percent nitrogen tetroxide and 10 percent nitric oxide (Mon 10) and a fuel composed of 72 percent monomethyl hydrazine and 28 percent water. The VPS consists of three regeneratively-cooled thrust chambers (TCAs) with radiation-cooled expansion cones. Each TCA has a variable thrust range from 30 to 104 pounds vacuum thrust.

Propellant is supplied to the TCAs from six tanks employing positive expulsion bladders. One fuel tank and one oxidizer tank supply each TCA and are located adjacent to the TCA near each of the three spacecraft landing legs.

Propellant expulsion is accomplished by pressurizing the propellant tanks on the gas side of the bladders with helium gas. The helium is stored under high pressure in a spherical pressure vessel. The helium tank, together with the pressure regulator and servicing connections, is mounted outboard of the spaceframe between landing legs 2 and 3. The dual check and relief valves are mounted on the spaceframe between landing legs 2 and 3.

Thermal control of the VPS is both active and passive. Electric heaters are installed on two oxidizer tanks, one fuel tank, and all propellant feedlines to the TCAs. Passive thermal control consists of polished aluminum or of the application of black and white paint and vapor-deposited aluminum to selected portions of the VPS, together with super insulation applied to the propellant tanks.

The feedlines are wrapped with aluminum foil to deter heat loss.

5.6.1.2 Purpose

The VPS has three main functions during the mission:

1) Midcourse velocity correction and attitude control
2) Attitude control during retro phase

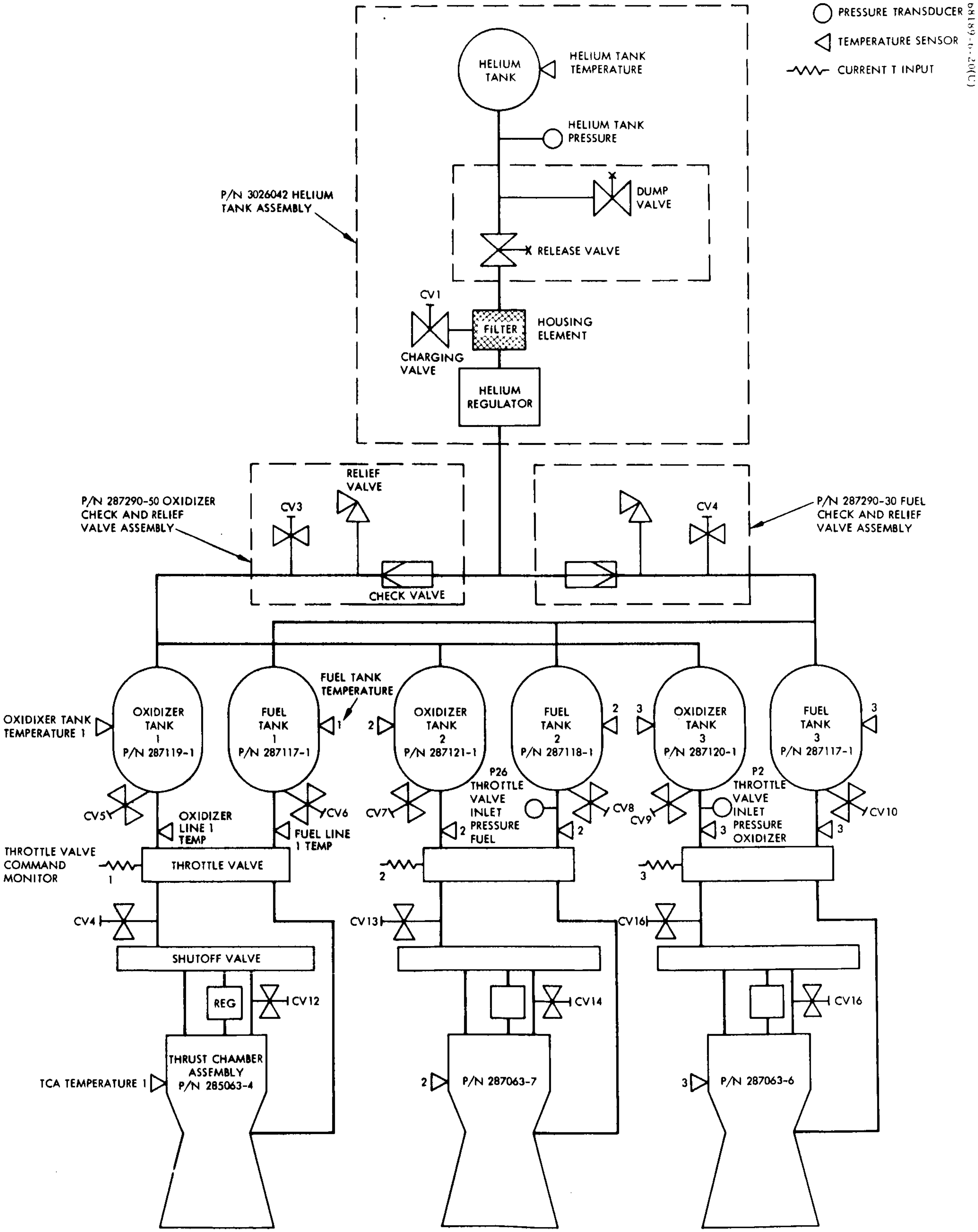

Figure 5.6-1. Vernier Propulsion System Schematic

3) Attitude control and velocity correction during the final descent maneuver

The midcourse velocity correction may be required to correct initial launching and injection errors. The VPS provides velocity corrections up to 50 m/sec with sufficient propellant remaining to successfully land the spacecraft on the moon. The required correction is transmitted to the spacecraft in the form of a desired burn time at a constant acceleration of 0.1 g, which results in a thrust level of approximately 75 pounds for each TCA. In addition to providing the required velocity change, the VPS also provides spacecraft attitude control during the maneuver.

Attitude control during firing of the spacecraft retro motor is provided by the VPS. The VPS is ignited approximately 1.1 seconds prior to retro ignition. Attitude control by the VPS is biased around a total vernier thrust level of either 150 or 200 pounds, depending on predictions of spacecraft attitude and velocity at retro burnout. The desired vernier thrust level is transmitted to the spacecraft several minutes prior to initiation of the retro maneuver sequence. Following retro burnout, the vernier thrust level is increased to 280 pounds total thrust to further slow the spacecraft to allow the ejected retro motor case to fall clear.

Following retro motor ejection, the VPS is throttled to approximately 110 pounds total thrust under radar control. When the spacecraft intersects the first descent segment, the VPS, operating in the closed-loop mode with the radar system, acquires the predetermined altitude-velocity profile and keeps the spacecraft on the profile. Each succeeding segment of the profile is acquired in a similar manner. At an altitude of 14 feet, the VPS is shut down, and the spacecraft free falls to the lunar surface.

5.6.2 ANOMALIES

No anomalies were observed during the earth/lunar transit.

5.6.3 SUMMARY AND RECOMMENDATIONS

The Surveyor VI vernier propulsion system performed in a nominal manner throughout launch, midcourse, and terminal descent. No modifications to procedures or components are recommended.

Table 5.6-1 lists the time of occurrence of the major events concerning or influencing the vernier engine system.

5.6.4 SUBSYSTEM PERFORMANCE ANALYSIS

5.6.4.1 Prelaunch

Final propulsion preparations for the Surveyor VI launch were begun on 16 October when propellant loading of the vernier system was initiated.

TABLE 5.6-1. SURVEYOR VI PROPULSION EVENTS

Event	GMT, day:hr:min:sec	Mission Time, hr:min:sec	Engine Burn Time, seconds
Pressurize propellant tanks	312:02:16:00	18:36:59	
Midcourse	312:02:20:03	18:41:02	10.3
Engine burn and terminal descent	314:00:58:03	65:19:02	
14-foot mark, (engines off)	314:01:01:04	65:22:03	183
Touchdown	314:01:01:05	65:22:04	
Liftoff and translation	321:10:32:02	177:30:56	2.5

The desired and actual loadings are given in Table 5.6-2 and show that the spacecraft was loaded within the specified tolerance in Reference 1. The helium tank was then charged with 2.41 pounds of helium.

Prelaunch telemetry readings of the tank temperature and pressure were taken over a 60-hour period and indicated a helium leakage rate of 4.45 psi/day which was within the 20 psi/day of Reference 2.

5.6.4.2 Launch (L-1 Hour to L+ 36 Minutes)

Prelaunch monitoring of the propulsion system was initiated at 06:42 GMT on 7 November when the helium tank pressure and temperature were 5200 psia and 80° F, respectively. At launch (311:07:39:01 GMT), the pressure had increased to 5219 psia, and the temperature was 81° F. All other propulsion data were also within the range specified for launch conditions. The prelaunch conditions of the propulsion system are given in Table 5.6-3.

5.6.4.3 Coast Phase I (L+ 36 Minutes to L+ 17 Hours)

Following launch, an assessment of the propulsion functions was made and all conditions were normal. At L+ 1 hour and 51 minutes, the line 2 temperature was down to 20.3° F and the heater started cycling between that temperature and 27.4° F. Fifteen hours after launch, the helium tank pressure had stabilized at 5182 psia, and the tank temperature

TABLE 5.6-2. PROPELLANT LOADING SURVEYOR VI (POUNDS)

	Predicted at 105° F		Predicted at Ambient		Actual at Ambient	
	Oxidizer	Fuel	Oxidizer	Fuel	Oxidizer	Fuel
Total loaded gross	110.08	75.18	113.60	76.67	116.13	76.75
3σ loading tolerance	0.75	0.75	0.75	0.75	0.75	0.75
Offload	0	0	3.52	1.49	5.47	1.17
Total loaded net	109.33	74.43	109.33	74.43	109.91	74.83
Unusable at 0° F	1.29	0.86	1.29	0.86	1.29	0.86
Total usable	108.04	73.57	108.04	73.57	108.62	73.97

was 83° F. During gyro drift checks, the altered shadow patterns on the leg 2 thrust chamber assembly, resulting from a positive yaw error, increased the assembly's temperature from a stabilized value of 82° F to a maximum of 99° F.

5.6.4.4 Midcourse (L+ 17 Hours to L+ 19 Hours)

Midcourse preparation of the propulsion system consisted of pressurizing the feed system and verification of system readiness for firing at that time. Pressurization was accomplished at 312:02:16 GMT. Propellant tank pressures rose and locked up at 764 psia, well below the relief valve cracking pressures of about 825 psia. The helium tank pressure decreased 179 psi during pressurization, a drop comparable to that seen on previous spacecraft. The commanded midcourse correction of 10.2 seconds duration was successfully completed at 312:02:20:13 GMT. Attitude transients at ignition and cutoff were less than 1 degree, indicating nominal thrust chamber assembly start and shutdown performance. The average corrected, commanded thrust levels for thrust chamber assembly's 1, 2, and 3 as determined from telemetry were 79.6, 72.0, and 70.4 pounds, respectively. All three values were within 3.4 pounds of the predicted values. For a summary of midcourse thrust command and strain gage data, see Table 5.6-4. A helium pressure decrease of 208 psi was noted during the midcourse correction. This compares to 205 psi predicted for Figure 5.6-2. A summary of premidcourse propulsion data is given in Table 5.6-3. Helium tank, fuel tank, and oxidizer tank pressure histories are shown in Figure 5.6-3.

TABLE 5.6-3. CRITICAL TIME VERNIER PROPULSION SYSTEM PARAMETERS

Parameter		Prelaunch Status	Midcourse Status	Terminal Status
Day		311	312	314
GMT, min:sec		07:15	01:40	00:45
Launch time, min:sec		-00:24	+ 18:02	+ 65:06
Mode		5/2/1	5/2/1	5/2/1
Bit rate		550	1100	550
P1	Helium tank pressure, psia	5219	5182	4853
P2	Oxidizer leg 3 pressure, psia	224	205	762
P3	Upper retro case temperature, °F	74	73	65
P4	Leg 2 oxidizer line temperature, °F	80	20	25
P5	Leg 2 fuel tank temperature, °F	74	43	33
P6	Leg 3 oxidizer tank temperature, °F	74	54	43
P7	Leg 1 TCA temperature, °F	80	63	67
P8	Leg 1 oxidizer line temperature, °F	80	54	74
P9	Leg 3 oxidizer line temperature, °F	80	–	44
P10	Leg 2 TCA temperature, °F	79	84	80
P11	Leg 3 TCA temperature, °F	79	74	86
P12	Lower retro case temperature, °F	75	55	41
P13	Leg 1 fuel tank temperature, °F	75	56	57
P14	Leg 3 fuel tank temperature, °F	74	56	58

Table 5.6-3 (continued)

	Parameter	Prelaunch Status	Midcourse Status	Terminal Status
P15	Leg 1 oxidizer tank temperature, °F	74	60	50
P16	Leg 2 oxidizer tank temperature, °F	74	37	28
P17	Helium tank temperature, °F	80	83	73
P18	Leg 1 strain gage, pounds	-147*	-147*	16**
P19	Leg 2 strain gage, pounds	-56*	-56*	2**
P20	Leg 3 strain gage, pounds	-45*	-45*	3**
P22	Retro nozzle temperature, °F	77	-188	-39
P23	Leg 1 fuel line temperature, °F	80	57	55
P24	Leg 2 fuel line temperature, °F	79	33	28
P25	Leg 3 fuel line temperature, °F	80	58	60
P26	Fuel leg 2 pressure, psia	266	256	770

*With strain gage power off.

**With strain gage power on.

5.6.4.5 Coast Phase II (L+19 Hours to L+64 Hours)

During this coast phase, the helium tank pressure and temperature remained at a constant 4866 psia and 85°F, respectively, to the terminal descent maneuvers. The line 3 heater started cycling at L+33 hours and 39 minutes. At L+55 hours, the heaters for the leg 2 and 3 oxidizer tanks and the leg 2 fuel tank were enabled. All temperatures and pressure remained within specified limits throughout the entire phase. A final estimate for retro T_{3500} of 39.60 seconds was made at L+62 hours.

TABLE 5.6-4. MIDCOURSE THRUST DATA

GMT	Engine 1, pounds			Engine 2, pounds			Engine 3, pounds		
	Predict	Thrust Command*	Strain Gage*	Predict	Thrust Command*	Strain Gage*	Predict	Thrust Command*	Strain Gage*
02 hr 20 min	0	65.0	0	0	66.0	0	0	65.5	0
3.16 seconds	0	65.0	0	0	66.0	0	0	65.5	0
3.88 seconds	76.3	82.0	85.4	74.6	75.5	68.0	71.1	71.8	72.2
4.58 seconds	76.3	80.2	84.8	74.6	72.2	66.5	71.1	70.5	72.1
5.28 seconds	76.3	79.6	85.1	74.6	72.0	67.1	71.1	70.3	71.6
5.99 seconds	76.2	79.5	85.8	74.5	72.0	67.6	71.0	70.3	72.1
6.69 seconds	76.2	79.6	85.7	74.5	71.9	68.7	71.0	70.1	72.7
7.39 seconds	76.2	79.6	85.6	74.5	71.9	69.5	71.0	70.4	72.2
8.10 seconds	76.2	78.6	86.3	74.5	71.9	69.8	71.0	70.3	72.1
8.80 seconds	76.1	79.1	86.5	74.4	71.5	70.4	70.9	70.3	73.0
9.50 seconds	76.1	79.4	86.4	74.4	71.5	69.4	70.9	70.5	72.0
10.23 seconds	76.1	78.6	86.7	74.4	71.5	69.0	70.9	70.4	71.2
10.92 seconds	76.1	78.6	86.5	74.4	71.5	69.0	70.9	70.3	71.0
11.63 seconds	76.0	78.6	86.4	74.3	71.5	68.9	70.8	70.3	70.7
12.34 seconds	76.0	78.3	87.1	74.3	71.5	68.4	70.8	70.3	70.4
13.03 seconds	76.0	78.2	86.1	74.3	71.4	69.0	70.8	70.4	70.3
13.74 seconds	0	65.0	0	0	67.5	0	0	65.5	0
Average during firing	76.2	79.6	86.1	74.5	72.0	68.7	71.0	70.4	71.7
Difference (predicted versus actual), percent	—	+3.4	+9.9	—	-2.5	-5.8	—	-0.6	+0.7

*Thrust commands and strain gage data corrected for offsets and zero shifts before and after.

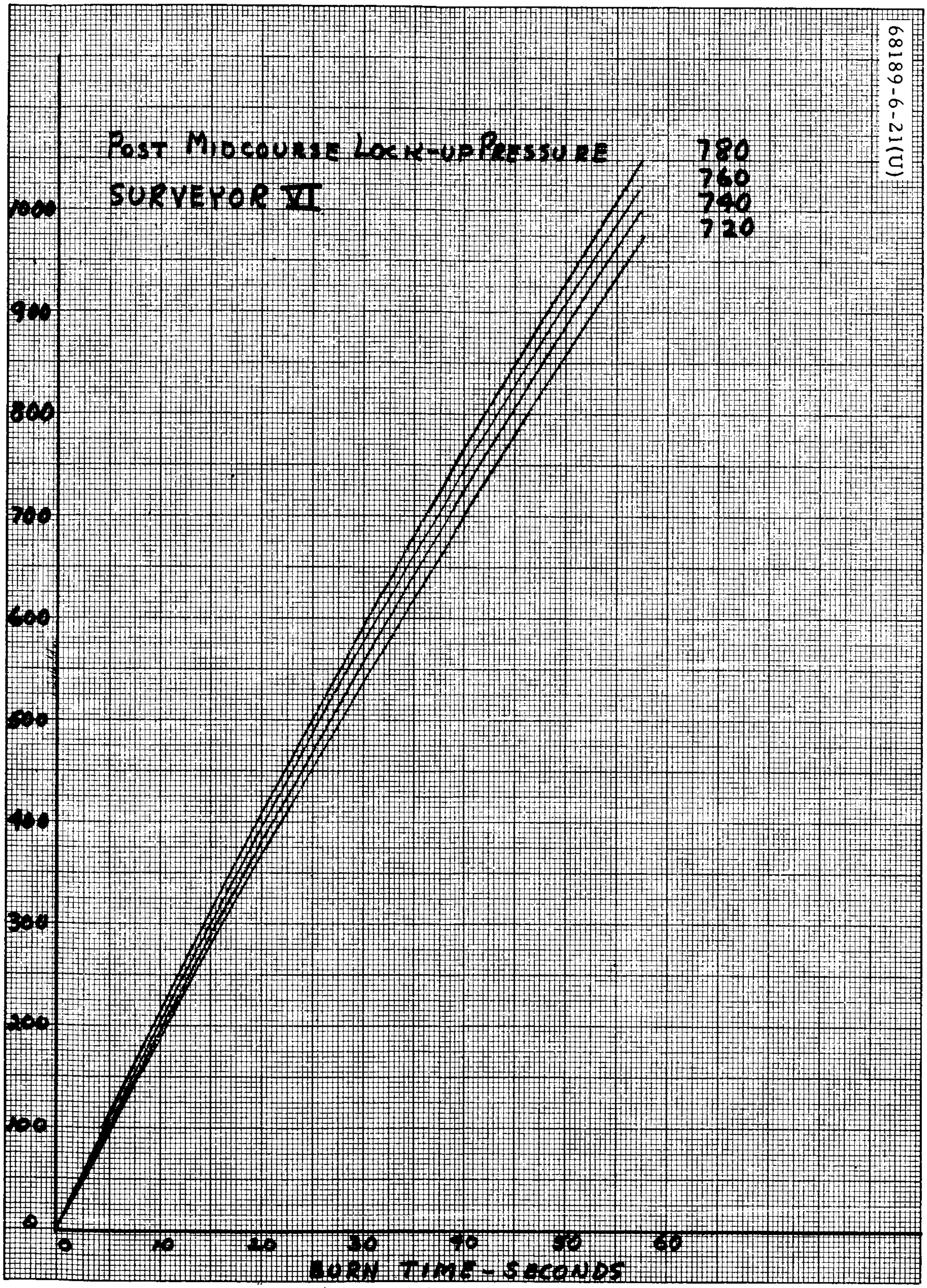

Figure 5.6-2. Predicted Helium Pressure at Midcourse

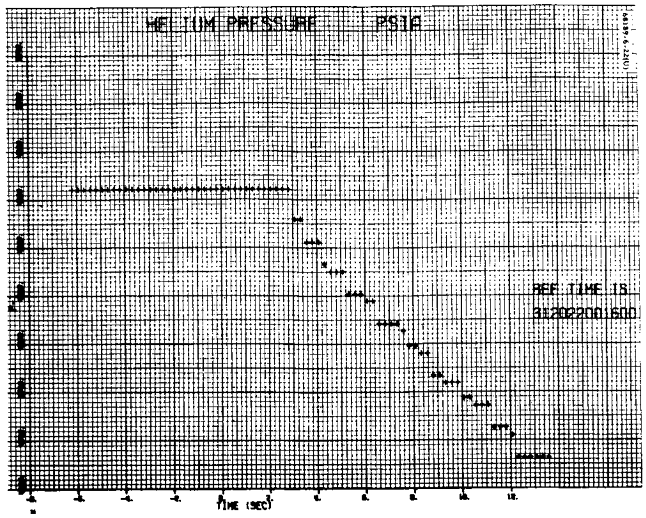

a) Helium Pressure (P-1)

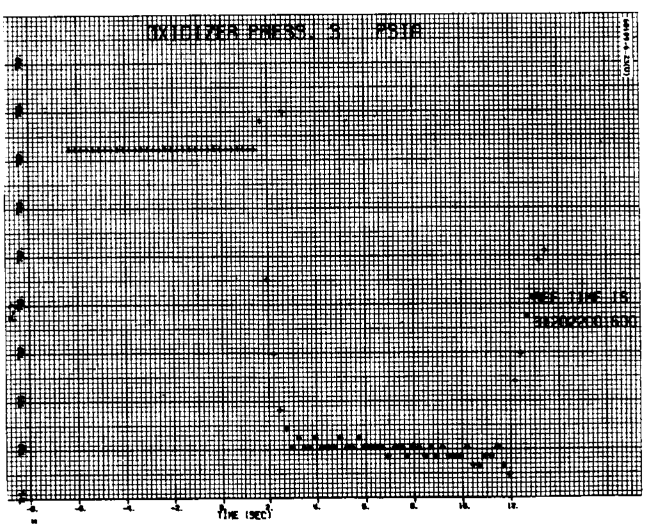

b) Oxidizer Pressure (P-2)

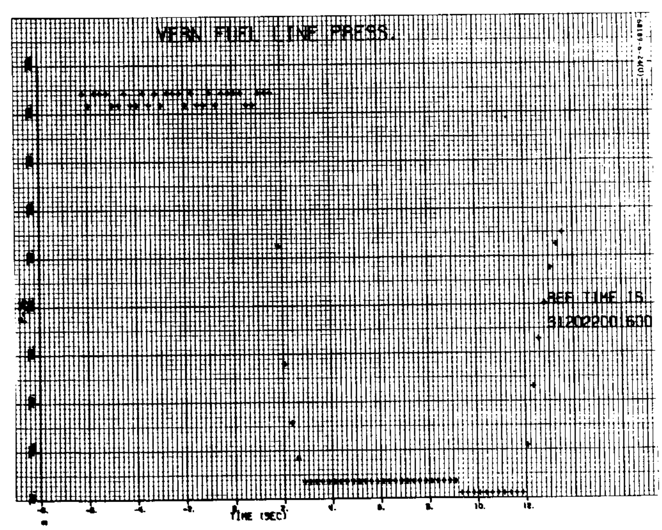

c) Vernier Fuel Line Pressure (P-26)

Figure 5.6-3. Midcourse

5.6.4.6 Terminal Descent (L+64 Hours to L+66 Hours)

Terminal descent operations were initiated at 314:00:07:31 GMT when the transmitter filament was turned on. At the initiation of terminal descent, all propulsion system parameters were normal. A summary of data at that time is contained in Table 5.6-3. Vernier ignition occurred at 314:00:58:03 GMT, followed by retro ignition at 58:04. Touchdown occurred at 314:01:01:06. All propulsion parameters were normal during the descent.

The observed total vernier thrust level of 196 pounds (corrected) from thrust command data agrees well with the 200-pound thrust predicted during retro burn.

Helium and oxidizer pressure histories during terminal descent are shown in Figure 5.6-4. Fuel pressure is not recorded in the descent mode.

Propellant usage is shown in Table 5.6-5.

TABLE 5.6-5. PROPELLANT USAGE (POUNDS)

Event	Propellant Used	Propellant Remaining
Launch	0	182.6
Midcourse	8.4*	174.2
Terminal descent	145**	29.2
Lunar hop	1.4*	27.8

*From engine performance data.
**From helium tank pressure decay data.

5.6.4.7 First Lunar Day

At touchdown, the helium pressure was 2314 psia; the oxidizer and fuel tank pressure was 728 psia. Subsequently, it was recommended that helium not be dumped since static fire operations were under consideration.

Both the propellant tank and helium tank pressures began to increase after touchdown as a result of lunar heating. At 315:01:30 GMT, the oxidizer pressure had reached 804 psia. Shortly thereafter, the oxidizer relief valve actuated, reseating at a pressure of 729 psia. The oxidizer relief then cycled five times at about 6- to 8-hour intervals. At 318:03:30 GMT, the solar panel was repositioned to shade both the oxidizer and fuel relief valves. The fuel relief valve relieved initially at 317:00 GMT

This page intentionally left blank.

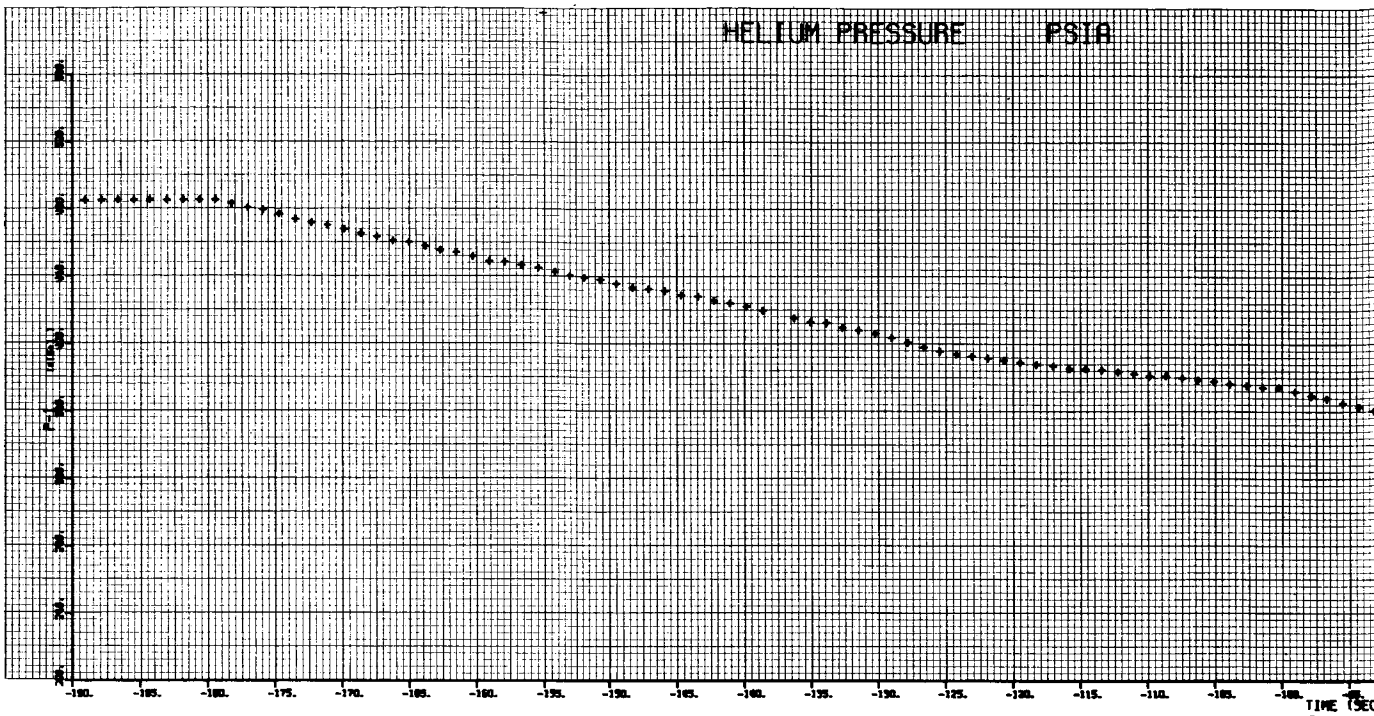

a) Helium Pressure (P-1)

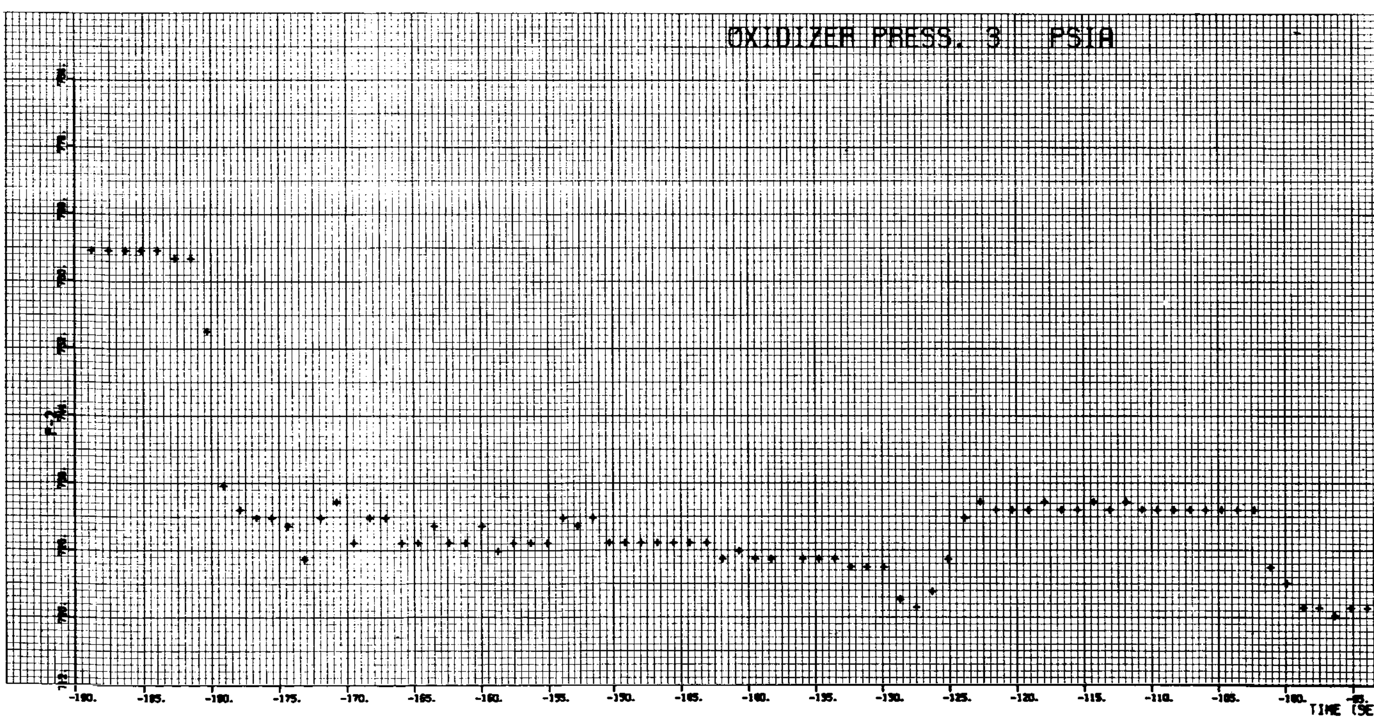

b) Oxidizer Pressure (P-2)

Figure 5.6-4. Terminal Descent

FOLDOUT FRAME

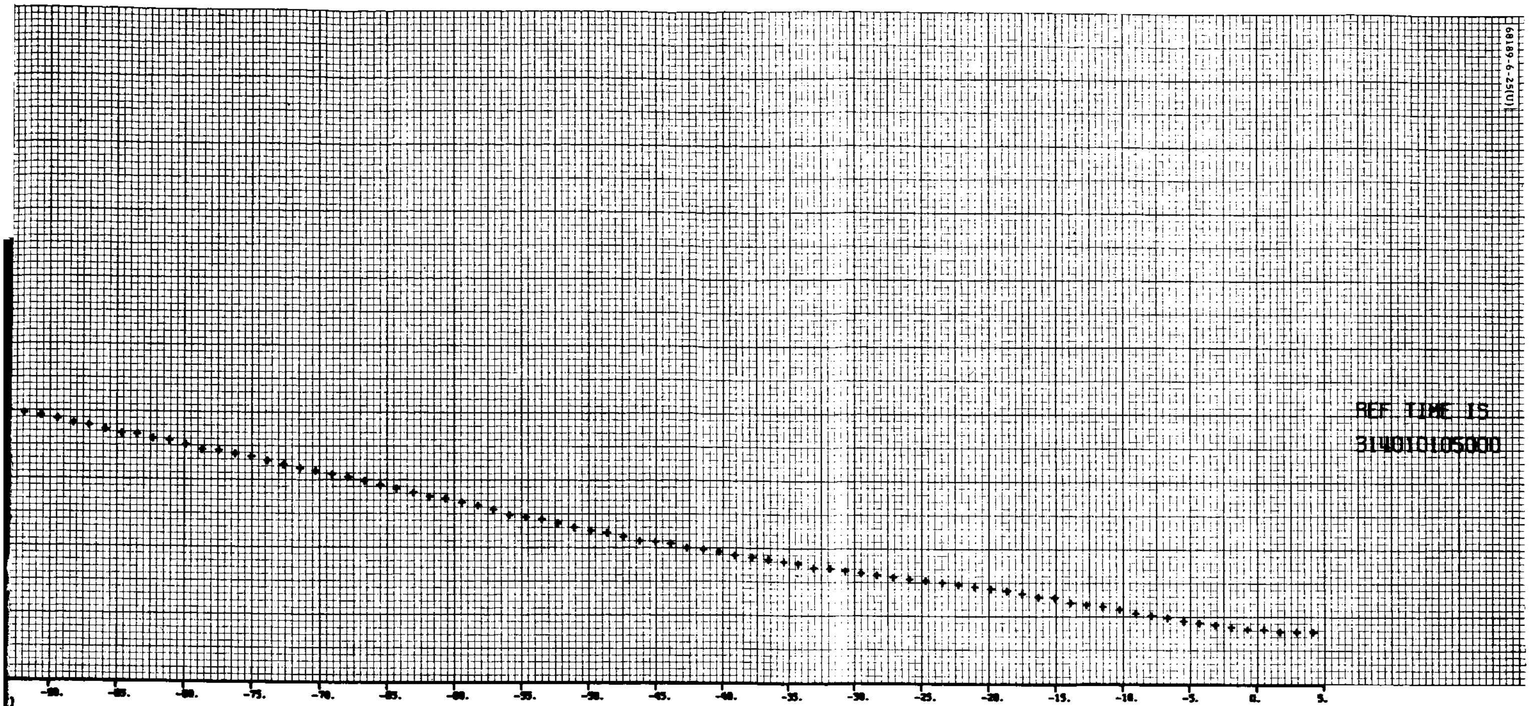

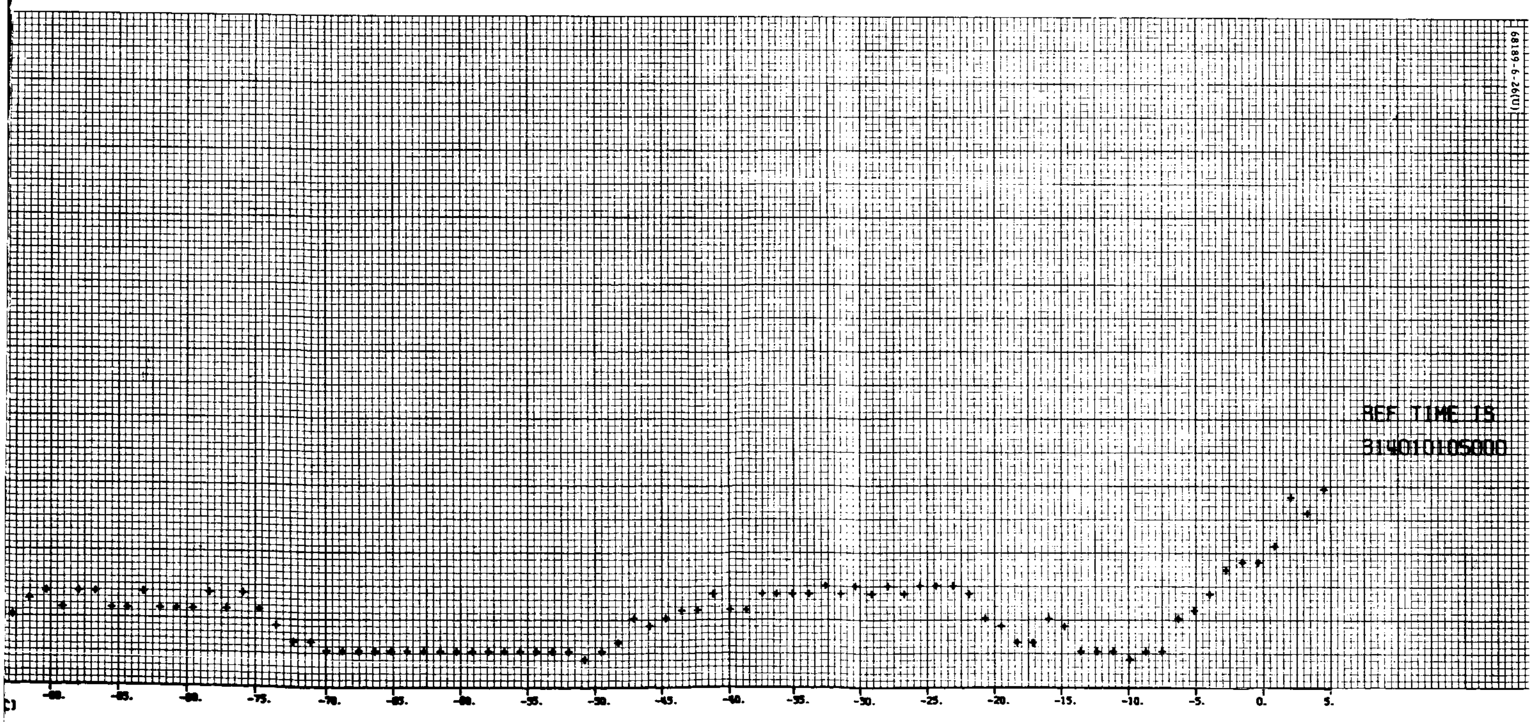

FOLDOUT FRAME

5.6-14

between 800 and 788 psia. It cycled three times prior to the repositioning of the solar panel at 318:03:30 GMT.

On day 321, it was decided to perform a spacecraft liftoff and translation. By selective positioning of the A/SPP, it was possible to bring all three thrust chamber assemblies within the 220°F maximum lunar operating limit. The maneuver was initiated at 321:10:32 GMT. The thrust chamber assembly preignition temperatures were as follows: leg 1, 204°F; leg 2, 191°F; and leg 3, 189°F. The commanded thrust level and duration was 150 pounds for 2 seconds. Post-translation data evaluation indicated an average thrust of 146 pounds for 2.5 seconds as the backup thrust cutoff command terminated thrust. Approximate individual thrusts were: leg 1, 50 pounds; leg 2, 50 pounds; and leg 3, 46 pounds. Maximum post-burn temperatures exhibited by TCAs 1, 2, and 3 were 335°, 323°, and 233°F, respectively. The TCA 3 temperature does not represent the maximum soak-back temperature but rather the temperature prior to the mode change and attendant temperature data loss. The sensor temperature rise rate of this assembly was also slower than the other two TCAs; either a delayed engine shutdown or a loose thermal sensor could have produced this behavior. A delayed fuel shutdown could result in a significant unbalanced thrust of 1 to 2 pounds due to fuel vaporization, whereas the flight control system sensed no perturbation within its sensitivity of about 0.05-pound thrust. Therefore, it may be concluded that a loose thermal sensor is the most probable cause of the observed behavior.

Due to the short burn duration, the oxidizer and fuel pressures (Figure 5.6-5) did not fall below the in-flight regulated pressure of 730 psia. Consequently, no helium was expelled from the helium tank, and the apparent rise in helium tank pressure is a hysteresis effect.

At approximately 323:10 GMT, a pressure decrease was noted in the oxidizer system. The oxidizer pressure decayed 115 psi in 25 hours to 740 psia, causing the helium regulator to open and allow helium to pass from the helium tank into the oxidizer system and then overboard. When the helium tank pressure decreased to the regulated pressure at about 325:16 GMT, the oxidizer pressure again began to decrease. By 329:16, both pressures had decayed to essentially zero.

Thermal data on the leg 1 oxidizer tank, taken at the time the leak was noted and also after lunar sunset, indicate that some, but not all, oxidizer was lost out of the leg 1 oxidizer tank. Additionally, gas leakage occurred as a partial loss of liquid could not account for the total noted pressure loss.

The most probable source of leakage is the standpipe-to-propellant tank seal O-rings which were degraded due to exposure to lunar temperatures.

The leakage signature was sufficiently different from that noted on Surveyor V, raising doubt, until post-sunset thermal data were evaluated as to the type of leak that had occurred. Consequently, for the purpose of future liftoff and translation planning, any pressure losses similar to those noted on Surveyor V and VI must be assumed to be partly liquid leakage.

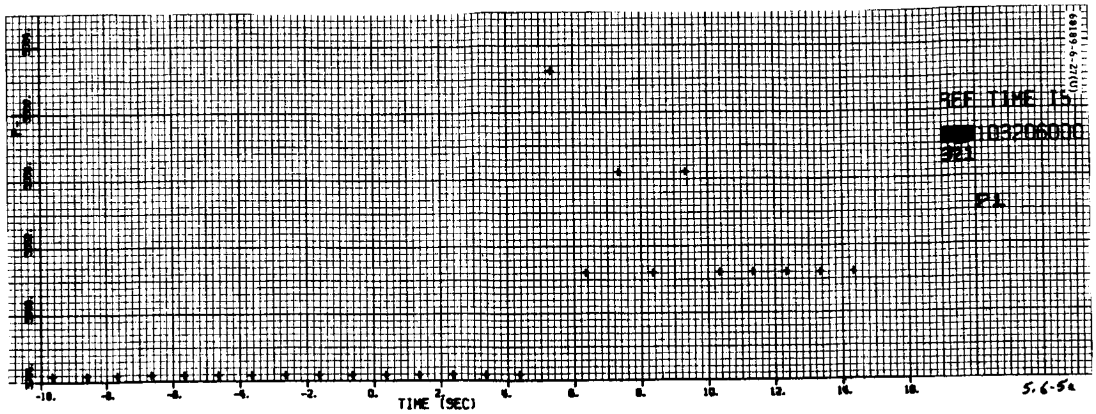

a) Helium Pressure (P-1)

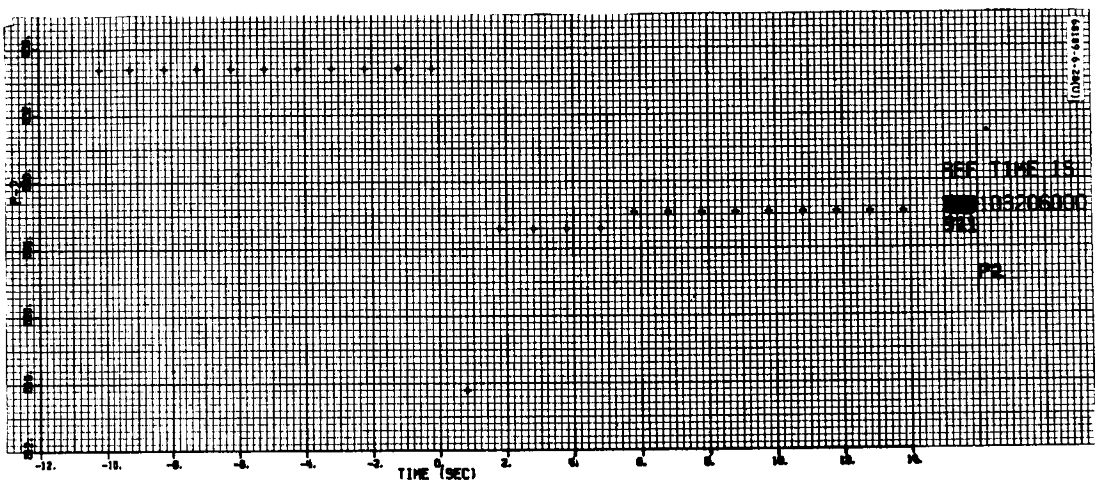

b) Oxidizer Pressure (P-2)

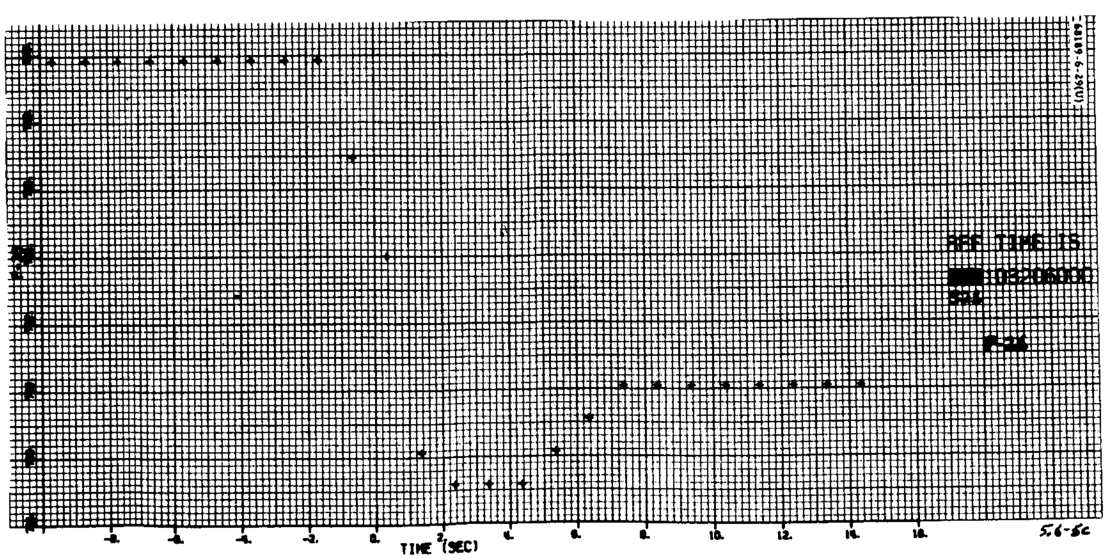

c) Vernier Fuel Line Pressure (P-26)

Figure 5.6-5. Lunar Translation

Final first lunar day data on fuel pressure were taken at 328:09 GMT when the pressure was 710 psia, indicating an integral fuel subsystem.

A detailed discussion of the oxidizer pressure loss is presented in Appendix A.

5.6.5 REFERENCES

1) R. Laird to Distribution, "A21 and A21A/114 Vernier Propulsion Systems Propellant Inventory," Hughes IDC 2227.1/1110, 29 September 1966.

2) G. F. Pasley to P.A. Donatelli, "Allowable Helium Leakage for SC-6," Hughes IDC 2227.2/1244, 3 October 1967.

3) T.B. Shoebotham to L. Gee, "Transmittal of Propulsion SPAC Mission F Report, " Hughes IDC 2227.2/1248, 15 November 1967.

4) T.B. Shoebotham to K. Filetti, "Transmittal of Propulsion SPAC Mission F First Lunar Day Report, " Hughes IDC 2227.2/2228, December 1967.

5.6.6 ACKNOWLEDGMENTS

Section 5.6 was coordinated by G. F. Pasley who also wrote Appendix A to Section 5.6. T.B. Shoebotham contributed to subsection 5.6.4 through References 3 and 4. J.P. Amelsberg did many of the figures.

APPENDIX A TO SECTION 5.6

FIRST LUNAR DAY VERNIER SYSTEM PRESSURE LOSS STUDY

INTRODUCTION

From lunar landing at 314:01:01 until 323:13:30 GMT, the vernier propulsion system exhibited normal thermal response to the changing radiation heat input (Figures 5.6-A1 and 5.6-A2). Helium tank, oxidizer, and fuel pressures had stabilized at 2761, 858, and 797 psia, respectively. At the next interrogation (323:16:22), the oxidizer pressure had dropped slightly to 857, and this rate of drop (0.8 psi/hr) continued until 324:00:30 when the loss rate increased to about 3 psi/hr. This pressure decay was attributed, at the time, to effects of component cooling occurring in the lunar afternoon. At 324:19:50, the helium tank, oxidizer tank, and fuel tank pressures were 2676, 805, and 791, respectively, but, at the next interrogation 2 hours later, the oxidizer pressure had dropped to 739 psia, the normal regulated pressure, and the helium tank pressure was dropping at about 2 psi/min. These data indicated that the oxidizer side of the vernier propulsion was leaking. Whether the leak was gas or liquid or a combination was not apparent from the data. The leak continued throughout the lunar day until the oxidizer and helium tank pressures reached zero on about 329:14:00. The length and uniformity of the pressure decay rate observed during this time interval indicated the rapid pressure loss commecing at about 324:22 was definitely a gas leak. However, the question of a prior liquid leak was still open to discussion. Propulsion system temperatures were subsequently monitored into the lunar night and, in conjunction with similar data from Surveyors I and V, are used to establish the leakage history of Surveyor VI.

CONCLUSIONS

The data available indicate that oxidizer tank 1 lost a significant amount of propellant in addition to the observed gas leak.

DISCUSSION

A review of the lunar day tank thermal histories (Figures 5.1-B23, 31, and 32) showed unexplained temperature fluctuations on oxidizer tank 1 starting at about the time the oxidizer pressure began to fall (323:13:30 GMT) and ending about the time the gas leak began (324:20). Similar fluctuations earlier in the lunar day on oxidizer tank 2 are the result of transient shadowing by the camera and A/SPP. Since similar, but larger, fluctuations seen on Surveyor V leg 1 oxidizer tank had been diagnosed as a liquid leak, this possibility was investigated.

An analysis of the expected pressure loss prior to the gas leak indicated that the thermal history of the propellant tanks (which changes ullage pressure and volume) could account for only 17 of the 54-psi pressure decay observed. This calculation confirmed that there was either a slow gas or liquid leak (or combination) prior to the rapid gas leak. The propellant quantities in each tank at sunset may be estimated from the tank cooling rates during lunar night. As seen in Figure 5.6-A2, oxidizer tank 1 is cooling much more rapidly than oxidizer tanks 2 and 3 during this period, indicating a lower propellant load. The relative amounts of propellant in tanks 1 and 2 were computed from the cooling rates prior to the "knee" in the curves caused by propellant freezing. Then, since inflight propellant consumption calculations predicted a propellant residual of 5.6 pounds in leg 2 oxidizer tank, the corresponding propellant in leg 1 was found to be 2.5 pounds from the above relationship. An alternative method of finding the residual propellant in leg 1 did not require knowledge of landed propellant but used the data from the freezing or "knee" portion of the curves to estimate propellant residual. This calculation gave an oxidizer tank 1 residual of 0.8 pound. Since there were inaccuracies in each of the above calculations (e.g., the landed propellant was not known to within ±1 pound), the conclusion drawn was that 1.5 ± 1 pound of propellant remained in oxidizer tank 1 at the end of the first lunar day.

The oxidizer tank 1 temperature profile produced by the Surveyor V liquid leak at 261:11:00 GMT is shown in Figure 5.6-A3 and, although it is more extreme, it is very similar to the erratic profile seen on the Surveyor VI oxidizer tank 1 in Figure 5.6-A1. A comparison of Surveyor V and VI lunar night oxidizer tank temperature profiles is shown in Figures 5.6-A2 and 5.6-A4. The striking similarity of the thermal histories indicates that the respective oxidizer tank had very similar propellant loadings. The knee in the first day temperature history of Surveyor V oxidizer tank 1 indicates that it also had some propellant remaining after the leak which occurred 7 days earlier. When the above analyses are applied to the Surveyor V data, the results agree closely with Surveyor VI residuals. The second lunar day profile on Surveyor V shows that most of the propellant remaining in oxidizer tank 1 leaked out during the second lunar day.

Further evidence of the type of leakage(liquid versus gas) is seen in data from Surveyor I (Figure 5.6-A5) where the gas leak is reflected in a gradual drop in oxidizer tank temperatures as the gas in all three tanks cools during expansion. This smooth type of temperature change is in contrast to the rapid fluctuations seen during propellant leakage on Surveyor V and VI.

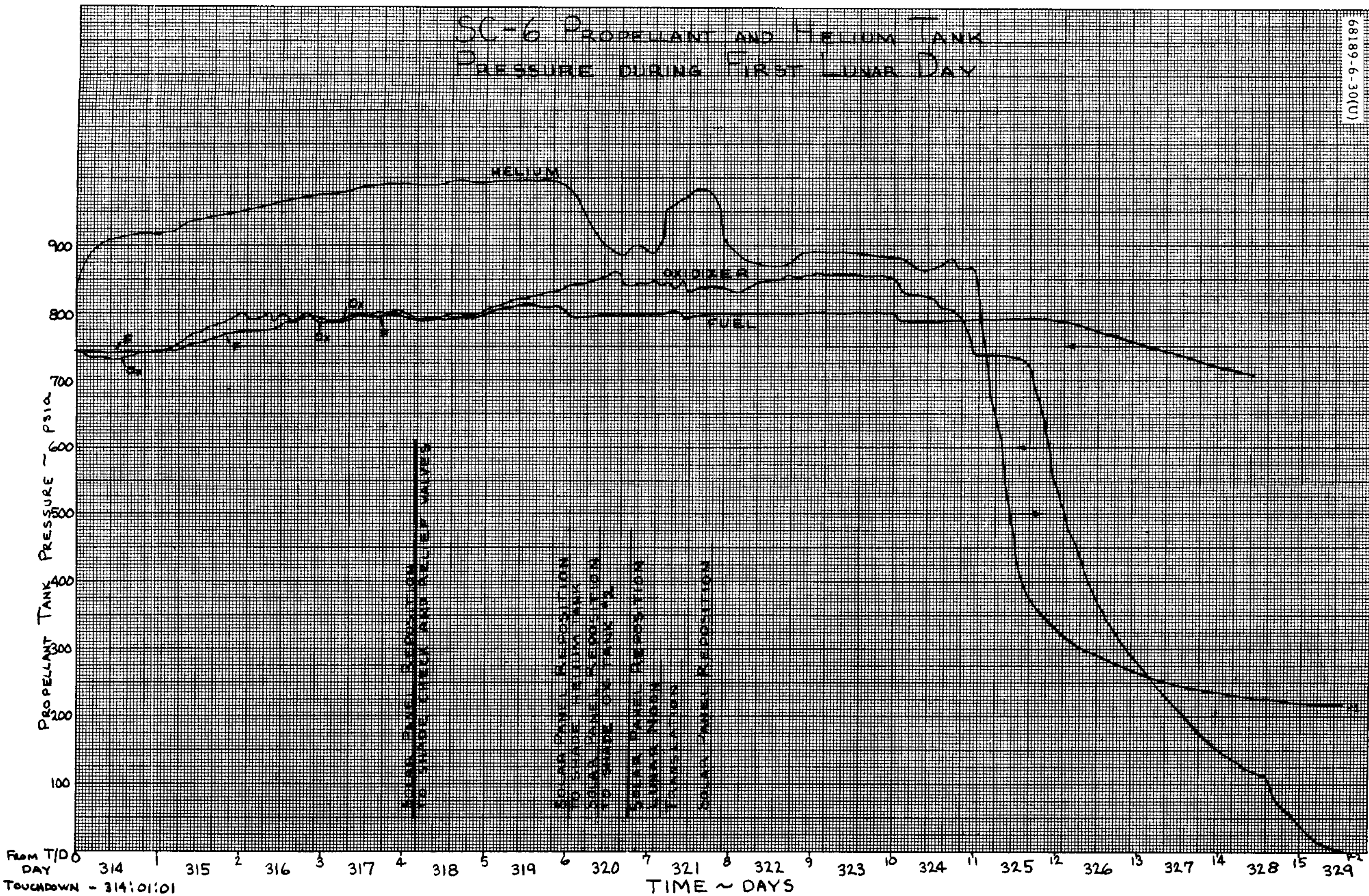

Figure 5.6-A1. Propellant and Helium Tank Pressure – First Lunar Day

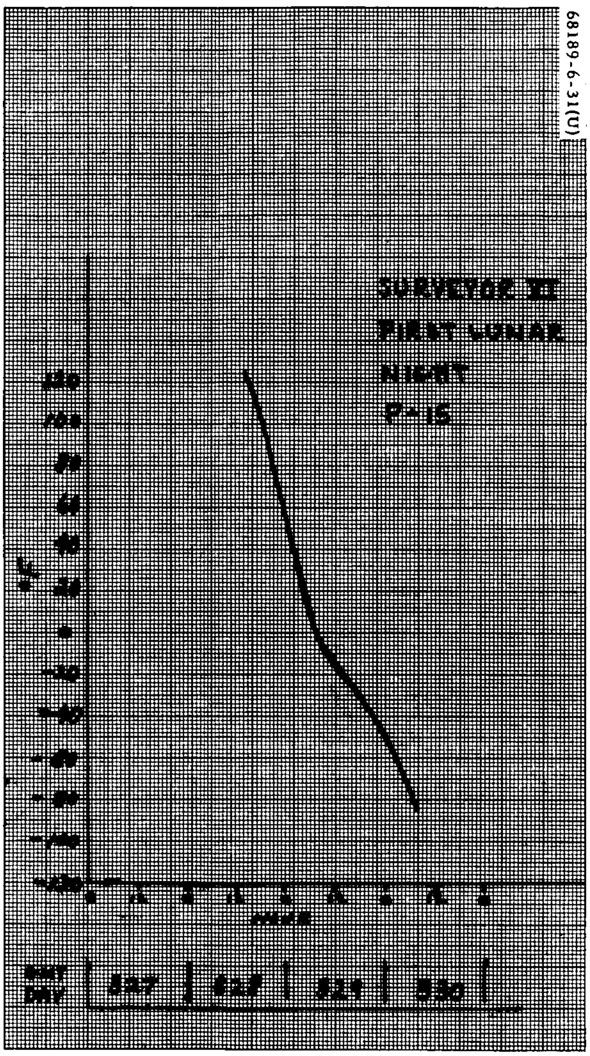

a) Vernier Oxidizer Tank 1 (P-15)

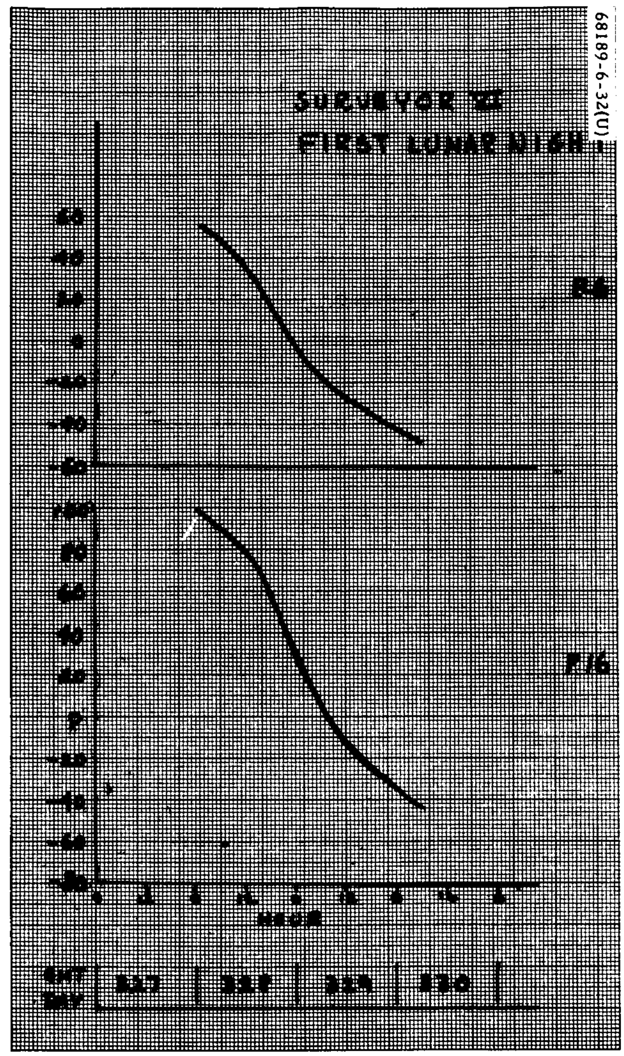

b) Vernier Oxidizer Tanks 2 (P-16) and 3 (P-6)

Figure 5.6-A2. Surveyor VI First Lunar Night Temperatures

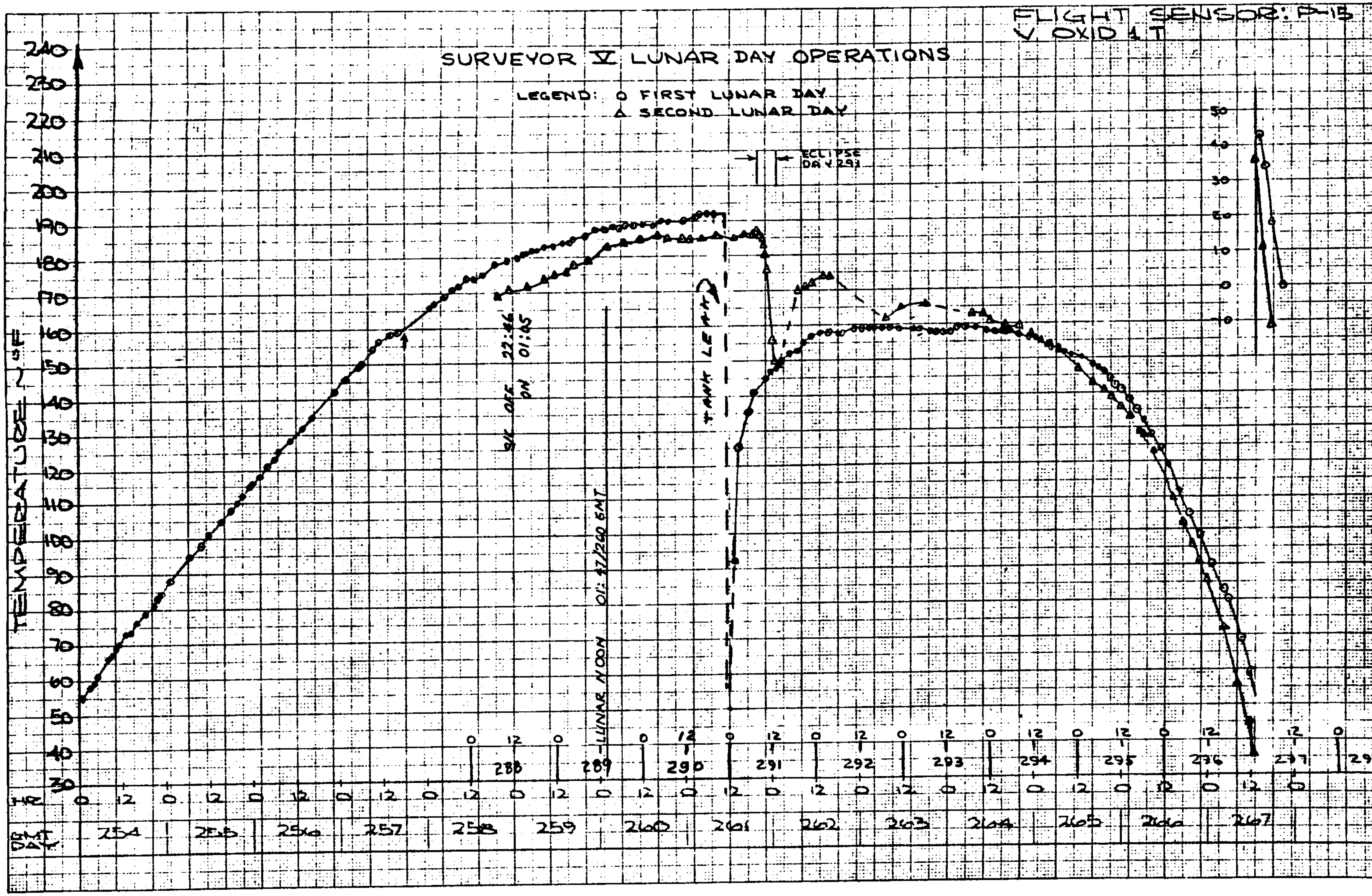

a) Tank 1

Figure 5. 6-A3. P-15 Vernier Oxidizer Tank Temperatures

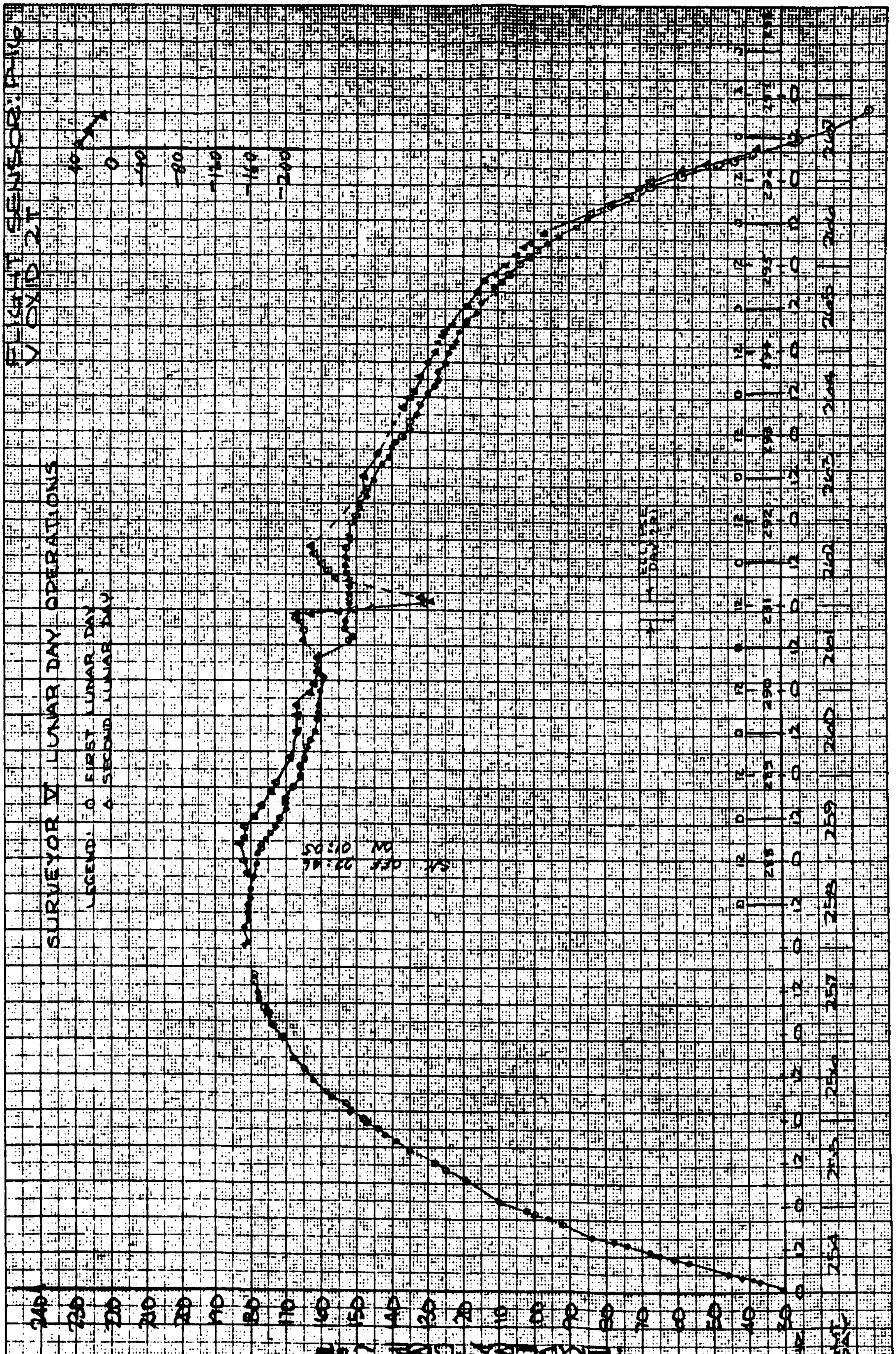

b) Tank 2

Figure 5.6-A3 (continued). P-15 Vernier Oxidizer Tank Temperatures

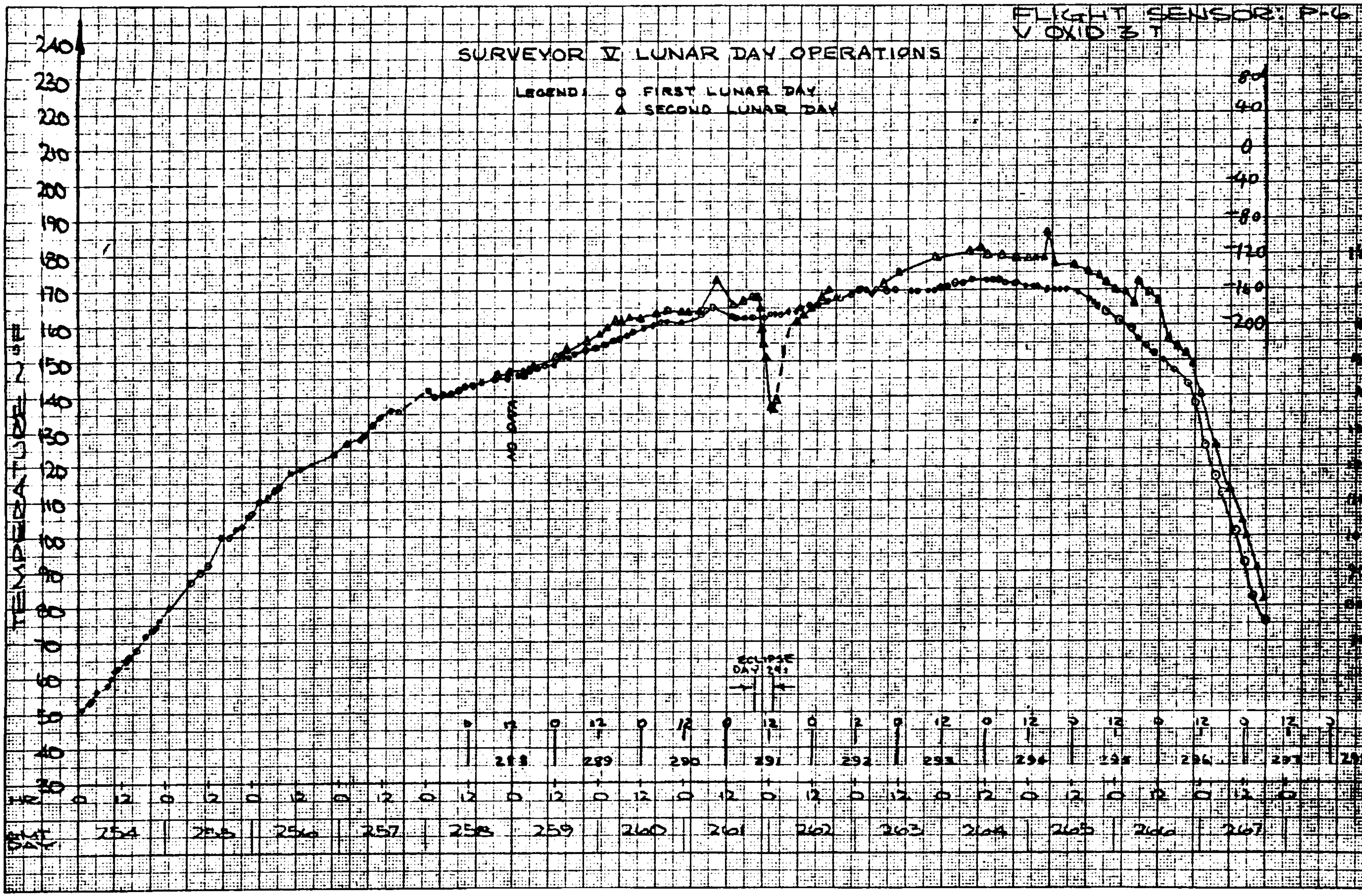

c) Tank 3

Figure 5.6-A3 (continued). P-15 Vernier Oxidizer Tank Temperatures

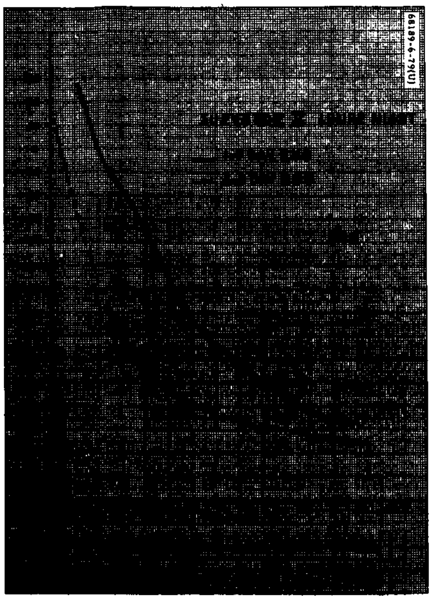

a) Vernier Oxidizer Tank 1 (P-15)

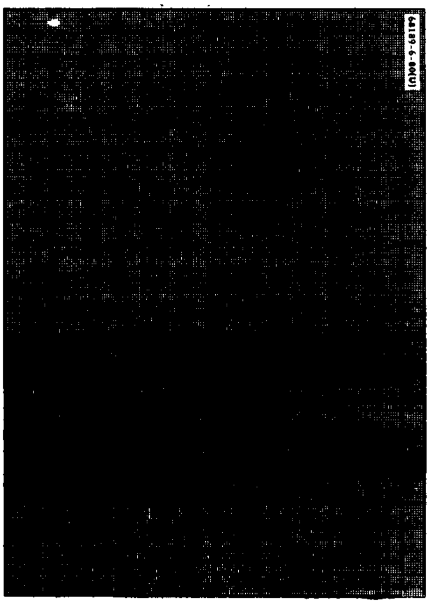

b) Vernier Oxidizer Tank 2 (P-16)

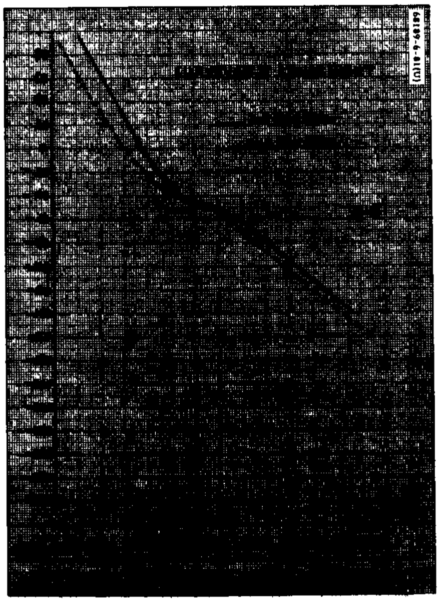

c) Vernier Oxidizer Tank 3 (P-6)

Figure 5.6-A4. Surveyor V Lunar Night Temperatures

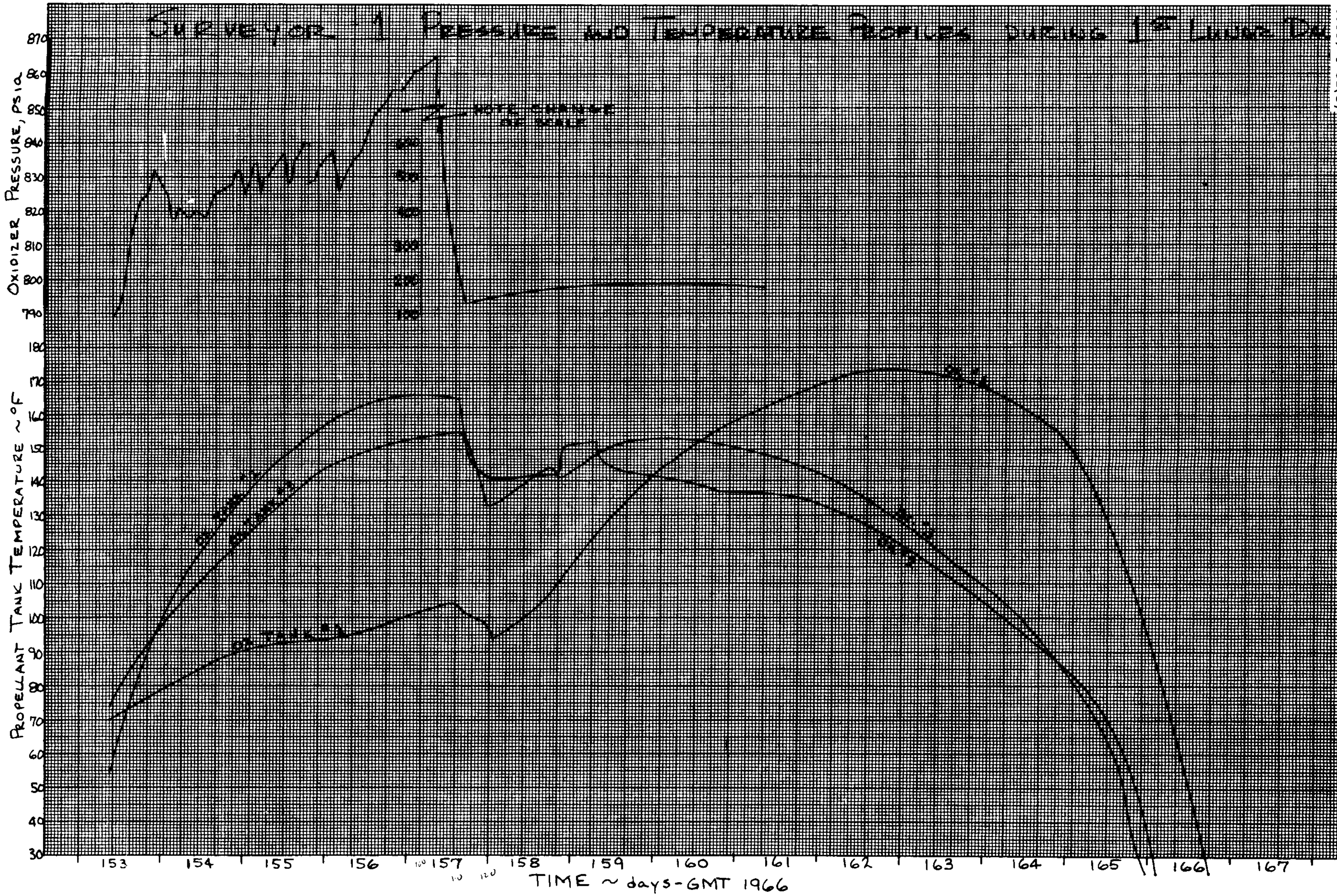

Figure 5.6-A5. Pressure and Temperature Profiles During Surveyor I First Lunar Day

An estimate of leakage hole sizes, based on a sharp edge orifice approximation and observed pressure decay rates, indicates that the Surveyor VI oxidizer hole size was increasing with time and was of the order of 0.001 inch in diameter.

Surveyor III data are incomplete due to the telemetry malfunction at touchdown and the early spacecraft shutdown time. Consequently, no meaningful comparisons can be made with its data.

In summary, all indications are that there was a slow liquid leak on the Surveyor VI oxidizer tank 1 prior to the rapid gas leak. Consequently, if on future spacecraft an oxidizer pressure decay in conjunction with a rapid tank temperature decay is observed, translation should be delayed until data can be thoroughly analyzed. To do otherwise could result in altitude loss during lunar translation and corresponding spacecraft destruction.

5.7 PROPULSION – MAIN RETRO

5.7.1 INTRODUCTION

The main retro-rocket, which performs the major portion of the deceleration of the spacecraft during terminal descent, is a spherical solid propellant unit with a partially submerged nozzle.

The unit is attached at three points to the spacecraft near the landing leg hinges, with explosive nut disconnects for postfiring ejection. Friction clips around the main retro-rocket engine nozzle flange provide attachment points for the altitude marking radar. The igniter gas pressure ejects the altitude marking radar when the retro firing sequence is initiated. The main retro-rocket engine ignition squibs and retro release explosive nuts operate from a pulsed, 19-ampere, constant-current source. Commands are initiated by the flight control system.

The nozzle is partially submerged to minimize overall length. The nozzle has a graphite throat insert backed up by laminates of carbon cloth phenolic with a fiberglass exit cone lined with bulk carbon phenolic. The case is of high strength steel and insulated with asbestos and inorganic fiber filled buna-N rubber to maintain the case at a low temperature level during burning.

The main retro-rocket engine with propellant weighs approximately 1394 pounds. The engine utilizes an aluminum, ammonium perchlorate, polyhydrocarbon, case-bonded, composite-type propellant, and conventional grain geometry. The engine thrust may vary between 8000 to 10,000 pounds over the temperature range of 50° to 70°F.

Two thermal sensors are installed on the main retro-rocket engine case for telemetering engine temperature during transit. The thermal sensor for monitoring nozzle temperature during transit is no longer used.

The main retro-rocket engine employs a safe and arm device that has dual firing and single bridgewire squibs for the engine igniter. In addition, provisions for local and remote safe and actuation and remote indication of inadvertent firing of the squibs are included. Both mechanical and electrical isolation exists between squib initiator and pyrogen igniter in the safe condition.

5.7.2 ANOMALY DESCRIPTION

No anomalies were noted in the main retro subsystem.

5.7.3 SUMMARY AND RECOMMENDATIONS

The Surveyor VI main retro-rocket engine operated within all required tolerances. No changes to the SC-7 retro-rocket engine or to the engine performance prediction models are recommended. Table 5.7-1 presents a summary of main retro performance parameters.

TABLE 5.7-1. SUMMARY OF MAIN RETRO PERFORMANCE PARAMETERS

Parameter	Predicted Main Retro Value	Required Main Retro Value or Tolerance	Actual Value	Uncertainty
Bulk temperature, °F	55	±15	52.5	±5
T3500, seconds	39.60	±0.4	39.37	±0.1
Maximum thrust, pounds	9650	<10,000	9700	±100
Total impulse, lb-sec	362,322	±3600	362,067	±1800
Specific impulse, seconds	289.5	±0.3	289.3	±1.5
Center of gravity excursion, inch	—	<0.030		
Thrust vector excursion			0.060*	±0.005
Displacement, inch	—	<0.040		
Angular, degree	—	<0.2		
Roll torque, in-lb	—	<80	12*	±6

*Total value from all sources.

5.7.4 SUBSYSTEM PERFORMANCE ANALYSIS

Table 5.7-2 gives the major events and times associated with the firing of the retro engine.

TABLE 5.7-2. MAJOR EVENTS AND TIMES FOR RETRO OPERATION

Event	Day 314:00, GMT, minutes:seconds	Maximum Error, second
Vernier ignition	58:02.938	±0.05
Retro ignition	58:04.038	±0.05
3500-pound thrust level	58:43.408	±0.05
3.5 g switch	58:43.397	±0.3
"Actual" 3.5 g	58:44.088	±0.05
Retro ejection signal	58:55.637	±0.05

Items constituting the analysis effort are as follows:

1) Reconstruction of thrust versus time curve from accelerometer and doppler data (Figure 5.7-1)

2) Calculation of engine specific impulse

3) Determination of thrust vector excursions and roll moments generated by the retro engine

4) Determination of T3500

5.7.4.1 Thrust Versus Time

The technique used in reconstruction of the thrust versus time trace from both accelerometer and doppler data is discussed in subsection 5.15.6.2 of Reference 1. This reconstructed trace varies from the predicted trace as shown in Figure 5.7-1. The maximum difference is 7 percent, and it occurs 8 seconds after ignition. This, however, is in an area of higher error for the accelerometer data since the spacecraft passes through a period of rapid change in acceleration to a fairly steady acceleration.

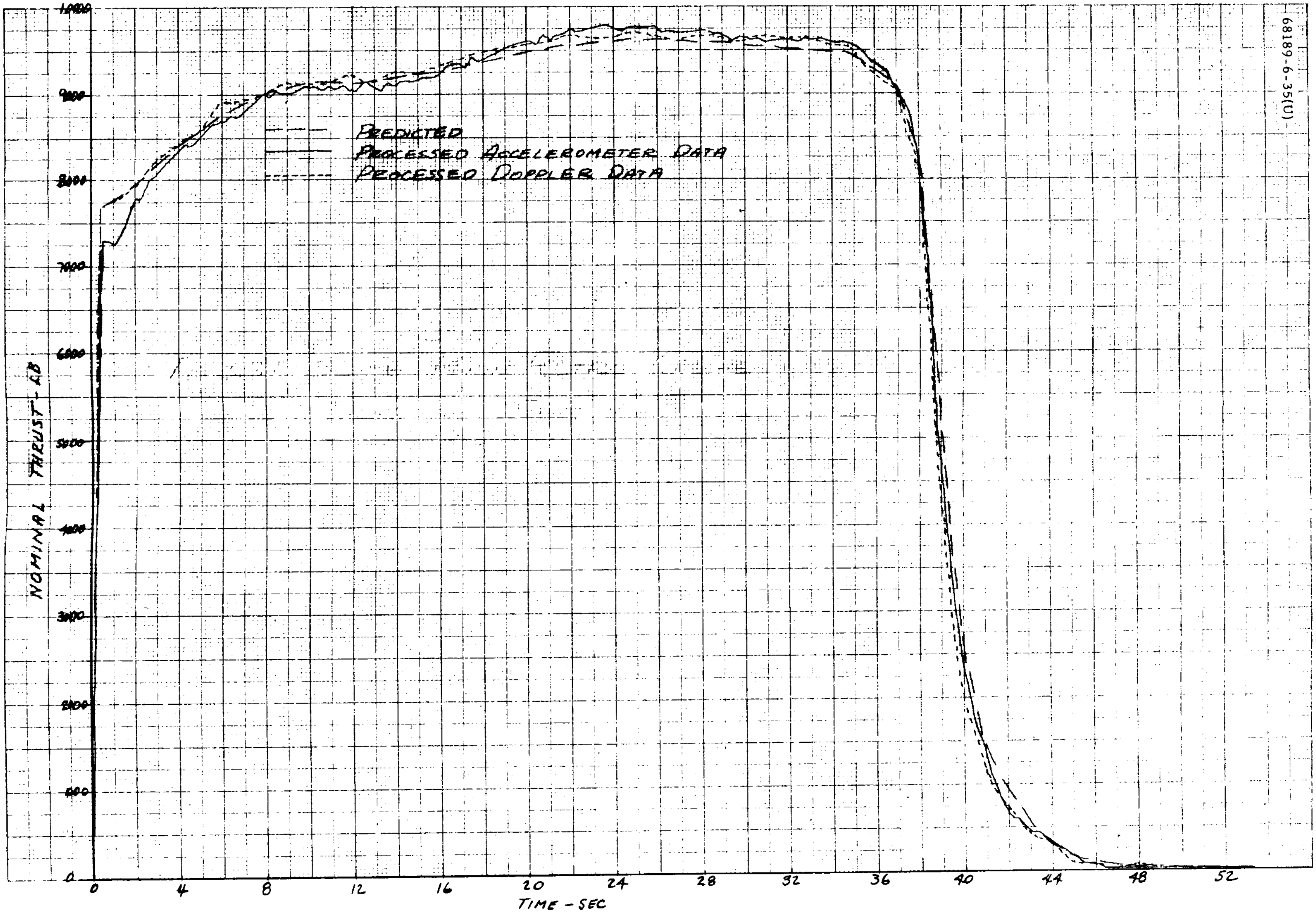

Figure 5.7-1. Surveyor VI Main Retro Engine Thrust Versus Time

5.7.4.2 Specific Impulse

The main retro-rocket engine specific impulse was obtained by correcting the predicted nominal specific impulse used in the preflight descent trajectory computer program by the change in velocity measured during retro burning on Surveyor V. The difference between the actual and predicted change in velocities, 8411 and 8414 fps, respectively, amounts to 0.03 percent low versus the 1 percent allowed. This approach is conservative from the retro-rocket engine point of view since the velocity difference is actually due to a number of sources in addition to the main retro-rocket engine. Some of these other sources are as follows:

1) Uncertainty in vernier engine specific impulse

2) Uncertainty in vernier engine thrust level

3) Uncertainty in vernier engine weight versus time

4) Uncertainty in retro-rocket engine specific impulse versus time

5) Uncertainty in retro-rocket engine weight versus time

6) Uncertainty in doppler data

5.7.4.3 Retro Disturbance Torques

The following retro disturbances were noted:

1) Retro ignition produced a short duration disturbance torque of approximately 60 ft-lb.

2) Following retro ignition, all three vernier engines settled near their mid-thrust condition and remained steady throughout retro burning, except for one disturbance of 15 ft-lb at 30 seconds into burning. This disturbance was quickly corrected.

3) The maximum required corrective roll torque produced by the vernier engines after accounting for bracket bending was 3 ft-lb at ignition and 1 ft-lb during burning. Assuming all this torque was required due to the retro engine, the engine roll torque was still well below the 7 ft-lb maximum moment allocated to the retro engine.

4) Retro engine ejection from the spacecraft was smooth and required no apparent corrective torque; however, a spike of 0.6 g was noted in the retro accelerometer. The spike could not be correlated to other data.

5.7.4.4 $\underline{T_{3500}}$

The T_{3500} (time from ignition to the time when thrust decays to 3500 pounds) prediction was acceptable. The total error of 0.5 percent is within the 1 percent tolerance for the prediction. This total error is the result of the actual engine temperature gradient uncertainty, the error in calculating the bulk temperature corresponding to that gradient, telemetry error, and prediction error.

5.7.5 REFERENCES

1) "Surveyor Spacecraft A21 Model Description," Hughes Aircraft Company, Document No. 224847B, 1 March 1965.

2) "Surveyor Main Retro Engine A21-29 Support Documentation," Thiokol Chemical Corporation.

3) "SC-6 Event Time from Teltab," Hughes Aircraft Company.

5.7.6 ACKNOWLEDGMENTS

The following people contributed to the main retro analysis:

L. M. Spicer, Coordinator

E. W. White, Systems Analysis

L. H. Davids, Systems Analysis

5.8 ALTITUDE MARKING RADAR

5.8.1 INTRODUCTION

The Surveyor altitude marking radar (AMR) is a small, conventional, pulsed, X-band, fixed dual range gate, marking radar designed and supplied by Hughes Aircraft Company. The purpose of the AMR is to provide, with high accuracy and reliability, a positive indication that slant range from the Surveyor spacecraft to the lunar surface has decreased through a preset value, nominally 60 statute miles for the A-21 series of engineering models. This signal starts an on-board timer whose run-out time is set by ground command earlier in flight to initiate vernier and main retro engine ignition. Since the AMR is installed in the exhaust cone of the main retro engine, it is forcibly jettisoned from the spacecraft when that engine is ignited, having served its purpose in providing ignition timing.

The AMR is a conventional, noncoherent radar employing a pulsed magnetron; single antenna; duplexed mixer; crystal-controlled, solid-state local oscillator; wideband IF amplifier; noncoherent detector; and video processing circuitry. Dynamic range is extended by IF amplifier AGC; AGC voltage is telemetered, and provides an indication of received signal power. The video circuitry is of special design to mark at a preset range with high accuracy and reliability. Two fixed, adjacent range gates continuously examine the video signal; their outputs are continuously summed and differenced. When the sum exceeds a fixed threshold and the difference simultaneously crosses zero with positive slope, the mark signal is generated. Sum threshold is set for an extremely low probability of marking on noise (false mark) throughout the operating time, while video integration, plus a very substantial radar gain margin, ensures a high probability of successful marking.

Two separate ground commands, whose timing is controlled, are required to fully activate the AMR. The first signal, called AMR on, commands on the primary power to the AMR, which includes all internal power except high voltage to the transmitter. The video signal is inhibited from reaching the marking circuits until the second command, thus eliminating any residual probability of false marking on noise during this warm-up interval. The second signal, called AMR enable, commands on the transmitter high voltage and also removes the video inhibit. This enabling function is timed, not only for favorable thermal conditions at the expected marking time, but also for the purpose of precluding premature marking on second-round echoes at much longer ranges. In a lunar mission, FPAC supplies a marking time prediction based upon trajectory data. The prescribed times for SPAC transmission for these two commands are: "on" at 280 ± 10 seconds, and "enable" at 100 ± 10 seconds before predicted marks.

For proper analysis, complete trajectory information is required. While either known or assumed for preflight predictions, it must be known or derived for postflight evaluation. Spacecraft attitude and velocity data are supplied by FPAC from tracking and trajectory computations. Residual range uncertainty, however, exceeds that of the AMR itself, which is assumed to have marked with mean value and dispersion predicted by radar analysis prior to each mission. In conjunction with approach velocity and attitude conditions from FPAC, the trajectory can then be extrapolated backward with high accuracy by a special two-body program. This program derives all the significant AMR parameters throughout the nominally 100-second interval from enable to mark, and calculates correction factors to be applied to observed telemetry data before comparison with predicted received signal power.

AMR telemetry includes three digital and three analog signals, plus analog temperature data. The digital signals confirm on-board discrete events: prime power application (R-1, AMR on), high voltage and video enabling (R-11, AMR enable), and slant range trigger (FC-64, AMR mark). It should be noted that FC-64 is telemetered only when the on-board mark is generated, and not in response to the backup command from earth. The three analog signals (besides temperature) are magnetron current (R-12), AGC voltage level (R-14), and late gate detected video voltage level (R-29). The AGC not only confirms receiver response to RF return, but is also useful in evaluating terrain reflectivity. The magnetron current confirms pulsing of the magnetron after enable, and is useful primarily as a transmitter failure mode indication. The late gate signal, primarily a receiver failure mode indication, normally confirms the presence of a gated video signal rising quickly to a peak at the time of mark and decaying quickly thereafter. All but a few of its values are normally at the quiescent noise level, and in no way constitute repeated events.

5.8.2 ANOMALIES

There were no anomalies in AMR operation during the Surveyor VI mission.

5.8.3 SUMMARY

The Surveyor VI AMR functioned normally. The true altitude mark was generated at the expected time and initiated the automatic terminal descent sequence as planned. The routine emergency mark backup command was received by the spacecraft after the on-board mark had been generated.

The AMR was turned on 277.44 ± 0.65 seconds before mark, acceptable within the 280 ± 10 seconds specified. It was enabled 97.44 ± 0.65 seconds before mark, acceptable within the 100 ± 10 seconds specified. EP-17 showed normal current drain characteristics throughout AMR operation and jettison, and AMR magnetron current (R-12) was normal before, during, and after enable operation. The late gate signal (R-29) was normal, confirming the presence of RF return signal and detected video within the gate at the time of the mark.

AGC-indicated signal strength, after proper evaluation, showed good correlation with the nominal predicted value (within 1 to 2 db). The initial telemetry data were considerably below the predicted value because of the response time of the circuit.

5.8.4 SUBSYSTEM PERFORMANCE ANALYSIS

5.8.4.1 Event Times

From the table of Surveyor VI events associated with radar operation (subsection 5.9.4), the following AMR events are repeated below. The times listed are GMT when recorded at DSIF-11.

Channel	Name	GMT at DSIF-14, day:hr:min:sec
R-1	AMR on	314:00:53:19.604 ± 0.6
R-11	AMR enable	314:00:56:19.600 ± 0.6
FC-64	AMR mark	314;00:57:57.038 ± 0.05
FC-28	Vernier ignition	314:00:58:02.938 ± 0.05
FC-29	Retro ignition	314:00:58: 04.038 ± 0.05
FC-64	AMR mark off	314:00:58:04.138 ± 0.05

The warmup time (on to enable) was 180.0 ± 1.2 seconds, well within the nominal 180 ± 20 seconds. The time from on to mark was 277.44 ± 0.65 seconds, acceptably within the 280 ± 10 seconds specified. The enabled time (enable to mark) was 97.44 ± 0.65, acceptably within the 100 ± 10 seconds specified.

From readings of the magnitude register (FC-18), actual mark time can be refined to 314:00:57:57.043 ± 0.045, and actual vernier ignition time can be refined further to 314:00:58:02.923 ± 0.025, still referred to GMT at DSIF-14.

5.8.4.2 Load Current Signals

Radar and squib current (EP-17) was normal. It was zero until AMR on when it rose to normal AMR warmup load, which continued until AMR enable. During the enabled interval, it properly cycled in the manner characteristic of magnetron pulsing, which is not synchronized with the telemetry data sampling. This continued until engine ignition, when the AMR load was removed (by jettison of the AMR) and replaced by the RADVS warmup load.

Magnetron current (R-12) (Figure 5.8-1) also was normal. It was zero until AMR enable, when it rose to normal high voltage load during magnetron pulsing. This continued until engine ignition, when the signal went to full scale as the AMR was forcibly jettisoned by the retro engine.

5.8.4.3 Late Gate Signal

The late gate video detected analog voltage signal (R-29) (Figure 5.8-2) was normal, confirming the presence of RF signal and detected video at the time of the mark.

From the trajectory reconstruction for AGC evaluation, the total stretched pulse length, as received, was about 16.7 microseconds and the effective closing rate was 8459.2 fps, both at the time of the mark. The corresponding video pulse closing rate was therefore about 17.19 microseconds per second. The video late gate has a nominal duration of 20 microseconds (20.0 ± 1.0 required). It should therefore have produced output within 3 db of peak for (16.7 + 20)/17.19 = 2.08 seconds.

With R-29 sampled at 1.2-second intervals, there should be at least one high level sample, and perhaps two, if the sampling time phase were right. In Surveyor VI, it happened that there was one high level sample that occurred at the proper time relative to the time of the mark.

5.8.4.4 DB Budget

The Surveyor VI AMR db budget, revised for the postflight parameters in the trajectory reconstruction for AGC evaluation, shows a 31.5-db margin above that required for a 0.999 cumulative probability of successful marking, as follows:

P_t (average)	+ 32.55 dbm
G^2	+ 69.0 db
β_1	- 13.57 db
σ (0 degree) = 0.065	- 1.17 db
R^{-3}	- 53.34 db
f^{-2}	-199.37 db
f_r^{-1}	- 25.44 db

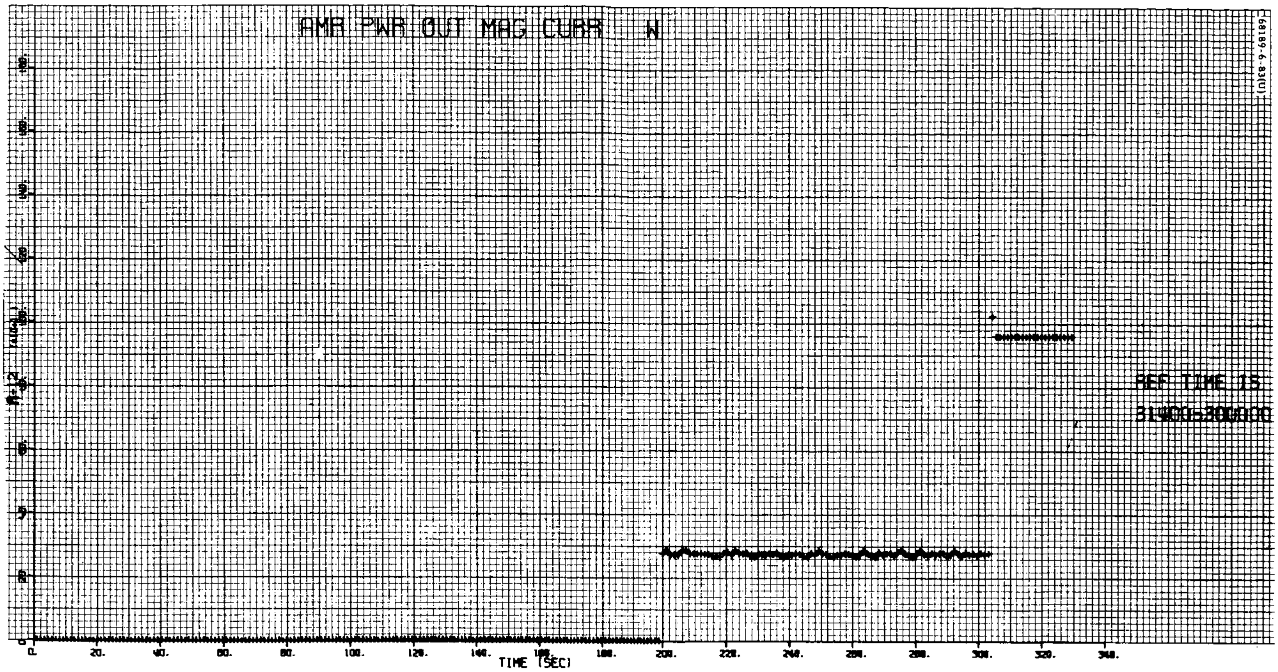

Figure 5.8-1. Magnetron Current (AMR)

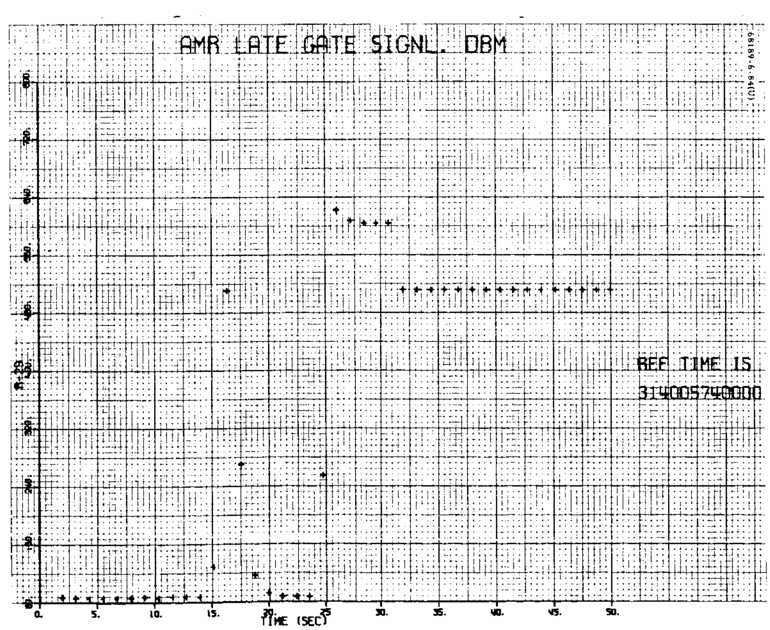

Figure 5.8-2. Late Gate Signal (AMR)

$\left(\frac{1}{2}\right)\left(\frac{c}{4\pi}\right)^3$	+122. 12 db
cotan 25. 5 degrees	+ 3. 27 db
F (25. 5 degrees)	- 9. 66 db
	+226. 88 dbm
	-302. 52 db
P_r	- 75. 64 dbm
P_{min} (10 microseconds)	- 97. 3 dbm (worst case)
P_{min} (10 microseconds)	-105 dbm (measured)
P_{min} (10 microseconds-worst case)-P_{min} (10 micro-seconds-measured)	+ 7. 7 db
P_{min} (30 microseconds)	-101. 5 dbm (worst case)
P_{min} (30 microseconds)	-109 dbm (measured)
P_{min} (30 microseconds-worst case)-P_{min}(30 micro-seconds-measured)	+ 7. 5 db
P_{min} (16. 7 microseconds)	- 99. 5 dbm (worst case)
P_{min} (16. 7 microseconds-worst case) -P_{min} (16. 7 micro-seconds-predicted)	+ 7. 6 db
P_{min} (16. 7 microseconds)	-107. 1 dbm (predicted)
	- 75. 6 dbm +107. 1 dbm
Total margin above threshold for 0. 999 cumulative probability:	+ 31. 5 db

5. 8. 4. 5 Expected Marking Range

The expected value of the slant range along the AMR antenna electrical axis when the mark is produced will vary slightly from the nominal value of 60 statute miles. This expected value is supplied before each mission to FPAC, which inserts this value and both mechanical alignment and electrical boresight data into its trajectory programs. These determine the time delay value to be commanded into the on-board magnitude register so that automatic engine ignition will occur at the altitude desired for that mission.

Previous study and experience, confirmed by Surveyor VI itself, have demonstrated that the expected marking range is affected significantly by only two parameters, according to the well-documented equation:

$$R_m = R_o + (2.02 \times 10^{-4})\,\varphi - (1.01 \times 10^{-4})\,\varphi^2$$

The operational parameter is the angle φ, the incidence angle in degrees off the local lunar vertical of the AMR beam at its intersection with the lunar surface. The equipment parameter is the value R_o, which is the expected marking range at vertical incidence characteristic of the specific AMR hardware aboard each spacecraft. The result R_m is the expected marking range in statute miles.

The value R_o is determined for each AMR as the measured gate setting (leading edge of late gate) minus the nominal analytical value of range bias at vertical incidence; the latter is equal to 12.20 microseconds. The former is measured in test.

The Surveyor VI AMR (283810, S/N 13) gate setting was 655.2 microseconds. The R_o value was therefore:

Gate (measured)	655.2 microseconds
Bias (analytical)	- 12.2 microseconds
R_o	= 643.0 microseconds
	= 59.89 statute miles

(at 10.737 microseconds per round-trip statute mile)

The trajectory reconstruction for AGC evaluation (Figure 5.8-3) showed an incidence angle of 25.5 degrees at the time of the mark. The expected marking range for Surveyor VI was therefore 59.82 statute miles.

5.8.4.6 Marking Range Dispersion

The standard budget of allowances for in-flight drifts of AMR parameters that affect marking range at any incidence angle has been documented as a rss total of ±893 feet, 3 σ.

From the calculations of AMR cumulative probability (Reference 1) of successful marking, the spread from 0.001 to 0.999 probability is ±525 feet at 25 degrees. The allowable pointing error (3 σ) contribution is ±1526 feet at 25 degrees.

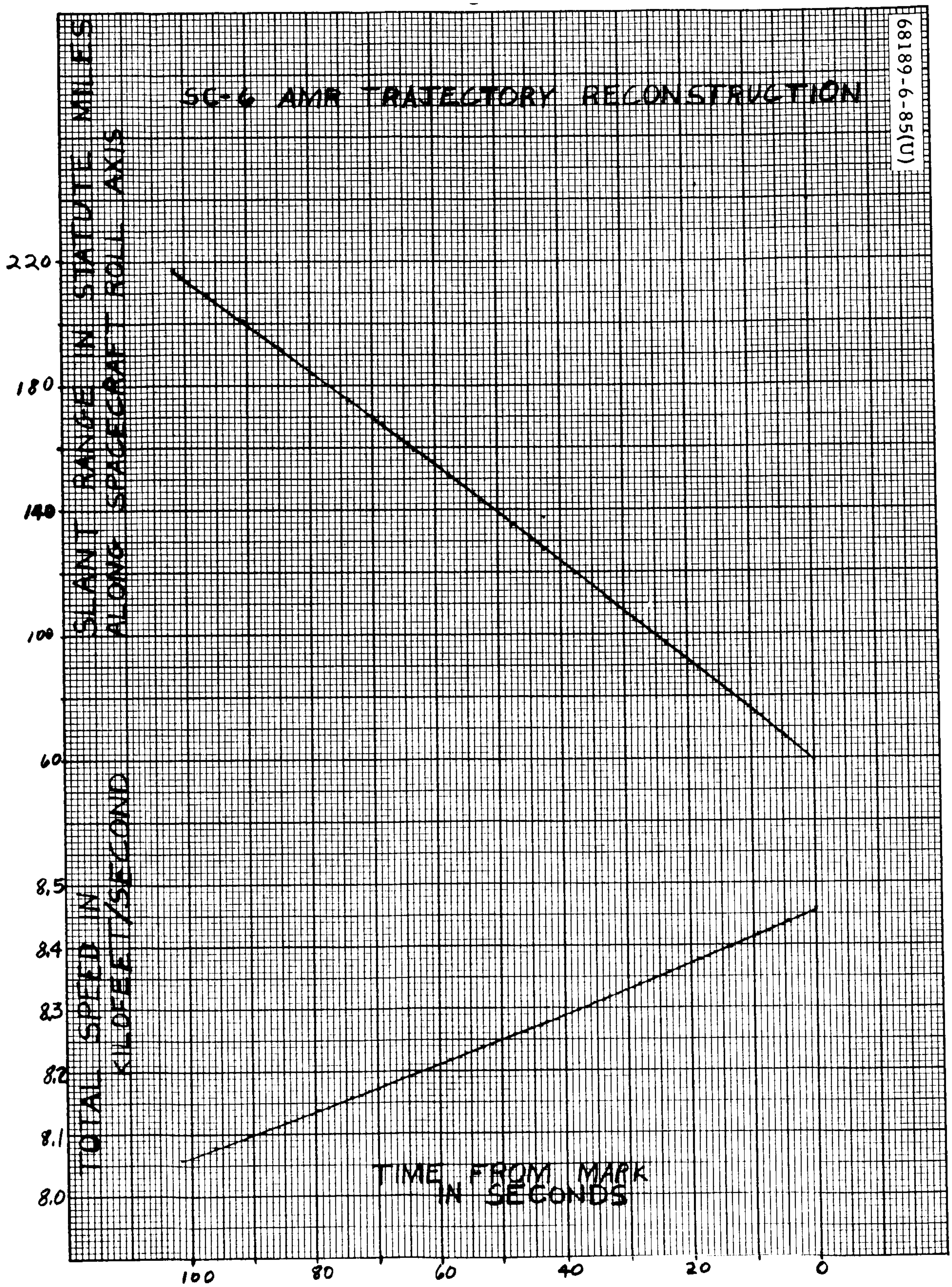

Figure 5.8-3. Trajectory Reconstruction (AMR)

The total (rss) marking range dispersion at 25 degrees is therefore ±1844 feet (3σ). (For perfect pointing error compensation in the guidance and trajectory programs, the actual dispersion would be only ±1040 feet (3σ) at 25 degrees, well within the specified maximum of 0.345 mile or 1820 feet (3σ).

At the Surveyor VI velocity of 8459.2 fps at the time of the mark, the total dispersion of ±1844 feet (3σ) would be a time error of ±0.218 second (3σ). By coast phase orbit determination from earth tracking, the a priori mark time uncertainty has been reported as 0.62 second (1σ), or almost five times larger. Hence, while orbit determination provides excellent velocity data, integration into position is less accurate, and the predicted value of expected marking range remains the best available estimate of actual conditions.

5.8.4.7 AMR Parameter Reconstruction

Because of the significant distance traveled during the nominal 100 seconds of enabled operation, the AMR parameters during this interval are evaluated accurately as functions of time and of the mission variables. This is done by a separate computer program developed for this purpose.

Trajectory constants are found from conditions at mark and/or at engine ignition. Velocity, velocity angle, and attitude angle are supplied by FPAC; slant range at mark is the predicted expected marking range. All quantities are then evaluated analytically without approximation at each of a number of two-body trajectory points determined by stepping speed in arbitrary increments. Negative increments of speed produce a backward extrapolation from mark, or from ignition to enable. The only approximation used is for the time interval between trajectory points, which assumes linearized distance and velocity between points. Adequate time accuracy results with the -20 fps increments normally used.

Of particular interest are the AMR slant range, the beam incidence angle at the surface, and the accompanying received pulse stretching effect (Figure 5.8-4). The latter is seen to vary quite significantly because of slant range variation over a dynamic range of about two octaves. Despite variation of both flight path and attitude angle relative to instantaneous local lunar vertical, however, the beam incidence angle remains remarkably constant as a result of the constant inertial attitude of the spacecraft in this phase.

The Surveyor VI trajectory conditions supplied by FPAC were as follows:

	At Mark
Velocity angle, degrees	24.18
Attitude angle, degrees	24.20
Speed, fps	8459.2

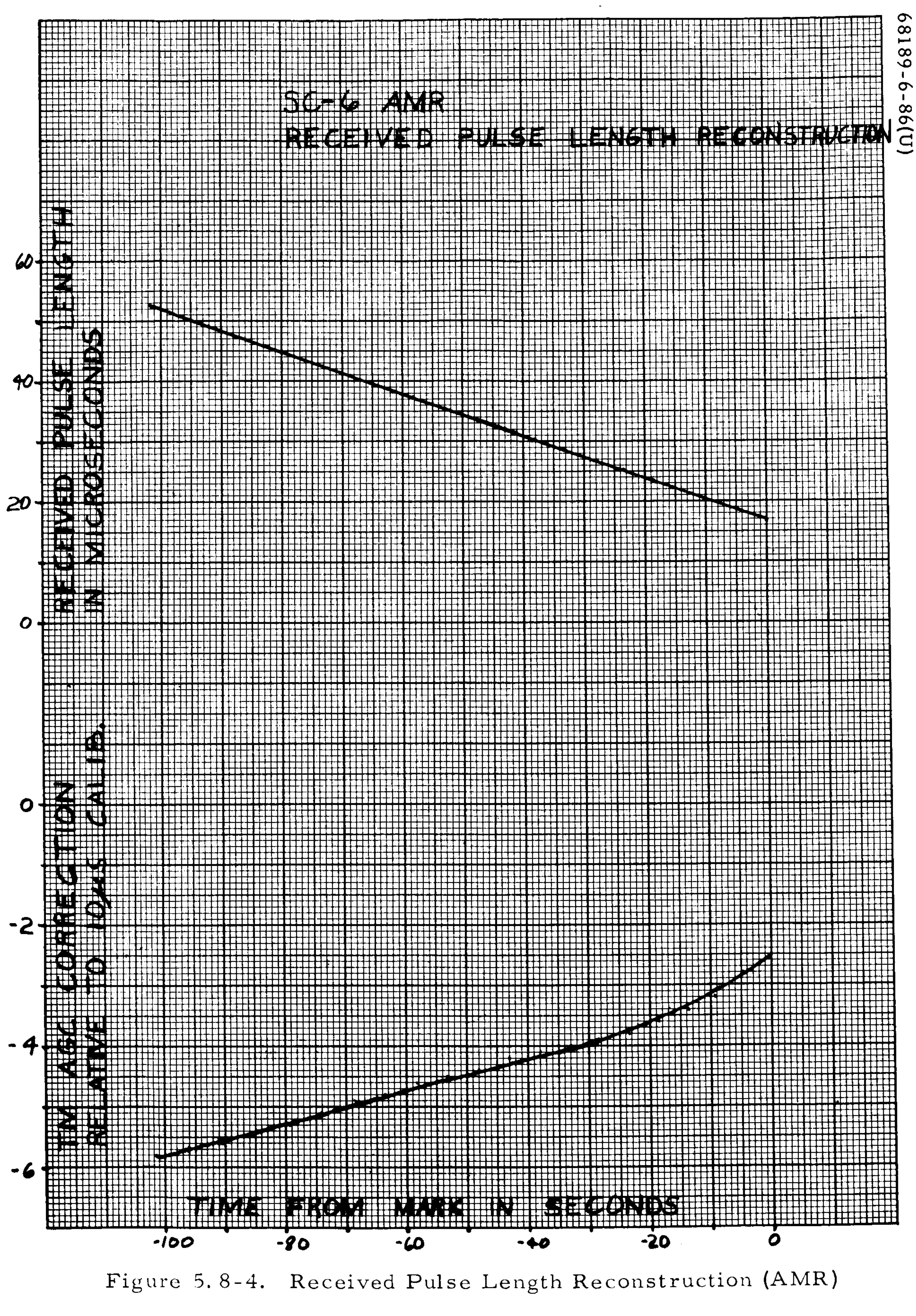

Figure 5.8-4. Received Pulse Length Reconstruction (AMR)

From these, it was determined that the AMR beam incidence angle was 25.50 degrees at mark, and varied less than 0.1 degree throughout the enabled time.

5.8.4.8 AMR AGC Evaluation

The original standard test conditions of 3, 10, and 30 microseconds for preflight AGC calibration (Figure 5.8-5) encompass approximately the region of stretched pulse lengths as received over the required range of A-21 approach angle (0 to 45 degrees) at the nominal marking range. The AGC response curves are nonlinear, however, and intermediate values are helpful for proper interpolation of a given approach angle even at the marking range. In addition, because of the appreciable variation in received pulse length during enabled operation prior to the mark, particularly at angles of more than several degrees, proper AGC interpretation at times other than the mark requires extended AGC calibration. The analysis was fully documented for Surveyor III (Reference 2).

Unfortunately, the extended AGC calibration was not carried out for Surveyor VI. From data available (maximum pulse length = 30 microseconds), the correction relative to 10-microsecond calibration was estimated (Figure 5.8-6). This correction was applied in the interpretation of AGC telemetry data (Figure 5.8-7). It should be noted that after the AMR was enabled, the telemetry data were initially low due to the response time of the circuit. After the initial period, the AGC data were in good agreement with the nominal predicted value.

5.8.5 REFERENCES AND DOCUMENTATION

1) R.A. Dibos, "Preliminary Study of AMR at Large Angles," (unpublished IDC), 4 November 1966.

2) "Surveyor III Flight Performance," Hughes Aircraft Company, SSD 68189-3, July 1967.

3) S. Thaler, "The AMR – Predicted Performance," Hughes IDC 2729.1/11, 29 March 1965.

4) I. Holtzman, "AMR Marking Range Bias as Function of Angle of Incidence," Hughes IDC 2253.3/294, 13 May 1965.

5) R.A. Dibos, "Post-Mission Analyses Involving Radar Data," (unpublished), 25 March 1966.

6) Lincoln Laboratory, "Radar Studies of the Moon," Quarterly Report No. 2, 15 May 1966, p. 11.

7) R.A. Dibos, "Radar Performance Evaluation," SC-1 Symposium (NASA at JPL), September 1966.

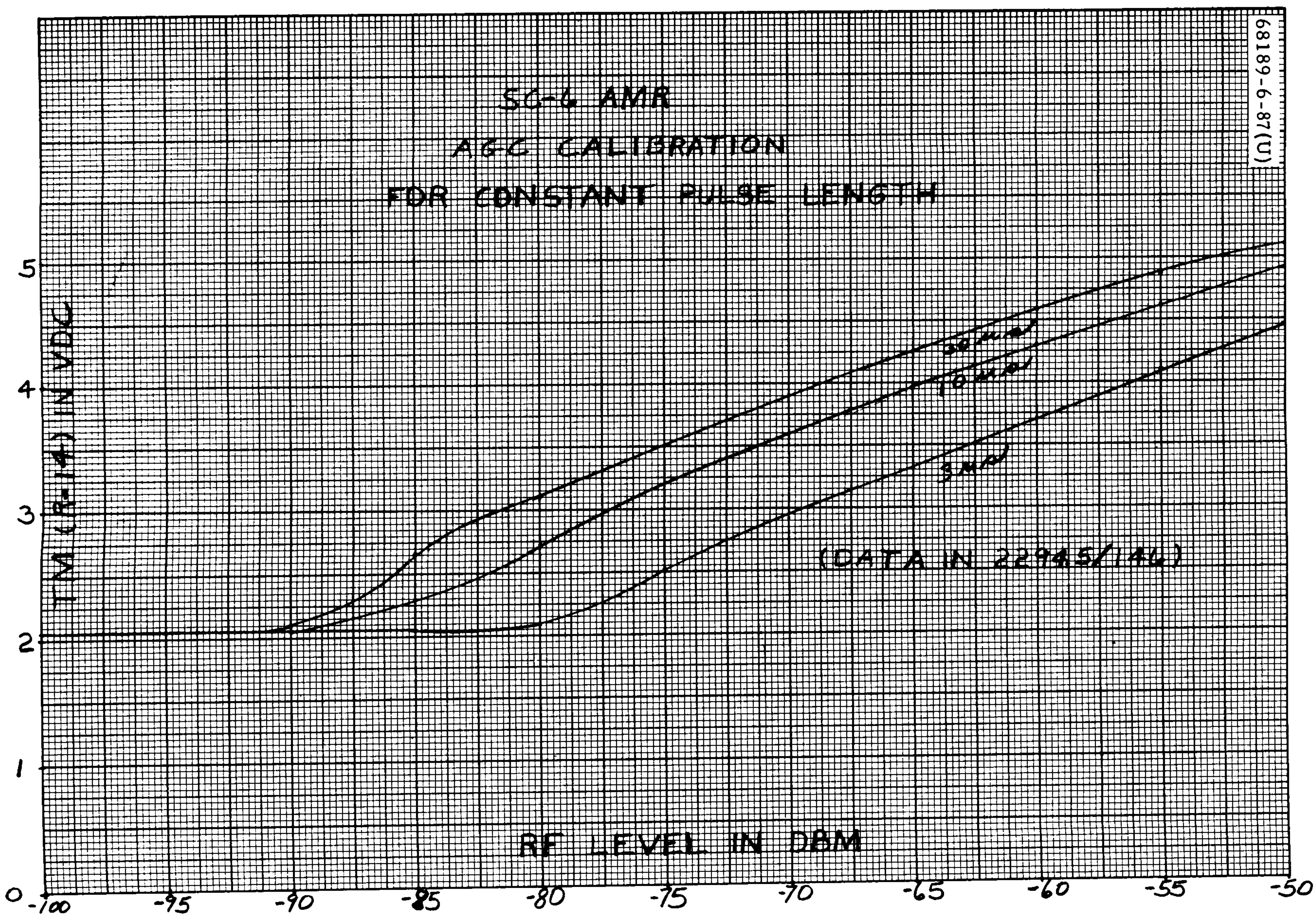

Figure 5. 8-5. AGC Calibration for Constant Pulse Length (AMR)

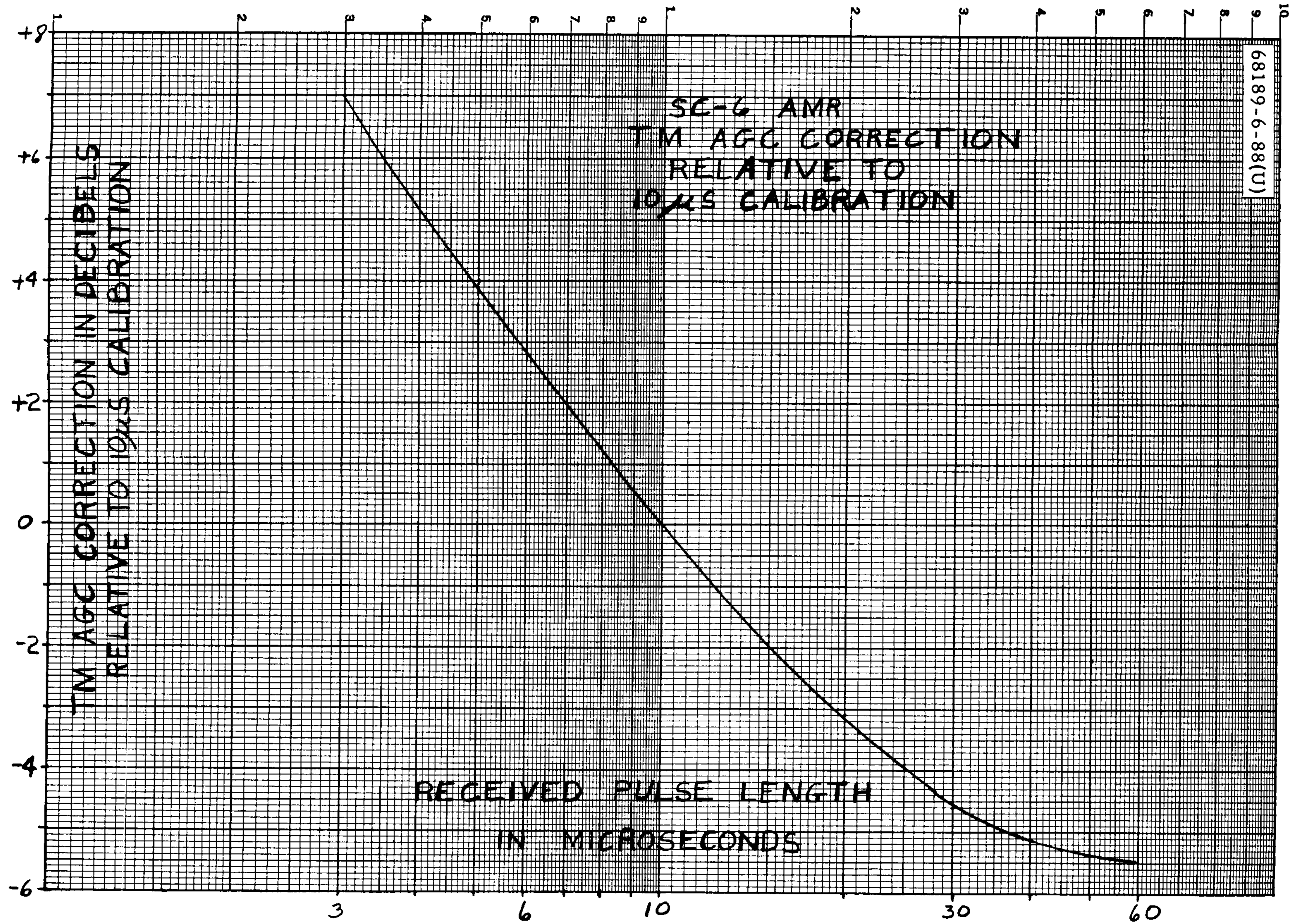

Figure 5. 8-6. Telemetry AGC Correction Relative to 10-Microsecond Calibration

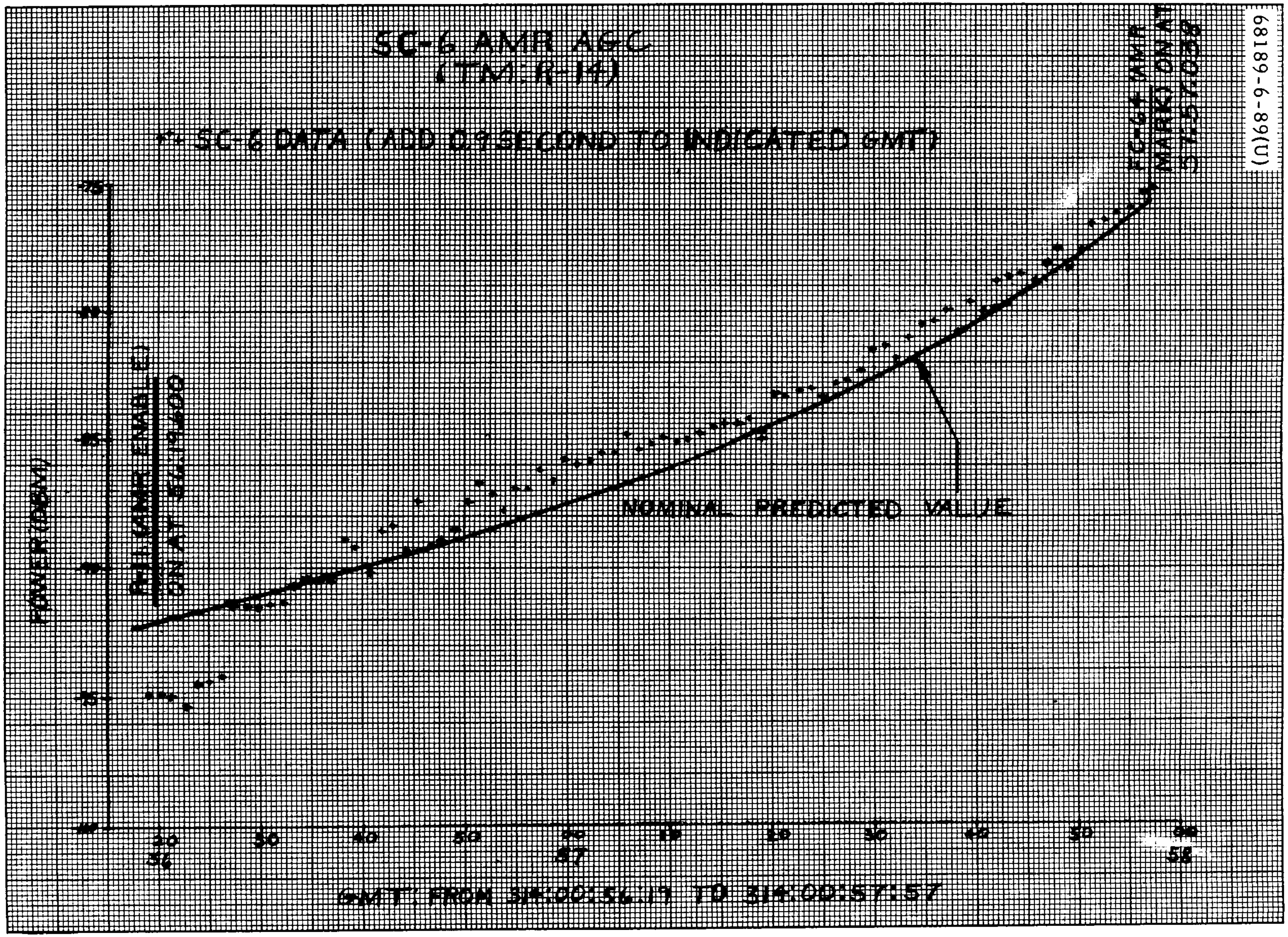

Figure 5.8-7. AMR AGC (TM: R-14)

8) "Surveyor I Flight Performance," Hughes Aircraft Company, SSD 68223R, Vol. III, October 1966.

9) "Decibel Allocation and Margin Summary," Hughes Aircraft Company, SSD 4021R-2, 28 November 1966.

10) R. A. Dibos, "AMR Test Data Required for Analyses," Hughes IDC 2253. 4/71, 20 March 1967.

11) R. A. Dibos, "SC-3 AMR (S/N-15) Predictions," Hughes IDC 2253. 4/79, 10 April 1967.

12) R. A. Dibos, "TM Mode 6 Data Relating to Radar Performance," Hughes IDC 2253. 4/84, 15 June 1967.

13) R. A. Dibos, "AMR AGC Post-Mission Evaluation," Hughes IDC 2253. 4/88, 27 June 1967.

14) "Surveyor IV Flight Performance," Hughes Aircraft Company, SSD 68189-4, September 1967.

15) "Surveyor V Flight Performance," Hughes Aircraft Company, SSD 68189-5, November 1967.

16) D. W. Demaree, "SC-6 AMR Marking Accuracy," Hughes IDC 2294. 5/142, 2 October 1967.

17) M. R. Weiner, "SC-6 AMR Marking Range Data," Hughes IDC 2292/413, 19 October 1967.

18) D. W. Demaree, "SC-6 Radar Calibration Data," Hughes IDC 2294.5/146, 23 October 1967.

5. 8. 6 ACKNOWLEDGMENTS

Calibration data were supplied by W. T. Black and D. W. Demaree. Telemetry data were supplied by W. McIntyre.

Guidance and trajectory data were supplied by T. L. Parker of FPAC.

This section was technically coordinated by M. R. Weiner.

5.9 RADVS PERFORMANCE

5.9.1 INTRODUCTION

The radar altimeter and doppler velocity sensor (RADVS) is a coherent CW microwave radar designed and supplied by Ryan Electronics, San Diego. Its primary function is to measure velocity and slant range relative to the lunar surface during the terminal descent of the Surveyor spacecraft. These quantities are measured directly in spacecraft coordinates, allowing direct utilization by the spacecraft flight control system for both attitude steering and deceleration thrust control.

The doppler velocity sensor (DVS) portion of the system is essentially a three-beam coherent CW autodyne doppler radar. A single klystron (two-cavity type) provides undeviated output at a nominal frequency of 13, 300 MHz. Its output is divided equally among the transmitting horns for beams 1, 2, and 3. Each beam has a separate receiving horn, with adequate RF isolation against direct leakage, and a separate and independent receiver utilizing a small sample of the transmitted signal as a local oscillator (bias). Associated with each receiver is a separate and independent frequency tracker capable of acquiring and tracking the doppler signal corresponding to that component of velocity associated with the spacecraft orientation of that particular beam. The spacecraft beam orientations are such that the nominal velocity components V_i $(i = 1, 2, 3)$ along the axes of these three beams are determined by the spacecraft coordinate components of velocity according to the matrix multiplication:

$$\begin{pmatrix} V_1 \\ V_2 \\ V_3 \end{pmatrix} = \begin{pmatrix} +A & +A & +B \\ -A & +A & +B \\ -A & -A & +B \end{pmatrix} \begin{pmatrix} V_x \\ V_y \\ V_z \end{pmatrix}$$

where

$$A = \sin 45 \text{ degrees} \sin 25 \text{ degrees} = 0.29884$$

$$B = \cos 25 \text{ degrees} = 0.90631$$

PRECEDING PAGE BLANK NOT FILMED.

and the spacecraft coordinates are a Cartesian right-handed triad with +z along the roll axis in the normally descending direction.

The frequency outputs of these three frequency trackers are properly scaled and summed in three converters whose outputs are analog voltages representing the spacecraft velocity components:

$$V_x = \frac{V_1 - V_2}{2A}; \quad V_y = \frac{V_2 - V_3}{2A}; \quad V_z = \frac{V_1 + V_3}{2B}$$

The radar altimeter (RA) portion of the system is basically a single-beam coherent FM-CW microwave radar altimeter. Beam 4, fixed along the spacecraft +Z axis, also contains separate transmit and receive horns, a fourth receiver, and a fourth frequency tracker. The same kind of transmitter-derived local oscillator (bias) signal configuration is used, but the RA uses a reflex klystron whose frequency is sawtooth deviated in standard FM-altimeter fashion. The operating portion of the sawtooth has negative slope (with time) to avoid any range-velocity ambiguities. The beam 4 receiver and frequency tracker therefore operate at a frequency which is the sum of scaled slant range and scaled doppler velocity inevitably appearing along that beam. The RA converter corrects the frequency output of the beam 4 tracker by a properly scaled term (V_z compensation), obtained from the DVS V_z converter, to provide an analog output voltage proportional to R_z, the slant range along the spacecraft +Z axis. (The nominal RA operating frequency is 12, 900 MHz. Deviation is nominally 40 MHz at 8000 MHz/sec below 1000 feet, and 4 MHz at 800 MHz/sec above 1000 feet.)

Each receiver is actually two parallel receiving channels, each with separate microwave mixers and audio preamplifiers. Microwave mixer signal and bias inputs are phased so that the parallel audio channels are essentially in phase quadrature, and with equal amplitudes, for all normal doppler signals. Each frequency tracker uses these quadrature audio signals to single-sideband modulate an internal reference signal held at 600 kHz, thus reproducing doppler frequencies unambiguously. In Surveyor, this serves primarily to reject negative velocity at tracker IF, thereby preserving the sense of the velocities. (In a more general application, this would permit measuring negative and positive beam velocities including the unwanted radar return from the main retro engine after separation from the spacecraft.) Each frequency tracking loop is closed by a voltage controlled oscillator whose frequency is controlled by a discriminator-integrator combination, whose output is a direct measure of the frequency being tracked.

To preserve the high degree of both amplitude and phase balance between the parallel quadrature channels of each receiver over the full dynamic range of signals and over the region of operating temperatures, the preamplifier gains are switched in discrete steps by wideband (at audio) gain-switching threshold circuits. Automatic gain control is <u>not</u> used. A set of discrete outputs is provided and telemetered to indicate the gain state of each receiver, as follows:

	Gain Switch 1	Gain Switch 2
High gain (DVS, 90 db; RA, 80 db)	Off	Off
Mid gain (DVS, 65 db; RA, 60 db)	Off	On
Low gain (DVS and RA, 40 db)	On	On

Other discrete outputs are also provided and telemetered. One is a confirmation of application of prime power. This initiates a warmup interval ended by an internal timer which applies high voltage to both klystrons. A set of tracker-lock signals indicates the search or track status of each of the four frequency trackers. A reliable operate doppler velocity sensor (RODVS) discrete indicates, both prior to 3.5 g + 3.7 seconds and subsequent to the 1000-foot mark, that all three DVS beams are locked; between these two times (in Surveyor IV and subsequent spacecraft), it indicates that any one or more of the DVS beams is locked. RODVS causes the flight control to switch attitude steering inputs from gyros to lateral velocities. A RORA (reliable operate radar altimeter) discrete is on when and only when beams 1, 3, and 4 are locked, thus providing reliable V_Z and R_Z for the flight control acceleration control loop. From the analog range output, the RADVS itself derives and supplies two discrete range mark signals, one at 1000 feet (used to change flight control loop parameters), and the other at 12 feet (used to cut off vernier engines).

The latter is termed the 14-foot mark for RADVS purposes, since it is measured from the RADVS antenna boresight reference, which is 24 inches above the legs-extended position of the landing pads on the spacecraft structure (whose position at vernier engine cut off, in turn, has been used in landing stability analyses).

The RADVS hardware is packaged in five units, each of which is a control item in Hughes Spacecraft Configuration Control. Since temperature is measured separately for most of these units, their basic composition is indicated below:

A/VS antenna	— beams 1 and 4 antenna, mixer, and preamplifier components
DVS antenna	— beams 2 and 3 antenna, mixer, and preamplifier components
Klystron power supply modulator (KPSM)	— includes all components for both DVS and RA
Signal data converter	— all frequency trackers and data converters
Waveguide assembly	

5.9.2 ANOMALIES

There were no radar anomalies in the Surveyor VI mission.

5.9.3 SUMMARY

Data at Station 14 was continuous during terminal descent. Therefore, the times for all mark events are within the accuracy determined by the bit rate.

All DVS beams locked during retro operation. This is normal and has occurred in all previous terminal descents.

RODVS was on from initial lock to touchdown.

Beam 4 was acquired after retro case separation. An explanation for this late acquisition is contained in subsection 5.9.4.3.

RORA was on from initial lock of beam 4 to touchdown.

There is good agreement between the processed telemetry data and the 6DOF terminal descent reconstruction for all RADVS parameters.

5.9.4 SUBSYSTEM PERFORMANCE ANALYSIS

5.9.4.1 RADVS Turn-on

RADVS power on occurred properly, within a second of retro ignition, as confirmed by EP-33, R-28, EP-17, and the altimeter search sweep pattern in FC-35. Subsequent time-in of the high voltage occurred approximately 21 seconds later, as indicated by EP-17 (Figure 5.2-8), a normal internal delay.

5.9.4.2 Velocity Acquisition Conditions

All three beams of the doppler velocity sensor (DVS) acquired and commenced tracking lunar reflected signals as soon as they came within each tracker's acquisition sweep frequency limits. From the 6DOF computer program reconstruction, conditions at initial acquisition for each beam are shown in Table 5.9-1 (assuming conditions at the most probable tracker lock times, whose telemetry time accuracies are ±0.6 second, or about ±140 fps in beam velocities).

Spacecraft conditions at the time of RODVS (all DVS beams locked, and converters reporting reliable V_x, V_y, and V_z), again from the 6DOF program reconstruction, were as follows:

V_x = -3.3 fps

V_y = +135.8 fps

V_z = +3200 fps

Range = 68,023 feet

Attitude = 25.34 degrees

Altitude = 64,402 feet

again assuming conditions at the most probable time of RODVS, whose telemetry time accuracy is also ±0.6 second.

TABLE 5.9-1. CONDITIONS AT RODVS

Beam	Slant Range Along Beam, 1000 feet	Velocity Component Along Beam, fps	Beam Incidence Angle, degrees	Doppler Frequency, kHz	Upper Search Limit, kHz
1	66.0	3168	10.89	86.08	≈ 85
2	72.2	3169	26.12	86.12	≈ 85
3	99.4	3091	48.97	84.03	≈ 85

5.9.4.3 Range Acquisition Conditions

From telemetry and terminal descent 6DOF program reconstruction, conditions at the time of range tracker lockon and RORA were:

V_x = +1.3 fps

V_y = +118.7 fps

V_z = +501.8 fps

Range = 36,622 feet

Attitude = 13.9 degrees

Altitude = 35,548 feet

Altimeter frequency = 72.7 kHz

Upper sweep limit ≈ 91 kHz

again assuming conditions at the most probable time, whose telemetry accuracy is also ±0.6 second.

It should be noted that acquisition occurred much lower than the upper sweep limit and after retro eject. It is believed that beam 4 locked up late for the following reasons:

1) Before retro eject and after RODVS, beam 4 switched to gain state 2. Acquisition could not occur in this gain state because the gain is too low. This change in gain state can be attributed to reflections from the retro engine gases.

2) Beam 4 returned briefly to gain state 3 prior to retro eject but after retro eject went back to gain state 2 due to reflections from the retro case. When the tracker returned to gain state 3 on the next telemetry frame, beam 4 locked up and RORA occurred.

5.9.4.4 Revised Nominal db Budget

The db budget for the revised Surveyor VI conditions is shown in Table 5.9-2.

5.9.4.5 Surveyor VI Event Times

The GMT at DSIF-14 at the time of data recording is shown. Table 5.9-3 gives a number of significant spacecraft and related radar events defining the major items in the terminal descent sequence. Table 5.9-4 shows the use of the magnitude register (FC-18) to refine the times of vernier ignition and AMR mark. In these tables, a signal is shown as going on at a time interpolated between its last absence and its first presence, plus or minus one-half the data sampling interval. Table 5.9-5 shows the RADVS gain states and tracker lock conditions from vernier ignition.

5.9.4.6 Descent Reconstruction

The set of graphs of R, V_x, V_y, and V_z (Figures 5.9-1 and 5.9-2) compare PREPRO processed telemetry data with the 6DOF program values for the revised nominal conditions. These graphs show a good correlation between the computed values and processed telemetry values.

5.9.4.7 Radar Reflectivity Analysis

RADVS gain-switching events and reflectivity signal amplitudes for the Muhleman reflectivity model were derived, described, and presented in a succession of radar description and Surveyor I prediction packages, and were presented again in the Surveyor I postmission report. The unusual difference in frequency responses seen by the signal circuits and by the gain-switching threshold circuits was treated in detail, with predictions of higher than necessary gain states at very low altitude, starting about 10 seconds before touchdown. This response was confirmed in the Surveyor I mission performance and again in Surveyor VI.

TABLE 5.9-2. RADVS INDIVIDUAL BEAM db BUDGETS BEFORE STEERING

Using measured Pt and G values and nominal reflectivity model

For φ = 25.4 degrees; ρ = +109.2 degrees; and R_z = 40,574 feet

Values	Beam 1	Beam 2	Beam 3	Beam 4
Pt, dbm	+34.70	+33.60	+33.05	+25.05
G, db	+28.2	+28.1	+27.7	+28.5
(1/2), db	- 3.01	- 3.01	- 3.01	- 3.01
λ^2, db	-22.64	-22.64	-22.64	-22.36
$(4\pi)^{-2}$, db	-21.98	-21.98	-21.98	-21.98
$(36.65 \text{ kilofeet})^{-2}$, db	-91.28	-91.28	-91.28	-91.28
$\cos^2 \theta i$, db	- 0.16	- 0.94	- 3.68	- 0.88
$F(\theta i)$, db	- 4.99	- 9.22	-12.41	- 9.05
$\eta(K/\alpha^3)$, db	- 1.72	- 1.72	- 1.72	- 1.72
Sum of + values	62.90	61.70	60.75	53.55
Sum of - values	-145.78	-150.79	-156.72	-150.98
P_r, dbm	-82.88	-89.09	-95.97	-97.43
θi, degrees	10.9	26.2	49.1	25.4
$\sigma(\theta)$, db	- 6.72	-10.94	-14.13	-10.77
R, kilofeet	37.31	40.85	56.13	40.57

TABLE 5.9-3. SURVEYOR VI EVENTS

Sensor	Event	GMT, Day 314, hr:min:sec
R-1	AMR on	00:53:19.604 ± 0.6
R-11	AMR enable	00:56:19.600 ± 0.6
FC-64	AMR mark	00:57:57.038 ± 0.05
FC-28	Vernier ignition	00:58:02.938 ± 0.05
FC-29	Retro ignition	00:58:04.038 ± 0.05
EP-33	RADVS pyro switch	00:58:04.396 ± 0.6
R-28	RADVS on	00:58:05.798 ± 0.6
FC-34	RODVS	00:58:34.098 ± 0.6
FC-63	Inertial switch	00:58:43.397 ± 0.3
FC-30	Retro burnout	00:58:43.637 ± 0.05
FC-78	Start maximum thrust	00:58:53.297 ± 0.6
FC-31	Retro eject signal	00:58:55.637 ± 0.05
V-4	Retro ejected	00:58:55.942 ± 0.255
FC-42	Start RADVS descent	00:58:57.737 ± 0.05
FC-33	RORA	00:58:59.297 ± 0.6
	Segment acquisition	00:59:21.276 ± 0.14
FC-37	1000-foot mark	01:00:40.534 ± 0.05
FC-36	10 fps	01:00:57.634 ± 0.05
FC-38	14-foot mark	01:01:04.133 ± 0.05
(Leg 1)	Touchdown	01:01:05.467 ± 0.003

TABLE 5.9-4. TIMING REFINEMENT

GMT, Day 314, hr:min:sec	Magnitude Register, BCD
Initially	118
00:57:57.198	115
00:58:01.998	19

Vernier ignition at 58:01.998
0.925 ± 0.025
58:02.923 ± 0.025

Actual delay = 118 BCD
= 5.875 ± 0.025 seconds

Clock started at 57:57.073 ± 0.025
FC-64 at 57:57.038 ± 0.050

Actual mark at 57:57.088 maximum
57:57.048 minimum
= 57:57:068 ± 0.025

This page intentionally left blank.

TABLE 5.9-5. SURVEYOR VI RADVS GAIN STATES AND TRACKER LOCK CONDITION FROM VERNIER IGNITION

Reference Vernier Ignition 314:00:58:02.938, seconds	Gain States				Beam Lock (Lock is 1)				
	B1	B2	B3	B4	T1	T2	T3	T4	
-0.270	3	3	3	3	0	0	0	1	
0.930					1	1			
2.130					0	0		0	
23.730	2								
29.730					1	1	1		RODVS occurred.
40.529		2							
48.929				2					
52.529				3					
53.729			2	2					Retro case has been ejected.
54.929				3					
56.129		3	3						
57.329		2						1	RORA occurred.
59.729		3							
60.929			2						
63.329		2	3						
64.528			2						
69.329			3						
70.529			2						
114.927				2					
116.127				3					
124.527				2					
129.327				3					
130.527				2					
131.727				3					
134.127				2					
135.327				3					
138.927				2					
140.127	2	2	2	3	1	1	1	1	

Table 5.9-5 (continued)

Reference Vernier Ignition 314:00:58:02.938, seconds	Gain States				Beam Lock (Lock is 1)				
	B1	B2	B3	B4	T1	T2	T3	T4	
141.327	2	2	2	2	1	1	1	1	
142.527				3					
143.726				2					
144.926				3					
146.126				2					
149.726				3					
150.926				2					
152.126	1								
153.326	2								
154.526		1							
155.726	1	2	1						
156.926	2	1		1					
158.126	1	2							
159.326		1	2						
160.526			1						
162.926				2					
164.126			2						
165.326			1	1					
168.926				2					
171.326		2	2						
172.526	2								
173.726	1								
174.926	2		3						10-fps mark occurred.
176.126		3	2						
177.326	3	2							
178.526	2		3						
179.726			2	3					
180.926	1		1	2					
182.125	2		2	3					
183.325	3	3	3	3	1	0	0	1	Touchdown occurred.
184.525	3	3	3	3	0	0	0	1	

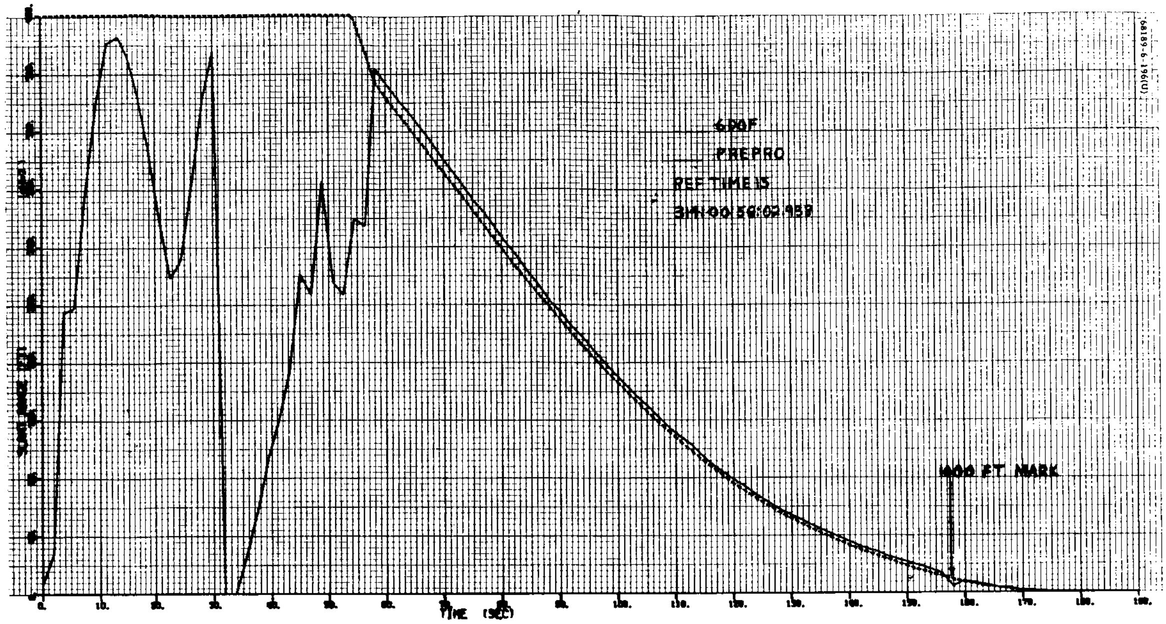

Figure 5.9-1. Slant Range — Reconstructed

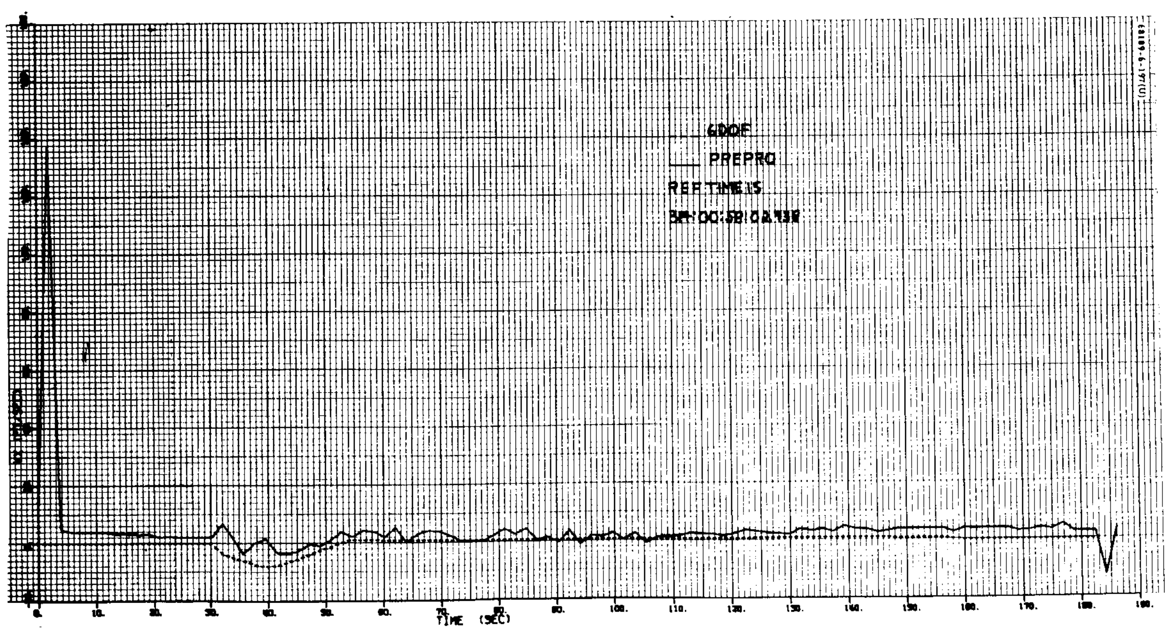

a) V_x

Figure 5.9-2. Spacecraft Velocities — Reconstructed

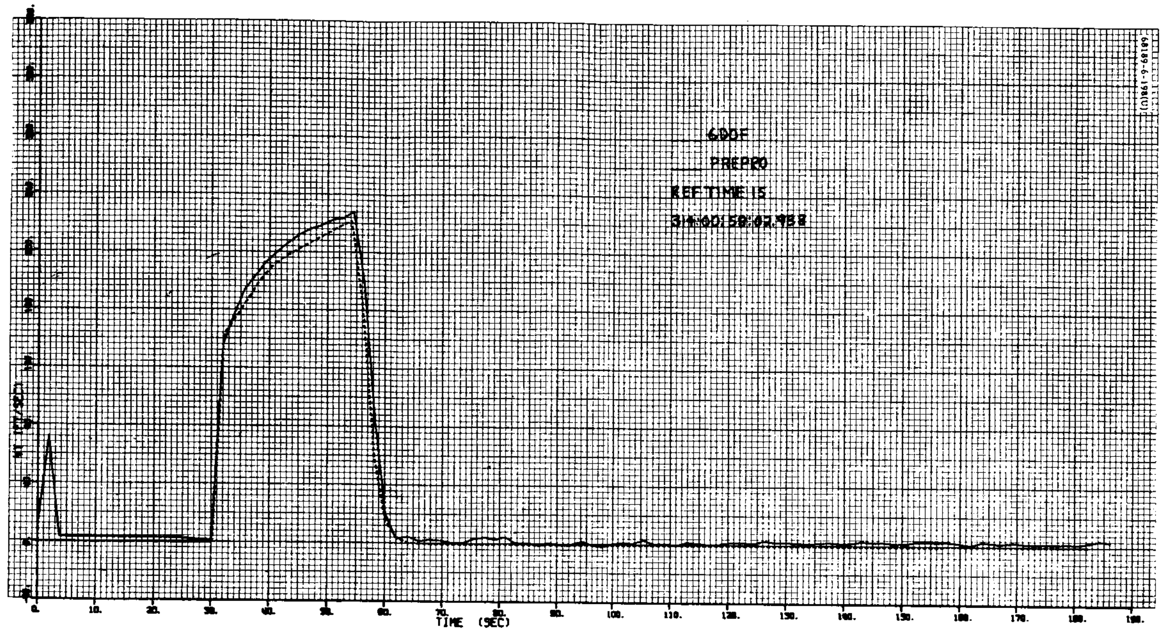

b) V_y

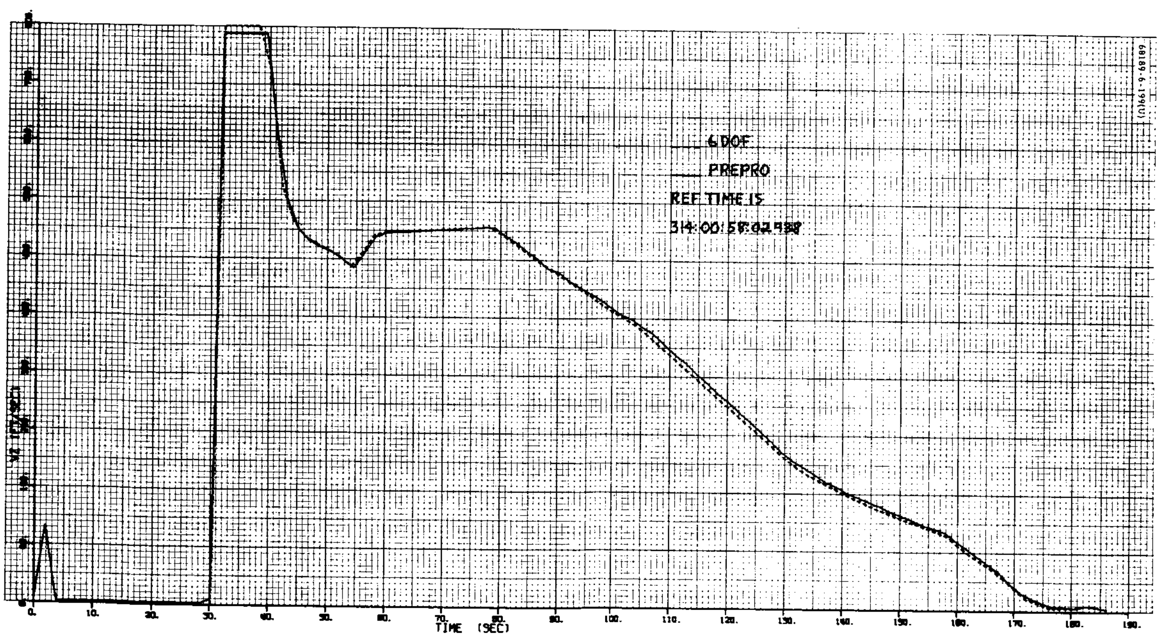

c) V_z

Figure 5.9-2 (continued). Spacecraft Velocities — Reconstructed

Not just for radar purposes, but for the larger analyses of the entire terminal descent of each mission, an appreciable effort is devoted to a complete and accurate nine-dimensional trajectory versus real time reconstruction. While this process is hampered by lack of direct data on spacecraft attitude once steering has started, it is possible to converge on an accurate and unique solution in which attitude is implicit by iteration of a precise spacecraft simulation against every significant telemetry channel, as described in the terminal descent discussion. Radar data aid in this reconstruction and, in return, the simulation provides expected or predicted reflectivity signal strengths throughout the descent. This process was almost trivial in the almost exactly nominal Surveyor I, but has proved its utility in matching Surveyors III, V, and VI.

The results were presented in subsection 5.9.4.6, and the received signal strength versus time plots are represented here (Figure 5.9.4) along with the processed telemetered received signal strength data for comparison. Figure 5.9-3 shows beam incidence angles and reflectivity factors from 6DOF versus time.

It should be noted that the reflectivity signal voltage is not always a true indicator of received signal strength when the preamplifier is switching between two gain states. The rapid sawtooth motion of the processed telemetry data during RADVS control is due to gain switching.

5.9.4.8 Reflectivity Model

The lunar radar reflectivity model used by Hughes and approved by JPL for design and evaluation of both Surveyor radars was developed by D.O. Muhleman. This model has been completely described in previous documentation. (See, for example, the "Surveyor III Flight Performance Final Report.")

5.9.5 RADVS DOCUMENTATION

R.A. Dibos, RADVS Design Review Material, 22 July 1965.

R.A. Dibos, "Behavior of Telemetered Range Near 1000-ft Scale Factor Charge," Hughes IDC 2253.1/523, 27 December 1965.

R.A. Dibos, "Post-Mission Analyses Involving Radar Data," 25 March 1966.

R.A. Dibos, "A-21 RADVS-Predicted Minimum Margin Performance," 30 May 1966.

"Surveyor III Flight Performance," Hughes Aircraft Company, SSD 68189-3, July 1967.

M.R. Weiner, "Least Square Polynominal Fit of the DVS Tracker Non-Linearity for SC-6," Hughes IDC 2292/398, 25 September 1967.

"Surveyor IV Flight Performance Final Report," Hughes Aircraft Company, SSD 68189-4, September 1967.

R.A. Dibos, "Radar Performance Evaluation," SC-1 Symposium (NASA at JPL), September 1966.

"Surveyor I Flight Performance Final Report," Hughes Aircraft Company, SSD 68223R, October 1966.

"Decibel Allocation and Margin Summary," Hughes Aircraft Company, SSD 4021R-2, 28 November 1966.

R.A. Dibos, "RADVS Lateral Velocity Saturation," Hughes IDC 2253.4/67, 9 March 1967.

R.A. Dibos, "Extended RADVS Equations for Six-Degree Digital Program," Hughes IDC 2253.4/69, 15 March 1967.

E. White, "Timetic Method for Determining Surveyor System Errors," Hughes IDC 2293/105, 14 April 1967.

R.A. Dibos, "TM Mode 6 Data Relating to Radar Performance," Hughes IDC 2253.4/84, 15 June 1967.

D.W. Demaree, "SC-6 Radar Calibration Data," Hughes IDC 2294.5/146, 23 October 1967.

"Surveyor V Flight Performance Final Report," Hughes Aircraft Company, SSD 68189-5, November 1967.

5.9.6 ACKNOWLEDGMENTS

M.R. Weiner — technical coordination

V. Marelia — terminal descent trajectory reconstruction

N.R. Krupa — PREPRO processing

E.R. Kopitzke — 6DOF processing

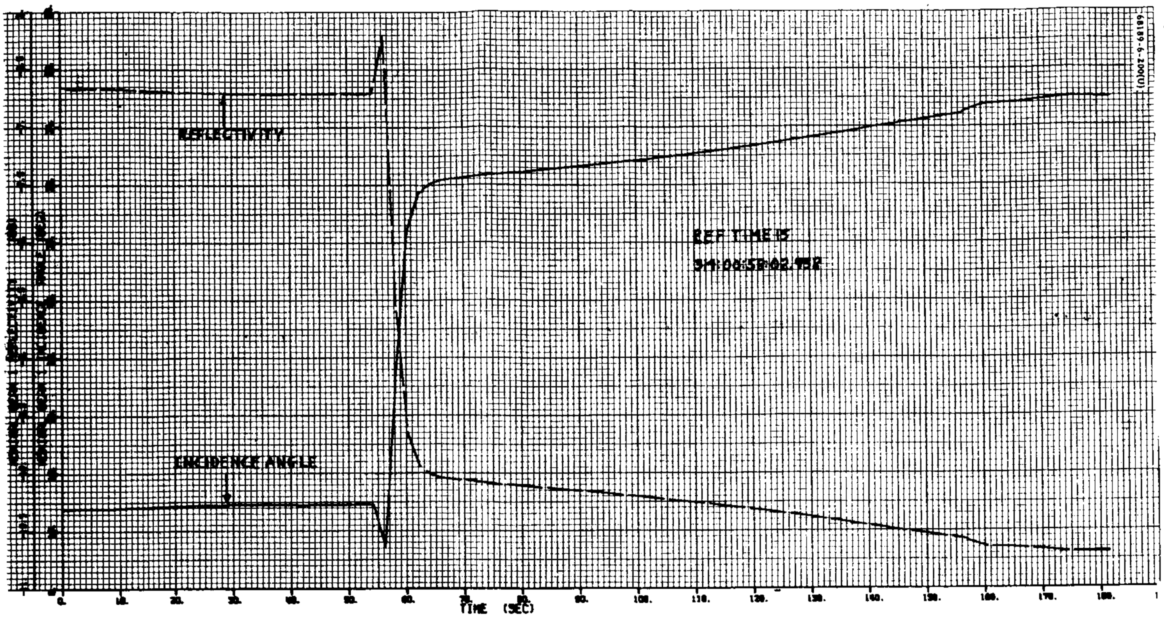

a) Beam 1

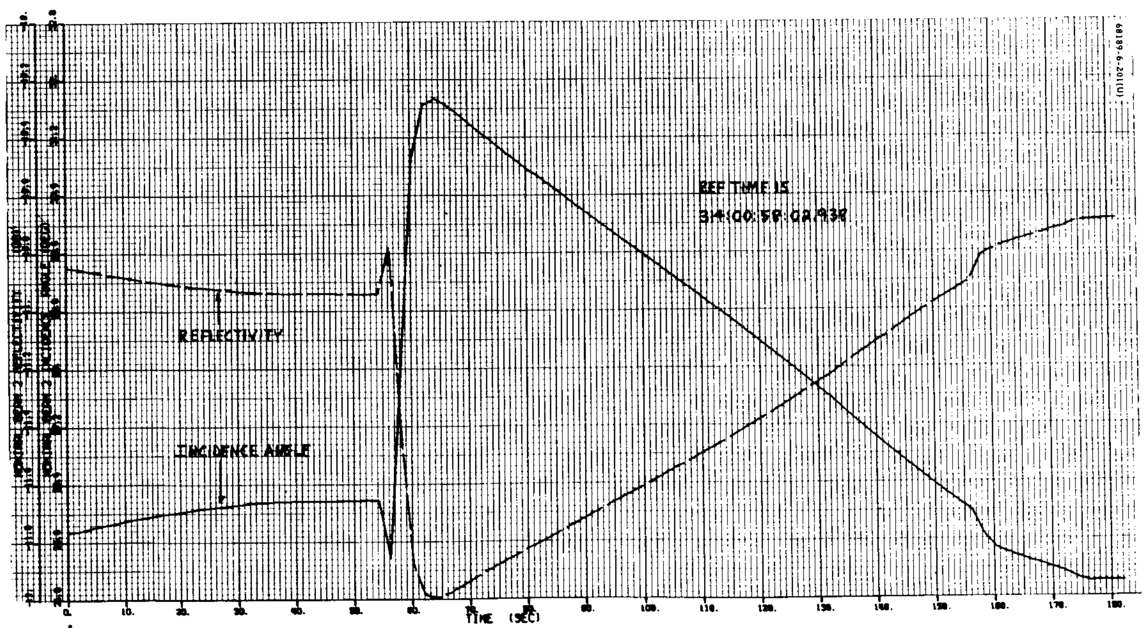

b) Beam 2

Figure 5.9-3. Beam Incidence Angles (θ) and Reflectivity Factors (σ) From 6DOF Program

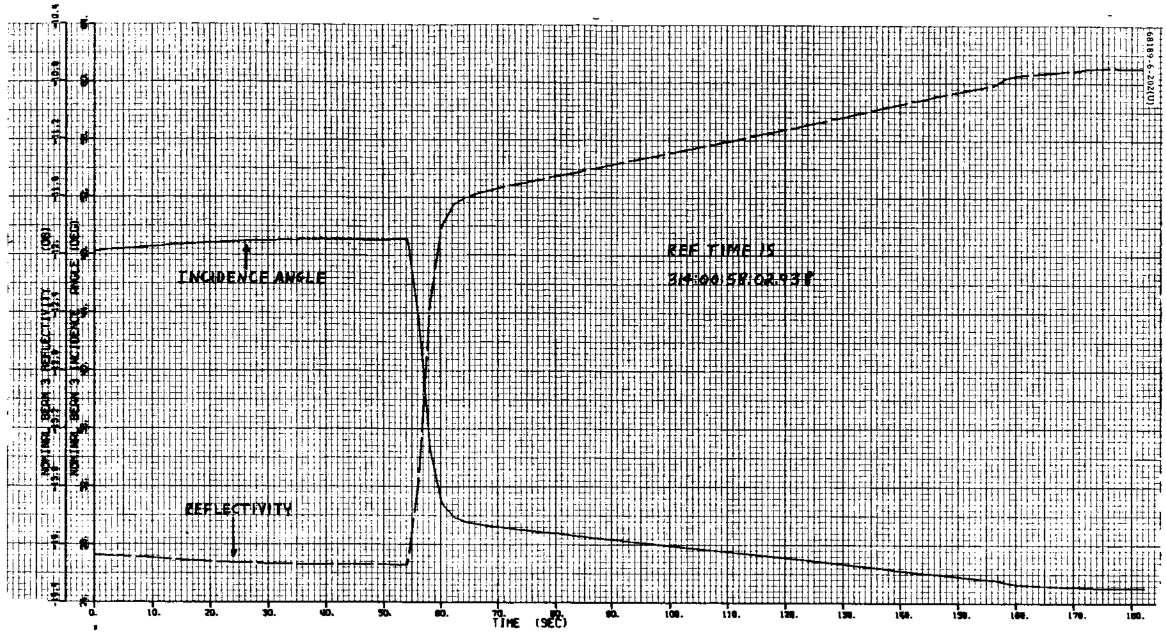

c) Beam 3

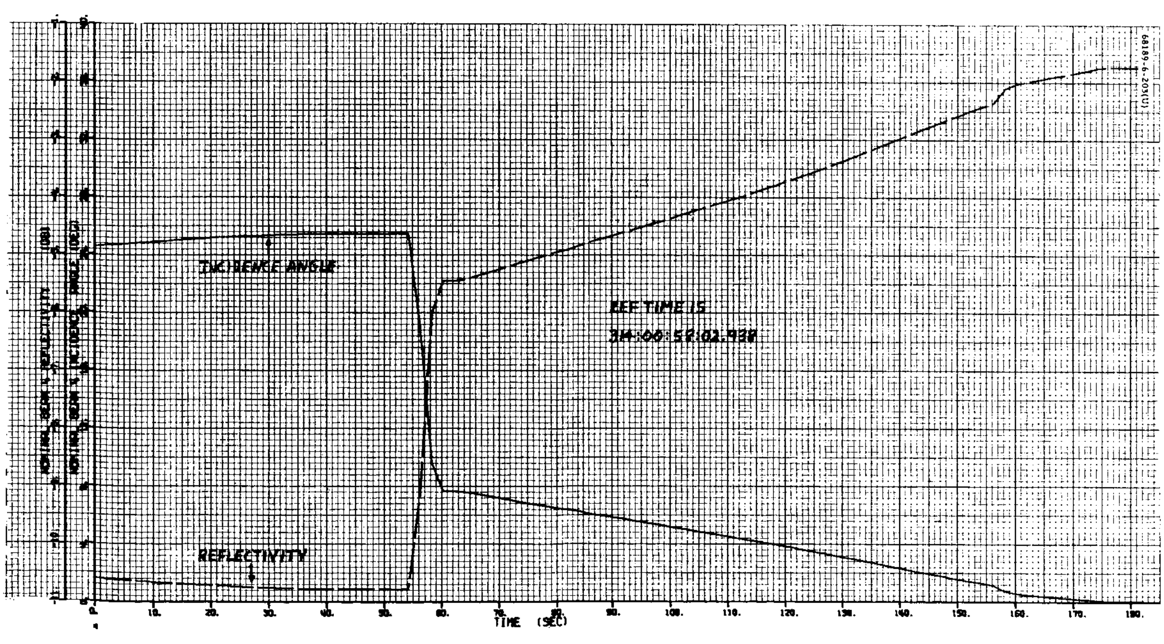

d) Beam 4

Figure 5.9-3 (continued). Beam Incidence Angles (θ) and Reflectivity Factors (σ) From 6DOF Program

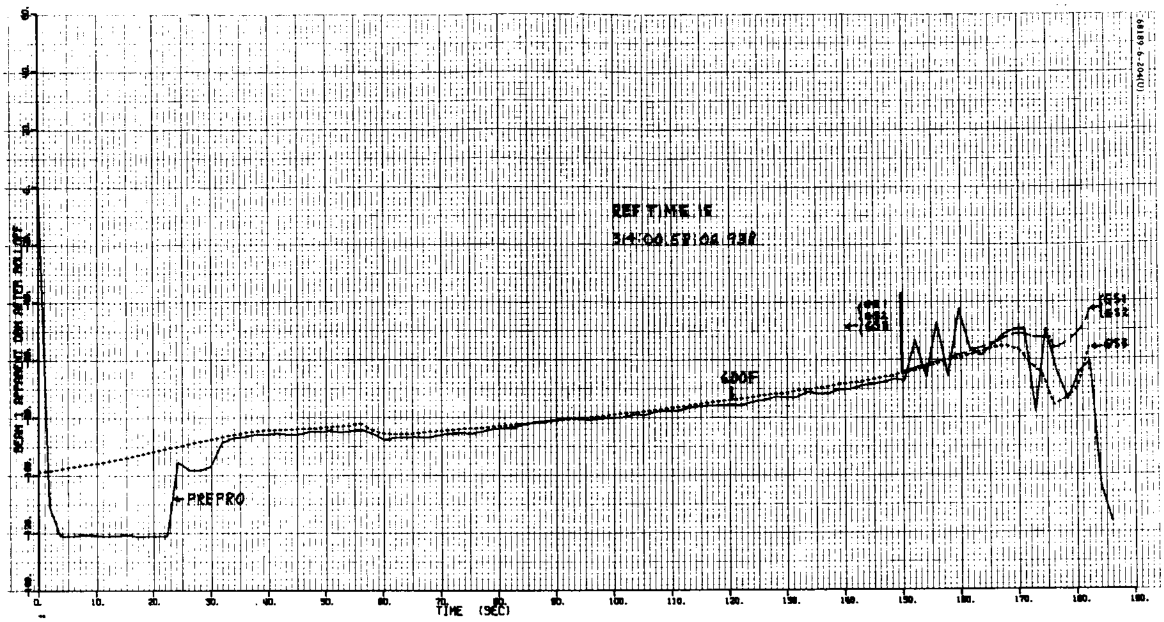

a) Beam 1

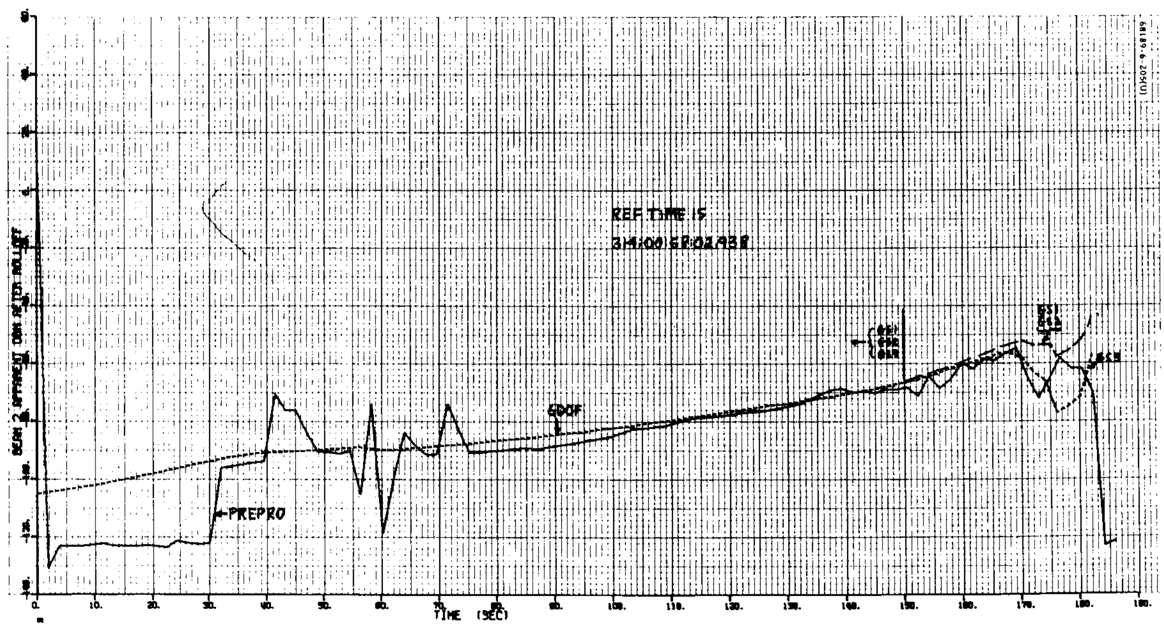

b) Beam 2

Figure 5.9-4. RADVS Reflectivity

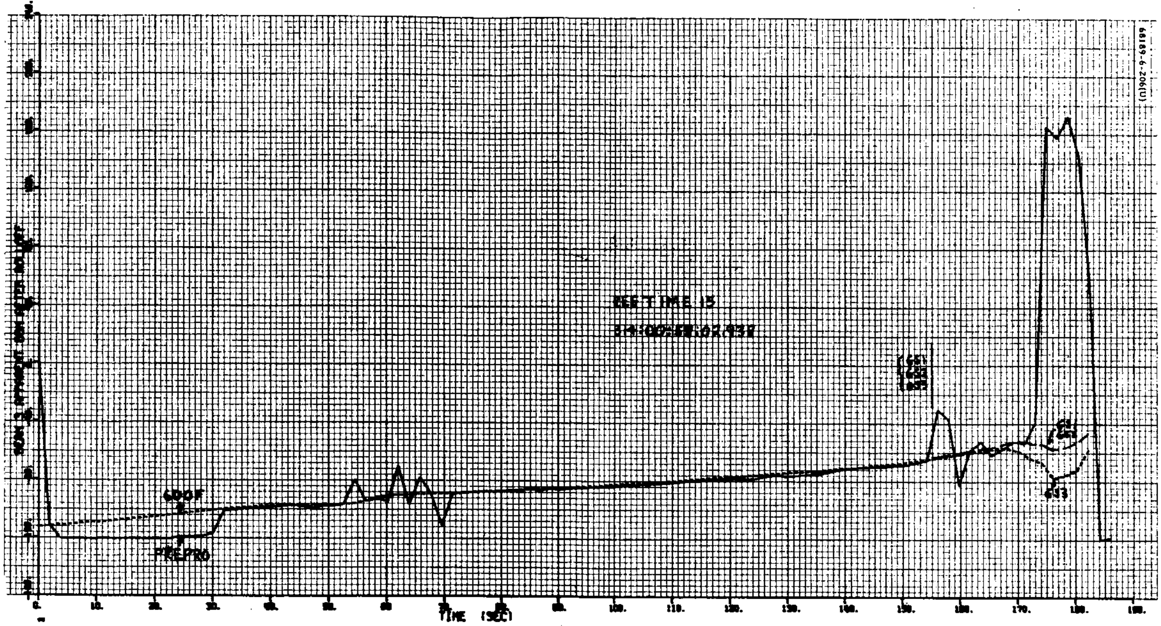

d) Beam 4

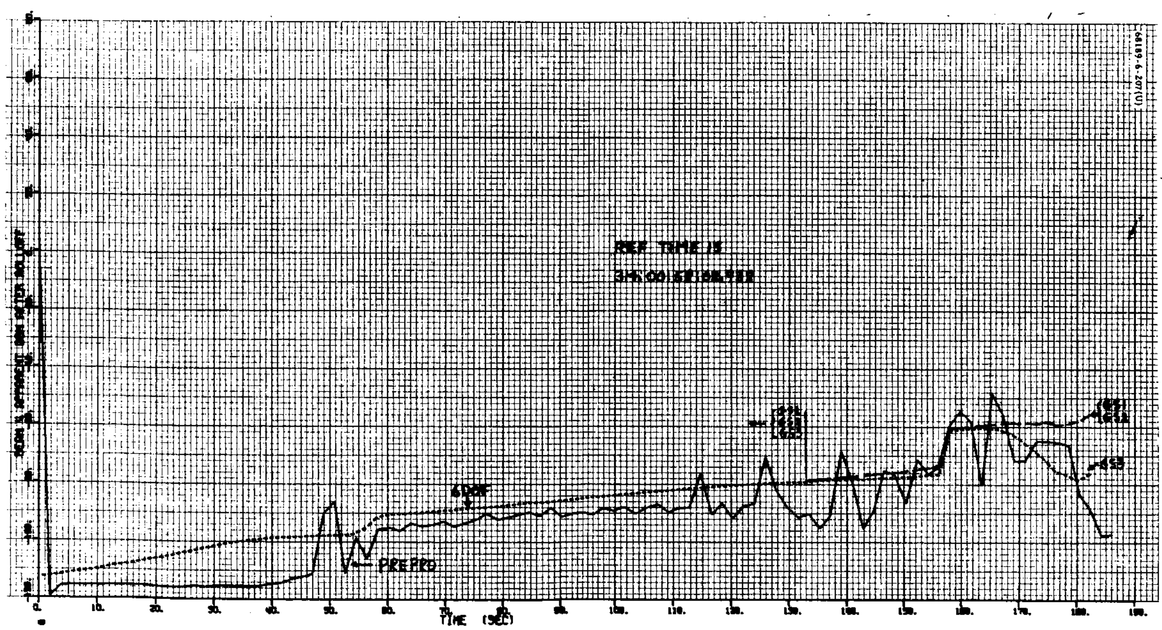

c) Beam 3

Figure 5.9-4 (continued). RADVS Reflectivity

5.10 STRUCTURES PERFORMANCE

5.10.1 INTRODUCTION

Structures postmission analysis is normally confined to launch and touchdown phases of the mission and the resulting structural loads, landing gear performance, and landing dynamics. Structures support is also required if vernier engine static firing or a hopping maneuver is performed.

During the launch phase, vehicle separation and extension of the landing gear were verified. During touchdown, shock absorber strain gages indicated the landing gear load time histories and enabled a prompt, but approximate, assessment of landing conditions, such as impact velocity and vehicle incidence relative to the lunar surface. Before and after a landing, leg deflections were monitored to establish whether or not the operating characteristics of the shock absorbers had been impaired during the mission.

Postmission analysis consists of analyzing 1) leg deflection potentiometer data, and 2) shock absorber strain gage data during landing. A mathematical model was used to simulate Surveyor VI landing conditions. The analytical results obtained from the mathematical model, combined with other data, can facilitate evaluation of lunar surface mechanical properties.

5.10.2 ANOMALY DESCRIPTION

There were no anomalies in the structures subsystem.

5.10.3 SUMMARY

Surveyor VI landing legs deployed in a normal fashion during the launch phase and operated normally during the landing and through the lunar day.

Analysis indicates that the spacecraft initially landed with an incidence relative to the surface of between 2 and 3 degrees at approximate impact velocities of 11.5 fps vertical and less than 1 fps lateral. In the analysis, these conditions resulted in footpad penetration of between 2 and 3 inches on a surface of 5 psi static bearing strength.

The structural loads experienced by Surveyor VI during the initial landing were low relative to design levels. This was also essentially true during the translation, but with the solar and roll axes unlocked it is considered that a tip-off rate at engine shutdown, which reduced the spacecraft incidence to approximately zero, was the basic reason for maintaining A/SPP loads at acceptable levels.

5.10.4 PERFORMANCE ANALYSIS

5.10.4.1 Launch Phase

Leg Extension and Vehicle Separation

Landing gear extension was confirmed by Structures at 08:03:54 GMT on day 311. Because of a data outage, vehicle separation was not confirmed by Structures until 08:10:25 GMT on day 311.

Leg Deflections

The landing gear position potentiometers were first monitored at 08:35:07 GMT on day 311 and were as follows:

Leg 1: V-5 = 0.1 degree

Leg 2: V-6 = 0.1 degree

Leg 3: V-7 = 0.0 degree

With the landing gear extended, the nominal value for these signals is 0.0 degree, with an allowable variation of ±5 percent, or ±1.2 degrees.

5.10.4.2 Touchdown

The actual landing process of the spacecraft can be reconstructed quite accurately from a variety of telemetry signals in connection with available dynamic landing simulations. Pertinent telemetry data are as follows:

1) Commutated indications of spacecraft altitude

2) Continuous analog signals monitoring three strain gage bridges, one being mounted on each leg shock absorber, indicating its axial loading

3) Postlanding television coverage of footpads, crushable blocks, and areas on the lunar surface in which these spacecraft elements contacted the surface and came to rest

4) Postlanding attitude determinations based on the high gain directional antenna position, horizon sightings, etc.

The above telemetry data and the dynamic landing simulations led to the conclusion that the vertical velocity of Surveyor VI at initial impact was approximately 11.5 fps, the horizontal velocity was less than 1 fps, the surface slope was approximately 0.8 degree, and the spacecraft incidence at landing was between 1 and 2 degrees relative to the lunar horizontal plane.

Figure 5.10-1 shows the time histories of the axial forces in the landing gear shock absorbers from prior to initial surface contact until after the spacecraft came to rest. Footpad 1 contacted first, followed by pad 2 at 25 milliseconds and pad 3 at 40 milliseconds after pad 1 impact. Initially, each shock absorber experienced a force for approximately 0.35 second and then zero force for approximately 1.1 seconds. This was followed by a low amplitude oscillatory force which rapidly damped out to a low constant value consistent with forces resulting from the static lunar weight of the spacecraft. These force-trace characteristics are consistent with those expected from an initial vehicle impact, during which maximum pressures are exerted on the lunar surface, followed by a relief of the load as the spacecraft rebounds under the action of landing gear spring forces, followed by a final low energy impact and oscillatory forces related to the elasticity of the spacecraft and the lunar surface. The frequency of the observed oscillation is approximately 6 cps which corresponds to the oscillation frequencies observed during Surveyor I and III touchdowns (approximately 6.5 cps).

Table 5.10-1 gives the maximum force levels experienced by each shock absorber, and also the footpad impact times for the initial landing.

TABLE 5.10-1. MAXIMUM SHOCK ABSORBER FORCES AND FOOTPAD IMPACT TIMES

Leg Assembly Number	Maximum Shock Absorber Force, pounds	Footpad Impact Time, seconds after 314:01:01:00 GMT
1	1590 ±80	05.467 ± 0.003
2	1810 ±80	05.490 ± 0.003
3	1590 ±80	05.506 ± 0.003

Computer simulation studies of landings have been performed to estimate the landing conditions and mechanical properties of a surface material that will yield surface penetration and shock absorber axial loads similar to those obtained during the Surveyor VI landings. Using the compressible soil model described in Reference 1, the best strain gage time history correlation achieved to date for the initial landing has been for a 5 psi static bearing strength soil and is shown in Figure 5.10-2. The impact velocities are 11.5 fps vertical and 0 fps lateral, with a 3-degree

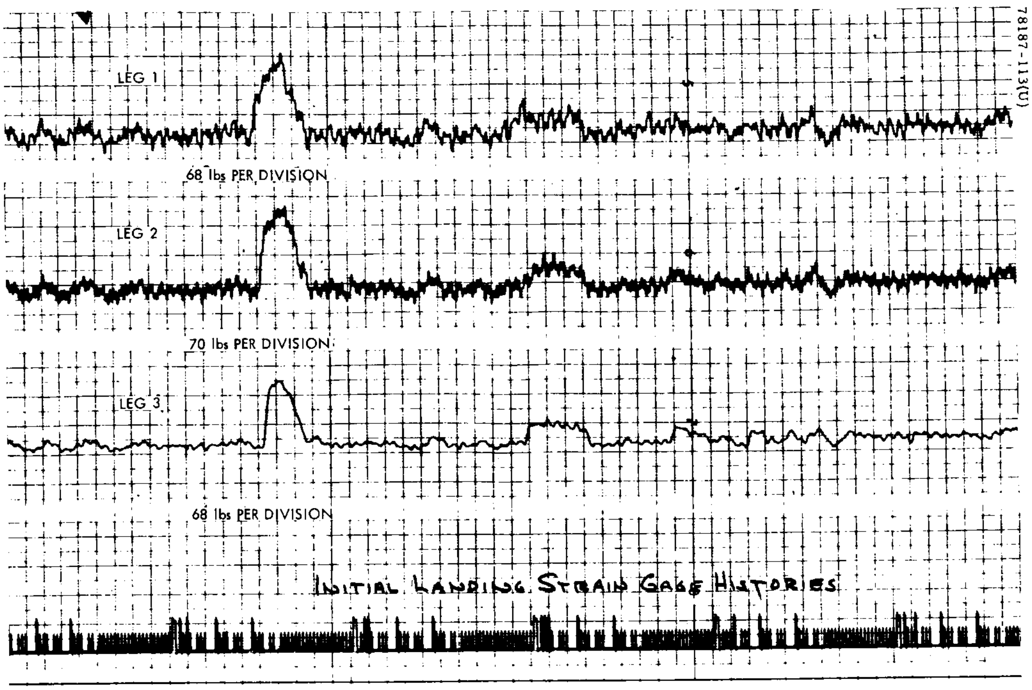

Figure 5.10-1. Initial Landing Strain Gage Histories

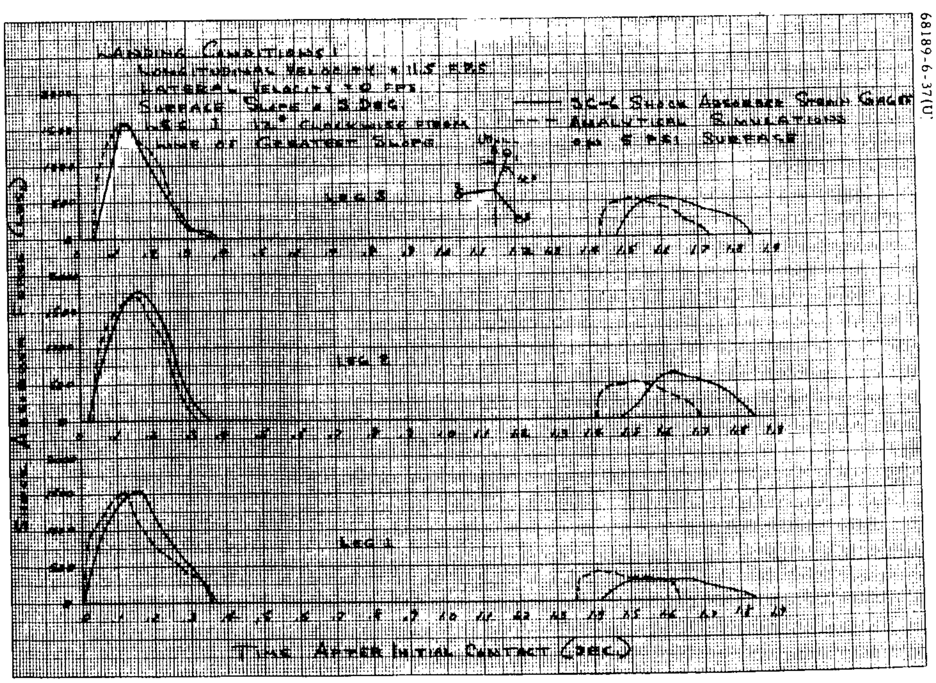

Figure 5.10-2. Analytical and Measured Shock Absorber Force Histories for Initial Landing

incidence relative to the surface. Leg 1 is oriented 12 degrees clockwise from the line of greatest surface slope. The penetration of footpads 1, 2, and 3 obtained in this simulation are 2.6, 2.7, and 2.7 inches, respectively. The penetrations of crushable blocks 1, 2, and 3 are 1.6, 2.0, and 2.3 inches, respectively. The initial and final densities used in the compressible soil analytical model were 2.36 and 3.04 slug/ft^3, respectively. It is significant that using the compressible surface model the best analytical reproduction of strain gage time histories for Surveyor I and III were obtained with the same values of psi and density (References 2 and 3), whereas for Surveyor V lower values were used for the best agreement (Reference 1).

Structural Loads

The impact velocities, spacecraft attitude, and surface conditions for Surveyor VI were very similar to those for Surveyor I. It is therefore considered that, as on Surveyor I, the structural loads experienced by Surveyor VI at initial touchdown were less than 20 percent of the design load levels.

Leg Deflections

Shortly after touchdown (01:01:05:48 GMT on day 314), the landing gear leg deflections were monitored and found to be as follows:

Leg 1: V-5 = 0.9 degree

Leg 2: V-6 = 0.9 degree

Leg 3: V-7 = 0.5 degree

Since these angles were not excessive, it was considered there was no necessity to lock the landing gear at that time. The decision not to lock the gear is made to facilitate gear actuation during any executed lunar hopping maneuver or during inadvertent hopping that could occur during a static firing experiment. Apart from the translation maneuver, no variations in leg deflections were observed. The legs were locked prior to lunar night, and no anomalous deflections such as occurred on Surveyor V (Reference 1) were observed upon entering lunar night.

5.10.5 REFERENCES

1) "Surveyor V Flight Performance Final Report," Hughes Aircraft Company, SSD 68189-5, November 1967.

2) "Surveyor I Flight Performance Final Report," Hughes Aircraft Company, SSD 68189R, October 1966.

3) "Surveyor III Flight Performance Final Report," Hughes Aircraft Company, SSD 68189-3, July 1967.

5.10.6 ACKNOWLEDGMENTS

This section was coordinated by R. H. Jones. The majority of the analytic effort was performed by C. D. Conaway. J. D. Hinchey also performed analysis and data reduction.

5.11 MECHANISMS SUBSYSTEM

5.11.1 INTRODUCTION

This section deals with the mechanical performance of the spacecraft landing legs, omnidirectional antennas, and antenna/solar panel positioner (A/SPP). For purposes of this report, these mechanisms are collectively defined as the mechanisms subsystem.

1) Landing gear deployment — When each landing gear is fully deployed, it opens an electrical switch on the telescoping strut. The actuation of these switches indicates that the landing gear is deployed, and is required for initiation of automatic sun acquisition at separation from Centaur. The telemetry designations for these functions are V-1, V-2, and V-3 for each landing leg, respectively.

2) Omnidirectional antenna deployment — When each omnidirectional antenna is fully deployed, it opens an electrical switch to produce a change of state for telemetry purposes only. The telemetry designation for omnidirectional antenna A is M-1, for omnidirectional antenna B, M-2.

3) A/SPP automatic solar panel deployment — The A/SPP function after separation is to deploy the solar panel surface perpendicular to the roll axis to achieve maximum receipt of solar energy during transit.

The A/SPP has four rotation axes which are moved in steps upon command from earth. The axes are polar, solar, elevation, and roll. The polar axis rotates 1/16 degree per command; the other axes rotate 1/8 degree per command. Figure 5.11-1 illustrates the A/SPP with the polarity of rotation for each axis. The telemetry designation for the A/SPP axis positions are as follows:

Solar panel	M-3
Polar axis	M-4
Elevation axis	M-6
Roll axis	M-7

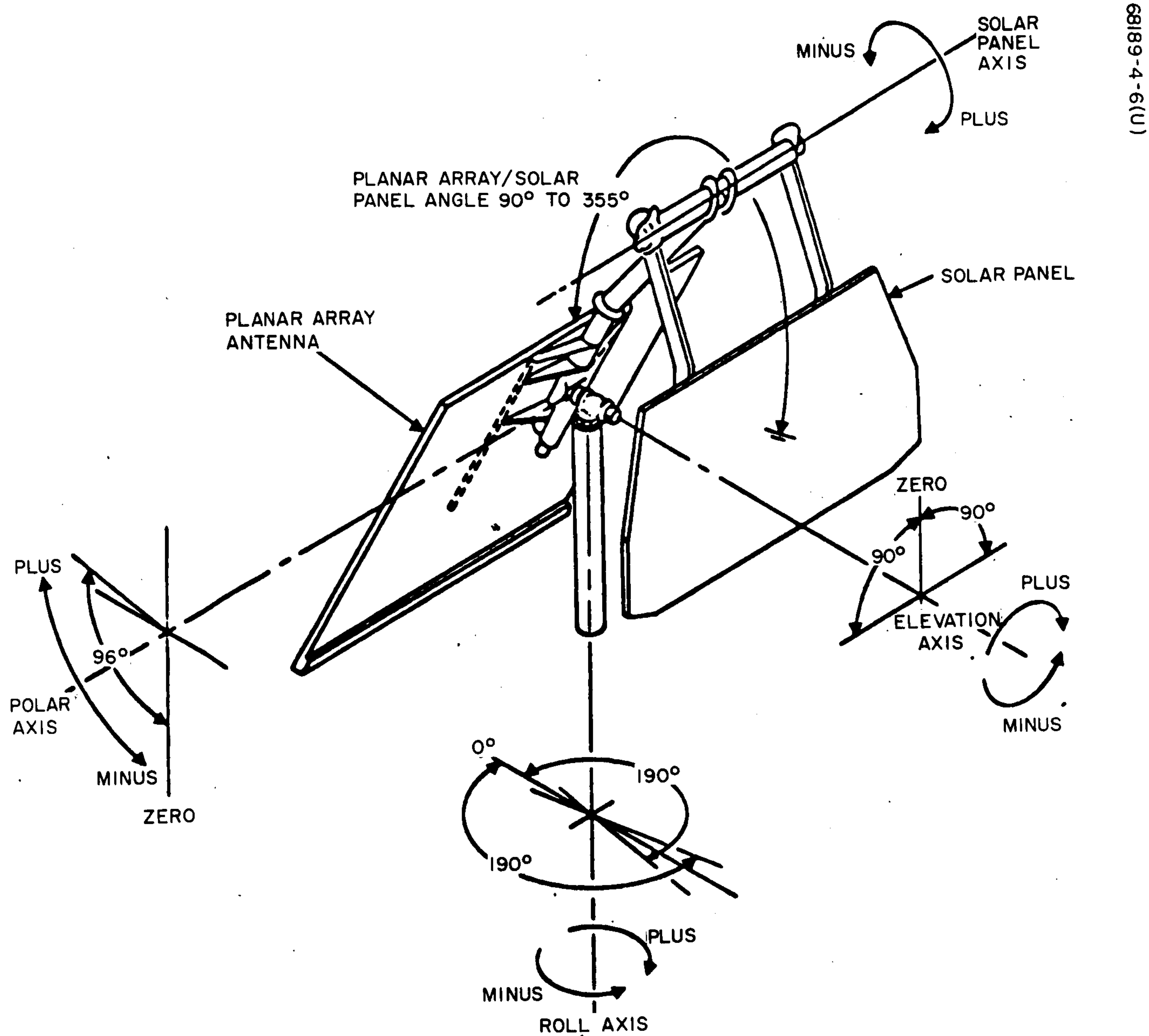

Figure 5.11-1. Antenna and Solar Panel Positioner

5.11.2 ANOMALY DESCRIPTION

No anomalies were detected in the mechanisms subsystem during separation. Telemetry data during transit indicated no anomalous conditions.

5.11.3 SUMMARY AND RECOMMENDATIONS

All mechanism functions performed properly and at the correct times.

5.11.4 SUBSYSTEM PERFORMANCE ANALYSIS

Table 5.11-1 shows the occurrence of major events for the mechanisms subsystem. Table 5.11-2 presents a summary of the subsystem parameters reduced from telemetry data. The expected values were obtained from flight acceptance, type approval, and solar thermal vacuum testing, and from specified design performance values.

5.11.4.1 Landing Gear Deployment

Table 5.11-2 shows the nominal expected deployment time for the landing gear to be about 2.3 seconds. Flight data show the deployment time to be 1.833 ±1.2 seconds, which indicates nominal deployment time. The leg deflection signals (V5-7) also indicated normal and complete extension of the landing gear.

5.11.4.2 Omnidirectional Antenna Deployment

The nominal expected omnidirectional antenna deployment time is 2.4 seconds. The mission deployment time was 2.733 ±1.2 seconds, which indicates nominal deployment time. Data show that both omnidirectional antennas were deployed at the same time.

5.11.4.3 A/SPP Performance

Automatic Solar Panel Deployment

Automatic solar panel deployment begins upon closure of the 22-volt switch in the separation sensing and arming device at vehicle separation. The solar panel launch lock is unlocked and the solar panel is stepped from 355 to 270 degrees where it is relocked. At this point, the roll axis is stepped from -60 to 0 degrees and relocked. Both positions are locked until after touchdown.

The Surveyor VI mission solar panel deployment time was 576 seconds. Comparing this mission deployment time to that in solar thermal vacuum phase A (579 seconds), the agreement is excellent.

TABLE 5. 11-1. MECHANICAL EVENTS AT SEPARATION

Event	Mission Time, GMT, Day 311, hr:min:sec
Launch	07:39:01.075
Extend landing gear (Centaur command)*	08:03:48.995
Landing gears extended (V-1, V-2, V-3 on)	08:03:50.828±1.2
Extend omnidirectional antennas (Centaur command)*	08:03:59.495
Omnidirectional antennas extended (M-1, M-2 on)	08:04:02.228±1.2
Spacecraft electrical separation (Centaur command)*	08:04:25.095
Spacecraft electrical separation (M-9 on)	08:04:24.426±1.2
Spacecraft mechanical separation*	08:04:29.995
A/SPP solar panel unlocked (M-14 on)	08:04:31.4±2.0
A/SPP solar panel locked in transit position (M-11 on)	08:10:07.4±2.0
A/SPP roll axis locked in transit position (M-13 on)	08:14:07.4±2.0

TABLE 5.11-2. PERFORMANCE PARAMETERS SUMMARY

Parameter	Expected Value, Nominal	Measured Value
Time from Centaur extend landing gear command to legs extended indications (V-1, V-2, and V-3 on)	<2.3 seconds	1.833±1.2
Time from Centaur extend omnidirectional antenna command to omnidirectional antennas extended (M-1 and M-2 on)	<2.4 seconds	2.733±1.2
Solar axis deployment time (A/SPP solar panel autodeployment)	337 seconds*	336 seconds
Roll axis deployment time (A/SPP solar panel autodeployment)	242 seconds*	240 seconds
Total A/SPP solar panel autodeployment time	579 seconds*	576 seconds
Solar axis launch position (355 degrees) (M-3)	356.2 degrees*	355.4 degrees
Polar axis launch position (0 degree) (M-4)	0.12 degree*	0.07 degree
Elevation axis launch position (0 degree) (M-6)	0.01 degree	-0.63 degree
Roll axis launch position (-60 degrees)(M-7)	-60.4 degrees*	-60.9 degrees
Solar axis transit position (M-3)	270 degrees	270.5 degrees
Roll axis transit position (M-7)	0 degree	-1.15 degrees
Leg deflection signals, prelaunch:		
Leg 1 (V-5)	24 degrees 0 BCD	25.4 degrees 2 BCD
Leg 2 (V-6)		23.6 degrees 1 BCD
Leg 3 (V-7)		23.4 degrees 2 BCD
Leg deflection signals, postlaunch:		
Leg 1 (V-5)	0 degree 950 BCD	0.00 degree 950 BCD
Leg 3 (V-6)	0 degree 953 BCD	0.17 degree 946 BCD
Leg 3 (V-7)	0 degree 953 BCD	-0.15 degree 959 BCD

*Solar thermal vacuum test phase 1A.

Table 5.11-3 shows the positions of the A/SPP axis before and after the automatic solar panel deployment. These all fall within the required limits when corrections are applied to the telemetry data.

TABLE 5.11-3. A/SPP AXIS POSITIONS FOR PRELAUNCH AND POST-AUTODEPLOYMENT CONDITIONS

	Prelaunch*				Post-autodeployment, Transit**			
	Raw Data		Corrected Data		Raw Data		Corrected Data	
	BCD	Indicated Angle, degrees	BCD	Angle, degrees	BCD	Indicated Angle, degrees	BCD	Angle, degrees
M-3 solar axis	937	356.8	934.7	355.4	721	271.1	720.1	270.5
M-4 polar axis	259	0.21	258.7	0.07	259	0.21	259.0	0.12
M-6 elevation axis	493	-0.01	492.1	-0.63	493	-0.01	492.5	-0.42
M-7 roll axis	345	-60.49	344.5	-60.90	495	-0.77	494.5	-1.15
S-1 reference voltage	1003	–	–	–	1002	–	–	–
S-2 reference return	0	–	–	–	0	–	–	–
S-5 commutator unbalance current	99	–	–	–	99	–	–	–

Note: Nominal reference voltage, 1000 (BCD)

*Prelaunch data time 311:07:19:41.556

**Post-autodeployment data time 314:00:09:20.505

Postlanding Performance

Table 5.11-4 presents the complete record of stepping commands during lunar operations. It also includes a statement of the functions being performed during stepping. Figure 5.11-2 presents this in graphical form.

Table 5.11-5 provides the number and direction of step commands sent for each A/SPP gimbal axis.

Drive Stepping Response

An evaluation of stepping count tallies for the first lunar day, as compared with telemetry readings, indicates that, as far as can be determined, the gimbal drives responded successfully to all commands.

TABLE 5.11-4. A/SPP STEPPING COMMAND LOG

Execution Time, day:hr:min	Command	Quantity	Function
314:02:55	403	876	Sun-earth acquisition
03:04	402	867	
03:13	405	470	
03:19	406	22	
03:21	402	231	
03:36	406	332	
03:40	403	387	
12:04	405	343	Fine positioning
12:07	402	72	
12:13	406	25	
12:19	402	60	
12:20	405	10	
12:22	401	10	
12:28	406	45	
12:30	405	15	
12:30	402	15	
12:31	401	30	
12:35	405	25	
12:36	402	15	
12:39	405	25	
12:42	401	22	
12:48	402	11	
12:49	405	2	
12:51	406	10	
13:07	406	345	
13:12	405	128	
13:14	406	32	
13:18	403	15	
13:24	404	40	
13:25	403	12	

Table 5.11-4 (continued)

Execution Time, day:hr:min	Command	Quantity	Function
314:19:35	405	91	Increase solar panel output
315:16:30	406	40	Decrease solar panel output
17:08	406	40	
19:22	401	469	
316:03:49	403	79	Reposition planar array
23:20	401	108	
23:20	410	36	
23:40	407	36	
317:14:16	401	36	
318:03:47	406	1016	Shade oxidizer relief valve
04:13	403	90	
04:21	401	361	
20:34	404	60	
319:02:57	403	20	
320:02:56	402	448	
09:46	406	144	Shade ASI and oxidizer tank 3
18:11	402	210	Shade oxidizer tank 3 and lower temperature on solar panel
18:15	410	8	
321:01:07	401	401	Shade engines 1 and 3; TV, relief valves, and ASI
01:30	405	1515	
03:37	405	651	
03:44	402	370	
05:53	405	58	
08:47	406	376	
08:53	401	289	

Table 5.11-4 (continued)

Execution Time, day:hr:min	Command	Quantity	Function
321:10:04	405	292	Step to fire safe position
10:12	404	358	
10:17	401	853	
10:46	402	571	Step to earth position
10:51	403	358	
12:59	405	70	
20:41	406	680	
322:06:25	406	482	
07:02	406	37	
07:03	405	519	
14:40	405	36	
15:30	404	45	
15:31	403	15	
18:21	405	416	
19:02	402	609	
19:32	405	48	
19:42	406	48	
19:44	404	40	
19:50	406	100	
323:07:44	405	58	
324:02:30	401	253	
02:30	406	145	
12:46	403	59	
12:51	405	37	
12:59	404	39	

Table 5.11-4 (continued)

Execution Time, day:hr:min	Command	Quantity	Function
324:13:24	401	37	
13:38	402	184	
13:43	406	20	
13:54	405	90	
18:49	401	432	Fine sun positioning
18:49	406	565	
18:49	403	30	
18:49	405	80	
19:15	403	24	Fine earth positioning
19:15	404	75	
19:15	405	759	
19:15	406	48	
325:09:46	406	56	
13:37	402	120	
20:35	406	400	
20:35	403	73	
20:35	405	400	
20:35	404	73	
326:04:12	406	171	
04:15	403	40	
04:18	406	397	
04:25	410	10	
04:30	406	600	
04:38	406	400	
04:43	406	400	
04:48	403	33	
04:49	410	44	

Table 5.11-4 (continued)

Execution Time, day:hr:min	Command	Quantity	Function
326:05:01	402	480	
06:04	401	40	
06:24	401	40	
20:23	402	30	
20:26	402	90	
327:07:01	402	120	
09:35	402	40	
328:10:09	402	120	
20:23	405	650	
20:29	404	17	
20:30	407	62	
20:31	401	650	
20:38	405	663	
20:44	401	308	
329:03:08	401	104	Reposition solar panel to second lunar day optimum position

TABLE 5.11-5. POSTLANDING A/SPP STEPPING COMMANDS SUMMARY

Axis	Solar		Polar		Elevation		Roll	
Direction	Plus	Minus	Plus	Minus	Plus	Minus	Plus	Minus
Command	0401	0402	0403	0404	0407	0410	0405	0406
Total	4443	4663	2111	747	98	98	7451	6976
Total plus and minus	9106		2858		196		14,427	
Grand total	26,587							

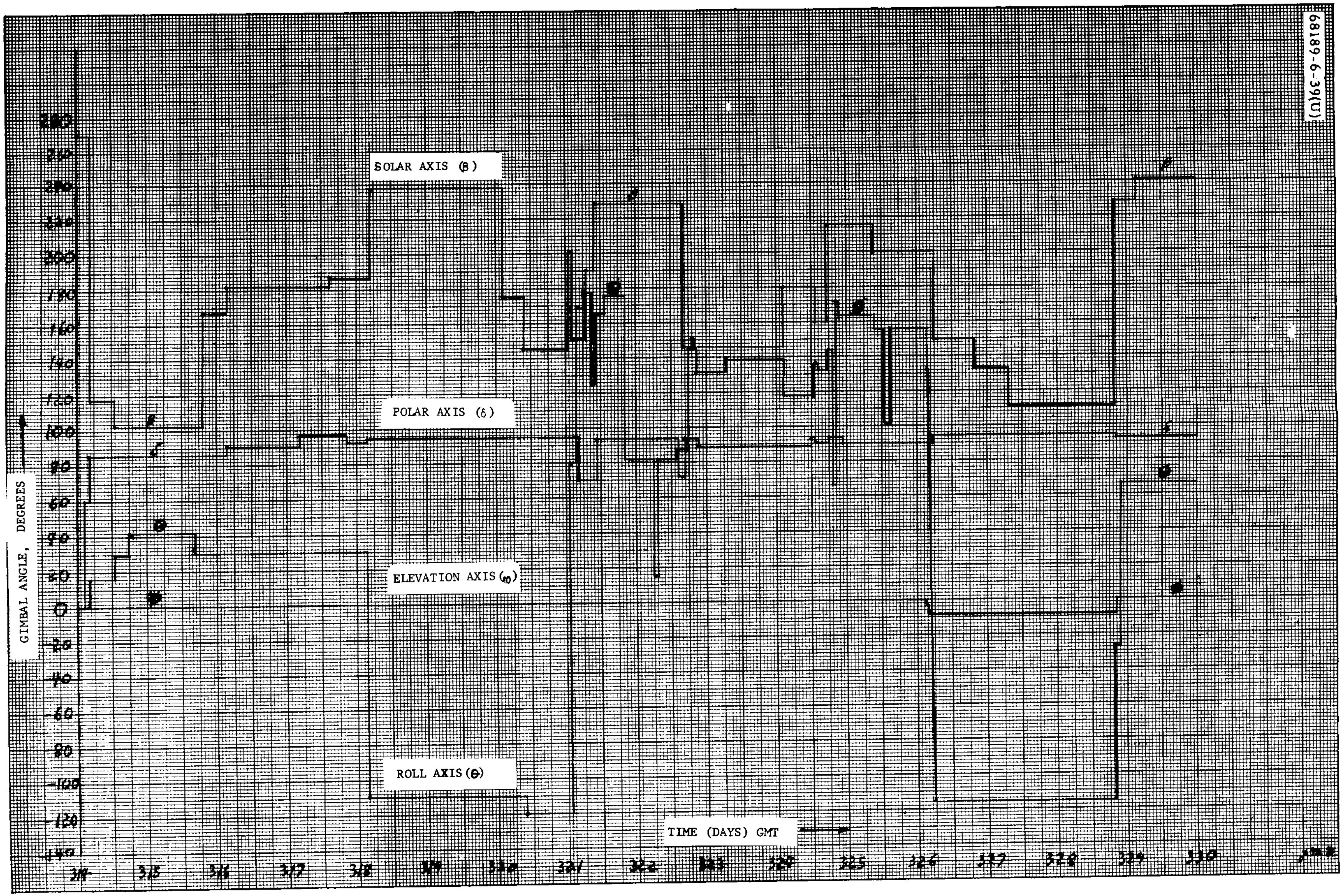

Figure 5. 11-2. A/SPP Gimbal Angles Versus Time During First Lunar Day

5.11.5 REFERENCES

1) "Surveyor VI Flight Path Analysis and Command Operations Report," Hughes Aircraft Company, SSD74176, 30 November 1967.

2) R.L. Lackman and W.R. Heathcote, "Error Analysis of the SC-3 Spacecraft Attitude on the Lunar Surface," Hughes Aircraft Company, IDC 2292/246, 4 April 1967.

5.11.6 ACKNOWLEDGMENTS

J.M. Berger, technical coordinator and author

L.L. Gamer, lunar performance analysis

5.12 TERMINAL DESCENT TRAJECTORY PERFORMANCE

5.12.1 INTRODUCTION

The terminal descent and landing phase begins with the transition from coast mode II to the terminal descent phase. Terminal descent itself starts with the preretro attitude maneuvers which reposition the attitude of the spacecraft from the sun-star reference so that the expected direction of the retro thrust vector will be aligned with respect to the velocity vector. This alignment achieves the desired retro burnout conditions. Following completion of the attitude maneuvers, the altitude marking radar (AMR) is activated. The AMR is preset to generate a mark signal when the range to the lunar surface is 60 miles. A backup mark signal, delayed a short interval after the time the AMR mark should occur, is transmitted to the spacecraft to initiate the automatic sequence in the event the AMR mark is not generated. The desired delay between the altitude mark and vernier ignition is stored in the flight control programmer by ground command. Retro engine ignition is automatically initiated 1.1 seconds after vernier ignition.

During the retro phase, spacecraft attitude is maintained in the inertial direction established at the end of the preretro maneuvers by the vernier attitude control system, and the total vernier thrust is maintained at mid-thrust. As the mass of the vehicle decreases due to expenditure of retro and vernier propellant, the spacecraft thrust to mass ratio (T/M) increases from approximately 4 g_e (g_e = 32.2 ft/sec^2) at ignition to 10 g preceding burnout. Prior to burnout, the inhibit is removed from the acceleration switch output, and the doppler radar and altimeter (RADVS) is activated.

As the thrust decays during retro burnout, the acceleration switch signals when the T/M level has dropped to 3.5 g_e. At this time, a counter in the flight control programmer is initiated and, after 10 seconds from this point, the vernier engines are commanded to high thrust. The explosive bolts attaching the retro to the spacecraft are activated 2 seconds following the high thrust command, allowing the retro case to separate from the spacecraft. Following a programmed delay of 2.15 seconds after separation begins, the vernier thrust command is changed from the open-loop mode to a closed-loop acceleration control mode. Nominal acceleration commanded at this point is 4.75 ft/sec^2.

Surveyor VI performance was near perfect; all events occurred according to specification. The preretro maneuvers properly oriented the spacecraft for the start of the retro phase sequence. The AMR mark occurred and the vernier engines ignited at the desired time delay of 5.9 seconds from AMR mark, indicating that the start of the terminal descent was generated by the true mark and not by the backup command. Approximately 23.5 seconds prior to the start of the RADVS-controlled descent, all three doppler velocity sensors acquired lock and remained reliable throughout the descent. The radar altimeter acquired lock approximately 1.5 seconds after the start of RADVS-controlled descent.

From postflight analysis, all spacecraft events and performances were near nominal, except for a larger than expected retro thrust misalignment during retro burn. However, the misalignment was within the maximum allowable. This situation is further discussed in subsection 5.12.4.5.

5.12.2 ANOMALY DESCRIPTION

There were no anomalies during this phase of the mission.

5.12.3 SUMMARY AND RECOMMENDATIONS

Table 5.12-1 lists the significant terminal descent events and time of occurrence. The DSS time is either plus or minus the one-way transit time delay (approximately 1.297 seconds), depending on whether the event is a command or a telemetered spacecraft action.

The significant terminal descent performance parameters are summarized in Table 5.12-2, along with the predicted values. From this table, it can be seen that Surveyor VI performed very well, except for the larger than expected retro thrust misalignment. This misalignment was the reason for differences in spacecraft velocities at the start of the RADVS-controlled descent (prediction and best estimation).

5.12.4 PERFORMANCE ANALYSIS

5.12.4.1 Introduction

The Surveyor VI terminal phase performance has been investigated and analyzed by comparing processed telemetry data by the PREPRO program (described in paragraph 5.12.4.2 along with other postflight analysis computer programs) with a precision six degree of freedom (6DOF) digital simulation reconstruction. Various nominal predicted preflight and preterminal in-flight parameters within the 6DOF were adjusted so as to coincide discrete time events with discrete telemetry time events. These events provide the 6DOF program with significant data points for constructing a best-fit trajectory. Table 5.12-3 shows the discrete time events determined from telemetry data and compared with the best match reconstruction by the 6DOF program.

TABLE 5.12-1. BEST ESTIMATE TIMES FOR SURVEYOR VI TERMINAL DESCENT

Event	GMT, Day 314, min:sec	
	At DSS-14	At Spacecraft
Hour 00		
AMR mark	57:57.038 ± 0.05	57:55.741 ± 0.05
AMR backup command	57:56.400 ± 0.1	57:57,697 ± 0.1
Vernier engine ignition	58:02.938 ± 0.05	58:01.641 ± 0.05
Retro ignition	58:04.038 ± 0.05	58:02.741 ± 0.05
RADVS on	58:05.798 ± 0.6	58:04.501 ± 0.6
RODVS on	58:34.098 ± 0.6	58:32.801 ± 0.6
3.5 g switch	58:43.647 ± 0.05	58:42.350 ± 0.05
Start maximum thrust	58:53.297 ± 0.6	58:52.000 ± 0.6
Retro eject	58:55.637 ± 0.05	58:54.340 ± 0.05
Retro ejected	58:55.942 ± 0.255	58:54.645 ± 0.255
Start RADVS-controlled descent	58:57.737 ± 0.05	58:56.440 ± 0.05
RORA on	58:59.297 ± 0.6	58:58.000 ± 0.6
Segment intercept	59:21.276 ± 0.14	59:19.979 ± 0.14
Hour 01		
1000-foot mark	00:40.534 ± 0.05	00:39.237 ± 0.05
10-fps mark	00:57.634 ± 0.05	00:56.337 ± 0.05
14-foot mark	01:04.133 ± 0.05	01:02.836 ± 0.05
Touchdown	01:05.467 ± 0.003	01:04.226 ± 0.15

TABLE 5.12-2. SUMMARY OF TERMINAL DESCENT PERFORMANCE PARAMETERS

Parameter	Predicted Value	Best Estimated Value
Vernier ignition conditions		
Time, hr:min:sec	00:58:01.96	00:58:01.641
Altitude, feet	240,787	239,484
Velocity, fps	8,488.9	8,489.0
Attitude, degrees	24.4	24.5
Misalignment angle during retro		
In-plane, degrees	0	0.632
Out-of-plane, degrees	0	0.488
Start RADVS-controlled descent		
Altitude, feet	37,005	36,625
Total velocity, fps	482	515
V_x	36	0.0
V_y	105	224.6
V_z	468	463
Attitude, degrees	25.29	25.4
Flight path angle, degrees	10.82	8.1
Retro burn time, seconds	39.88	39.57
Segment intercept conditions		
Slant range, feet	23,000	24,730
Velocity (V_z), fps	494	522
1000-foot mark conditions		
Slant range, feet	1,000	1,000
Total velocity, fps	106	106.1
V_z	—	106.0
Attitude, degrees	1.3	1.04
10-fps mark conditions		
Slant range	43.0	50.0
Velocity (V_z), fps	8.6	10.0
Attitude, degrees	0.02	0.03
Vernier engine cutoff conditions		
Slant range, feet	13.0	14
Velocity (V_z), fps	5.02	5.01
Attitude, degrees	0.01	0.03
Touchdown conditions		
Longitudinal velocity, fps	12.5	12.5
Lateral velocity, fps	0.0	0.0
Total vernier propellant used, pounds	143.61	146.33

TABLE 5.12-3. 6DOF DISCRETE TIME EVENTS VERSUS TELEMETERED

Event	6DOF Time (Figures 5.12-7 to 5.12-14), seconds	GMT, Day 314, min:sec	
		Converted Figure Time to GMT	Actual GMT at DSS-14
Hour 00			
Vernier engine ignition	0.0	58:02.938	58:02.938 ± 0.05
Retro ignition	1.1	58:04.038	58:04.038 ± 0.05
RODVS on	31.0	58:33.938	58:34.098 ± 0.6
3.5 g mark	40.73	58:43.668	58:43.647 ± 0.05
Start maximum thrust	50.73	58:53.668	58:53.297 ± 0.6
Retro eject	52.74	58:55.678	58:55.637 ± 0.05
Start RADVS-controlled descent	54.88	58:57.818	58:57.737 ± 0.05
RORA on	56.4	58:59.338	58:59.297 ± 0.6
Segment intercept	78.3	59:21.238	59:21.276 ± 0.14
Hour 01			
1000-foot mark	157.53	00:40.468	00:40.534 ± 0.05
10-fps mark	174.89	00:57.828	00:57.634 ± 0.05
14-foot mark	181.61	01:04.548	01:04.133 ± 0.05
Touchdown	183.00	01:05.938	01:05.523 ± 0.15

The one-way doppler data, as received by the tracking station, provides information for reconstructing a highly accurate retro thrust-time curve. These data, utilized by the DOPP program, also allow determination of the retro specific impulse, retro performance, and characteristic velocity (total ΔV removed) during the retro and vernier phases. From the retro accelerometer telemetry data, a thrust-time curve is also reconstructed by the TTC program, and comparison is made with the DOPP program reconstruction.

The doppler data are also utilized to determine the radial velocity (the velocity in the direction of the earth tracking station-spacecraft line of sight). The same parameter is computed within the 6DOF program. The two methods of reconstructing the radial velocity are then compared, thus providing an additional confidence measurement in the 6DOF reconstruction.

The total vernier propellant consumption is determined by utilizing vernier engine flight acceptance test data of mixture ratio and specific impulse as a function of vernier engine thrust for the midcourse, retro, and vernier phases. The spacecraft landing location is determined from postflight orbit determination data.

The best-estimate terminal descent trajectory reconstruction scheme employed for Surveyor VI was similar to that of previous successful flights. Again, the scheme depends on establishing a good reference point near the end of the retro phase in which the spacecraft V_x, V_y, and V_z telemetry data are reliable. The point selected was at the start of the RADVS-controlled descent in which all three doppler velocity sensor beams were reliable. Based on postmission assessment of the RADVS and telemetry system, the calibrated V_x, V_y, and V_z velocities at the start of the RADVS-controlled descent were determined to be:

$$V_x = 0.0 \text{ fps}$$

$$V_y = 224.6 \text{ fps}$$

$$V_z = 463.0 \text{ fps}$$

These values are corrected for biases determined in the telemetry data as indicated in subsection 5.12.4.9.

With the DOPP program retro thrust-time curve as input into the 6DOF program, the initial conditions at vernier ignition of velocity, altitude, and retro thrust vector misalignment (as determined from orbit determination postflight data) were perturbed within the 6DOF program until the above velocities at the start of the RADVS-controlled descent and the elapsed time from start of RADVS-controlled steering to the command descent contour intercept (as indicated by telemetry) and the 1000-foot mark were matched.

With the velocities at the start of RADVS-controlled descent and the discrete time events matched, the 6DOF reconstruction provided a fairly close comparison to the telemetry data. Therefore, the 6DOF reconstruction was considered a good estimate of the actual Surveyor VI performance. This reconstruction is discussed further in paragraph 5.12.4.9.

5.12.4.2 Postflight Analysis Computer Programs

PREPRO

The PREPRO program converts an input tape of processed telemetry data into appropriate engineering units. The tape is preprocessed by Hughes into raw BCD counts and appears in commutator sequence. The spacecraft preflight telemetry calibration coefficients are utilized within the program for the conversion into engineering units. Prior to the conversion, the flight control reference return (FC-77 telemetry signal) correction is made to the appropriate signals. The program interpolates engineering data significant to terminal descent reconstruction into preselected equal time intervals. PREPRO then writes two output tapes: tape No. 1 of the interpolated engineering data, and tape No. 2 of all the input signals in proper engineering units as they appear in commutator sequence.

POSTPR

POSTPR provides machines plots (CALCOMP) of any combination of variables from the following input data tapes: PREPRO tape No. 1, 6DOF data tape, and both PREPRO tape No. 1 and the 6DOF tape, thus providing a superimposed plot of the best estimated 6DOF reconstruction and the telemetered data.

6DOF

6DOF is a precision six degree of freedom digital program simulating the Surveyor terminal phase from vernier ignition to touchdown. The program assumes rigid body dynamics, including spacecraft weight and moment of inertia changes. The program also models the spacecraft flight control and radar subsystems. The flexibility of the data input is such that preflight and postflight reconstructions of the terminal phase can be made. By matching significant time events with telemetry discrete times, a fairly accurate reconstruction of the terminal phase trajectory can be established by the 6DOF program in the absence of gross system errors or telemetry errors in spacecraft V_x, V_y, and V_z velocities. The program outputs are velocity, position, acceleration, attitude, moments, weight, inertia, angular velocity, control loop states, engine commands and thrusts, and radar system states. The program also writes a tape that can be used for machine plots (CALCOMP) of any combination of variables. The tape can also be set up for input into the POSTPR program.

TD1

TD1 is a two-dimensional, three degree of freedom simulation of the terminal phase of the Surveyor mission. The main use of TD1 is to determine the vernier propellant consumption. The program can also be used to a limited extent for terminal descent trajectory reconstruction since it is restricted to a planar case. However, the program models the spacecraft to the extent necessary for accurate propellant consumption determination, that is, if no apparent degradation appears in the vernier engine performance.

TTC

TTC reconstructs the retro thrust-time curve from raw accelerometer telemetry data. Corrections are made to the telemetry data by removing bias, scale factor, and hysteresis errors. This reconstruction is used for comparison with the DOPP program reconstruction.

DOPP

DOPP reconstructs the main retro thrust-time curve from the spacecraft transmitter's one-way doppler data. This reconstruction technique is especially accurate since the frequency of the spacecraft transmitter is very stable. The program accounts for errors introduced by the transmitter's temperature sensitive drift, variation in retro thrust vector direction during retro burn, and flight control sensor deflection. The program is also utilized for determining the main retro specific impulse and the characteristic velocity (total ΔV removed) during the retro and vernier phases.

5.12.4.3 Velocity Change Due to Thrusting During Retro Phase

Determination of Ignition Conditions

Ignition velocity V_o, flight path angle γ, and roll angle φ serve as initialization parameters and are determined from tracking data. The 3σ uncertainty in free flight velocities is <0.5 fps. Since ignition altitude has a calculated 3σ inaccuracy of 1640 feet due to marking range errors (with a $V_o = 8500$ fps and an incidence angle with respect to local vertical of 25 degrees), the equivalent ignition velocity uncertainty due to this error source is

$$\Delta V = g \cos \gamma \, t = 5 \times \frac{1640}{8500} = 1.0 \text{ fps}$$

Hence, the total uncertainty in ignition velocity is 1.1 fps when these two independent error sources are combined. The direction of V_o at ignition has an uncertainty of <0.07 degree. Therefore, the best estimate ignition conditions are

$$V_o = 8488.9 \pm 1.1 \text{ fps}$$

$$\gamma_o = -65.6 \pm 0.07 \text{ degree}$$

Gravity-Induced Component of Velocity

During the retro phase (from vernier ignition to start of RADVS-controlled descent), gravity contributes to the spacecraft velocity by an amount $\int \underline{g}\, dt$. Lunar gravity varies in magnitude from 4.92 ft/sec^2 (at vernier ignition) to 5.27 ft/sec^2 (at start of RADVS). In addition, $\underline{g}$ varies in direction since the spacecraft has horizontal motion. The change in direction of $\underline{g}$ over the retro phase (to RADVS control) is about

$$\int_0^t \sin^{-1}\left[\frac{V \sin \psi \, dt}{R_{\ell}}\right] = 0.89 \text{ degree}$$

where

t = retro time

ψ = velocity vector

V = spacecraft velocity incidence angle

R_{ℓ} = moon centered radial distance

The time duration of the retro phase is 54.8 seconds (see Table 5.12-1). Actual numerical integration of $\int g\, dt$ gives dt = 283.7 ± 1 fps.

Thrust-Induced Velocity Change

The two methods used to calculate velocity change during the retro phase due to the thrusting of the engines are as follows:

1) ΔV from vector addition — The vector equation (Figure 5.12-1a) $\underline{V}_{BO} = \underline{V}_o + \underline{gt} + \underline{\Delta V}$ can be solved to find $\underline{\Delta V}$. $\underline{V}_o$ and $\underline{gt}$ are available as discussed above; the spacecraft axis components of $\underline{V}_{BO}$ (the velocity at start of RADVS) are available from calibrated telemetry data. The axial velocity V_z is known to an estimated accuracy of better than 1 percent at a given time, based on correlation of simulated versus actual discrete time events such as the 1000-foot mark and the 10-fps mark. V_x and V_y at start of RADVS-controlled descent have calculated uncertainties of 3.0 and 4.6 fps, respectively, based on 3σ telemetry and RADVS sensor errors. At the start of RADVS-controlled descent, the velocity components are:

$$V_{BO_x} = 0.0 \pm 3 \text{ fps}$$

$$V_{BO_y} = 224.6 \pm 4.6 \text{ fps}$$

$$V_{BO_z} = 463 \pm 4.6 \text{ fps}$$

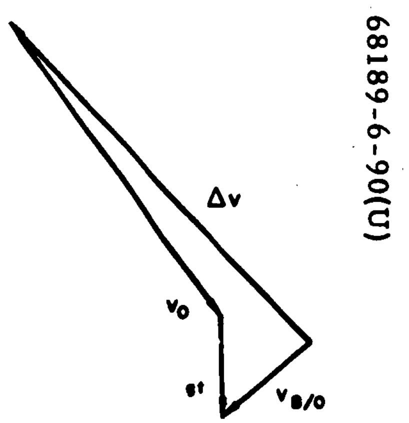

a) Vector Diagram

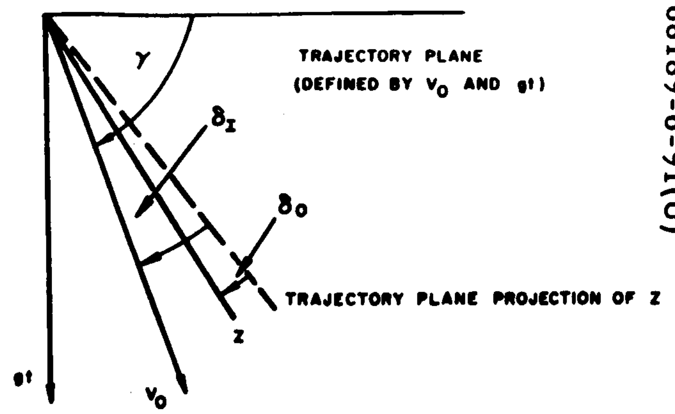

b) Trajectory Plane

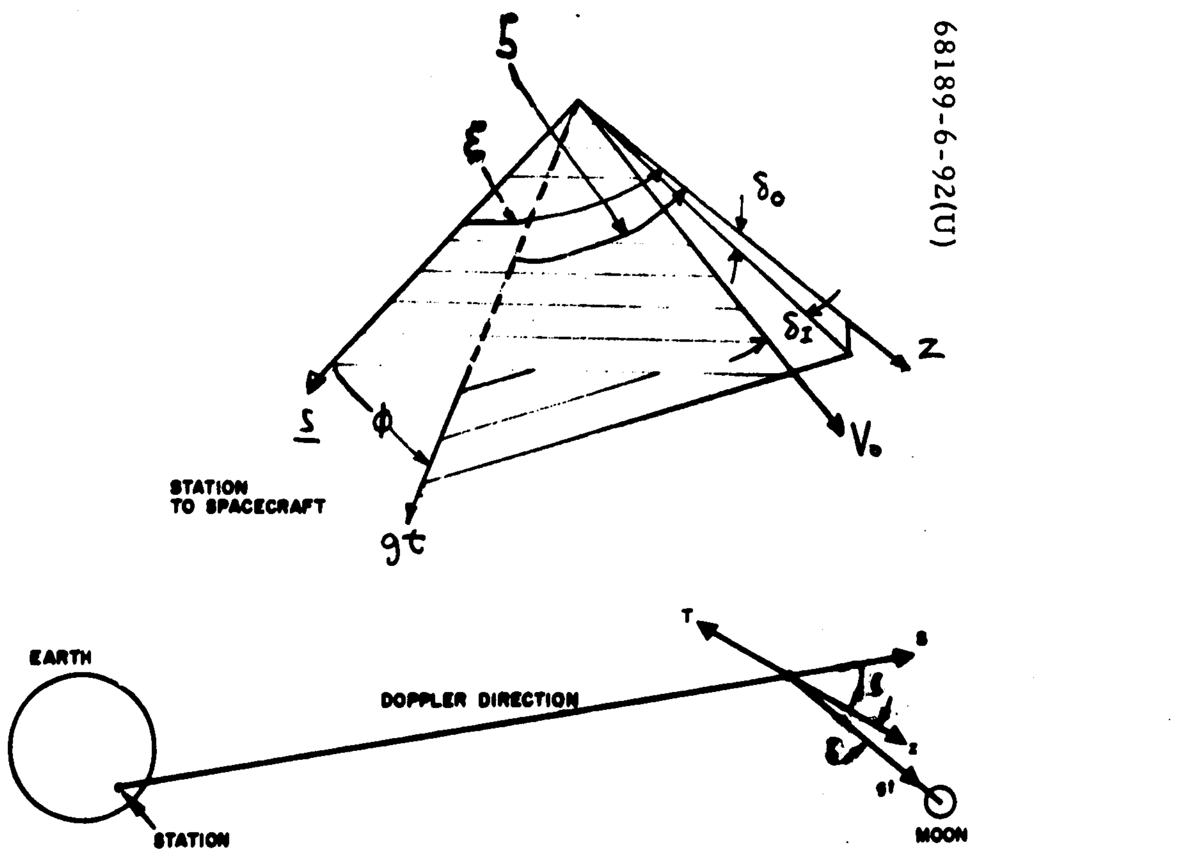

c) Doppler Geometry

Figure 5.12-1. Spacecraft Velocity During Retro Phase

This method will yield ΔV to an accuracy of ±5.0 fps. δi, the in-plane thrust misalignment angle (Figure 5.12-1b) between $\underline{V}_o$ and z, defined as positive when z is "above $\underline{V}_o$" as shown, is known to be within ±0.02 degree based on uncertainties in V_{BO_x}, which is primarily in-plane. δo, the out-of-plane angle between these two directions, is known to be within ±0.03 degree based on uncertainties in V_{BO_y}. δo is positive when z has a component out of the paper. This method yields ΔV at the start of RADVS-controlled descent of

$$\Delta V = 8273.6 \pm 5.0 \text{ fps}$$

also,

$$\delta i = +0.632 \pm 0.02 \text{ degree}$$

$$\delta o = +0.488 \pm 0.03 \text{ degree}$$

$$\text{total misalignment} = 0.798 \pm 0.036 \text{ degree}$$

Values of the other angles in degrees shown in Figure 5.12-1c are as follows:

$$\xi = 33.98$$

$$\zeta = 24.93$$

$$\varphi = 11.41$$

2) ΔV from doppler data — The thrust-induced velocity change of the spacecraft is determined from the spacecraft one-way doppler data by the DOPP program. These data are input into DOPP and are corrected for the transmitter's temperature-dependent frequency drift within the program. This correction is determined by comparing postflight doppler data prior to vernier ignition with a simulated determination of the expected doppler shift since, at this period in the flight, the actual doppler shift is well defined.

The ΔV during this phase is found by dividing the sum of the radial velocity change as determined from the doppler data and the gravity-induced velocity component in the same radial direction by the cosine of the angle between the tracking station-spacecraft line and the spacecraft thrust axis. A correction is made to the doppler data to account for the radial velocity change, ΔV_{ROT}, due to the earth's rotation. The thrust-induced velocity change, ΔV, can therefore be determined as follows:

$$\Delta V = \frac{\Delta V_{DOPP} + gt \cos \varphi + \Delta V_{ROT}}{\cos \xi}$$

where

ΔV_{DOPP} = velocity change seen by tracking station

φ = angle between tracking station-spacecraft line and lunar gravity direction

ξ = angle between tracking station-spacecraft line and thrust direction

Therefore,

$$\Delta V = \frac{6579 + 278.2 + 4.2}{\cos 33.98} = 8274.4 \text{ fps}$$

An uncertainty exists in the angle ξ of ±0.04 degree due to uncertainties in δi and δo, the thrust misalignment angles. An uncertainty also exists in the temperature-dependent doppler frequency drift of ±5 fps. The above uncertainties result in an uncertainty of ±8 fps in ΔV.

Comparison of ΔVs and Retro Performance Implications

It is interesting to note that not only do the absolute magnitudes of ΔV check surprisingly well, but, out of necessity, so does the inertial thrusting direction as computed from burnout conditions. The doppler data are inherently one-dimensional and, to be useful in computing the retro thrust ΔV, the angular information supplied by the vector addition method of computing ΔV must be accurate. Thus, due to the geometric relation of the earth vector and trajectory plane, an uncertainty of 0.1 degree in the in-plane angle (δi) would cause an 8.0-fps variation in the total ΔV as computed by doppler. Since the two ΔVs check to within 1 fps, this would give added confidence in the thrusting direction computed from the telemetered and corrected burnout conditions.

Assuming a nominally performing main retro and vernier system, the main retro phase ΔV should have been 8279.8 fps as compared to 8274.0 fps actual (average of the two methods). Of the nominal 8279.8 fps total ΔV, a nominal performing vernier system would have contributed 290.3 fps. Based on a retro phase trajectory reconstruction by DOPP, the nominal vernier system would have contributed 289.0 fps due to the slight decrease in actual time from vernier ignition to the beginning of RADVS control from that predicted.

The retro performance, based upon the ΔV which it took out, was very nearly nominal. The slight decrease in actual total impulse over nominal ($\delta T_{imp}/T_{imp}$) is given by

$$\frac{\delta T_{imp}}{T_{imp}} = \frac{\delta \Delta V}{\Delta V retro} \times 100 \text{ percent}$$

$$= \left(\frac{8274 - 289.0}{8279.8 - 290.3} - 1 \right) \times 100 \text{ percent} = 0.06 \text{ percent loss}$$

The above percent decrease in total impulse results in a retro specific impulse of 289.19 seconds as compared to the nominal predicted value of 289.35 seconds. The predicted and calculated specific impulses are both computed from a retro propellant weight which is corrected for buoyancy.

5.12.4.4 Main Retro Thrust Versus Time Curve

Two independent methods used to calculate the retro's thrust versus time curve are as follows:

1) Thrust/time from retro accelerometer data — Before being used to calculate a thrust curve, the raw accelerometer data are given the following three corrections:

   a) Biases are removed by comparing telemetered values with known values of acceleration which occur at times such as those prior to vernier ignition (zero g), after retro separation $\approx$ (0.9 g), etc.

   b) A scale factor error is removed. This is done by integrating the unbiased accelerometer data over time and comparing the resulting integral with the retro phase ΔVs found by the other two methods of computing ΔV described above. The scale factor is then the integral divided by the mean of the other two ΔVs. The unbiased acceleration divided by this scale factor is then assumed free of bias and scale factor errors.

   c) A hysteresis error is removed by actually determining two biases: one for the rising part of the acceleration curve, and the other for the falling part.

   The bias on each part of the curve can be removed to an accuracy of 0.1 g_{earth}, and the accuracy of the scale factor is 0.1 percent.

   The corrected acceleration a(t) is then used in the equation

$$T(t) = \frac{a(t)}{g_o} \left[W_o - \int_o^t \frac{T(t)}{I_{sp}} \, dt \right]$$

which is integrated numerically to obtain total thrust (W_o is weight at retro ignition). Vernier thrust is then subtracted to obtain the retro thrust.

I_{sp} for this calculation is found from the following relationship where W_L is the weight lost from retro ignition to burnout.

$$I_{sp} = \frac{\Delta V}{g_o \ \ell_n \dfrac{W_o}{W_o - W_L}}$$

Figure 5.12-2 shows the Surveyor VI thrust-time curve as determined from accelerometer data. Also shown is the predicted thrust-time curve along with the raw accelerometer data and the corrected accelerometer data.

2) Thrust/time from doppler data — Figure 5.12-3 shows the main retro thrust curve as constructed from doppler counts received at Goldstone. Also shown is the predicted thrust-time curve.

To construct the curve, a retro phase simulation trajectory program, using a nominal thrust curve, calculates nominal radial velocities relative to the tracking station and converts these to doppler counts that the station would receive from a stable spacecraft transmitter on a nominal trajectory.

The nominal thrust curve is then perturbed until the doppler data from the perturbed curve are arbitrarily close to the doppler data actually received. For each point considered on the thrust curve, a difference between actual and perturbed counts over a 1-second interval of two counts (i.e., about 0.4 fps) is considered close enough. In addition, the sum of such differences is constrained to be within 10 counts (2.2 fps).

Radial velocity divided by the cosine of the angle between the tracking station and the thrust direction (33.98 ± 0.04 degrees) gives total velocity. When $gt \cos \varphi$ is added, the remaining velocity differences are entirely due to thrusting and give the thrust acceleration. Multiplication by the mass then gives the thrust level.

Comparison of Two Methods for Retro Thrust/Time Curve

Both the doppler and accelerometer reconstructed curves agree well with the predicted curve, with both deviating from the predicted by generally less than 200 pounds. The accelerometer reconstructed curve appears rough because of accelerometer stiction.

The only discrepancy between the two reconstructions is an unexplained difference in the calculated burn time from retro ignition to the 3.5-g point.

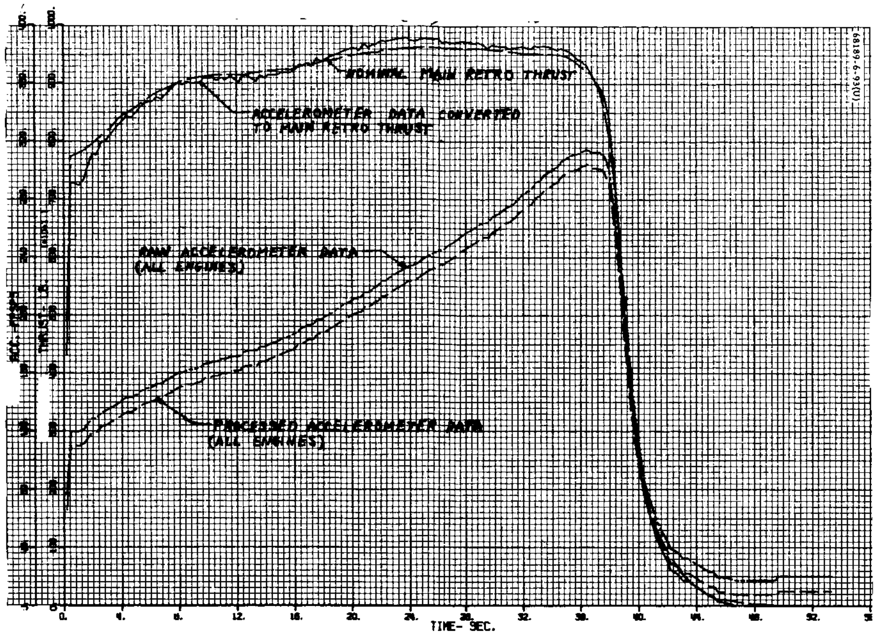

Figure 5. 12-3. Main Retro Thrust Versus Time (Doppler Data)

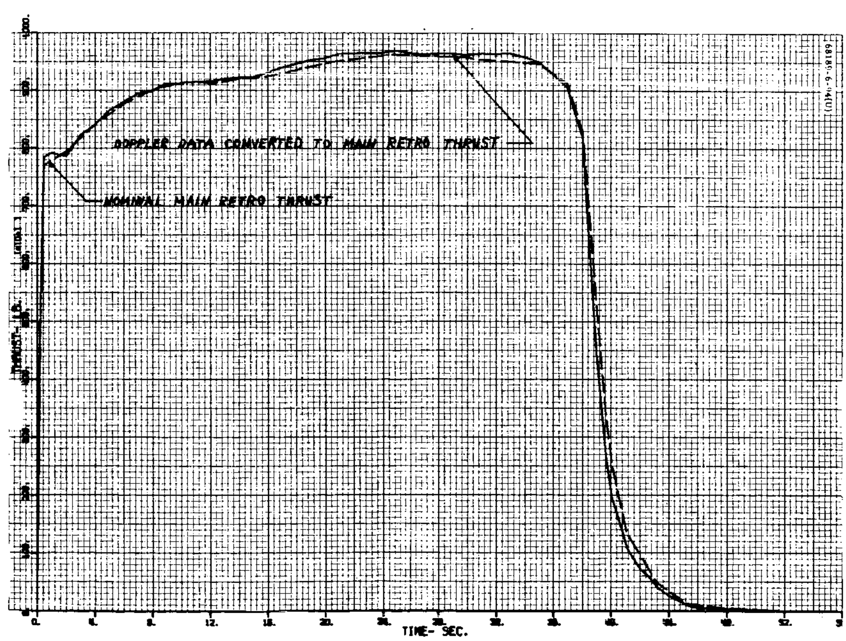

Figure 5. 12-2. Retro Phase Thrust and Acceleration Versus Time (From Retro Acclerometer Data)

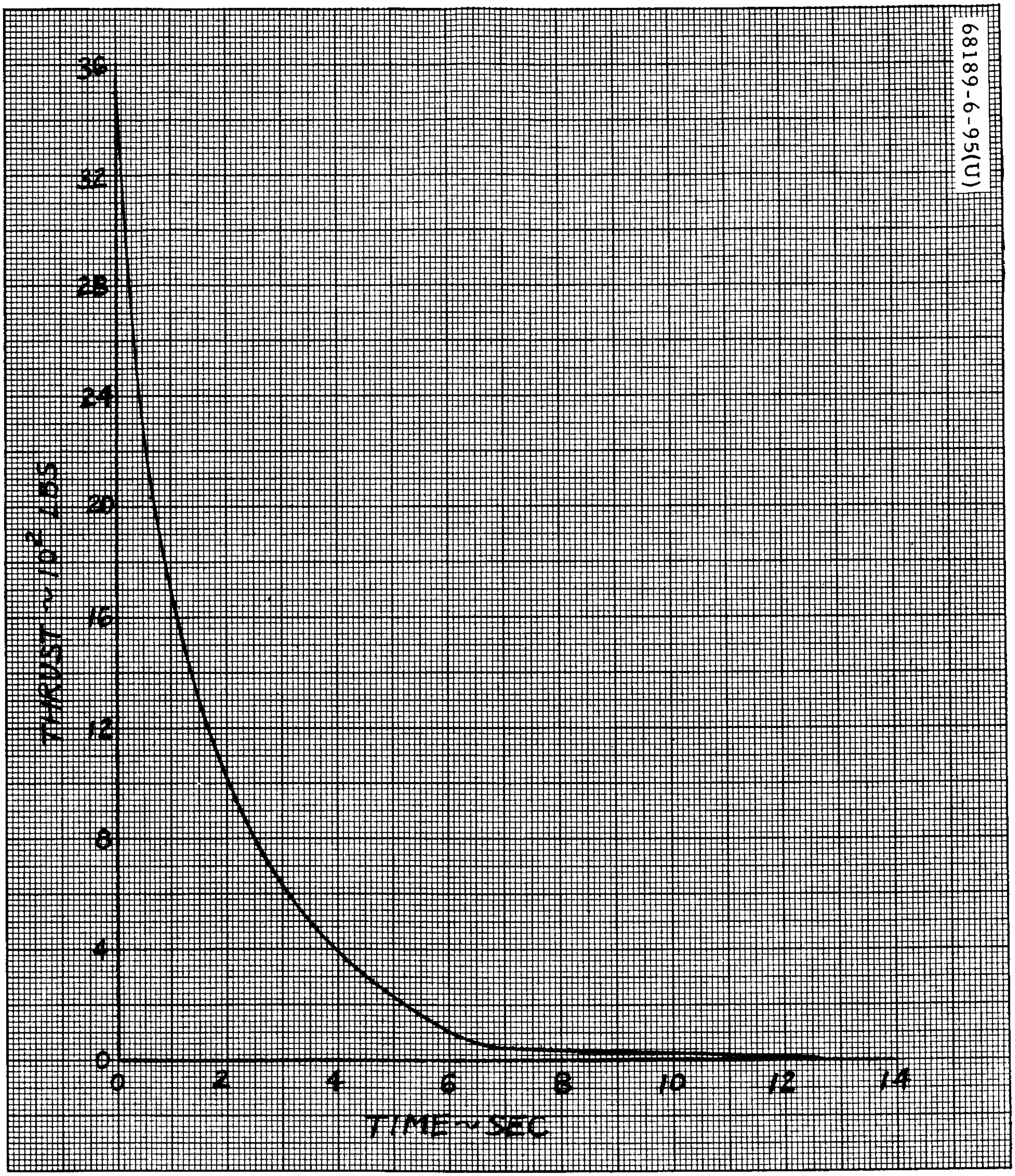

Figure 5.12-4. Main Retro Tailoff Versus Time
(Doppler Data)

The doppler reconstruction gives 39.52 ± 0.08 seconds as compared to 39.75 seconds from the accelerometer reconstruction. The predicted time was 39.88 seconds. The doppler reconstructed burn time of 39.52 seconds is believed to be the best reconstruction of burn time since it agrees with discrete telemetry events between the retro ignition signal and the retro burnout signal (39.6 ± 0.1 seconds).

The 39.52 seconds obtained from the doppler reconstruction is more accurate than the 39.6 seconds obtained from discrete telemetry events because the latter time is known to be slightly long since a small delay exists between the actual 3.5 g point and generation of the retro burnout signal.

Main Retro Tailoff from Doppler Data

Figure 5.12-4 shows an enlargement of the thrust tailoff region of Figure 5.12-3 (doppler reconstruction of main retro thrust). The data used in this reconstruction were first corrected for a constant temperature-dependent frequency drift which can be determined accurately by comparing preignition flight data to preignition simulated data. Since the data also contained a small random noise, it was then smoothed by fitting a second order curve through the data points since this tailoff shape has been determined from test results. If high frequency thrust oscillations were present during retro tailoff, the doppler data would not show it since these data are available only at 1-second intervals. However, the chance of such oscillations being present is small since all previous retro pressure test data have generally shown a smooth tailoff.

Assuming a normal noise distribution, the 1σ deviation (68 percent) of the data from this fitted curve was computed to be 1.82 doppler counts, which corresponds to a retro thrust deviation at any point of 13 pounds. However, the total integrated thrust after the 200-pound point has been reached is in error by 8 percent or less due to noise uncertainties which yield an average thrust error over the total length of the curve past the 200-pound point of less than 4 pounds.

5.12.4.5 Retro Thrust Misalignment

From postflight analysis, a larger than expected retro thrust misalignment of 0.798 degree during the retro phase was determined (previous spacecraft misalignments were <0.4 degree). This is the total misalignment due to a possible initial pointing error at retro ignition and attitude errors developed during the retro burn phase from such contributors as initial spacecraft center of gravity to thrust vector offset, retro thrust vector wander, larger than expected flight control sensor group deflections, and so forth. Figure 5.12-11, the vernier engine thrust command telemetry data, shows a definite center of gravity to thrust vector offset at retro ignition. The possible resultant pointing error at retro ignition determined from known measured errors is discussed below.

Resultant Pointing Error From Known Measured Errors

A digital program reconstruction of the actual terminal attitude maneuver simulating the initial attitude errors and measured gyro drift rates was used to determine any resultant attitude pointing error from these sources. The results indicate an ignition attitude error of approximately 0.26 degree.

A compilation of the data used in the analysis is given below and is documented in subsection 5.5 of this report.

Desired terminal attitude rotations (actual values in parentheses):

Roll = + 81.62 (81.82) degrees

Yaw = +111.67 (111.71) degrees

Roll = +120.55 (120.55) degrees

Sensor attitude errors:

Roll = -0.06 degree (Canopus sensor)

Yaw = +0.20 degree (primary sun sensor)

Pitch = 0.0 degree (primary sun sensor)

Final preignition measured gyro drift rates:

Roll = -0.64 deg/hr

Yaw = +1.4 deg/hr

Pitch = 0.0 deg/hr

Computation of the desired attitude rotations was based upon a determination to compensate for the attitude pointing error due to the gyro drift rates. This was done by computing rotations such that implementation of these rotations in the presence of the gyro drift rates would essentially lead to no pointing error. Hence, it is noted that the 0.26-degree pointing error obtained in this analysis is primarily due to the 0.2-degree error in the first roll rotation and to the 0.2-degree offset in the yaw reference at initiation of the yaw rotation due to limit cycle error. Uncertainties of approximately 10 percent in the determination of the drift rates and limit cycle errors lead to a maximum attitude error of approximately 0.35 degree. In this analysis, a uniform 0.5 deg/sec rotation rate was assumed. During the mission, the roll rate was measured and determined to be 0.5009 deg/sec.

5.12.4.6 6DOF Simulation of Doppler Data

The 6DOF determination of radial velocity relative to the moon (velocity component along the earth tracking to spacecraft vector), as compared to the doppler data reconstruction of this velocity, is shown in Figures 5.12-5 and 5.12-6 for the retro and vernier phases. As can be seen in the figures, excellent matches are obtained for both phases of the descent. This close correlation increases the confidence in the 6DOF reconstruction.

The maximum and minimum spacecraft accelerations can be determined from vernier phase doppler data by the equation

$$a_{dopp} = g \cos \varphi - a \cos \xi$$

where

a_{dopp} = doppler acceleration (slope of doppler curve)

φ = angle between lunar gravity and tracking station to spacecraft direction

a = actual spacecraft acceleration

ξ = angle between spacecraft thrust direction and tracking station to spacecraft direction

Thus,

$$a = \frac{g \cos \varphi - a_{dopp}}{\cos \xi}$$

In determining the minimum spacecraft thrust acceleration, a_{min}, the value for a_{dopp} is taken during the minimum acceleration phase just prior to first segment acquisition.

$$a_{min} = \frac{5.29 \cos 10 \text{ degrees} - 0.523}{\cos 17 \text{ degrees}} = 4.90 \text{ ft/sec}^2$$

The 6DOF simulation used a value for the nominal minimum thrust acceleration command of 4.75 ft/sec^2 which resulted in a simulated thrust acceleration value of a_{min} = 4.82 ft/sec^2.

The value of a_{dopp} used in determining the maximum spacecraft thrust acceleration, a_{max}, is taken just after the second segment intercept since the spacecraft acceleration is saturated for a period of time along the second segment.

$$a_{max} = \frac{5.30 \cos 10 \text{ degrees} + 6.95}{\cos 14 \text{ degrees}} = 12.52 \text{ ft/sec}^2$$

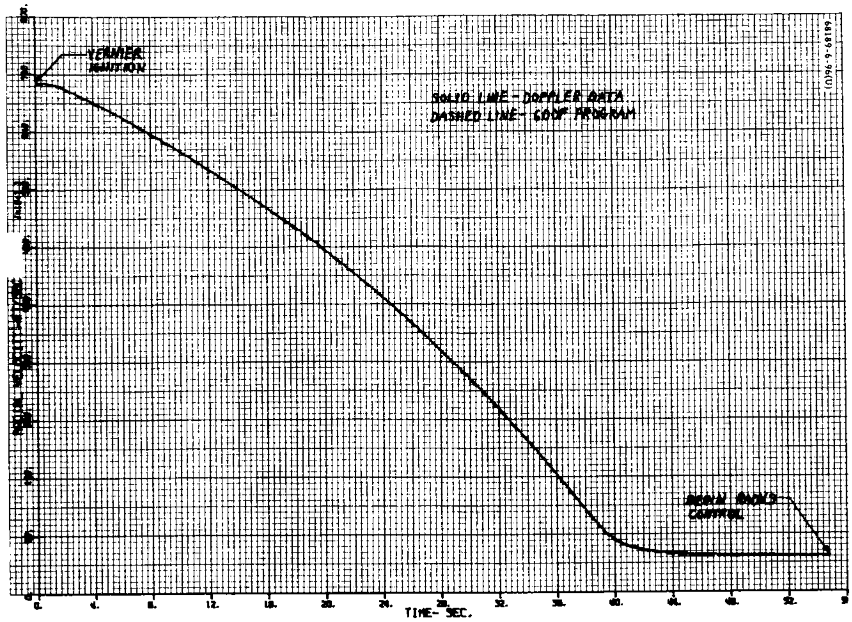

Figure 5. 12-5. Radial Velocity — Retro Phase Doppler Data

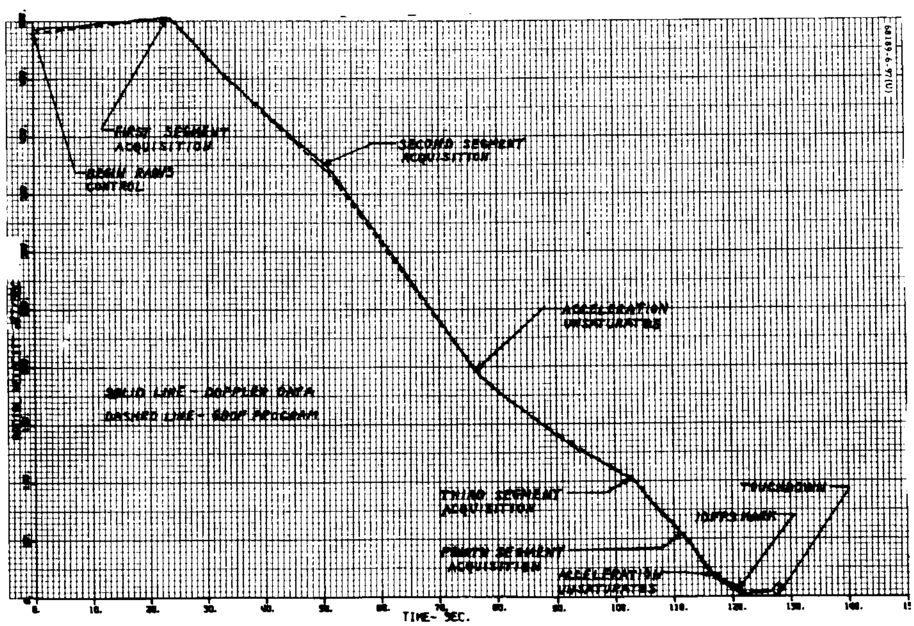

Figure 5. 12-6. Radial Velocity — Vernier Phase Doppler Data

The 6DOF simulation used a value for the nominal maximum thrust acceleration command of 12.47 ft/sec^2, resulting in a simulated thrust acceleration of a_{max} = 12.41 ft/sec^2.

5.12.4.7 Vernier Propellant Consumption

Table 5.12-4 presents a tabulation of the propellant consumption from the individual engines based on vernier engine flight acceptance test data of both specific impulse and mixture ratio as a function of engine thrust.

For the midcourse and retro phases, the propellant consumption was obtained from the TD1 program. This program models all three engine flight acceptance performance characteristics individually. For the vernier phase portion, the propellant consumption was determined from the best-estimate 6DOF program reconstruction. However, the 6DOF program assumes that all three engines have the same specific impulse and mixture ratio performance. The input of the engine performance characteristics to the 6DOF program was the average performance of the three Surveyor VI vernier engine flight acceptance test data.

TABLE 5.12-4. VERNIER PROPELLANT CONSUMPTION (POUNDS)

Phase	Engine 1	Engine 2	Engine 3	Total	Preterminal Mission Predictions
Midcourse	2.90	2.74	2.73	8.37	8.37
Main retro	14.29	13.46	13.38	41.13	41.22
Vernier phase	32.93	32.67	31.23	96.83	94.02
Total used	50.12	48.87	47.34	146.33	143.61
Total loaded	61.51	61.51	61.51	184.53	184.53
Trapped (lines and expulsion efficiency)	0.71	0.71	0.71	2.13	2.13
Usable loaded (total minus trapped)	60.80	60.80	60.80	182.40	182.40
Remaining propellant (usable and unusable)	10.68	11.93	13.46	36.07	38.79

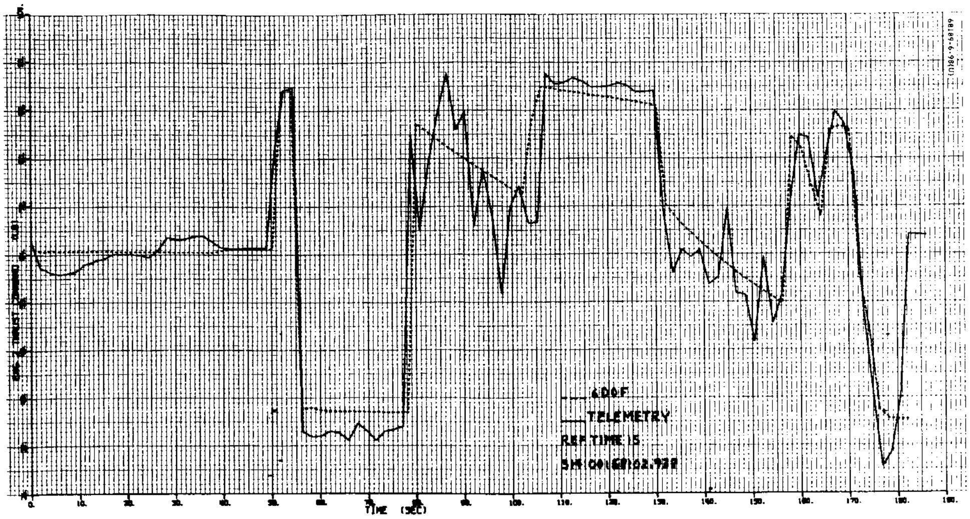

a) Engine 2

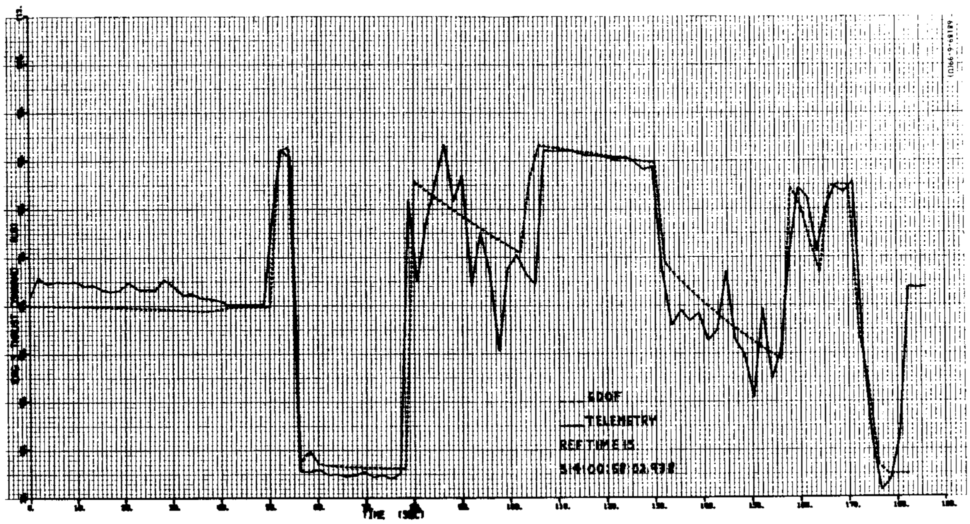

b) Engine 3

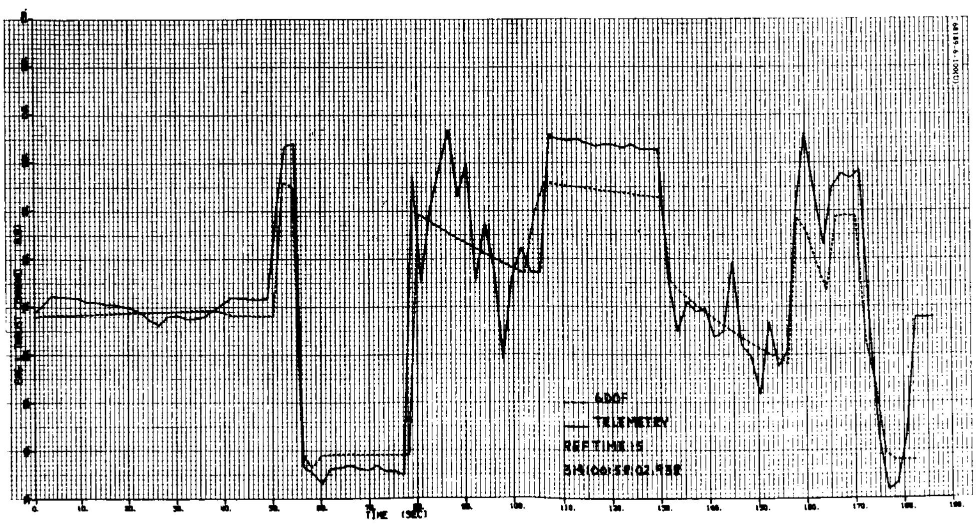

c) Engine 1

Figure 5.12-7. Vernier Engine Thrust Commands

The propellant consumption for the midcourse maneuver was based on postflight determination of burn time and preflight data of engine thrust for the midcourse maneuver.

The main retro phase propellant consumption computations are inherently the most inaccurate because of the open-loop nature of the thrust commands. While at midcourse, the change in spacecraft velocity is a very accurate measure of engine impulse; during the retro phase, the main retro engine overshadows any expected variation in vernier performance.

The telemetered values of engine thrust commands disagreed with premission computations of the vernier engine total thrust level of 196.4 pounds during retro burn and 276.4 pounds during retro separation.

The 6DOF program assumed the premission calculation of vernier engine thrust levels, and the difference between telemetry data and the premission values can be seen in Figure 5.12-7. The 6DOF program assumed preflight calculations of spacecraft center of gravity and retro thrust vector offset at the start of the retro phase sequence. The 6DOF models the center of gravity change during the terminal descent. Figures 5.12-7a and 5.12-7b show almost identical commands between the 6DOF reconstruction and the telemetry data: however, the engine 1 (Figure 5.12-7c) thrust command does not compare in magnitude during command of high and low thrust. These comparisons imply that the telemetry data are probably in error with respect to the actual engine thrust levels. Consequently, the total engine thrust level during the retro phase was assumed to be equal to the premission calculations for the propellant consumption calculations. Further discussion is given in subsection 5.12.4.9.

5.12.4.8 Spacecraft Landing Location

The original targeted landing site for Surveyor VI was 0.417°N latitude and 1.133°W longitude. The computed midcourse maneuver to enable the spacecraft to land at the desired landing site was 10.06 m/sec. Based on orbit determination postflight analysis data, the computed landing site was determined to be 0.437°N latitude and 1.373°W longitude. This results in a miss of 7.2 km from the original targeted landing site. However, a review of the Lunar Orbiter and Surveyor VI photographs of the touchdown area revealed the probable landing site to be 0.470°N latitude and 1.480°W longitude. From this determination, a miss of 10.5 km is indicated.

5.12.4.9 Trajectory Reconstruction

This subsection discusses the reconstruction of the vernier phase of the terminal descent trajectory from the 6DOF program to provide a best estimate of the actual trajectory parameters. The DOPP program reconstruction of the retro thrust-time curve was input into the 6DOF program. The DOPP reconstructed retro burn time (from retro ignition to the 3.5-g point) was 39.52 ± 0.08, which is the same time duration as indicated by telemetry data (see Table 5.12-1). The nominal Surveyor VI subsystem parameters from preflight assessment were input to the 6DOF program.

Initial conditions at vernier ignition of velocity, altitude, and retro thrust vector misalignment, as determined from orbit determination postflight data, were perturbed until the start of the RADVS-controlled descent conditions of velocity coincided with the calibrated telemetry data values indicated in paragraph 5.12.4.1. Further perturbations had to be made to the ignition altitude to arrive at the telemetry discrete time events of the 1000-foot mark and the descent segment acquisition. With these conditions matched, the 6DOF reconstruction from vernier ignition to segment acquisition agreed very well with postflight analysis of the telemetry data. Also, the telemetry discretes of the 10-fps and the 14-foot marks resulted in perturbing the nominal values within the 6DOF program. The final reconstruction by the 6DOF program compared favorably with telemetry data, as indicated by Table 5.12-3, and the close correlation between significant subsystem parameters, as indicated by the POSTPR machine plots in Figures 5.12-7 through 5.12-14.

POSTPR Program Plots

Figures 5.12-7 through 5.12-14 are plots of important parameters for trajectory reconstruction. The processed telemetry data from PREPRO (solid lines) and the best-fit 6DOF trajectory (dashed lines) are superimposed on the plots. The time scale starts at 0.0 second, which corresponds to vernier ignition (314:00:58:02.938 GMT). The spacecraft touchdown at 314:01:01:05.523 GMT corresponds to 182.6 seconds on the time scale. After 182.6 seconds, the magnitude changes on the PREPRO curves are the direct result of spacecraft touchdown. The PREPRO curves are plots of interpolated telemetry data in equal time intervals of 2 seconds designed to coincide with the 6DOF intervals. Therefore, part of the transients within the telemetry data will not be plotted on the PREPRO curves.

Table 5.12-3 lists the time occurrences of pertinent events as reconstructed by the 6DOF program. The PREPRO curves are referenced to the actual GMT as listed in the table.

Figure 5.12-8a shows the 6DOF true slant range and the telemetered slant range as a function of time. Figure 5.12-8b shows the 6DOF simulated slant range as output from the telemetry conditioning circuit along with the actual telemetry data. Comparison of the two figures shows an error between the actual slant range and the simulated telemetry circuit output of slant range within the 6DOF program. This error is due to the lag within the telemetry conditioning circuit. The oscillations in the PREPRO curves between 2 and 56 seconds are due to the tracker sweeping. At approximately 56.4 seconds, RORA occurred, resulting in reliable slant range data from this point to touchdown.

Figures 5.12-9a and 5.12-9b show an almost identical V_x and V_y reconstruction between the 6DOF and telemetry data. As indicated in Table 5.12-3, start of RADVS-controlled descent occurred at 54.8 seconds. It took approximately 7 seconds to steer out the V_y component of velocity developed by the retro burn phase, whereas the V_x component was essentially zero at this time. Approximately 2 seconds after vernier ignition, the RADVS is turned on, resulting in the spikes in the V_x and V_y plots.

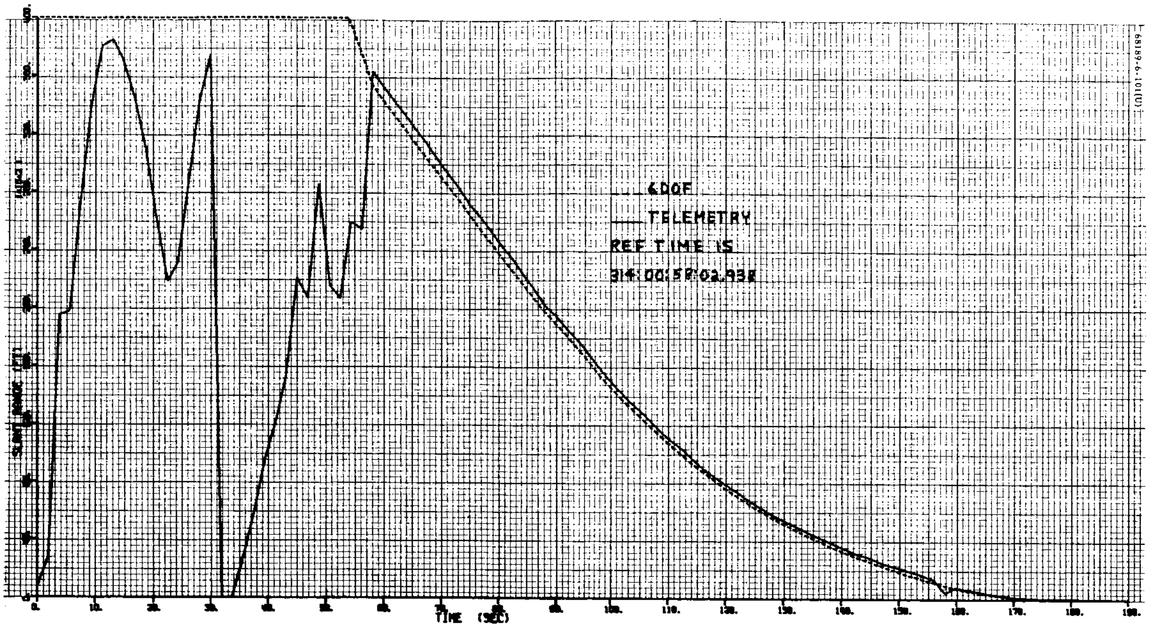

a) 6DOF Actual

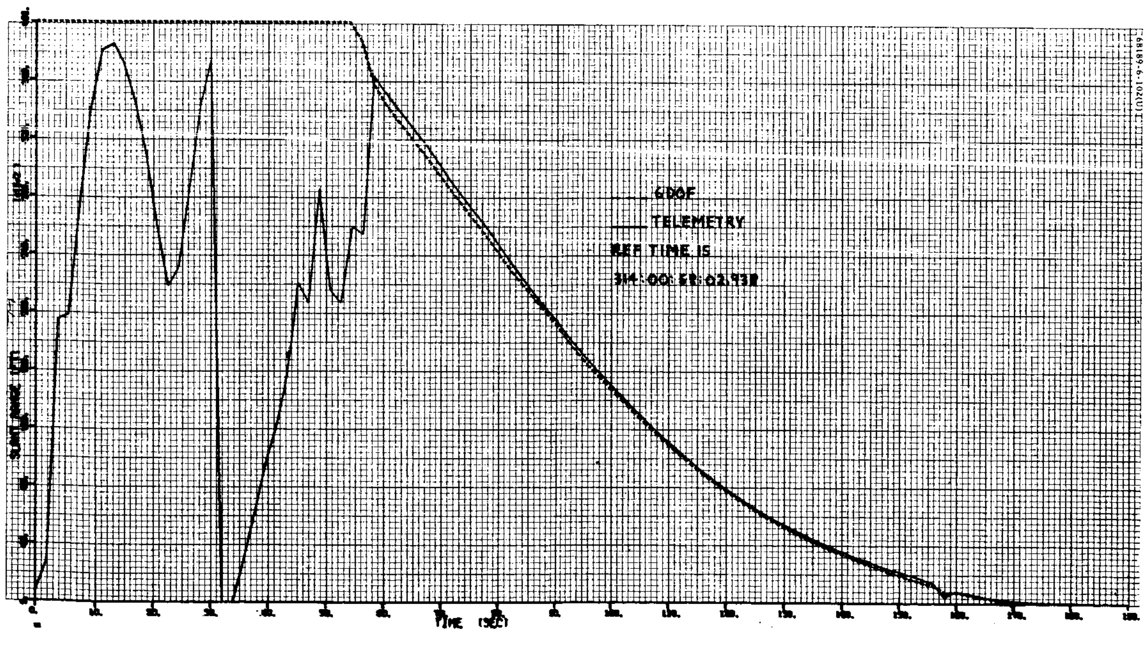

b) 6DOF Simulated Slant Range Telemetry Circuit

Figure 5.12-8. Slant Range

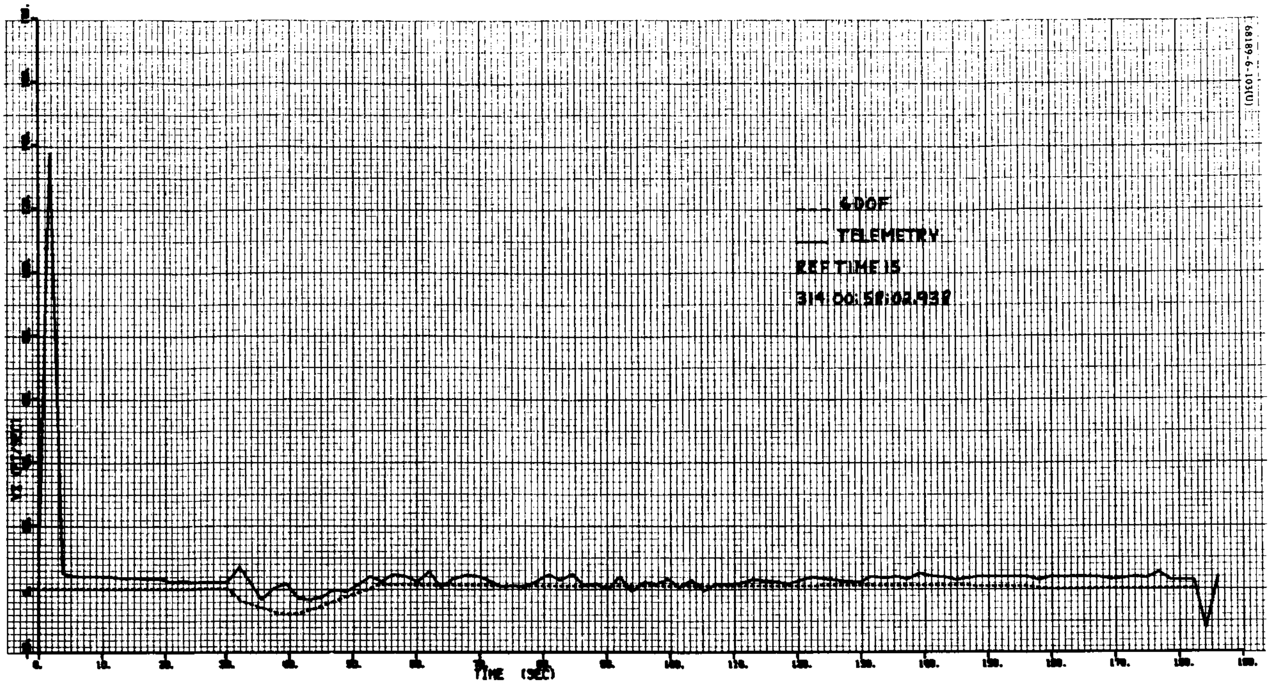

a) X-axis

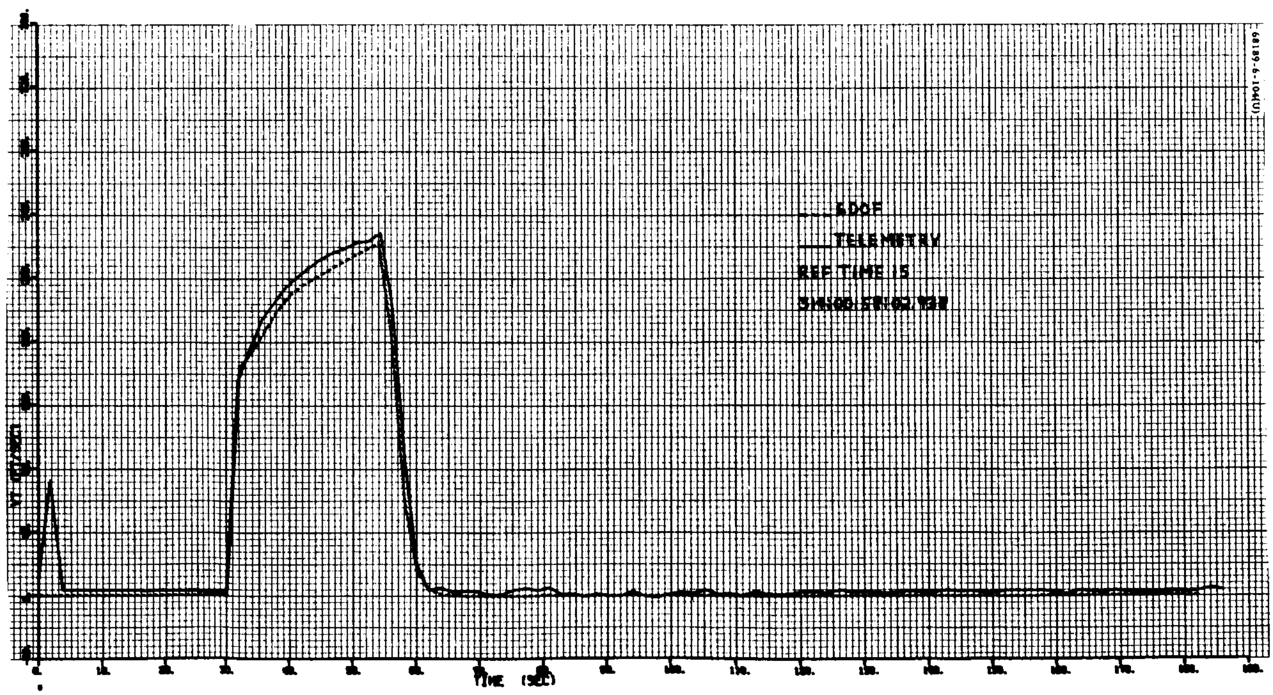

b) Y-axis

Figure 5.12-9. Spacecraft Velocity

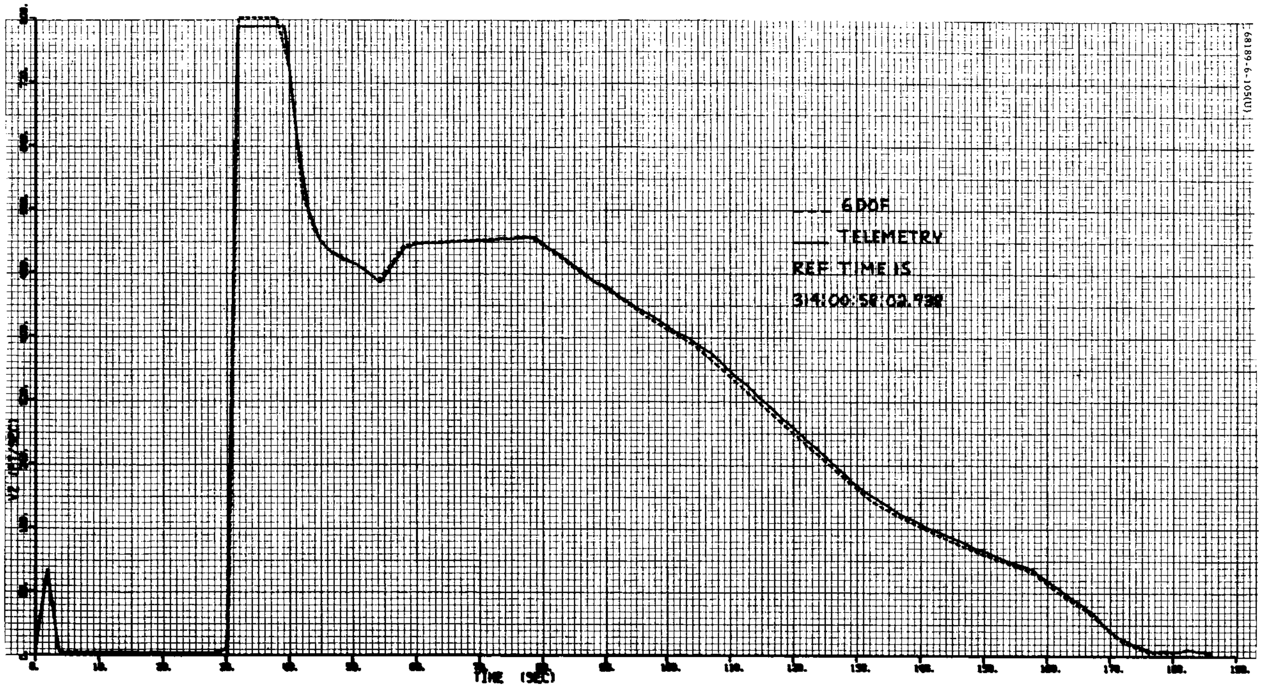

c) Z-axis (Actual 6DOF)

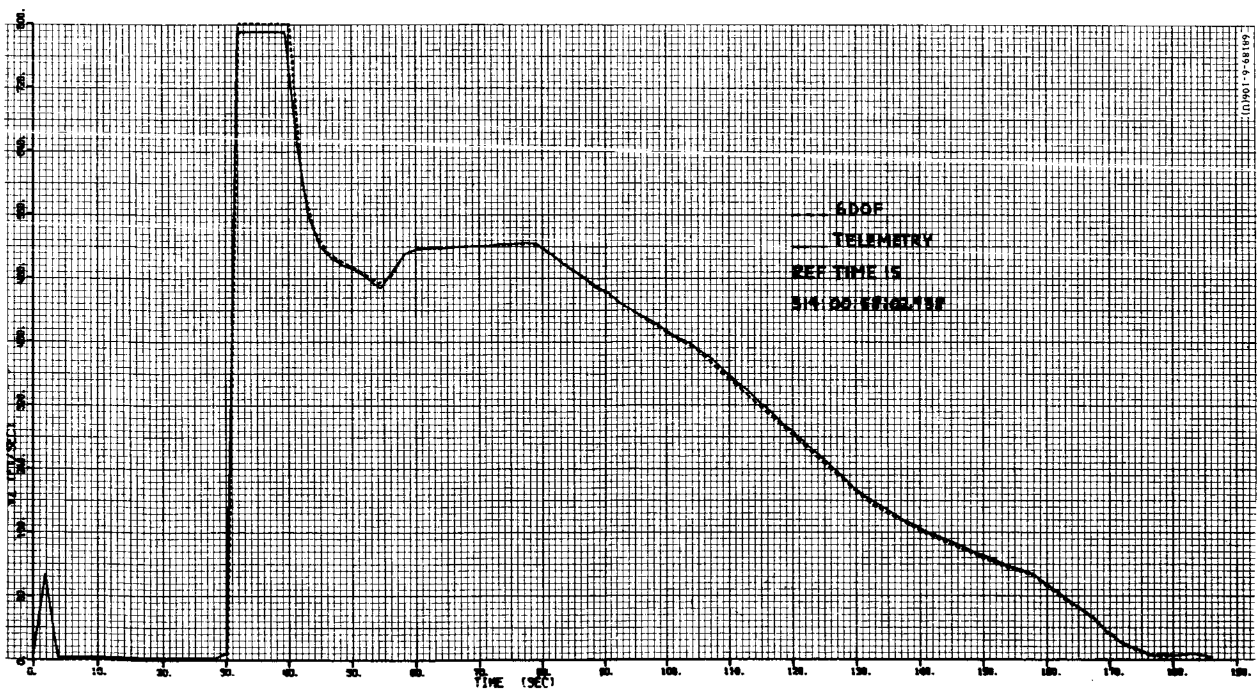

d) Z-axis (Simulated 6DOF V_z Telemetry Circuit)

Figure 5.12-9 (continued). Spacecraft Velocity

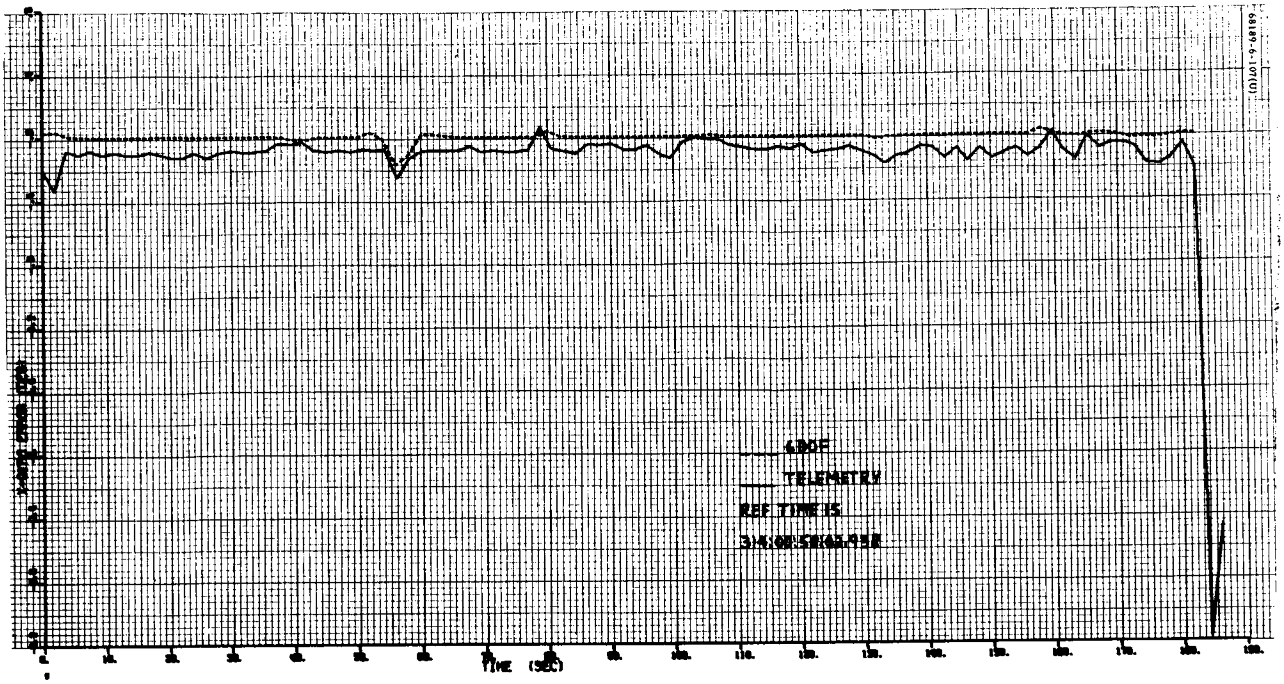

a) X-gyro

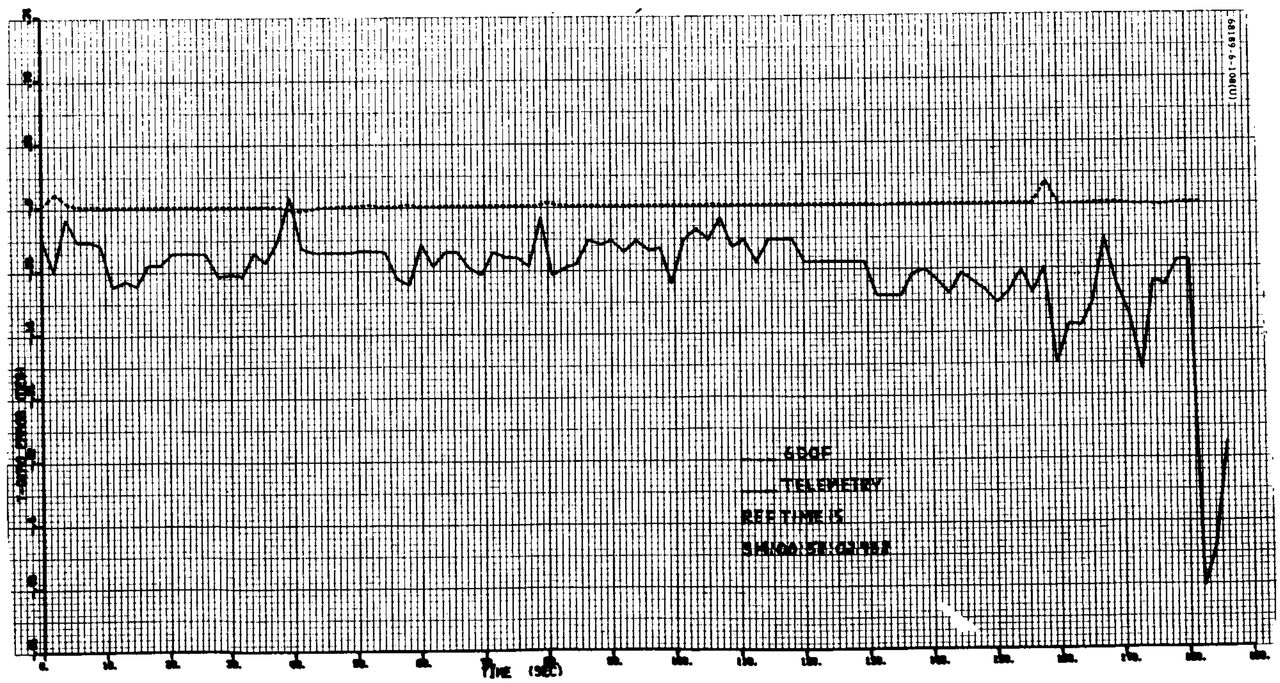

b) Y-gyro

Figure 5.12-10. Gyro Error Signal

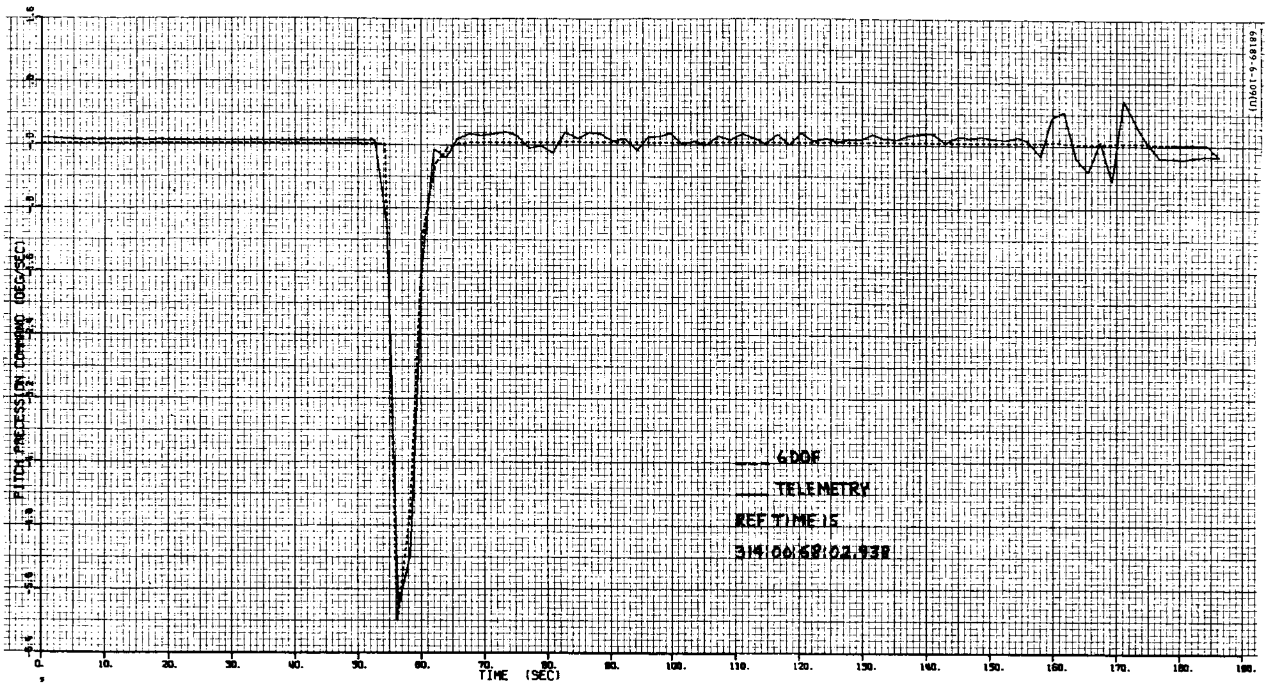

a) Pitch

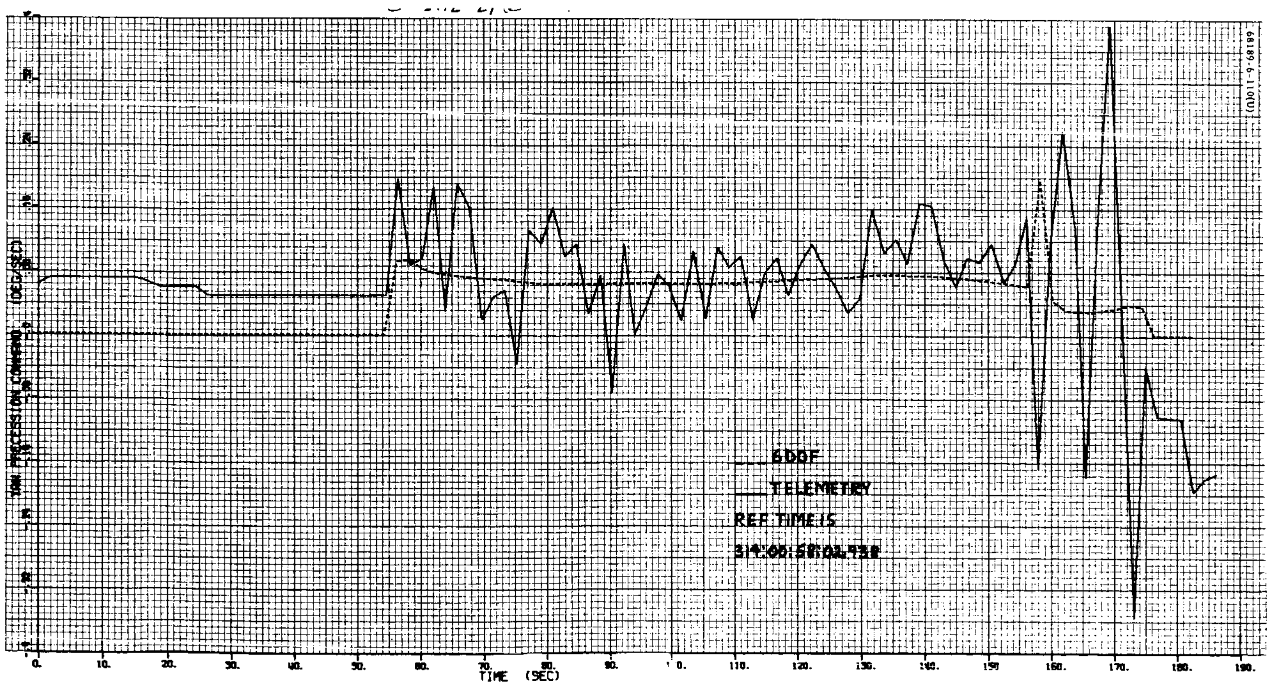

b) Yaw

Figure 5.12-11. Spacecraft Precession Commands

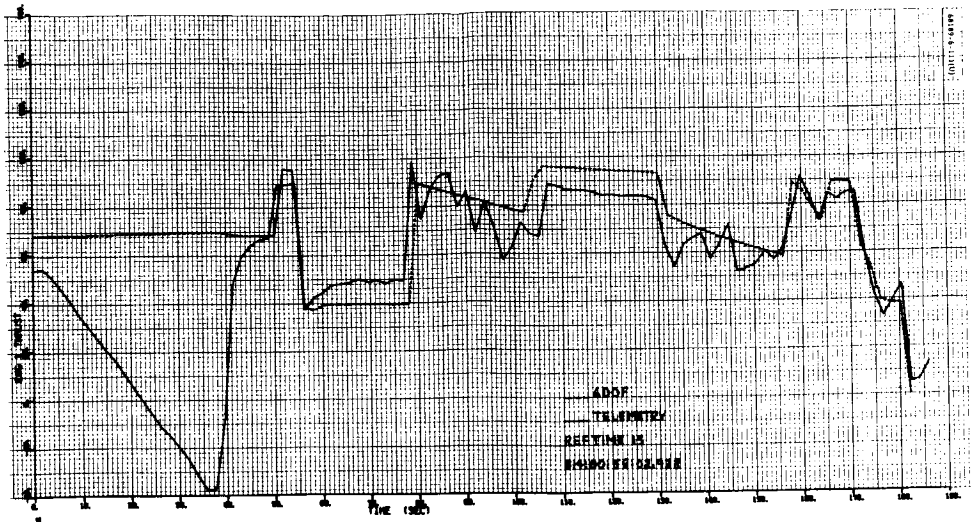

a) Engine 1

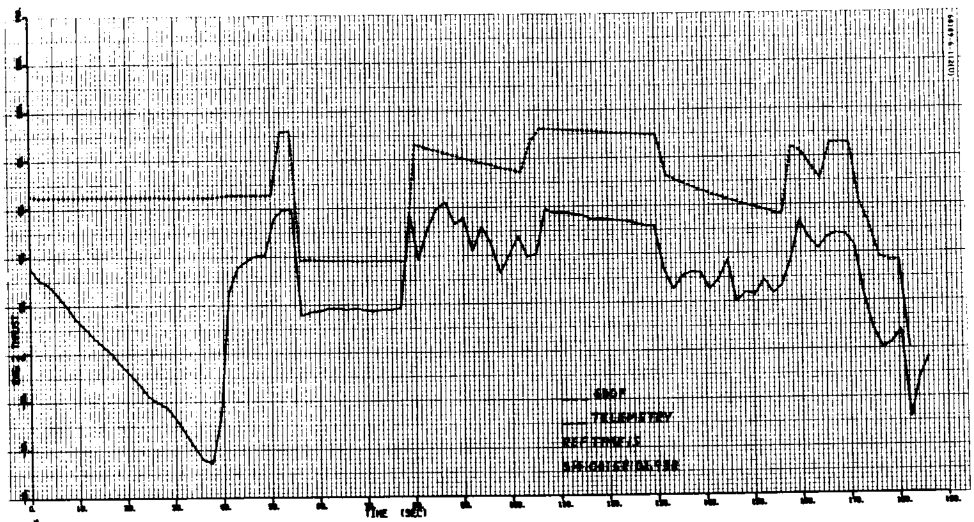

b) Engine 2

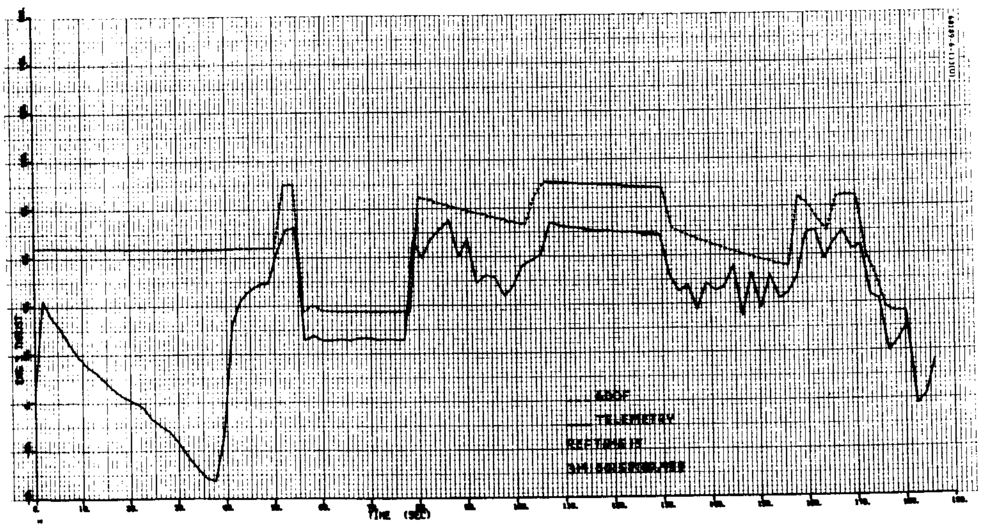

c) Engine 3

Figure 5.12-12. Telemetry Engine Strain Gage Data and 6DOF Engine Thrust Level Versus Time

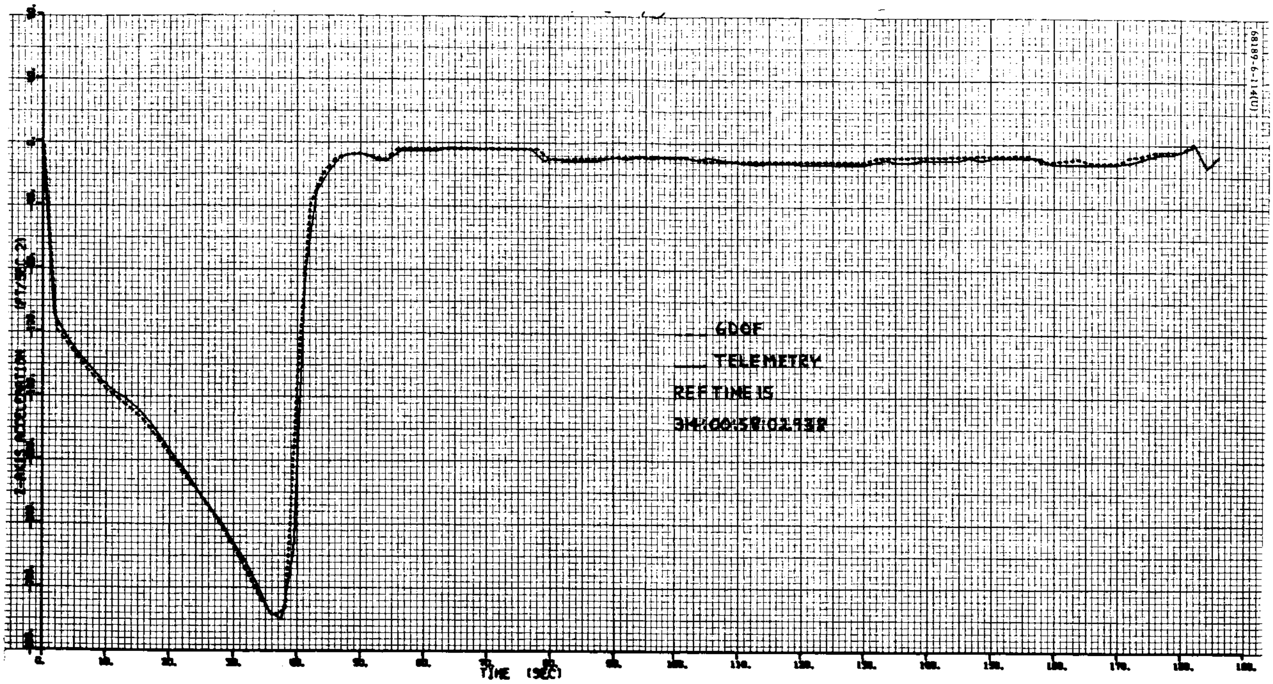

Figure 5.12-13. Telemtry Retro Accelerometer Data and 6DOF Z-axis Acceleration Versus Time

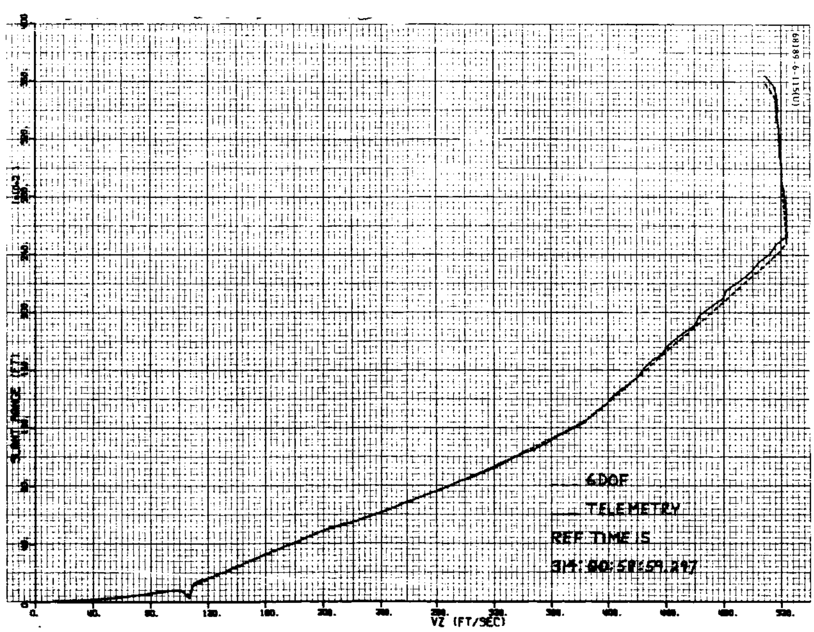

Figure 5.12-14. Slant Range Versus Z-axis Velocity

Figure 5.12-9c is a plot of the actual V_z component of velocity as reconstructed by the 6DOF program, whereas Figure 5.12-9d is a plot of the 6DOF simulation of the telemetry conditioning circuit for V_z. Both Figures 5.12-9c and 5.12-9d indicate an almost identical match with the telemetry data. Slight differences can be seen between the two 6DOF curves on Figures 5.12-9c and 5.12-9d from 40 to 60 seconds during which V_z changes most rapidly. This is a result of the lag network in the V_z telemetry circuit.

Figure 5.12-9 shows biases in the V_x, V_y, and V_z telemetry data. From observing the data, the following biases appeared:

$$V_x = 3.77 \text{ fps}$$

$$V_y = 3.19 \text{ fps}$$

$$V_z = 3.00 \text{ fps}$$

Corrections to the velocity components at the start of RADVS-controlled descent, as outlined in subsection 5.12.4.1, were made to compensate for these biases.

Figures 5.12-10a and 5.12-10b show both telemetry gyro error signals to be biased about -0.1 degree beyond that determined by preflight calibration. The spike in both signals at 54 seconds is a result of the change from inertial hold mode to RADVS-controlled steering mode.

Figure 5.12-11 shows the pitch and yaw precession commands. The pitch precession command compares favorably with the reduction in the V_y component of velocity during the minimum acceleration phase.

Figure 5.12-7 shows the vernier engine thrust commands. The roughness in the telemetry data is due to RADVS noise. The 6DOF curves are smooth since the RADVS noise was not simulated.

The premission computations of total vernier engine thrust during retro burn is 196.4 pounds, and for the high thrust phase, 276.4 pounds. The 6DOF program assumed these levels as can be noted from the sum of the three engine commands; however, the sum of the telemetered commands is approximately 202 pounds during the low thrust phase, a 6-pound difference between 6DOF and telemetry. Also, during the high thrust phase (retro separation), there is a difference between premission thrust level computations and telemetry data of 9 pounds. Engines 2 and 3 compare favorably between the 6DOF program and the telemetry data, whereas engine 1 does not.

During the vernier phase, the three engine commands should be equal to within 1 to 2 pounds. This is not so in the case of engine 1 in comparison to engines 2 and 3. Therefore, the engine 1 telemetry data becomes suspect, implying a probable bias or scale factor error in the calibrated telemetry data for this engine. For this reason, the premission computations of engine thrust during the retro phase were used in determining the propellant consumption specified in subsection 5.12.4.7.

Figure 5.12-12 shows the 6DOF engine thrust levels superimposed on the processed vernier engine strain gage data. Although the strain gage data are not an accurate source for indicating the actual engine thrust magnitude, they are suitable for indicating the engine thrust variation characteristics. The telemetry data have almost the same characteristic changes in thrust as does the 6DOF program. The rapid change in slope of the telemetry data between 2 and 38 seconds is caused by the main retro thrust.

Figure 5.12-13 compares the retro accelerometer telemetry data with the 6DOF spacecraft Z-axis acceleration. The peak acceleration of approximately 10 g occurs at 37.5 seconds, which compares with the strain gage data of Figure 5.12-12 and the retro accelerometer reconstruction on Figure 5.12-2.

Figure 5.12-14 is a plot of slant range versus velocity from the time of RORA to the 10-fps mark.

5.12.5 ACKNOWLEDGMENTS

Victor Marelia, coordinator and writer.

Eddy White, retro thrust-time curve reconstruction, main retro tailoff, retro ΔV determination, and 6DOF doppler reconstruction.

Ed Kopitzke, 6DOF reconstruction.

Tom Parker, retro thrust vector pointing error from known measured errors.

Nancy Krupa, POSTPR machine plots.

5.13 TELEVISION

5.13.1 INTRODUCTION

A short time after landing on the moon on day 314, GMT, the television camera began taking the first of more than 30,000 good quality pictures (30,065 when turned off at lunar night). This feat is enhanced by the absence of any television malfunctions.

5.13.2 ANOMALIES

During the first lunar day, no anomalies occurred in the television camera or the television camera supporting equipment.

5.13.3 SUMMARY

The success of the Surveyor VI camera system proves out the capability of the upgraded camera (290512 series). Mirror assembly redesign was most significant. Television camera system performance was excellent, enabling accomplishment of all mission objectives.

5.13.4 SUBSYSTEM PERFORMANCE

Table 5.13-1 is a summary time and events log for the first lunar day. After taking about 12,000 pictures from the initial landing site, the spacecraft was commanded into a short powered translation. This hop was quickly determined to be a spectacular success when the television camera again began surveying the lunar landscape. Footpad impressions at the initial touchdown position exhibited soil movement due to vernier engine ignition.

In taking the more than 30,000 pictures, the camera mirror was stepped more than 46,000 times in azimuth and more than 13,000 times in elevation.

TABLE 5.13-1. SURVEYOR VI TELEVISION OPERATIONS — FIRST LUNAR DAY

Post TD Pass	Station CMDG	Survey Number	Activity	Time GMT Start	Time GMT End
1	DSS-11	010	Post TD 200 Line Mode	314-0150	314-0235
		020	W/A 360 Pan (600 Line Mode)	-0402	-0500
		030	Special Area (CT-801B)	-0502	-0749
	DSS-42	Started CMDG oven DSS-42 at 0741			
		040	Aux. Mirrors	-0754	-0807
		-	Special Area	-0812	-0824
		-	Magnets, N/A	-0831	-0835
		-	Polarmetric - Pad 2 P.T.	-0840	-0843
		-	N/A - Segment 3	-0851	-0910
		-	N/A - Segment 2	-0925	-1027
		-	N/A - Segment 2, ?	-1029	-1042
		-	P.A. and S.P.	-1044	-1048
		-	Polarmetric	-1049	-1053
		-	N/A Segment	-1054	-1134
		-	Alpha Scat.	-1135	-1140
	DSS-61	-	Alpha Scat. TV Support	-2100	-2130
2	DSS-11	010	Polarimetric Survey	314-2247	314-2328
		020	Special Area and Aux. Mirrors	-2328	-2358
		010	Polarmetric Survey (cont.)	-2358	315-0029
		020	Special Area	315-0029	-0118
		021	Aux. Mirrors	-0118	-0130
		030	N/A Segment 3	-0130	-0150
		031	N/A Segment 5	-0150	-0213
		032	N/A Segment 2	-0213	-0229
		040	Magnets, N/A	-0229	-0238
		050	A/C Jet Exp. - TV Support	-0240	-0356
		060	W/A 360 Pan. (C1202)	-0412	-0431
		070	Star Survey - Sirius, Canopus, Capella	-0431	-0443
3	DSS-11	010	Filter Interrogation	315-2319	315-2337
		020	Polarimetric Survey	-2337	316-0100
		030	Focus Ranging, AZ=0	316-0102	-0201
		031	Focus Ranging, AZ=36	-0202	-0229
		032	Focus Ranging, AZ=72	-0230	-0300
		033	Focus Ranging, AZ= -72	-0300	-0337
		040	W/A 360 Pan.	-0340	-0433
		050	N/A Segment 4	-0437	-0524
		060	Special Area	-0525	-0646
		061	Aux. Mirrors	-0649	-0710
		070	N/A Segment 3	-0710	-0738

Table 5.13-1 (continued)

Post TD Pass	Station CMDG	Survey Number	Activity	Time GMT Start	- End
4	DSS-11	010	Polarimetric Survey	317-0002	317-0115
		020	Special Area and Magnets	-0115	-0226
		021	Aux. Mirrirs	-0227	-0244
		030	Focus Ranging, Az= -36	-0246	-0333
		031	Focus Ranging, Az= 90	-0333	-0354
		032	Focus Ranging, Az= 108	-0355	-0411
		040	N/A Segment 5	-0411	-0500
		041	N/A Segment 2	-0500	-0528
		042	N/A Segment 1	-0544	-0600
		050	W/A 360 Pan.	-0603	-0651
		060	Star Survey - Alpha Cm-1	-0652	-0712
		070	N/A Segment 1, Supplement on Stop	-0715	-0732
		080	N/A Segment 3	-0732	-0758
		081	N/A Segment 4	-0829	-0855
		071	N/A Segment 5, Supplement on Stop	-0858	-0917
		071	Aux. Mirror - Surface Focus Range	-0917	-0920
		071	Earth View Test	-0925	-0928
	DSS-42	-	Special Area	-1209	-1246
		-	Aux. Mirrors	-1253	-1311
5	DSS-11	010	Iris Interrogation	318-0033	318-0103
		020	Polarimetric Survey	-0103	-0254
		030	Special Area and Magnets	-0256	-0332
		031	Aux. Mirrors	-0431	-0442
		040	W/A 360 Pan.	-0443	-0512
		050	N/A Segment 1 and Supplement	-0515	-0601
		051	N/A Segment 2	-0601	-0625
		051	N/A Segment 3	-0630	-0648
		052	N/A Segment 4	-0648	-0713
		053	N/A Segment 5 and Supplement	-0737	-0807
		060	Star Survey, Jupiter (neg), Vega (neg)	-0808	-0846
		070	Selected Polarimetric	-0851	-0916
		080	He Check and Relief Valve	-0920	-0939
	DSS-42	-	Special Area	-1306	-1343
		-	Aux. Mirrors	-1348	-1359
6	DSS-11	010	Filter Interrogation	319-0053	319-0117
		020	Polarimetric Survey	-0117	-0227
		030	W/A 360 Pan.	-0228	-0244
		040	Special Area	-0324	-0343
		041	Aux. Mirrors	-0344	-0347
		050	Aux. Mirror-Focus Range	-0348	-0351
		041	Aux. Mirrors (cont.)	-0351	-0354
		050	Aux. Mirror - Focus Range	-0355	-0358
		041	Aux. Mirrors (completion)	-0359	-0402
		060	N/A Segment 1 and Supplement	-0408	-0443
		061	N/A Segment 2	-0444	-0500
		062	N/A Segment 3	-0502	-0523
		063	N/A Segment 4	-0539	-0600
		064	N/A Segment 5 and Supplement	-0600	-0625

Table 5.13-1. (continued)

Post TD Pass	Station CMDG	Survey Number	Activity	Time GMT Start	End
6	DSS-11 (con.)	070	Star Survey, Vega (neg.)	-0625	-0628
		071	Star Survey, Jupiter	-0628	-0633
		080	Selected Polarimetric	-0633	-1002
		090	He Check and Relief Valve	-1002	-1010
		100	Star Survey, Vega	-1010	-1020
		110	Magnets	-1020	-1029
		081	Polarimetric, Pad 2 Chart	-1029	-1033
	DSS-42	-	Special Area	-1303	-1336
7	DSS-11	010	He Check and Relief Valve	320-0125	320-0129
		020	Polarimetric Survey	-0129	-0240
		030	Earth Picture	-0240	-0246
		040	Special Area 2nd	-0246	-
		041	Magnets	-	-0357
		042	Aux. Mirrors	-0357	-0410
		050	W/A 360 Pan.	-0414	-0428
		060	N/A Segment 1 and Supplement	-0429	-0457
		061	N/A Segment 2	-0458	-0513
		062	N/A Segment 3	-0514	-0553
		063	N/A Segment 4	-0556	-0614
		064	N/A Segment 5 and Supplement	-0618	-0700
		070	Selected Polarimetric	-0700	-0734
		080	Earth Picture	-0735	-0751
		090	Iris Calib. Interrogation	-0818	-0900
		100	Alpha Scat. Survey	-0900	-0915
		-	Earth Picture (Approx.)	-1200	-
8	DSS-11	010	Video Test on Omni and Planar Ant.	321-0428	321-0438
		020	Selected Polarimetric in Seg. 3	-0440	-0525
		021	Selected Polarimetric in Seg. 4	-0525	-0643
		022	Selected Polarimetric in Seg. 5	-0643	-0714
		023	Selected Polarimetric in Seg. 2	-0714	-0921
		030	Special Area - Selected	-0921	-0925
		031	Aux. Mirrors	-0925	-0940
		040	W/A 360 Pan. (Post Translation)	-1107	-1122
		050	N/A Segment 4	-1122	-1153
		060	Special Area	-1154	-1245
	DSS-42	070	Aux. Mirrors	321-1323	321-1333
		-	Aux. Mirrors	-1437	-1441
		-	N/A Segment 3, Filter 2	-1521	-1543
		-	N/A Segment 3, Filter 3	-1657	-1714
		-	N/A Segment 3, Filter 4	-1716	-1749
	DSS-61	-	N/A Segments, 4 and 5 in Filter 2,3,&4	-1835	-2307
9	DSS-11	010	Polarimetric Survey	322-0250	322-0407
		020	W/A 360 Pan.	-0409	-0425
		030	Special Area and Magnets	-0427	-0601
		031	Aux. Mirrors	-0602	-0611

Table 5.13-1 (continued)

Post TD Pass	Station CMDG	Survey Number	Activity	Time GMT Start	End
9	DSS-11 (con.)	040	Inside ASI	-0633	-0700
		050	N/A Segment 1	-0748	-0822
		051	N/A Segment 2	-0824	-0840
		060	Solar Corona Calib. Seg.	-0840	-1011
		070	Polarimetric, Pad 3 Area	-1012	-1103
		080	Star Survey, Venus	-1104	-1121
		090	N/A Segment 3, not complete	-1122	-1137
	DSS-42	090	N/A Segment 3 (cont.)	-1231	-1247
		091	N/A Segment 4	-1247	-1308
		092	N/A Segment 5	-1308	-1340
		100	Shadow Progression A	-1341	-1344
		-	Special Area	-1606	-1626
		-	Aux. Mirrors	-1628	-1655
		-	Shadow Progression A	-1759	-1805
	DSS-61	-	Shadow Progression A, 5 Times (Each hour)	- 322-2003	- 323-0242
10	DSS-11	010	Polarimetric Survey	323-0337	323-0443
		020	Special Area and Magnets	-0447	-0524
		021	Aux. Mirrors	-0524	-0532
		030	360 W/A Pan.	-0532	-0608
		040	N/A Segment 1	-0608	-0639
		041	N/A Segment 2	-0642	-0709
		042	N/A Segment 3	-0815	-0918
		050	Star Survey, Venus, Alpha ERI	-0920	-0946
11	DSS-11	010	Polarimetric Survey	324-0430	324-0542
		020	W/A 360 Pan.	-0548	-0606
		030	N/A Segment 3 W/Polarimetric	-0608	-0714
		031	N/A Segment 4 W/Polarimetric	-0718	-0803
		040	Star Survey, α Cent., α ERI, Vega	-0917	-0958
		050	N/A Segment 1	-1000	-1026
		051	N/A Segment 2 W/Polarimetric	-1027	-1056
		060	Shadow Progression	-1119	-1124
		052	N/A Segment 5	-1124	-1148
		070	Special Area	-1148	-1212
		071	Aux. Mirrors	-1213	-1221
	DSS-42	-	Shadow Progression, 4 times	-1415	-1931
	DSS-61	-	Shadow Progression	-2333	-2344
12	DSS-11	010	W/A 360 Pan.	325-0530	325-0542
		020	Shadow Progression	-0543	-0553
		030	Focus Ranging Az = -90	-0556	-0618
		031	" " Az = -108	-0621	-0645
		032	" " Az = -126	-0645	-0709
		033	" " Az = -144	-0712	-0805
		021	Shadow Progression	-0807	-0818

Table 5. 13-1 (continued)

Post TD Pass	Station CMDG	Survey Number	Activity	Time GMT Start	Time GMT End
12	DSS-11 (con.)	040	Polarimetric Survey and Selected	-0821	-0931
		022	Shadow Progression	-1025	-1039
		040	Polarimetric Survey (cont.)	-1041	-1059
		050	Special Area	-1102	-1125
		051	Aux. Mirrors	-1125	-1131
		060	N/A Segment 3	-1133	-1159
		061	N/A Segment 4	-1221	-1238
		062	N/A Segment 5	-1238	-1306
		063	N/A Segment 2	-1307	-1325
	DSS-42	070	Star Survey, Saturn	-1435	-1501
		023	Shadow Progression	-1501	-1507
	DSS-11	080	Selected Polarimetric	-1529	-1626
	DSS-42	-	Shadow Progression	-1728	-1735
	DSS-61	-	Shadow Progression- 2 times	325-2119	326-0225
13	DSS-11	010	Polarimetric Survey	326-0644	326-0821
		020	W/A 360 Pan.	-0826	-0841
		030	N/A Segment 3 and Polarimetric	-0842	-0944
		031	N/A Segment 4 " "	-0946	-1048
		040	Focus Ranging, Az= -72	-1052	-1127
		041	" " Az= -54	-1144	-1212
		050	Shadow Progression	-1213	-1218
		042	Focus Ranging, Az= -36	-1220	-1240
		043	" " Az= 108	-1241	-1336
		060	Aux. Mirror	-1339	-1344
		070	Selected Polarimetric	-1345	-1417
		051	Shadow Progression	-1418	-1422
		080	Special Area (not complete)	-1424	-1431
	DSS-42	080	Special Area (cont.)	-1532	-1600
		090	Star Survey, α Cent., α ERI, α LVR	-1615	-1651
		052	Shadow Progression	-1652	-1659
		100	N/A Segment 5	-1700	-1747
		101	N/A Segment 2	-1751	-1811
			- DSS-11 Set -		
		-	Shadow Progression	-1909	-1914
		-	Shadow Progression	-2104	-2109
	DSS-61	-	Shadow Progression, 4 times	-2300	327-0509
14	DSS-11	010	Polarimetric Survey	327-0721	-0837
		020	W/A 360 Pan.	-0839	-0857
		030	N/A Segment 3 and Polarimetric	-0906	-1036
		031	N/A Segment 4 " "	-1038	-1131
		040	Focus Ranging, Az = 90	-1136	-1149
		041	" " Az = 72	-1220	-1238
		042	" " Az = 0	-1240	-1325
		043	" " Az = -18	-1329	-1359

Table 5. 13-1 (continued)

Post TD Pass	Station CMDG	Survey Number	Activity	Time GMT Start	- End
14	DSS-11	050	Shadow Progression A	-1423	-1428
	(con.)	060	" " B	-1428	-1444
		070	Special Area	-1448	-1508
		071	Aux. Mirrors	-1510	-1514
		080	Star Survey, αERI, α Cent., α LYR	-1516	-1521
	DSS-42	080	Star Survey (Cont.)	-1621	-1639
		090	N/A Segment 5	-1642	-1659
		051	Shadow Progression A	-1701	-1709
		091	N/A Segment 2 and Polarimetric	-1709	-1811
		100	Filter Interrogation	-1812	-1820
		-	Shadow Progression	-1826	-1901
		-	" "	-2106	-2204
		-	" "	-2305	-2312
		-	" "	-2312	-2333
	DSS-61	-	Shadow Progression	328-0131	328-0138
		-	" "	-0328	-0336
		-	" " , A	-0607	-
		-	Special Area	-	-
		-	Aux. Mirrors	-	-
		-	Shadow Progression, B	-	-0714
15	DSS-11	010	W/A 360 Pan.	-0757	-0818
		020	N/A Segment 3 and Polarimetric	-0821	-0914
		021	N/A Segment 4	-0915	-0956
		022	N/A Segment 5	-1020	-1041
		023	N/A Segment 2	-1043	-1104
		011	W/A 360 Pan.	-1110	-1130
		030	Shadow Progression B	-1132	-1139
		040	N/A Horizon Scan	-1143	-1207
		012	W/A 360 Pan.	-1233	-1244
		041	N/A Horizon Scan	-1245	-1310
		013	W/A 360 Pan.	-1314	-1323
		042	N/A Horizon Scan (sunset)	-1324	-1352
		050	Solar Corona	-1411	-1426
		060	W/A Eastern Horizon	-1426	-1434
		070	Solar Corona	-1436	-1520
		080	Star Survey, Anterus	-1520	-1534
		071	Solar Corona	-1536	-1622
		090	Earth Shine, Pad 2	-1623	-1650
		100	Solar Corona	-1651	-1806
		081	Star Survey, αLYR	-1808	-1826
		110	Solar Corona	-1828	-1904
		091	Earth Shine, Pad 2	-1905	-1928
		111	Solar Corona, 20 min. integrate, "Lost in Low Power"	-1929	-2004

End of First Lunar Day SC-6

5.13.5 REFERENCE

1) SSAC Operation Log.

5.13.6 ACKNOWLEDGMENTS

This section was compiled by W. E. Drake with inputs from J. N. Lindsly and R. C. Hayes of JPL.

5.14 ALPHA SCATTERING EXPERIMENT

5.14.1 INTRODUCTION

5.14.1.1 Purpose

The alpha scattering experiment was added to Surveyor VI in order to perform a compositional analyses of the lunar surface. The alpha scattering technique of surface chemical analysis takes advantage of the characteristic interactions of α particles with matter to provide information on the chemical composition. The energy spectrums of the large-angle, elastically scattered α particles are characteristic of the nuclei doing the scattering. In addition, certain elements, when bombarded with α particles, produce protons, again with characteristic energy spectrums. Consequently, these energy spectrums and intensities of scattered α particles and protons can be used to determine the chemical composition of the material being exposed to the α particles.

The method has good resolution for the light elements expected to be contained in rocks (unfortunately, however, it can give only indirect information about hydrogen). The resolution under this technique decreases as the atomic weight increases (Fe, Co, and Ni cannot easily be resolved), even though the sensitivity is greater for heavy elements than for most light elements. (The sensitivity for elements heavier than lithium is approximately 1 atomic percent.)

The absence of an atmosphere on the moon made practical the use, for such chemical analyses, of the relatively low-energy α particles from a radioactive source. Cm^{242} ($t_{1/2}$ = 163 days, T_a = 6.11 mev) is a convenient nuclide for this purpose. The use of low-energy α particles, however, restricts the information obtained to that pertaining to the uppermost few microns of material, i.e., the method is one of surface chemical analysis. Moreover, using practical source intensities ($\sim$100 mc), the rate of analysis is rather slow: a relatively complete analysis requires about 1 day. In spite of these disadvantages, the simplicity of the instrumentation associated with using a radioactive source made this a feasible, attractive method.

5.14.1.2 Description

The alpha scattering subsystem consisted of five principal units: sensor head, digital electronics, electronic auxiliary, thermal compartment/heater assembly, and deployment mechanism/standard sample, having a total weight (including mechanical and electrical spacecraft interface substructure and cabling) of approximately 13.1 kg (28.8 pounds). Power dissipation of the subsystem was normally 2.1 watts (approximately) which increased to 17.1 watts, when both the thermal compartment and the sensor head heaters were active. A brief description of each of the principal units follow.

Sensor Head (GFE)

The sensor head is a box measuring 17.1 by 16.5 by 13.3 cm which contains a 30.5-cm-diameter plate on the bottom. The main purpose of this plate is to minimize the probability of the box appreciably sinking into a soft (lunar) surface. At the bottom of the head is a 10.8-cm circular opening, and recessed 7.0 cm above the opening are six α sources, which are orientated in such a way that the α particles are directed only at the opening of the head. Close to the α sources are two silicon semiconductor detectors arranged to detect α particles scattered back at an average angle of 174 degrees from the sample. Also contained in the head are four detectors (~ 1 cm^2 area each) designed to detect protons produced in the sample by the α particles. A gold foil of ~ 21 mg cm^{-2} prevents scattered α particles from reaching these detectors. Because the proton rates were expected to be low, and because these detectors are particularly sensitive to solar protons, the proton detectors were backed by guard detectors. The electronics associated with the guard detectors was arranged so that an event registered in both detectors (and, therefore, due to space radiation) will not be counted as coming from the sample. The anticoincidence arrangement had the effect of significantly reducing the backgrounds of the instrument when operating in the proton mode.

In addition to the sources, detectors, and associated electronics, the head contained a temperature sensor, a 5-watt heater, and an electronic pulser. The electronic pulser was used to calibrate the electronics of the instrument by introducing electrical pulses of known magnitudes (two) into the detector stages of the system. The calibration mode is initiated by earth command.

The output of the head characterizes the energy of an event, in either the scattered α or proton mode of the instrument, by a signal in time analog (pulse) form.

Digital Electronics (GFE)

The time analog output signal of the sensor head is processed by the digital electronics unit and converted into a nine-bit digital word that has seven information bits. Stated differently, the event energy spectrum is analyzed and expressed, in terms of channels, by 128-channel pulse-height analyzers having a threshold of about 600 kev and a gain of about 54 kev per channel. The nine-bit digital words characterizing each event are transmitted in near-real time (essentially no spacecraft storage) to earth at a rate of 2200 bits/sec for the α mode and 550 bits/sec for the proton mode.

The digital electronics unit contains, in addition to the digital processing electronics, the necessary power supplies and the logical electronic interfaces between the GFE and the Hughes spacecraft equipment. The digital electronics unit contained circuits so that the output of any one individual detector, together with its associated guard detector, could be inhibited by earth command; the temperature of the sensor head, as well as other monitoring voltages, could be transmitted to earth. Finally, a crude ratemeter provided information on the number of events occurring in the guard (anticoincidence) detectors.

Electronics Auxiliary (Hughes)

The electronics auxiliary unit provided the necessary command decoding, signal processing, and power management so that the GFE equipment could interface with the basic spacecraft bus. Basic items interfacing directly with the sensor head and the digital electronics are 1) the central signal processor that provides 2200 and 550 bits/sec sync to the digital electronics clocks, and 2) the engineering signal processor that provides temperature sensor excitation current and commutation of the GFE engineering data outputs.

The electronics auxiliary also provides the two data channels employed by the alpha scattering subsystem for the alpha and proton counts. The characteristics of these two subcarrier oscillator channels are as follows:

	Alpha Counts	Proton Counts
Data input to electronic auxiliary	Digital, NRZ	Digital, NRZ
Input data rate	2200 bits/sec	550 bits/sec
Subcarrier oscillator center frequency	70,000 Hz	5400 Hz

Thermal Compartment/Heater Assembly

The digital electronics and the electronic auxiliary units were contained in a thermal compartment attached to the spacecraft. Thermal control was obtained by compartment thermal design in conjunction with a 10-watt compartment heater assembly, which was operated by the engineering signal processor.

Deployment Mechanism/Standard Sample

The deployment mechanism provides for the operation of the experiment in any of the following three positions:

1) Stowed position where the standard sample was utilized for calibration of the system

2) Background position where the solar and surface natural radiation was calibrated

3) Lunar surface position where the lunar surface compositional analysis was performed

The standard sample is a sample of known chemical composition that was attached to the deployment mechanism and was used to assess subsystem performance prior to launch and after lunar landing. The standard sample covers the sensor head viewing part when in the stowed position, and is removed when the sensor head is in either the background or the lunar surface positions. Operation in this manner minimizes the entrance of both dust and light during spacecraft launch, transit, and landing and/or until the experiment is to be operated.

5.14.2 ANOMALIES

The operation of the alpha scattering experiment was completely successful with a total operating time of 108 hours and 41 minutes during which 59 hours of science data were accumulated, including 30-1/2 hours of lunar surface analysis.

During flight and all lunar operations, the essential telemetry data remained within predicted limits except for the sensor head temperature, which exceeded the maximum operating temperature limit for a period of approximately 82 hours. A/SPP shading was used to reduce the sensor head temperature to within operating limits.

Proton detector No. 3 became noisy on an intermittent basis at a head temperature of 110°F, but cleared up when the temperature was reduced to 90°F.

After spacecraft translation on GMT day 321, the alpha scattering experiment was turned on at 12:48. A subsequent investigation indicated that the experiments had been turned on when the head temperature was 144°F, which is above the operational limit. Consequently, the experiment was turned off at 12:52 and was not turned on again until the temperature had decreased to operating limits.

5.14.3 RECOMMENDATIONS

It is recommended that temperature function always be checked prior to commanding the alpha scattering experiment on.

5.14.4 SUBSYSTEM PERFORMANCE ANALYSIS

The Lunar Operations plan called for four modes of operation: 1) standard sample, 2) background, 3) lunar surface, and 4) calibration. There were, however, five actual modes of operation provided with the addition of a post-translation mode after the alpha sensor was turned over and the detectors were viewing space. Data accumulated during the post-translation period may provide information regarding proton activity from space.

Two forms of science data were recorded during operation: the uncorrected spectra, received via teletype from the stations, which were used for near-real time analysis; and the FR-1400 prime data tapes for use during the postmission analysis. The uncorrected spectra, while not reflecting all data transmitted from the alpha scattering subsystem, did contain the vast majority of data recorded on the FR-1400 tapes. Table 5. 14-1 presents a summary of the science data accumulation time in each of the five operational configurations.

TABLE 5. 14-1. SCIENCE DATA ACCUMULATION SUMMARY

Operational Configuration	Accumulation Time, minutes
Standard sample	318
Background	367
Lunar surface position	1834
Post translation (instrument upside down)	796
Calibration	216
Total	3531 ≈ 59 hours

Operation of the alpha scattering subsystem was initiated during lunar phase approximately 4 hours and 38 minutes after touchdown while the spacecraft was in view of DSS-11. Lunar operations continued during days 314 through 316, 320, 322, 324, and 326 through 328. During lunar operations, the science data were accumulated while the sensor head was within its operational temperature limits of -40° to 122°F. All data were accumulated while the thermal compartment was within its operational temperature limits of -4° to 131°F. When it was discovered that proton detector No. 3 was noisy, it was turned off. The experiment successfully accumulated data using three detectors until the noisy detector corrected itself when the sensor temperature decreased to 90°F. The approximate 3 hours of proton data were unusable, due to the time required to determine that a detector was noisy and to isolate the noise to detector 3.

During spacecraft translation the alpha scattering sensor head was turned upside down, thus terminating further lunar soil analysis. In the upside down position, the detectors were exposed to space and an additional 13 hours of data were accumulated for possible use in investigating space proton activity.

Approximately 450 commands were transmitted, received, and executed without a single error.

In general, the communications link from the spacecraft was excellent, and the bit error rate of 10^{-6} was at least a factor of 100 better than the predicted worst-case value. Deviations from this high quality data reception generally occurred when the spacecraft was being tracked near the earth's horizon.

For ancillary information, Table 5. 14-2 is a summary of preliminary results of the chemical analysis of the moon at the Surveyors V and VI landing sites (Reference 1). Table 5. 14-3 is a detailed account of SSAC alpha scattering operations during the first lunar day, and Table 5. 14-4 outlines the overall operation of the alpha scattering experiment.

TABLE 5. 14-2. CHEMICAL COMPOSITION OF LUNAR SURFACE AT SURVEYORS V AND VI SITES

Element	Surveyor V Atomic, percent*	Surveyor VI Atomic, percent*
Carbon	< 3	< 3
Oxygen	58 ± 5	57 ± 5
Sodium	< 2	< 2
Magnesium	3 ± 3	3 ± 3
Aluminum	6. 5 ± 2	6. 5 ± 2
Silicon	18. 5 ± 3	22 ± 5
28 < A < 65**	13 ± 3	
Calcium		6 ± 2
(Fe, Co, Ni)	< 3	
Iron		5 ± 2
A > 65	< 0. 5	

*Excluding hydrogen, helium, and lithium. These numbers have been normalized to approximately 100 percent.

**This group includes, for example, S, K, Ca, Fe, Co, and Ni.

TABLE 5.14-3. ALPHA SCATTERING DETAILED DATA ACCUMULATION

DSS	Day	Position	Record Number	Calibration Period	Accumulation Period	GMT, hr:min:sec Start	GMT, hr:min:sec End	Comments
11	314	Stowed	1		10M	05:41:40	05:51:40	
			2-6	10M		05:53:10	06:09:00	
			7		10M	06:10:30	06:20:30	
42			2		15M	09:52:50	10:07:50	
			3		20M	11:54:00	12:14:00	
			4		20M	12:15:00	12:35:00	
			5		20M	12:35:30	12:55:30	
			6		20M	12:56:00	13:16:00	
			7-11	10M		13:18:10	13:32:30	
			12		19M50S	13:34:20	13:54:17	
			13		22M51S	14:24:30	14:47:21	
61			1		24M30S	15:21:00	15:45:30	
			2		20M	16:10:20	16:40:20	
			3-7	10M		16:45:00	17:00:10	
			8		30M	17:30:40	18:00:40	
			9		30M	18:00:40	18:30:40	
			1A		30M	19:54:20	20:24:20	
			2A		25M20S	20:30:10	20:55:30	
		Background	3A		20M	21:37:45	21:57:45	
			4A-8A	10M		21:59:10	22:14:45	
			9A		13M30S	22:16:30	22:30:00	
11	315		2		20M	05:06:40	05:26:40	
			3		20M	05:29:00	05:59:00	
			4		20M	05:49:00	06:09:00	
			5-13	18M		06:11:15	06:45:00	
			14		40M	06:46:45	07:26:45	
			15		40M	07:27:45	08:07:45	
			16		35M	08:07:45	08:42:45	

Table 5. 14-3 (continued)

DSS	Day	Position	Record Number	Calibration Period	Accumulation Period	GMT, hr:min:sec Start	End	Comments
42			8		40M	08:56:30	09:36:30	
			9		38M20S	09:36:30	10:14:50	
			1A		10M	10:47:00	10:57:00	
			2A		30M	10:57:00	11:27:00	
			3A		40M	11:27:00	12:07:00	
		Lunar surface	4A		20M	12:08:30	12:28:30	
			5A		30M	12:28:30	12:58:30	
			6A		12M	12:58:30	13:10:30	
			7A		20M	14:14:00	14:34:00	
			8A-9A	4M		14:36:00	14:44:00	
			1B-3B	6M		14:59:00	15:09:00	
			4B		15M	15:10:30	15:25:30	
			5B		10M	15:25:30	15:35:30	
61			1		40M	15:38:32	16:18:32	
			2		40M	16:18:32	16:58:32	
			3		38M28S	16:58:32	17:37:00	
			4		40M	17:44:00	18:24:00	
			5		40M	18:24:00	19:04:00	
			6		40M	19:04:00	19:44:00	
			7		10M	20:32:20	20:42:20	
			8		20M	20:42:21	21:02:21	
			9-13	10M		21:04:25	21:18:35	
			14		40M	21:20:10	22:00:10	
			15		30M	22:00:10	22:30:10	
			16		30M	22:30:10	23:00:10	
11	316		2		20M	07:52:45	08:12:45	
			3		10M	08:12:45	08:22:45	
			4-12	18M		08:25:50	08:59:05	

Table 5. 14-3 (continued)

DSS	Day	Position	Record Number	Calibration Period	Accumulation Period	GMT, hr:min:sec Start	End	Comments
11	316 cont		13		20M	09:02:40	09:22:40	
			14		20M	09:22:40	09:44:40	
42			2		20M	09:37:40	09:57:40	
			3		20M	09:57:40	10:17:40	
			4		15M	10:17:40	10:32:40	
			5		20M30S	10:33:45	10:54:15	A_1, A_2, P_1, P_2, P_4 on
			6		20M	10:54:15	11:14:15	A_1, A_2, P_1, P_2, P_4 on
			7		20M	11:14:15	11:34:15	A_1, A_2, P_1, P_2, P_4 on
			8		20M	11:34:15	11:54:15	A_1, A_2, P_1, P_2, P_4 on
			9		20M	11:54:15	12:14:15	A_1, A_2, P_1, P_2, P_4 on
			10		20M	12:14:15	12:34:15	A_1, A_2, P_1, P_2, P_4 on
			11		20M	12:34:15	12:54:15	A_1, A_2, P_1, P_2, P_4 on
			12		20M	12:54:15	13:14:15	A_1, A_2, P_1, P_2, P_4 on
			13		20M	13:14:15	13:34:15	A_1, A_2, P_1, P_2, P_4 on
			14		20M4S	13:34:15	13:54:19	A_1, A_2, P_1, P_2, P_4 on
			15		20M	14:06:00	14:26:00	A_1, A_2, P_1, P_2, P_4 on
			16		20M	14:26:00	14:46:00	A_1, A_2, P_1, P_2, P_4 on
			17		20M	14:46:00	15:06:00	A_1, A_2, P_1, P_2, P_4 on
			18		20M	15:06:00	15:26:00	A_1, A_2, P_1, P_2, P_3
			19-23	10M		15:28:30	15:44:45	
			24		14M	15:46:00	16:00:00	A_1, A_2, P_1, P_2, P_3
61			1		20M	16:15:03	16:35:03	A_1, A_2, P_1, P_2, P_3
			2		20M	16:35:03	16:35:03	A_1, A_2, P_1, P_2, P_3
			3		20M	16:55:03	17:15:03	A_1, A_2, P_1, P_2, P_3
			4		20M	17:15:03	17:35:03	A_1, A_2, P_1, P_2, P_3
			5		20M	17:35:03	17:55:03	A_1, A_2, P_1, P_2, P_3
			6		20M	17:55:03	18:15:03	A_1, A_2, P_1, P_2, P_3
			7		3M43S	18:22:40	18:18:46	A_1, A_2, P_1, P_2, P_3
			8		19M40S	18:26:23	18:46:03	A_1, A_2, P_1, P_2, P_3
			9		20M	18:46:03	19:06:03	A_1, A_2, P_1, P_2, P_3

Table 5.14-3 (continued)

DSS	Day	Position	Record Number	Calibration Period	Accumulation Period	GMT, hr:min:sec Start	GMT, hr:min:sec End	Comments
61	316 cont		10		20M	19:06:03	19:26:03	A_1, A_2, P_1, P_2, P_3
			11		28M57S	19:26:03	19:46:03	A_1, A_2, P_1, P_2, P_3
42	320		2		10M	12:59:00	13:09:00	
			3-11	18M		13:17:00	13:46:30	
			12		30M	13:49:00	14:19:00	A_1, A_2, P_1, P_2, P_3
			13		10M	14:20:30	14:30:30	A_1, A_2, P_1, P_2, P_3
			14		40M	14:35:00	15:25:00	A_1, A_2, P_1, P_2, P_3
			15		10M	15:37:00	15:47:00	A_1, A_2, P_1, P_2, P_3
			16		40M	15:47:40	16:27:40	A_1, A_2, P_1, P_2, P_3
			17		20M	16:27:40	16:47:40	A_1, A_2, P_1, P_2, P_3
			18		30M	16:50:00	17:20:00	
			19-23	10M		17:21:35	17:33:50	
			24		10M	17:34:25	17:44:25	
61			1		30M	17:59:40	18:29:40	
			2		20M	18:29:40	18:49:40	
			3		20M	18:49:40	19:09:40	
			4		20M	19:09:40	19:29:40	
			5		20M	19:29:40	19:49:40	
			6	2M		19:53:15	19:55:15	
			7		20M	19:57:30	20:17:30	
			8		20M	20:17:30	20:37:30	
			9		20M	20:37:30	20:57:30	
			10		20M	20:57:30	21:17:30	
			11		20M	21:17:30	21:37:30	
			12		40M	21:37:30	22:17:30	
			13		20M	22:17:30	22:37:30	
			14		20M	22:37:30	22:57:30	
			15		20M	22:57:30	23:17:30	
			16-20	10M		23:19:00	23:33:20	
			21		29M59S	23:34:40	00:04:39	

Table 5.14-3 (continued)

DSS	Day	Position	Record Number	Calibration Period	Accumulation Period	GMT, hr:min:sec Start	GMT, hr:min:sec End	Comments
61	321 cont		22		40M17S	00:04:39	00:44:56	
			23		11M30S	00:45:50	00:57:20	
			24		15M	01:00:30	01:15:30	
			25		14M30S	01:15:30	01:30:00	
11			2		30M	01:46:45	02:16:45	
			3		29M50S	02:20:00	02:46:35	
			4		40M	02:50:30	03:30:30	
42		post-translation	2		2M19S	12:50:15	12:52:34	
61	322		1		5M	00:53:30	00:58:30	
			2-6	10M		01:04:00	01:20:25	
			7		10M	01:25:30	01:35:30	A_1, P_1
			8		10M	01:39:00	01:49:30	A_2, P_2
			9		10M	01:52:00	02:02:00	A_1, A_2, P_3
			10		10M	02:06:00	02:16:00	A_1, A_2, P_4
42			2		10M	14:04:00		
			3-7	10M		14:15:30	14:30:10	
			8		15M	14:34:20	14:49:20	A_1, P_1
			9		15M	14:52:00	15:07:00	A_2, P_2
			10		15M	15:09:00	15:24:00	A_1, A_2, P_3
			11		15M	15:25:30	15:40:30	A_1, A_2, P_4
			12		30M	17:03:46	17:33:46	A_1, P_1, P_2, P_3, P_4
			13		20M	17:33:46	17:53:46	A_1, P_1, P_2, P_3, P_4
61			1		30M	18:59:00	19:29:00	A_1, P_1, P_2, P_3, P_4
	324		2		10M	02:55:00	03:05:00	
			3-7	10M		03:07:25	03:23:05	
			8		15M	03:26:30	03:41:30	A_1, P_1

Table 5. 14-3 (continued)

DSS	Day	Position	Record Number	Calibration Period	Accumulation Period	GMT, hr:min:sec Start	GMT, hr:min:sec End	Comments
61	324 cont		9		15M	03:44:30	03:59:30	A_2, P_2
			10		15M	04:02:45	04:17:45	A_1, P_3
	326		1		10M	04:58:30	05:08:30	
			2-6	10M		05:11:05	05:26:50	
			7		15M	05:29:20	05:44:20	A_1, A_2
			8		15M	05:48:20	06:03:20	A_2, P_2
42			2		18M35S	18:28:00	18:46:35	
			3-7	10M		18:48:55	18:59:20	
			8		15M	19:23:20	19:38:20	A_1, P_1
			9		15M	19:40:20	19:55:20	A_2, P_2
			10		15M	19:57:30	20:12:30	A_1, P_3
			11		15M	20:20:20	20:35:20	A_1, P_4
			12		20M	20:38:00	20:58:00	A_1, P_1, P_2, P_3, P_4
			13		20M	21:19:00	21:39:00	A_1, P_1, P_2, P_3, P_4
61			1		20M	23:18:30	23:38:30	A_1, P_1, P_2, P_3, P_4
	327		2		20M	23:57:10	00:17:10	A_1, P_1, P_2, P_3, P_4
			3		20M	00:23:00	00:43:00	A_1, P_1, P_2, P_3, P_4
			4-8	10M		00:50:20	01:05:20	
			9		15M	01:26:30	01:41:30	A_1, P_1
			10		15M	01:43:45	01:58:45	A_2, P_2
			11		15M	02:11:00	02:26:00	A_1, P_3
			12		15M	02:29:00	02:34:00	A_1, P_4
			13		15M	02:46:15	03:01:15	A_1, P_1, P_2, P_3, P_4
			14		20M	03:21:40	03:41:40	A_1, P_1, P_2, P_3, P_4
			15		20M	03:43:10	04:03:10	A_1, P_1, P_2, P_3, P_4
			16		30M	04:05:05	04:35:05	A_1, P_1, P_2, P_3, P_4
			17		20M	04:36:30	04:56:30	A_1, P_1, P_2, P_3, P_4

Table 5. 14-3 (continued)

DSS	Day	Position	Record Number	Calibration Period	Accumulation Period	GMT, hr:min:sec Start	End	Comments
	328		1		10M	02:14:10	02:24:10	
			2-6	10M		02:32:20	02:49:15	
			7		30M	02:52:35	03:22:35	A_1, A_2
			8		30M	03:41:25	04:11:25	A_2, P_2
			9		30M	04:22:15	04:52:15	A_1, P_3
			10		30M	04:55:25	05:25:25	A_1, P_4
			11		30M	05:27:55	05:57:55	A_1, P_1, P_2, P_3, P_4

TABLE 5. 14-4. ALPHA SCATTERING EXPERIMENT SURVEYOR VI SEQUENCE OF OPERATION

Day	GMT, hr:min:sec	Function
313	20:25:06	Compartment C heater commanded on
	22:37:25	Sensor head heater commanded on
314	00:52:25	Compartment C heater commanded off
	00:52:28	Sensor head heater commanded off
	01:09:23	Compartment C heater commanded on
	01:09:32	Sensor head heater commanded on
	05:47:00	Compartment C heater commanded off
	05:39:40	Alpha scattering power commanded on
	21:17:45	Deploy to background
315	12:07:52	Deploy to lunar surface
	20:26	Alpha scattering power commanded off
	20:29	Alpha scattering power commanded on
	23:01	Alpha scattering power commanded off
316	07:48	Alpha scattering power commanded on
	19:57	Alpha scattering power commanded off
	22:38	Alpha scattering power commanded on
	23:39	Alpha scattering power commanded off
320	12:57	Alpha scattering power commanded on
321	03:32	Alpha scattering power commanded off
	12:48	Alpha scattering power commanded on
	12:53	Alpha scattering power commanded off
322	00:40	Alpha scattering power commanded on
	02:19	Alpha scattering power commanded off
	14:00	Alpha scattering power commanded on
	19:30	Alpha scattering power commanded off
324	02:44	Alpha scattering power commanded on
	04:21	Alpha scattering power commanded off
326	04:52	Alpha scattering power commanded on
	06:05	Alpha scattering power commanded off
	18:26	Alpha scattering power commanded on
327	05:06	Alpha scattering power commanded off
328	02:11	Alpha scattering power commanded on
	17:28	Alpha scattering power commanded off

5.14.5 REFERENCE

1) A. L. Turkevich, E. J. Franzgrote, and J. H. Patterson, "Chemical Analysis of the Moon at the Surveyor V Landing Site: Preliminary Results."

5.14.6 ACKNOWLEDGMENT

This section was compiled by H. H. Barker.